INDIAN JOURNAL OF PHYSICS

VOL. XXI

AND

PROCEEDINGS

OF THE

Indian Association for the Cultivation of Science, Vol. XXX

(Published in Collaboration with the Indian Physical Society)

Indian [illegible] Physics

With Nineteen Plates)

PRINTED BY NISHITCHANDRA SEN, SUPERINTENDENT (OFFG.), CALCUTTA
UNIVERSITY PRESS, 48, HAZRA ROAD, BALLYGUNGE, CALCUTTA, AND
PUBLISHED BY THE REGISTRAR, INDIAN ASSOCIATION FOR
THE CULTIVATION OF SCIENCE
210, Bowbazar Street, Calcutta

1947

Price Rs. 12 *or* £1-2-6

INDIAN JOURNAL OF PHYSICS VOL. XXI (1947)

CONTENTS.

PART I

Page

1. On the Evaluation of the Parameter σ_0 in Chapman's formula for Determining the Ionic density of the E layer—By M. M. Sen Gupta and S. K. Dutt. 17
2. Melt Viscosity. Part I-Shellac and its Constituents—By Sadhan Basu.
3. Ring deposits on Surfaces bombarded by Canal rays—By V. T. Chiplonkar. 17
4. On the After-glow of Sodium Chloride and its Decay—By H. N. Bose. 29

PART II

5. Absorption Bands of Iodine in Quartz Ultra-Violet—By Putcha Venkateswarlu. 43
6. Relationship between Wind velocity and Temperature in the free Atmosphere—By S. K. Banerji. 50
7. Distribution of Molecular and Atomic Oxygen in the Upper Atmospere—By H. Rakshit. 57
8. The effect of Spin-Spin interaction on High Veloctiy Scattering—By K. C. Kar. 69
9. On the continuous Emission bands of ICl and IBr.—By R. K. Asundi and P. Venkateswarlu. 76

PART III

10 Melt Viscosity—Part II. Esters, Acetyl derivatives of Shellac and its Constituents—By Sadhan Basu. 83
11. A Circuit for the Control of Ionizing current by a Saturable Core Transformer—By B. M. Banerjee and A. Mukhejee. 90
12. Spectra of Halogens, I_2, Br_2 and Cl_2—By R. K. Asundi and P. Venkateswarlu. 111
13. The purification of Carbon rods for Spectrographic analysis by Cathode layer Arc—By B. Mukherjee. 119
14. Second order Chlorine K-Valence Band Spectra of Chlorides—By K. Das Gupta. 129

PART IV

15. Quantum number, Atomic mass number and Atomic Forces—By M. F. Soonawala. 137
16. Ultra-violet Band systems of Mercury Iodide molecule-Part III—By C. Ramasastry and K. R. Rao. 143
17. Inter-electrode Capacitances of Triode valves at Ultra-high Frequency and their dependence on the Operating condition—By D. K. Ganguli and S. R. Khastgir. 153
18. Some directional observations of Atmospherics on 1000 metres during Sun-set time.—By S. R. Khastgir, M. K. Das Gupta and D. K. Ganguli. 169
19. On the propagation of E. M. waves through the Upper Atmosphere—By M. N. Saha, B. K. Banerjea and U. C. Guha. 181

PART V

20. On the condition of Escape of Microwaves of Radio frequency range from the Sun.—By M. N. Saha, B. K. Banerjea and U. C. Guha. 190
21. X-ray studies of Alkali Chlorides dissolved in B_2O_3-Glass.—By Subodh Kumar Majumdar and Bhupati Kumar Banerjee. 222
22. On the Raman Spectra of Solutions of Ethylene-dibromide in different Solvents—By B. M. Bishui and S. B. Sanyal. 233
23. Measurement of Inherent noise in Radio Receivers—By M. K. Das Gupta, J. Ray and S. R. Khastgir. 239

PART VI

24. X-ray study of some Vegetable Fibres—By Bhupati Kumar Banerjee. 259
25. The Band Spectrum of Cadmium Chloride—By C. Ramasastry. 267
26. A source of Continuous Spectrum in the Ultra-violet—By C. Ramasastry. 272
27. A new Cryostat of the Gas-flow type and a Quartz-fibre Microbance for adopted for Magne-crystalline measurements—By A. Bose. 275
28. Extra Reflections in Laue Photographs of Benzil—By R. K. Sen. 285
29. Comparative studies of the *Joshi-effect* under Single and Bi-phase Half-wave detection—By Bind Bansi Prasad. 295
30. Studies of the Optical properties of some Organic Crystals—By M. N. Datta. 302
31. A note on Thermal Fluctuations—By Duleh Singh Kothari and Laxman Singh Kothari. 307
32. Band Spectrum of Carbon-disulphide—By C. Ramasastry and K. R. Rao. 313

AUTHOR INDEX

Author	Subject	Page
Asundi, R. K. and Venkateswarlu, P.	On the continuous Emissions bands of ICl and IBr.	76
,, ,, ,,	Spectra of Halogens, I_2, Br_2 and Cl_2	111
Banerjee, Bhupati Kumar	X-ray study of some Vegetable Fibres	259
,, ,, B. M. and Mukherjee, A.	A Circuit for the Control of Ionizing current by a Saturable core Transformer	90
Banerji, S. K.	Relationship between Wind velocity and Temperature in the free Atmosphere	50
Basu, Sadhan	Melt-Viscosity Part I—Shellac and its Constituents	7
,, ,,	Melt Viscosity Part II. Esters, Acetyl derivatives of Shellac and its Constituents	83
Bishui, B. M. and Sanyal S. B.	On the Raman Spectra of solutions of Ethylene didromide in different Solvents	233
Bose, A.	A new Cryostat of the Gas-flow type and Quartz-fibre Microbalanc adopted for Magne-crystalline measurements	275
,, H. N.	On the After-glow of Sodium Chloride and its Decay	29
Chiplonker, V. T.	Ring deposits on Surfaces bombarded by Canal rays	17
Datta, M. N.	Studies of the Optical properties of some Organic Crystals	302
Das Gupta, K.	Second order Chlorine K-Valence Band Spectra of Chlorides	129
,, M. K., Ray, J. and Khastgir, S. R.	Measurement of Inherent noise in Radio Receivers	239
Ganguli. D. K. and Khastgir, S. R.	Inter-electrode Capacitances of Triode valves at Ultra-high frequency and their dependance on the Operating condition	153

Author	Subject	Page
Kar, K. C.	The effect of Spin-spin interaction on High velocity Scattering	69
Khastgir, S. R., Das Gupta, M. K. and Ganguli, D. K.	Some directional observations of Atmospherics on 1000 metres during Sun-set time	169
Kothari, D. S. and Kothari, L. S.	A note on Thermal Fluctuations	307
Majumdar, S. K. and Banerjee, B. K.	X ray studies of Alkali Chlorides dissolved in B_2O_3-Glass	222
Mukherjee, B.	The purification of Carbon rods for Spectrographic analysis by Cathode layer Arc	119
Prasad, B. B.	Comparative studies of *Joshi-effect* under Single and Bi-phase Half-wave detection	295
Rakshit, H.	Distribution of Molecular and Atomic Oxygen in the Upper Atmosphere	57
Ramasastry, C.	A source of Continuous Spectrum in the Ultra-Violet	272
	The Band Spectrum of Cadmium Chloride	267
,, and Rao, K.R.	The Band Spectrum of Carbon-disulphide	313
	Ultra-violet Band systems of Mercury Iodide molecule, Part III	143
Saha, M. N., Banerjea, B. K. and Guha, U. C.	On the propagation of E. M. waves through the Upper Atmosphere	181
	On the condition of Escape of Micro-waves of Radio-frequency range from the Sun	109
Sen, R. K.	Extra Reflections in Laue Photographs of Benzil	285
Sen Gupta, M. M. and Dutt, S. K.	On the evaluation of the Parameter σ_0 in Chapman's formula for determining the Ionic density of E-layer	1
Soonawala, M. F.	Quantum number, Atomic mass number and Atomic forces	137
Venkateswarlu, P.	Absorption bands of Iodine in Quartz Ultra-violet	43

SUBJECT INDEX

Subject	Author	Page
Absorption Bands of Iodine in Quartz Ultra-violet	P. Venkateswarlu	43
After-glow of Sodium Chloride and its Decay. On the	H. N. Bose	29
Atmospherics on 1000 metres during Sun-set time. Some directional observations of	S. R. Khastgir, M. K. Das Gupta and D. K. Ganguli	169
Band Spectrum of Cadmium Chloride	C. Ramasastry	267
Band Spectrum of Carbon Disulphide	C. Ramasastry and K. R. Rao	313
Carbon rods for Spectrographic analysis by Cathode layer Arc. The purification of	B. Mukherjee	119
Chlorine K-Valence Band Spectra of Chlorides. Second order	K. Das Gupta	129
Cryostat of the Gas-flow type and a Quartz-fibre Micro-balance adopted for Magne-crystalline measurements. A new	A. Bose	275
Emission Bands of ICl and IBr. On the continuous	R. K. Asundi and P. Venkateswarlu	76
E. M. waves through the Upper Atmosphere. On the propagation of	M. N. Saha, B. K. Banerjea and U. C. Guha	11
Ionic density of the E-layer. On the evaluation of the Parameter σ_0 in Chapman's formula for determining the	M. M. Sen Gupta and S. K. Dutt	1
Ionizing current by a Saturable core Transformer. A Circuit for the control of	B. M. Banerjee and A. Mukherjee	90
Joshi-effect under Single and Bi-phase Half-wave detection. Comparative studies of	B. B. Prosad	295
Laue Photographs of Benzil. Extra Reflections in	R. K. Sen	285
Microwaves of Radio frequency Range from the Sun. On the condition of Escape of	M. N. Saha, B. K. Banerjea and U. C. Guha	199

Subject	Author	Page
Optical properties of some Organic Crystals. Studies of the	M. N. Dutta	302
Quantum number, Atomic mass-number and Atomic forces	M. F. Soonawala	137
Radio Receivers. Measurement of Inherent noise in	M. K. Das Gupta, J. Ray and S. R. Khastgir	239
Raman Spectra of Solutions of Ethylene Dibromide in different Solvents. On the	B. M. Bishui and S. B. Sanyal	233
Ring deposits on Surfaces bombarded by Canal rays	V. T. Chiplonkar	17
Spectrum in the Ultra-violet. A source of Continuous	C. Ramasastry	272
Spin-spin interaction on High velocity Scattering. The effect of	K. C. Kar	69
Spectra or Halogens, I_2, Br_2 and Cl_2	R. K. Asundi and P Venkateswarlu	111
Thermal Fluctuations A note on	D. S. Kothari and L. S. Kothari	307
Triode Valves at Ultra-high frequency and their dependence on the Operating condition. Inter-electrode Capacitances of	D. K. Ganguli and S. R. Khastgir	153
Ultra-violet Band Systems of Mercury Iodide molecule. Part III	C. Ramasastry and K. R. Rao	143
Upper Atmosphere. Distribution of Molecular and Atomic Oxygen in	H. Rakshit	57
Viscosity-Melt. Part I—Shellac and its constituents	S. Basu	7
Viscosity-Melt Part II. Esters, Acetyl derivatives of Shellac and its constituents	S. Basu	83
Wind Velocity and Temperature in the free Atmosphere. Relationship between	S. K. Banerji	50
X-ray studies of Alkali Chlorides dissolved in B_2O_3-Glass	S. K. Majumdar and B. K. Banerjee	222
X-ray study of some Vegetable Fibres	B. K. Banerjee	259

ON THE EVALUATION OF THE PARAMETER σ_0 IN CHAPMAN'S FORMULA FOR DETERMINING THE IONIC DENSITY OF THE E LAYER

By M. M. SENGUPTA[*] and S. K. DUTT

(*Received for publication Nov. 29, 1946*)

ABSTRACT. In our previous paper it has been mentioned that the discrepancy of the theoretical values of ionic densities from experimental ones for E layer is due mainly to the assumption of taking σ_0 constant during day and night. In the present paper the authors give the values of σ_0 which seem to give the best agreement possible.

In a previous paper (Sengupta and Dutt, 1941) it was shown by the authors that in the early part of the night of winter months of 1940-41 radio waves of frequency 810 kc/s transmitted from the Calcutta Station (Lat. 22°34'N, Long. 88°55'E) reached Patna (Lat. 25°30'N, Long. 85°15'E) after reflection from the E layer while in the same period of night of summer months of 1941 those waves penetrated the E layer. It was also pointed out that our results were in agreement with those obtained at Watheroo (Lat. 30° 19'S, Long. 115° 53'E) which has almost the same latitude as Patna but in the opposite hemisphere. This type of result could not be predicted from Chapman's (1931) formula with a constant value of the parameter σ_0 in the formula throughout day and night and for all seasons. In the present work an attempt has been made to find suitable day-time and night-time values of σ_0 for summer and winter months.

Curves showing the variation of ion density with time (ν, ϕ) for June and December of Watheroo, are given in Figs. 1 and 2. Tables I and II give the values of the critical frequencies (f_c) for E layer at Watheroo observed by Parkinson and Prior (1939, 1940, 1941) by the modern automatic multi frequency equipment for June of years 1938 to 1941 and for December of years 1938 to 1940 respectively. Square values of the critical frequencies are calculated and finally the squares reduced to fractions by a suitable choice of a factor such that the midday value (obtained from the graph of hours and squares of critical frequency) corresponded to the theoretical value of ν where

$\nu = n/n_0$; n = ion-density at any time.

n_0 = the maximum steady value of n if the rate of production of ions were to remain constant at its maximum possible value.

All the critical frequencies f_c in Mc/s are for the E layer at Watheroo (lat. 30° 19'S, Long. 115° 53'E).

---

[*] Fellow of the Indian Physical Society.

TABLE I

(Winter)

120°E mean time Hours	June, 1938		June, 1939		June, 1940		June, 1941		Mean* ν
	f_c	ν	f_c	ν	f_c	ν	f_c	ν	
12	3.43	0.773	3.51	0.773	3.37	0.773	3.04	0.773	0.773
13	3.36	0.742	3.44	0.742	3.30	0.741	3.03	0.768	0.748
14	3.25	0.603	3.37	0.713	3.07	0.641	2.96	0.733	0.675
15	3.04	0.607	3.05	0.584	2.86	0.557	2.74	0.628	0.594
16	2.69	0.475	2.61	0.427	2.47	0.415	2.33	0.454	0.443
17	2.05	0.270	1.91	0.229	1.85	0.233	1.65	0.228	0.242
18			1.17	0.086					
19			1.00	0.063					
20			.94	.055					
21			.81	.041					
22			.73	.033					
23			.75	.035					
00			.70	.031					
01			.69	.030					
02			.67	.028					
03			.66	.027					
04			.68	.029					
05			.79	.039					
06			.85	.045	0.78	0.041			0.043
07	1.65	0.179	1.74	.190	1.61	.176	1.52	0.193	.184
08	2.57	.433	2.55	.408	2.50	.425	2.28	.435	.425
09	2.93	.564	3.02	.572	2.90	.572	2.57	.552	.565
10	3.21	.676	3.27	.672	3.11	.658	2.90	.704	.677
11	3.34	.732	3.41	.730	3.25	.719	3.00	.753	.734

*Hourly critical frequencies for the whole night are available for June, 1939 and December, 1938 only

Prof Chapman's theory (1931) of ionization of the upper atmosphere has been applied to construct curves for Watheroo showing the variation of ionic density with time (ν, ϕ). (The notation is according to Chapman's paper). In actual construction the simple approximate method of Millington (1932) together with his envelope correction (1935) has been made use of for solving the fundamental differential equation and obtaining the upper limit of theoretical ν values. Attempts were made to find the best fit with the experimental values by taking different constant values for both day and night of parameter σ_0 such as 0.01, 0.02, 0.03, etc. and the results for December and June are shown in Figs. 1 and 2. Here the average declination of the sun for the respective months has been considered and for greater accuracy points were obtained at close intervals by making $\phi_2-\phi_1=0.1$ for a few hours around noon and $\phi_2-\phi_1=0.05$ for the hours near sunset and sunrise. These results indicate that by taking σ_0 constant for day and night there is no good fit. It may be noted that for a few hours round about noon, curves drawn with different values of σ_0 practically overlap. The effect of alteration in the value of σ_0 is most pronounced during an hour or so before sunset. The value of σ_0 corresponding to the best agreement between the theoretical

TABLE II

(Summer)

120°E mean time Hours	December, 1938		December, 1939		December, 1940		Mean ν
	f_E	ν	f_E	ν	f_E	ν	
12	4.02	0.996	3.74	0.996	3.59	...	0.996
13	3.96	.967	3.74	.996	3.64	0.974	.979
14	3.83	.904	3.59	.918	3.58	.943	.922
15	3.80	.890	3.61	.877	3.45	.875	.881
16	3.50	.755	3.26	.757	3.21	.757	.756
17	3.10	.592	2.90	.599	2.85	.597	.596
18	2.44	.367	2.23	.354	2.22	.362	.361
19	1.46	.131	1.39	.137	1.45	.154	.141
20	.75	.0345					
21	.63	.0247					
22	.58	.0210					
23	.53	.0173					
00	.54	.0179					
01	.53	.0173					
02	.56	.0191					
03	.57	.0197					
04	.60	0.022	0.65	0.030			0.026
05	1.46	.131	1.44	.147	1.43	0.150	.143
06	2.45	.370	2.29	.373	2.19	.353	.365
07	3.06	.577	2.82	.566	2.69	.532	.558
08	3.47	.742	3.20	.729	3.12	.716	.729
09	3.79	.885	3.46	.852	3.42	.860	.866
10	3.95	.962	3.66	.923	3.55	.927	.937
11	4.01	.991	3.70	.975	3.67	.991	.986

and experimental curves during this period, was, therefore, taken as the value giving a good fit. The value of $\sigma_0 = 0.01$ no doubt agrees closely with the summer month of December of Watheroo and 0.03 for winter month of June for day-time only ; but during night-time the agreement fails.

Now, according to the theory there should be continuous decay of ionic density during the night. The proper values of σ_0, therefore, for the night were obtained directly from the experimental observations of continuous decay of the ionic density during night. It may be noted, however, that for the evaluation of the above, observations were confined to early part of night only to avoid complications due to replenishing of the ionization which has been observed by Mitra (1938) and by Best, Farmer and Ratcliffe (1938) in the later part of night about 4 hours before sunrise. The values of night-time σ_0 that were obtained directly are given in Table III and are found to be different for different seasons. They are also found to differ from day-time values ($\sigma_0 = 0.01$ for December and $\sigma_0 = 0.03$ for June) giving the best fit.

TABLE III

Summer		σ_0	Winter	σ_0
December, 1938	...	0.029	June, 1939	0.059
January, 1939	...	0.023	July, 1939	0.064

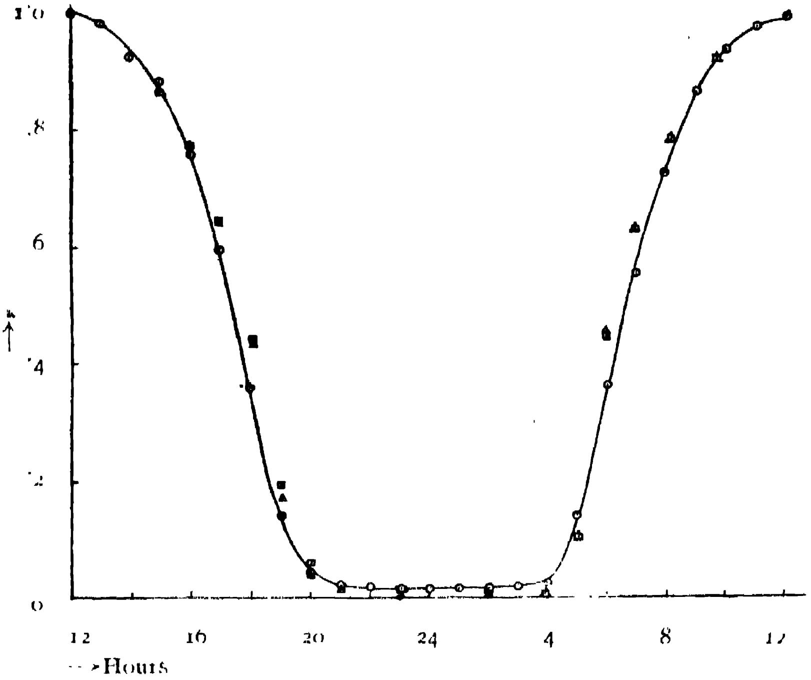

Fig. 1

December Curves

⊙ Experimental curve (mean for years 1938-40)

□ ..Points of theoretical curve with $\sigma_0=0.02$

△...Points of theoretical curve with $\sigma_0=0.01$

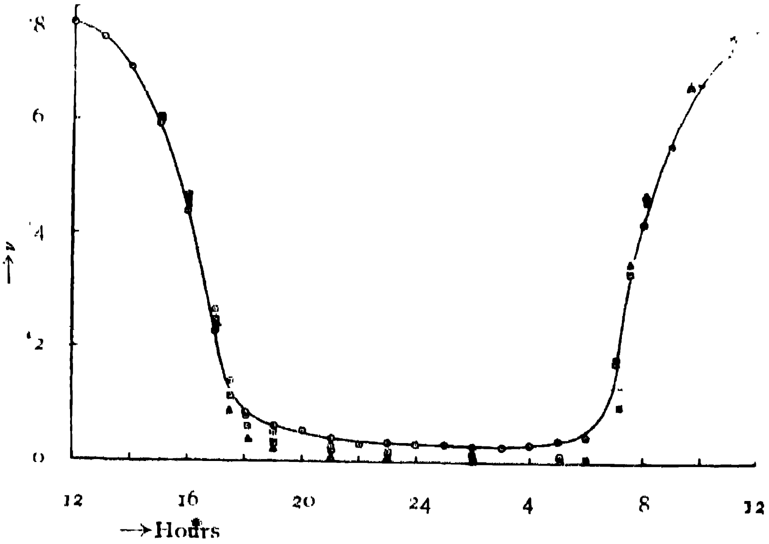

Fig. 2

June Curves

⊙...Experimental curves (mean for years 1938-41)

∵ ...Points of theoretical curve with $\sigma_0=.03$

□ ..Points of theoretical curve with $\sigma_0=.02$

△...Points of theoretical curve with $\sigma_0=.01$

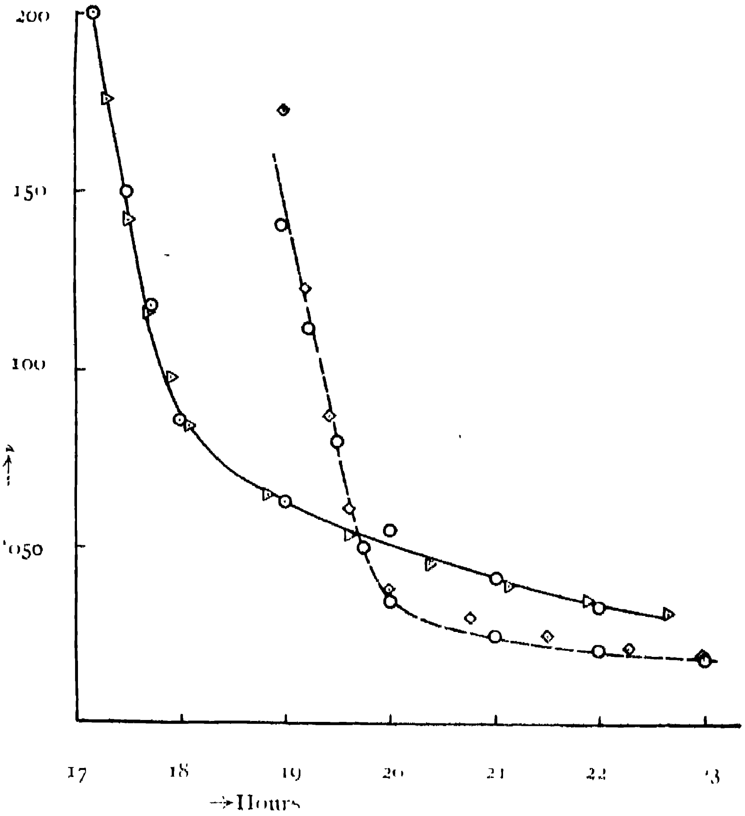

FIG. 3

△, △ ...Theoretical curve

⊙ ..Experimental curve

June, 39 curve (full line)
$\sigma_0 = 0.03$ (day time)
$\sigma_0 = 0.059$ (night-time)
December, 38 curve (broken line)
σ_0 0.01 (day-time)
$\sigma_0 = 0.029$ (night-time)

To obtain the best fit, therefore, it is necessary to take different values of σ_0 for seasons as well as for day and night. The theoretical curves of Fig. 3 are drawn with $\sigma_0 = 0.01$ (day-time), $\sigma_0 = 0.029$ (night-time) for December (summer) and with $\sigma_0 = 0.03$ (day-time), $\sigma_0 = 0.059$ (night-time) for June (winter) in which the experimental data are also plotted for comparison ; the agreement comes out to be very close both for day and night and for seasons also.

Summer and winter (ν, ϕ) curves derived from Chapman s formula with a constant values of σ_0 for day and night throughout the year, will not intersect each other as the rate of ionization at any hour in summer is greater than that in winter for the same hour. But with different values of σ_0 the theoretical curves (Fig. 3) do intersect and agree with the experimental observations. The net result of different values of σ_0 is that the night-time ionic density of E layer for winter is larger than that for summer, though the noon value for the latter season is much higher than that for the winter.

That σ_0 has different values for night and day has been observed by Best, Farmer and Ratcliffe (*loc. cit.*). They found that for both summer and winter the night-time value of σ_0 is 0.098 corresponding to recombination co-efficient $\alpha=4\times10^{-9}$ and day-time value of σ_0 a little greater than 0.032 corresponding to $\alpha=1.2\times10^{-8}$. That it is necessary to assume a greater rate of recombination during the day than during the night, is confirmed by some curves calculated by Wilkes (1939) from observations made at Washington (Lat. 38° 50′ N, Long. 77° 00′ W) on 31st August, 1932, when an eclipse of the sun took place, δ by Kirby, Gilliland and Judson (1936). He points out that the day-time curves on eclipse day with $\sigma_0=0$, α very large or $\sigma_0=0.032$, fit in with the experimental curves better than the one for $\sigma_0=0.098$. Hulburt (1939) concludes that during day-time the available data favour $\sigma_0=0.019$ ($\alpha=2\times10^{-8}$) but do not preclude an even lower value of σ_0, *i.e.*, a higher rate of recombination.

Another point to be noted is that the summer night time value of σ_0 for Watheroo is found to be approximately 3 times the day-time value of σ_0 while winter night-time value is twice that during day-time. The night-time and day-time values of σ_0 as observed by Best, Farmer and Ratcliffe are in the ratio of 3 : 1.

From the above it is clear that the values of σ_0 obtained from the data of Watheroo are quite probable in view of the determinations of Hulburt, and of Best, Farmer and Ratcliffe. It has been shown by us (Sengupta and Dutt, 1944) that the behaviour of the ionosphere in the Patna-Calcutta region (about 24° N latitude) has been experimentally found to be similar to that of Watheroo, so far as the ionic densities of summer and winter are concerned; it, therefore, seems that the most probable values of σ_0 for latitudes 24° to 30° North or South, may be taken as given above.

PHYSICS LABORATORY,
SCIENCE COLLEGE,
PATNA

REFERENCES

Best, Farmer and Ratcliffe, 1938, *P.R.S. (A)*, **164**, 96.
Chapman, 1931, *Proc. Phy. Soc. (Lond.)*, **43**, 26 and 483.
Hulburt, 1939, *Phy. Rev.*, **56**, 639.
Kirby, Gilliland and Judson, 1936, *Proc. I.R.E.*, **24**, 1027.
Millington, 1932, *Proc. Phy. Soc. (Lond.)* **44**, 580.
Millington, 1935, *Proc. Phy. Soc, (Lond.)*, **47**, 263.
Mitra, 1938, *Science and Culture*, **3**, 496.
Parkinson and Prior, 1939, *Terr. Mag. & Atmos. Elec.* **44**, 199, 341 & 401; 1940, *Ibid.*, **45**, 45 & 471; 1941, *ibid.*, **46**, 79.
Sengupta and Dutt, 1944, *Ind. Jour. Phy.*, **18**, 88.
Wilkes, 1939, *Proc. Phy. Soc.*, **51**, 138.

2

MELT VISCOSITY PART I—SHELLAC AND ITS CONSTITUENTS

By SADHAN BASU

(Received for publication, Aug. 5, 1946)

ABSTRACT. The activation energy for viscous flow for dewaxed shellac, hard resin and soft resin have been found to be 38.13, 33.34, 47.07 K-cal respectively. These high activation energy values have been explained as due to the aggregation of polar molecules to give bigger 'micelles'

The value of the viscous volume for dewaxed shellac, (7.023×10^{-18} c.c.) has been found to be nearer to the value of soft resin (7.50×10^{-18}) than to that of hard resin (4.56×10^{-18}). A tentative explanation for this has been offered

It is also found that of all the molecules that are activated only a small fraction are suitably oriented for flow.

INTRODUCTION

A really efficient use of a plastic material for moulding purposes demands a thorough knowledge of its structural properties. The factors on which ultimately such properties rest are the chemical units, length, flexibility, orientation, the nature of the side groups and the effective forces between the units. The forces between the building units, for instance, vary within wide limits, being very strong for the primary valency bonds and relatively weak for secondary van der Waals' forces. They also vary greatly depending on whether the attraction is between polar groups or between non-polar groups, the attraction in the former case being stronger than in the latter case. It has been shown by Grunberg and Nissan that the activation energy for viscous flow is a measure of the cohesive forces between the non-polar units, but in the case of polar substances the energy is much greater owing to association which leads to the formation of aggregated 'micelle'. The significance of this activation energy for viscous flow has been given by Eyring and others (1936, 1937a, 1937b), and Smallwood (1937) and its relationship with the size of the moving unit as also its orientation has been clearly brought out. Though shellac has long been used in the production of moulded articles not much is known about its structural units, particularly the state of the molecules as also the forces between the units. To fill up this gap in our knowledge, a series of investigations have been planned and partly carried out on shellac and its various modifications that are used in moulding operations; the present paper, which is the first of a series, summarises the results of viscosity studies on molten shellac resins.

THEORETICAL

The ground-stone in Eyring's deduction lies in the recognition of the fact that in most cases flow takes place by movement of activated or energy-rich molecules which allow all transport phenomena, such as viscosity, diffusion etc., to be treated logically by the theory of reaction rate, considering the flow process as a unimolecular chemical reaction.

Quantum-mechanically speaking, the molecules in a liquid are confined by Van der Waal's forces to a region of minimum potential energy. In course of statistical fluctuation, some molecules may acquire energy in excess of the average and as a result may escape from one potential minimum to another adjacent potential minimum corresponding to a different energy value. In the state of equilibrium the jumping of the molecules will take place uniformly in all directions. The application of a shearing stress to the liquid, however, causes a lowering of activation energy corresponding to motion in one particular direction, *i.e.*, the number of jumps along the direction of applied stress preponderates over that in the opposite one, which is the same thing as saying that the liquid flows along the direction of applied stress.

Deducing the rate of forward and backward flow from the above consideration Smallwood (*loc. cit.*,) has obtained an expression for the viscosity, namely,

$$\eta=\tfrac{1}{2}\,f\,\frac{\lambda_1}{\lambda},\ \frac{1}{k_0}\cdot\frac{h}{kT}\ \exp.{E_0/kT}\Big/\sinh\frac{f\lambda\lambda_2\lambda_3}{kT}\qquad\ldots\quad(1)$$

where f = applied stress, k_0 = equilibrium constant, E_0 = depth of the potential height, *i.e.*, the activation energy in absence of shearing stress, λ_2 and λ_3 distances between moving units in two given directions, λ_1 distance between two moving parallel layers, λ the distance through which each molecule jumps, k = Boltzmann's constant, T = absolute temperature, and h = Planck's constant.

In the case of non-Newtonian liquids, equation (1) changes into

$$\eta=f.\frac{\lambda_1}{\lambda}.\ \frac{1}{k_0}\cdot\frac{h}{kT}\ .\ \exp.\ \frac{E_0-\frac{1}{2}f\lambda\lambda_2\lambda_3}{kT}\qquad\ldots\quad(2)$$

which may be written as

$$\eta=A.\ f.\ \exp.\frac{a-bf}{T}\qquad\ldots\quad(3)$$

This equation has been applied by Smallwood (*loc. cit.*,) as also by Ewell (1938) to the case of rubber in elucidating the flow process and calculating its structural constants. In the present paper an attempt has been made to apply this method to the case of shellac and its constituents and examine the results with a view to throwing light on the structural problem.

EXPERIMENTAL

Apparatus.—The measurement of viscosity of the molten resin was done by means of a modified form of Ostwald's viscometer first suggested by Lee (1934) for tar. The original apparatus of Lee was modified for the present investigation since without modification the filling up of the Viscometer proved very difficult and complete elimination of air bubbles from the melt was found almost impossible. Further, a single measurement with Lee's unmodified apparatus would require a very much longer time and therefore involve some possibility of shellac undergoing polymerisation. With the modified apparatus, however, a period of about half an hour was found sufficient for the measurement to be complete, which, since the temperature was below 100°C, reduced the chance of polymerisation to an insignificant degree.

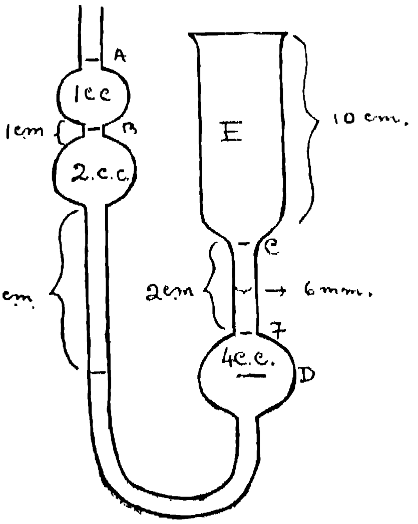

FIG. 1

The diagram of the modified apparatus is shown in Fig. 1. The driving pressure was applied by means of a mercury column, the free surface of which served as an index to the flow of resin. The viscometer was made of glass, the approximate dimensions of various parts of which are indicated in Fig. 1. Sufficient mercury was poured into the viscometer so as to fill it up to C or from A to D. The amount of molten resin, required to fill the viscometer from C to E, was found out by trial. The viscometer was placed in an oil thermostat and when a steady temperature had been attained, suction was applied at the upper end of A. The resin from CE moved down into the bulb D. The movement of mercury was observed in the tube AB and the time taken by it to move from A to B was noted when connection was established with atmospheric pressure.

The apparatus was first calibrated with technical glucose jelly of Baker, the viscosity of which had been first determined with a falling sphere viscometer. The viscosity measurements were done at the same temperature with both the instruments. The viscosity in Ostwald viscometer is given by $\eta = kt$ where t is the time taken by the mercury to move from A to B, and k is a constant for the apparatus. The value of k was found out by calibrating the viscometer with technical glucose.

To measure viscosity at various shearing stresses a three-way stop-cock was attached at the upper end of A by which both suction and high pressure could be applied as required, the pressure being registered by means of a mercury manometer. The shearing stress was calculated from the following equation

$$f = \frac{r\Delta P}{2l}$$

where ΔP = driving pressure, r = the radius of the tube CF, and l = length of CF.

Procedure.—The evaluation of the constants in equation (3) was effected by a graphical method. The equation (3) was first transformed into

$$\log_{10}\eta/f = \log_{10} A + \frac{a-bf}{2.3T} \qquad \ldots \text{(4a)}$$

$$\text{and } \log_{10}\eta = (\log_{10} A + \log_{10} f) + \frac{a-bf}{2.3T} \qquad \text{(4b)}$$

The slope of the curve obtained by plotting $\log_{10}\eta$ against $1/T$ at a constant stress gave the value $(a-bf)/2.3$; similarly, $b/2.3T$ was obtained by plotting $\log_{10}\eta/f$ against 'f' at a constant temperature. The values of a, b and A in equation (3) thus obtained could be employed in finding out $\lambda\lambda_2\lambda_3$ (viscous volume) and E_0 (activation energy) from the relation $b = \lambda\lambda_2\lambda_3/kT$, and $a = E_0/k$. Further E_0 being the activation energy for a molecule, the value of molar activation energy E'_0 is given by aR, where R is the gas constant.

RESULTS

The experimental values of viscosity at different temperatures for hard

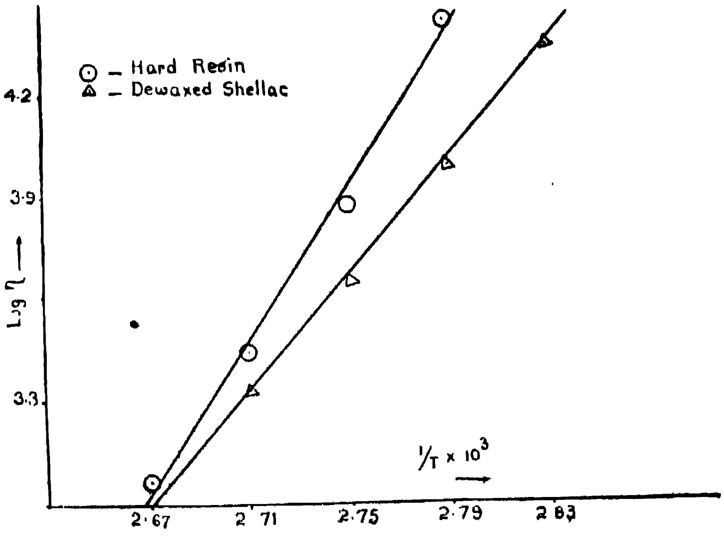

FIG

resin, dewaxed shellac and soft resin are given in Tables I, II and III, and the corresponding $\log_{10} \eta - 1/T$ curves are shown in Figs. 2 and 3.

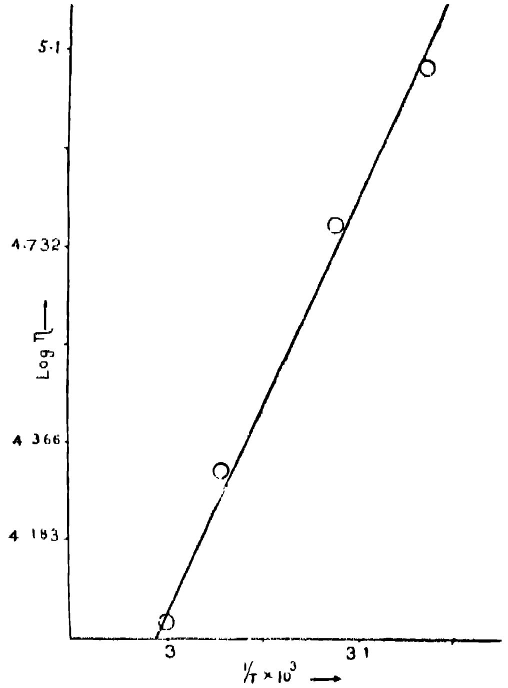

FIG. 3

○ Soft resin

TABLE I

$f = 6.5214 \times 10^3$ dynes/cm^2

Hard Resin

Temperature			Viscosity in	
t°c	T°K	$1/T \times 10^{-3}$	pois (η)	$\log_{10}$
85	358	2.79	27,229.55	4.4349
90	363	2.75	7,526.80	3.8766
95	368	2.71	2,787.48	3.4451
100	373	2.67	1,316.31	3.1182

TABLE II

$f = 6.5214 \times 10^3$ dynes/cm^2

Soft Resin

Temperature			Viscosity in	
t°c	T°K	$1/T \times 10^{-3}$	pois (η)	$\log_{10}$
45	318	3.14	117,912	5.0715
50	323	3.09	58,956	4.7705
57	330	3.03	20,810	4.3183
60	333	3.00	10,405	4.0191

TABLE III

$f = 6.5214 \times 10^3$ dynes/cm^2

Dewaxed Shellac

Temperature		$1/T \times 10^{-3}$	Viscosity in pois (η)	$\log_{10}$
t°c	T°K			
80	353	2.83	22,505.00	4.3522
85	358	2.79	10,062.95	4.0024
90	363	2.75	4,533.15	3.6561
95	368	2.71	2,154.05	3.3304

The viscosity data at different shearing stresses are shown in Tables IV, V and VI, and the corresponding $\log_{10} \eta/f - f$ curves in Figs. 4 and 5 respectively.

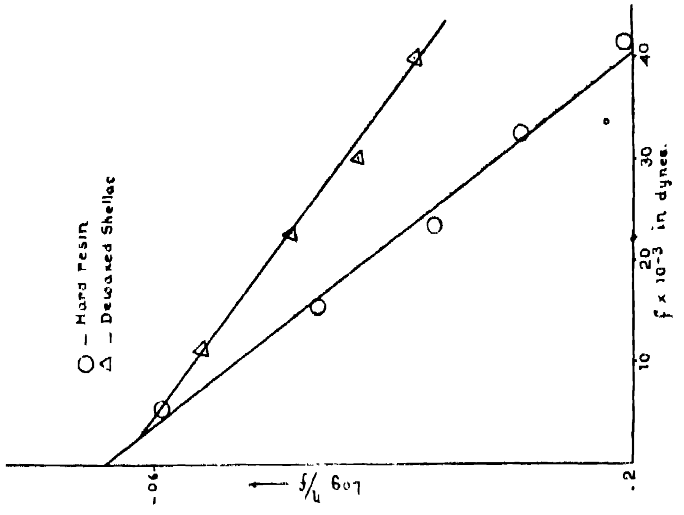

FIG. 2

TABLE IV

Temperature = 365°K

Hard Resin

f in dynes/cm$^2 \times 10^{-3}$	Viscosity in pois (η)	η/f	$\log_{10}(\eta/f)$
6.5214	5,591.10	0.8570	−0.0670
15.4300	2,636.30	0.1707	−0.7520
23.7400	1,639.65	0.0690	−1.1612
32.7500	932.35	0.0284	−1.5467
41.7400	450.10	0.0107	−1.9706

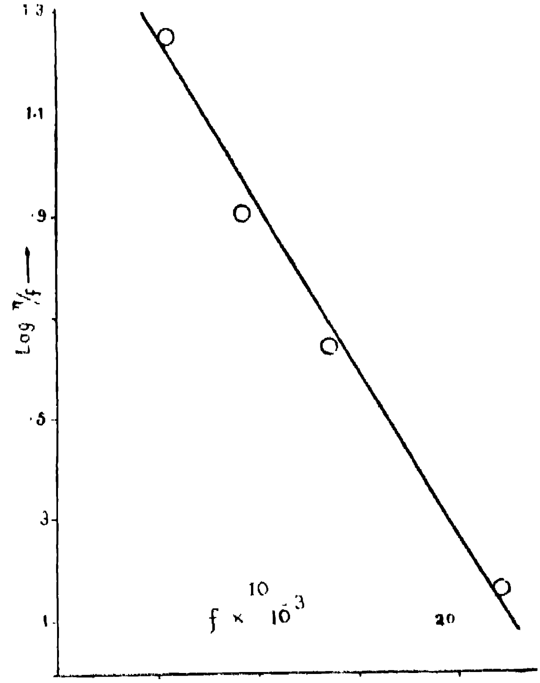

FIG. 5

○ Soft resin.

TABLE V

Temperature = 318° K

Soft Resin

f in dynes/cm^2 × 10	Viscosity in pois (η)	η/f	$\log_{10} \eta/f$
6.5214	117,912	18.080	1.2572
10.6960	84,966	7.943	0.9000
14.9940	65,892	4.390	0.6425
22.1910	32,946	1.480	0.1703

TABLE VI

Temperature = 356°K

Dewaxed Shellac

f in dynes/cm^2 × 10^{-3}	Viscosity in pois (η)	η/f	$\log_{10} \eta/f$
6.5214	18,518.40	2.8420	0.4535
14.6170	8,584.05	0.5970	−0.2314
22.9910	5,304.75	0.2300	−0.6383
30.2880	3,922.30	0.1290	−0.8894
40.4840	3,150.70	0.0778	−1.1090

The values of *a*, *b* and Λ as obtained from the graphs (2 – 5) and above data as also E'_0 and $\lambda\ \lambda_2\ \lambda_3$ calculated therefrom are given in Table VII.

TABLE VII

	a	b	Λ	E'_0(K-cal)	$\lambda\ \lambda_2\ \lambda_3$ in c.c.	Molecular volume in c c.
Hard resin	4,5224.0	1.656×10^{-3}	9.882×10^{-31}	47.673	4.557×10^{-19}	2.96×10^{-21}
Soft resin	1,7108.8	2.764×10^{-2}	1.807×10^{22}	33.335	7.5624×10^{-18}	0.97×10^{-21}
Dewaxed shellac	1,9764.4	2.775×10^{-2}	2.656×10^{24}	38.133	7.623×10^{-18}	1.59×10^{-21}

DISCUSSION

Constant b—For all the three substances used in the above experiments the value of $\lambda\ \lambda_2\ \lambda_3$ is found to be much higher than the actual molecular volume. If, as an explanation of this, it is assumed that a molecule taking part in the flow has to move through a distance much greater than its own linear dimensions then the activation energy for such flow process must be higher than the vaporisation energy (Kauzmann and Eyring, 1940), which would mean that activation would lead to vaporisation rather than to flow. Thus the only probable explanation seems to be that the moving units themselves are much bigger than the individual molecules, *i.e.*, they exist in the form of micelles These micelles are, in the broadest sense, defined as clusters of molecules held together by secondary valency forces. This, however, does not suggest that the micelles, during the course of flow, move bodily through a distance equal or nearly equal to their length in any direction. In fact, this cannot happen in shellac resins which contain a number of active polar groups. For as a 'micelle' flows, secondary or dipole bonds between adjacent micelles are broken, but before it can go very far the broken bonds will recombine with the loose ends of another micelle. As a result the micelle will move by jumps between successive polar gorups *i.e.*, flow takes place by segments. The smaller the number of polar groups and the more widely they are distributed on the surface of the micelles the greater will be the distance jumped by the micelle. Thus in soft resin, where the number of polar groups is smaller, the viscous volume is relatively large, *i.e.*, the distances between the successive polar groups are great, whereas in hard resin, with its larger number of polar groups, the encounter between the broken ends will be more frequent, resulting in a smaller viscous volume for it than in case of soft resin.

Coming to the case of shellac, if it were a simple mixture of hard and soft resin without mutual interaction, it might be expected to obey the ideal mixture law and accordingly, the values of these or any other constants would be strictly deducable as a weighted mean, from the corresponding values of its constituent resins. Actually, however, the value of $\lambda \lambda_2 \lambda_3$ for shellac is found to be much greater than such a weighted mean. This is either because in shellac, the soft resin is included in the hard resin micelle, or because the soft resin brings about some modification in the orientation of the hard resin such that spatial separation of polar groups on the surface of the micelles is somehow increased.

Constant E'_0.—The values of E'_0, *i.e.*, the activation energy per mole as calculated for shellac, hard resin and soft resin appear to be too high to be caused by the usual type of weak van der Waals' forces. A probable explanation for this may be found in the presence of a large number of highly active polar groups, *i.e.*, hydroxyl and carboxyl groups in the molecules, which means that any flow process involving transport of such molecules must require, besides the usual energy to overcome van der Waal's forces, considerable additional energy on account of a relatively large number of secondary or inter-molecular hydrogen bonds that must be broken in bringing about the activated state. The activation energy, in other words, would be partly 'structured'.

It has been shown by Kauzmann and Eyring (*loc. cit*) that for non-associated substances; increase in molecular weight causes but a small increase in the activation energy; but the difference in the activation energy of hard resin and soft resin is too large to be accounted for merely on ground of their difference in molecular weight and may be explained only on the assumption that both hard and soft resins are associated or aggregated, the extent of aggregation being much greater in the former than in the latter.

Constant A.—The value of A from the equation (3) comes out to be equal to

$$\frac{\lambda_1}{\lambda} \cdot \frac{1}{k_0} \cdot \frac{h}{kT} \cdot$$

which from the theory of reaction rate becomes

$$A = P(\lambda_1/\lambda)\ (F_n/F_n^*)\ \left(\frac{h}{kT}\right) \qquad \ldots \quad (4)$$

where P is the probability factor, F_n and F_n^* are the partition functions of the initial and the activated states respectively, the other terms having the same significance as stated previously. Since λ_1 and λ will have the same order, if not the same value, λ_1/λ may be taken as approximately unity. Hence from (4) we get

$$P(F_n/F_n^*) = A/\frac{n}{kT} \qquad (5)$$

The values of the right hand side of the equation (5) as obtained for hard and soft resins are 2.05×10^{-18} and $3{\cdot}7 \times 10^{-10}$ respectively. This is evidently a very low value and may be due to the fact that either both **P** and (F_n/F_n^*)

are small or one of the factors very small in comparison with the other. Since, however, (F_n/F_n^*) cannot be less than unity in which case the activated state would be more favoured than the normal state, P must be very low. This means that of all the molecules that are activated, only a few satisfy the spatial requirement to jump from one potential minimum to another. In other words, the molecules must be favourably oriented before they can 'jump' on activation.

ACKNOWLEDGMENT

The author wishes to express his gratefulness to Dr. P. K. Bose, D.Sc., F N I., Director, Indian Lac Research Institute, for his great interest in the work and constant encouragement.

Indian Lac Research Institute,
Namkum, Ranchi.

REFERENCES

Ewell, 1938, *Jour. Appd. Phys*, **9**, 252.
Eyring and others, 1936, *Jour. Chem. Phys*, **4**, 283.
Eyring and others, 1937a *Jour. Chem. Phys.*, **5**, 726.
Eyring and others, 1937b *Jour. Phys. Chem*, **41**, 249.
Grunberg and Nissan, 1944, *Nature*, **153**, 146
Kauzmann and Eyring, 1940, *Jour. Amer. Chem. Soc.*, **62**, 3113.
Lee, 1934, *Jour. Soc. Chem. Ind.*, **53**, 69.
Smallwood, 1937, *Jour. Appd. Phys*, **8**, 505.

3

RING DEPOSITS ON SURFACES BOMBARDED BY CANAL RAYS

By V. T. CHIPLONKAR

(Received for publication, December [illegible])

(Plates IA and IB)

ABSTBACT The paper deals with a detailed investigation on the formation of the deposits with the ring structure, obtained on surfaces, due to bombardment by positive rays, in the observation chamber of a canal ray tube of the usual simple type (when hydrocarbon substances are present in the discharge tube). The phenomenon has been studied as a function of the nature and condition of the surface bombarded, nature of the gas in the discharge tube, energy of the rays, time for which the bombardment takes place, etc. Special experiments are reported which were carried out to elucidate the mechanism of (1) the deposit formation, (2) origin and development of the ring structure. The results obtained have been finally discussed and a mechanism suggested for the deposit formation.

INTRODUCTION

The formation of deposits, in discharge tubes under different forms of discharge, has often proved of interest and has led to interesting results on the space distribution of the potential in the tube. The formation of deposits, on surfaces bombarded by canal rays in the observation chamber of a canal ray tube, takes place under conditions which are much simpler, as this space is free of the electric field. Black deposits are known to form on plates of glass or metal when bombarded by canal rays which have not been passed through an analysing field prior to the impact. An examination of these deposits by electron diffraction led Raether (1933) to ascribe them to carbon, produced from the decomposition of the hydrocarbon vapours usually present in the discharge tubes. That these deposits show a ring structure under certain circumstances was shown by Dasannacharya, Chiplonkar and Sapre (1934). As the phenomenon did not appear to have been investigated in sufficient detail, the following experimental work was undertaken which it is the object of the present paper to report.

The experimental arrangement used for this investigation (Chiplonkar, 1939 a) consisted of three canal ray units with modifications to suit the particular aspect of the problem in hand. The first one of these is 3.5 cms. in diameter with a cathode of brass faced with aluminium and a canal 20 mms. in length and 2 mms. in diameter. The anode is made of aluminium and is fitted in a side tube at a distance of 16 cms. from the cathode. The observation chamber is 10 cms. long and into this is introduced the material to be bombarded, which usually consisted of plates 15 cms. × 20 cms. on a metal carrier. This observation chamber is closed with a glass window fixed with sealing wax. The second unit differs from the first in having a cathode of moulded aluminium 8 mms. long with a canal 2 mms. in diameter; all the other measurements are identical. The third unit has a discharge tube 2.5 cms. in diameter with a canal 7.0 mms. long and 2 mms. in diameter. This is provided with ground joints at both its ends. Through one of these is introduced the material to be bombarded and through the other the anode.

Different gases were used in the discharge tube. The gases hydrogen and nitrogen were obtained from cylinders and were purified and dried by passing successively through alkaline pyrogallol and a train of drying tubes before being admitted into the apparatus. Oxygen and carbon-dioxide were obtained by heating pure potassium-permanganate and sodium-bicarbonate respectively in vacuum. Evacuation was obtained by means of a set of mercury diffusion pumps of the Waran type backed by a Cenco Hyvac oil pump. Liquid air traps were used for preventing the diffusion of mercury vapour into the discharge tube and when permissible for purifying the gases.

The H. T. voltage was obtained from a transformer coupled with a single Kenotron circuit. The anode was connected to H. T. the cathode being earthed through a milliammeter. The H. T. voltage was measured by means of an electrostatic voltmeter of the Kelvin-Whyte type. This potential, as well as the earth current, were kept constant by regulating the gas-pressure and the filament current of the Kenotron respectively. A wattmeter of the dynamometer type was introduced into the primary of the H. T. transformer; the constancy of the energy input to which, was ensured by maintaining the wattage reading constant throughout the course of the experiment.

In a series of experiments gas streaming was used. Apparently this made no difference in the final results.

EXPERIMENT AND RESULTS

The nature of the rings observed in the first instance coupled with Raether's observations suggested the presence of a hydrocarbon substance (which would ultimately serve as a source of carbon) as necessary for the deposit formation. This was confirmed by the observation that the intensity of the deposits increased enormously when picein was introduced in the discharge tube. The effect of introducing this in (1) the observation chamber, (2) the discharge chamber, was first observed. In the former the face of the cathode itself (away from the discharge side) was painted with picein; in the latter its vapour was mixed with the streaming gas. The behaviour of the deposits under the two modes of observation is quite different; whereas in (1) only ten to twenty minutes sufficed for a visible deposit to appear, in (2) exposures of the order of 2-3 hours were required. The object of the experiment was to decide whether the association of the deposit forming particles with the main canal ray beam takes place in the observation or the discharge chamber. Later experiments revealed that the diffusion of the vapours from the observation to the discharge chamber, took place to an appreciable extent although the direction of gas streaming was such as to oppose this. Merck's pure paraffin wax and iodine were also tried in place of picein for painting the cathode. In the former copious amounts of carbon were released which escaped to the discharge side and were found to effect the main discharge in such a manner as to make it unsteady. The receptacle plate in this case showed only an ill-formed brown deposit. Iodine, on the other hand, was not found to form deposits as shown by microchemical tests.

The effect of variation of the nature and the condition of the bombarded plate was next investigated by successively exposing plates of aluminium, copper, mica, polished graphite (Pl. 2) ground glass (Pl. 1) to positive rays of hydrogen. In all these cases, except the last, sharp ring deposits were obtained. The rings are easier formed and better defined on the metals than on the non-metals. The ring pattern in all these cases with the above exception is essentially similar. The condition of the surface affects both the time for deposit formation as also the pattern, for the ground glass. One gets only a central transparent spot after long exposures--presumably corresponding to the spread of the positive rays, surrounded by a dark annular patch, the outer edge of which gradually fades in intensity. In some experiments, plates initially covered with soot (from sealing wax) were exposed to positive rays of hydrogen. In this case a central circular region was made bare by the impacting rays and at a distance of few millimeters from the edge of the central region a thin sharp ring grey in color was formed on the deposit already there.

Different gases like carbon dioxide (Pl. 3), oxygen (Pl. 4) nitrogen (Pl. 5) air (Pl. 26), mixture of hydrogen and nitrogen produced essentially the same ring pattern except nitrogen and oxygen. In the case of these latter, patterns are produced which are characteristic of the other gases with longer times of exposure and higher voltages (*vide infra*). The intensity of the deposits shows a certain dependence on the nature of the gas in the discharge tube appearing quickest with hydrogen and comparatively with less ease in the other gases in the order, nitrogen, oxygen, carbon dioxide and air. One might have expected them to appear quickest in carbon dioxide for the gas itself might be expected to supply the deposit-forming material.. The above observation is supported by another experiment in which picein was made to predominate in the discharge chamber (Pl. 14) when no great difference in the intensity of the deposits was brought about. The observation that they appear with the least ease in air suggested the possibility that its constituents might have mutually disturbing influence. It was shown by taking observations with a mixture of hydrogen and nitrogen that no such influence existed. Experiments were also made in which iodine and mercury were used in the discharge tube with traces of hydrogen. With mercury alone (without the presence of picein) irregular deposits were obtained either on metallic or glass plates. The effect of temperature on the deposit formation was investigated by cooling the bombarded glass plate with liquid air. For this purpose, a vertical discharge tube was devised with a ground joint closing the observation chamber. This was partly filled with mercury, the level coming to within a distance of 6-7 cms. from the cathode. On the mercury surface was placed the glass plate and liquid air was applied over the whole of the mercury column. Again no change in the density of the deposits was observed. All these observations taken together show that the deposit formation is not merely a condensation of the deposit-forming material but is a process intimately connected with discharge reactions taking place on the other side of the canal.

The deposits obtained under conditions of spark and high frequency discharge were also observed. In the latter a sleeve electrode was used round the discharge tube connected to a high frequency tension source, the cathode being earthed as usual. Under these circumstances, one gets a fairly intense beam through the canal which to judge by the light emitted by it, consists of hydrogen particles. That this was not a more rectification effect was shown by the null reading in the D.C. ammeter connected to the cathode A glass plate exposed to these rays showed the usual form of deposit (Pl. 6). Under conditions of spark discharge, we get short intense streamers whitish red in color which have been regarded to consist of slow metallic ions. Glass plates exposed to these have been known to show deposits (Bareford 1935) but any structure in them does not find mention. On exposing a plate to these, one obtains a deposit which shows itself as a single well-defined ring which is slightly bigger than the aperture of the canal, when the plate is kept practically in contact with the cathode. This is very similar to the one obtained with positive rays at this distance. Some observations during these experiments suggested that the shape and material of the anode might have some influence on the deposit formation. Subsequent experiments with canal rays, with different anode materials of the different shapes showed the absence of any such influence. It may be mentioned that the condition of the discharge does affect the deposit formation and distorted ring patterns are obtained under conditions where there is an unsteady discharge or when it creeps under the electrode. Observations were also made by splitting the canal into two by an aluminium plate. Two patterns were obtained corresponding to the two portions of the canal though overlapping took place to a certain extent. That the deposits take the shape of the positive ray beam was again clearly shown on exposing a plate tilted at 45° with the plane of the cathode when elliptically-disposed rings were obtained (Pl. 20).

The cathode faces, on the observation as well as the discharge side (Pl. 27) sometimes showed deposits with a structure. A possibility of some type of reflection of the positive ray particles between the exposed plate and the cathode surface was suggested. To test this a fine mesh was introduced between the canal and the plate. The deposits obtained (Pl. 21) consisted of fine spots which were themselves distributed in the form of an annular zone. This incidentally shows the absence of any creeping on the part of the deposits. This was further confirmed by heating a plate on which this ring formation was obtained directly over a burner when no change was found in their disposition. This observation, however, does not preclude the possiblity of 'creeping' while in the act of formation This, we believed, is shown by the mesh experiment

The variation in the structure of the deposits with the energy of the bombarding rays is interesting. This was investigated under both the modes of introducing the picein vapour (*vide infra*). In the case where it is streamed along with the gas, one finds that at low voltage (both 4 KV), the plate shows a translucent spot in the centre surrounded by a thin deposit which gradually fades towards the edges (Pl. 9) Near the edge of the central spot, one can just see a faint ring. This gets more and more marked till about 7 KV there is a sharp ring formed there. As one increases the voltage the diameter of the central spot decreases and the rings stand out prominently on the back ground (8 KV) (Pl. 8). When viewed in reflected light one observes a number of delicate regular rings almost like interference rings except for their colour In the case of the alternative mode of introducing the picein plates 10, 11, 12, 13, show the results for voltages 4, 6, 8, 10 KV respectively. Here the structure is perceptible even at low voltages of the order of 4 KV. With increase of voltage the number of rings increases and also the diameter apparently. A measurement of the diameter of the rings in these plates shows, however, that with increase of voltages the rings are successively destroyed starting from the centre and the maximum of intensity shifts gradually from the innermost to the outer rings. This probably is due to the thermal effect of the bombarding rays and we infer that at very high voltages and long times of exposure the structure should be absent and the intensity of the deposits also must become small. This was supported by observation of the deposits obtained with positive rays of carbon dioxide at 16 KV. Thus it is possible that there is an optimum voltage and time of exposure with which the structure is best obtained. The variation in these deposits with different times of exposure lends further support to this deduction. Plates 11, 17, 18, show the deposits obtained with times of exposure 12 minutes 1 hour and 2½ hours Here also we can see the progressive destruction of the rings and the gradual shifting of the maximum of intensity towards the outer rings. It may be mentioned that variation of the earth current is without effect on the structure and what is more curious, on the intensity of the deposits. Plates 11, 10, are obtained with earth currents of 1. mA and 0.2 ma respectively.

Variation of the distance of the bombarded plate from the cathode between values ranging from 0 to 20 mms. was next tried in another series of observations. The deposit, when the plate is kept in contact with the cathode, shows itself as a single ring (Pl. 16) not unlike that obtained under spark discharge. As the distance of the plate from the cathode is increased (Pl. 25) the characteristic multiple ring structure makes its appearance. At greater distances the rings obtained are less distinct, they naturally have greater dimensions

(Pl. 15) but they lose regularity to some extent. In most of the above experiments the plates were kept at a distance of 5 mms. from the cathode. It may be mentioned that the ring effect was first observed on a plate at a distance of 110 mms. from the cathode. A reference may, however, be made to a phenomenon which was observed (Chiplonkar, 1939 b) during the course of this work, which appears to be of interest for the purposes of the present investigation. In some experiments 'gas streaming' was not used but picein vapor was added from time to time. Each such addition was followed by a rapid rise in the voltage across the tube though no change was observed in the earth current. This was presumbaly an effect of the so-called 'clean-up' since the voltage becomes a rough index of the pressure in the tube when the discharge current remains constant. This rapid rise of the voltage was followed by a subsequent gradual decrease which was marked by a number of periodic fluctuations of small magnitude. Significant changes in the colour of the discharge accompany these fluctuations. In the absorption regime when the voltage is rising, the colour is that of hydrogen pure rose red, in the desorption regime, when the voltage is falling, there is a preponderence of bluish white color. This observation suggests that when the release of the absorbed hydrogen takes place, the hydro-carbons accompany it It has been mentioned before that every value of the external voltage has got a characteristic ring structure corresponding to it. The idea, therefore, suggested itself that the multiplicity of the ring structure might be due to these fluctuations. In all the experiments thus far mentioned, in which streaming was not used, the voltage was kept constant by continuously manipulating the pressure. In one experiment this was not done and the voltage was allowed to fluctuate without interference to test the above hypothesis. The exposed plate (Pl. 22), however, failed to show any increase in the number of rings. The deposit was kept under observation, while in the course of formation, to see if it showed corresponding changes in the increase of intensity in the two stages of absorption and desorption. The difference was not very marked but one could see that the increase in the intensity of the deposits took place in the latter but not in the former stage.

Observations with electron beams recorded by other workers (*vide supra*) suggested the possibility of a structure in the positive ray beam itself. Such a structure is known in the case of positive rays and has been generally ascribed to the effect of stray magnetic fields. To test whether a similar structure was responsible for the deposits described here, a transverse magnetic field was applied on the discharge side of the canal (Konigsberger and Kutschewski, 1910) which extended practically over the whole length of the cathode dark space In this case, the discharge was twisted and struck a place in the middle of the discharge tube where glass fluorescence was obtained. Here a dark brown deposit was produced. The deposit obtained on the plate is shown (Pl. 24). Similar results were obtained with different

PLATE IA

1

2

3

4

5

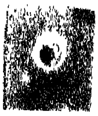
6

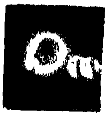
7

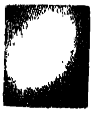
8

9

10

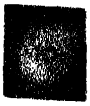
11

12

13

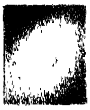
14

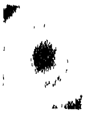
15

16

17

18

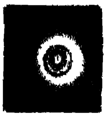
19

20

21

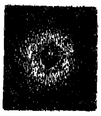
22

23

24

25

26

27

magnetising currents in the electro-magnet. Observations were also made with a receptacle plate raised to 220 volts when similar results were obtained

DISCUSSIONS

The general nature of the phenomenon is shown by its appearance under greatly varied conditions, with different bombarded materials, different gases in the discharge tube etc. It shows, however, a definite dependence on the excitation voltage, the structure making its appearance above a certain value of the latter. This value, however, varies from tube to tube and seems to depend on the way in which the deposit forming material is introduced as well (vide infra p 3). For voltages below this there is deposition but no structure. Certain experiments tend to show that for very high voltages also, the structure can be absent. The fact that the deposits follow the shape of the beam, form on plates placed in contact with the cathode, get distorted under unsteady discharge, fairly make it certain that they originate in the discharge space.

It is generally accepted that the positive ray particles suffer no collisions in their passage across the cathode dark space which result in the transfer of kinetic energy (Chaudhri and Oliphant 1932). To explain the kinetic energy of the hydrocarbon particles one is left only with two possibilities (1) they are carried along the positive rays through some type of association or (2) form positive rays themselves Two possible types of association are due to (*a*) electron exchange or (*b*) due to the formation of loose chemical complexes. A process of electron exchange takes place in which an atom gets neutralised and fresh ion produced without there being necessarily a transfer of the kinetic energy. Kallman and Rosen (1930) have shown that the probability of transfer depends on $N-I$ where N is the neutralising energy of the ion and I the ionisation potential. It is probably this type of reaction that makes it possible to get canal rays of mercury or iodine by the addition of traces of hydrogen. Another possible type of association has already been suggested, *i.e.*, the formation of loose complexes between hydrogen and adsorbing hydrocarbon. The reason why some type of association is suggested is based on the observation (1) the dependence of the intensity of the deposits on the gas in the discharge tube (2) non-influence of the amount of hydrocarbon vapours on the intensity. One can explain, on this basis, the above mentioned dependence in terms of the ease of association between the gas and the hydrocarbons. Hydrocarbon particles are known to occur in the canal rays. On the other hand one expects that the presence of the hydrocarbon, whatever the type of association, will appreciably affect the velocity distribution among the canal rays. Investigations on the Doppler effect show that such an effect exists when a foreign gas like helium (Wien 1927 (c) etc., is introduced into the discharge space but not when it is only introduced in the observation chamber. In the deposit phenomenon under consideration, it has been shown that introducing the picein in the observation chamber increases enormously the intensity of the deposits There is no doubt that there is considerable diffusion of this vapour to the discharge side, and the increase in intensity is probably due to the fact that by this mode it is introduced directly into the dark space where the beam formation takes place. In the other mode, there is the possibility of its being deposited before it comes in the dark space. The considerations thus far given do not preclude the possibility of the existence of the positive rays of the hydro-carbons but make it less likely. Raether (1933) has observed that these deposits are not found when the positive ray beam is passed through an analysing field prior to the impact. The evidence that has been given thus far, especially that with transverse magnetic field indicates that the phenomenon is not characteristic of the charged particles

To find an explanation for the peculiar ring structure observed, one has to settle beforehand whether it is the result of a primary action due to an inherent structure in the beam or a secondary action caused by a redistribution of these deposits through the agency of either the impacting rays or merely surface forces called into play by condensation. Data on molecular beams, do not lend support to this last possibility (Cockroft, 1928). The second hypothesis assumes that a deposit formed on the plate, suffers a redistribution into the characteristic ring structure by some specific action of the impacting rays When positive rays strike a surface in vacuum, many types of reactions can take place involving various kinds of energy exchanges. These range from the very small transfer of energy accompanying reflection to the violent destruction of the surface by bombardment. The production of thermal or chemical action, the emission of electrons, positive particles (Wien, 1927, (a)) or under special conditions the release of occluded gases (Johnson, 1930) from the surface comprise the main reactions produced by canal ray bombardment. That the redistribution does not mean any surface motion has been demonstrated by the mesh experiments. Observations on the tilted plate (*vide infra*) rule out the possibility of selective reflection, for the presence of this effect would have brought about a difference in the intensity of the deposits in the different regions. The existence of rings on both metallic and non-metallic plates invalidates the view that it is due to characteristic charging up of the surface. The possibility of chemical action is ruled out by the generality of the phenomenon. We are therefore only left with the possibility of mechanical action. The existence of such a mechanical action is shown by the observations of Stark and Wendt (1912) who report that glass plates exposed to positive ray bombardment develop a depression at the point of impact due to a partial penetration by the rays. Berliner, (1926) has shown the possibility of microscopic explosions of the loose metallic complexes (in which form the impacting ions are held bound on the cathodic surface) due to positive ionic bombardment. Bush and Smith (*ibid*) explain this on the supposition that the bound ions on the cathode reach such a high pressure as to become unstable. It is not unlikely that a similar effect is taking place

Fig. 1

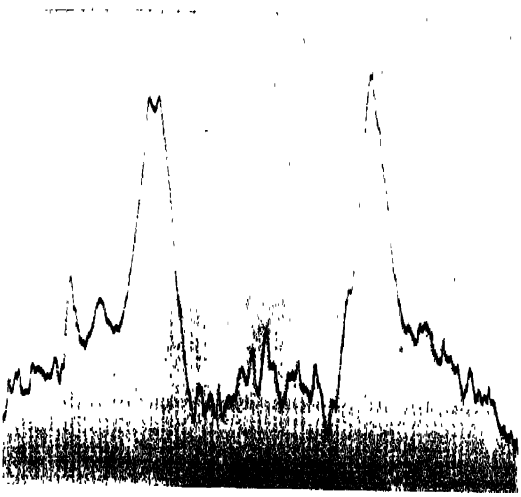

Microphotometer curve of the plate showing the deposit (cf. Fig. 15, Plate IA)
Magnification 1 X 10

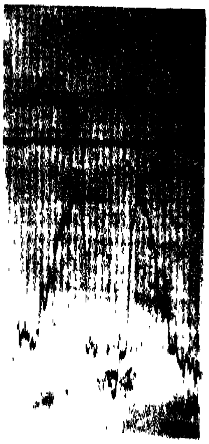

Microphotometer curve of the plate showing the deposit (cf. Fig. 5, Plate IA)
Magnification 1 X 3

Fig. 3

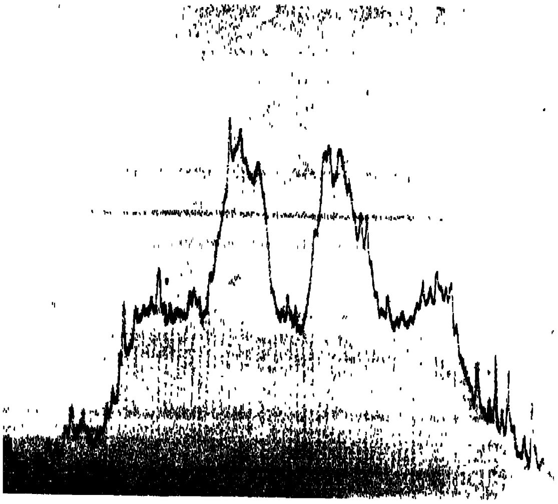

Microphotometer curve of a plate showing the deposit obtained with canal rays of [illegible], with C.K.7, 0.6 m.a. d = 0.5 cms, T = 2[illegible] minutes, Magnification 1 X 10

here, for the observations given in this paper clearly show that the deposition is accompanied by adsorption effects. Accordingly we can think of the deposition as proceeding along the following stages: (1) a primary deposition of the particles from the associated beam on the bombarded surface, (2) adsorption of the impacting ions by this primary deposit which ends in (3) a mechanical explosion in which the deposit forming material is scattered. On account of the central symmetry of the primary deposit, it is reasonable to suppose that the secondary deposition will also show a similar symmetry. This hypothesis, although it suggests a likely reaction, does not explain the ring structure. The dependence on the nature of the gas in the discharge tube, the existence of a threshold value etc. make it probable that the phenomenon under consideration, is closely bound up with the allied phenomenon of cathode sputtering.

There is the other probability of an inherent structure in the beam of the hydrocarbon particles themselves. Such a structure is known to exist in the case of electron beams, brought about by a variety of causes depending on the form and disposition of the apparatus. Thus McFarlane (1936) reports that a beam of electrons passed through earthed slits shows a structure which he finds reason to ascribe to certain charges developed by the irregularities on the slits. Curran (1936) reports a case in which this was brought about by the geometry of the collimating slits. Lastly we have the inherent structure (Clay, 1928) showed by high velocity electron beams in Röntgen ray tubes. Rüchardt (Wien, 1927, b) has mentioned that a structure in a positive ray beam is brought about by the action of stray magnetic fields. This suggested the possibility of an inherent structure in the positive ray beam. The experiments with the transverse magnetic field, however, show that the ring structure is not to be ascribed to any similar effect. The distortion of the rings in the case of an unsteady discharge shows, however, that the phenomenon is intimately connected with the process of beam formation in the cathode dark space.

Note on the microphotometer curves.—The microphotometer curves of the original plates on which the deposits were formed were taken at the suggestion of Dr. Asundi on a Zeiss recording Microphotometer. The plates were run on the microphotometer with a point source along a diameter of the ring deposits. The curves, therefore, represent the distribution of the particle-density along the diameter and exhibit in a remarkable way, the multiplicity in the ring structure of these deposits.

ACKNOWLEDGMENTS

I take this opportunity of expressing my indebtedness to Dr. Md. Ishaq, Chairman, Physics Department, Muslim University of Aligarh for facilities for *taking the microphotograms*.

In the end, I offer my sincere thanks to Prof. Dr. S. S. Joshi for giving the facilities for work and constant encouragement. I am also indebted to Prof. Dr. Asundi for useful discussions.

COLLEGE OF SCIENCE,
BENARES HINDU UNIVERSITY.

REFERENCES

Bareford, 1935, *Phil. Mag.* London, **20**, 845.
Berliner, 1926, *Ann. d. Phys.*, **81**, 1044
Chaudhri and Oliphant, 1932, *Proc. Roy. Soc.* (A), **137**, 662
Chiplonkar, a 1939, *Proc. Ind. Sc. Congress, Phys. Math. Section*, p. 25.
Chiplonkar, b 1939, *Current Science*, **7**, 160.
Clay, 1928, *Proc. Phys. Soc. London*, **40**, 223.
Cockroft, 1928, *Proc. Roy. Soc. London* (A), **119**, 293.
Curran, 1936, *Phil. Mag. London*, **21**, 406.
Dasannacharya, Chiplonkar, and Sapre, 1934, *Nature*, **42**, 642.
Johnson, 1930, *Proc. Phys. Soc. London*, **42**, 490
Konigsberger and Kutschewski, 1910, *Verh. d. Deutsch Phys. Ges.*, **12**, 514
Kallman and Rosen, 1930, *Zeits. f. Phys.*, **61**, 61.
McFarlane, 1936, *Phil. Mag. London*, **22**, 149.
Raether, 1933, *Phys. Zeits.*, **34**, 492.
Stark and Wendt, 1912, *Ann. d. Phys.*, **38**, 921.
Wien, 1927, *Kanalstrahlen Handbuch der Experimental Physik*, **14**.

(a) p. 458, 463, 475, 539
(b) p. 576, 527.
(c) p. 655

EXPLANATION OF THE PLATES IA, IB

All the photographs except plate (23) show the deposits as seen in reflected light of a size slightly greater than the original. Plate (23) depicts a direct contact print of the glass plate on which the deposit was obtained. The same plate as seen in reflected light is shown for comparison in plate (14). In the following data, unless specific mention is made to the contrary the plate exposed should be taken to be a smooth glass plate. Plates marked W. S. are taken with picein vapour streamed along with the gas; all the rest with the other mode of introducing it (*vide infra*). 'd' represents the distance of the plate behind the cathode, T the time of exposure. All the other symbols are self explanatory.

Pl. 1. Ground glass plate, canal rays of hydrogen, 8 KV, 1.2 ma, d = 1.5 cms. T = 60 min.

Pl. 2. Polished graphite, canal rays of hydrogen 6.0 KV, 1.0 ma, d = 0.5 cms. T = 60 min.

Pl. 3. Smooth glass plate, canal rays of hydrogen 7 KV, 1.0 ma, d = 0.5 cms. T = 120 min.

Pl. 4. Canal rays of oxygen, 6 KV, 1.0 ma, d = 0.5 cms. T = 20 min.

Pl. 5. Canal rays of nitrogen, 8. KV, 0.9 ma, d = 0.5 cms. T = 14 min.

Pl. 6. High frequency discharge in hydrogen, 0.5 ma, d = 0.5 cms. T = 32 min.

Pl. 7. Canal rays of air, 6 KV, 0.5 ma, d = 0.4 cms. T = 1.3 min. split canal.

Pl. 8. W. S. Canal rays of hydrogen, 8 KV, 1.0 ma, d = 0.5 cms. T = 30 min.

Pl. 9. W. S. Canal rays of hydrogen 4.0 KV, 1.0 ma, d = 0.5 cms. T = 130 min.

Pl. 10. Canal rays of hydrogen, 4.0 KV, 0.8 ma, d = 0.5 cms. T = 20 min.

Pl. 11. Canal rays of hydrogen, 6. KV, 1.0 ma, d = 0.5 cms. T = 12 min.

Pl. 12. Canal rays of hydrogen, 8 KV, 1.0 ma, d = 0.5 cms. T = 20 min.

Pl. 13. Canal rays of hydrogen, 10 KV, 0.8 ma, d = 0.5 cms. T = 20 min.

Pl. 14. W. S. Canal rays of hydrogen, (Picein predominating), 3 KV, 1.0 ma, d = 0.5 cms. T = 120 min.

Pl. 15. Canal rays of hydrogen, 5 KV, 0.5 ma, d = 2.0 cms. T = 20 min.

Pl. 16. Canal rays of hydrogen, 6. KV, 0.5 ma, d = 0.5 cms. T = 20 min.

Pl. 17. Canal rays of hydrogen, 6 KV, 1.0 ma. d = 0.5 cms. T = 60 min.

Pl. 18. Canal rays of hydrogen, 6 KV, 1.0 ma, d = 0.5 cms. T = 120 min.

Pl. 19. Canal rays of hydrogen, 6 KV, 0.2 ma, d = 0.5 cms. T = 20 min.

Pl. 20. Canal rays of hydrogen, 3 KV, 1.2 ma, d = 0.0 cms. T = 120 min, tilted at 45^0 to face of canal.

Pl. 21. Canal rays of hydrogen, 8 KV, 0.8 ma, d = 1.0 cms. mesh 0.5 cms, from cathode. T = 50 min.

Pl 22. Canal rays of hydrogen, fluctuating voltage, d = 0.5 cms. T = 180 min.

Pl 23. Canal rays of hydrogen, 6.0 KV, 1.0 ma, d = 0.5 cms. T = 42 min with transverse magnetic field.

Pl 25. Canal rays of hydrogen, 6 KV, 0.5 ma, d = 0.5 cms. T = 20 min

Pl 26. Canal rays of air, 4 KV, 1.2 ma, d = 0.5 cms. T = 120 min.

Pl. 27. Cathode face on discharge side

4

ON THE AFTER-GLOW OF SODIUM CHLORIDE AND ITS DECAY

By H. N. BOSE[†]

(Received for publication, February [illegible], 1957)

ABSTRACT The decay of luminescence after-glow excited by X-rays has been investigated in the case of sodium chloride (single crystal), pressed powdered sample of sodium chloride, and sodium chloride with 0·1 % of copper. The effect of annealing the pressed samples at different temperatures as well as of heating the sample during emission has also been studied.

The suitability of various mechanisms and the corresponding decay laws has been discussed. The ideas of trap mechanism as developed by Randall and Wilkins have been utilised to deduce the expected decay law in the present case.

Phosphorescence in the gaseous state can occur only through the presence of an intermediate metastable state; it is therefore understandable that no afterglow of measurable duration occurs in gases as the metastable states in gases generally possess a relatively short duration. After-glows have been observed in denser media, the intensity and duration increase with the viscosity of the medium in general. It is thus reasonable to suppose that there exists an interaction between the electronic transition of the excited particle and the surrounding medium. From general ideas and previous investigations we can state, in short, that (*i*) no after-glow occurs if the medium does not influence the emission process appreciably, *i.e.*, the process occurs entirely within the atom or molecule in a sphere of about 10^{-8} cm. diameter; (*ii*) after-glow occurs when the configuration of the surrounding molecular structure plays a part; for this may change as a result of the absorption process and some time must elapse before the configuration falls back into its former state. After-glow will be accompanied by photo-conductivity if the electron is completely set free as it occurs in certain phosphors. Phosphorescence is therefore generally characterised by photo-conductivity but the reverse is not necessarily true.

A large amount of work has been done about the decay of after-glow of solid phosphors under ultraviolet excitation. The solid solutions of organic dyes were some of the first to be investigated; fluorescein in sugar possesses a fluorescence, originating from an excited state, with a life of 10^{-8} sec and shows an after-glow of a few seconds. The intensity of fluorescence varies with the concentration almost in the same way in solids as in liquid solution which is rather a puzzle because, in solids collisions do not occur as it is supposed in solutions. This indicates that chemical change of some type takes place during preparation. The emission of these phosphors decays according to

---

[*] Fellow of the Indian Physical Society.

the mono-molecular reaction law $I = I_0 e^{-at}$. Generally speaking, a reduction of temperature increases the time of decay while increase in concentration diminishes the time of decay. Jablonsky (1935) has explained many features of this kind of phosphors by assuming the existence of at least one metastable level lower than the unstable level reached by absorption.

Zinc sulphide is the only phosphor which has been investigated thoroughly by many workers. The decay of luminescene of impurity activated zinc sulphide in general follows a bimolecular law which may be written for simple cases as

$$\frac{1}{\sqrt{I}} = \frac{1}{\sqrt{I_0}}(1 + An_0 t)$$

where A is a constant and n_0 is the number of electrons per unit volume in the conduction band at $t = 0$.

Antonow—Romanowsky (1935) and De Groot (1939) have observed in case of copper activated zinc sulphide that high intensity gives a rapid decay; this also follows from the bimolecular law given above. De Groot has further observed a more rapid decay with shorter wavelength of exciting radiation; according to him this is due to the higher absorbability of shorter wavelength by the medium.

In case of photo-conducting phosphors with stoichiometric excess of either constituent, Mott and Gurney (1940) suggest a different decay law,

$$N_q = An\,(n + \nu)\ ; \quad n = \frac{\nu}{B\exp.(\nu At) - 1}$$

$$B = 1 + \frac{\nu}{n_0}\ .$$

ν = the number of normally unoccupied impurity centres in addition to the ordinary impurity centres.

The slow bimolecular decay may have superposed on it a much more rapid decay in certain cases. The measurements of Strange in case of copper and silver activated phosphors indicate such possibility.

Mott and Gurney (1940) have given the following types of decay for photo-conducting impurity activated phosphors :

"1. For very high emitted intensities an exponential decay with a decay period of the order of fraction of a microsecond, independent of temperature.

2. As the intensity decreases this should change over to a rapid bimolecular decay independent of temperature.

3. For still lower intensities this should change to a slow bimolecular decay with a value of 'A' strongly dependent on temperature.

4. Finally the decay law may change over again to an exponential form dependent on temperature, due to the presence of frozen-in ions. This should only occur when the activating impurity is a stoichiometric excess of one of the constituents."

More recently, Randall and Wilkins (1945) have carried out extensive investigations on the decay curve of phosphors of the recombination type with traps, and allied phenomena; they have also developed formulae to explain the decay curves on the basis of trapping mechanisms. Klasens and Wise (1946) have calculated in a more generalised way the luminescence intensity over the whole period and have shown that the decay becomes bimolecular at high temperatures.

The measurement of decay of luminescence under X-rays has as yet attracted little attention from the experimental workers. Levy and West (1939) in their attempts to improve the suitability of zinc sulphide screens by minimising the after-glow, measured the decay of luminescence of zinc sulphide under X-rays with certain impurities. They found that the addition of very small quantities of nickel greatly reduces the phosphorescence without affecting the fluorescence intensity to a great extent. They also found out the optimum amount. The addition of iron does not affect the intensity much while traces of cobalt greatly reduces the fluorescence intensity. The addition of impurities in case of zinc sulphide also affects the quality of the fluorescence and phosphorescence light.

In the present investigation the nature of the long period decay of phosphorescence after-glow of sodium chloride with and without impurity by X-ray excitation has been studied under different conditions; the various decay laws have been discussed with respect to the present case and the probable mechanism suggested.

EXPERIMENTAL PROCEDURE

The pressed substance in the form of thin plate was excited to luminescence by X-rays coming out from the window of the Hadding tube with copper anticathode run at 35-40 K.V. with 10 m.A. The photovoltaic cell connected to a galvanometer, was placed almost in contact with sample on the side opposite to that of the X-ray tube. Two lead covers, both connected to a single lever, were arranged in such a way that when X-rays were incident on one side of the sample, the light and transmitted X-rays from the other side were stopped by one of them and could not reach the photocell; on the other hand, when that cover was raised by pressing the lever, the second lead cover at once intercepted the X-rays incident on the front side of the sample. In this way the light from the back side of the luminescent sample fell on the photocell simultaneously with the cutting off of the incident X-rays. The deflections could be marked off on the scale at regular intervals of time with the help of a stop watch.

The low intensity of luminescence is a great trouble in the measurement of the decay curve. After the lapse of a small interval of time the intensity falls too low to be measured with high accuracy.

that the sodium chloride crystal shows no increase in electrical conductivity under X-rays as is demanded by the zone picture of the crystal, calls for the formulation of other mechanism to explain the phenomena of luminescence in such crystals.

It is now known that the presence of impurity or lattice defects in general causes a number of localised levels between the allowed band of the normal energy spectrum. The electron or the hole may be trapped in any one of these states. This trapping process will lead to a release of a part of the energy which may or may not be in the form of emission. The trapped electrons may be thermally excited to upper bound levels or to the conduction band. In the first case energy may be emitted when the electrons come back to the ground state. In the latter case the electron is free to find out a hole for recombination ; on the other hand, the impurity atom with trapped electrons may bodily move through the lattice encountering another with trapped hole and neutralise it with the emission of a quantum of phosphorescence light.

Since pure sodium chloride does not show any fluorescence under ultra-violet radiation, emission is to be supposed to be taking place in some special position of the lattice, *i.e.*, centres.

Different types of centres are possible in a crystal like sodium chloride :

1 A foreign negative or positive ion may replace one of the negative or positive ions of the regular lattice.

2. An electron may be trapped at a lattice point where a negative ion is missing (F & F′ centres).

3. There are bound levels associated with an ion in the interstitial position of the lattice.

4. At the surface of a crystal crack, where the periodic field is broken off, there exists bound levels in which electrons can exist without being free to move through the crystal.

In the case of the presence of a foreign ion in the lattice (*viz.* KBr KH, KCl Th) the emission is characteristic of the activation and there is no reason why the sample should not be luminescent under ultraviolet radiations. Substances used in the present investigation had little chance of containing any such activator. As regards surface levels, though they are predicted from theoretical consideration, there is no direct experimental evidence of their presence in the crystal. In a normal crystal, at any temperature there are present a number of vacant lattice points. Trapping of electrons into positions, where there are missing negative ions, is possible and actually takes place in alkali halide crystals under suitable circumstances, *viz.*, the crystal in contact with Na or K vapour at high temperature. These are called F centres which give rise to the new absorption bands in the crystals termed as F bands. Tibbs (1939) has calculated the wave function of the ground state for such an electron in case of sodium chloride with some approximation. He finds it to be 3 e.v. below the level of the conduction band and the first excited state. 0.6 e.v. below it. As the ions move into new position of equilibrium after absorption the energy of the electron is raised and there is indirect evidence that the excited state is 0.1 e.v below the conduction band after the absorption process. The filled up F centre is neutral but the wave function of the electron in the centre should extend over a greater volume than that of the replaced negative ion. If now another electron is brought to this centre, the surrounding medium gets polarised pushing adjacent ions into new positions of equilibrium This causes a spherical field which varies as $1/r$; a set of stationary states is therefore possible so that it is quite possible that two electrons can be trapped at a vacant lattice point. This type of centres are F′ centres and the F′ band obtained in absorption is due to this mechanism When sodium chloride is exposed to X-rays. the crystal is coloured due to the trapping of electrons in these centres for the same absorption bands are also obtained when the F and F′ centres are created by other means On irradiation therefore at first F and F′ centres are created and then the photoelectrons produced inside the crystal go on exciting and ionising different centres which give rise to luminescence

Now luminescence may be excited in two ways:

1. The emitting centres are directly excited but not ionised

2. The electron from the centres or valence band are raised to the conduction band which will presumably find some centres and be captured; it will in all probability be captured into an excited state causing emission on its return to the ground state.

In case of (1) electrons on absorption of photons are raised to higher states but not freed so that they cannot contribute towards electrical conductivity; if '*n*' be the number of electrons in excited states per unit volume at any time '*t*', then during illumination the rate of decay of electrons in the excited state will be .

$$\frac{dn}{dt} = p - \alpha n \qquad .$$

which, on solution, yields

$$n - p/\alpha = A\,e^{-\alpha t}$$

$$At\ t = 0, \quad n = 0,$$

$$\therefore \qquad n = p/\alpha(1 - e^{-\alpha t})$$

α, being a constant for the particular crystal at a given temperature, and p, being the number of electrons raised to higher states per sec. per unit volume.

The intensity of luminescence at any instant is proportional to the number of electrons in the excited state; hence the intensity grows exponentially to a steady value when an equilibrium is established between the number of electrons raised to excited states and of those coming to the ground state per second.

For decay, $p=0$ and $n=n_0$ at $t=0$, so that $n=n_0e^{-at}$. Hence $I=I_0e^{-at}$. Since sodium chloride crystals do not show any increase in conductivity under X-rays, it is natural to infer that luminescence of sodium chloride under X-rays will be of type (1). But for forbidden transition 'a' is of the order of 10^4 sec.$^{-1}$, so that decay law in no case can be slower than $I=\dfrac{I_0}{\exp.(10^4 t)}$; hence the long duration of after-glow as is found in case of sodium chloride cannot be explained by this. Besides, the high temperature dependence of decay rate as has been found in the present case is also difficult of explanation by the simple mechanism, for 'a' should not be much influenced by temperature.

Assuming, on the other hand, that the second type of luminescence occurs in the case of sodium chloride, let us suppose that the crystal contains a number of radiative centres where the electrons are trapped, presumably in the higher states, in order to be able to cause phosphorescence; besides, the crystal may contain a large number of non-radiative trapping centres where the electrons may return to the valence band whence it was originally released without any emission; the last assumption is justified by the fact that the pure crystals do not show any luminescence under ultraviolet radiations.

Let 'm' be the number of radiative centres per unit volume of the crystal and is more or less unaffected by X-ray irradiation. Let 'ν' be the number of non-radiative centres per unit volume also constant for the crystal; if 'n' be the number of electrons at any instant in the conduction band per unit volume the number of vacant holes in the filled band may also be taken as 'n', for the concentration of trapped electrons obtainable by X-ray irradiation of sodium chloride is small even at saturation value. Further when the steady state is reached an equilibrium is established between the number of electrons released to the conduction band per second and those coming back to different positions from the conduction band per second, so that number of electrons trapped in special positions inside the crystal at any instant should have a constant value at a particular temperature of the crystal and inclusion of 'm' and 'ν' will have accounted for those. Hence the number of electrons in the conduction band will decay at the rate given by,

$$\frac{dn}{dt}=-Anm-Bn(n+\nu)$$

so that, $$n=\frac{2a}{N\exp.(2aBt)-1} \qquad \text{where } a=\frac{Am+\nu B}{2B}$$

at $t=0$. $n=n_0$.

$$N=1+\frac{2a}{n_0}$$

After sufficiently long time,

$$n = \frac{Am + \nu B}{n_0 B + Am + \nu B} \cdot n_0 e^{-(Am+\nu B)t}$$

and,

$$I = I_0 e^{-(c+\nu B)t} .$$

Thus the decay is exponential

If n_0 is very large compared to $(Am + \nu B)$,

$$n = \frac{n_0}{1 + n_0 Bt},$$

so that the decay law can be written as

$$I = \frac{I_0}{1 + bt}, \quad \text{where } b = n_0 B.$$

As a matter of fact, luminescence in sodium chloride should consist of fluorescence and phosphorescence; for the probability of direct excitation of centres is much greater than that of ionisation of the centres. The fluorescence part will decay too quickly to be noticed in the present measurement. Assuming total luminescence intensity to be 'p' times as great as the phosphorescence intensity, the decay law for our purpose should be

$$I = \frac{I_0}{p(1+bt)} \quad \text{or} \quad \frac{I}{I_0} = \frac{1}{p(1+bt)}$$

It is easy to see that the experimental curve is widely different from this as much as from the bimolecular law. In order that this may explain the long duration of after-glow, 'b' is necessarily very small; assuming $\frac{I}{I_0} \sim \frac{1}{20}$ at $t = 1000$ seconds approximately we have,

$$b = \frac{20-p}{p} \times 10^{-3}, \quad i.e., \; b \sim 10^{-3} .$$

Besides, the absence of any increase in conductivity under X-rays is not clearly understood.

On the other hand, it appears more reasonable to assume that the long after-glow is due to the time the electrons spend in a trap. Mott and Gurney have shown that the probability of capture of electrons in the conduction band by the traps is very large, so that during irradiation by X-rays the electrons are trapped as soon as they are released to the conduction band and the fluorescence is mostly due to the direct excitation of the radiative centres (which may be filled up F and F′ centres caused by X-rays itself or otherwise). In the equilibrium state the crystal contains a fixed number of electrons trapped inside it depending upon the temperature and nature of the crystal. During irradiation a steady state is reached between the supply of electrons to the conduction band and their decrease by trapping mechanism or other transitions; when the illumination is stopped, the release of secondary electrons into the conduction band no longer takes place; the trapped electrons released by thermal energy escape to the conduction band at a rate depending upon the temperature and the depth of the traps; some of these electrons at least meet with radiative centres resulting in emission; proceeding with these ideas, Randall (1945) has explained the long duration decay curve of many phosphors and some other allied phenomena. In a similar way, we can arrive at the decay law expected in the present case.

Let, 'ν' be the number of trapped electrons at any instant per unit volume of the crystal, 'n' be the number of electrons in the conduction band and 'd' the total number of trapping centres, then we have, 'm' having the same meaning as before,

$$\frac{d\nu}{dt} = -A\nu e^{-E/kT} + a(d-\nu)n$$

$$\frac{dn}{dt} = A\nu e^{-E/kT} - a(d-\nu)n - cnm.$$

Assuming that the contribution of retrapping to phosphorescence is small,

$$\frac{d\nu}{dt} = -\nu A e^{-E/kT}$$

and,

$$\nu = \nu_0 e^{-A\exp.(-E/kT)t}$$

where,

$$\nu = \nu_0 \quad \text{at} \quad t = 0.$$

$$\frac{dn}{dt} = A\nu_0 e^{-A\exp.(-E/kT)t}.\, e^{-E/kT} - cnm.$$

Hence,

$$n = \frac{\alpha}{cm-\beta} e^{-\beta t} + K e^{-cmt}.$$

where,

$$\alpha = A\nu_0 e^{-E/kT}$$

$$\beta = A e^{-E/kT}.$$

$$K = \text{a constant}.$$

$$\text{At} \quad t = 0, \quad n = n_0.$$

$$\therefore \quad n = n_0 \left\{ \left(1 - \frac{\alpha/n_0}{cm-\beta} \right) e^{-cmt} + \frac{\alpha/n_0}{cm-\beta} e^{-\beta t} \right\}.$$

The value of cm is necessarily large so that the first term will be negligible within a short time; the intensity is proportional to 'n'.

Hence

$$I = I_0 \frac{\alpha}{n_0 cm} e^{-\beta t}$$

The after-glow period will therefore be highly temperature dependent, for both 'a' and 'β' vary with temperature. In considering the decay we have so far taken into aocount only one type of trapping centres of depth E; if there be a number of them of different depths,

$$I = I_0 \sum \frac{a}{n_0 cm} e^{-\beta t} .$$

The effect of retrapping which has been neglected so far is expected to make the decay curve still slower. The long after-glow period, temperature dependence, and the nature of the decay, specially at the late portion of the curve, can thus be satisfactorily accounted for without any difficulty about the absence of photo-conductivity (under X-rays).

The slope of the decay curve for a single crystal of sodium chloride is perceptibly greater than that for the pressed powder samples. The dependence of the slope of decay curve on the particle size of the phosphor (zinc sulphide) was noticed by Antonow Romanowsky ; he found that for powders with grain size of the order of 50μ, the slope is almost double of that for particle size of the order of 10μ. In the present case the particle size was not so small; single crystal used was a colourless transparent sodium chloride crystal (1 cm × 1 cm × 5 mm. approximately) and the powdered sample consisted of particles of average size 10^{-2} cm. It has been further observed in the present investigation that the samples need be pressed into sheets before they exhibit this longer afterglow. This way of preparing samples entails generation of intense local heating followed by cooling producing internal cracks and strain ; these will all go to produce a larger number of trapping centres of different depths, which are probably deeper than those present in an unstrained single crystal. These traps will therefore lose their electrons less readily than the other and the decay of after-glow will be thereby slowed down. The inclusion of copper ions in the lattice is also found to be unimportant. This only shows that the copper ions do not play any important role in the mechanism of luminescence ; they probably produce local strains in the crystal causing new trapping centres which may account for the comparatively slower decay in the case of NaCl + Cu phosphors.

ACKNOWLEDGMENTS

The investigation was carried out in the Khaira Laboratory of Physics, University of Calcutta. My thanks are due to Prof. S. N. Bose, Khaira Prof. of Physics for the encouragement and helpful discussions.

My thanks are also due to Mr. N. Sen Gupta, M.Sc., Palit Laboratory of Physics, for many helpful discussions.

Khaira Laboratory of Physics,
Calcutta University.

REFERENCES

Antonow—Romanovsky, W. W. (1935). *Phys. Zeit. d. Sowjetunion*, **7**, 366.

Groot, W. de (1939), *Physica*, **6**, 275.

Jablonsky, A. (1935), *Zeits f. Phys.*, **94**, 38.

Klasens, H. A. and Wise, M. E. (1946), *Nature*, **158**, 483.

Levy, L. and West, D. W. (1939), *Trans. Farad. Soc.*, **35**, 87.

Mott, N. F., and Gurney, R. W. (1940), " Electronic Processes etc." Oxford, 218.

Mott, N. F. and Massey, H. S. W. (1939), " Theory of Atomic Collision " Oxford.

Randall, J. T. and Wilkins, M. H. F. (1945), *Proc. Roy. Soc., A*. **184**, 366, 390.

Tibbs, S. R. (1938), *Trans. Farad. Soc.*, **35**, 1471.

The following special publications of the Indian Association for the Cultivation of Science, 210, Bowbazar Street, Calcutta, are available at the prices shown against each of them :—

No.	Subject	Author	Price Rs.	A.	P.
III	Methods in Scientific Research ...	Sir E. J. Russell	0	6	0
IV	The Origin of the Planets ..	Sir James H. Jeans	0	6	0
V	Separation of Isotopes ...	Prof. F. W. Aston	0	6	0
VI	Garnets and their Role in Nature. ...	Sir Lewis L. Fermor	2	8	0
VII	(1) The Royal Botanic Gardens, Kew. ...	Sir Arthur Hill	1	8	0
	(2) Studies in the Germination of Seeds. ...				
VIII	Interatomic Forces ..	Prof. J. E. Lennard-Jones	1	8	0
IX	The Educational Aims and Practices of the California Institute of Technology ..	R. A. Millikan	0	6	0
X	Active Nitrogen A New Theory .	Prof. S. K. Mitra	2	8	0

A discount of 25% is allowed to Booksellers and Agents.

RATES OF ADVERTISEMENTS

Third page of cover	Rs.	32, full page
do. do.	,,	20, half page
do. do.	,,	12, quarter page
Other pages	,,	25, full page
do.	,,	16, half page
do.	,,	10, quarter page

15% Commissions are allowed to bonafide publicity agents securing orders for advertisements.

We are now manufacturing :

* **KIPP'S APPARATUS of one litre capacity,**
* **DESICCATOR of 4", 5" and 6" diameter,**
* **MEASURE GLASSES of 2 drams, 1 oz., 4 oz. and 8 oz. cap. accurately calibrated**

AND

ALL TYPES OF GRADUATED GLASSWARE
such as Measuring Flasks, Measuring Cylinders,
Burettes, Pipettes, etc., etc.

Manufactured by :

INDUSTRIAL & ENGINEERING APPARATUS CO., LTD.

CHOTANI ESTATES, PROCTOR ROAD, BOMBAY, 7.

THE SCIENTIFIC APPARATUS & CHEMICAL WORKS, LIMITED.

CIVIL LINES, AGRA,

(Originally founded in 1918

GOLDEN OPPORTUNITY

The Company's Managing Director Mr. S. P. Khandelwal has brought with him from America and Europe a number of Schemes for the Scientific development in India. Hence the Company invites,

TEMPORARY DEPOSITS

on interest as detailed below :

For one year Rs. 5/4/- p.c. per annum.
For two years Rs. 6/- p.c. per annum.

For long periods please write or see personally the Managing Director.

ABSORPTION BANDS OF IODINE IN QUARTZ ULTRAVIOLET *

By PUTCHA VENKATESWARLU

(*Received for publication, January 10, 1947.*)

ABSTRACT. Review of the absorption spectrum of iodine in quartz ultraviolet and fluorite region is made. The analysis of all the bands from 1950-2760A is given here. The position of the 0-0 band, which gives the position of the excited level is extrapolated to be 44900 cm^{-1}. The convergence limit of the excited state is about 58000 ± 1000 cm^{-1}. These quartz ultraviolet bands are due to transition from the ground state to an excited state σ_g, Π_u^4, Π_g^4, $\sigma_u . 1_u(^3\Sigma_u^+)$ at 44900 cm^{-1} which has a frequency of about 90 cm^{-1}. The fluorite region bands from 1950-1770A are due to transition from the ground state to an excited state σ_g, Π_u^4, Π_g^4, $\sigma_u . 0_u^+(^1\Sigma_u^+)$ at 51683 cm^{-1} having a frequency of 165 cm^{-1}. The two excited states have the same convergence limit and have as their dissociation products $I^-(^1S_0)+I^+(^3P_2)$. The two continua at 3413 and 3263A which occur in absorption at high temperature are explained. The narrow diffuse bands overlapping these two continua are also discussed.

INTRODUCTION

During the course of an investigation and interpretation of the emission bands of iodine, it has become necessary to make a complete review of the extensive absorption data collected by different authors in the quartz ultraviolet and fluorite regions, at temperatures ranging from −30° to 1100°C. In a previous communication (Venkateswarlu, 1946*a*) an analysis and interpretation of the discrete absorption bands (Cordes bands) in the region 1770-1950A is given. In this paper it is proposed to present a complete analysis of the bands from 1950 to 2760A. Incidentally the continua at 3413, 3263A and the narrow diffuse bands overlapping the continua are also discussed.

REVIEW OF WORK DONE IN ABSORPTION IN QUARTZ ULTRAVIOLET

The absorption of iodine vapour has been investigated by many different workers. Warren (1935) has given a brief summary of the work done till 1934. Pringsheim and Rosen (1928) investigated the region 2760 to 2080A, using a sphere of 6 cm. diameter, and temperatures in the range 200-800°C and a pressure of about one atmosphere. They found two series of bands, one in the region 2500-2760A, spaced uniformly at 90 cm.$^{-1}$, the second in the region 2080-2200A, spaced at 70 cm^{-1}. They designated these as $v'=0$ and $v''=0$ progressions respectively of a transition between two electronic levels, and analysed the intervening group of bands according to these two frequencies. Thus they explained the observed absorption bands as due to the transition from a lower initial state having $\omega=90$ cm^{-1}, which is not the ground state but a state lying higher than it, to an upper final state with a frequency of 70 cm^{-1}. Kimura and Miyanishi (1929) extended the absorption data, obtaining bands with an absorption tube 15 cm. long at temperatures 35-120°C in the region 1950-2150A. They obtained 157 bands, some of which on the long wave side can be identified with the bands of $v''=0$ progression of P-R bands. They developed for their bands an equation

---

* Communicated by Dr. R. K. Asundi.

$$\nu=52800+78\ v'-v'^2-210\ v''.$$

The upper state with the frequency 78 cm^{-1} was identified with the upper state ($\omega'=70$) of P-R bands and the lower state with the ground state of the iodine molecule. Their $v'v''$ scheme, as pointed out by Sponer and Watson (1929), gave the analysis of K-M and P-R bands in two tables with the following alternative suggestions : (1) the two are different band systems, the bands on the longwave side of K-M being identical with the bands of $v''=0$ progression of P-R band system, and so these bands belong to P-R band scheme and not to the scheme of K-M band system. (2) The two schemes given in the two tables belong to one system, being connected by a long thin bridge which consists of bands with mutual separation of 70 cm^{-1}. They are of the opinion that the connection by such a long thin bridge makes the second suggestion insecure. Further Sponer and Watson's arrangement does not include the P-R bands with $v'=0$ progression. They suggest that because these bands occur in single series in contrast to the other bands, they belong to a different system.

Later Warren (*loc. cit.*) has investigated the absorption spectrum at gradually increasing temperatures, in fact from room temperature up to 1100°C. He suggests that P-R, K-M bands, which he also obtains, belong to one system involving the ground level of the molecule, and that the single series which forms the bridge between the two groups of bands is not a single progression but belongs to three or four progressions. According to him, because $\omega'=70$ and $\omega''=210$, the bands of different progressions overlap one another, giving the appearance of a single series. Similarly he explains the single series on the long-wave side (*i.e.*, bands of $v'=0$ progression of P-R which have a separation of 90 cm^{-1}) as belonging to different progressions the bands of which overlap because of a single ratio 2 : 1 between ω''_{180} and ω'_{90}. By increasing the temperature and hence pressure of the iodine vapour, he obtained also two continua at 3413 and 3263A, thus confirming Skorko's observations. By a further increase in temperature (at 1150°C) Warren finds that the absorption bands increase towards longer waves and ultimately reach 3413A, overlapping the two continua.

Skorko (1933, 34) working in absorption at high temperatures has obtained the following results. At a temperature of 775°C he obtains the continuum at 3413A and at 885°C another continuum at 3263A. With further increase of temperature up to 1050°C, diffuse narrow bands appear overlapping the continua. The wavelengths of the diffuse bands from 3419 to 2974 are given. He does not, however, mention that these bands unite with the bands of P-R on the short wave side. These bands do not appear to belong to the P-R, K-M bands. Their origin is discussed later.

Explanation of continua at 3413 and 3263A :—Warren is of the opinion that the continuum at 3413A belongs to the same transition as all the discrete absorption bands, and that it forms the long wave limit of the (P-R, K-M) absorption bands. The experiments of Skorko as well as of Warren show, however, that the continua at 3413 and 3263A are the first to appear, and only with further increase of temperature, do they become overlapped on the short wave side by narrow bands. If the continuum is to form the long wave end of the apsorption bands, then one would expect a gradual development of P-M, K-R bands towards the long wave side as the temperature is increased and the continuum to appear finally. As this is not so, it is not correct to say that the continuum at 3413A forms the long wave edge of the P-R, K-M bands. According to us the continuum and the bands are due to quite different electronic transitions. A continuum at 3416A, which obviously is identical with that observed in absorption, occurs in emission also where it is unaccompanied by the narrow bands or the P-R, K-M bands. As is shown elsewhere (Venkateswarlu, 1946*b*) this continuum is due to a transition from a stable state $\sigma_g, \pi_u^4, \pi_g^3, \sigma_u^3.1_g(^3\Pi_{1g})$ to a repulsive state $\sigma_g^2, \pi_u^3, \pi_g^3, \sigma_u^2.0_u(^1\Sigma_u^-)$ which dissociates into $^2P_{\frac{1}{2}} + {}^2P_{\frac{3}{2}}$ iodine atoms. The occurrence of this continuum in absorption at high temperatures is explained as due to a transition from the repulsive state $0_u^-(^1\Sigma_u^-)$ to the stable state $1_g(^3\Pi_{1g})$, the repulsive state having been reached by the recombination* of two iodine atoms $^2P_{\frac{3}{2}} + {}^2P_{\frac{1}{2}}$ which are obtained by thermal dissociation of molecules at such temperatures. Similarly the continuum at 3263A in absorption can be explained as due to a transition from the repulsive part of the state 0_u^+ (reached by recombination of $^2P_{\frac{3}{2}} + {}^2P_{\frac{1}{2}}$) to the state $1_g(^3\Pi_{1g})$ at 51528 cm^{-1}. This continuum is reported by Skorko to be narrower than that at 3413A. We have not got this continuum at 3263A on our plates in emission. Probably, if it is narrow, it might have been overlapped by one of the diffuse bands which are present there. But the continuous band recorded by Strutt and Fowler (1912) at 3270A in the glow excited by active nitrogen is very probably identical with this band. Thus the two continua are due to the following transitions in I_2 molecule.

---

* This view has been stated to be supported by the fact that at such high temperatures Utchida (1936), Wood (1906) and others have obtained in emission the visible bands of iodine which could be explained only as being brought out by thermal luminescence on the supposition that the initial state of the bands *viz.*, 0_u^+ at 15583 cm^{-1} is formed by combination of $^2P_{\frac{3}{2}} + {}^2P_{\frac{1}{2}}$ iodine atoms.

Continuum at 3413A . $\sigma_g^2, \pi_u^3, \pi_g^3, \sigma_u^2 . O_u^-(^1\Sigma_u^-) - \sigma_g, \pi_u^4, \pi_g^3, \sigma_u^2, 1_g(^3\Pi_{1g})$

Continuum at 3263A : $\sigma_g^2, \pi_u^4, \pi_g^3, \sigma_u . O_u^+ (^3\pi_{g,u}) \succ \sigma_g, \pi_u^4, \pi_g^3, \sigma_u^2, 1_g(^3\Pi_{1g})$.

Analysis of the Bands from 2760-1950A :—Warren does not give the measurements of the absorption bands or their analysis, but he is of the opinion that all the bands in the quartz ultraviolet belong to one system. Sponer and Watson (1929) do not include the bands from 39815 to 36190 cm.$^{-1}$ in their analysis. In view of these facts, having given a complete review of the work done on absorption, we feel it worth while to give the analysis of all the bands in this paper and calculate the approximate position of the excited level which will be useful for the interpretation of some of the emission bands. This analysis is given in Table I. All the values from 36190 to 47756 cm.$^{-1}$ are due to Pringsheim and Rosen and those from 47756 to 51298 cm.$^{-1}$ are due to Kimura and Miyanishi. As between 46592 and 47756 cm^{-1} the bands obtained by Kimura and Miyanishi and Pringsheim and Rosen are identical, in Table I K-M values are given in brackets beside the P-R values. The analysis of the bands from 39815 to 51298 cm^{-1} is almost the same as that given by Sponer and Watson except for the following differences. The single series which forms the thin bridge between the two groups of K-M and P-R is given, in agreement with Warren's suggestion in three progressions. The bands in the fluorite region are not included in this scheme, as they form quite a different system. The long series bands (v′=0 progression of P−R) from 34815 to 36190 cm^{-1} which are not included in the analysis of Sponer and Watson are also given in the v′v″ scheme. There is some difference in the v″=0, 1 progressions also. According to the analysis given here, about 46 levels of the ground state are excited which is probable at the high temperatures used. The wave number differences are very irregular and it does not serve any useful purpose to deduce an equation. The vibrational frequency in the excited state is of the order of 90 cm^{-1}. The position of the O−O band has been extrapolated to be 44900 cm^{-1}. The convergence limit of the excited state is extrapolated to roughly 58000 ± 1000 cm^{-1}.

Bands in Fluorite Region.—Sponer and Watson (1929) have worked in the fluorite region by using a spectrograph giving a dispersion of about 9A/mm at 1700A. Cordes (1935) has worked with a higher dispersion fluorite spectrograph (2.3A/mm at 1700A) and obtained bands in the region 1950-1500A which are more in number than those obtained by Sponer and Watson. In the region 1770−1542A the bands are irregular and Cordes has grouped them into seven systems. Cordes suggested that the rest of the bands on the long wave side of 1770 up to 1950A form a single progression which probably is an extension of K−M bands. If these bands are to be arranged as a single progression according to this suggestion, the wave number differences will be very spasmodic. We have, therefore, given in an earlier communication (Venkateswarlu, *loc. cit.*) a different analysis of all the bands between 1776 and 1948A. The proposed v′v″ scheme is deemed satisfactory, particularly when

M bands These bands, which
s due to a transition from the
$^{-1}$, having a vibration frequency
by the fact that we have five
10466) with successive separa-
y be explained by transition
table states dissociating into
s.

9. 51007 and 50942 cm^{-1}, which
heme of Cordes bands with (v′v″)
5) respectively. Further a few
of v″ = 0 and 1 progressions of the
ds. Thus it appears that the
reme side of the quartz ultra-
e excited states of the Cordes
discussed (by the author)
5 and 90 cm^{-1}, are respec-
ectively with $^1\Sigma_u^+$ and $^3\Sigma_u^+$ of
tion is $\sigma_g, \pi_u^4, \pi_g^4, \sigma_u$. Also
viz., ~ 59000 cm^{-1} and the

Δγ	Group
111	
93	
93	
95	
76	
66	
96	
87	
77	
117	III
108	
78	
90	
99	
101	
101	
91	
92	
113	

λ_{air}	ν_{vac}	Δ_ν
3105	32197	
3095	32301	104
3084	32416	115
3076	32500	84
3067	32596	96
3059	32681	85
3052	32756	75
3042	32864	108
3035	32939	75
3029	33005	66
3019	33114	109
3009	33224	110
3001	33313	89
2994	33390	77
2984	33502	112
2974	33615	113

2974A.—As stated above, Skorko
lapping the continua at very
wavelengths of the bands from
3419-2974A (see Table II). The wave number separations are very irregular.

These cannot be placed in the v′v″ scheme of Table I. It is difficult to say what relation these bands have with P-R, K-M absorption bands. Future measurements of all the bands from 2000-3415A, on high dispersion instruments will probably throw light in this direction. However, the following may be given as one probable explanation. As these bands are diffuse they may be considered as arising in transitions from unstable states (reached by recombination of atoms) having nearly flat potential energy curves to stable states. The bands apparently occur in three groups. The second and the third groups consist of bands with an average wave number separation of 90 cm^{-1}. They may be considered to be due to transitions from unstable states $0_g^+(^3\Pi_{0_g^+})$* and $1_g(^3\Pi_1)$ formed by combination of two $^2P_{\frac{3}{2}}$ atoms to the stable state $1_u(^3\Sigma_u^+)$ which is the excited state of the P-R, K-M bands. The points

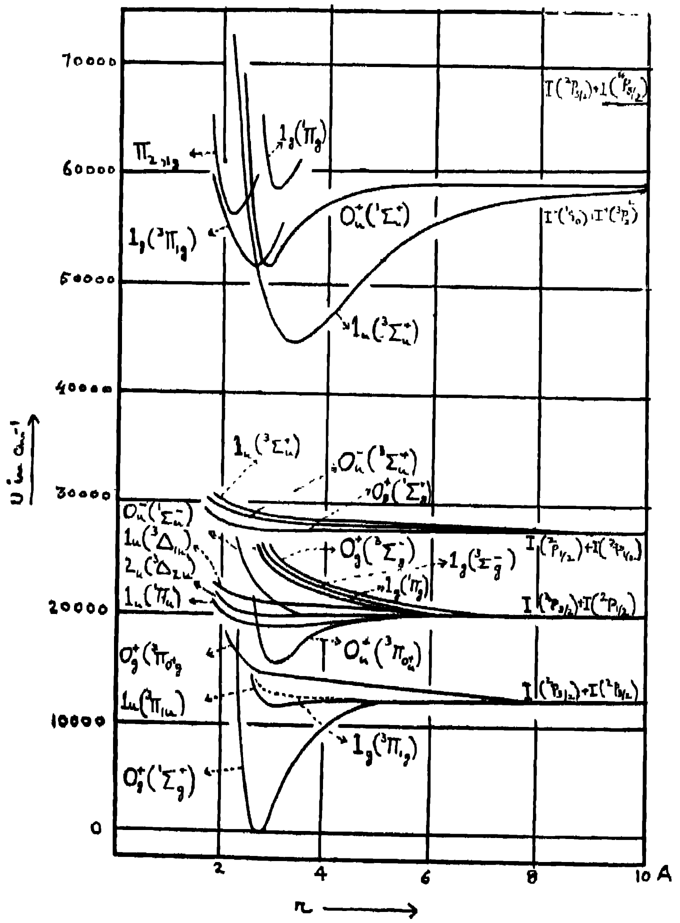

FIG. 1

Potential energy curves for I_2 molecules on the curves O_g^+ and 1_g below the state 1_u will be at $(44900-30340)=14560$, $(44900-32197)=12700$ cm^{-1}. The first group consists of bands with wave number separation of the order of 130 cm^{-1}. They may be considered to be arising in a transition from the state O_g^+ (formed by combination of two I ($^2P_{\frac{1}{2}}$) atoms) to that part of the state $O_u^+(^1\Sigma_u^+)$ where ω will be about 130 cm^{-1}. These may also be explained as due to a transition from the state $1_u(^3\Sigma_u^+)$ (formed from two $^2P_{\frac{1}{2}}$ atoms) to a state $1_g(^1\Pi_g)$ at 58572 cm^{-1}, with a frequency of the order of 120 cm^{-1}. This latter state is involved in the production of the three groups of diffuse emission bands below 2685A having a separation of 120 cm^{-1}, discussed elsewhere (Venkateswarlu, 1947).

---

* The state $0_g^+(^3\Pi_{0_g^+})$ forms the final level of the fifth group of diffuse emission bands, which are explained as arising in transitions from 0_u^+ state at 51683 cm^{-1} to this unstable state 0_g^+ which dissociates into two $^2P_{\frac{3}{2}}$ iodine atoms.

Figure 1 gives the potential energy curves of iodine molecule. The way of drawing these curves is already explained in papers "Emission Bands of Halogens Parts II and III" (Venkateswarlu, 1947).

ACKNOWLEDGMENT

The author wishes to express his thanks to Prof. R. K. Asundi for guidance and to Kamalapat Singhania Trust for the award of a scholarship.

PHYSICS DEPT.
HINDU UNIVERSITY
BENARES.

REFERENCES

Asundi and Venkateswarlu, 1946, *Science and Culture*, **12**, 153.

Cordes, 1935, *Zs. f Phys* , **97**, 603.

Kimura and Miyanishi, 1929, *Sci. Papers Inst. Phys Chem. Res. (Tokyo)*, **10**, 33

Pringsheim and Rosen, 1928, *Zs. f. Phys* , **50**, 1.

Skorko, 1933, *Nature*, **131**, 366

,, 1934, *Acta Physica Polonica*, **3**, 191.

Sponer and Watson, 1929, *Zs. f. Phys.*, **56**, 184.

Strutt and Fowler, 1912, *Proc. Roy. Soc* , **86A**, 105.

Uchida, 1936, *Sci. Papers Inst. Phys. Chem. Res. Tokyo)*, **30**, 71.

Venkateswarlu, 1946(*a*), *Proc. Ind. Acad. Sci.*, **24**, 473.

,, 1946(*b*), *Proc. Ind. Acad. Sci* , **24**, 480.

,, 1947, *Proc. Ind. Acad. Sci.*, **25A**, 119 and 133

Warren, 1935. *Phys. Rev.*, **47**, 1.

Wood, 1906, *Phil. Mag.*, **12**, 324.

6

RELATIONSHIP BETWEEN WIND VELOCITY AND TEMPERATURE IN THE FREE ATMOSPHERE *

By S. K. BANERJI†

(*Received for publication, Feb. 12, 1947*)

ABSTRACT. In this paper, a number of formulae have been given for the computation of upper air temperature from the known distribution of velocities of upper winds as given by pilot balloon observations. Sir Napier Shaw's formulae giving the relationship between temperature and velocity hold only when geostrophic conditions are satisfied. They are not applicable to tropical regions. For tropical regions, a closer approximation is obtained by the use of the formulæ

$$\frac{g}{T^2}\frac{\partial T}{\partial x} = -2\varpi \cos\phi \frac{\partial}{\partial x}\left(\frac{u}{T}\right) + 2\varpi \sin\phi \frac{\partial}{\partial z}\left(\frac{v}{T}\right),$$

$$\frac{g}{T^2}\frac{\partial T}{\partial y} = -2\varpi \cos\phi \frac{\partial}{\partial y}\left(\frac{u}{T}\right) - 2\varpi \sin\phi \frac{\partial}{\partial z}\left(\frac{u}{T}\right),$$

where T is the temperature in absolute scale, u, v the horizonal components of wind towards east and north, ϖ the angular velocity of earth's rotation, and ϕ the latitude.

1. Sir Napier Shaw's formulae giving the relationship between temperature and velocity are frequently used to compute upper air temperature from the known distribution of velocities of upper winds as given by pilot balloon observations. These formulae assume geostrophic relationship and do not therefore hold for tropical regions. The best formulae to be used for such computations in tropical regions received the consideration of the present writer some time ago. Starting from the rigorous hydrodynamical equations, a series of formulae were worked out, with the underlying assumptions clearly defined. In this paper, these formulae have been given, and the best formulae for tropical regions have been indicated. The results of certain computations made of the upper air temperature in India from the pilot balloon winds and their comparison with actual observed temperature will be published in a separate paper.

2. Let the axes refer to east, north and vertical respectively, and let u, v, w be the components of wind velocity at (x, y, z).

The equations of motion are—

$$\frac{Du}{Dt} + 2\varpi(w \cos\phi - v \sin\phi) = -\frac{1}{\rho}\frac{\partial p}{\partial x} + K\frac{\partial^2 u}{\partial z^2}$$

$$\frac{Dv}{Dt} + 2\varpi u \sin\phi = -\frac{1}{\rho}\frac{\partial p}{\partial y} + K\frac{\partial^2 v}{\partial z^2}$$

This paper was read at the Indian Science Congress, 1939.

† Fellow of the Indian Physical Society.

$$\frac{Dw}{Dt} - 2\varpi u \cos\phi = -\frac{1}{\rho}\frac{\partial p}{\partial z} - g$$

$$\frac{Du}{Dt} = \frac{\partial u}{\partial t} + u\frac{\partial u}{\partial x} + v\frac{\partial u}{\partial y} + w\frac{\partial u}{\partial z}$$

$$= \frac{\partial u}{\partial t} + \frac{1}{2}\frac{\partial q^2}{\partial x} + \eta w - \zeta v, \quad \text{etc.,}$$

where $$q^2 = u^2 + v^2 + w^2,$$

and $$\xi = \frac{\partial w}{\partial y} - \frac{\partial v}{\partial z}, \quad \eta = \frac{\partial u}{\partial z} - \frac{\partial w}{\partial x}, \quad \zeta = \frac{\partial v}{\partial x} - \frac{\partial u}{\partial y}$$

are the components of vorticity vector. ϕ denotes the latitude, ϖ the angular velocity of rotation of the earth, and K the coefficient of eddy viscosity.

3. If we write

$$\beta = 2\varpi \cos\phi, \quad \gamma = 2\omega \sin\phi,$$

the equations of motion become

$$\frac{\partial u}{\partial t} + \frac{1}{2}\frac{\partial q^2}{\partial x} + (\eta + \beta)w - (\zeta + \gamma)v = -\frac{1}{\rho}\frac{\partial p}{\partial x} + K\frac{\partial^2 u}{\partial z^2} \qquad \ldots (1)$$

$$\frac{\partial v}{\partial t} + \frac{1}{2}\frac{\partial q^2}{\partial y} + (\zeta + \gamma)u - \xi w = -\frac{1}{\rho}\frac{\partial p}{\partial y} + K\frac{\partial^2 v}{\partial z^2} \qquad \ldots (2)$$

$$\frac{\partial w}{\partial t} + \frac{1}{2}\frac{\partial q^2}{\partial z} + \xi v - (\eta + \beta)u = -\frac{1}{\rho}\frac{\partial p}{\partial z} - g \qquad \ldots (3)$$

4. If the motion is steady

$$\frac{\partial u}{\partial t} = \frac{\partial v}{\partial t} = \frac{\partial w}{\partial t} = 0 \qquad \ldots (4)$$

But in the atmosphere, we seldom see a steady state. To take account of the non-steady state, we can assume either

$$u = \lambda t + u_0, \quad v = \mu t + v_0, \quad w = \nu t + w_0 \qquad \ldots (5)$$

or

$$u = u_0 e^{\lambda t}, \quad v = v_0 e^{\mu t}, \quad w = w_0 e^{\nu t}, \qquad \ldots (6)$$

where λ, μ, ν are functions of x, y, z.

5. Taking $p = R\rho T$, where T is the temperature, we get, by eliminating p from the equations (1), (2), and (3), the following results on the second assumption, namely (6) :—

$$\frac{g}{T^2}\frac{\partial T}{\partial x} = K\frac{\partial}{\partial z}\left(\frac{1}{T}\frac{\partial^2 u}{\partial z^2}\right) + \frac{1}{2}\frac{\partial}{\partial x}\left(\frac{1}{T}\frac{\partial q^2}{\partial z}\right) - \frac{1}{2}\frac{\partial}{\partial z}\left(\frac{1}{T}\frac{\partial q^2}{\partial x}\right) - \frac{\partial}{\partial x}\left(\frac{(\eta + \beta)u - \xi v - \nu w}{T}\right)$$

$$- \frac{\partial}{\partial z}\left(\frac{\lambda u - (\zeta + \gamma)v + (\eta + \beta)w}{T}\right) \qquad \ldots (7)$$

$$\frac{g}{T^2}\frac{\partial T}{\partial y}=K\frac{\partial}{\partial z}\left(\frac{1}{T}\frac{\partial^2 v}{\partial z^2}\right)+\frac{1}{2}\frac{\partial}{\partial y}\left(\frac{1}{T}\frac{\partial q^2}{\partial z}\right)-\frac{1}{2}\frac{\partial}{\partial z}\left(\frac{1}{T}\frac{\partial q^2}{\partial y}\right)-\frac{\partial}{\partial y}\left(\frac{(\eta+\beta)u-\xi v-\nu w}{T}\right.,$$

$$\left.-\frac{\partial}{\partial z}\left(\frac{(\zeta+\gamma)u+\mu v-\xi w}{T}\right. \quad \ldots \quad (8)$$

If we make the first assumption, namely (5), the equations are obtained by writing λ, μ, ν for λu, μv, νw respectively in the terms involving the operator

$$\frac{\partial}{\partial t}.$$

6. If the air-mass is supposed to move adiabatically, we have

$$\frac{D}{Dt}\left(\frac{T^{\alpha}}{p^{\alpha-1}}\right)=0,$$

α being the ratio of specific heats,

or,
$$\frac{\partial T}{\partial t}+u\frac{\partial T}{\partial x}+v\frac{\partial T}{\partial y}+w\frac{\partial T}{\partial z}=\frac{\alpha-1}{\alpha}\frac{T}{p}\left(\frac{\partial p}{\partial t}+u\frac{\partial p}{\partial x}+v\frac{\partial p}{\partial y}+w\frac{\partial p}{\partial z}\right) \quad \ldots \quad (9)$$

If the motion is along an isotherm,

$$u\frac{\partial T}{\partial x}+v\frac{\partial T}{\partial y}+w\frac{\partial T}{\partial z}=0 \quad (10)$$

If the motion is along an isentropic surface that is, the surfacs $\Phi=$ constant, we get

$$u\frac{\partial \phi}{\partial x}+v\frac{\partial \phi}{\partial y}+w\frac{\partial \phi}{\partial z}=0,$$

or,
$$\left(u\frac{\partial T}{\partial x}+v\frac{\partial T}{\partial y}+w\frac{\partial T}{\partial z}\right)-\frac{T}{p}\frac{\alpha-1}{\alpha}\left(u\frac{\partial p}{\partial x}+v\frac{\partial p}{\partial y}+w\frac{\partial p}{\partial z}\right)=0. \quad \ldots \quad (11)$$

The two equations (7) and (8), coupled with any of the above, as the circumstances may be, may be used to calculate

$$\frac{\partial T}{\partial x}, \frac{\partial T}{\partial y}, \frac{\partial T}{\partial z},$$

if we know the velocity distribution.

These are very general equations, and are not easily amenable to numerical computation.

7. If the fluid elements move along stream lines in such a way that the angular rotation can be neglected, we get

$$\xi=0,\ \eta=0,\ \zeta=0.$$

If in addition, the viscosity is neglected, we get

$$\frac{g}{T^2}\frac{\partial T}{\partial x}=\frac{1}{2}\frac{\partial}{\partial x}\left(\frac{1}{T}\frac{\partial q^2}{\partial x}\right)-\frac{1}{2}\frac{\partial}{\partial z}\left(\frac{1}{T}\frac{\partial q^2}{\partial x}\right)-\frac{\partial}{\partial x}\frac{\beta u-\nu w}{T}-\frac{\partial}{\partial z}\frac{\lambda u-\gamma v+\beta w}{T} \quad (12)$$

$$\frac{g}{T^2}\frac{\partial T}{\partial y}=\frac{1}{2}\frac{\partial}{\partial y}\left(\frac{1}{T}\frac{\partial q^2}{\partial z}\right)-\frac{1}{2}\frac{\partial}{\partial z}\left(\frac{1}{T}\frac{\partial q^2}{\partial y}\right)-\frac{\partial}{\partial y}\frac{\beta u-\nu w}{T}-\frac{\partial}{\partial z}\frac{\gamma u+\mu v}{T}. \quad \ldots \quad (13)$$

8. *Sir Napier Shaw's equations.*

If the motion is steady,

$$\lambda=\mu=\nu=0,$$

and if the vertical velocity and the square of the velocity can be neglected,

$$w=0,\quad q=0.$$

On these assumptions, we get

$$\frac{g}{T^2}\frac{\partial T}{\partial x}=-\beta\frac{\partial}{\partial x}\left(\frac{u}{T}\right)+\gamma\frac{\partial}{\partial z}\left(\frac{v}{T}\right). \qquad \ldots \quad (14)$$

$$\frac{g}{T^2}\frac{\partial T}{\partial y}=-\beta\frac{\partial}{\partial y}\left(\frac{u}{T}\right)-\gamma\frac{\partial}{\partial z}\left(\frac{u}{T}\right). \qquad \ldots \quad (15)$$

These two equations reduce to Sir Napier Shaw's equations* when $\beta=0$, that is, $2\bar{\omega}\cos\phi=0$.

All these collectively constitute very large assumptions which are not justified, particularly in tropical regions. It is, therefore, little wonder that the correlation coefficient between the observed variations of temperature and those deduced by use of Sir Napier Shaw's equations has been found to be low, little less than 0.5, even in high latitudes. In latitudes near the equator, the assumption $\cos\phi=0$ completely invalidates the equations. Moreover, the vertical velocity, even though small compared with the horizontal, makes a very large contribution to temperature variation, and cannot, therefore, be neglected in such equations.

9. At latitude 25°,

$$\beta=2\times7\times10^{-5}\times0.9 \text{ cm./s}$$

$$\gamma=2\times7\times10^{-5}\times0.4 \text{ cm./s}.$$

In latitudes near the equator, Shaw's equations are approximately true, provided u/T undergoes no variation in either horizontal direction, that is, u/T remains constant in the entire horizontal field.

If the motion is north-south, then

$$\frac{g}{T^2}\frac{\partial T}{\partial x}=\gamma\frac{\partial}{\partial z}\left(\frac{v}{T}\right). \qquad \ldots \quad (16)$$

The temperature gradient is in the east-west direction; temperature is increasing or decreasing eastwards according as the ratio of velocity to temperature is increasing or decreasing upwards.

If the motion is east-west, we get

$$\frac{g}{T^2}\frac{\partial T}{\partial x}=-\beta\frac{\partial}{\partial x}\left(\frac{u}{T}\right)$$

or

$$\frac{g}{T}=\frac{\beta u}{T}+\text{const.},$$

that is,

$$u=AT+B. \qquad \ldots \quad (17)$$

---

* Manual of Meteorology, *see* reference 2 at end.

In a purely east-west motion, therefore, the temperature and velocity become linearly related along the same east-west line. That is, if velocity is constant along a line, temperature is also constant along that line. In illustration of this, see the upper wind and temperature charts for all levels, 2 km. and above, for the months November to March, in the Memoir on the General Circulation of the atmosphere over India and its neighbourhood by Dr. Ramanathan and Mr. Ramakrishnan (1939).

10. If we assume the motion to be steady, that is $\lambda=\mu=\nu=0$, we get, on simplifying the generalised equations (7) and (8),

$$\left(g-\beta u+\tfrac{1}{2}\frac{\partial q^2}{\partial z}\right)\frac{\partial T}{\partial x}+\left(\gamma v-\beta w-\tfrac{1}{2}\frac{\partial q^2}{\partial x}\right)\frac{\partial T}{\partial z}=T\left(\beta\frac{\partial v}{\partial y}+\gamma\frac{\partial v}{\partial z}\right) \qquad (18)$$

and

$$\left(g-\beta u+\tfrac{1}{2}\frac{\partial q^2}{\partial z}\right)\frac{\partial T}{\partial y}+\left(\gamma u-\tfrac{1}{2}\frac{\partial q^2}{\partial y}\right)\frac{\partial T}{\partial z}=T\left(-\beta\frac{\partial u}{\partial y}+\gamma\frac{\partial u}{\partial z}\right)\ldots \qquad (19)$$

If $w=0$, and if the velocities do not undergo variation in the horizontal direction,

$$\left(g-\beta u+\tfrac{1}{2}\frac{\partial q^2}{\partial z}\right)\frac{\partial T}{\partial x}+\gamma v\frac{\partial T}{\partial z}=T\gamma\frac{\partial v}{\partial z} \qquad \ldots \quad (20)$$

$$\left(g-\beta u+\tfrac{1}{2}\frac{\partial q^2}{\partial z}\right)\frac{\partial T}{\partial y}+\gamma u\frac{\partial T}{\partial z}=T\gamma\frac{\partial u}{\partial z} \qquad \ldots \quad (21)$$

or,

$$\left(g-\beta u+\tfrac{1}{2}\frac{\partial q^2}{\partial z}\right)\left(\frac{\partial T}{\partial x}+\frac{\partial T}{\partial y}\right)+\gamma(u+v)\frac{\partial T}{\partial z}=T\gamma\frac{\partial}{\partial z}(u+v) \qquad \ldots \quad (22)$$

or,

$$\left(g-\beta u+\tfrac{1}{2}\frac{\partial q^2}{\partial z}\right)\times\text{(mean horizontal lapse rate)}$$

$$+\gamma\frac{u+v}{2}\times\text{(vertical lapse rate)}$$

$$=T\gamma\frac{\partial}{\partial z}\frac{u+v}{2}. \qquad \ldots \quad (23)$$

If velocity does not vary with height,

$$\frac{\text{mean hor. lapse rate}}{\text{vertical lapse rate}}=-\frac{(u+v)\gamma}{2(g-\beta u)} \qquad (24)$$

If $u=v=20m/s=72$ km/hr, we have at $\phi=25°$,

$$\frac{\text{mean hor. lapse rate}}{\text{vertical lapse rate}}=-\frac{0\cdot112}{981-0\cdot252},$$

When there is no horizontal or vertical variation of wind velocity, the horizontal lapse rate is a very small fraction of the vertical lapse rate. For adiabatic lapse rate in the vertical, the horizontal lapse rate becomes 1.2°C per 1000 km., under the conditions stipulated.

11. In a region where the gradient equation holds,

$$\frac{1}{\rho}\frac{\partial p}{\partial n} = 2\bar{\omega}\,V\sin\phi \pm \frac{V^2}{r}, \qquad \ldots \quad (25)$$

∂n being an element of normal to the isobar.

Also,

$$\frac{\partial p}{\partial z} = -g\rho,\ p = R\rho T,\ \frac{1}{p}\frac{\partial p}{\partial z} = -\frac{g}{RT}, \qquad \frac{g}{RT^2}\frac{\partial T}{\partial n} = \frac{\partial}{\partial n}\left(\frac{1}{p}\frac{\partial p}{\partial z}\right)$$

$$= \frac{\partial^2}{\partial n\partial z}\log p = \frac{\partial^2}{\partial z\partial n}\log p = \frac{\partial}{\partial z}\left(\frac{1}{p}\frac{\partial p}{\partial n}\right) = \frac{\partial}{\partial z}\left(\frac{2\omega V\sin\phi}{RT} \pm \frac{V^2}{RTr}\right).$$

Therefore,

$$\frac{1}{T^2}\frac{\partial T}{\partial n} = \frac{2\bar{\omega}\sin\phi}{g}\cdot\frac{\partial}{\partial z}\left(\frac{V}{T}\right) \pm \frac{1}{g}\frac{\partial}{\partial z}\left(\frac{V^2}{rT}\right). \qquad \ldots \quad (26)$$

$$\bar{\omega} = 7\times 10^{-5}\ \text{cm./sec., and at } \phi = 25^\circ,\ \sin\phi = 0.4$$

Therefore,

$$\frac{1}{T^2}\frac{\partial T}{\partial n} = \frac{5.6\times 10^{-10}}{981}\left(\frac{V_2}{T_2} - \frac{V_1}{T_1}\right) \pm \frac{10^{-5}}{981}\left(\frac{V_2^2}{r_2T_2} - \frac{V_1^2}{r_1T_1}\right),$$

where V_1, T_1, r_1 and V_2, T_2, r_2 are velocity, temperature, and radius of curvature of isobar at height z and one kilometre higher up, ∂n being measured in units of kilometre.

If $\qquad r_1 = r_2 = 100\ \text{km.} = 10^7\ \text{cm},$

$$V_1 = 15m./s. = 53\ \text{km./hr.}, \qquad T_1 = 276^\circ A.$$

$$V_2 = 20m./s. = 72\ \text{km./hr.}, \qquad T_2 = 270^\circ A.,$$

we get

$$\frac{\partial T}{10^{-5}\partial n} = \begin{array}{c} 0.05 \text{ for cyclone,} \\ \text{and} \\ -0.03 \text{ for anticyclone.} \end{array}$$

With these data temperature is increasing outwards at the rate of 5°C per 100 km., in the case of cyclone, and decreasing outwards at the rate of 3°C in the case of anticyclone.

If, in a cyclone, velocity decreases upwards in such a way that $\frac{V_2}{T_2} < \frac{V_1}{T_1}$, and, therefore, also $\frac{V_2^2}{T_2} < \frac{V_1^2}{T_1}$, we have $\frac{\partial T}{\partial n}$ negative, and therefore, temperature increasing towards the centre. Or, air on the axis is at a higher temperature than the surrounding air.

Reverse condition holds when the velocity increases upwards so that

$$\frac{V_2}{T_2} > \frac{V_1}{T_1}\text{ , and, therefore, also }\frac{V_2^2}{T_2} > \frac{V_1^2}{T_1}\,.$$

In an anticyclone, if velocity increases or decreases fairly rapidly with height, then the term involving

$$\frac{V_2^2}{T_2} - \frac{V_1^2}{T_1}$$

is the dominant term. In this case the axis is cold or warm according as the velocity is decreasing or increasing upwards.

12. For the computation of temperature from the distribution of winds in tropical regions, a better approximation is obtained by the use of the equations

$$\frac{g}{T^2}\frac{\partial T}{\partial x} = -\beta\frac{\partial}{\partial x}\left(\frac{u}{T}\right)+\gamma\frac{\partial}{\partial z}\left(\frac{v}{T}\right)$$

$$\frac{g}{T^2}\frac{\partial T}{\partial y} = -\beta\frac{\partial}{\partial y}\left(\frac{u}{T}\right)-\gamma\frac{\partial}{\partial z}\left(\frac{u}{T}\right)\,.$$

than by Sir Napier Shaw's equations, because the assumption that $2\omega\cos\phi=0$, which does not hold in the tropical region, is not made.

METEOROLOGICAL OFFICE,
NEW DELHI.

REFERENCES

[1] Ramanathan and Ramakrishnan, 1939, *Ind. Met. Memoirs*, **26**, Part 10.

[2] Shaw, Sir N., 1931, Manual of Meteorology, Vol. IV, Ch. 7.

7

DISTRIBUTION OF MOLECULAR AND ATOMIC OXYGEN IN THE UPPER ATMOSPHERE

By H. RAKSHIT*

(Received for publication, April 28, 1947)

ABSTRACT. The identification of the auroral green line λ 5577 has established beyond doubt the presence of oxygen in the atomic state in the upper atmosphere. For various reasons a knowledge of the distribution of molecular and atomic oxygen with height, particularly in the region of transition in which the atmospheric composition changes from one of N_2 and O_2 to one of N_2 and O, is important. Attempts at determining the distribution have been made by Chapman (1931), by Wulf and Deming (1938) and by Majumdar (1938). Unfortunately the results obtained by these authors are based upon data which are not corroborated by recent observations.

In the present paper attempt has been made to determine the distribution by adapting Pannekoek's method of studying the distribution of ionisation in the earth's atmosphere by the action of solar ultraviolet radiation. The method is in its essentials the same as that adopted by Majumdar in his analysis. In carrying out the calculations recent data based on radio and other observations have been used and the results may thus be expected to represent more accurately the actual state of affairs.

It has been found that the density of O_2 molecules decreases very rapidly with height above 100 km. The density of the O atoms, which is almost zero at 80 km., increases rapidly with height, attains a maximum at about 105 km. and then gradually decreases.

Decrease in the density of O atoms at night due to recombination has also been considered. It is shown that the atoms will be in sufficient density at night to emit the green radiation with the observed intensity.

INTRODUCTION

The identification of the auroral green line λ 5577 by McLenan (1925) as due to the transition ($O^1S \rightarrow O^2D$) established beyond doubt the presence of atomic oxygen as one of the constituents of the upper atmosphere. Since direct measurements with the help of sounding balloons show that up to 22 km. the oxygen is in the molecular state, the atmospheric composition, a mixture of N_2 and O_2, must begin to change to one of N_2 and O at some higher level. Accurate determination of the distribution of the atmospheric gases with height in the region of transition, as also above it, is important for more than one reason.

It is now generally accepted that the different ionospheric regions, E, F_1, F_2, etc., are produced by the ionisation of the different upper atmospheric constituents O_2, N_2, O (it is not yet known with certainty if N_2, like O_2, is also dissociated in the upper atmosphere). The maximum of absorption of the ionising solar radiation by the different gases takes place at different levels because the positions of these maxima are dependent not only on the absorption coefficient of the radiation but also on the distribution with height of the absorbing gas.

---

* Fellow of the Indian Physical Society.

In particular it has been shown by Mitra (1938) and by Bhar (1938) and also by Wulf and Deming (1938) that the problem of the formation of Region E (100-120 km.) which presents difficulties, is solved if it is imagined that this layer is formed by the ionisation of O_2 in the region where its density undergoes rapid diminution with height due to its dissociation by the absorption of solar radiation in the region λλ 1751-1250 (Runge-Schumann continuum). An accurate knowledge of the distribution of O_2 with height in the region of transition is therefore very important in the theory of the formation of the E layer. Again, it is believed that Region F_2 is formed by the ionisation of O; also the rate of decay of electron density in the ionospheric regions has been found by Bates, Buckingham, Massey and Unwin (1939) to be controlled by the so-called *effective recombination coefficient* in which the negative ion concentration (O^-) plays an essential part. For the ionospheric studies, as also for understanding certain features of distribution of light intensity in auroral streamers, a knowledge of the distribution of atomic oxygen with height is extremely important

The first attempt in this direction was made by Chapman (1931); the next was by Wulf and Deming (1938), and Majumdar in 1938 undertook a rigorous solution of the problem. In what follows brief accounts of these investigations are first given.

Chapman, on the basis of some tentative assumptions, concluded that below 80 km the concentration of oxygen atoms should be very small compared with that of oxygen molecules. According to this estimate there is only one oxygen atom for every 300 O_2 molecules at 80 km., while at 120 km. there is one for every three O_2 molecules. Chapman emphasised that although his results are only approximate, there is nothing improbable in them.

Wulf and Deming (1936) derived an expression for the concentration of O atoms as a function of the number of quanta absorbed by O_2 molecules, the concentration of O_2 molecules as they would have existed prior to irradiation, the concentration of total molecules and the specific rate of the postulated three-body recombination of oxygen atoms. As the density of total molecules at any level depends upon height, this gave a method of estimating the degree of dissociation at different heights. In a later paper (Wulf and Deming, 1938) they gave results of their computation of dissociation at different heights for an atmosphere as advocated by Chapman and Milne (1920) in which diffusion starts at 20 km. and the temperature is 219° K throughout. Assuming solar radiation to be that of a black-body at 6000° K, Wulf and Deming estimated that dissociation starts from about 70 km., increases very rapidly beyond 80 km. and is practically complete at about 100 km. In regard to these results it may be mentioned that the present accepted model of the atmosphere is quite different from that assumed by Wulf and Deming. Moreover the pressure in the upper regions of the atmosphere is so low that three-body collision may be a rare phenomenon.

Majumdar adapted Pannekoek's method of studying the distribution of ionisation in the earth's atmosphere by the action of solar ultraviolet radiation. Since the case of dissociation of molecules into atoms by absorption of radiation is analogous to that of ionisation, the method of Pannekoek is applicable to the dissociation problem. On the basis of certain simplified assumptions Majumdar estimated that dissociation of O_2 which is negligibly small at 147 km. is practically complete above 167 km. Majumdar assumed that the molecular absorption coefficient of O_2 molecules remains constant for frequencies within the absorption band, being equal to the maximum value.

For the sake of simplicity, a constant temperature of 300°K was also assumed for the entire atmosphere. Majumdar, however, realised the limitations of his preliminary results in view of such approximations and promised to give a more quantitative account of the problem. Unfortunately no further investigation on the subject has yet been published. In the mean time certain new problems of the upper atmosphere have necessitated more precise knowledge of the distribution of O_2 and O in the upper atmosphere.

In the present paper a fresh attack on the problem is therefore being made. The method, in its essentials, is the same as that of Majumdar but some of his approximations have been avoided. Further, the calculations are based on recent radio and other observations. As such, the results are different from those obtained by Majumdar and are believed to represent more accurately the actual state of affairs. Simplifying approximations have, of course, been made, because a rigorous solution of the problem is beyond the present state of our knowledge. The effect of these simplifications is, however, considered to be unimportant.

DISSOCIATION OF GAS AT A CERTAIN TEMPERATURE BY RADIATION AT HIGHER TEMPERATURE

Consider a gas, at a temperature T say, being traversed by radiation from an external source at a very much higher temperature T_1, *e.g*, from the sun considered as a black body at 6500°K. Some of the molecules, composed of atoms A and B say, will be dissociated by absorption of radiation. These atoms will in turn recombine and a steady equilibrium state will be reached in which the rate of dissociation is equal to the rate at which the molecules are formed by recombination.

If $I_\nu d\nu$ be the amount of energy in the dissociating radiation within the frequency range ν and $\nu + d\nu$ passing through unit area of the gas per second, then the number of absorption processes per second per unit volume is

$$n_{AB}\psi_\nu I_\nu d\nu / h\nu \qquad \ldots \quad (1)$$

where n_{AB} is the number of molecules AB per unit volume of the dissociating gas and ψ_ν is the molecular absorption coefficient.

The dissociated atoms A and B will separate with a relative velocity V given by

$$\tfrac{1}{2}\mathrm{M}\mathrm{V}^2 = h\nu - h\nu_0 . \qquad (2)$$

where M is the reduced mass of the molecule given by

$$\mathrm{M} = \frac{m_A m_B}{m_A + m_B},$$

m_A, m_B being the masses of the corresponding atoms,

and $h\nu_0 = \mathrm{D}$, the energy of dissociation,

ν_0 being the threshold frequency for dissociation.

In case of oxygen the absorption of solar ultraviolet radiation in the Runge-Schumann continuum ($\lambda\lambda$ 1751 – 1250) dissociates O_2 molecules into one normal and another excited atom as follows:

$$O_2 + h\nu \longrightarrow O(^3P) + O(^1D).$$

In general, when one of the dissociated atoms, say A, is in an excited state A′ and E is the energy of excitation, then

$$h\nu_0 = \mathrm{D} + \mathrm{E}. \qquad (3)$$

The atoms thus formed will, in turn, recombine to form back the original molecule AB. We assume that the mass of the gas absorbing radiation is raised in temperature and that in spite of the fact that the dissociated atoms are ejected with velocities according to equation (2), the velocities of the particles settle down to Maxwellian distribution corresponding to the equilibrium temperature of the gas.

Now the total number of collisions of the atoms with relative velocity between V and V + dV is

$$\alpha . 4\pi n_{A'} n_B \left(\frac{\mathrm{M}}{2\pi k\mathrm{T}} \right)^{\frac{3}{2}} e^{-\mathrm{M}\mathrm{V}^2/2k\mathrm{T}}\, \mathrm{V}^3 d\mathrm{V}, \qquad (4)$$

where $n_{A'}$ and n_B are respectively the numbers per unit volume of the free atoms $A^{\prime}$ (excited) and B. In equation (4) α is a coëfficient having the dimension of an area which is a function solely of the atoms and the relative velocity with which they collide. But every one of these collisions does not result in recombination. The total number of spontaneous recombinations, due to collisions, per unit volume per second, may be written as

$$4\pi n_{A'} n_B \beta_\nu \left(\frac{\mathrm{M}}{2\pi k\mathrm{T}} \right)^{\frac{3}{2}} e^{-\mathrm{M}\mathrm{V}^2/2k\mathrm{T}}\, \mathrm{V}^3 d\mathrm{V}. \qquad \ldots \quad (5)$$

The quantity β_ν is proportional to ψ_ν by the Einstein relation connecting the absorption and emission coefficients. This will be discussed later. Besides spontaneous recombinations there may be recombinations stimulated by the radiation field, given as usual by

$$\frac{\text{stimulated recombinations}}{\text{spontaneous recombinations}} = \frac{c^2 I_\nu}{8\pi h\nu^3}.$$

Therefore the grand total number of recombinations is

$$4\pi n_{A'} n_B \beta_\nu \left(\frac{M}{2\pi kT}\right)^{\frac{3}{2}} \left(1+\frac{c^2 I_\nu}{8\pi h\nu^3}\right) e^{-MV^2/2kT}\, V^3 dV. \qquad (6)$$

It should be noted that expressions (1) and (6) will not be equal for every frequency $\nu > \nu_0$ but the total energy involved in all the absorption processes taken together must be equal to that for all the recombinations. This is fulfilled by multiplying both (1) and (6) by $h\nu$, integrating and equating as follows:

$$\int_{\nu_0}^{\infty} n_{AB}\psi_\nu I_\nu d\nu = \int_{V=0}^{V=\infty} 4\pi n_{A'} n_B \beta_\nu \left(\frac{M}{2\pi kT}\right)^{\frac{3}{2}} \left(1+\frac{c^2 I_\nu}{8\pi h\nu^3}\right) e^{-MV^2/2kT}\, V^3 h\nu dV$$

or

$$\frac{n_{A'} n_B}{n_{AB}} = \frac{\int_{\nu_0}^{\infty} \psi_\nu I_\nu d\nu}{4\pi h \int_{V=0}^{V=\infty} \beta_\nu \left(\frac{M}{2\pi kT}\right)^{\frac{3}{2}} \left(1+\frac{c^2 I_\nu}{8\pi h\nu^3}\right) e^{-MV^2/2kT}\, V^3 \nu dV}. \qquad (7)$$

The expression for β_ν is easily obtained from the ratio $n_{A'}n_B/n_{AB}$ for the case of thermodynamic equilibrium. In such a case, if neither of the dissociated atoms be in an excited state the equilibrium condition is given by the so-called *reaction isochore*:

$$\frac{n_A n_B}{n_{AB}} = \frac{Gs}{h r_0^2}\left(\frac{MkT}{8\pi}\right)^{\frac{1}{2}} e^{-D/kT}\left(1 - e^{-h\omega/kT}\right), \qquad \ldots \quad (8)$$

where

$G = G_A G_B / G_{AB}$,

G_A, G_B—the statistical weights of the normal quantum states of the free atoms,

G_{AB}—the statistical weight of the ground state of the electronic configuration of the molecule, the nuclei being regarded as fixed,

s—the symmetry number of the molecule and is equal to 2 when the two atoms produced by dissociation are identical (as in case of oxygen), but when the atoms are not so, $s = 1$,

r_0—the mean separation between the atoms,

ω—the fundamental vibration frequency of the molecule.

If one of the dissociated atoms, say A, be in an excited state A′, then for the relative numbers of the excited and unexcited atoms we have, from Boltzmann's law,

$$\frac{n_{A'}}{n_A} = \frac{G_{A'}}{G_A} e^{-E/kT},$$

where E is the energy of excitation of the atom A. This is justified in cases where the life time of the excited atoms is large compared with the time between successive atomic collisions. Substituting in (8) we have

$$\left[\frac{n_{A'}n_{B}}{n_{AB}}\right]_0=\frac{G's}{hr_0^2}\left(\frac{MkT}{8\pi}\right)^{\frac{1}{2}}e^{-(D+E)/kT}\left(1-e^{-h\omega/kT}\right). \quad . \quad (9)$$

where the suffix (o) refers to the case of thermodynamic equilibrium, and $G'=G_{A'}G_B/G_{AB}$.

It will be noted that equations (8) and (9) giving the degree of dissociation of the molecules are derived from the condition that in the equilibrium state the rate at which the molecules dissociate into atoms is equal to the rate at which they are formed by recombination. They do not make any reference to the details of the mechanism by which the equilibrium is maintained.

By taking into account the details of the absorption and recombination processes as in (1) and (6) and remembering that in case of thermodynamic equilibrium these should be identically equal for any frequency $\nu>\nu_0$, we have,

$$\frac{G's}{hr_0^2}\left(\frac{MkT}{8\pi}\right)^{\frac{1}{2}}e^{-(D+E)/kT}\left(1-e^{-h\omega/kT}\right)$$

$$=\frac{\psi_\nu I_\nu d\nu/h\nu}{4\pi\beta_\nu\left(\frac{M}{2\pi kT}\right)^{\frac{3}{2}}\left(1+\frac{c^2I_\nu}{8\pi h\nu^3}\right)e^{-MV^2/2kT}V^3dV}.$$

For this case of isotropic radiation,

$$I_\nu=\frac{8\pi h\nu^3}{c^2}\cdot\frac{1}{e^{h\nu/kT}-1}.$$

On substituting this value of I_ν and remembering that from (2)

$$MVdV=hd\nu \quad \text{and} \quad e^{-MV^2/2kT}=e^{-h\nu/kT}e^{(D+E)/kT},$$

we get, after simplification,

$$\beta_\nu'=\psi_\nu\frac{8\pi^2r_0^2}{c^2G's}\cdot\frac{kT}{\frac{1}{2}MV^2}\cdot\frac{\nu^2}{1-e^{-h\omega/kT}}.$$

Putting this value of β_ν in (7) and converting V in terms of ν by (2), we find

$$\frac{n_{A'}n_B}{n_{AB}}=\frac{r^2}{8\pi h}\left[\frac{n_{A''}n_B}{n_{AB}}\right]_0\frac{\int_{\nu_0}^{\infty}\psi_\nu I_\nu d\nu}{\int_{\nu_0}^{\infty}\psi_\nu\nu^3\left(1+\frac{c^2I_\nu}{8\pi h\nu^3}\right)e^{-h\nu/kT}d\nu}. \quad \ldots \quad (10)$$

For the case of dissociation in the earth's atmosphere it will be noted that the atmosphere is receiving diffuse dilute radiation within a small solid angle Ω

from the black body (sun at $T_1 = 6500^\circ K$) at a large distance. The value of I_ν at the top of the atmosphere is given by

$$I_\nu = W \frac{8\pi h\nu^3}{c^2} \cdot \frac{1}{e^{h\nu/kT_1} - 1},$$

where W—the dilution factor $= \frac{\Omega}{4\pi} = R^2/4r^2$,

R—radius of the sun $= 6{\cdot}95 \times 10^{10}$ cms.,

r—sun's distance from earth $= 1{\cdot}494 \times 10^{13}$ cms.

The intensity is further weakened as the radiation penetrates into the atmosphere. If **N** be the total number of absorbing gas molecules above one sq. cm. at the desired level having absorption coefficient ψ_ν, the reduced intensity at that level is

$$I_\nu = W \frac{8\pi h\nu^3}{c^2} \cdot \frac{1}{e^{h\nu/kT_1} - 1} e^{-\psi_\nu \mathbf{N}}.$$

Thus finally

$$\frac{n_{A'} n_B}{n_{AB}} = \left[\frac{n_{A'} n_B}{n_{AB}} \right]_0 W \frac{\displaystyle\int_{\nu_0}^{\infty} \frac{\psi_\nu \nu^3}{e^{h\nu/kT_1} - 1} e^{-\psi_\nu \mathbf{N}} \, d\nu}{\displaystyle\int_{\nu_0}^{\infty} \psi_\nu \nu^3 \left(1 + \frac{W e^{-\psi_\nu \mathbf{N}}}{e^{h\nu/kT_1} - 1} \right) e^{-h\nu/kT} \, d\nu} . \quad \dots \quad (11)$$

If x denotes the degree of dissociation, *i.e.*, the fraction of molecules AB dissociated into atoms A′ and B, then for N molecules/c.c. before dissociation, we get

N(1 − x) molecules AB,
Nx atoms A′,
and Nx atoms B,

i.e., a total of N(1 + x) particles/c.c. after dissociation. Therefore if p_d represents the equilibrium pressure due jointly to AB, A′ and B after dissociation, then

$$p_d = p(1 + x),$$

where p = pressure due to AB *before* dissociation, expressed in dynes/cm^2. Therefore

$$\frac{n_{A'} n_B}{n_{AB}} = \frac{N x^2}{1 - x} = \frac{x^2}{1 - x} \cdot \frac{p}{kT},$$

i.e., $$\frac{x^2}{1 - x} = \frac{kT}{p} \cdot \frac{n_{A'} n_B}{n_{AB}}$$

$$= \frac{kT}{p} \left[\frac{n_{A'} n_B}{n_{AB}} \right]_0 W \frac{\displaystyle\int_{\nu_0}^{\infty} \frac{\psi_\nu \nu^3}{e^{h\nu/kT_1} - 1} e^{-\psi_\nu \mathbf{N}} \, d\nu}{\displaystyle\int_{\nu_0}^{\infty} \psi_\nu \nu^3 \left(1 + \frac{W e^{-\psi_\nu \mathbf{N}}}{e^{h\nu/kT_1} - 1} \right) e^{-h\nu/kT} \, d\nu} . \quad \dots \quad (12)$$

The integral in the denominator on the right hand side is practically

$$=\int_{\nu_0}^{\infty} \psi_\nu \nu^3 e^{-h\nu/kT} d\nu$$

on account of the extreme smallness of W. To evaluate this we must know the values of absorption coefficient ψ_ν, for all frequencies within the absorption band. Our only knowledge of this in case of oxygen is from the experimental results of Ladenburg and Van Voorhis (1933) and the values of ψ_ν in Table I are obtained from their paper. Further, considering the rapid variation of $e^{-h\nu/kT}$ with ν as seen from Table I, the quantity $\psi_\nu \nu^3$ may, for the purpose of integration, be regarded as a constant having the value corresponding to ν_0 for which the value of $e^{-h\nu/kT}$ is a maximum.

TABLE I

$T=300°K$ (average value for the region concerned)

$\nu\times10^{-15}$	$e^{-h\nu/kT}$	$\psi_\nu\times10^{17}$	$\psi_\nu\nu^3\times10^{-28}$
1·71	$1{\cdot}26\times10^{-117}$	0·13	0·67
1·75	$4{\cdot}51\times10^{-121}$	0·22	1·18
1·80	$1{\cdot}97\times10^{-126}$	0·37	2·16
1·90	$2{\cdot}07\times10^{-131}$	0·80	5·49

Hence $\displaystyle\int_{\nu_0}^{\infty} \psi_\nu\nu^3 e^{-h\nu/kT} d\nu = \Big[\psi_\nu\nu^3\Big]_{\nu=\nu_0} \times \int_{\nu_0}^{\infty} e^{-h\nu/kT} d\nu$

$$=\Big[\psi_\nu\nu^3\Big]_{\nu=\nu_0} \times \frac{kT}{h} e^{-h\nu_0/kT} = 6{\cdot}702\times10^{27}\cdot\frac{kT}{h}e^{-h\nu_0/kT} \quad \ldots \quad (13)$$

Substituting in Eq. (12) and introducing the numerical values of the quantities involved, we finally get

$$\frac{x^2}{1-x} = 8{\cdot}588\times10^{-37}\frac{\sqrt{T}}{p}\int_{\nu_0}^{\infty}\psi_\nu\nu^3\frac{e^{-\psi_\nu N}}{e^{h\nu/kT_1}-1}d\nu.$$

In this equation p the partial pressure of O_2 at the level considered is expressed in dynes/cm^2. Expressing p in mm. of mercury, the formula reduces to

$$\frac{x^2}{1-x} = \frac{6{\cdot}527\times10^{-40}\sqrt{T}}{p}\int_{\nu_0}^{\infty}\psi_\nu\nu^3\frac{e^{-\psi_\nu N}}{e^{h\nu/kT_1}-1}d\nu. \quad \ldots \quad (14)$$

In order to find the value of x at different levels a knowledge of temperature and partial pressure of O_2 at each level is necessary. These data are not known with certainty but those that are best available and are considered as most plausible will be used.

Regarding temperature we assume, after Martyn and Pulley (1936), a value of 160°K at 80 km. and a linear temperature gradient, increasing with height at the rate of 4°K per km. This is in accordance with the latest view that the temperature in the vicinity of E_1 layer is about 250°K.

Regarding partial pressure we assume that if O_2 were not dissociated, the condition of thorough mixing of N_2 and O_2 would have been maintained up to at least 130 km. as exists at lower levels. This is justified because even up to this height the tendency for diffusive separation is, as shown by Mitra and Rakshit (1938), negligibly small. Our only knowledge of pressure in this region is that obtained from radio observations, being 10^{-3} mm. at 100 km. Since this corresponds to about 0.2 cm. of O_2 at S. T. P. above this level, most of the dissociating radiation will be absorbed higher up. We can therefore assume that the atmospheric composition at 100 km. is practically N_2 and O_2 and also that they exist almost in the same proportion as near the ground, 20 per cent O_2 and 80 per cent N_2 in round figures. Starting with this pressure and assuming the temperature distribution as indicated above, the partial pressure of O_2 at different heights (if there were no dissociation) can be calculated.

The initial total pressure P_z due to N_2 and O_2 at any level z cm. above 80 km. (in the 80-130 km. region) is thus given by

$$P_z = P_0(1+\alpha z)^{-\frac{gm}{\alpha T_0 k}},$$

where P_0 is the pressure and T_0 the temperature at the 80 km. level; α is the coefficient of increase of temperature with height above this level ($=2.5\times10^{-7}$°K per cm. per degree); g is the acceleration due to gravity; m is the mean molecular mass of the air in the region and k the universal gas constant. On substitution,

$$P_z = P_0(1+\alpha z)^{-8\cdot5}.$$

Assuming $P_{100km} = 10^{-3}$mm., we find $P_0 = 3{\cdot}14\times10^{-2}$mm., and hence

$$P_z = 3{\cdot}14\times10^{-2}(1+\alpha z)^{-8\cdot5}\text{mm}.$$

Table II gives the values of P_z and p_z, the partial pressure due to O_2, at different heights above 80 km.

TABLE II

$z\times10^{-5}$	T	$P_z(mm)$	$p_z(mm)$	$z\times10^{-5}$	T	$P_z(mm)$	$p_z(mm)$
5	180	$1{\cdot}15\times10^{-2}$	$2{\cdot}30\times10^{-3}$	30	280	$2{\cdot}70\times10^{-4}$	$5{\cdot}40\times10^{-5}$
10	200	$4{\cdot}71\times10^{-3}$	$9{\cdot}42\times10^{-4}$	35	300	$1{\cdot}50\times10^{-4}$	$3{\cdot}00\times10^{-5}$
15	220	$2{\cdot}09\times10^{-3}$	$4{\cdot}18\times10^{-4}$	40	320	$8{\cdot}68\times10^{-5}$	$1{\cdot}74\times10^{-5}$
20	240	$1{\cdot}00\times10^{-3}$	$2{\cdot}00\times10^{-4}$	45	340	$5{\cdot}19\times10^{-5}$	$1{\cdot}04\times10^{-5}$
25	260	$5{\cdot}05\times10^{-4}$	$1{\cdot}01\times10^{-4}$	50	360	$3{\cdot}19\times10^{-5}$	$6{\cdot}38\times10^{-6}$

DISSOCIATION AT DIFFERENT LEVELS

The quantity **N** in Eq. (14) is given by $\mathbf{N}=p\mathrm{HN}$, where p is the partial pressure of O_2 before dissociation expressed in atmospheres, H the height of the homogeneous atmosphere for O_2 and N the number of molecules of gas per c.c. at S. T. P. Hence $\mathbf{N}=2{\cdot}861\times10^{22}p$, where p is expressed in mm. of mercury. Eq. (14) thus finally reduces to

$$\frac{x^2}{1-x}=\frac{6{\cdot}527\times10^{-40}\sqrt{T}}{p}\int_{\nu_0}^{\infty}\psi_\nu\nu^3\frac{e^{-2{\cdot}861\times10^{22}\psi_\nu}}{e^{h\nu/kT_1}-1}d\nu. \qquad \ldots \quad (15)$$

The values of p and T for any level are obtained from Table II and the integral is evaluated by graphical method. Table III gives the values of the fraction x of O_2 molecules dissociated at various heights, the equilibrium concentrations n_{O_2} of O_2 and n_O of O and also the total amounts of O_2 and O above each level in the region studied.

TABLE III

Height above ground (km)	Degree of dissociation x	n_{O_2}	n_O	Amount of gas (cm. at S. T. P.)	
				O_2	O
85	0·00	$1{\cdot}243\times10^{14}$	0·00	2·302	0·260
90	$2{\cdot}96\times10^{-8}$	$4{\cdot}581\times10^{13}$	$2{\cdot}712\times10^{6}$	0·866	0·260
95	$7{\cdot}10\times10^{-4}$	$1{\cdot}847\times10^{13}$	$2{\cdot}624\times10^{10}$	0·313	0·258
100	$6{\cdot}70\times10^{-2}$	$7{\cdot}561\times10^{12}$	$1{\cdot}086\times10^{12}$	$8{\cdot}570\times10^{-2}$	0·251
105	0·6302	$1{\cdot}398\times10^{12}$	$4{\cdot}761\times10^{12}$	$1{\cdot}177\times10^{-2}$	0·190
110	0·9561	$8{\cdot}250\times10^{10}$	$3{\cdot}585\times10^{12}$	$5{\cdot}885\times10^{-4}$	0·115
115	0·9941	$5{\cdot}835\times10^{9}$	$1{\cdot}752\times10^{12}$	$5{\cdot}254\times10^{-5}$	$6{\cdot}33\times10^{-2}$
120	0·9988	$5{\cdot}288\times10^{8}$	$1{\cdot}057\times10^{12}$	$6{\cdot}336\times10^{-6}$	$3{\cdot}68\times10^{-2}$
125	0·9997	$8{\cdot}925\times10^{7}$	$5{\cdot}95\times10^{11}$	$1{\cdot}383\times10^{-6}$	$2{\cdot}20\times10^{-2}$
130	0·9999	$1{\cdot}724\times10^{7}$	$3{\cdot}45\times10^{11}$	$4{\cdot}000\times10^{-7}$	$1{\cdot}34\times10^{-2}$

The variations of n_{O_2} and n_O are shown plotted in Fig. 1. It will be seen that the density of O_2 molecules decreases very rapidly with height above 100 km. At the same time the density of the oxygen atoms, which is almost zero at 80 km., increases rapidly with height, attains a maximum at about

105 km. and then gradually decreases. The transition layer in which the density of O_2 rapidly decreases plays an extremely important part in the production of the E_1 layer of the ionosphere as mentioned in the Introduction.

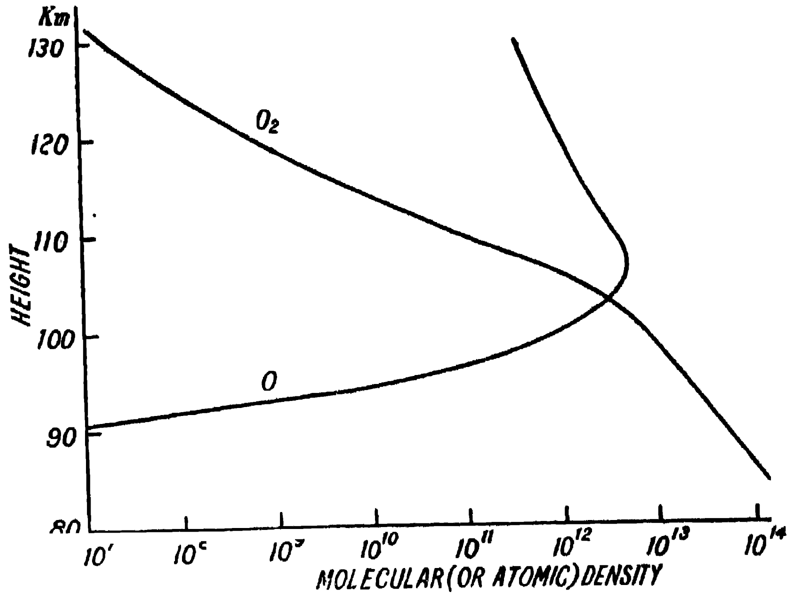

Fig. 1

RECOMBINATION PROCESSES

Finally the decrease in density of atomic oxygen in the upper atmosphere at night due to recombination of oxygen atoms to form oxygen molecules may be considered. The two different ways by which neutral O atoms may disappear are as follow :—

(*i*) Radiative recombination : $O + O \rightarrow O^* + h\nu$

(*ii*) Three-body collision : $O + O + M = O_2 + M$,* where M is the third body.

Regarding the first process the coefficient of recombination has been shown by Herzberg (1939) to be of the order of 10^{-16} cm.^{3}/sec. At 105 km. level, where the density of atomic oxygen is the maximum (4.76×10^{12} per c.c), the fall in 10 hours will be 2.63×10^{11} per c.c.

The contribution by the second process may be neglected on account of the low pressure. According to Herzberg, even at a pressure of 0.1 mm., recombination by the two-body process predominates.

There is also a third process by which the O atoms may recombine and which ought to be considered. The atmospheric region where atomic oxygen predominates is also rich in ionisation. Since atomic oxygen has considerable electron affinity, we may expect copious formation of negative ions of atomic oxygen and the following reaction is possible :

$$O + O^- \rightarrow O_2^* + e.$$

Here the attached electron acts as the third body carrying away the extra energy and momentum. The probability of this reaction has been examined by Massey (1938) and is found to be of the same order as that of radiative recombination of O atoms. Hence the loss of O atoms due to this action is also of the same order as that by radiative recombination of O atoms.

It is to be noted that this decrease in density—of about one order—is in the region of maximum density of the O atoms at 105 km. In higher regions (250 km), the fall in the density of O will be much less. In any case, there will always be sufficient atomic oxygen left throughout the dark hours of the night to account for the emission of the atomic oxygen lines.

ACKNOWLEDGMENT

It is a pleasure to record my sincere thanks to Professor S. K. Mitra for suggesting the problem to me and for his kind interest and helpful discussions throughout the progress of the work.

UNIVERSITY COLLEGE OF SCIENCE,
CALCUTTA.

REFERENCES

Bates, D. R., Buckingham, R. A., Massey, H. S. W., and Unwin, J J., 1939, *Proc. Roy. Soc.*, **A 170**, 322.
Bhar, J. N., 1938, *Ind. Jour. Phys.*, **12**, 363
Chapman, S., 1931, *Proc Roy. Soc.*, **A 132**, 353.
Chapman, S. and Milne, E. A., 1920, *Q. J. R. Met. Soc.*, **46**, 357.
Herzberg, G., 1939, *Astrophys. Jour.*, **89**, 290.
Ladenburg, R., and Van Voorhis, C. C., 1933, *Phys. Rev.*, **43**, 315.
Majumdar, R. C., 1938, *Ind Jour. Phys.*, **12**, 75.
Martyn, D F., and Pulley, O. O., 1936, *Proc. Roy. Soc.*, **A 154**, 455.
Massey, H. S W., 1938, *Negative Ions* (Cambridge University Press), p 74.
McLenan, J. C., 1925, *Proc Roy. Soc.*, **A 108**, 501.
Mitra, S. K , 1938, *Nature*, **142**, 914.
Mitra, S. K., and Rakshit, H., 1938, *Ind. Jour. Phys.*, **12**, 47.
Wulf, O. R., and Deming, L S , 1936, *Terr. Mag.*, **41**, 299.
Wulf, O. R., and Deming, L. S., 1938, *Terr. Mag.*, **43**, 283.

8

THE EFFECT OF SPIN-SPIN INTERACTION ON HIGH VELOCITY SCATTERING

By K. C. KAR

(Received for publication, Dec. 12, 1946)

ABSTRACT. The complete Mott formula of high speed electron scattering by atoms has been derived wavestatistically by assuming a spin-spin interaction potential somewhat similar to that taken by Dirac and Van Vleck in magnetism. The spin-orbit interaction is taken as in the well-known Thomas effect. The theory has been applied to electron-electron scattering. The formula thus derived agrees with Möller's formula only at the important limiting cases where the velocity in the relativistic region is (*i*) small and (*ii*) extremely high. The case of electron-positron scattering has also been considered.

In dealing with the problem of scattering of fast electrons by atoms, it was pointed out (Kar, 1946) that the complete Mott formula (Mott, 1929) of scattering, namely,

$$I=\left(\frac{Ze^2}{2m_0v^2}\right)^2\left(1-\frac{v^2}{c^2}\right)\left(\operatorname{cosec}^4\tfrac{1}{2}\theta-\frac{v^2}{c^2}\operatorname{cosec}^2\tfrac{1}{2}\theta+\pi.\frac{v}{c}.\frac{2\pi Ze^2}{hc}\,\frac{\cos^2\frac{1}{2}\theta}{\sin^3\frac{1}{2}\theta}+\text{higher terms}\right)\quad\ldots\quad(1)$$

could not be derived by the wavestatistical method unless some sort of spin-spin interaction was assumed between the interacting particles.

In the present paper it is proposed to derive the complete Mott formula by taking the spin-spin interaction somewhat similar to that taken by Dirac (*Principles of Quantum Mechanics*) and Van Vleck (*Electric and Magnetic Susceptibilities*) in the theory of Magnetism. The theory is also applied to electron-electron scattering and the formula thus derived is found to be in agreement with Möller's formula at very low and high velocities of incidence.

It has been shown in the previous paper that the relativistic wave equation is

$$\Delta\chi+\frac{4\pi^2}{h^2c^2}[(E-V)^2-E_0{}^2-(\tfrac{1}{2}V^2)_{s\text{-}o}]\chi=0 \qquad (2)$$

when the spin-orbit interaction potential $(\frac{1}{2}V^2)_{s\text{-}o}$ is taken into consideration. If the spin-spin interaction $(V_{s\text{-}s})$ is taken into account, the above wave equation is further modified and becomes

$$\Delta\chi+\frac{4\pi^2}{h^2c^2}[(E-V-V_{s\text{-}s})^2-E_0{}^2-(\tfrac{1}{2}V^2)_{s\text{-}o}]\chi=0 \qquad (3)$$

On proceeding in the usual manner we have, for the differential equation satisfied by the first order scattering function $(\lambda_1\chi_1)$,

$$\Delta(\lambda_1\chi_1)+k^2(\lambda_1\chi_1)=\frac{4\pi^2}{h^2c^2}\chi_0[2EV+2EV_{S\text{-}S}-V^2+(\tfrac{1}{2}V^2)_{S\text{-}O}]$$

$$k^2=\frac{4\pi^2}{h^2c^2}[E^2-E_0^2] \qquad (3.1)$$

where it is assumed that the effect of the potential $V_{S\text{-}S}$ is so small that its square is negligible.

It has been shown, in the previous paper referred to above, that the first term within bracket in (3.1) gives after solution the usual cosec^4-term in (1) whereas the third and fourth terms, namely, $-V^2$ and $(\frac{1}{2}V^2)_{S\text{-}O}$, give the third term in Mott formula (1). Let us find in the following the contribution of the second term, namely, $2EV_{S\text{-}S}$ of (3.1), in the formula for the intensity of scattering.

Now, Dirac and also Van Vleck have shown that the effective coupling between spins due to the exchange effect is equivalent to a potential energy of the form

$$V_{S\text{-}S}=-2s_1s_2J_{12} \qquad \dots \quad (4)$$

where J_{12} is the exchange integral for the interacting particles 1 and 2, while s_1, s_2 are the spin angular momenta in quantum units. We shall, however, take the instantaneous value of the potential in the form

$$V_{S\text{-}S}=\pm 2\,s_1s_2.\frac{Ze^2}{r} \qquad (5)$$

where the upper sign denotes that the Coulomb force between the interacting particles is repulsive. In the case of electron scattering by atom nuclei as considered by Mott, the force is attractive. So the negative sign should be taken in (5).

Thus, on proceeding as before we have for the first order scattering function (Kar, 1946) due to $V_{S\text{-}S}$

$$\lambda_1\chi_1=+2s_1s_2\frac{Ze^2}{2m_0v^2}(1-\beta^2)^{\frac{1}{2}}\text{cosec}^2\tfrac{1}{2}\theta\; A.\frac{e^{ikr}}{r}\cos k'r_0 \qquad (6)$$

Now, the incident electron may have the same or the opposite spin after scattering. In the former case the spin factor is evidently unity while in the latter case it is shown to be $-\cos\theta$ (Kar, *loc. cit*). Hence, the total spin factor is

$$\delta_S=1-\cos\theta=2\sin^2\tfrac{1}{2}\theta \qquad \dots \quad (7)$$

It is obvious that to include the two classes of events mentioned above, we must multiply (6) by the spin factor δ_S.

Again, we have good reasons to believe that the spin-spin interaction is effective only at high velocity of incidence. In other words, the spin-spin interaction is intimately connected with the relativity effect. Therefore the scattering function should be multiplied by yet another factor which may be called the 'relativity factor' (δ_{re}). It may be taken as

$$\delta_{re} = \frac{I_{relat} - I_{non\text{-}relat}}{I_{non\text{-}relat}} = \frac{I_{relat}}{I_{non\text{-}relat}} - 1 \qquad \dots \quad (8)$$

It is evidently a measure of the percentage of relativistic departure of the probability of scattering. On substituting the relativistic and non-relativistic values of the intensity we find that in the case of Mott scattering

$$\delta_{re} = -\beta^2 \qquad \dots \quad (8.1)$$

Thus from (6), (7) and (8.1) we have for the scattering function due to the spin-spin interaction

$$\lambda_1 X_1 = -4 s_1 s_2 \frac{Ze^2}{2m_0 v^2}(1-\beta^2)^{\frac{1}{2}} \beta^2 A \frac{e^{ikr}}{r} \cos k' r_0 \qquad \dots \quad (9)$$

Hence the total scattering function from (3.1), considering the relativity effect and the spin-spin and spin-orbit interactions, would be (*vide* Kar, *l.c.*)

$$\lambda_1 X_1 = \frac{Ze^2}{2m_0 v^2}(1-\beta^2)^{\frac{1}{2}} A \frac{e^{ikr}}{r} \Big\{ \operatorname{cosec}^2 \tfrac{1}{2}\theta \cos k' r_0 - 4 s_1 s_2 \beta^2 \cos k' r_0$$

$$+ (\pi - 2k' r_0)\beta \frac{\pi Z e^2}{hc} \operatorname{cosec} \tfrac{1}{2}\theta \cos^2 \tfrac{1}{2}\theta \Big\} \qquad (10)$$

Hence we have for the relative intensity of scattering

$$I = \left(\frac{Ze^2}{2m_0 v^2} \right)^2 (1-\beta^2)(\operatorname{cosec}^4 \tfrac{1}{2}\theta \cos^2 k' r_0 - 8 s_1 s_2 \beta^2 \operatorname{cosec}^2 \tfrac{1}{2}\theta \cos^2 k' r_0$$

$$+ (\pi - 2k' r_0)\beta \frac{2\pi Z e^2}{hc} \cos k' r_0 \frac{\cos^2 \frac{1}{2}\theta}{\sin^3 \frac{1}{2}\theta} + \text{higher terms}) \qquad (11)$$

Now, for parallel spins $s_1 = +\frac{1}{2}$, $s_2 = +\frac{1}{2}$ while for antiparallel spins $s_1 = -\frac{1}{2}$, $s_2 = +\frac{1}{2}$. Also the weights for parallel and antiparallel spins are as 3:1, *i.e.*, $I = \frac{3}{4} I_1 + \frac{1}{4} I_2$.

Hence

$$I = \left(\frac{Ze^2}{2m_0 v^2} \right)^2 (1-\beta^2)(\operatorname{cosec}^4 \tfrac{1}{2}\theta \cos^2 k' r_0 - \beta^2 \operatorname{cosec}^2 \tfrac{1}{2}\theta \cos^2 k' r_0$$

$$+ (\pi - 2k' r_0)\beta \frac{2\pi Z e^2}{hc} \cos k' r_0 \frac{\cos^2 \frac{1}{2}\theta}{\sin^3 \frac{1}{2}\theta} + \text{higher terms}) \qquad \dots \quad (12)$$

If the critical approach be neglected the above formula evidently reduces to Mott formula (1). It may be mentioned that in a recent note Kar and Sengupta (1942) have tentatively taken in Mott formula a correction factor for the critical approach, namely, $\cos^2 k' r_0$, and have found decidedly better agreement with Sengupta's (1939) experiment on electron scattering by xenon. However, the actual correction should be that given in (12) and it is evident it would give even a better agreement with the actual experiment.

ELECTRON-ELECTRON SCATTERING

In the case of electron-electron interaction the Coulomb potential is $+\frac{e^2}{r}$ and so from (5) the spin-spin interaction potential should be

$$V_{s-s} = +2s_1s_2\frac{e^2}{r} \qquad \dots \quad (13)$$

Now, it has been already shown by Kar and Mrs. Basu (1944) that the first order scattering function without taking into account the effect of spin-spin or spin-orbit interaction is

$$\lambda_1\chi_1' = -\frac{e^2\gamma}{2m_0c^2(\gamma-1)\gamma^*}\operatorname{cosec}^2\tfrac{1}{2}\theta^*\frac{1}{\sqrt{v}}\frac{e^{ikr}}{r}\cos k'r_0' \qquad \dots \quad (14.1)$$

before exchange, and after exchange

$$\lambda_1\chi_1' = -\frac{e^2\gamma}{2m_0c^2(\gamma-1)\gamma^*}\sec^2\tfrac{1}{2}\theta^*\frac{1}{\sqrt{v}}\frac{e^{ikr}}{r}\cos k''r_0'' \qquad \dots \quad (14.2)$$

where $\gamma = 1\Big/\left(1-\frac{v^2}{c^2}\right)^{\frac{1}{2}}$ and $\gamma^* = \sqrt{\tfrac{1}{2}(\gamma+1)}$. Thus the relativity factor as defined in (8) should be in this case

$$\delta_r = \frac{\gamma+1}{2\gamma^2} - 1 = \frac{(1-\gamma)(1+2\gamma)}{2\gamma^2} \qquad \dots \quad (15)$$

As (14.1) and (14.2) give the relativistic scattering functions before and after exchange due to the Coulomb potential, the corresponding scattering functions due to the spin-spin interaction will be obviously obtained by simply multiplying (14.1) and (14.2) by the factor $2s_1s_2$. The spin factors before and after exchange are respectively

$$\left.\begin{aligned} \delta_s &= 1-\cos\theta^* = 2\sin^2\tfrac{1}{2}\theta^* \\ \delta_s &= 1+\cos\theta^* = 2\cos^2\tfrac{1}{2}\theta^* \end{aligned}\right\} \qquad (16)$$

Thus the total scattering functions before and after exchange are respectively

$$\lambda_1\chi_1' = -\frac{e^2\gamma}{2m_0c^2(\gamma-1)\gamma^*}\frac{1}{\sqrt{v}}\frac{e^{ikr}}{r}\left(\operatorname{cosec}^2\tfrac{1}{2}\theta^*\cos k'r_0' + 2s_1s_2\frac{(1-\gamma)(1+2\gamma)}{\gamma^2}\cos k'r_0'\right), \text{ and}$$

$$\lambda_1\chi_1'' = -\frac{e^2\gamma}{2m_0c^2(\gamma-1)\gamma^*}\cdot\frac{1}{\sqrt{v}}\frac{e^{ikr}}{r}\left(\sec^2\tfrac{1}{2}\theta^*\cos k''r_0'' + 2s_1s_2\frac{(1-\gamma)(1+2\gamma)}{\gamma^2}\cos k''r_0''\right) \qquad (17)$$

neglecting the spin-orbit interaction which is small because $Z=1$ in this case.

Now, for parallel spins $s_1 = +\frac{1}{2}$, $s_2 = +\frac{1}{2}$. Therefore the total scattering function, after taking into account the effect of exchange, is

$$(\lambda_1\chi_1)_1 = -\frac{e^2}{2m_0v^2}\frac{\sqrt{2(\gamma+1)}}{\gamma}\frac{1}{\sqrt{v}}\frac{e^{ikr}}{r}\Big[\operatorname{cosec}^2\tfrac{1}{2}\theta^*\cos k'r_0' - \sec^2\tfrac{1}{2}\theta^*\cos k''r_0''$$
$$+\frac{(1-\gamma)(1+2\gamma)}{2\gamma^2}(\cos k'r_0' - \cos k''r_0'')\Big] \quad \ldots \quad (18.1)$$

Again, for antiparallel spins $s_1 = +\frac{1}{2}$, $s_2 = -\frac{1}{2}$ and so the total scattering function, after taking into account the effect of exchange, is

$$(\lambda_1\chi_1)_2 = -\frac{e^2}{2m_0v^2}\frac{\sqrt{2(\gamma+1)}}{\gamma}\frac{1}{\sqrt{v}}\frac{e^{ikr}}{r}\Big[\operatorname{cosec}^2\tfrac{1}{2}\theta^*\cos k'r_0' + \sec^2\tfrac{1}{2}\theta^*\cos k''r_0''$$
$$-\frac{(1-\gamma)(1+2\gamma)}{2\gamma^2}(\cos k'r_0' + \cos k''r_0'')\Big] \quad \ldots \quad (18.2)$$

Because the ratio of intensities for parallel and antiparallel spins are as 3:1, *i.e.*, $I_1 : I_2 = 3:1$, we have for the total relative intensity of scattering $I = \frac{3}{4}I_1 + \frac{1}{4}I_2$. Hence we have from (18.1) and (18.2)

$$I = \left(\frac{e^2}{2m_0v^2}\right)^2 . \frac{2(\gamma+1)}{\gamma^2}\Big[\operatorname{cosec}^4\tfrac{1}{2}\theta^*\cos^2 k'r_0' + \sec^4\tfrac{1}{2}\theta^*\cos^2 k''r_0''$$
$$-\operatorname{cosec}^2\tfrac{1}{2}\theta^*\sec^2\tfrac{1}{2}\theta^*\cos k'r_0'\cos k''r_0''$$
$$+\tfrac{3}{4}\frac{(1-\gamma)(1+2\gamma)}{\gamma^2}(\operatorname{cosec}^2\tfrac{1}{2}\theta^*\cos k'r_0' - \sec^2\tfrac{1}{2}\theta^*\cos k''r_0'')(\cos k'r_0' - \cos k''r_0'')$$
$$+\tfrac{1}{4}\frac{(\gamma-1)(2\gamma+1)}{\gamma^2}(\operatorname{cosec}^2\tfrac{1}{2}\theta^*\cos k'r_0' + \sec^2\tfrac{1}{2}\theta^*\cos k''r_0'')(\cos k'r_0' + \cos k''r_0'')$$
$$+\frac{(\gamma-1)^2(2\gamma+1)^2}{16\gamma^4}(\cos k'r_0' + \cos k''r_0'')^2 + \text{higher terms}\Big].$$

Because the fourth term of the above equation involves the difference of $\cos k'r_0'$ and $\cos k''r_0''$, each of which is very nearly equal to unity, the term may be neglected. Therefore

$$I = \left(\frac{e^2}{2m_0v^2}\right)^2 . \frac{2(\gamma+1)}{\gamma^2}\Big[\operatorname{cosec}^4\tfrac{1}{2}\theta^*\cos^2 k'r_0' + \sec^4\tfrac{1}{2}\theta^*\cos^2 k''r_0''$$
$$-\operatorname{cosec}^2\tfrac{1}{2}\theta^*\sec^2\tfrac{1}{2}\theta^*\cos k'r_0'\cos k''r_0''$$
$$+\frac{(\gamma-1)(2\gamma+1)}{4\gamma^2}(\cos k'r_0' + \cos k''r_0'')\{\operatorname{cosec}^2\tfrac{1}{2}\theta^*\cos k'r_0'$$
$$+\sec^2\tfrac{1}{2}\theta^*\cos k''r_0'' + \frac{(\gamma-1)(2\gamma+1)}{4\gamma^2}(\cos k'r_0' + \cos k''r_0'')\} \quad (19)$$

Special Cases.—

Case I: If the velocity is small so that $\gamma \rightarrow 1$, we have from (19)

$$I=\left(\frac{e^2}{2m_0v^2}\right)^2.\frac{2(\gamma+1)}{\gamma^2}\left[\operatorname{cosec}^4\tfrac{1}{2}\theta^*\cos^2k'r_0'+\sec^4\tfrac{1}{2}\theta^*\cos^2k''r_0''\right.$$
$$\left.-\operatorname{cosec}^2\tfrac{1}{2}\theta^*\sec^2\tfrac{1}{2}\theta^*\cos k'r_0'\cos k''r_0''\right]\quad\dots\quad(20)$$

If the critical approach be neglected, *i.e.*, $\cos k'r_0'=\cos k''r_0''=1$, eq. (20) reduces to the corresponding formula of Möller (1932).

Case II. If the velocity be great so that $\gamma >> 1$, we have from (19)

$$I=\left(\frac{e^2}{2m_0v^2}\right)^2.\frac{2}{\gamma}\left[\operatorname{cosec}^4\tfrac{1}{2}\theta^*\cos^2k'r_0'+\sec^4\tfrac{1}{2}\theta^*\cos^2k''r_0''\right.$$
$$-\operatorname{cosec}^2\tfrac{1}{2}\theta^*\sec^2\tfrac{1}{2}\theta^*\cos k'r_0'\cos k''r_0''+\tfrac{1}{2}(\cos k'r_0'+\cos k''r_0'')\{\operatorname{cosec}^2\tfrac{1}{2}\theta^*\cos k'r_0'$$
$$\left.+\sec^2\tfrac{1}{2}\theta^*\cos k''r_0''+\tfrac{1}{2}(\cos k'r_0'+\cos k''r_0'')\}\right]\dots\quad(21)$$

It may be seen without difficulty that because of the factor $2/\gamma$, which is very small in the present case, the critical approach is negligible. Thus the formula is very much simplified and we have

$$I=\left(\frac{e^2}{2m_0v^2}\right)^2.\frac{2}{\gamma}\left[\operatorname{cosec}^4\tfrac{1}{2}\theta^*+\sec^4\tfrac{1}{2}\theta^*+1\right]\quad\dots\quad(22)$$

which is Möller's formula at high velocity

It is thus shown that the general formula (19) reduces to Möller's formulae in the two special cases considered if the critical approach is neglected. But for intermediate values of the incident velocity, lying of course in the relativistic region, (19) becomes on neglecting the critical approach,

$$I=\left(\frac{e^2}{2m_0v^2}\right)^2.\frac{2(\gamma+1)}{\gamma^2}\left[\operatorname{cosec}^4\tfrac{1}{2}\theta^*+\sec^4\tfrac{1}{2}\theta^*-\operatorname{cosec}^2\tfrac{1}{2}\theta^*\sec^2\tfrac{1}{2}\theta^*\right.$$
$$\left.+\frac{(\gamma-1)(2\gamma+1)}{2\gamma^2}\left\{\operatorname{cosec}^2\tfrac{1}{2}\theta^*\sec^2\tfrac{1}{2}\theta^*+\frac{(\gamma-1)(2\gamma+1)}{2\gamma^2}\right\}\right]\quad\dots\quad(23)$$

which is different from Möller's formula.

ELECTRON-POSITION SCATTERING

In this case the effect of exchange should not be considered. Thus we have from the first equation of (17)

$$\lambda_1\lambda_1=-\frac{e^2\gamma}{2m_0c^2(\gamma-1)\gamma^*}\;\frac{1}{\sqrt{v}}\;\frac{e^{ikr}}{r}\left(\operatorname{cosec}^2\tfrac{1}{2}\theta^*\pm\frac{(1-\gamma)(1+2\gamma)}{2\gamma^2}\right)\cos k'r_0\dots\quad(24)$$

where the + sign is for parallel and − for antiparallel spins. Remembering that the weights for parallel and antiparallel spins are as 3:1, we have for the intensity of scattering

$$I=\left(\frac{e^2}{2m_0v^2}\right)^2.\frac{2(\gamma+1)}{\gamma^2}\left[\operatorname{cosec}^4\tfrac{1}{2}\theta^*+\frac{(1-\gamma)(1+2\gamma)}{2\gamma^2}\operatorname{cosec}^2\tfrac{1}{2}\theta^*\right]\cos k'r_0\quad\dots\quad(25)$$

neglecting higher terms. At low velocity but in the relativistic region the second term in bracket representing the spin-spin interaction is negligible and we get Bhaba's (1938) formula.

Again, if the velocity is extremely high, so that $\gamma >> 1$, we have from (25)

$$I = \left(\frac{e^2}{2m_0 v^2} \right)^2 \cdot \frac{2}{\gamma} \operatorname{cosec}^2 \tfrac{1}{2}\theta^* \cot^2 \tfrac{1}{2}\theta^* \tag{25.1}$$

neglecting the critical approach which is small.

DISCUSSION

It may be mentioned that in electron-electron and electron-positron scattering, the approximate value of the relativity factor given in (15) has been used. The rigorous value is more complicated. From the definition of δ_{re} given in (8) we should have strictly

$$\delta_{re} = \frac{\gamma + 1}{2\gamma^2} \cdot \frac{(\operatorname{cosec}^4 \tfrac{1}{2}\theta^*)\text{relat.}}{(\operatorname{cosec}^4 \tfrac{1}{2}\theta^*)\text{non-relat.}} - 1 \tag{26}$$

In the approximate value of δ'_{re} used before, the relativistic and non-relativistic values of $\operatorname{cosec}^4 \tfrac{1}{2}\theta^*$ have been taken approximately the same. However, on taking their exact values it may be easily shown that

$$\delta_{re} = \frac{2}{\gamma^2(\gamma + 1)} \left\{ 1 + (\gamma - 1)\sin^2\theta \right\}^{-} - 1 \tag{27}$$

If the velocity is too small so that $\gamma \rightarrow 1$, then $\delta_{re} \rightarrow 0$ as in the approximation. Again, if the velocity is very great so that $\gamma >> 1$, $\delta_{re} \rightarrow -1$ as before. Thus the limiting values of δ_{re} rigorously evaluated are exactly the same as in the approximations used before.

Lastly, the question of correction for the critical approach has not been discussed in the present paper as it is too small. The uncorrected value may be used.

PHYSICAL LABORATORY
RAJSHAHI COLLEGE, BENGAL.

REFERENCES

Bhaba, H. J., 1938, *Proc. Roy. Soc.*, **164**, 257.
Dirac, P. A. M., The Principles of Quantum Mechanics.
Kar, K. C., 1945, *Ind. Jour. Phys.*, **19**, 146.
Kar, K. C. and Mrs. Basu, C., 1944, *Ind. Jour. Phys.*, **18**, 223
Kar, K. C. and Sengupta, R. L., 1942, *Science and Culture*, **8**, 191
Mott, N. F., 1929, *Proc. Roy. Soc.*, **124**, 425.
Sengupta, R. L., 1939, *Pro. Phy. Soc. (Lond.)*, **51**, 355.
Van Vleck, Electric and Magnetic Susceptibilities.

ON CONTINOUS EMISSION BANDS OF ICl AND IBr

By R. K. ASUNDI* AND P. VENKATESWARLU

(Received for publication April 18 1947)

ABSTRACT. A number of new continuous bands have been recorded in the spectra of the mixed haolgens ICl and IBr excited by uncondensed discharge from a transformer. These are established by taking juxtaposed spectra of the halogens and the mixed halogens. A tentative explanation of the origin of the bands is given which ascribes them to transitions from stable electronic states to a number of repulsive states that arise from a combination of normal and $^2P_{\frac{1}{2}}$ excited states of the individual halogen atoms.

INTRODUCTION

The absorption spectra of mixed halogens have been studied in some detail by different workers, Cordes and Sponer (1930), Brown and Gibson (1932), Brown (1932), Mulliken (1934), Sponer (1935). But our knowledge of the emission spectra of these molecules is rather meagre. Filippov (1928), by irradiating a mixture of ICl and N_2 vapour with light from an aluminium spark, has recorded, in fluorescence, a single band with a maximum at 4350A which is also the only one band recorded by him in excitation of a mixture of ICl and N_2 by high frequency Tesla coil discharge. He has also recorded, by the same kind of electrical excitation in a mixture of IBr and N_2, four maxima at 4120, 3860, 3425 and 3045A. By irradiating IBr vapour and a mixture of IBr and N_2 vapour by ultraviolet light (below 2000A), he observed some diffuse bands. Loomis and Allen have reported, in fluorescence of IBr, the presence of groups of lines below 2500A and of diffuse bands between 2500 and 3700A, but they have not recorded the wavelength data of these bands. They also reported that pure ICl vapour did not show any fluorescence.

(I) IODINE CHLORIDE

Preparation and Experimental Procedure.—Iodine mono-chloride is prepared by mixing iodine and chlorine in equal proportions to their atomic weights. Dry chlorine from a liquid chlorine cylinder is passed through 127 gms. of resublimed iodine till about 35 gms. of chlorine vapour are dissolved, when the solid iodine becomes completely liquid. This liquid is distilled to obtain liquid iodine mono-chloride which was reddish brown in colour.

A 30 cm. long glass tube (with aluminium internal electrodes 20 cm. apart), to one end of which is fixed a clear quartz window while the other end is drawn flat, forms the discharge tube. To one side of the discharge tube is connected, through a stopcock, a bulb containing ICl and the side at the opposite end is connected through a stopcock and long absorption tubes containing KOH (to absorb ICl vapour) to a Cenco High Vacuum pump. The tube is first evacuated and the stopcock connected to ICl bulb is slightly opened. By adjusting the stopcock, the vapour is kept flowing and excited by an uncondensed discharge from a transformer. The glow obtained, which is bluish violet in colour, is so dazzling and repulsive to the eye that one cannot look at it for a long time. An observation of this glow with a direct vision spectroscope shows the presence of a strong green continuous band and indicates its difference from the nature of the individual glows of iodine and chlorine excited in a similar manner. As the iodine and iodine chloride bands (but not the chlorine bands) lie almost in the same region, juxtaposed spectra are taken for I_2 and ICl using the same type of discharges, the apparatus used for I_2 being similar to that for ICl.

---

* Fellow of the Indian Physical Society.

In the visible region the spectrum is photographed on a two-prism glass spectrograph and in the ultraviolet region, Hilger medium and E_3 quartz spectrographs are used. The two-prism spectrograph is the one set up recently in this laboratory and has a dispersion of 44 A/mm at 5500A and 15 A/mm at 4300A Gevart ultra-panchromatic and orthochromatic plates, Kodak P-150 process plates and Ilford ordinary plates have been used.

EXPERIMENTAL RESULTS

The spectrum consists entirely of continuous bands and atomic lines. Most of the atomic lines are identical with those which are also obtained in iodine. The discrete bands of iodine, and chlorine (parts of which are due to Cl_2^+) are entirely absent in the spectrum of ICl thus obtained. In the green region, there is a broad continuous band extending from 5640 to 5120A with a maximum intensity at about 5330A. Between 4800 and 3400A there are a number of continuous bands. In the same region iodine possesses a number of diffuse bands but in this region chlorine does not show any continuous (or diffuse) bands but only discrete bands. Hence juxtaposed spectra for I_2 and ICl only are taken on all the spectrographs used. These show the difference between ICl spectrum and I_2 spectrum and thus enable one to establish the existence of ICl bands. Plate IIA Spectrogram 1 of these spectra gives the necessary illustrations.

The wavelengths and wavenumbers of the maxima of the continuous bands obtained and their shortwave and longwave limits are given in Table I. The wavelengths are the mean values obtained from measurements of a number of plates. The accuracy of the wavelengths of the maxima will probably be about ±2A. All the bands given in Table I are recorded for the first time and are different from the bands of I_2 and Cl_2. As such they can, with confidence, be attributed to ICl. The single band, with a maximum at 4350A recorded by Filippov, is probably the same as the intense band between 4383 and 4175A, having a maximum at 4275A.

TABLE I

Emission Bands of ICl

Intensity	Extent of the band in A.U.	Position of the maximum	
		λ_{air}	ν_{vac}
8	5610–5120	5330	18757
6	4623–4583	4603	21719
6	4552–4512	4532	22059
6	4480–4407	4455	22440
10	4383–4175	4275	23385
8	4075–3935	4006	24956
5	3877–3799	3844	26007
3	...	3700	27019

(II) IODINE BROMIDE

Preparation and Experimental Procedure.—Resublimed iodine crystals and liquid bromine are mixed in equal proportions to their atomic weights. The mixture is heated and the vapours condensed to give pure iodine bromide (dark gray crystals). These crystals have the appearance of iodine and the smell of bromine. If a little excess of bromine is added, the crystals become liquefied, probably giving IBr_3.

The discharge tube and the evacuating apparatus used are exactly similar to those used for ICl. The tube is first evacuated and the IBr bulb slightly heated. The vapour is kept flowing and the tube is excited by an uncondensed discharge from a transformer. The glow obtained is bluish in colour which is different from the individual glows of I_2 and Br_2 excited in a similar manner. Observation with a small direct vision spectroscope already indicates the difference in the nature of the IBr spectrum from those of iodine and bromine. The spectra are photographed on the same instruments as those used for ICl. Juxtaposed spectra are taken for IBr and I_2, and for IBr and Br_2, to establish the identity of the bands due to IBr.

Experimental Results.—In the visible region from 6700-5000A iodine and bromine give discrete bands degraded towards the longer waves, but IBr gives only a strong continuous band from 5194 to 5008A with two maxima at 5153 and 5059A. A number of continuous (or diffuse) bands are obtained in the iodine spectrum from 4800-2400A and in bromine from 4250 to 2000A, Venkateswarlu (1946). IBr shows also diffuse bands from 4800-2300A. The difference of the spectrum of IBr from those of iodine and bromine is well brought out by a comparison of the respective spectra taken in juxta-

TABLE II

Iodine Bromide Bands

Filippov's results in fluorescence		Present experiments with transformer discharge			
$IBr+N_2$ λ_{air}	IBr λ_{air}	Intensity	Position of maxima λ_{air}	ν_{vac}	Extent of band in A. U
5100	...	5	5153	19401	5194–5008
		6	5059	19761	
4900	4850				
4675*	4675*				
4495	4495	10	4442	22506	4500–4410
4370	4365	5	4348	22993	4375–4299
4220	4210	4	4242	23567	4253–4231
		4	4198	23814	4210–4186
4140	4160	4	4150	24090	4163–4140
		4	4120	24265	4132–4108
4085	4055	4	4056	24648	4070–4045
		4	4007	24949	4019–3995
3860	3855, 3770,	10	3855	25933	3900–3800
3715	3705				
	3650	8	3650	27389	3695–3605
3550	3500	6	3533	28296	3570–3510
3425*	3400*				
3160 3045	3325, 3265, 3205, 3160, 3120, 3050, 3015, 2995, 2960, 2935, 2915, 2890				
		4	2752	36326	2766–2738
		4	2646	37782	2658–2626
		4	2556	39112	2564–2546
		3	2477	40359	2482–2470
		3	2423	41259	2428–2416
		2	2363	42306	2369–2356

* These are probably due to I_2.

position (*vide* Spectrograms II and III). The wavelengths and wavenumbers of the maxima of the bands which are probably accurate to ± 2A are obtained from calculations on a number of plates. The shortwave and longwave limits of the bands along with their maxima are given in Table II. The intensity values represent the relative intensities visually estimated from the bands obtained on Kodak P-150 and B-20 process plates. A comparative study of the juxtaposed spectra allows one to conclude with confidence that all the bands given in Table II are to be attributed to IBr (except those marked *).

From Table II, which contains also the data on the fluorescent bands recorded by Filippov, it can be seen that there is no apparent agreement among the values recorded by Filippov in fluorescence and those obtained in the present experiments in emission by electrical excitation. For example, between 3325 and 2890A Filippov has recorded twelve bands in fluorescence which do not appear on our plates. It is, however, not necessary that there should be one to one coincidence between bands obtained in fluorescence and those obtained in electrical excitation. But taking into consideration the fact that Filippov has used only a small quartz spectrograph which, on account of low dispersion and resolution, necessarily introduces considerable error in the values of wavelengths particularly on the longwave side of the spectrum as pointed out by Filippov himself, it is likely that the bands obtained by him in the region 3500-4850A can be identified with some of the bands obtained in present experiments as indicated in Table II.

Filippov has excited a mixture of IBr and N_2 by Tesla coil high frequency discharge and recorded wavelengths of the maxima of only four bands at 3425, 3860, 4120 and 3045A. Of these probably 3425A is identical with the well-known iodine continuum at 3416A. 3860 and 4120A may be identified with bands at 3855 and 4120A of Table II. But we shall not lay any stress on these coincidences as it is not excitation of pure IBr that Filippov has employed.

(III) A PROBABLE EXPLANATION OF THE RESULTS OBTAINED

The bands given in Table I for ICl and those in Table II for IBr do not show any structure under the dispersion and resolution of the instruments used, and they appear to be identical in nature to the continuous (or diffuse) bands in the halogens (Venkateswarlu, 1946, 1947). Hence it should be possible to explain them in an analogous manner. In other words, there is the possibility that they are due to transitions from excited stable electronic terms to a set of repulsive states.

From among the stable states till now known from absorption data we select two in the fluorite region, for each of the molecules ICl and IBr. These are at 53478 and 58190 cm^{-1} for ICl and at 51700 and 56370 cm^{-1} for IBr (Sponer). In ICl there is at least one more level in the fluorite region which is indicated by the third system of bands (Cordes and Sponer). But

Spectrogram I

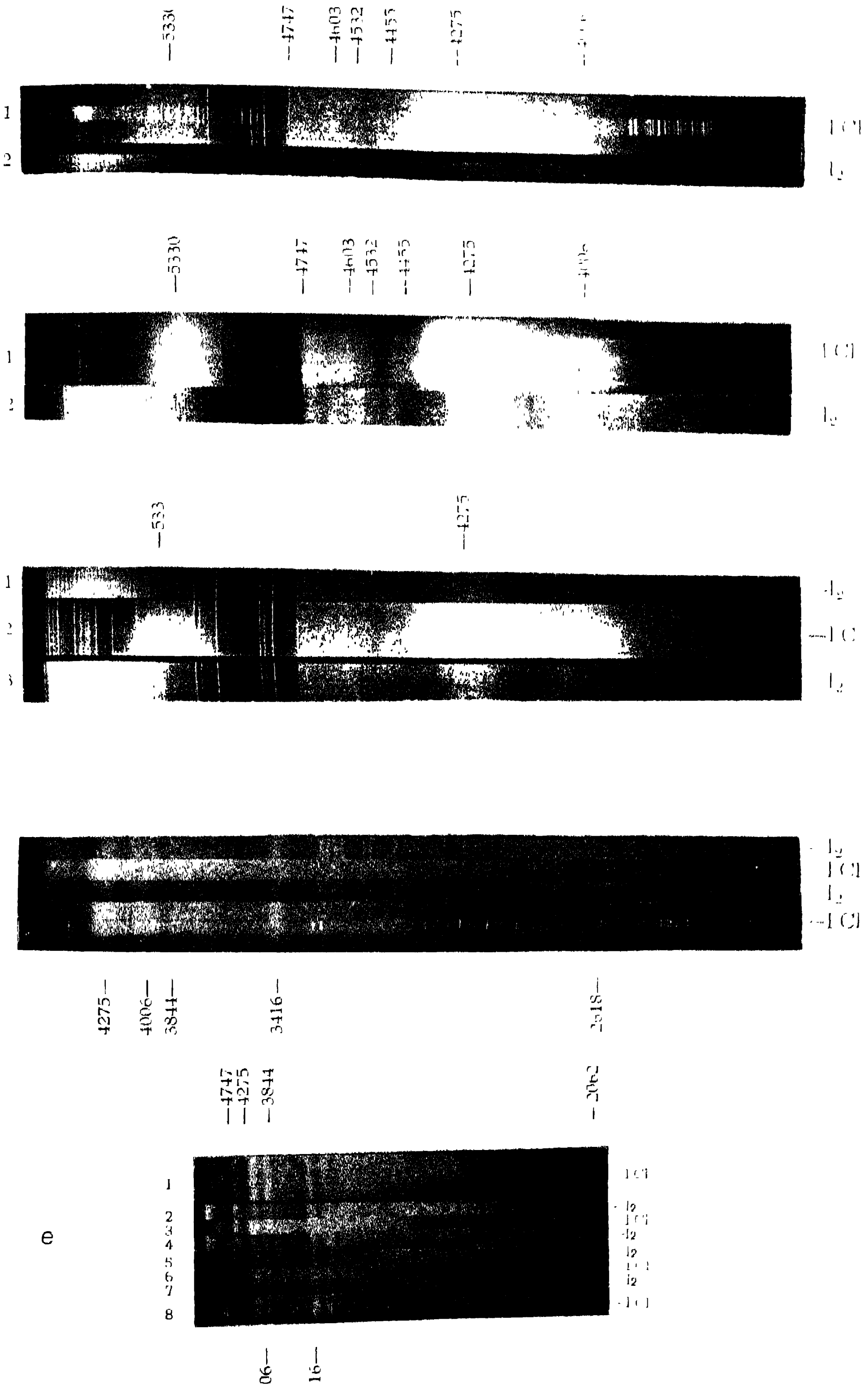

Spectrogram II

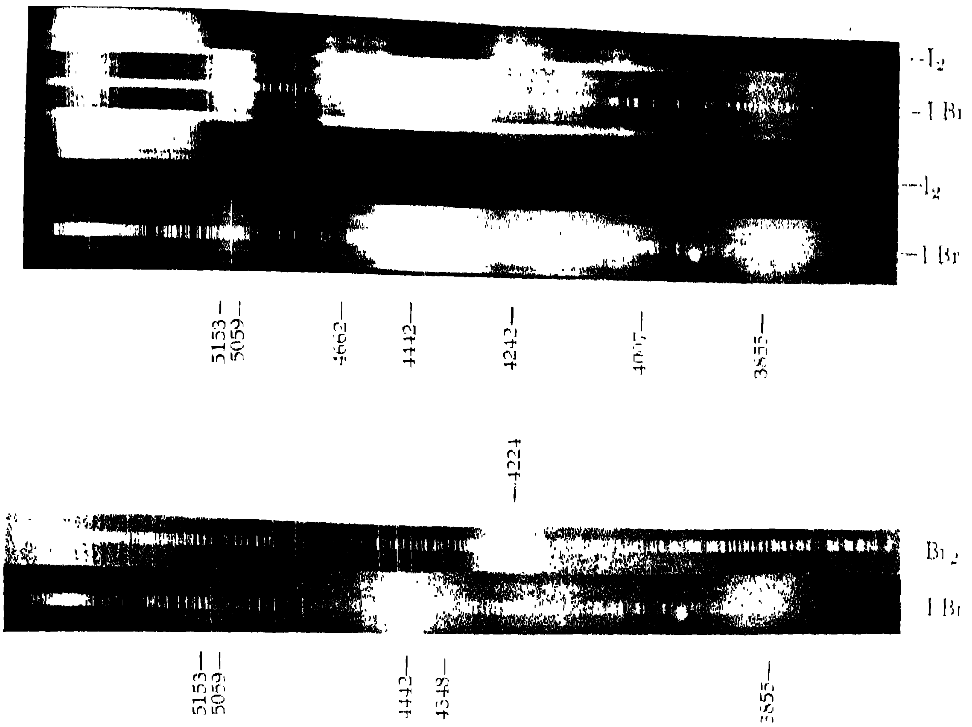

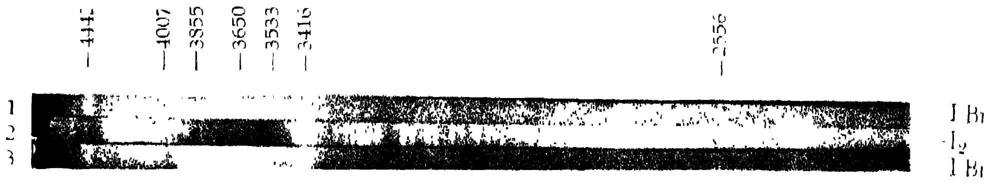

Spectrogram III

a

b

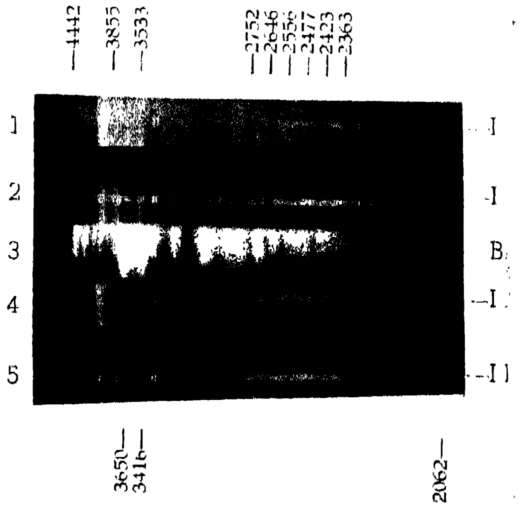

this has not been measured. The number and approximate positions of the repulsive states arising from combinations of the separated atoms can be easily calculated in each case. The dissociation energies of ICl and IBr involving atoms in the normal states are 17371 cm^{-1} and 14656 cm^{-1} respectively. The dissociation levels of other combinations involving Cl, Br and I in their $^2P_{\frac{1}{2}}$ states can be easily calculated. The range in which the dissociation levels lie is thus between 17371 and 25852 cm^{-1} for ICl and between 14656 and 25941 $cm.^{-1}$ for IBr. The range of the repulsive states being thus known, transitions from the stable states mentioned above to those repulsive states will then give rise to emission bands of the observed diffuse type in a range between 27626 and 40810 cm^{-1} in the case of ICl and between 25759 and 41614 $cm.^{-1}$ in the case of IBr The region in which the observed bands in ICl lie is from 19000 to 29000 cm^{-1}. It is likely that the third, as yet not measured, stable level in ICl is also involved in the production of these bands. In IBr the observed bands occupy the region between 19000 and 42000 $cm.^{-1}$ in close correspondence with the calculated range.

It is thus possible to offer a tentative explanation of the bands along the lines already successfully applied for similar bands in the halogens. A detailed treatment of such an explanation, however, is expected to be undertaken when the further experimental work on the absorption and emission spectra of ICl, IBr and BrCl, which is now in progress in this laboratory, is completed.

ACKNOWLEDGMENTS

We express our thanks to Principal S. S. Joshi, of Benares Hindu University, for lending us the E_3 quartz spectrograph and to Prof. S. Bageshwar, of Fine Chemicals Section, for the chlorine cylinder used in this investigation.

DEPARTMENT OF PHYSICS,
BENARES HINDU UNIVERSITY.

REFERENCES

Brown, 1932, *Phys. Rev.*, **42**, 355.

Brown and Gibson, 1932, *Phys. Rev.*, **40**, 529.

Cordes and Sponer, 1930, *Zs. f. Phys.*, **63**, 334; 1932, *ibid.*, **71**, 34; 1932, *ibid.*, **79**, 17[illegible].

Filippov, 1928, *Zs f. Phys*, **50**, 861.

Loomis and Allen, 1929, *Phys. Rev.*, **33**, 639.

Mulliken, 1934, *Phys Rev.*, **46**, 549.

Sponer, 1935, *Molekül Spektren*, Vol. I.

Venkateswarlu, 1946, *Proc. Ind. Acad. Sci*, **24A**, 480 (Pt I); 1947, *ibid.*, **25A**, 119 (Pt. II), 133 (Pt. III), 138 (Pt. IV); and Pt V of the same series to appear in the same Journal

ILLUSTRATIONS TO PLATES IIA AND IIB

Spectrogram I

a(1) and *a*(2) are the spectra of ICl and I_2 respectively taken in juxtaposition on a 2-prism, glass spectrograph, using Gevart ultra-panchromatic plate.

b(1) and *b*(2) are the spectra of ICl and I_2 respectively, taken on a 2 prism glass spectrograph using P-150 Kodak Process Plate.

c(1) and *c*(3) are the spectra of I_2 and *c*(2) that of ICl taken in juxtaposition on a 2-prism glass spectrograph The continuous band in *c*(2) between 5640 and 5120A, with a maximum at about 5330A, shows the absorption bands of free I_2 molecules which are probably present in the free space between the discharge glow and the quartz window of the apparatus. This absorption of free iodine molecules is absent in *a*(1) and *b*(1) where the free space between the discharge glow and the window of the discharge tube are eliminated. *d* (1) and *d*(3) are the iodine spectra and *d*(2), *d*(4) are the ICl spectra taken on a Medium Hilger quartz spectrograph, using Ilford Ordinary Plate.

e(1) to *e*(8) are the spectra of ICl, I_2, ICl, I_2, I_2, ICl, I_2 and ICl respectively, on an E_3 Hilger quartz spectrograph using B-20 Kodak Process Plate.

Spectrogram II

a(1) and *a*(3) are the spectra of I_2 and *a*(2) that of IBr taken in juxtaposition on a 2-prism glass spectrograph, using P-150 Kodak Process Plate. *b* is the IBr spectrum taken on the same instrument using the same plate

c(1) and *c*(2) are the spectra of Br_2 and IBr respectively, taken on a 2 prism glass spectrograph, using P-150 Kodak Process Plate.

d(1) and *d*(3) are the spectra of IBr and *d*(2) that of I_2 taken in juxtaposition on a Medium Hilger quartz spectrograph, using Ilford Ordinary Plate.

Spectrogram III

a(1) and *a*(3) are the spectra of IBr and *a*(2) that of I_2 taken in juxtaposition on an E_3 Hilger quartz spectrograph, using Kodak B 20 Process Regular Plate.

b(1), *b*(2), *b*(4) and *b*(5) are the spectra of IBr and *b*(3) that of bromine taken on an E_3 quartz spectrograph, using B-20 Kodak Process Regular Plates.

ACKNOWLEDGMENTS

We thankfully acknowledge the receipt of a grant of Rupees one thousand only from the Rockefeller Foundation Trust of America and a grant of Rupees Two hundred and fifty only from the Government of India, through the National Institute of Sciences, India.

The following special publications of the Indian Association for the Cultivation of Science, 210, Bowbazar Street, Calcutta, are available at the prices shown against each of them :—

Subject	Author	Price Rs.	A.	P
Methods in Scientific Research	Sir E. J. Russell	0	6	0
The Origin of the Planets	Sir James H. Jeans	0	6	0
Separation of Isotopes	Prof. F. W. Aston	0	6	0
Garnets and their Role in Nature.	Sir Lewis L. Fermor	2	8	0
(1) The Royal Botanic Gardens, Kew. (2) Studies in the Germination of Seeds.	Sir Arthur Hill	1	8	0
Interatomic Forces	Prof. J. E. Lennard-Jones	1	8	0
The Educational Aims and Practices of the California Institute of Technology	R. A. Millikan	0	6	0
Active Nitrogen A New Theory	Prof. S. K. Mitra	2	8	0
Theory of Valency and the Structure of Chemical Compounds ...	Prof. P. Ray	3	0	0

A discount of 25% is allowed to Booksellers and Agents.

RATES OF ADVERTISEMENTS

Third page of cover	Rs.	32, full page
do. do.	,,	20, half page
do. do.	,,	12, quarter page
Other pages	,,	25, full page
do.	,,	16, half page
do.	,,	10, quarter page

15% Commissions are allowed to bonafide publicity agents securing orders for advertisements.

We are now manufacturing :

- **KIPP'S APPARATUS of one litre capacity,**
- **DESICCATOR of 4", 5" and 6" diameter,**
- **MEASURE GLASSES of 2 drams, 1 oz., 4 oz. and 8 oz. cap. accurately calibrated**

AND

ALL TYPES OF GRADUATED GLASSWARE
such as Measuring Flasks, Measuring Cylinders,
Burettes, Pipettes, etc., etc.

Manufactured by :

INDUSTRIAL & ENGINEERING APPARATUS CO., LTD.

CHOTANI ESTATES, PROCTOR ROAD, BOMBAY, 7.

MELT VISCOSITY : PART II

Esters and Acetyl Derivatives of Shellac and its Constituents

By SADHAN BASU

(Received for publication, April 28, 1947)

ABSTRACT. The results of viscosity measurements of esters and acetyl derivatives of shellac resins have shown that both hydroxyl and carboxyl groups exert their influence in micelle formation of the individual resins, but the influence which soft resin exerts on the micelle formation of hard resin in shellac is mainly due to its hydroxyl group.

INTRODUCTION

As reported in a previous communication (Basu, 1947) the results of viscosity measurements on molten shellac resins have shown that the resin molecules are greatly aggregated owing to the presence of a large number of active polar groups in them. In the present paper an attempt has been made to find out the role of the various functional groups, namely, hydroxyl and carboxyl groups in "micelle" formation. This end has been achieved by protecting the polar groups by esterification and acetylation, and examining their effect on the energy of activation and viscous volume.

EXPERIMENTAL

Apparatus.—The viscometer used was the same as described in a previous paper (Basu, *loc. cit.*) and the same procedure was adopted in calculating the values of activation energy and viscous volume.

Preparation : Acetyl derivative.—Acetyl derivatives were prepared in each case by refluxing the weighed quantity of powdered resin with a mixture of 1 : 3 acetic anhydride : pyridine mixture (5 c.c. of mixture per gramme of substance) for 2-3 hours. The resulting solution was poured into water, and the precipitated resin thoroughly washed, and dissolved in a 1 : 1 benzene-alcohol mixture. The last trace of acid was removed by neutralising the benzene-alcohol solution with solid bicarbonate. The solution thus neutralised was poured into water, washed thoroughly and then dried at 50°C in vacuum. The product thus obtained corresponded to 6.83 acetylated derivative for hard resin, 4.79 acetylated derivative for shellac and 1 acetylated derivative for soft resin. Use of hot water should be avoided since this leads to decomposition of the acetylated products especially in the case of hard resin and shellac.

Ethyl ester.—20% ethyl alcoholic solution of the dried sample was saturated with dry hydrochloric acid gas, left overnight and then refluxed for

2-3 hours. The resulting solution was cooled, neutralised with bicarbonate and then poured into water. The precipitated resin was repeatedly washed with distilled water and then dried in vacuum at 60°C. The acid value for soft resin ester was zero, but in the case of shellac and hard resin it varied from 3 to 5.

The separation of hard and soft resin was effected by ether extraction method.

RESULTS

The results of viscosity determination of acetyl derivatives of shellac, hard resin and soft resin are summarised in Tables I-VI and the corresponding curves given in Figs. 1-3.

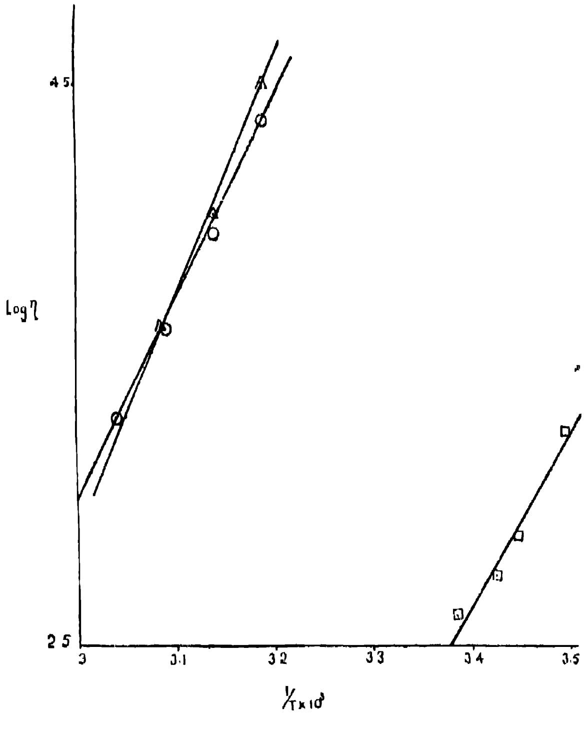

Fig. 1

Acetyl derivative

○ hellac △ Hard Resin □ Soft Resin

ACETYL DERIVATIVES

Table I

Shellac

$f = 5.495 \times 10^3$ dynes/cm²

$1/T \times 10^{-3}$	η (pois)	$\log \eta$
3.09	4340.25	3.6375
3.14	1,0448.75	4.0190
3.19	3,3339.55	4.5229

Table II

Hard Resin

$f = 5.495 \times 10^3$ dynes/cm²

$1/T \times 10^{-3}$	η (pois)	$\log \eta$
3.04	2057.60	3.3133
3.09	4404.55	3.6440
3.14	9259.20	3.9665
3.19	2,3437.35	4.3699

TABLE III

Soft Resin

$f = 5{\cdot}495 \times 10^3$ dynes/cm^2

$1/T \times 10^{-3}$	η (pois)	log η
3·508	1832·55	3.2629
3·448	771.60	2.8874
3·424	546·55	2·7376
3·389	417·95	2.6210

TABLE IV

Shellac

T°K = 323

f (dynes/cm^2)	η (pois)	log η/f
11.988×10^3	2186.2	−0.7391
20.149×10^3	1350.3	−1.1480
$25{\cdot}475 \times 10^3$	964·5	−1.4219
$30{\cdot}969 \times 10^3$	710.3	−1.6397

TABLE V

Hard Resin

T°K = 321

f (dynes/cm^2)	η (pois)	log η/f
11.988×10^3	5465·50	−0.3412
21.711×10^3	2893·50	−0.8391
$25{\cdot}475 \times 10^3$	2250.50	−1.0538
28.472×10^3	1961.15	−1.1619

TABLE VI

Soft Resin

T°K = 284

f (dynes/cm^2)	η (pois)	log η/f
$5{\cdot}495 \times 10^3$	2025·45	−0.4335
8.492×10^3	1286.00	−0.8198
10.489×10^3	1093.10	−0.9820
12.488×10^3	868.05	−1.1580

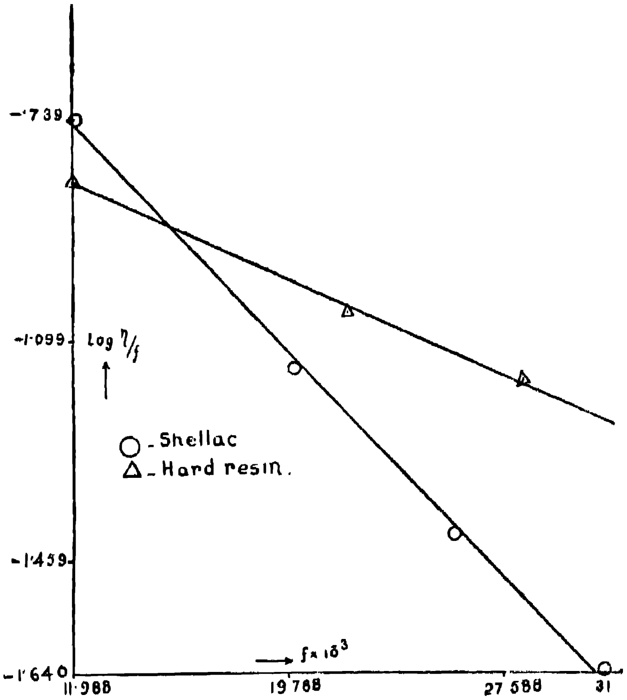

FIG. 2

Acetyl derivative

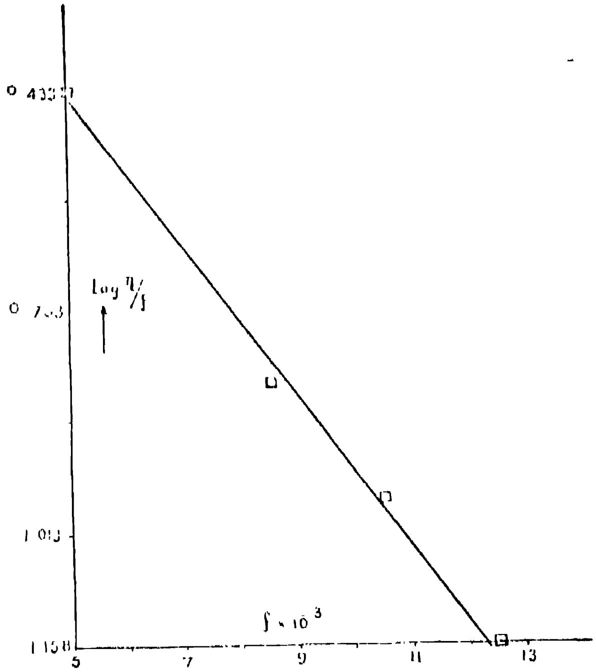

FIG. 3
Acetyl derivative. Soft Resin

Similar results for esters are given in Tables VII-XII and the corresponding log η-1/T and log η/f-f curves are given in Figs. 4-5.

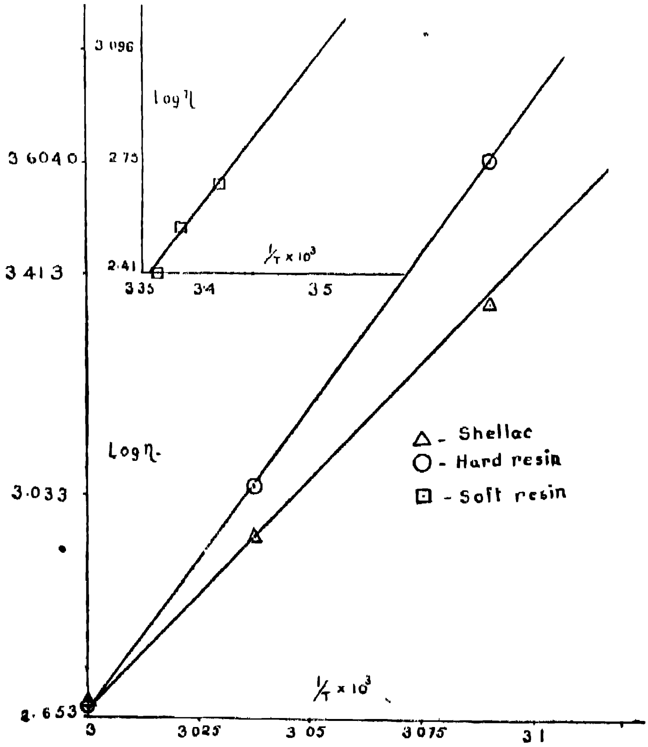

FIG. 4
Ethyl Ester

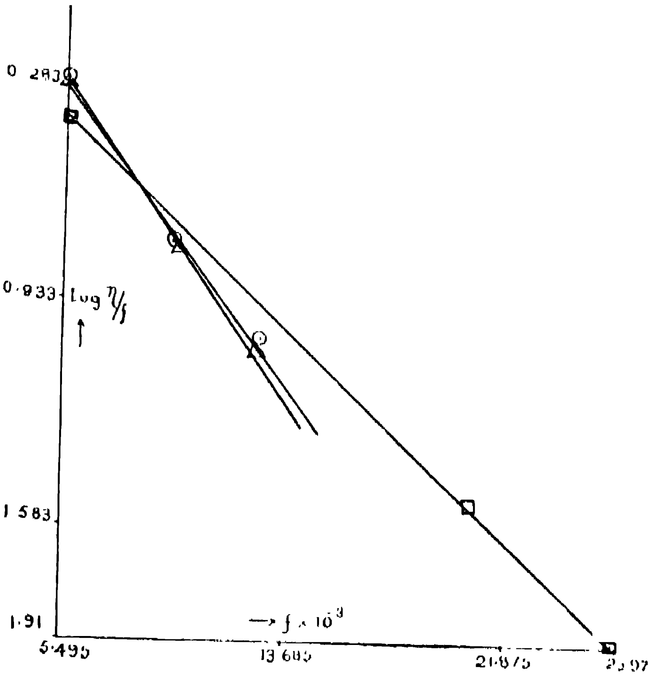

FIG. 5

Ethyl Ester

⊙ Hard Resin △ Soft Resin □ Shellac

ETHYL ESTERS

TABLE VII

Shellac

$f = 5{\cdot}495 \times 10^3$ dynes/cm^2

$1/T \times 10^{-3}$	η (in pois)	log η
3·09	2057 60	3 3133
3·04	932 35	2 9696
3.00	450.10	2 6532

TABLE VIII

Hard Resin

$f = 5{\cdot}495 \times 10^3$ dynes/cm^2

$1/T \times 10^{-3}$	η (in pois)	log η
3 09	2535 00	3.4040
3 04	1093 10	3 0386
3.00	450 15	2.6533

TABLE IX

Soft Resin

$f = 5\ 495 \times 10^3$ dynes/cm^2

$1/T \times 10^{-3}$	η (in pois)	log η
3·546	2797 05	3 4467
3 424	546·55	2 7376
3·389	353·65	2·5487
3·367	257 20	2·4102

TABLE X

Shellac

$T°K = 323$

f (dynes/cm^2)	η (pois)	log η/f
$5{\cdot}495 \times 10^3$	2057.60	−0 4267
12.488×10^3	932·35	−1.1270
20.979×10^3	417·95	−1.7017
25.974×10^3	321·50	−1 9073

TABLE XI

Hard Resin

T°K = 325

f (dynes/cm²)	η (pois)	log η/f
5.4950×10^3	2862.2	−0.2833
9.4910×10^3	1546.2	−0.7881
12.4875×10^3	1157.4	−1.0329

TABLE XII

Soft Resin

T°K = 282

f (dynes/cm²)	η (pois)	log η/f
5.495×10^3	2797.05	−0.2933
9.491×10^3	1511.05	−0.7980
12.488×10^3	1125.25	−1.0450

The values of a, b, E_0' and $\lambda\lambda_2\lambda_3$ for esters and acetyl derivatives as obtained from the above Tables and the corresponding graphs are given in Tables XIII and XIV.

TABLE XIII

Acetyl Derivatives

		a	b	E_0' (K-cal)	$\lambda\lambda_2\lambda_3$ (in cc.)
Hard resin	...	1.6403×10^4	2.443×10^{-2}	31.81	10.154×10^{-18}
Shellac	..	1.3714×10^4	3.694×10^{-2}	28.74	10.292×10^{-18}
Soft resin	...	1.2782×10^4	6.767×10^{-2}	25.32	18.622×10^{-18}

TABLE XIV

Ethyl Esters

		a	b	E_0' (K-cal)	$\lambda\lambda_2\lambda_3$ (in cc.)
Hard resin	...	1.8100×10^4	8.013×10^{-2}	35.94	22.07×10^{-18}
Shellac	...	1.5086×10^4	6.117×10^{-2}	29.89	16.83×10^{-18}
Soft resin	...	1.3606×10^4	4.944×10^{-2}	27.08	13.61×10^{-18}

DISCUSSION

A glance at Tables XIII and XIV will show that on protecting the polar groups the activation energy for viscous flow is greatly reduced. In the case of esters, this is evidently due to the difference in cohesive forces between ester groups and carboxyl groups. Mark and Meyer (1930) have shown that cohesive forces in K-cal/mole for carboxyl and ester groups are respectively 8.97 and 5.60. Hence the lower value of cohesive force between ester groups is responsible for the lower activation energy, *i.e.*, lower degree of association of shellac esters.

An anomalous case is presented by the acetyl derivatives. The cohesive force between acetyl groups is not actually so low as (Mark and Meyer, *loc. cit.*) to cause such a great reduction in the activation energy of the acetylated products. But since the acetyl group is much bulkier than the hydroxyl group and cannot therefore fit in tightly in the original micelle of shellac, the whole structure becomes extended, easily deformable and less aggregated owing to the greater average distance through which the cohesive forces have now to operate.

Another interesting observation that can be made from the values of activation energy and viscous volume for acetyl derivatives is that these values for shellac in every case are nearly the weighted averages of those of hard and soft resin. Thus we may assume that the effect which soft resin exerts on hard resin in micelle formation is mainly due to its own hydroxyl groups interacting with those of the hard resin. Naturally we may assume that aggregation is mainly due to attraction between the hydroxyl groups, *i.e.*, the OH groups are responsible for intramiceller forces, while the intermiceller forces are due to COOH groups. If these assumptions be true then the difference between the activation energy for pure resin and that of its ester will be equal to the difference between the same quantities for carboxyl groups and ester groups. Taking, for example, the case of soft resin, the difference between the activation energy for soft resin and that of its ester is 6.35 K-cal/mole, while that between esters and carboxyl groups is 3.3 K-cal/mole. The difference is too high to be ascribed to experimental error. Thus we can conclude that both hydroxyl and carboxyl groups exert their influence in micelle formation of individual resins but it is the hydroxyl group which is responsible for mutual interaction of resins.

The interpretation of the values for viscous volume as obtained for esters and acetyl derivatives is difficult. Since esterification and acetylation cause some strong polar attraction to vanish from the molecule, the molecules get an entirely new orientation in the micelle and the same idea as expressed in the previous communication as regards the jumping of the micelle between polar groups, cannot be applied here.

ACKNOWLEDGMENT

The author wishes to express his gratefulness to Dr. P. K. Bose, Director, Indian Lac Research Institute, for his kind interest in the present work.

INDIAN LAC RESEARCH INSTITUTE,
NAMKUM, RANCHI.

REFERENCES

Basu, S , 1947, *Ind. J. Phys.*, **21**, 7.

Mark and Meyer, 1930, Der Aufbau der Hochpolymeren Organischen Naturstoffe, Leipzig, p. 27.

11

A CIRCUIT FOR THE CONTROL OF IONIZING CURRENT BY A SATURABLE CORE TRANSFORMER

By B. M. BANERJEE * AND AMBUJ MUKERJEE

(*Received for publication, April 30, 1947*)

ABSTRACT A simpler version of the Overbeck Meyer circuit for automatic control of ionizing current is described. A mathematical analysis for the circuit is presented. Theoretical calculations in a practical case are checked against experimental observations.

The discovery of a simple and interesting relation between A. C. permeability and D. C. magnetizing current is reported.

A new phenomenon—self oscillation of the D. C. current in such a circuit is reported. An explanation about the mechanism of such oscillations is also suggested.

The design of this circuit is discussed in detail. A step by step method of design outlined.

Finally the advantages and disadvantages of this type of circuit is compared with other types of control circuits.

INTRODUCTION

In devices † where a stream of electrons are used to ionize a gas, the necessity of keeping this ionizing current constant, frequently arises. The ionizing current in such devices is inherently unstable, being greatly dependent on the gas pressure and the surface conditions of the electron emitting filament. Means must therefore be provided for continuous adjustment of the filament current so as to compensate for, by altering the filament temperature, the effects of cumulative ionization at high pressures and of surface activation and poisoning with different types of gases. Many circuits have been proposed. We give below another. This is a simplified version of the Overbeck and Meyer (1934) circuit. This circuit, like the Overbeck and Meyer circuit, is primarily meant for use with ionization gauges although it may be used in any of the other devices mentioned below with suitable modification.

Circuit.

The circuit diagram is given below. It will be seen that here we have only a series resonating capacity in place of the series inductance and parallel resonating capacity of the Overbeck Meyer circuit. From the circuit point of view both circuits are intrinsically the same as both lead effectively to the same equivalent circuit which is analysed below :

---

* Fellow of the Indian Physical Society.

† (1) Ionization gauge, (2) Ion tubes and sources, (3) Mass spectrometer, -

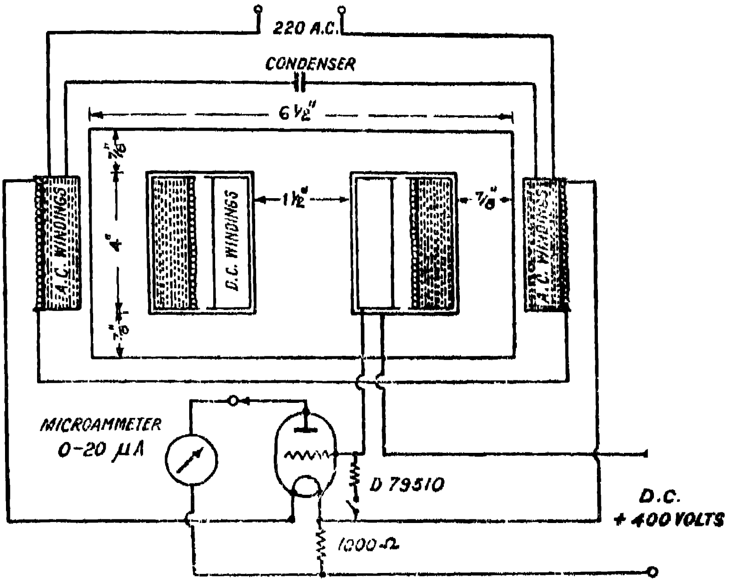

FIG. 1

Saturable Core transformer and control circuit.

Details of saturable core transformer: Core of 26 S.W.G. transformer sheets; core thickness 1¼″; Two a.c. windings on two outer limbs; Primary: (3500+3500) turns of No. 30 S.W.G. enamelled wire, total d.c. resistance 220 ohms insulating paper between layer to layer. Secondary: (20+15)+(20+15) turns of No. 16 S.W.G. D.C.C. wire wound in a single layer above the primary winding, three layers of empire cloth insulation between primary and secondary. D.C. winding on central limb, 50,000 turns of No. 42 S.W.G. enamelled wire, total resistance 20,000 ohms, no insulating paper between layer to layer. All formers made with thick presspahn paper.

Ion gauge tube is a Western Electric D79510 tube.

For reactivation of the oxide coated filament of this gauge, the resistance between the grid and filament may be switched on. A current will then pass through the d.c. winding and a maximum filament voltage will be developed and maintained across the filament so long as the emission does not appear. Appearance of emission will be accompanied by an automatic reduction in the filament voltage and the switch may be thrown off to get the normal stabilized value (10 5 mA) of the emission current.

Analysis: The mode of operation of the circuit may be understood from an analysis of the equivalent circuit.

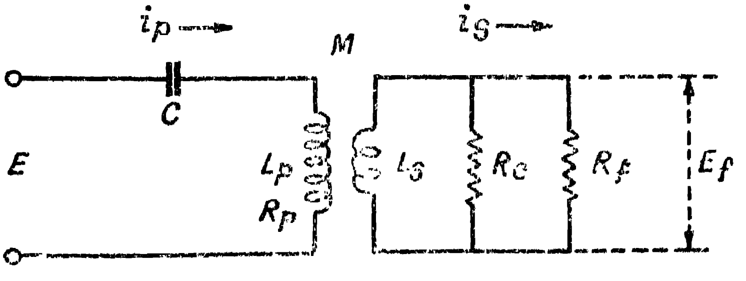

FIG. 2

Fig. 2. Equivalent Electrical Circuit. R_p = D. C. resistance of the A. C. windings. R_f = Resistance of the ion tube filament and the resistance of the secondary windings; R_e = Resistance coming about due to eddy current losses in the core.

The voltage induced in the secondary windings is given by the relation

$$E_s = jpMi_p \qquad \ldots \quad (1)$$

And

$$i_p = \frac{E}{-j/pc + jpL_p + R_p + \left(\dfrac{p^2M^2}{R_s^2 + p^2L_s^2}\right)R_s - jpL_s\left(\dfrac{p^2M^2}{R_s^2 + p^2L_s^2}\right)} \qquad (2)$$

where $R_s = \dfrac{R_e R_f}{R_e + R_f}$.

Now $L_p = \dfrac{4\pi n_1^2 A\mu}{l.10^9}$ Henries :

$$M = \frac{4\pi n_1 n_2 A\mu}{l.10^9} \quad ,,$$

$$L_s = \frac{4\pi n_2^2 A\mu}{l.10^9} \quad ,,$$

and turns ratio

$$T = \frac{n_1}{n_2}. \qquad \ldots \quad (3)$$

n_1 = Primary turns.

n_2 = Secondary turns.

A = Area of cross section of the core.

μ = A. C. permeability.

l = length of A. C. flux path in core.

Putting $\alpha = \dfrac{4\pi n_2^2 A}{l.10^9}$, we get

$$\left.\begin{aligned} L_s &= \alpha\mu \\ M &= \alpha T\mu \\ L_p &= \alpha T^2\mu. \end{aligned}\right\} \qquad \ldots \quad (4)$$

Also putting $R_s = (k/\mu) \quad pL_s = kp\alpha$
and remembering $M^2 = L_p L_s$ and $T^2 = L_p/L_s$
we obtain from (1) and (2)

$$|E_s| = \frac{p\alpha TE\mu}{\left[\left\{\left(\dfrac{k^2/\mu^2}{k^2/\mu^2+1}\right)p\alpha T^2\mu - \dfrac{1}{pc}\right\}^2 + \left\{R_p + \dfrac{T^2R_s}{k^2/\mu^2+1}\right\}^2\right]^{\frac{1}{2}}}$$

whence

$$|i_s| = \frac{p\alpha TE\mu}{\left[\left\{\left(\dfrac{k^2/\mu^2}{k^2/\mu^2+1}\right)p\alpha T^2\mu - \dfrac{1}{pc}\right\}^2 + \left\{R_p + \dfrac{T^2R_s}{k^2/\mu^2+1}\right\}^2\right]^{\frac{1}{2}}\left[R_s^2 + p^2\alpha^2\mu^2\right]^{\frac{1}{2}}}$$

and

$$E_f = \frac{p\alpha TE\mu . R_s}{\left[\left\{\left(\dfrac{k^2/\mu^2}{k^2/\mu^2+1}\right)p\alpha T^2\mu - \dfrac{1}{pc}\right\}^2 + \left\{R_p + \dfrac{T^2R_s}{k^2/\mu^2+1}\right\}^2\right]^{\frac{1}{2}}\left[R_s^2 + p^2\alpha^2\mu^2\right]^{\frac{1}{2}}} \qquad \ldots \quad (5)$$

E_f is the ion gauge tube filament voltage.

DISCUSSION ON RESULTS OF ANALYSIS AND EXPERIMENT

Equation (5) expresses E_f as a function of μ, the A. C. permeability. As is well known, the A. C. permeability of the iron core changes with D. C. magnetisation. The D. C. magnetisation of the transformer core is caused by the ionizing current of the ion gauge tube which passes through the D. C. winding on the central limb of the transformer. Thus a change in the ionizing current will cause a change in the A. C. permeability of core and hence a change in the filament voltage. In other words the filament voltage will be a function of the ionizing current as it is a function of μ.

A set of five theoretical curves will be found in Fig. 3. These represent Eq. (5)— filament voltage as a function of μ — the A. C. permeability. The ordinates in the curves of Fig. 3 are drawn proportional to $1/\mu$. The curves are for a transformer of the dimensions given in Fig. 1.

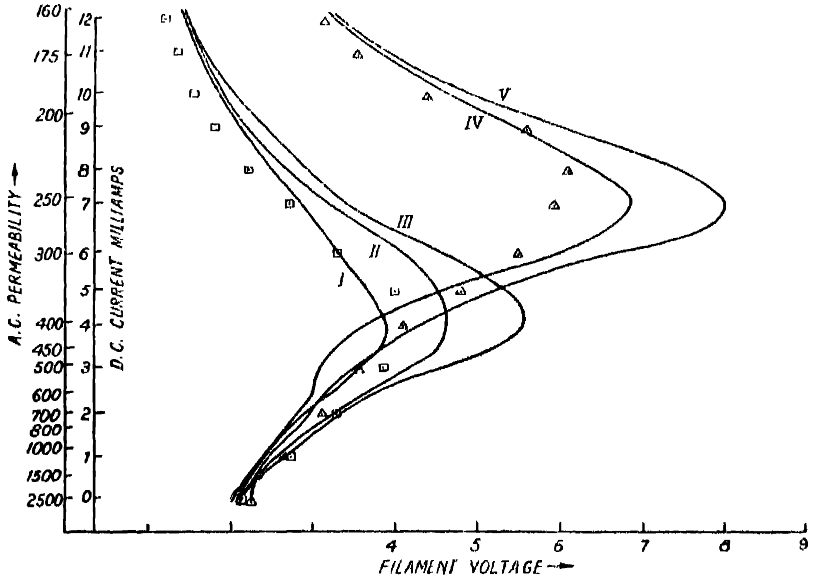

FIG. 3

Theoretical curves for a saturable core transformer of the dimensions given in Fig. 1. All the curves are for a turns ratio of 100 (Primary = 7000 turns, Secondary = 70 turns). Filament voltage plotted is 90% of that given by equation (5) to allow for the drop in the resistance and leakage inductance of the secondary.

curve I, $c = .33\mu f$;	$R = 2.0$ ohm
curve II, $c = .33\mu f$;	$R = 2.5$ ohm.
curve III, $c = .33\mu f$;	$R = 3.0$ ohm
curve IV, $c = \frac{1}{2}\mu f$;	$R = 2.5$ ohm.
curve V, $c = \frac{1}{2}\mu f$;	$R = 3.0$ ohm.

The squares are the experimental points for $c = .33\mu f$. The triangles are the experimental points for $c = \frac{1}{2}\mu f$. Secondary load D7951O tube. This tube takes 1.4 amps at 3.4 volts and 2.2 amps at 7.5 volts on the filament.

The curves were drawn as a function of $1/\mu$, rather than μ, because it was found that μ — the A. C. permeability (at constant A. C. flux density in the core) varies with the D. C. magnetizing current (*i.e.*, the D. C. magnetization) such that the relation between $1/\mu$ and the D. C. magnetizing current is almost a straight line. See curves in Fig. 4. This interesting relation appears not to have been observed or reported to previously by any other worker. The relation means that the admittance of an iron cored reactor increases linearly with the D. C. magnetization. The simplicity of the relation makes it important.

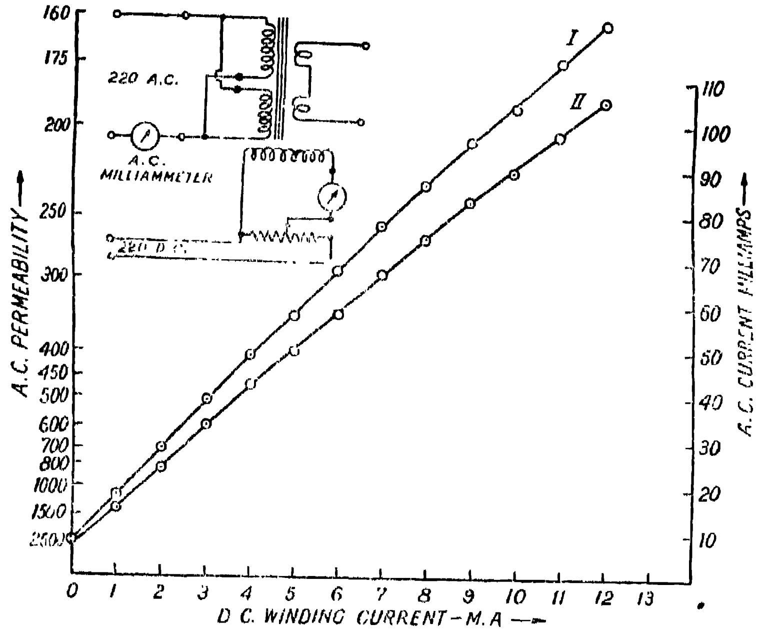

FIG. 4

A.C. permeability at constant flux density vs D.C. magnetization curve I. The ordinates in curve I are proportional to $1/\mu$. The A.C. flux density in the core was approximately 4000 gauss. The D.C. magnetization would amount to 1.7 gilberts per cm per milliampere if leakage were neglected. It will be observed that an almost linear relation exists between $1/\mu$ and D.C. magnetization. This discovery will be of great help in future designs of reactors and transformers where a D.C. magnetization takes place. (A.C. current in curve II is half the total current).

A set of four experimental curves—filament voltage vs. D. C. winding current—are given in Fig. 5. They have the same general nature as the theoretical curves in Fig. 5. The experimental points of the curves I and II are also plotted in Fig. 3. as small triangles and squares. It will be appreciated that the experimental points correspond to a curve for a secondary resistance lying between 2 and 2.5 ohms. The agreement between the theoretical and experimental values is good. The discrepancy that is observed is due to the following reasons :—

(1) The filament resistance is a variable one in the experimental case. The resistance of the ion-gauge tube filament varies with temperature. So it is smaller for a smaller voltage and greater for a larger one. The filament voltage in the experimental curves may therefore be expected to drop off more sharply and down to lower values than predicted by the theoretical curves.

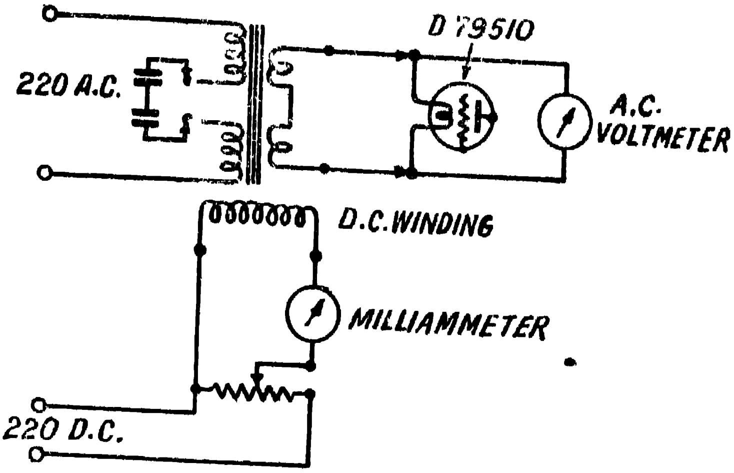

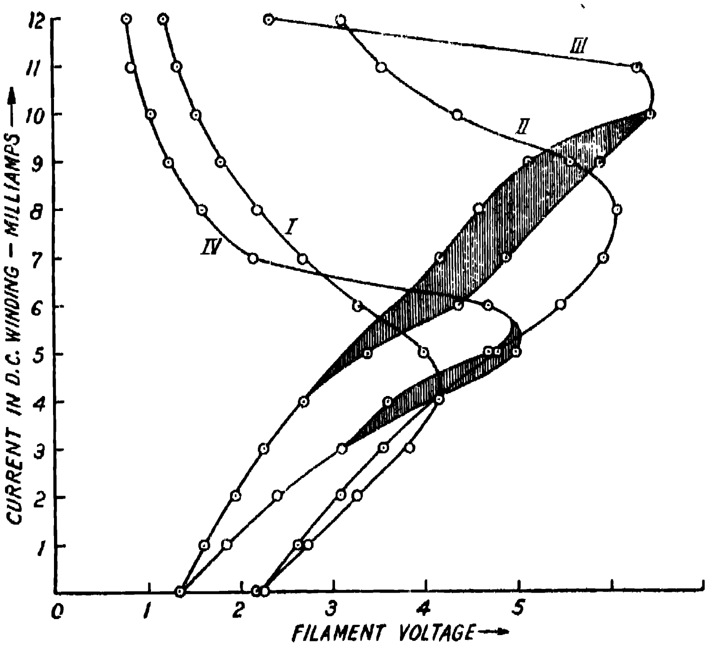

FIG. 5

Experimental curves for a saturable core transformer control circuit. Circuit, Ion gauge tube and transformer data given in Fig 1,

Curve I—for $c = \frac{1}{3}\mu f$, secondary turns 70
Curve II—for $c = \frac{1}{2}\mu f$, secondary turns = 70
Curve III—for $c = \frac{1}{2}\mu f$; secondary turns = 10
Curve IV—for $c = \frac{1}{3}\mu f$; secondary turns = 40

In the circuit of Fig. 1 with the constants for curve III, the stabilized value of the current is near about 10 5 m.A. With the constants of curve IV, the stabilized current is about 6 M.A. So, if it is desired to change the operating current of the ion-gauge tube, the resonating capacity may be changed to achieve this over a limited range. Shaded area in curves III and IV represent regions of oscillation.

(2) In the experimental case the A. C. permeability drops off beyond the resonance point by virtue of two causes

(*a*) the increasing D. C. magnetization.

(*b*) the reducing A. C. magnetization.

The latter is not taken into account in fixing the points for the experimental curves. Hence the experimental values of voltage are found to be smaller than the calculated ones for they actually correspond to lower values of μ.

(3) The effect of magnetic leakage is not taken into account in the calculations. As leakage increases with decrease of μ, the voltages observed are smaller than the calculated ones, in the region where μ is small.

STABILIZATION OF IONIZING CURRENT

The device will stabilize the ionizing current flowing also through the D. C. winding in the region where the secondary voltage decreases with increase of D. C. winding current. For, an increase in the ionizing current will also result in an increase of the D. C. winding current which will produce a decrease in the secondary voltage and thus the filament temperature and emission and *vice versa*. Thus a tendency of a change in the ionizing current will be suppressed. The stable point is given by the intersection of the filament voltage—emission current curve of the ion gauge tube with the secondary voltage—saturating current curve of the saturable core transformer circuit. Changes in the ionizing current may take place due to changes in pressure and composition of the gas in the ion-gauge tube and due to line voltage fluctuations. These will respectively modify the filament voltage—emission current curve of the ion gauge tube and the D. C. current—secondary voltage curve of the saturable core transformer circuit and so alter the stable point.

The stabilizing control will be more efficient if the slope of the secondary voltage—D. C. winding current be steep. Thus the control becomes increasingly efficient as we pass on to curves I, II, IV, III in order. It will be noticed from the theoretical as well as the experimental curves, that the slope is greater and stabilizing action more powerful for,

(*a*) a secondary load of higher resistance.

(*b*) a series capacity of ·5μf — which resonates the transformer at a permeability of 250-300.

(*c*) for a higher turns ratio.

Oscillation.—The experimental curves III and IV show that there is a region of oscillation—the D. C. winding current and the filament voltage (in the circuit of Fig. 5) oscillating at a frequency lying between 40 to 100 cycles per minute. Such a phenomenon was not reported by Overbeck and Meyer. It appears to be quite a common phenomenon when the resonance is sharp. It can be explained away in the following way :—

A. C. permeability depends on D. C. winding current ; A. C. permeability also depend on A. C. magnetization.

Further,

D. C. Flux density depends on D. C. winding current ; D. C. Flux density also depend on A. C. magnetization.

Thus a change in D. C. winding current will produce a change in A. C. permeability and a change in A. C. winding current and so a change in A. C. magnetization. The change in A. C. magnetization, will produce a change in D C. flux density, which may reinforce the original change in the D. C. winding current, and result in an oscillation of the D. C. winding current and an oscillation of the amplitude of the secondary voltage.

The period of oscillation will depend on :—

(*a*) Time taken for the establishment of a change in the A. C. winding current and consequent change in A. C. magnetization. In the resonant circuit formed by the A. C. winding with the capacity C some time must elapse before the current can alter its magnitude. This time is of the order of a fraction of a second.

(*b*) Time taken for the establishment of the current in the D. C. winding. This depends upon the time constant of the D. C. winding. This is also a fraction of a second.

The overall period is the sum of the two. It was found to lie between half a second to one and a half seconds depending upon whether load was connected to the secondary or not. This fits in well with what may be expected. The correctness of the explanation was further verified by putting a resistance in series with the D. C. winding. This shortened the time period as expected.

DESIGN OF THE TRANSFORMER

It was pointed out earlier that the stabilizing action becomes more perfect,

(*a*) with a secondary load of higher resistance,

(*b*) for a greater turns ratio, T,

(*c*) for a resonating permeability lying between 250-400.

The secondary load will have a higher resistance value if the eddy current losses are minimized. This may be achieved by using thin laminations of high specific resistance transformer sheets to form the core. Wooden core clamps should be used to eliminate eddy current losses in the clamps and also to reduce leakage of D. C. and A. C. magnetic flux. Leakage of both D. C. and A. C. flux lines tend to reduce the efficiency of control.

The turns ratio T cannot be increased indefinitely. With a greater value the secondary voltage will be smaller. Most useful design results when the maximum secondary voltage of the secondary voltage—D. C. winding current curve of the circuit coincides with the maximum rating of the ion gauge tube.

The capacity value chosen should be sufficiently large so that *resonance is possible, i.e.,* the reactive volt-amperes be several times (at least three) greater than the filament power. The dimensions of the transformer core should be big enough to secure the resonance inductance at a permeability not smaller than 250, otherwise the system will fail to give satisfactory stabilizing action.

The D. C. winding should have sufficient number of turns to reduce the a. c. permeability to values below the resonance permeability.

A method of step by step design of the transformer is outlined below:

1. Find out the maximum filament power (w) required by the ion-gauge tube.

2. Set upon a suitable value Q, for the ratio reactive volt amperes (W) to filament power (w). It should have a value not less than three for good stabilizing action.

3. The maximum voltage across the series capacity will then be approximately Q times the supply voltage. Calculate the capacity from the relation,

$$(QE)^2\, p.c. = Q.w$$

4. The maximum primary voltage is also QE approximately. The maximum secondary voltage is to be equal to the maximum rating of the Ion-gauge tube. So

$$\text{Turns ratio} = \frac{Q.\ E.}{\text{Max. rated ion tube filament voltage}}.$$

5. Calculate the size of the transformer from the relations

$$W = \tfrac{1}{2} pLI^2$$

and
$$\tfrac{1}{2}LI^2 = VB^2/8\pi\mu$$

where B is the flux density, μ the A. C. permeability and V the volume of iron in the A. C. limbs of the core.

So that
$$W = pVB^2/8\pi\mu$$

whence
$$V = W.8\pi\mu/pB^2 = 8Qw\pi\mu/pB^2$$

This sets the volume of iron in the A.C. limbs of the core and thus the size of the transformer.

V increases and so the size becomes greater as

(*a*) w—the filament power increases

(*b*) Q increases.

Since control becomes more efficient with higher values of Q, *efficient control means increased size.*

Smaller size results when the resonating permeability is small and B is large. But as has been remarked earlier, it is not practical to use μ values less than 250 and B greater than 10,000 gauss.

6. Calculate the number of turns required in the primary and secondary for the dimensions of the core (calculated in step 5) from the relations

(*a*) $\text{volts per turn} = \dfrac{4{\cdot}44\ B.\ A.\ f.}{10^8}$

where B = Maximum flux density in core.

A = Area of cross section of core.

f = supply frequency.

(*b*) Maximum primary voltage—Q. E.

(*c*) Maximum secondary voltage = Maximum rated ion tube voltage.

7. From the wire tables select suitable wire sizes for the primary and secondary. The maximum secondary current is equal to the maximum rating of the gauge tube filament. The maximum primary current is obtained from the relation

Maximum primary current = Q. E. *p*. c.

8. The D. C. winding of the transformer should be put on the central limb. This eliminates A. C. voltages from the D. C. turns. The central limb should have an area of cross-section approximately twice the outer A. C. limbs.

From the wire tables select the wire size for the D. C. winding. The current it has to pass is equal to the ionizing current of the ion-gauge tube. Calculate the number of turns that may be put in the space available. Hence calculate the resistance of the winding and also the D. C. voltage drop across it If this is excessive a thicker gauge must be used.

Steps 6, 7 and also 8 may point towards an increased size for the transformer. In that case the calculations are to be repeated assuming a greater value of resonance μ in step 5.

PERFORMANCE

The performance of an actual circuit is described in the curves of Fig. 5. The curves themselves cannot give an exact idea of the actual stabilization obtained against line voltage fluctuations and gas pressure variations. The variation of the ionizing current with line voltage fluctuations and gas pressure variations were therefore separately studied and the results are as follows :

1. For a change of line voltage from 226 volts to 240 volts, the change in the ionizing current was only 0.5 m. A. in 10.5 m. A. This variation of line voltage affected both the saturable core transformer circuit as well as the rectified D. C. supply for the ionizing current.

2. Change in the ionizing current was not discernible for gas pressure changes from the "blue glow" region (pressure higher than 10^{-3} mm.) to lower than 10^{-4} mm. However, the filament voltage dropped and glow of the filament disappeared as the vacuum worsened from 10^{-4} mm. to the "blue glow" region.

CONCLUSION

The circuits that appear to be generally adopted as a control circuit of ionizing current is some variation of the circuit described by Ridenour and Lampson (1937). This circuit uses many valves and components. The

The second division in the region 4800-2370A consists of diffuse bands which apparently occur in groups except for the continuum at 3416A and three other broad bands at 4747, 4662 and 4575A, which may also be regarded as continua (*vide* Papers I, II and III). These groups of diffuse bands, together with the continua can be explained as arising in stable states and having for their final levels different repulsive states. In general, the constituent bands of different groups are well separated from one another with wavenumber differences which approximately agree with the vibrational frequencies of the stable states that form the initial levels of these groups.

number of compon

the saturable core transformer. This makes

or carbon resistors to age and spoil performance.

The difficulty with this circuit is perhaps **the sat**

itself. It is not a component which may be readily **bought from**

However, construction of one even in the average **laboratory is not too** difficult. Any transformer manufacturer or rewinding shop can turn out these things (even a single unit) with very little difficulty. It will be found that the transformer is of rather big size and the condensers must be of high voltage. This may be considered a draw-back of this circuit. But again we find that a Ridenour Lampson circuit of equivalent performance could not be assembled in a smaller space and at a lower cost. It is expected that in *future the circuit will be adopted by manufacturers and experimenters as frequently as any other circuit.*

ACKNOWLEDGMENT

The authors are grateful to Prof. M. N. Saha, D.Sc., F.R.S., for his kind interest and continued encouragement during the progress of the work.

PALIT LABORATORY OF PHYSICS,
CALCUTTA UNIVERSITY.

REFERENCES

Hoag, J. B., and Smith N. M., (1936)—*Rev. Sci. Inst.*, **7**, 497.

Jay Cox. E. K., and Wienhart H. W., (1931)—*Rev. Sci Inst.*, **2**, 401.

Overbeck, W. P., and Meyer F. A., (1934)—*Rev. Sci. Inst.*, **5**, 287.

Rainwater, J., (1942)—*Rev. Sci. Inst.*, **13**, 118.

Ridenour, L. N., and Lampson C. W., (1937)—*Rev. Sci. Inst.*, **8**, 162.

Ridenour, L. N., (1941)—*Rev. Sci. Inst.*, **12**, 134.

and others may be due to the transitions which are theoretically possible, notably $0_u^+ (^1\Sigma_u^+) \rightarrow 1_g(^3\Pi_{1g})$; $1_g(^3\Pi_{1g}) \rightarrow 1_u(^3\Pi_{1u})$ and $1_g(^3\Pi_{1g}) \rightarrow 0_u^-$ $(^3\Pi_{0_u^-})$, where the three final levels dissociate into two $I(^2P_{\frac{3}{2}})$ atoms. (See Table III and Fig. 1).

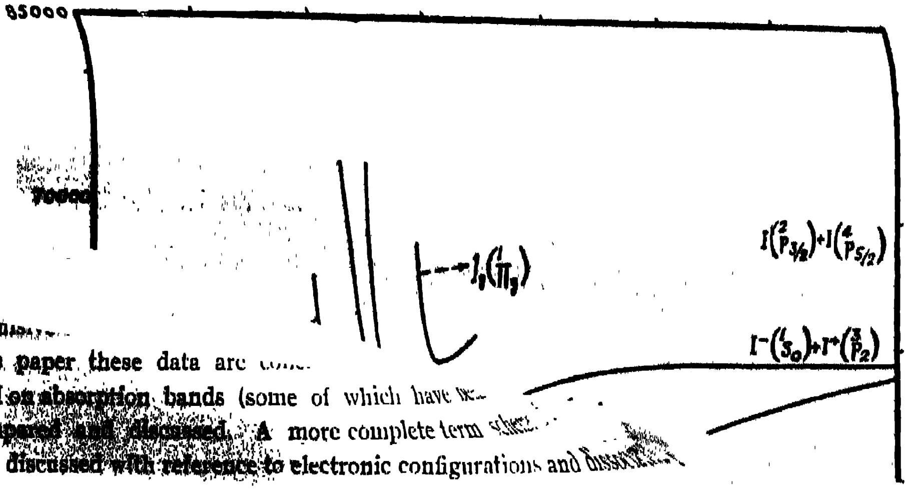

repuls…
this paper these data are …
and on absorption bands (some of which have …
compared and discussed. A more complete term …
and discussed with reference to electronic configurations and dissoc…

INTRODUCTION

In a series of papers entitled "Emission spectra of Halogens, Parts I-V" (Venkateswarlu, I-V, 1946-47)† detailed accounts of the emission bands of the fluctuation continuous or diffuse type observed, many of them for the first time have been given and interpretations of them are offered which have enabled us to obtain a fairly accurate *knowledge regarding the repulsive curves of the molecules. In the absorption spectrum of iodine, two systems of discrete bands have also been newly reported (Venkateswarlu 1946, 47, VI-VII).‡ All these data along with the knowledge previous to these investigations have* been utilised in the present paper in which it is proposed to give a general

The second division in the region 4800-2370A consists of diffuse bands which apparently occur in groups except for the continuum at 3416A and three other broad bands at 4747, 4662 and 4575A, which may also be regarded as continua (*vide* Papers I, II and III). These groups of diffuse bands, together with the continua can be explained as arising in stable states and having for their final levels different repulsive states. In general, the constituent bands of different groups are well separated from one another with wavenumber differences which approximately agree with the vibrational frequencies of the stable states that form the initial levels of these groups. The different stable states which are involved in giving rise to the bands in the region 4800 to 2370A are $\sigma_g, \pi_u^4, \pi_g^4, \sigma_u. 1_u^+ ({}^3\Sigma_u^+)$; $\sigma_g, \pi_u^4, \pi_g^3, \sigma_u^2. 1_g({}^3\Pi_{1g})$; $\sigma_g, \pi_u^4, \pi_g^3, \sigma_u. 0_u^+({}^1\Sigma_u^+)$; $\sigma_g, \pi_u^4, \pi_g^3, \sigma_u^2. 1_g({}^1\Pi_g)$ and $\{(\sigma_g^2, \pi_u^4, \pi_g^3. {}^2\Pi_{\frac{3}{2}g})\sigma_u^x\}\Pi_{2,1g}$ at 44900, 51528, 51683, 58572 and 56000 cm^{-1} with ω values 90, 215, 165, 120 and 360 cm^{-1} respectively (*vide* Fig. 1). Of these the first and the third are observed in absorption as forming the final levels of the Pringsheim-Rosen, Kimura-Miyanishi (P-R, K-M) bands between 2760-1950A (Paper VII) and Cordes bands (Paper VI) in the fluorite region 1950-1770A respectively. The other three states cannot combine with the ground state $\sigma_g, \pi_u^4, \pi_g^4; 0_g^+ ({}^1\Sigma_g^+)$ because of the $g \leftarrow\mid\rightarrow g$ rule, and as such they are not observed in absorption.

There are five groups with wavenumber differences of the order of 165 cm^{-1} among the constituent bands, which arise in the state $0_u^+ ({}^1\Sigma_u^+)$ at 51683 cm^{-1} with $\omega = 165{\cdot}1$ cm^{-1} (Paper I). These five groups have for their final levels the following repulsive state: $0_g^+ ({}^1\Sigma_g^+)$, $0_g^+ ({}^3\Sigma_g^-)$, $1_g ({}^3\Sigma_g^-)$, $1_g({}^1\Pi_g)$ and $0_g^+ ({}^3\Pi_{0_g^+}$(of which the first dissociates into $I({}^2P_{\frac{1}{2}}) + I({}^2P_{\frac{1}{2}})$ atoms at 27637 cm^{-1}; the second, third and fourth into $I({}^2P_{\frac{3}{2}}) + I({}^2P_{\frac{1}{2}})$ atoms at 20037 cm^{-1} and the fifth into $I({}^2P_{\frac{3}{2}}) + I({}^2P_{\frac{3}{2}})$ at 12437 cm^{-1}, (*vide* Fig. 1).

Five groups with a wavenumber separation of about 215 cm^{-1} among the constituent bands (Paper II), arise in the state $1_g ({}^3\Pi_{1g})$ with $\omega \backsim 215$ cm^{-1} at 51528 cm^{-1}. They have for their final levels the following repulsive states: $1_u({}^3\Sigma_u^+)$, $0_u^-({}^3\Sigma_u^+)$, $1_u({}^3\Delta_{1u}$), $2_u({}^3\Delta_{2u})$ and $1_u({}^1\Pi_u)$ of which the first two dissociate into two $I({}^2P_{\frac{1}{2}})$ atoms, and the remaining into $I({}^2P_{\frac{3}{2}}) + I({}^2P_{\frac{1}{2}})$ atoms. The state $\Pi_{2,1g}$ forms the initial state of the five groups of bands with a wavenumber separation of the order of 360 cm^{-1} among the constituent bands. The final levels of these groups are the same as those of the groups arising in the $1_g({}^3\Pi_{1g})$ state. The state $1_g({}^1\Pi_g)$ at 58572 cm^{-1} with $\omega \backsim 120$ cm^{-1} forms the initial level of three groups of bands from 2685-2448A which have for their final levels the same repulsive states as the last three groups arising in $1_g({}^3\Pi_{1g})$ and $\Pi_{2,1g}$ (Paper III). Between 2500-2370A there are some bands which are difficult to be measured and some of which may be extensions of the three groups of bands arising in $1_g({}^1\Pi_g)$

and others may be due to the transitions which are theoretically possible, notably O_u^+ $(^1\Sigma_u^+)\rightarrow 1_g(^3\Pi_{1g})$; $1_g(^3\Pi_{1g})\rightarrow 1_u(^3\Pi_{1u})$ and $1_u(^3\Pi_{1g})\rightarrow O_u^-$ $(^3\Pi_{0^-_u})$, where the three final levels dissociate into two $I(^2P_{\frac{3}{2}})$ atoms. (See Table III and Fig. 1).

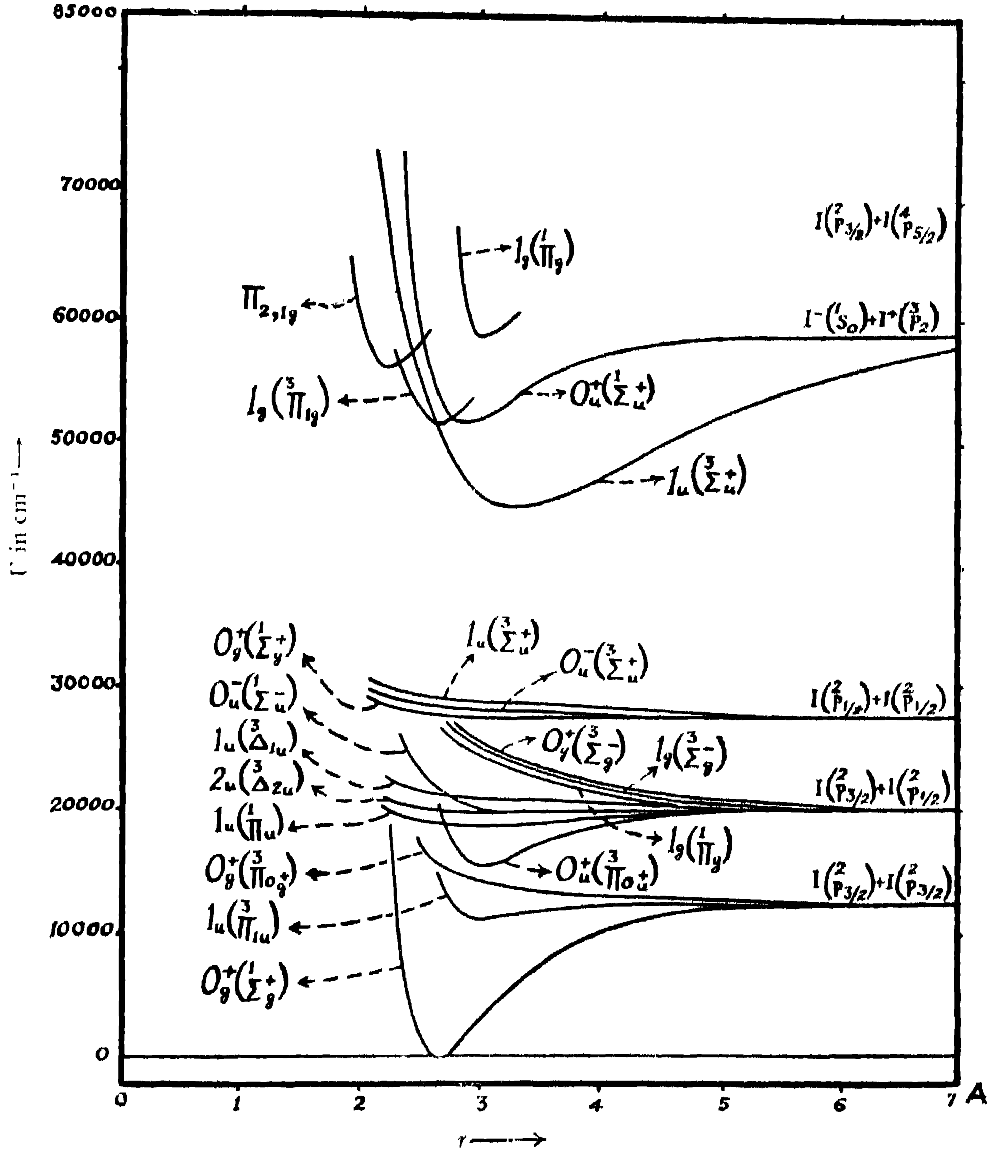

FIG. 1

Potential energy curves for I_2 molecule

Of all the various transitions, the following determine the coupling for iodine molecule as of case (*c*) type :

(1) O_u^+ $(^1\Sigma_u^+)\rightarrow O_g^+$ $(^3\Sigma_g^-)$; (3) 1_u $(^3\Sigma_u^+)\rightarrow O_g^+$ $(^3\Sigma_g^-)$

(2) O_u^+ $(^1\Sigma_u^+)\rightarrow 1_g$ $(^3\Sigma_g^-)$; (4) 1_u $(^3\Sigma_u^+)\rightarrow 1_g$ $(^3\Sigma_g^-)$.

The second division in the region 4800-2370A consists of diffuse bands which apparently occur in groups except for the continuum at 3416A and three other broad bands at 4747, 4662 and 4575A, which may also be regarded as continua (*vide* Papers I, II and III). These groups of diffuse bands, together with the continua can be explained as arising in stable states and having for their final levels different repulsive states. In general, the constituent bands of different groups are well separated from one another with wavenumber differences which approximately agree with the vibrational frequencies of the stable states that form the initial levels of these groups. The different stable states which are involved in giving rise to the bands in the region 4800 to 2370A are $\sigma_g, \pi_u^4, \pi_g^4, \sigma_u . 1_u^+ (^3\Sigma_u^+)$; $\sigma_g, \pi_u^4, \pi_g^3, \sigma_u^2 . 1_g(^3\Pi_{1g})$; $\sigma_g, \pi_u^4, \pi_g^4, \sigma_u . 0_u^+(^1\Sigma_u^+)$; $\sigma_g, \pi_u^4, \pi_g^3, \sigma_u^2 . 1_g(^1\Pi_g)$ and $\{(\sigma_g^2, \pi_u^4, \pi_g^3 . {}^2\Pi_{\frac{3}{2}g})\sigma_g^*\}\Pi_{2,1g}$ at 44900, 51528, 51683, 58572 and 56000 cm^{-1} with ω values 90, 215, 165, 120 and 360 cm^{-1} respectively (*vide* Fig. 1). Of these the first and the third are observed in absorption as forming the final levels of the Pringsheim-Rosen, Kimura-Miyanishi (P-R, K-M) bands between 2760-1950A (Paper VII) and Cordes bands (Paper VI) in the fluorite region 1950-1770A respectively. The other three states cannot combine with the ground state $\sigma_g, \pi_u^4, \pi_g^4$; $0_g^+ (^1\Sigma_g^+)$ because of the $g \leftarrow | \rightarrow g$ rule, and as such they are not observed in absorption.

There are five groups with wavenumber differences of the order of 165 cm^{-1} among the constituent bands, which arise in the state $0_u^+ (^1\Sigma_u^+)$ at 51683 cm^{-1} with $\omega = 165.1$ cm^{-1} (Paper I). These five groups have for their final levels the following repulsive state: $0_g^+ (^1\Sigma_g^+)$, $0_g^+ (^3\Sigma_g^-)$, $1_g (^3\Sigma_g^-)$, $1_g(^1\Pi_g)$ and $0_g^+ (^3\Pi_{0_g^+}$(of which the first dissociates into $I(^2P_{\frac{1}{2}}) + I(^2P_{\frac{1}{2}})$ atoms at 27637 cm^{-1}; the second, third and fourth into $I(^2P_{\frac{3}{2}}) + I(^2P_{\frac{1}{2}})$ atoms at 20037 cm^{-1} and the fifth into $I(^2P_{\frac{3}{2}}) + I(^2P_{\frac{3}{2}})$ at 12437 cm^{-1}, (*vide* Fig. 1).

Five groups with a wavenumber separation of about 215 cm^{-1} among the constituent bands (Paper II), arise in the state $1_g (^3\Pi_{1g})$ with $\omega \backsim 215$ cm^{-1} at 51528 cm^{-1}. They have for their final levels the following repulsive states: $1_u(^3\Sigma_u^+)$, $0_u^-(^3\Sigma_u^+)$, $1_u(^3\Delta_{1u})$, $2_u(^3\Delta_{2u})$ and $1_u(^1\Pi_u)$ of which the first two dissociate into two $I(^2P_{\frac{1}{2}})$ atoms, and the remaining into $I(^2P_{\frac{3}{2}}) + I(^2P_{\frac{1}{2}})$ atoms. The state $\Pi_{2,1g}$ forms the initial state of the five groups of bands with a wavenumber separation of the order of 360 cm^{-1} among the constituent bands. The final levels of these groups are the same as those of the groups arising in the $1_g(^3\Pi_{1g})$ state. The state $1_g(^1\Pi_g)$ at 58572 cm^{-1} with $\omega \backsim 120$ cm^{-1} forms the initial level of three groups of bands from 2685-2448A which have for their final levels the same repulsive states as the last three groups arising in $1_g(^3\Pi_{1g})$ and $\Pi_{2,1g}$ (Paper III). Between 2500-2370A there are some bands which are difficult to be measured and some of which may be extensions of the three groups of bands arising in $1_g(^1\Pi_g)$

and others may be due to the transitions which are theoretically possible, notably $0_u^+ \, (^1\Sigma_u^+) \rightarrow 1_g(^3\Pi_{1g})$; $1_g(^3\Pi_{1g}) \rightarrow 1_u(^3\Pi_{1u})$ and $1_g(^3\Pi_{1g}) \rightarrow 0_u^-$ $(^3\Pi_{0_u^-})$, where the three final levels dissociate into two $I(^2P_{\frac{3}{2}})$ atoms. (See Table III and Fig. 1).

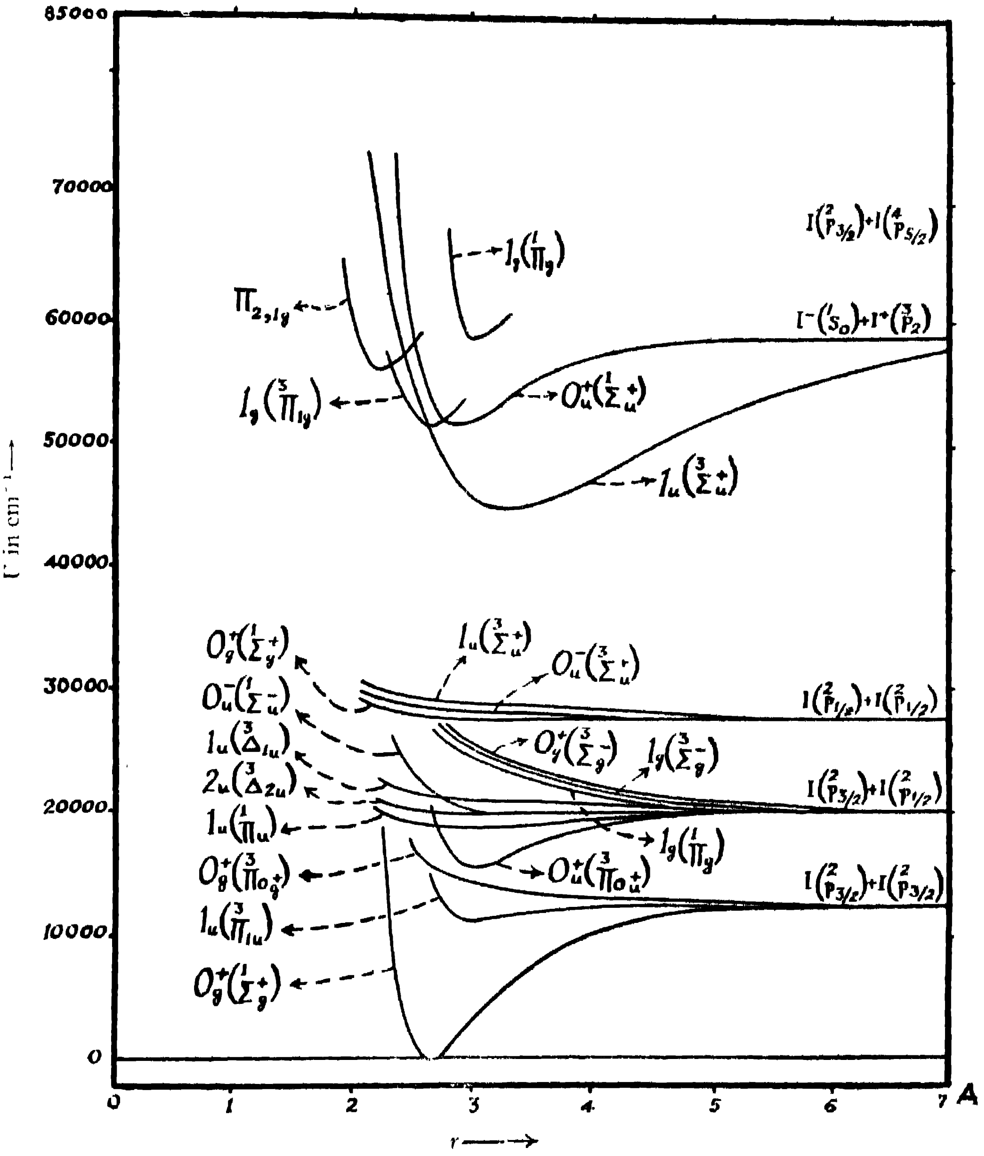

FIG. 1

Potential energy curves for I_2 molecule

Of all the various transitions, the following determine the coupling for iodine molecule as of case (*c*) type :

(1) $0_u^+ \, (^1\Sigma_u^+) \rightarrow 0_g^+ \, (^3\Sigma_g^-)$; (3) $1_u \, (^3\Sigma_u^+) \rightarrow 0_g^+ \, (^3\Sigma_g^-)$

(2) $0_u^+ \, (^1\Sigma_u^+) \rightarrow 1_g \, (^3\Sigma_g^-)$; (4) $1_u \, (^3\Sigma_u^+) \rightarrow 1_g \, (^3\Sigma_g^-)$.

Of these the first two represent the second and third groups arising in the state 0_u^+ ($^1\Sigma_u^+$) (Paper I) and the remaining two represent the two broad bands at 4747, 4662A arising in 1_u ($^3\Sigma_u^+$) (Paper III). These transitions would not have been possible if the coupling is case (*a*) or (*b*) type, because of $\Sigma^+ \leftarrow\!|\!\rightarrow \Sigma^-$ rule. The fact that these transitions are present is a clear proof of the existence of case (*c*) type coupling in these states of iodine. All the other transitions will be possible for case (*c*) type coupling as well as case (*a*) or (*b*) type coupling provided the singlet←|→triplet rule is not strict.

(2) *Bromine* : The spectrum of bromine, as that of iodine can also be divided broadly into two divisions (Paper IV). The first division between

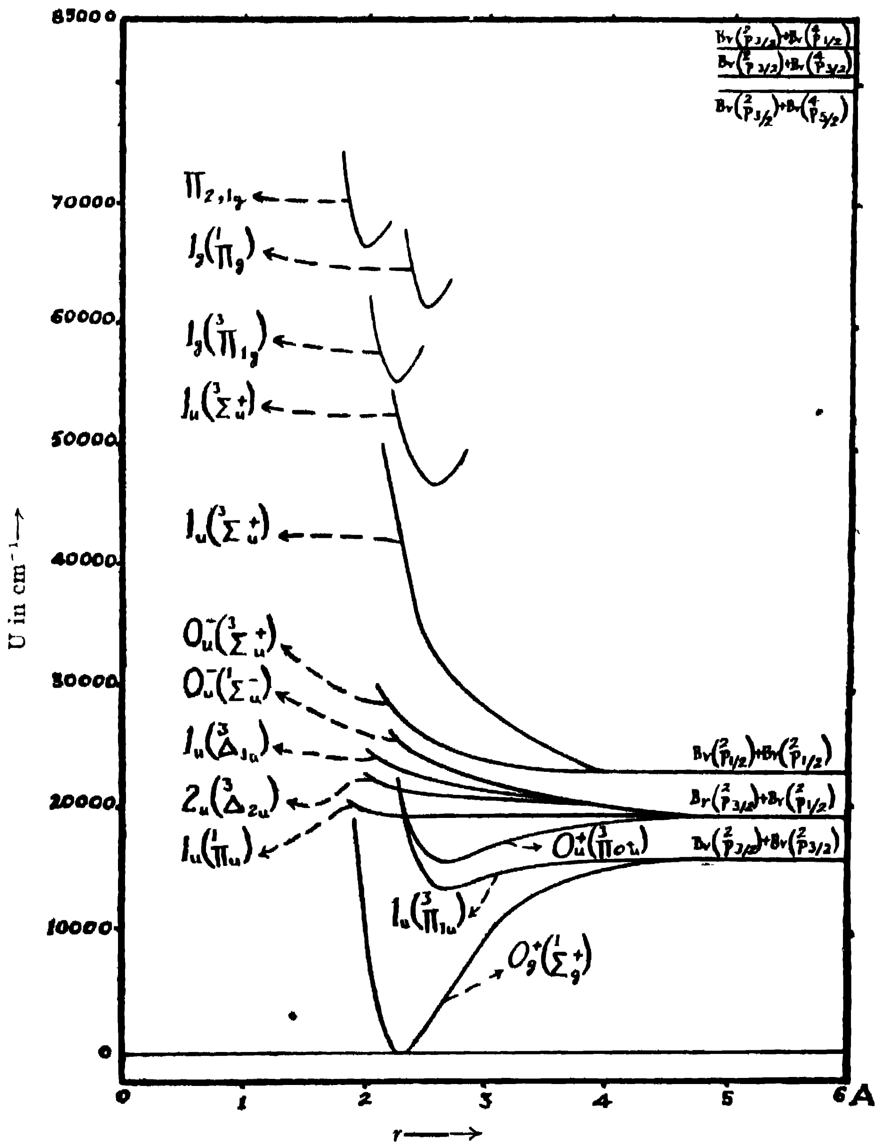

FIG. 2

Potential energy curves for Br_2 molecule

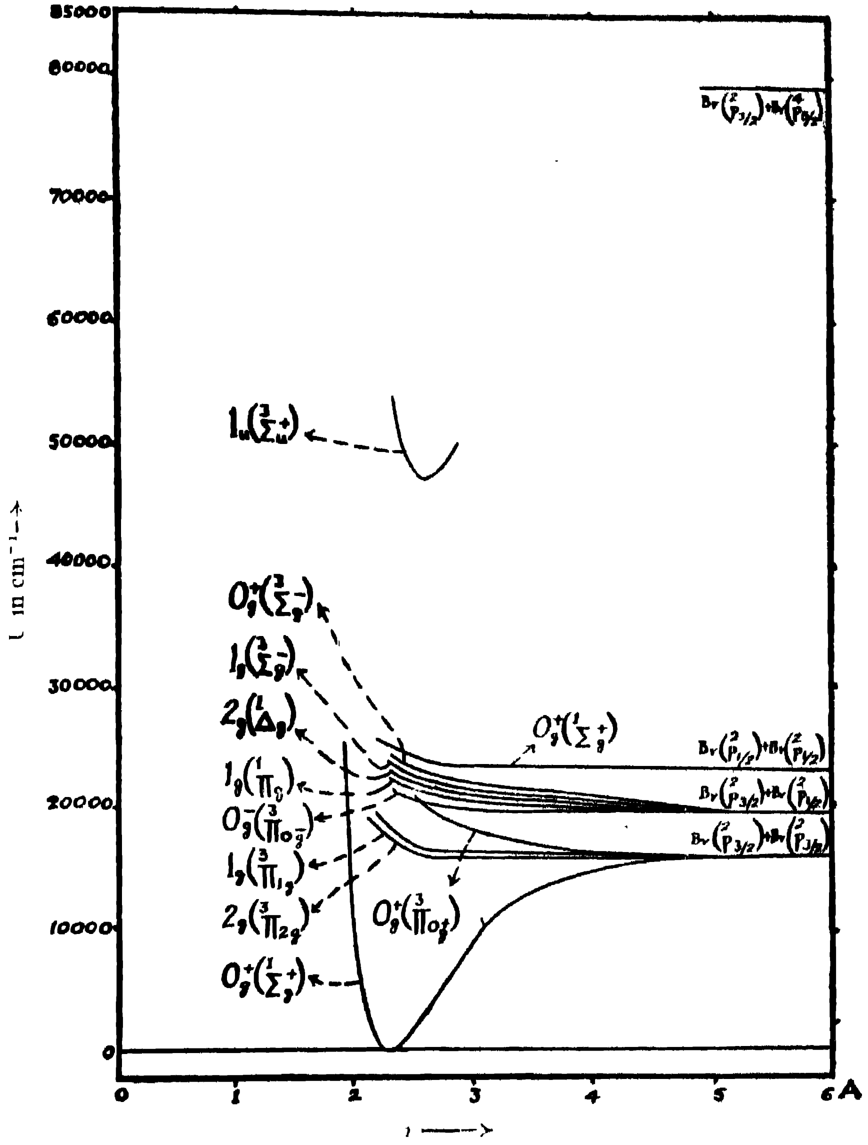

FIG. 3

Potential energy curves for Br_2 molecule

6700-5000A consists of bands degraded towards red. According to Uchida and Ota, these bands occur in two systems which arise from two different initial states having frequencies of 192 and 151 cm^{-1} to a common final level which is different from the ground state and which has a frequency of about 360 cm^{-1}. Unlike in iodine, therefore, these emission bands do not coincide with absorption bands. This fact is confirmed from the spectra taken for absorption and emission on a 3-prism glass Steinheil spectrograph Uchida and Ota indicate also the probability that the discrete emission bands may not be due to the neutral bromine molecule.

The second division from 4250 to 2000A consists of diffuse bands (Paper IV) which like those in iodine occur in groups, the difference being that the constituent bands in different groups in bromine overlap one another. In general, these groups appear as continua superposed by different maxima whereas the constituent bands of different groups in iodine are well separated and appear like sequences.

These groups also can be explained as arising in stable levels, and having repulsive states for their final levels. The various stable states are $1_u(^3\Sigma_u^+)$ at 47000 cm^{-1} and $1_g(^3\Pi_{1g})$, $1_g(^1\Pi_g)$ and $\Pi_{2,\,1g}$ with frequencies 330, 220 and 480 cm^{-1} respectively at 55534, 61444 and 66500 cm^{-1}. Of these four states only $1_u(^3\Sigma_u^+)$ at 47000 cm^{-1} can combine with the ground state O_g^+ $(^1\Sigma_g^+)$ and so we expect in the extreme quartz ultraviolet, absorption bands in bromine corresponding to P-R, K-M bands in iodine. In fact Aickin and Bayliss (1938) have indicated the presence of a weak band system accompanying the continuous absorption in the ultraviolet. As can be seen from the potential energy curves of bromine molecule (Fig. 2) the repulsive curve $\sigma_g^2, \pi_u^3, \pi_g^3, \sigma_u^2$. 1_u $(^3\Sigma_u^+)$ and the stable curve 1_u $(^3\Sigma_u^+)$ at 47000 cm^{-1} arising from the configuration σ_g, π_u^4, π_g^4, σ_u, run close together on the left hand side. So it is likely that the band absorption will be so overlapped by strong continuous absorption as not to be observed easily. Besides the four stable states observed in bromine, there is a fifth state O_u^+ $(^1\Sigma_u^+)$ occurring in absorption and emission in iodine. Probably the corresponding bands of bromine arising in O_u^+ $(^1\Sigma_u^+)$ lie in the vacuum ultraviolet region.

There are five groups arising in 1_g $(^3\Pi_{1g})$ with an average wavenumber separation of about 330 cm^{-1} among the constituent bands which represents the vibrational frequency of the initial state. These groups have for their final levels the repulsive states O_u^- $(^3\Sigma_u^-)$, O_u^- $(^1\Sigma_u^-)$, 1_u $(^3\Delta_{1u})$, 2_u $(^3\Delta_{2u})$ and 1_u $(^1\Pi_u)$ of which the first dissociates into $Br(^2P_{\frac{1}{2}}) + Br(^2P_{\frac{1}{2}})$ atoms at 23266 cm^{-1} and the remaining into $Br(^2P_{\frac{3}{2}}) + Br(^2P_{\frac{1}{2}})$ at 19581 cm^{-1}. The 1_g $(^1\Pi_g)$ state at 61444 cm^{-1} forms the initial level of four groups of bands with a wavenumber separation of 220 cm^{-1} among the constituent bands, (which represents the ω value of the initial state) and of a broad band at 20230 cm^{-1}. The final states of the four groups are the same as those of the second to fifth groups arising in 1_g $(^3\Pi_{1g})$ and the broad band has for its final level, $1_u(^3\Sigma_u^+)$ dissociating into $Br(^2P_{\frac{1}{2}}) + Br(^2P_{\frac{1}{2}})$ atoms, (*vide* Figs. 2, 3).

The $\Pi_{2,\,1g}$ state at 66500 cm^{-1} forms the initial level of the two groups of bands in the extreme ultraviolet region which have a wavenumber separation of about 480 cm^{-1} which roughly represents the vibrational frequency of the initial state. The final levels of these groups are the same as those of the last two groups arising in 1_g $(^3\Pi_{1g})$ state.

Finally the state 1_u $(^3\Sigma_u^+)$ at 47000 cm^{-1} forms the initial level for nine broad bands which are too broad and irregularly separated from one another to be regarded as a single group. These nine bands have for their final levels the following repulsive states: 0^+_u ($^1\Sigma^+_u$), 0^+_u ($^3\Sigma^-_u$), 1_u ($^3\Sigma^-_u$), 2_u ($^1\Delta_u$), 1_u ($^1\Pi_u$), 0^-_u ($^3\Pi_{0^-_u}$), 0^+_u ($^3\Pi_{0^+_u}$), 1_u ($^3\Pi_{1u}$) and 2_u ($^3\Pi_{2u}$). Of these the first dissociates into $Br(^2P_{\frac{1}{2}})+Br(^2P_{\frac{1}{2}})$ atoms. The five states from second to sixth, dissociate into $Br(^2P_{\frac{3}{2}})+Br(^2P_{\frac{1}{2}})$ and the last three into $Br(^2P_{\frac{3}{2}})+Br(^2P_{\frac{3}{2}})$. It should be noted that the transitions from the stable state to the second, third and fourth repulsive states will not be possible if there is case (*a*) or (*b*) type coupling, because of $\Sigma^+\longleftarrow$ and $\Sigma\longleftarrow|\longrightarrow\Delta$ rules and they will be possible only if there is case (*c*) type coupling. The existence of these transitions which alone explains the experimental data is a proof of the existence of the case (*c*) type coupling in these states of bromine molecule as in iodine where Ω becomes a good quantum number and Λ and Σ lose their significance.

(3) *Chlorine.*—The spectrum of chlorine, similarly to that of iodine and bromine can also be divided into two divisions (Paper V). The first division in the region 5000 to 3000A consists of discrete bands degraded towards red, only part of which have been analysed by Cameron and Elliot as due to Cl_2 (1937-38-39). The discrete emission bands, like those of bromine do not coincide with absorption bands. The second division in the region 3063-1850A consists of continuous bands which can be divided easily into three sets. Paper V deals with these bands. These three sets of continua arise in three different stable states 1_u ($^3\Sigma_u$), 1_u ($^3\Pi_{1u}$) and 1_u ($^1\Pi_u$) at 58000, 67700 and 75000 cm^{-1} respectively. The bands due to the state Π_2, $_{1u}$ which occur in bromine and iodine and those due to 0^+_u ($^1\Sigma^+_u$) which occur in iodine will probably lie in the vacuum region in chlorine.

The first set consisting of six continua between 3063-2715A will arise in 1_u ($^3\Sigma^+_u$) and will have for their final levels the following repulsive states: 0^+_u ($^1\Sigma^+_u$), 0^+_u ($^3\Sigma^-_u$), 1_u ($^3\Sigma^-_u$), 2_u ($^1\Delta_u$), 1_u ($^1\Pi_u$), 0^-_u ($^3\Pi_{0^-_u}$) of which the first dissociates into $Cl\ (^2P_{\frac{1}{2}})+Cl\ (^2P_{\frac{1}{2}})$ atoms at 21784 cm^{-1} and the remaining into $Cl\ (^2P_{\frac{3}{2}})+Cl\ (^2P_{\frac{1}{2}})$ at 20903 cm^{-1}. It should be mentioned that these six states can combine with 1_u ($^3\Sigma^+_u$) if there is case (*c*) type coupling. If the coupling is akin to case (*a*) type, transitions from 1_u ($^3\Sigma^+_u$) to the second, third and fourth states will not be possible because of $\Sigma^+\longleftarrow|\longrightarrow\Sigma^-$ and $\Sigma\longleftarrow|\longrightarrow\Delta$ rules. The six continua can, however, be explained according to case (*a*) type coupling as due to transitions from the stable state $^3\Sigma^+_u$ to the repulsive states $^1\Sigma^+$ $^1\Pi_u$, $^3\Pi_{0^-_u}$, $^3\Pi_{0^+}$, $^3\Pi_{1u}$, and $^3\Pi_{2u}$ of which the first dissociates into two $Cl\ (^2P_{\frac{1}{2}})$ atoms, second and third into $Cl\ (^2P_{\frac{3}{2}})+Cl\ (^2P_{\frac{1}{2}})$ atoms and the remaining two into two $Cl\ (^2P_{\frac{3}{2}})$ atoms at 20022 cm^{-1}.

1_u ($^3\Pi_{1u}$) at 67700 cm^{-1} forms the initial level of the seven continuous bands in the second set from 2565 to 2007A which have for their final levels the following repulsive states: 0^-_u ($^1\Sigma^-_u$), 1_u ($^3\Delta_{1u}$), 2_u ($^3\Delta_{2u}$), 1_u ($^1\Pi_u$),

0_u^- ($^3\Pi_{0^-u}$), 1_u ($^3\Pi_{1u}$) and 2_u ($^3\Pi_{2u}$) of which the first four dissociate into Cl ($^2P_{\frac{3}{2}}$) + Cl ($^2P_{\frac{1}{2}}$) and the remaining three into Cl ($^2P_{\frac{3}{2}}$) + Cl ($^2P_{\frac{3}{2}}$) atoms. 1_u ($^1\Pi_u$) forms the initial state of the three continua in the third set from 1997 to 1855Å which have their final levels the same as those of the first three bands of the second set. (*Vide* Figs. 4 and 5).

(4) *General Remarks*.—Taking the experimental results in the three spectra we come to the following conclusions: (*a*) the emission spectra of

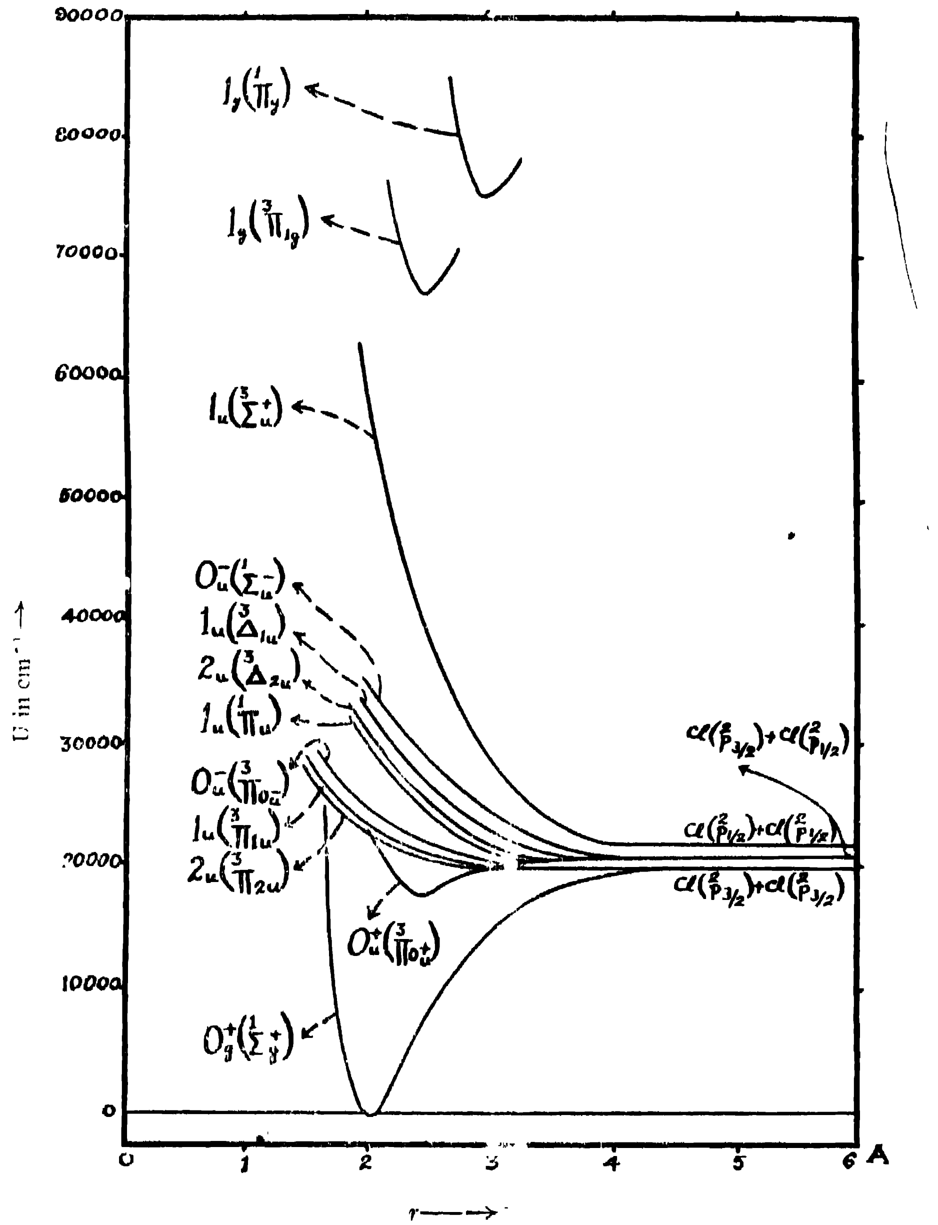

FIG. 4

Potential energy curves for Cl_2

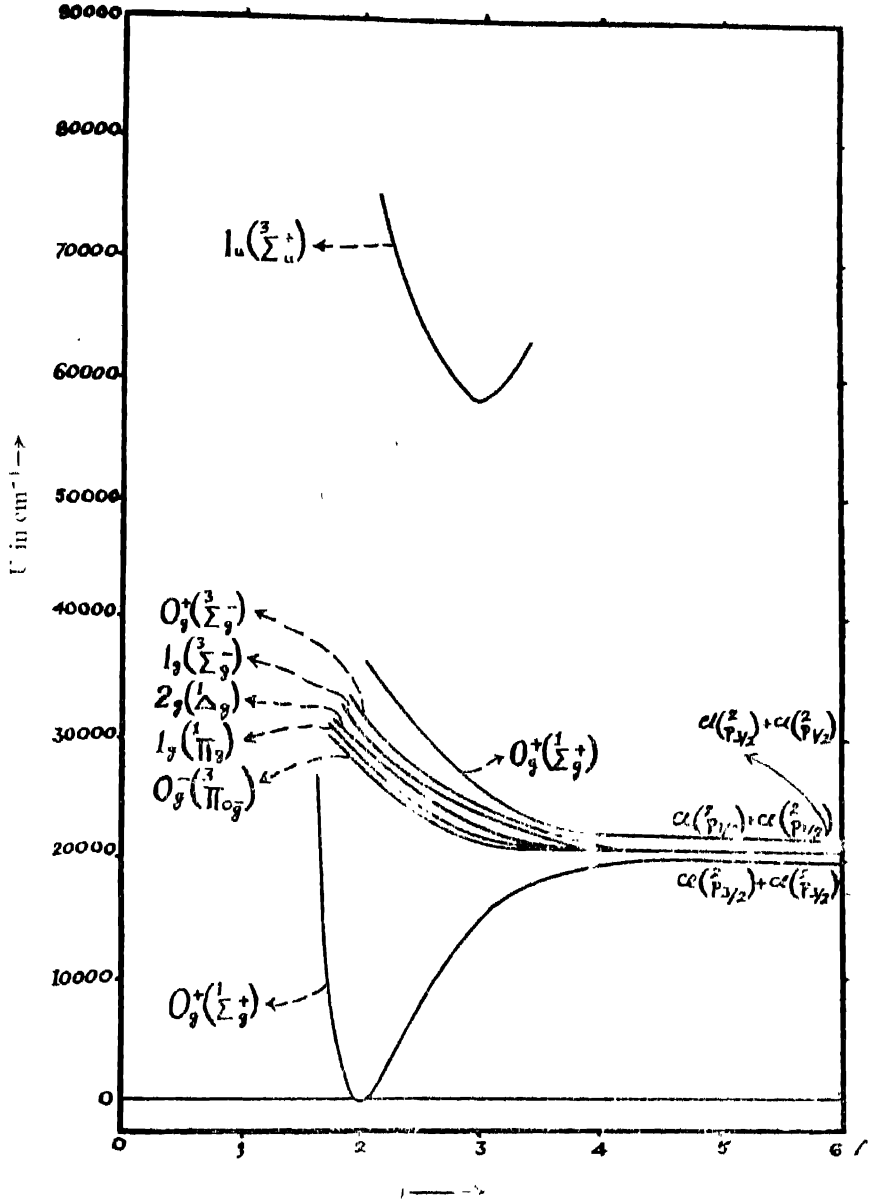

FIG. 5

Potential energy curves for Cl_2 molecule

these three molecules can be divided broadly into two divisions ; the first (visible region) consists of discrete bands degraded towards red, the origin of the bands being, however, different in the three cases. The second division consists of diffuse bands. (*b*) The three spectra apparently appear to be similar though the chlorine spectrum is displaced towards shorter wavelengths compared to that of bromine and the spectrum of bromine to that of iodine. (*c*) One striking difference in these three spectra is that the constituent bands in different groups in general are well separated from one another in iodine and appear like sequences; whereas in bromine they merge into one another and in fact the different groups of bromine generally appear as continua superposed by different maxima. This tendency appears to have been developed still further in chlorine where we get only broad continuous bands. (d) All the bands in the second division in the three molecules can be explained as arising in different stable states and having various repulsive states for their final levels. The difference in the nature of the diffuse bands in the three spectra can be well explained as due to the following nature of the repulsive states. Mostly the repulsive states in iodine are nearly flat and so the bands in every group due to transitions from different vibrational levels of the initial stable state to the flat potential energy curve are well separated from one another by wavenumber differences which represent the spacings of the vibrational levels in the initial state. In bromine the repulsive states are slightly steep and so different bands in every group overlap one another. Finally in chlorine the repulsive curves are still more steep and therefore, we get only broad continua.

(B) ABSORPTION SPECTRA

(1) *Iodine*: Iodine has absorption bands in the near infra-red region from 8375-9300A. They are due to a transition from the ground state $\sigma_g^2, \pi_u^4, \pi_g^4, 0_g^+ ({}^1\Sigma_g^+)$ having a frequency of 214 cm^{-1} to a state $\sigma_g^2, \pi_u^4, \pi_g^3, \sigma_u . 1_u ({}^3\Pi_{1u}$ at 11803 cm^{-1} with $\omega = 44$ cm^{-1}. There is a continuous maximum at 7370A observed by Brown (1931) which is due to a transition from the ground state to the repulsive part of $1_u ({}^3\Pi_{1u})$ state. There are also bands in the visible region, which converge to a limit at about 4995A followed by continuous absorption. The absorption curve has a maximum at 5200A according to Rabinowitch and Wood (1930). These bands together with the continuum are due to a transition from the ground state to $\sigma_g^2, \pi_u^4, \pi_g^3, \sigma_u ; 0_u^+ ({}^3\Pi_{0_u^+})$ at 15598 cm^{-1} with $\omega = 128$ cm^{-1}. Besides the bands in the visible and infrared, iodine shows absorption bands in the quartz ultraviolet and fluorite regions. Bands in the quartz ultraviolet region 2150-1950A are measured by Kimura and Miyanishi (K-M) and those from 2760 to 2090A by Pringsheim and Rosen (P-R). They have analysed these bands but a more satisfactory analysis is given by Sponer and Watson (1929). The analysis of Sponer and Watson is, however, not complete and does not include all the bands of Pringsheim and Rosen.

A complete review of the experimental work on absorption in the quartz ultraviolet is given in Paper VII. The analysis proposed there includes all the bands in the quartz ultraviolet (P-R, K-M bands). From this analysis it has been shown that the bands from 2760 to 1950A are due to a transition from the ground state to a state $\sigma_g, \pi_u^4, \pi_g^4, \sigma_u . 1_u ({}^3\Sigma_u^+)$ at 44900 cm^{-1} and with $\omega = 90$ cm^{-1}. The convergence limit of these bands by extrapolation comes out as 58000 ± 1000 cm^{-1}.

Cordes has measured a number of bands in the fluorite region from 1950 to 1500A. In the region 1770-1500A the bands are irregular and Cordes has grouped them into seven systems. The bands on the long wave side of 1770A up to 1950A are not analysed by Cordes, but he was of the opinion that they form the extension of K-M bands in the ultraviolet region. In Paper VI it is shown that they do not form the extension of K-M bands but that they belong to a separate system. The analysis of these bands proposed in that paper leads to the location of a new electronic level (O_u) at 51683 cm^{-1} with a frequency of 165 cm^{-1}. The dissociation limit of this state is at 59000 ± 800 cm^{-1} which coincides with that of the state 1_u ($^3\Sigma_u^+$). Both these states O_u^+ ($^1\Sigma_u^+$) and 1_u ($^3\Sigma_u^+$) thus arise from the same electronic configuration, *viz* :— σ_g, π_u^4, π_g^4, σ_u and have for their dissociation products two ions I^- ($^1S_0$) + I^+ ($^3P_2$).

The absorption data and molecular constants of iodine are given in Table I. Besides the bands in the regions given in Table I, I_2 shows absorption bands between 1770 and 1500A which have been grouped into seven systems by Cordes. He explained six of the systems as due to transitions from the ground level to $^3\Pi_{1u}$, $^3\Pi_{0u}$, $\Pi_{2,1u}$, $\Pi_{1,0u}$ and two other levels $^3\Pi_{1u}$ and $^3\Pi_{0u}$ above 56000 cm^{-1}. His analysis is, however, not satisfactory and these levels have not been observed in emission. Cordes has reported a continuum with a longwave end at 1505A which extends slightly to longer wavelengths with increase of pressure. This continuum, according to Cordes, is not similar to the short wave continuum of Br_2, Cl_2 and other halogens. (Probably this is due to a transition from the ground state to a steep potential energy curve possibly of σ_g, π_u^3, π_g^4, σ_u^2, 1_u ($^1\Pi_u$) dissociating into atomic products one of which will be an excited atom or into two ions I^- ($^1S_0$) + I^+ ($^3P_2$) at about 59000 cm^{-1}).

At very high temperatures Skorko (1933, 1934) has obtained two continua in absorption at 3413 and 3263A. By further increasing the temperature a number of diffuse narrow bands is developed overlapping the continua. The continuum at 3413A which is also observed in emission is due to a transition from the repulsive state O_u^- ($^1\Sigma_u^-$) to the stable state 1_u ($^3\Pi_{1u}$) at 51528 cm^{-1}. The continuum at 3263A is due to a transition from the repulsive part of the state O_u^+ ($^3\Pi_{0_u^+}$) to the state 1_u ($^3\Pi_{1u}$) at 51528 cm^{-1} (Paper VII). The states O_u^- ($^1\Sigma_u^-$) and O_u^+ ($^3\Pi_{0_u^+}$) are reached by the recombination of $^2P_{\frac{3}{2}}$ + $^2P_{\frac{1}{2}}$ iodine atoms into which the molecule dissociates at such high temperatures. A probable explanation for the diffuse bands which could be arranged into three groups has been suggested in Paper VII.

(2) *Bromine*.—Bromine, similar to iodine, is known to have two band systems in absorption, one in the region 7600-6450A and the other between 6950 and 5110A (Brown 1931, 1932). Darbyshire (1936) has reported extensions of both the systems. In the first system he has recorded bands up to 8150A (12221.5 cm^{-1}) and in the second system up to 8672A (11528 cm^{-1}). The

TABLE I

Region A.U.	Transition	ν_{00}, cm^{-1}	ω'_e	ω''_e	$\omega'_e x'_e$	$\omega''_e x''_e$	D'_0	D''_0	r''_e	r'_e
9300–8375	$\sigma^2_g, \pi^4_u, \pi^4_g\ 0^+_g(^1\Sigma^+_g) \rightarrow \sigma^2_g, \pi^4_u, \pi^3_g, \sigma_u\ 1_u(^3\Pi_{1u})$	11803	44	214.3	1.0	0.59	0.68	1.535	2.66	(3.2)
8600–4300	,, $\rightarrow$,, $0^+_u(^3\Pi_{0u})$	15598	128	,,	0.85	,,	0.85	,,	,,	3.01
2700–1950	,, $\rightarrow \sigma_g, \pi^4_u, \pi^4_g, \sigma_u\ 1_u(^1\Sigma^+_u)$	44900	90	,,	…	,,	1.9	,,	,,	3.33
1950–1770	,, $\rightarrow$,, $0^+_u(^1\Sigma^+_u)$	51683	165.1	,,	0.59	,,	1.95	,,	,,	2.8

TABLE II

Region	Electronic Transition	ν_{00}, cm^{-1}	ω'_e	ω''_e	$\omega'_e x'_e$	$\omega''_e x''_e$	D'_0	D''_0	r''_e	r'_e
8180–6450A	$\sigma^2, \pi^4_u, \pi^4_g\ 0^+_g(^1\Sigma^+_g) \rightarrow \sigma^2_g, \pi^4_u, \pi^3_g, \sigma\ 1_u(^3\Pi_1)$	13737	170.7	324.3	3.60	1.145	0.209	1.961	2.28	(2.64)
8672–5110A	,, $\rightarrow$,, $0^+_u(^3\Pi_{0^+_u})$	15840	167.9	,,	1.84	,,	0.459	,,	,,	(2.65)

first system is due to a transition from the ground state O_g^+ ($^1\Sigma_g^+$) to 1_u ($^3\Pi_{1u}$) at 13737 cm^{-1} and the second system to a transition from the ground state to O_u^+ ($^3\Pi_{0_u^+}$) at 15840 cm^{-1}. The bands in the second system have a convergence limit at 5107A after which they are followed by continuous absorption. This continuous absorption has, according to Acton, Aickin, and Bayliss (1936) two maxima at 4150A and 4050A In Paper IV it is suggested that the two may be due to transitions from the ground state to two repulsive states $1'_u$ ($^3\Delta_{1u}$) and 1_u ($^1\pi_u$) respectively. 4950A may also be considered as due to a transition from the ground state to the repulsive parts of 1_u ($^3\Pi_{1u}$) and O_u^+ ($^3\Pi_{0_u^+}$) which meet vertically above the minimum of the ground level (view of Darbyshire). In short, from the potential energy curves of bromine it is evident that the absorption maximum due to transitions from the ground state to the repulsive parts of 1_u ($^3\Pi_{1u}$) and O_u^+ ($^3\Pi_{0_u^+}$) and to 1_u ($^1\Pi_u$) and 1_u ($^3\Delta_{1u}$) lies between 5000 and 4000A which region is experimentally observed to be having continuous absorption. Though Acton, Aickin and Bayliss report two maxima and so many different views are expressed by different authors for their origin, probably it may not be easily possible to get the maxima due to the four transitions resolved and separately observed.

Besides the absorption in the visible region followed by a continuum, bromine shows a strong continuous absorption between 3000 and 1560A with a maximum at about 2250A (Cordes and Sponer (1930) Aickin and Bayliss, 1938). This continuum is explained in Paper IV as due to a transition from the ground state to a steep repulsive state $\sigma_g^2, \pi_u^3, \pi_g^3, \sigma_u^2\ 1_u\ (^3\Sigma_u^+)$ dissociating into two $^2P_{\frac{1}{2}}$ bromine atoms. The transitions of the two main systems in the visible region together with the molecular constants are given in Table II.

(3) *Chlorine*: Chlorine shows absorption bands only in the region 5760 to 4800A which are due to a transition from the ground state ($\omega=565$, $D=2.47$ e.v.) to O_u^+ ($^3\Pi_{0_u^+}$) state at 17711 cm^{-1} with a vibrational frequency of 261 cm^{-1} and $D_e=.39$ e.v. (Sponer). These absorption bands have a convergence limit at 4785A which is followed by a continuous absorption having a maximum at 3300A (Finkelnburg). This maximum is probably due to a transition from the ground to the repulsive state 1_u ($^1\Pi_u$). Besides the strong maximum, Aickin and Bayliss have indicated the probable presence of an extremely weak maximum at 4250A in the continuous absorption. If it is real, the secondary maximum is probably due to a transition from the ground state to 1_u ($^3\Pi_{1u}$). The secondary maximum may also be due to a transition from the ground state to the repulsive part of O_u^+ ($^3\Pi_{0_u^+}$). In fact what is said about the continuous absorption following the visible absorption bands of bromine will hold good for chlorine, *i.e.*, from the potential energy diagrams of chlorine we expect continuous maxima due to transitions from the ground state to 1_u ($^3\Pi_{1u}$), to the repulsive part of O_u^+ ($^3\Pi_{0_u^+}$) to

1_u ($^3\Delta_{1u}$) and to 1_u ($^1\Pi_u$) in the region 4800-3000A in which region a strong continuous absorption is observed. Probably it may not be easily possible to resolve these maxima.

Besides the absorption bands followed by continuous absorption already stated, chlorine shows a continuum below 1950A extending into the vacuum region. This continuous absorption similar to the corresponding absorption in bromine is due to a transition from the ground state to a repulsive state σ_g^2, π_u^3, π_g^3, σ_u^2; 1_u ($^3\Sigma_u^+$), dissociating into two $^2P_{\frac{1}{2}}$ chlorine atoms.

(C) ELECTRONIC CONFIGURATION AND ENERGY LEVELS OF HALOGEN MOLECULES

The configuration of all the halogen molecules can be represented by the 10 outer electrons of the np shell as $(\sigma_g np)^2$ $(\pi_u np)^4$ $(\pi_g np)^4$ where $n = 2$, 3, 4, and 5 for F_2, Cl_2, Br_2 and I_2 respectively. This configuration gives the term $^1\Sigma_g^+$ which is to be correlated with 0_g^+ of case (c) type and which represents the ground state of all the halogen molecules. Leaving off np which is common the ground state of the halogen molecules can also be generally represented as σ_g^2, π_u^4, π_g^4, 0_g^+ ($^1\Sigma_g^+$). The various excited states are then obtained by suitable excitation of the inner electrons. Thus by removing one π_g electron to the next state σ_u of the same shell we get two ungerade terms $^1\Pi$ and $^3\Pi$ which under case (c) type of coupling resolve into one (1) and four (0^+, 0^-, 1, 2) terms respectively. Similarly by the excitation of an electron in π_u and σ_g states various other terms are obtained. The nature and properties of these terms and their probable products of dissociation arrived at in the light of the observed experimental data are contained in Table III. The data regarding the observed stable states in the three molecules are included in Table IV.

Table III shows the electronic term scheme of halogen molecules. The electronic configurations, the electronic terms and their dissociation products, mean vertical energies estimated by Mulliken for I_2 and those estimated on similar lines for Br_2 and Cl_2 and the mean vertical energies obtained from experimental data are given. The estimated mean vertical energies for I_2, Br_2, and Cl_2, however rough they may be, will indicate in a right way the nature of all electronic states (except that of 1_u ($^3\Pi_{1u}$) dissociating into two $^2P_{\frac{3}{2}}$ atoms which is repulsive in Cl_2 and slightly stable in Br_2 and I_2 and which will be expected from the estimated energies to be repulsive in all the three molecules). For example, if the mean estimated vertical energy for a state is less than the energy of the dissociation products into which the particular state dissociates, we can say that the state will be stable; and if it is greater the state will be repulsive. This criterion is often experimentally available. Theoretically, another factor which counts in the nature of the relative stability of electronic states is the relative number of the so-called bonding (σ_g, π_u) and antibonding (σ_u, π_g) electrons, *i.e.*, of the two possible

Tern

Mean vertical energies						Electronic Configuration				
Experimental			Estimated							
I_2	Br_2	Cl_2	I_2	Br_2	Cl_2	σ_g	Π_u	Π_g	σ_u	Parity
			12.2	13	14.4	0	4	4	2	g
7.5			7.3			2	3	4	σ_g	u
7.3			8.8	9.5	10.5	1	3	4	2	u
0	8.2					2	4	3	σ_g'	g
8	7.2	8.8	8.1	8.7	9.6	1	4	3	2	g
1	6.5	7.2	6.1	6.5	7.2	1	4	4	1	u
.	...	.	5.6	6.0	6.6	2	2	4	2	g
0	4.5	5.2	4.9	5.2	5.7	2	3	3	2	u
3	3.1	4.0	4.2	4.4	4.8	2	4	2	2	g
4	2.5	3.3	2.8	3.0	3.3	2	3	4	1	g
9	2.0	2.8	2.1	2.2	2.4	2	4	3	1	u
	...	...	...	...	...	2	4	4	0	g

* (C)—State established by

† Stable in I and Br and

TABLE IV

Stable Electronic States of Halogens Occurring in Emission of Diffuse or Fluctuation Bands

Electronic configuration	Electronic term	Iodine		Bromine		Chlorine	
		ν cm^{-1}	ω	ν cm^{-1}	ω	ν cm^{-1}	ω
$\{(\sigma_g^2, \pi_u^4, \pi_g^3, {}^2\Pi_{g\frac{3}{2}})\sigma^+\}$	$\Pi_{2, 1g}$	56000	360	66500	480	...	...
$\sigma_g, \pi_u^4, \pi_g^3, \sigma_u^2$	$1_g\ ({}^1\Pi_g)$	58578	120	61444	220	75000	...
,,	$1_g\ ({}^3\Pi_{1g})$	51528	215	55534	330	67700	...
$\sigma_g, \pi_u^4, \pi_g^4, \sigma_u$	$0_u^+\ ({}^1\Sigma_u^+)$	51683	165	...	...		...
,,	$1_u\ ({}^3\Sigma_u^+)$	44900	90	47000	...	58000	...
ground state: $\sigma_g^2, \pi_u^4, \pi_g^4$	$0_g^+\ ({}^1\Sigma_g^+)$	0	214	0	324	0	565

TABLE V

Figures represent ν cm^{-1}

Molecule	Average energies of the unstable states dissociating into $^2P_{\frac{3}{2}}+{}^2P_{\frac{3}{2}}$ atoms A	Energy of the dissociation products $^2P_{\frac{3}{2}}+{}^2P_{\frac{3}{2}}$ B	(A−B) indicating repulsive nature	Average energies of the states dissociating into $^2P_{\frac{3}{2}}+{}^2P_{\frac{1}{2}}$ C	Energy of the dissociation products $^2P_{\frac{3}{2}}+{}^2P_{\frac{1}{2}}$ D	(C−D) indicating repulsive nature	Average energies of the states dissociating into $^2P_{\frac{1}{2}}+{}^2P_{\frac{1}{2}}$ E	Energy of the dissociation products $^2P_{\frac{1}{2}}+{}^2P_{\frac{1}{2}}$ F	(E−F) indicating repulsive nature
I_2	13400	12437	963	21900	20037	1863	28244	27637	507
Br_2	17694	15896	1798	22070	19581	2489	32500	23266	9234
Cl_2	23000	20022	2978	29078	20903	8175	47500	21784	25716

states the one having the greater number of bonding electrons will be the more stable. The conception of stability on the pair-bond theory also leads to similar results.

From experimental data it is observed that the repulsive nature of most of the unstable states increases from I_2 to Cl_2, the relative change being, however, great for the states dissociating into ${}^2P_{\frac{1}{2}} + {}^2P_{\frac{1}{2}}$ atoms. Table V indicates the average energy of the unstable states and of the dissociation products into which the unstable states dissociate. The difference in energy indicates the repulsive nature of the states.

All the unstable states dissociate into ${}^2P_{\frac{3}{2}} + {}^2P_{\frac{3}{2}}$, ${}^2P_{\frac{3}{2}} + {}^2P_{\frac{1}{2}}$, ${}^2P_{\frac{1}{2}} + {}^2P_{\frac{1}{2}}$ atoms. The energy of the molecular terms increases from I_2 to Cl_2. The energy of the dissociation products ${}^2P_{\frac{1}{2}} + {}^2P_{\frac{1}{2}}$ decreases from I_2 to Cl_2 and that of ${}^2P_{\frac{3}{2}} + {}^2P_{\frac{1}{2}}$ is practically the same for the three molecules. Therefore it is natural to expect the repulsive nature to increase from I_2 to Cl_2, the relative change being to some extent greater for the states dissociating into ${}^2P_{\frac{1}{2}} + {}^2P_{\frac{1}{2}}$ atoms. As stated above, this is what we observe from the experimental results. The energy of the dissociation products ${}^2P_{\frac{3}{2}} + {}^2P_{\frac{3}{2}}$, however, increases from I_2 to Cl_2 as does also the energy of the molecular terms. Hence large variations in the repulsive nature of the curves in the three molecules here is not expected. But, however, there is a slight increase in the repulsive nature from I_2 to Cl_2 which is due to the reason that the increase in the molecular energy from I_2 to Cl_2 is slightly greater than the increase in the energy of dissociation products from I_2 to Cl_2.

NOTES FOR TABLE III

Column 7 shows the various electronic configurations of the halogen molecules in terms of the ten outer electrons which are of *np* shell. σ^1 represents an electron that has gone to $(n+1)$s shell. Eighth column shows the parity of the electronic terms that can be derived from the respective configurations. They are even (gerade) if the number of the odd electrons (σ_u, π_u) is even, whereas they are odd (ungerade) if the number of odd electrons is odd. Ninth column gives the electronic terms that can be derived from the respective configurations, according to case (*a*) type coupling, and tenth column shows the terms according to case (*c*) type coupling, and they are written in a line with those of case (*a*) type with which they should be correlated. Eleventh column shows the dissociation products into which the electronic terms will dissociate. *aa* means np^5 (${}^2P_{\frac{3}{2}} + {}^2P_{\frac{3}{2}}$) atoms, *ab* represents np^5 (${}^2P_{\frac{3}{2}} + {}^2P_{\frac{1}{2}}$) atoms and *bb* represents np^4 (${}^2P_{\frac{1}{2}} + {}^2P_{\frac{1}{2}}$) atoms, ex represents excited atoms or ions.

The term scheme here is practically the same as that worked out by Mulliken (1934) for I_2, except that the following few states are now found to have dissociation products of greater energy than those predicted by Mulliken. Thus 1_u (${}^3\Sigma_u^+$), 0_u^- (${}^3\Sigma_u^+$) dissociate into ${}^2P_{\frac{1}{2}} + {}^2P_{\frac{1}{2}}$ instead of ${}^2P_{\frac{1}{2}} + {}^2P_{\frac{3}{2}}$ atoms ; 1_u (${}^1\Pi_u$) and 0_u (${}^1\Sigma_u^-$) into ${}^2P_{\frac{1}{2}} + {}^2P_{\frac{3}{2}}$ instead of ${}^2P_{\frac{3}{2}} + {}^2P_{\frac{3}{2}}$ atoms. It may be mentioned, however, that Mulliken has indicated that there is always a possibility that the state may tend to dissociate into products of more energy than those predicted by him. Besides the above four states, σ_g, π_u^4, π_g^4, σ_u, 1_u (${}^3\Sigma_u^+$) dissociates into excited neutral atoms or ions, instead of two ${}^2P_{\frac{1}{2}}$ atoms (*bb*). This also has been already foreseen by Mulliken. for I_2, case (c) type component of ${}^1\Sigma_u^+$ of the configuration σ_g, π_u^4, π_g^4, σ_u may dissociate into two atoms at least one of which may not be np^5 ${}^2P$ type in order to avoid crossing a similar curve 1_u from the configuration σ_g^2, π_u^3, π_g^4, σ_u.

The nature of the electronic states is indicated in column 13. Fourteenth column gives the names of the molecules in which the respective states are observed The first three columns deal with the average vertical energies of the molecular terms from the experimental data. For molecular terms having stable states, the position of the stable levels give the vertical energies of the terms For those terms giving repulsive states, the heights of the repulsive curves vertically above the ground state are taken to represent their vertical energies. So the vertical energies for different observed terms arising from a particular configuration, are known and their average is taken to represent the mean excitation energy. In this way the average energies are given for the three molecules in the first three columns.

Fourth column gives the mean energy values for I_2 estimated by Mulliken by taking that the excitation energy for $\pi_g \rightarrow \sigma_u$ as 2.1 volts, $\sigma_g \rightarrow \sigma_u$ as 6.1, and $\pi_u \rightarrow \pi_g$ as 0.7 volts. 2.1 volts was based on the visible absorption bands, 6.1 was a rough value based on the bands in the quartz ultraviolet region and 0.7 was a guess Following similar lines the mean energies have been estimated for Br_2 and Cl_2 in fifth and sixth columns. For Br_2 the energy for $\pi_g \rightarrow \sigma_u$ is 2.2, $\sigma_g \rightarrow \sigma_u$ is 6.5 and $\pi_u \rightarrow \pi_g$ is .8 and for Cl_2 $\pi_g \rightarrow \sigma_u = 2.4$, $\sigma_g \rightarrow \sigma_u = 7.2$ and $\pi_u \rightarrow \pi$, is 0.9. The values for $\pi_g \rightarrow \sigma_u$ are based on visible absorption bands, $\sigma_g \rightarrow \sigma_u$ based on the position of the level σ_g, π_u^4, π_g^4, σ_u, 1_u (${}^3\Sigma_u^+$) and $\pi_u \rightarrow \pi_g$ value is a guess as that of I_2.

PHYSICS DEPARTMENT,
HINDU UNIVERSITY, BENARES.

REFERENCES

Acton, Aickin and Bayliss (1936), *Jour Chem Phys.*, **4**, 474.

Aickin and Bayliss (1937), *Trans. Farad. Soc.*, **33**, 1333

,, (1938), *ibid*, **34**, 1371.

Brown (1931), *Phys Rev* , **38**, 709 and 1187.

,, (1932), *ibid*, **39**, 777.

Cameron and Elliot (1937), *Proc. Roy. Soc. Lond.*, **158A**, 681.

,, (1938), *ibid*, **164A**, 531.

,, (1939), *ibid*, **169A**, 463.

Cordes (1935), *Zeit. fur Phys.*, **97**, 603.

Cordes and Sponer (1930), *Ibid*, **63**, 334.

Darbyshire (1936), *Jour. Chem. Phys.*, **4**, 747.

,, (1937), *Proc. Roy. Soc. Lond.*, **159A**, 93.

Finkelnburg (1938), Kontinuerliche Spektren pp. 161, 295.

Kimura and Miyanishi (1929), *Sc. Papers, Inst. Phys. Chem. Res.* (Tokyo) **10**, 33.

Mulliken (1934), *Phys. Rev.*, **46**, 549

,, (1940), *ibid*, **57**, 500.

,, (1936), *Jour. Chem Phys.*, **4**, 620.

Pringsheim and Rosen (1928), *Zeit. fur Phys* , **50**, 1.

Rabinowitch and Wood (1936), *Trans. Farad. Soc.*, **32**, 540.

Skorko (1933), Nature, **131**, 366.

,, (1934), *Acta Physica Polonica*, **3**, 191.

Sponer (1935), Molekülspektren (I).

Sponer and Watson (1929), *Zeit. fur Phys.*, **56**, 184.

Uchida and Ota (1928), *Jap. Jour. Phys.* (Tokyo), **5**, 59

Venkateswarlu :—

(I) 1946, *Proc. Ind. Acad. Sc.*, **24A**, 480.
(II) 1947, *ibid*, **25A**, 119.
(III) ,, *ibid*, **25A**, 133.
(IV) ,, *ibid*, **25A**, 138.
(V) ,, *ibid*, 26A, 22.
(VI) 1946, *ibid*, **24A**, 473.
(VII) 1947, *Ind. Jour. Phys.*, **21.**

THE PURIFICATION OF CARBON RODS FOR SPECTROGRAPHIC ANALYSIS BY CATHODE LAYER ARC

By B. MUKHERJEE

(*Received for publication, March 10, 1947*)

(Plate III)

ABSTRACT Different methods of purification of carbon rods which can be used as electrodes in the carbon arc cathode layer method of spectrographic analysis have been studied and suitable conditions for purification have been worked out by combinations of both chemical and thermal methods and by the method of resistance heating as employed by Gatterer. The degree of purification of the carbon rods has always been studied in the E_1 spectrograph with Twyman-Simeon lens arrangement by the cathode layer method with an arc current of 11 amp. at 220 volts, D C.

INTRODUCTION

In the carbon arc cathode layer method of spectrographic analysis developed by Mannkopff and Peters (1931) carbon electrodes of very high purity must have to be used. The line spectra of most elements in the cathode layer are 10 to 100 times stronger than in the main arc gas column (Strock, 1936). Spectrum lines of the impurities in concentrations down to 0.0001% (a concentration of 0.0001% in 1 mg. is 10^{-9} gm.) present are clearly recorded in the cathode layer photograph. Lines of the impurities below this amount also distinctly appear in the region adjoining the cathode. These requirements are not satisfied by the methods of purification generally followed.

The methods of purification developed so far can be classified broadly under two heads, *viz.* (1) method of chemical treatment followed by heat treatment and (2) method of resistance heating under heavy current. Early investigators first tried to purify carbon rods by subjecting them to heat treatment either in vacuum or in atmospheres of certain gases, and later, chemical treatment was combined with heat treatment.

Moissan obtained graphite from impure carbon rods by the method of electric arc treatment and observed that the graphite so obtained was purer the higher the temperature in the arc. Lebeau and Picon (1924) started with graphite containing 0.1 to 0.2% ash and after heating it for three hours in vacuum at 2000°C obtained graphite containing only 0.005% to 0.006% ash. They further observed that graphite containing sulphurous matters could not be purified by heating it even at 2200°C, and impurities amounting to 0.185% persisted after this heat treatment. Heyne (1930) tried to purify carbon rods by heating them in an electric tube furnace at 2500°C-3000°C in atmospheres of air, nitrogen and hydrogen. He observed that even at 3000°C Ca, Mg, Ti, V and above all B were not eliminated completely. He also found that the rods heated at 2000°C for 15 minutes in an atmosphere of Cl_2 were superior to those heated at 3000°C in the atmosphere of N_2 and H_2. Zurer and Treadwell (1935) purified parts of carbon electrodes by arcing in an atmosphere of nitrogen or argon containing 5% chlorine. The best purification was obtained by arcing for 3 minutes, but ultimate lines of Mg, Ca, Co and B were found to be present in the spectrum of the arc formed between carbon rods thus purified. Standen and Kovach (1935) worked out two methods for the elimination of impurities except Si and B. The chemical treatments followed in the second method were found to be satisfactory and were developed in the present investigation. Next Staud (1938) tried to purify carbon rods by first treating them in acids and then heating in oxy-gas burner He tried to remove Si by treating the carbon rods in hydrofluoric acid but the method proved a failure. Pierce, Torres and Marshall (1940) tried to purify Acheson graphite rods by refluxing them first in nitric and hydrochloric acids and then in 6M hydrochloric acid. Graphite thus purified contained B, Si, Cu, Ca, Mg and Na. The amount of Cu, Na, Mg and Ca was, however, reduced greatly on arcing the rods at 10 amps for 1 minute. The spectrographic examination of the purified carbon rods was not carried out so far by the sensitive cathode layer method.

As regards the second method, *viz.*, that of resistance heating, Russanow (1934) first observed that by resistance heating the purification began at 2250°C and when the temperature went up to even 3000°C traces of Ca, Mg and B persisted, allowing the maximum time of heating to be 3 minutes. Preuss (1935) developed the method of passing currents of 180A-200A through carbon rods 35 cm. in length and 5 mm. in diameter placed in vertical position. Traces of impurities of Ca, Mg, Ti, Al, Fe, Si, B and Ba were still found to be present. Gatterer (1941) passed currents of 300-320A maximum at 70 volts for 30-60 seconds through carbon rods 14 cm. in length and 6 mm. in diameter, held between graphite blocks by a spring arrangement to allow free expansion. For uniform heating a weak current of air was blown during heating. The maximum temperature attained was about 3000°C but still traces of B, Cu, Mg, Ca, Ti and V were present in the purified product, Hoogland (1946) passed still higher current *e.g.*, 400-650A maximum at 30-60 V for 15-60 seconds through carbon rods held horizontally with proper arrangement for free expansion. The main advantage of the horizontal position of the carbon rod was that in the direction of the length the rod not being irregularly heated, the extra cooling by the current of air as used by Gatterer was avoided. The main disadvantage during heating was that the long carbon rod (200 mm. in length, 7 mm. in diameter) which became soft at high temperature attained sagged a little. Starting with " Siemens-Plania Superbio Negative Homogen Kohle " carbon the best product was obtained with a maximum current of 650A passed for 60 secs. The purified carbon rods were analysed in the Hilger-Fully spectrograph by the cathode layer method with a current of 5.5A and a separation between the electrodes of 5 mm. in the region 2450A°-3000A and his results of analysis are given in Table 2. Trombe, Foex and Bardet (1945) obtained carbon rods of very high purity by the method of resistance heating with a current of 600A maximum (temperature maximum 2050°C) passed through carbon rods (length 300 mm. diameter 8 mm.) for 5 minutes in the atmosphere of nitrogen, hydrogen and also air in a specially constructed chamber. But the method of analysis of the purified carbon rods was not the sensitive cathode layer method. The light of the arc was photographed in the Hilger large dispersion quartz spectrograph for 1 min., the arc functioning between carbon electrodes placed horizontally at 12 amps., 40 volts.

The object of the present investigation was to make an attempt to develop a method combining chemical treatment with heat treatment for the purification of carbon rods and to examine its purity by the cathode layer method. It was further intended to investigate under what conditions the method of resistance heating give the best results.

EXPERIMENTAL

(A) *Chemical method combined with heat treatment*

In the present investigation "Kino-Homogen" (Germany) carbon rods were used as the starting material The spectrum of the impurities in a heavily exposed cathode layer photograph in the region 2500A°-3500A° of the carbon electrodes under a current of 11 amps. at 220 V revealed the presence of the following impurities: Fe, B, Si, Cu, Ni, Ti, Al, Mg, Na, Ca, Mn in large amounts and Ag, V, Zn, Bi, Cd, Sn, Ga, Pb, Cr, As, K and Co in small traces. (See Plate III).

The carbon rods were each 20 cm. in length and 7 mm. in diameter. Each was cut into three pieces and 100 such pieces were boiled in 1 : 1 mixture of concentrated HCl and HNO_3 for 5 hours in a flask, fitted with a reflux condenser. The acids were then replaced by fresh quantity and boiled for 4 hours. The flask was placed over a lamp at 80°C for 12 hours and subsequently washed by decantation with distilled water. These carbon rods were next boiled in pure conc. H_2SO_4 for 3 hours and placed over the lamp at 80°C for 12 hours. The process of washing with distilled water was repeated. Then they were boiled for 1 hour in liquor ammonia and placed over the lamp at 60°C for 12 hours. Subsequently the rods were washed with distilled water, then boiled in glacial acetic acid for 3 hours and placed over the lamp at 80°C for 12 hours. The carbon rods were washed with distilled water, boiled in it for 2 hours and again washed by decantation. Then they were heated to boiling pt. in liquor ammonia and again washed with distilled water. Finally the carbon rods were dried in an electrical furnace at 100°C. After each heat treatment the rods were allowed to cool before the next operation. The whole chemical process and specially the glacial acetic acid and pure conc. H_2SO_4 treatment was very effective for the preliminary purification.

The principle of the next thermal treatment was to remove the easily volatile compounds in the chemically treated carbon rods by high temperature heat treatment. Some of the carbon rods were next placed on a silica dish which was heated to redness in oxy-acetylene flame for 30 seconds. The flame was then allowed to play on the rods from all sides for 30 seconds. The carbon rods first gave out black smoke and then became red hot. The temperature as measured by an optical pyrometer was between 1800°C-2000°C. Sometimes it was still higher. The rods when cooled were found to be used up with a surface layer of small black globules.

A simple arrangement for heating these carbon rods again at high temperature in a current of nitrogen bubbled through carbon tetrachloride was made. A Pyrex glass tube with a large bulb at the centre was used as the heating chamber. Two copper rods with arrangements in each for holding a carbon rod horizontally at one end and for electrical connections at the other were used as electrode holders. The copper rods were fitted within two Pyrex glass tubes, each having one side tube for outside connections. These glass tubes, were fitted within the central glass tube using bored corks as sockets. All the leak points were sealed with plasticin and pecien. The heating chamber was evacuated by a Cenco pump connected to a side tube. Nitrogen from the cylinder was bubbled through CCl_4 and then introduced into the heating chamber through the other side tube. Two carbon rods were taken out from the silica dish and clamped into the holders horizontally within the heating chamber. They were burned as electrodes in the arc with 15 amps current for 2 minutes. The arc gap which could be adjusted from outer arrangements was kept small in order to have the temperature through a greater length (1.5 cm.) of the rods near the arc points very high. The chamber was evacuated by the Cenco pump and a continuous current of N_2-gas bubbled through CCl_4 was passed through it. Due to the high temperature near the arc the concentration of the gas at that region was high. The temperature in the carbon electrodes was found to fall abruptly at a distance of nearly 1.5 cm. from the arc gap.

The heating process in the electric arc was carried out in different conditions: (*a*) at 15 A. in air for 2 mins., (*b*) at 15 A. in vacuum for 2 mins., (*c*) at 15 A. in the current of N_2 bubbled through CCl_4 for 2 mins. In each of these conditions part of the carbon rods (about 1.5 cm. at the ends) of high purity were obtained. The best products were obtained in the current of N_2 bubbled through CCl_4. Due to the heat treatment for one minute in oxy-acetylene flame the diameter of the carbon rod was reduced from 7 mm. to 5.5 mm. and the surface layers were found to be in a very porous condition. The heat treatment in oxy-acetylene flame (temperature nearly 2000°C) reduced the impurities throughout the carbon rods and in two minutes arcing the impurities from the part of the carbon rods were greatly reduced.

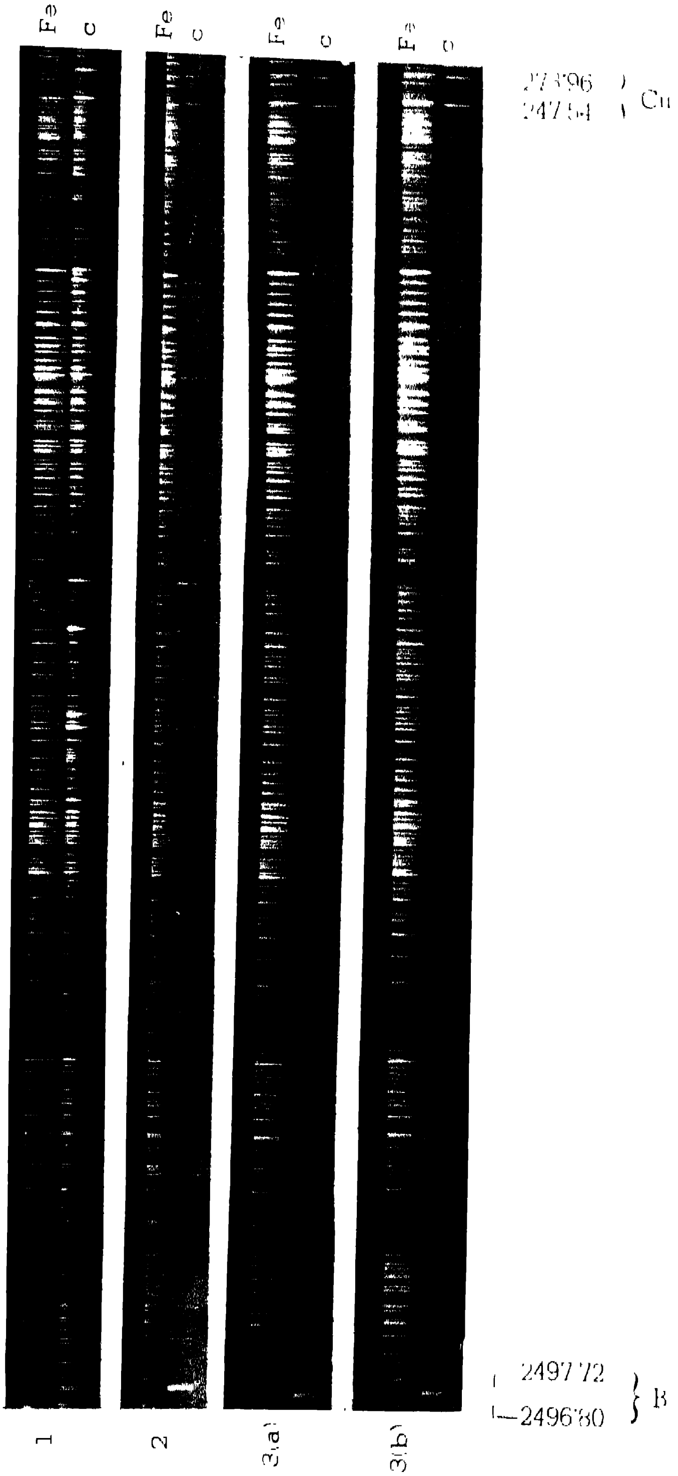
Fe
C
Fe
C
Fe
C
Fe
C
2473·96
2475·4
Cu
2497·72
2496·80
B
1
2
3(a)
3(b)

TABLE I

Results of analysis of the purified carbon rods by the cathode layer method (Plate III, 2). Arc current 11 A at 220 v.(d.c.)

Element	Sensitive line * λ in I. A°	Intensity	Present
B	2497. 72 2496. 80	++	Almost entire amount
Si	2516. 12 2881. 59	+	Considerable traces
Mg	2795. 54 2802. 71 2852. 12	→o	Faint traces
Mn	2794. 82 2798. 27 2801. 08	o	None
Ti	3088. 03 3371. 45 3354. 63	→o←	None to faint traces
Al	3082. 16 3092. 71	→o	Faint traces
Ca	3158. 88 3179. 34	→o←	None to faint traces
Cu	3247. 54 3273. 96	(+)	Traces
Na	3302. 34 3302. 94	o	None
V	3183. 42 3183. 96	o	None
Fe	3020. 64 3021. 07	(+)	Small traces

(* Wave lengths of the elements according to the table of H. Kayser and R. Ritschl.)

++ = strong line; + = medium line; (+) = faint line;

→o = extremely faint line, a faint point at the base with a faint prolongation.

→o← = None to faint point at the base of the cathode layer; o = undetectable.

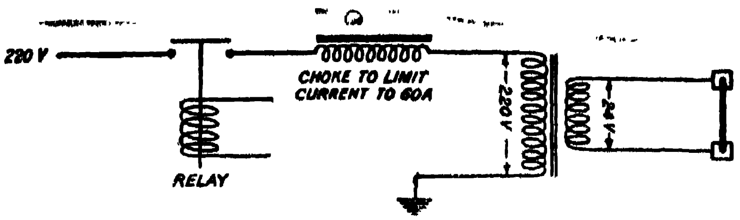

FIG. 1

The final products were analysed by the cathode layer method using a Hilger E_1 quartz spectrograph of very suitable dispersion. An electric supply of up to 15A. at 220 V. (D.C.) together with tapped resistance and an ammeter to control the current through the arc was used. In order to produce an image of the cathode layer effect on the spectrographic plate the lens arrangement of Twyman and Simeon (1929) was found very satisfactory. The arc was focussed sharply with a quartz condensing lens (F. 278, Adam Hilger) over a screen in which there was an adjustable circular diaphragm. The diaphragm was adjusted so that it allowed to pass only the edge of the cathode (negative crater) and the overlying arc column, *i.e.*, an opening of about 4 5 mm. The light image of the illuminated opening was again focussed and enlarged by another spherical quartz condensing lens (F. 17, Adam Hilger) on the slit of the spectrograph. During an exposure the arc gap was best controlled by means of an enlarged image thrown at right angles to the former arrangement over a graduated screen by another condensing lens. The cathode image was held just on the edge of the circular aperture and any slight lack of alignment was adjusted by the position of the image of both cathode and anode on the graduated screen. For the purpose of analysis the arc of the purified carbon rods was drawn at 11 A, separation between electrodes being 8 mm. With the spectrum of the purified carbon an iron spectrum was taken below which served as a reference wavelength scale. The spectrum photograph was studied under a "Comparator" for the identity of all the lines in the carbon spectrum with the help of "Atlas De Spectres D'Arc" of J. Bardet.

All other impurities originally present in the starting material were absent in the final product. As the method of analysis of the previous investigators was not the same the results were not compared.

B. Method of Resistance Heating.

Gatterer's method in a slightly modified form was employed in the present investigation for purifying carbon rods by resistance heating. It was not possible to copy the apparatus used by Gatterer and Hoogland in this laboratory. Figure 1 shows the arrangement used for resistance heating. The type of holder used though very simple was found to be inconvenient for higher currents.

Two copper blocks were drilled in the middle in order to make a hole whose diameter was slightly less than that of the carbon rod. Both of the blocks were cut into two halves through the centres of the holes. On each block the two halves could be screwed tightly in order to clamp the end of the carbon rod into the hole. On one side of each block, there was an arrangement for connection to the lids of the secondary terminals of the transformer. There was no extra spring arrangement for free expansion and contraction during the process of heating. The blocks were light and could slide freely over a smooth plain surface of mica sheet. Chemically treated carbon rod (by the method given before) of 95 mm. length, 7 mm. in diameter was clamped horizontally on both ends into the holes of the blocks. At both the ends only 5 mm. of the carbon rod was introduced into the holes. The carbon rod was heated by allowing the current of 550 amps. maximum to pass through the rod from the transformer, the current being limited by a choke in the circuit (primary voltage 220 V. secondary voltage 24 V). The contacts between the rod and the blocks and the electrical connections to the blocks were sufficiently good enough to minimise the high transition resistances.

As the relay was started, during the first 5 secs only black vapour came out from the surface of the carbon rod. Suddenly the rod began to glow, the temperature being nearly 1200°C. The brightness of the glow increased very rapidly and the temperature went up to 1800°C within 10 secs. At about 30 secs. the glow was very intense when the temperature went higher than the maximum temperature range of the optical pyrometer used (*i.e.*, higher than 2000°C) and carbon flames (named by Catterer) appeared in the bright glow. Suddenly at about 50 secs. the circuit was broken with the formation of an arc at one end. The metal block was found to be melted at the end. The copper blocks must have to be replaced by graphite blocks or there should be an arrangement for cooling the blocks during heat treatment.

This resistance heated carbon rod when cooled, was found to be covered on the surface with loose black globules. Probably due to oxidation the surfaces were used up, which could be avoided, as found in the method (A) if the heating by the passage of current was carried out in the current of nitrogen bubbled through CCl_4. The lengths of the carbon rod used being small, the sag (as found by Hoogland) due to high temperature attained during heating was small.

The resistance heated carbon rod was cut into two equal halves and then used as electrodes in a current of 11A at 220 V with a separation of 8 mm. between them. The light of the cathode layer arc was then analysed in the spectrograph with the lens arrangement as before. During an exposure when the negative crater (cathode) was adjusted just below the edge of the circular diaphragm ultimate lines of Fe and Si were recorded as faint dots at the origin of the cathode layer. But when the cathode was placed just touching the edge of the diaphragm these faint dots were not present at all (Plate 3a and 3b). Thus the faint traces of Fe and Si present were undetectable. By visual inspection under the comparator the percentage of B in this carbon was found to be slightly less than that present in the carbon purified by the previous method, but the percentage of Cu present was greater. During analysis the time of exposure was always 60 secs. the current was 11 A and the separation between the carbon electrodes was 8 mm. Ilford (H. & D. 100) plates and metol hydroquinone developer were always used, the times of development and fixation were 2.5 minutes and 10 minutes respectively at 18°C. Due to a consistent operating technique, the same rocking arrangements during development and the use of fresh developing solution for each plate, spectrum plates of almost identical character were obtained.

In the purification by this method of resistance heating it was found that the carbon rods with preliminary chemical treatment were better purified (as given in Table 2) than the rods without any chemical treatment.

TABLE II

Results of analysis of the purified carbon rods (resistance heated for 50 secs. with i_{max} = 550A). Arc current 11 A.

Element	Sensitive line λ in I.A°	Intensity	Hoogland's results I_{max} = 650 A, Arc current 5.5 A. Time of heating 60 secs.
B	2497. 72 2496. 80	++	+
Si	2516. 12 2881. 59	→o←	?
Mg	2795. 54 2802. 71 2852. 12	→o	+
Mn	2794. 82 2798. 27 2801 08	o	
Ti	3088. 03 3371. 45 3354. 03	→o	?
Al	3082. 16 3092. 71	→o	?
Ca	3158. 88 3179. 34	→o←	(+)
Cu	3247. 54 3273. 96	+	?
Na	3302. 34 3302. 94	o	
V	3183. 42 3183. 96	o	–
Fe	3020. 64 3021. 07	→o	+

Symbols in column 3 are explained as :

++ = almost entire amount ; + = considerable traces ;

o = absent ; →o = faint traces ;

→o← = none to faint traces.

According to Hoogland the symbols in column 4 are given as :

+ = present, ? = presence uncertain ;

– = absent ; (+) = just barely observable.

In the analysis of the purified carbon rods by the cathode layer method while Hoogland (1946) used a current of 5.5 amps.. the author used 11 amps. current, because the spectrographic analysis is usually carried out at 9 to 11 amps. current.

DISCUSSION

The method of chemical treatment conjugated with heat treatment tried in the present investigation in oxy-acetylene flame and in 15 amps. arc in the atmosphere of N_2-Cl_2 mixt. is recommended for the purification of carbon rods in a laboratory. The presence of N_2 and Cl_2 gives more volatile compounds than the oxides. Boron usually forms very non-volatile compounds. As to the properties of the purified carbon rods, they can easily be made into proper shape with new high speed steel machine tools and give steady arc without much flickering, when used as supporting electrodes for spectrographic analysis.

As regards the method of resistance heating, better purification is expected with higher currents passed through the carbon rod for longer times (3 mins. or more) in the atmosphere of N_2 and Cl_2. Deinum (1946) found that $i_{max} = 650$ A was the limiting value up to which the carbon rod (20 cm. length, diameter 7 mm.) could be heated and that the axial temperature attained must be of the order of 3500°C. Hoogland (1946) found that all carbon rods broke at $i_{max} = 650$ A and that a cavity was formed in the middle of the rod, the 'central canal' which indicated that carbon was sublimated in the core of the rod due to high vapour pressure in the centre. In order to study these points the simple arrangement used in the present investigation is inadequate for reasons stated before.

EXPLANATION OF PLATE III

Cathode layer spectrum at 11 A, 220 v. (d. c.) of the

No. 1. Impure 'Kino-Homogen' carbon rods.
" 2. Purified carbon rods by the method (A).
" 3. Purified carbon rods by the method of resistance heating (method B).
(a) when the cathode is adjusted just below the edge of the circular diaphragm.
(b) when the cathode is adjusted just touching the edge of the diaphragm.

In the photograph attached the cathode layer spectrum of the carbon rods is found to be inverted which is not actually the case in the original negative plate. In each plate the iron spectrum is shifted due to the movement of the plate holder. Lines of the elements which show the " Glimmschicht " or cathode layer effect are wedge-shaped with maximum intensity at the base of the cathode layer. For boron the effect is scarcely apparent. The two doublet lines of B (2497.72, 2496.80) approach equal intensity over the entire height of the spectrum.

ACKNOWLEDGMENT

The author wishes to express his sincere and grateful thanks to Prof. P. B. Sarkar for discussions on the subject and for providing all laboratory facilities and to the Director, C.S.I.R. for having granted him a research scholarship. He also expresses his thanks to Prof. M. N. Saha for his kind permission to use the transformer and to Mr. A. Ghosh for his help in the electrical connections.

INORGANIC CHEMISTRY LABORATORY,
UNIVERSITY COLLEGE OF SCIENCE AND TECHNOLOGY,
CALCUTTA.

REFERENCES

Deinum, H, W., 1946, *Rec. Trav. Chim.*, **65**, 270.

Gatterer, 1941, *Spectrochemica Acta*, **2**, 2.

Heyne, 1930, *Z Anorg. Chem* , **43**, 711.

Hoogland, P. L., 1946, *Rec. Trav. Chim.*, **65**, 257.

Lebeau and Picon, 1924, *C.R.*, **179**, 264

Mannkopff, R. and Peters, C., 1931, *Zeits. f. Physik.*, **70**, 444.

Pierce, W. C., Torres, O.R. and Marshall, W. W., 1940, *Ind. Eng. Chem.* (*Anal Edn.*), **12**, 41.

Preuss, E., 1935, *Chem Erde*, **9**, 377.

Russanow, 1934, *Z anorg. chem.*, **219**, 332

Standen, G. W. and Kovach, L., 1935, *Proc Am. Soc.*, **35**, 79.

Staud, A, H.. 1938, *Ind. Eng. Chem.* (*Anal. Edn.*), **10**, 59.

Strock, L. W., 1936, *(May)*, Spectrum Analysis with the Carbon Arc Cathode Layer, Adam Hilger, London.

Trombe, F., Foex. M., and Bardet, J., 1945, *Annales De Chimie*, **20**, 701.

Twyman. F. and Simeon, F., 1929-30, *Trans Opt. Soc.*, **31**, 179.

Zurer, T., and Treadwell, W. D, 1935, *Helv. Chim. Acta*, **18**, 1181.

14

SECOND ORDER CHLORINE K-VALENCE BAND SPECTRA OF CHLORIDES

By K. DAS GUPTA*

(Received for publication, June 20, 1947)

(Plate IV)

ABSTRACT. Chlorine K-valence band spectra (3p->1s) in the second order *i.e*, in the region of 9 A. U. were studied by a concave (gypsum crystal) spectrograph for the alkali-chlorides, alkaline-earth chlorides, $CdCl_2$, $ZnCl_2$, $CuCl_2$, AgCl etc. The resolving power is about 2X. U. per mm. or 1.0 e.v. per mm. on the photometer records. The energy differences of '3p' emission structures from the chlorine K-absorption edge of the corresponding chloride obtained from Stelling's data have been calculated for various chlorides and the differences are found to agree well with the ultra-violet absorption bands obtained by Pohl and Hilsch for the corresponding chlorides As to the origin of ultra-violet absorption bands in various chlorides, a new explanation has been offered and that put forward by Von Hippel has been criticised. The 3p band widths of various chlorides have been estimated and are related to the ratio of ionic diameters of the constituent elements of the chlorides. The experimental results obtained are better explained by the band scheme due to Bloch than by atomic model due to Heitler-London.

INTRODUCTION

In the first paper (K. Das Gupta, 1946) of the series, an account of the soft X-ray absorption and emission spectra of Mg, Al, Si and their oxides has been given. In the present paper, second order emission spectra of chlorine from LiCl, NaCl, KCl, RbCl, CsCl ; $CaCl_2$, $SrCl_2$, $BaCl_2$; $CdCl_2$, $ZnCl_2$, $CuCl_2$, AgCl in the region of about 9 A. U. have been described.

Chlorine $L_{2,3}$ spectra (3, 1s→2p, p being doublet) have been studied by Siegbahn and Magnusson, O'Bryan and Skinner (1940). They have found that $L_{2,3}$ lines of these chlorides *viz.*, η and l lines are accompanied by other two lines η' and l' in the neighbourhood. The intensities of η' and l' are found to be different for various chlorides but the voltage difference between them (η' and l') is the same as that found for η and l *viz.*, 1.6 volts. There is no doubt as to the presence of other satellites on both sides of the main lines for which no satisfactory explanation has been offered. O'Bryan and Skinner suggest that of the two groups (η, l and η', l') the strongest pair η, l are from ionic chlorine centres, while the other which is relatively displaced to the shorter region are from 'neutral atomic centres' of chlorine in the lattice. It has, however, been observed by O'Bryan and Skinner that the third order $L_{2,3}$ spectrum of chlorine in LiCl consist of two bands only and of Cl in CsCl taken by Siegbahn and Magnusson consists of two bands with a very faint band near about the middle. The absence of weak band in CsCl has been ignored in the 'neutral atomic hypothesis' of Skinner and in the case of LiCl the absence of satellites has been attributed to the lack of resolution due to the greater breadth of lines.

---

* Fellow of the Indian Physical Society

The K level in compounds is very much sharper than that of the valence band and thus the structure of K band (3p→1s) gives us a direct measure of the influence of the lattice on the energy breadth of 3p level. O'Bryan and Skinner have drawn some '3s' bands of Cl from $L_{2,3}$ spectra (3s→2p) assuming that the breadth of the levels 2p is small compared to that of 3s. Our experimental results throw some new light on Cl K-valence spectra (3p-1s) and in the case of 3p band one is more justified to neglect the width of 1s level due to chemical binding.

The energy differences of 3p emission structure from the Cl K-absorption edge of the corresponding chloride obtained from Stelling's data have been calculated for NaCl, KCl, RbCl, CsCl, $CaCl_2$, $BaCl_2$, $CuCl_2$, AgCl and it is very interesting to note that the differences are found to agree well with the ultra-violet absorption bands obtained by Pohl and Hilsch for the corresponding chlorides.

Slater and Schockley (1936) have theoretically calculated the total breadth of Cl 3p band of NaCl which comes out about 4.5 e.v. for which experimentally observed data are not available. The present experimental data on the chlorides give 3p band width and it has been found that the observed 3p band width of Cl in NaCl is 6.5 volts, resolving power in this region being 1 e.v. per mm. More accurate experiments in third order spectra, with better resolution are necessary to measure accurately the 3p band width. It has been found that the structure of all alkali chlorides are similar while it is different from those of alkaline-earth chlorides. For alkaline-earth chlorides, however, 3p band spectra are similar amongst themselves.

EXPERIMENTAL RESULTS AND TECHNIQUE

In the previous paper (K. Das Gupta, *loc.cit.*) the experimental details have been given. It must be mentioned here that the emission spectra taken by direct excitation by electron impact are not satisfactory. It has been found that the effect of a particular metal forming the anti-cathode target on the investigating sample can be practically avoided, but still the electrons from the filament strike the substance causing some undesirable change. Most of the alkali-chlorides become coloured green, blue, violet etc., due to the electron impact in the X-ray tube, the colour is also formed by X-ray irradiation. Secondary fluorescence method has just been adopted to study the emission spectra of chlorides in the second order, that is in the region of about 9 A. U. to avoid electron impact. For some less stable chlorides it is very difficult to maintain the order of vacuum of the spectrograph, as the electron impact under the

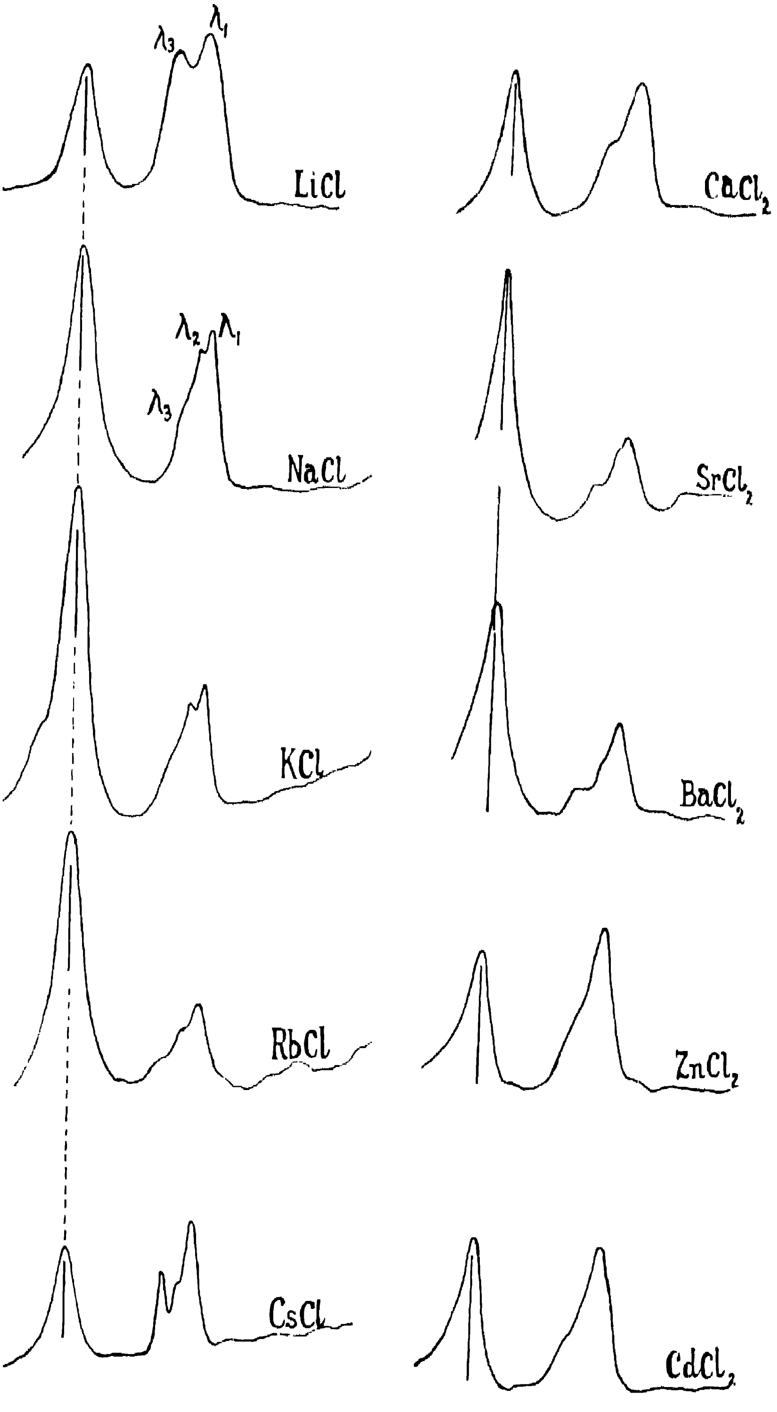

2nd order Cl K-valence band Spectra.
Sc Lβ_1 reference line on extreme left

experimental conditions cause some reduction of the sample and Cl gas comes out. In such cases there is always a discharge current in the tube and the rate of suction of the pump, as well as, the cooling of the anticathode had to be increased to minimise the discharge. The blackening of the film due to exposure to the discharge glow was avoided by using a very thin aluminium foil screen. To study the effect of metal target on the Cl spectra, NaCl was pressed on copper target and silver target successively and there was no detectable change of Cl 3p band structure.

TABLE I

K-Valence Band Spectra of Chlorine in Chlorides

Specimen	Wavelength in X. U.		
	λ_1	λ_2	λ_3
LiCl	4395.8 S (Strong)	...	4386.9 W (Weak)
NaCl	4398.1 S	4395.2 W	4390.1 V. W. (Very Weak)
KCl	4399.1 S	4396.1 W	4391.2 V. W.
RbCl	4899.0 S	4395.1 V. W.	4387.1 W.
CsCl	4397.1 S	4392.7 V. W.	4388.1 W.
$CaCl_2$	4396.9 S	4388.7 W	4370.8 V. W.
$SrCl_2$	4397.0 S	4391.2 W	4387.7 V. W.
$BaCl_2$	4397.1 S	4394.0 W	4385.6 V. W.
$CdCl_2$	4395.9 S	...	4385.6 V. W.
$ZnCl_2$	4395.1 S	......	4386.6 V. W.
$CuCl_2$	4397.3 S	4391.8 W	V. V. W.
AgCl	4398.0 W	4393.6 S	4387.7 W.

GENERAL INTERPRETATION OF RESULTS

Kβ or K-valence band spectra of Cl give a direct measure of the influence of the lattice on the energy breadth of 3p level, neglecting the breadth of 1s of Cl in chlorides. Plate IV shows original microphotometer records and in Table I, wavelengths of Kβ band of various chlorides have been given.

In LiCl, the peaks of the two bands λ_1 and λ_3 are separated by 5.7 e.v. and the stronger one is on the lower energy side. Intensities of the two bands are approximately of the same order of magnitude. If we assume the stronger one (low energy part) to be due to Cl ion, the other must be assumed, according to O'Bryan and Skinner, to have emitted from neutral Cl. The question of relative intensity between the bands raises a serious doubt whether in these ionic crystals, percentage of neutral chlorine can be so large.

In NaCl, beginning from the low energy part of the spectrum, of the three bands the first *viz.*, λ_1 is the strongest while the last one λ_3 is distinctly weaker than the middle one. In NaCl spectrum, the energy difference between the two extreme bands is almost the same as found for the two bands for Cl in LiCl. If we explain the origin of the band on the short wave side due to neutral Cl centres we are faced with difficulty to explain the intermediate band.

The structure of K band of Cl in KCl is similar to that found for NaCl. In CsCl, which is body centred cube, the number of bands is the same as found for NaCl and KCl with the difference that the band having shortest wavelength is stronger than the middle one. The main point of similarity in Cl $K\beta$ spectra of alkali halides is that the spectra begin for each of them with the strongest band on the long wavelength side and its wavelength in chlorides in the same periodic column is almost the same. The wavelength and intensity of the remaining band in each spectra differ. It means that the influence of the lattice is much more felt by the outer portion of the 3p level while the energy value of the deepest part of the valency level remains less affected.

TABLE III

Total Band-width of Cl $K\beta$ band in Chlorides

Width in e.v.	LiCl	NaCl	KCl	RbCl	CsCl
e.v.	9.18	7.71	7.10	6.37	5.40
Ratio of ionic diameters ...	Cl^-/Li^+	Cl^-/Na^+	Cl^-/K^+	Cl^-/Rb^+	Cl^-/Cs^+
....	3.0	1.90	1.36	1.22	1.07
Width in electron volt .	$CaCl_2$	$SrCl_2$	$BaCl_2$	$ZnCl_2$	$CdCl_2$
.... .	10.0	9.2	7.71	10.72	9.72
Ratio of ionic diameters ...	Cl^-/Ca^{++}	Cl^-/Sr	Cl^-/Ba^{++}	Cl^-/Zn^{++}	Cl^-/Cd^{++}
......	1.82	1.60	1.34	2.40	1.86

Ca, Sr and Ba are in the same column of the Periodic Table, having same crystal structure for their chlorides and their spectra are similar. This is also the case with Cd and Zn. In the case of $CdCl_2$ and $ZnCl_2$, the $K\beta$ spectra of Cl are similar, but they are different from those of alkali-chlorides and alkaline-earth chlorides. Thus different groups of elements have different structure of K-band but the structure for the chlorides of elements in the same column and having same crystal structure are similar.

It has been found that within 5-10 minutes the alkali halides become coloured green, blue, violet under electron impact in the existing condition of the tube. Cl in the form of gas comes out of chlorides and stoichiometric excess of alkali metals thus produced is responsible for the development of colour. Similar colour can be developed if the particular halide be heated for a sufficient time in presence of the corresponding alkali vapour

The widths of chlorine Kβ band of chlorides, have been calculated and in Table III, the values as against the ratios of ionic diameters Cl^-/R^+ are given. It will be seen that as the ratio of ionic diameters increases, the width of Cl Kβ band also increases. When the radii of the metal ion are large, the halide ions are pushed farther apart and they overlap less with each other, the width depending on the amount of overlapping. A similar interpretation applies to the oxide and fluoride band widths obtained by Skinner. In alkaline-earth chlorides the width of K band is greater compared to alkali-chlorides for the same value of the ratio of ionic diameters, showing thereby that the overlapping does not depend only on the ratio of the ionic diameters but also on the arrangements of the atoms in the crystal.

TABLE II

Soft X-ray K-Absorption and Emission Spectra and Ultra-violet Absorption bands of Chlorides

Specimen	K-valence band spectra of Cl		Cl K-absorption edge in e.v. (Stelling)	K-edge-E_2 in e.v.	1st Ultra-violet absorption band (Hilsch & Pohl)	K-edge E_1 in e.v.	2nd Ultra-violet absorption band (Hilsch & Pohl)
	E_1 e.v.	E_2 e.v.					
NaCl	2806.0	2808.7	2815.9	7.2	7.8	9.0	9.6
KCl	2806.2	2808.1	2815.2	7.1	7.6	9.0	9.1
RbCl	2806.3	2808.8	2815.1	6.3	7.4	8.8	8.9
CsCl	2807.5	2810.3	2815.0	4.7	......	7.5	7.6
$CaCl_2$	2807.0	2812.9	2815.6	2.7	......	8.6	8.1
$BaCl_2$	2807.0	2809.5	2815.9	6.4	7.7	8.3	9.1
$CiCl_2$	2807.3	2810.9	2816.0	5.1	6.4	8.7	8.2
AgCl	2807.0	2809.7	2811.3	1.6	1.8	7.3	......

Table II shows that the ultra-violet absorption bands of various chlorides can be indirectly obtained, if we know accurately the K-absorption edge of Cl in different chlorides, the latter being taken by Stelling. If we calculate the energy difference of the peak λ_1 and of the peak λ_2 of Cl emission spectra of a chloride from Cl K-absorption edge of the corresponding chloride, we get the values of the two ultra-violet absorption bands. The energy difference between λ_1 and λ_2 peaks of Cl spectra in a chloride agrees well with the difference between the first and second ultra-violet absorption bands of the corresponding chloride.

An explanation as to the origin of Cl Kβ spectra in various chloride is put forward In solid physics, mainly there are two schemes, the Heitler-London scheme, in which the solid is pictured as being made up of separate atoms or ions which interact with each other. The second is due to Bloch in which the electrons in the outermost shell of the atoms concerned are not supposed to be bound to their individual atoms, but are supposed to be free to move through the lattice. This is known as the collective electron model.

In an atomic picture, the eight valence electrons per unit cell of the alkali-halides completely occupy the outer 's' and 'p' shells of the negative ions. In the band scheme, the same electrons occupy four zones, one of which connect with the ionic 's' level and the three others of which connect with ionic 'p' level. Fig. 1 illustrates the manner in which the ionic level broaden into bands of the zone theory, as the ions are brought together. The levels of the negative ions are depressed and those of the positive ions are raised because of the Madelung field. In addition, the levels break into bands when ions begin to overlap. At the observed lattice distance of NaCl, the 's' and 'p' bands are separated from one another and from the higher unfilled band which connects with the lowest level of the metal ion. The ionic level does not split into bands in the Heitler-London approximation but remains discrete, roughly following the centre of gravity of the bands. The chlorine '3p' band is superposition of $3p_1$ and $3p_2$ electrons and thus the

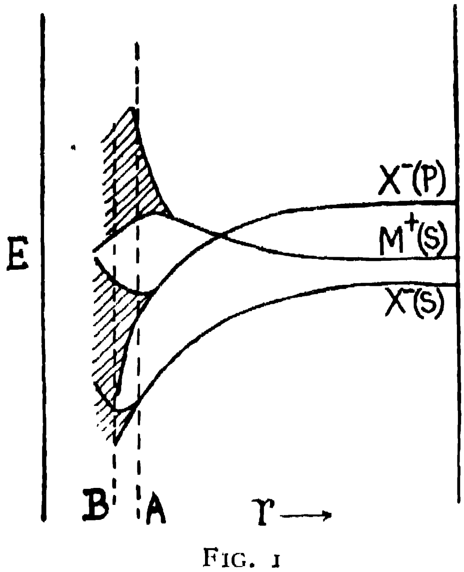

Fig. 1

Schematic representation of the manner in which the ionic levels of the constituents of ionic crystals break into the bands in the band approximation. At A the s and p bands of the negative ions are separate, whereas at B they overlap.

transition probability to vacant K level for them are different. This gives rise to two peaks, the longest wavelength peak of Cl spectra is due to the transition of electrons from the bottom of the valence 3p band having $3p_1$ characteristic and the next one, on the short wave side is due to '$3p_2$' electrons from the top of the 3p band. The energy difference between the two consecutive peaks beginning from long wave side is found to be fairly constant for all the alkali chlorides and is of the order of 2 e. v. In the band scheme $3p_1$ level, as well as, $3p_2$ level broaden into band and the width of 3p band determined experimentally in the case of NaCl spectra is of the order of 6.5 e. v. Although, in the ground state the doublet separation for Cl atom is 0.11 e. v. only, considering both the transition probability, as well as, the density of state of $3p_1$ and $3p_2$ electrons in 3p band it is quite possible to get two peaks at the observed 2 volts energy difference. In chemical combination, both $3p_1$ and $3p_2$ level are affected and displaced downwards in the energy (negative) scale and it is quite possible that $3p_1$ and $3p_2$ electrons are not equally affected when chemical combination takes place. This is supported by the experimental fact that the longest peak for most of the chlorides has got nearly the same wavelength. The width of 3p band, which depends on to what extent the electrons overlap, will also be different for $3p_1$ and $3p_2$ electrons. The absence of two peaks having energy difference equal to 2 volts in LiCl is attributed to the overlapping of $3p_1$ and $3p_2$ bands, centres of gravity of p_1 and p_2 band possibly come very close to each other. The width of Cl long wave band in LiCl being greater than 5 e. v.

The origin of the weakest band having shortest wavelength may be due to electrons coming from the colour band above the 3p band. The colour is formed due to stoichiometric excess of alkali metals. The energy gap between the short wavelength band and the 3p band qualitatively accounts for the green, blue, violet colours observed with different halides. To establish definitely this point, sample of KCl was changed at an interval of 10 minutes so that Cl Kβ spectra may be taken mostly from uncoloured salt. From the microphotometer record it was seen that the weakest band on short wave side has almost disappeared.

This explanation as to the origin of the structure of Cl K-valence band spectra *viz.*, from $3p_1$, $3p_2$ and the 'colour band' electrons may also be extended to explain the ultra-violet absorption bands of chlorides. Of course, in the same apparatus, by the same experimenteer both the emission and absorption spectra are to be obtained, which work has already been undertaken. Von Hippel (1936) has calculated the position of the first absorption band in the alkali-halides on the assumption that an electron is removed from a halogen ion to a neighbouring metal ion. Passing to the absorption band of shorter wavelength, attempts have been made to assign these to a process in which an electron is transferred from a halogen ion to one of the next nearest metal ions. According to Mott and Gurney (1940) there is no reason why the electron should stay on a particular one of these more distant ions. Theory put forward as to the origin of the ultra-violet absorption bands in chlorides (at least) is that electrons in the valence band, which is superposition of $3p_1$ and $3p_2$ electrons, absorb energy and jump into the first vacant band, which according to the zone scheme, is the 's' band of metal ion. In X-ray K absorption spectra, the absorption begins at an wavelength corresponding to the transition of K electrons to the same vacant 's' band of metal ion. From above explanation it is at once evident that the energy difference between p_1 and p_2 peaks in Cl K-spectra will agree with the energy difference between the first and second ultra-violet absorption bands.

DISCUSSION

The second order Cl K-valence band spectra with gypsum crystal is unsatisfactory because of poor resolving power *viz.*, 1 e. v per mm. To establish definitely the theory put forward to explain the ultra-violet absorption bands in chlorides, third order spectra in emission, as well as, in absorption are being taken with a concave mica grating spectrograph. The longwave band in LiCl has been attributed to the overlapping of $3p_1$ and $3p_2$ band and the energy difference between the peaks as obtained in other chlorides is so small in LiCl that the peaks are not resolved by the spectrograph. This conclusion is supported by the fact that amongst the alkali-chlorides it is only in LiCl that the two ultra-violet absorption bands are least separated and the separation is 1 e. v. which, according to the theory put forward, is the energy difference between $3p_1$ and $3p_2$ peaks of LiCl. The resolving power of the spectrograph in this region being 1 e. v. per mm. on the microphotometer record. It is expected that in the third order spectra with better resolving power some fluctuation of intensity in the long wave band of Cl in LiCl will be observed.

ACKNOWLEDGMENT

I take this opportunity of expressing my indebtedness to the late Prof. B. B. Ray, under whom I began my work. I am grateful to Prof. S. N. Bose, University College of Science, Calcutta, under whose guidance I am continuing my work on soft X-ray spectroscopy. I am thankful to Mr. H. N. Bose, of the Department of Physics, Calcutta University, who has encouraged me much during the progress of the work.

KHAIRA LABORATORY OF PHYSICS,
CALCUTTA UNIVERSITY.

REFERENCES

Das Gupta, K. (1946), *Ind. Jour. Phys.*, **20**, 226.
Mott and Gurney (1940), 'Electronic Processes in Ionic Crystals.'
O'Bryan and Skinner (1940), *Proc. Roy. Soc.*, **176**.
Slater and Shockley (1936), *Phys. Rev.*, **50**, 705.
Von Hippel (1936), *Zeits. f. Physik*, **101**, 680.

We are now manufacturing :

- **KIPP'S APPARATUS of one litre capacity,**
- **DESICCATOR of 4″, 5″ and 6″ diameter,**
- **MEASURE GLASSES of 2 drams, 1 oz., 4 oz. and 8 oz. cap. accurately calibrated**

AND

ALL TYPES OF GRADUATED GLASSWARE
such as Measuring Flasks, Measuring Cylinders,
Burettes, Pipettes, etc., etc.

Manufactured by :

INDUSTRIAL & ENGINEERING APPARATUS CO., LTD.

CHOTANI ESTATES, PROCTOR ROAD, BOMBAY, 7.

15

QUANTUM NUMBERS, ATOMIC MASS NUMBERS AND ATOMIC FORCES

By M. F. SOONAWALA[1]

(*Received for publication, May 8, 1947*)

ABSTRACT. By a simple extension of the elementary quantum theory, a relation is derived between the quantum numbers of the orbits of particles and their atomic mass numbers. The force between the constituents of a system of atomic dimensions is derived in terms of the mass numbers of the constituents and the distance between them. There follows a similar derivation of the energy of the system. The application to the cases of the hydrogen-like atoms and the deuteron is considered,

INTRODUCTION

The quantum numbers are characterized by their integral values, and so are the atomic mass numbers. By atomic mass number we mean the atomic weight expressed in terms of the mass of the proton or the neutron as the unit. The atomic mass numbers are known to be integers from the results of the experiments with the mass-spectrograph; and, therefore, they are taken to represent the number of protons and neutrons in the atomic nucleus.

The fundamental quantum relation in the elementary Bohr theory of the hydrogen atom is

$$2\pi m v r = nh,$$

where m is the mass of the electron, r the radius of the orbit, and v the velocity of the electron in the orbit. n is the quantum number, and it is an integer. We may expect a similar relation to hold for the electron's partner, the proton, which is also moving in a circular orbit round the common centre of gravity. Generalising still further, consider any two such particles, A and B, of atomic mass numbers m_1 and m_2, bound together by a common force of attraction, and revolving in circular orbits round the common centre of gravity. Let r_1 and r_2 be their distances from the centre of gravity, so that the distance between them is $r_1 + r_2 = r$; and let ω be the common angular velocity of the two particles. Their masses would be Mm_1 and Mm_2, where M is the mass of the proton. Then, we have the following relations.

$$m_1 r_1 = m_2 r_2 \tag{1}$$

$$2\pi M m_1 r_1 v_1 = 2\pi M m_1 \omega r_1^2 = n_1 h, \tag{2}$$

and

$$2\pi M m_2 r_2 v_2 = 2\pi M m_2 \omega r_2^2 = n_2 h, \tag{3}$$

---

[1] Fellow of the Indian Physical Society

where n_1 and n_2 are the quantum numbers. Substituting in (1) from (2) and (3), we have

$$\frac{n_1 h_1}{2\pi M\omega r_1} = \frac{n_2 h}{2\pi M\omega r_2} \qquad \ldots \quad (4)$$

Or,

$$\frac{n_1}{r_1} = \frac{n_2}{r_2} \qquad \ldots \quad (5)$$

which gives

$$\frac{r_1}{r_2} = \frac{n_1}{n_2} = \frac{m_2}{m_1} \qquad (6)$$

This can be also expressed as

$$n_1 = sm_2,$$

and

$$n_2 = sm_1. \qquad (7)$$

If n_1, n_2, m_1, and m_2 are to be integers, we can see that s can have only a discrete set of values. These would be, (*i*) any integer ; (*ii*) a fraction equal to the reciprocal of any factor common to m_1 and m_2 ; which we may call $1/f$ in general ; (*iii*) all numbers expressed by $n + 1/f$, where n is an integer. Thus, for example, for $m_1 = 20$ and $m_2 = 40$, the values of s would be, $\frac{1}{2}$, $\frac{1}{4}$, $\frac{1}{5}$, $\frac{1}{10}$, $\frac{1}{20}$, 1, $1\frac{1}{2}$, $1\frac{1}{4}$, $1\frac{1}{5}$, $1\frac{1}{10}$, $1\frac{1}{20}$, 2, $2\frac{1}{2}$, $2\frac{1}{4}$, etc. We may also put it this way : n_1 and n_2 are integers because m_1 and m_2 are integers. n_1 and n_2 express the multiples of the number of protons and neutrons in the particles, or their numbers in the equal sub-groups which they can form in the two particles.

The moment of inertia of the system would be given by

$$J = Mm_1 r_1^2 + Mm_2 r_2^2 = \frac{h}{2\pi\omega}(n_1 + n_2) \text{ from (2)}$$

$$= \frac{hs}{2\pi\omega}(m_1 + m_2) \text{ from (7)} \qquad \ldots \quad (8)$$

The energy of the system would be given by

$$\tfrac{1}{2}J\omega^2 = \frac{h\omega s}{4\pi}(m_1 + m_2) \qquad \ldots \quad (9)$$

The centrifugal force acting on A is

$$\frac{Mm_1 v_1^2}{r_1} = Mm_1 r_1 \omega^2 \qquad \ldots \quad (10)$$

and that on B is, similarly,

$$Mm_2 r_2 \omega^2$$

Each of them is equal to the force of attraction, F, between A and B, and the two balance, holding A and B together. Therefore,

$$F = \frac{M\omega^2}{2}(m_1 r_1 + m_2 r_2)$$

$$= \frac{M\omega^2}{2}\left(\frac{m_1 r_1^2}{r_1} + \frac{m_2 r_2^2}{r_2}\right)$$

$$= \frac{h\omega}{4\pi}\left(\frac{n_1}{r_1} + \frac{n_2}{r_2}\right), \text{ from (2) and (3)}$$

$$= \frac{h\omega}{2\pi}\,\frac{n_1 + n_2}{r_1 + r_2}, \text{ from (5)}$$

$$= \frac{h^2}{4\pi^2 J}\,\frac{(n_1 + n_2)^2}{(r_1 + r_2)}, \text{ from (8)}$$

$$= \frac{h^2}{4\pi^2 M}\,\frac{(n_1 + n_2)^2}{(r_1 + r_2)}\,\frac{1}{(m_1 r_1^2 + m_2 r_2^2)}$$

$$= \frac{h^2}{4\pi^2 M m_1 r_1}\left(\frac{n_1 + n_2}{r_1 + r_2}\right)^2, \text{ from (1)}$$

$$= \frac{h^2 s^2}{4\pi^2 M m_1 r_1}\left(\frac{m_1 + m_2}{r_1 + r_2}\right)^2, \text{ from (7)}$$

$$= \frac{h^2 s^2}{4\pi^2 M m_1 m_2}\left(\frac{m_1 + m_2}{r_1 + r_2}\right)^3, \text{ from (6)}$$

$$= \frac{h^2 s^2}{4\pi^2 M m_1 m_2}\left(\frac{m_1 + m_2}{r}\right)^3 \qquad \ldots \quad (11)$$

This is an expression of the force between A and B in terms of their masses and the distance between them, but it cannot be called a gravitational force for that reason, as it only gives the centrifugal force upon A or B. It is only a general expression of the force between A and B, irrespective of its nature. If this is known, r can be expressed as a function of s; *i.e.*, it will have discrete values; and it is only for these sets of values of s and the corresponding values of r that (11) holds.

The energy of the system would be given by

$$E = \tfrac{1}{2}J\omega^2 = \tfrac{1}{2}\frac{(J\omega)^2}{J} = \frac{h^2(n_1 + n_2)^2}{8\pi^2 J}$$

$$= \tfrac{1}{2}F.r = \frac{h^2 s^2}{8\pi^2 M m_1 m_2}\,\frac{(m_1 + m_2)^3}{r^2} \qquad \ldots \quad (12)$$

If A and B are spinning with angular velocities ω_1 and ω_2 and J_1 and J_2 are moments of inertia about the axes of spin, the total moment of momentum would be

$$J\omega + J_1\omega_1 + J_2\omega_2$$

By a simple extension of (8), this becomes,

$$\frac{h}{2\pi}\{s(m_1+m_2)+s_1m_1+s_2m_2\} \quad \ldots \quad (13)$$

where s_1 and s_2 are integers.

Also,

$$E = \tfrac{1}{2}J\omega^2 + \tfrac{1}{2}J_1\omega_1^2 + \tfrac{1}{2}J_2\omega_2^2$$

and

$$\tfrac{1}{2}J_1\omega_1^2 = \frac{h^2m_1^2s_1^2}{8\pi^2Mm_1k_1^2} \qquad (14)$$

where k is the radius of gyration about the axis of spin.

APPLICATIONS

(a) *The Hydrogen-like Atom*

This consists of a nucleus of atomic mass number m_1, and a positive charge Ze, with an electron of charge $-e$ and mass number $m_2 = 1/1839$ revolving round it. The centre of gravity practically coincides with the nucleus. This is, of course, a departure from the picture of the general system described above in that one of the atomic mass numbers is not an integer. The limitations set out above for the values of s will no longer hold in this case, the only limitation being the integral values of n_1 and n_2; *i.e.*, of sm_1 and sm_2. From (11), the force between the nucleus and the electron is

$$F = -\frac{h^2m_1^2s^2}{4\pi^2Mm_2r^3} \qquad (15)$$

The force is the Coulomb force of attraction, $\frac{Ze^2}{r^2}$.

Therefore,

$$\frac{h^2(sm_1)^2}{4\pi^2Mm_2r^3} = \frac{Ze^2}{r^2} \qquad (16)$$

giving

$$r = \frac{h^2n_1^2}{4\pi^2mZe^2} \qquad (17)$$

where $Mm_2 = m$, the electronic mass.

The energy of the system, as also seen from (12) and (17) is

$$E = \frac{Ze^2}{2r} = \frac{2\pi^2mZ^2e^4}{h^2n_1^2} \qquad (18)$$

which is the familiar Bohr formula.

(b) *The Deuteron*

Here $m_1 = m_2 = 1$, and hence the values of s are all integral. From (12), the energy of the system is

$$E = \frac{h^2 s^2}{\pi^2 r^2 M} \qquad \dots \quad (19)$$

The potential function is very probably of the form $\frac{Ve^{-\lambda r}}{r}$. The general procedure would be to solve the equation

$$\frac{h^2 s^2}{\pi^2 r^2 M} = \frac{Ve^{-\lambda r}}{r}$$

or

$$\log r - \lambda r = \frac{h^2 s^2}{\pi^2 V M} \qquad \dots \quad (20)$$

to obtain r as a function of s; and using these values of r and s to obtain the energies for the different levels. As this does not seem feasible, we may take particular values of s, find the corresponding value of r by trial or otherwise, and calculate the energy. Thus, for $s = 1$,

$$re^{-\lambda r} = \frac{h^2}{\pi^2 V M} \qquad \dots \quad (21)$$

Assuming the values $\frac{1}{\lambda} = 3.8 \times 10^{-13}$, and $V = 7.7 \times 10^{-18}$ as deduced elsewhere, (Soonawala, 1942) this becomes

$$\log r - 1.1 \times 10^{12} \times r = -12.5 \qquad \dots \quad (22)$$

where $\log r$ is to the base 10. We can see that the maximum value of r is attained for $r = 1/1.1 \times 10^{12}$, and is equal to about -13. This nearly but not quite fits into (22). Assuming it to be a close enough approximation, $E = 2.6 \times 10^{-6}$ erg, which is near enough to the accepted value. This is not altogether surprising as the values of λ and V were originally deduced from a similar value of E.

We can hardly be justified in improving the fit by selecting a suitable value of λ, as this would involve a corresponding correction for V; but our present knowledge of the nucleus is too meagre. However, it would illustrate some interesting features. Thus assume $\frac{1}{\lambda} = 4.3 \times 10^{-12}$ leaving V the same as before. Then,

$$\log r - 1 \times 10^{11} \times r = -12.5 \qquad \dots \quad (23)$$

The maximum of $\log r - 1 \times 10^{11} . r$ is reached for $r = 10^{-11}$ as well as $r = 10^{-12}$, and is about equal to -12. But, while with $r = 10^{-12}$ the second term is of small significance, it is not quite so insignificant when $r = 10^{-11}$.

For $s = 2$, we have

$$\log r - 1 \times 10^{11} r = -11.9 \qquad \dots \quad (24)$$

As before, with $r = 10^{-12}$ approximately, the second term is of small importance, and then r varies as the second, or almost the second, power of s. The energy varies as $\frac{s^2}{r^2}$, as seen from (12), or nearly as $\frac{1}{s^2}$. On the other hand, if values of r are chosen which make the term λr of greater significance than log r, it can follow that the energy of binding would increase with s.

Another important feature which becomes illustrated is a certain upper limit set on s. This happens because the right hand side of (20) can, for large enough values of s, attain a value corresponding to which no value of r is possible, the maximum of $\log r - \lambda r$ exceeding $\frac{h^2 s^2}{\pi^2 VM}$. The energy levels would then be few and discrete. The tightest binding is for $s = 1$, and diminishes with higher values of s.

MAHARAJA'S COLLEGE,
JAIPUR, (RAJPUTANA)

REFERENCE

Soonawala, M. F., (1942), *Ind. Jour. Phys*, **16**, 391.

16

ULTRAVIOLET BAND SYSTEMS OF THE MERCURY IODIDE MOLECULE. PART III

By C. RAMASASTRY and K. R. RAO *

(*Received for publication, June 9, 1947*)

(Plate V)

ABSTRACT. The band spectrum of the mercury iodide molecule has been investigated further in the ultra-violet in the region between λ 2400 – 2000 Å as excited by a specially constructed high frequency oscillator. The G and H systems are considerably extended ; the G-system is analysed for the first time and a new vibrational scheme is suggested for the H-system, different from that proposed by Prileshcjewa The vibrational constants are

G-system	...	88.4	0.2	125.7	1.2
H-system	...	97.1	1.05	125.3	1.15
		ω_e'	$x_e'\omega_e'$	ω_e''	$x_e''\omega_e''$

The two systems have a common final level which is the same as that for the C and D systems. In the H-system, the progressions are abruptly cut off after $v'=2$; this is considered as an instance of predissociation not found in any of the systems of the mercury halides so far analysed.

INTRODUCTION

The emission spectrum of the mercury iodide molecule was found to consist of seven band systems in the region λλ 4400 – 2100 as listed by Rao, Sastry and Krishnamurty (1944) in Part I of these papers which contains a review of the work done by previous investigators on these bands. The systems were designated as B, C, D, E, F, G, and H in the order of decreasing wavelength, the H system occurring at the most refrangible end of the spectrum. Three more systems, were later discovered by Ramkrishna Rao and K. R. Rao (1946) and described in Part II ; they lie in the region between the F and G systems and hence designated as F_1, F_2 and F_3. The systems B, C, D, and E are extensive, each consisting of quite a large number of bands, while the others extend over shorter regions and are somewhat fragmentary. Vibrational analysis was suggested only for C and D and F_1 and F_3, all of which were shown to have a common lower state, probably the ground state of the molecule with the approximate vibrational constants $\omega_e = 125.2$ and $x_e\omega_e = 1.1$. it was shown further that the two systems C and D whose (0,0) bands have a wavenumber separation of 3510 cm^{-1} might form the components of the electronic transition $\pi^2 \longrightarrow \Sigma^2$, analogous to similar systems established by Howell (1943) in the HgF bands and by Rao and Ramchandra Rao (1944) in the HgCl bands.

---

* Fellow of the Indian Physical Society

With a view to the elucidation of the entire band system of the Hg I molecule, further work is carried out and in this part, the results relating to the G and H systems will be described. When the structure of the entire band systems is completely known, it would be of interest to examine why many systems are emitted by this molecule while only a few are known to exist in each of the corresponding molecules HgF, HgCl and HgBr, as well as in the halides of the other elements, zinc and cadmium of the same periodic group. It is hoped that some of the ten characteristic systems of Hg I might prove to be intercombination bands due to transitions between excited states of the molecule.

EXPERIMENTAL

A pure sample of mercury iodide is taken in a thin-walled pyrex tube about 8″ long and half-inch internal diameter. The tube is continuously evacuated by a Cenco Hyvac pump and excited by a radio frequency voltage, available at the ends of the tank circuit of a Hartley shunt-fed valve oscillator of 1 to 10 Mega cycles range. The heat of the discharge is sufficient to vaporise the mercury iodide in the tube. Within a minute of switching on the oscillator, the colour of the discharge turns intense blue, characteristic of the Hg I vapour. The spectrum is photographed by a Hilger Quartz E 315 spectrograph, using an exceedingly narrow slit This narrow width has proved to be worthwhile in resolving some close band heads, in spite of their general diffused nature. Ilford Special Rapid plates sensitised by high grade mobil oil served well to photograph the spectrum below λ2300. Zenith 'Fast Ultra-Violet' plates of high speed and Ilford plates type Q III are also employed. Exposures of even two hours duration gave very good spectra. The copper arc standards are adopted for reducing the plates.

As pointed out in Part II, in view of the peculiarly large number of systems attributed to Hg I molecule, special care is taken to establish first, as far as possible, from an experimental standpoint the origin of these band systems and to examine that they are not due to other molecules or to the products of dissociation of mercury iodide. Comparison is made with spectra obtained under identical experimental conditions of various other halides and chifley iodides. The band spectra of the two molecules, mercury and iodine, have also been studied in detail in this respect. There is evidence on the plates of bands attributable to Hg_2 and Hg_2^+ but they occur in regions remote from that of G and H systems. As iodine is known to have an extensive band system observed in absorption and in emission below λ 3500 down to the vacuum ultra-violet, plates have been taken with iodine alone in the discharge tube and the data are compared with the bands ascribed to iodine by the previous investigators, Curtis and Evans (1933), Warren (1935), Venkateswarlu (1946). It is found that under the conditions adopted in our experiments no trace of iodine emission bands appeared in the region where the G and H systems of HgI occur. On the other hand, a general continuous spectrum is obtained extending down

PLATE V

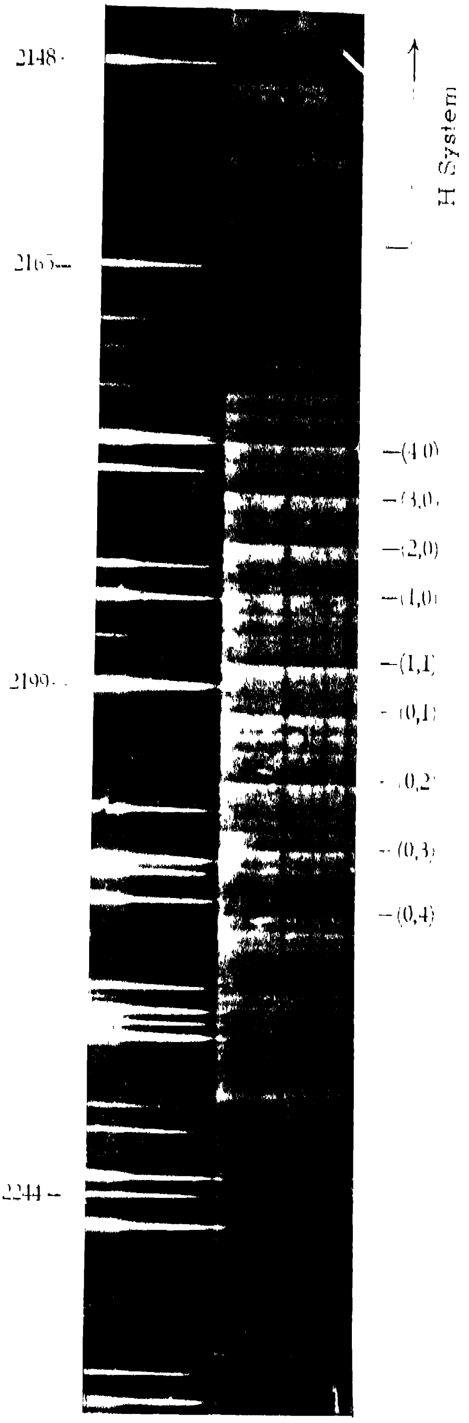

a

(*a*) G System with Culture.

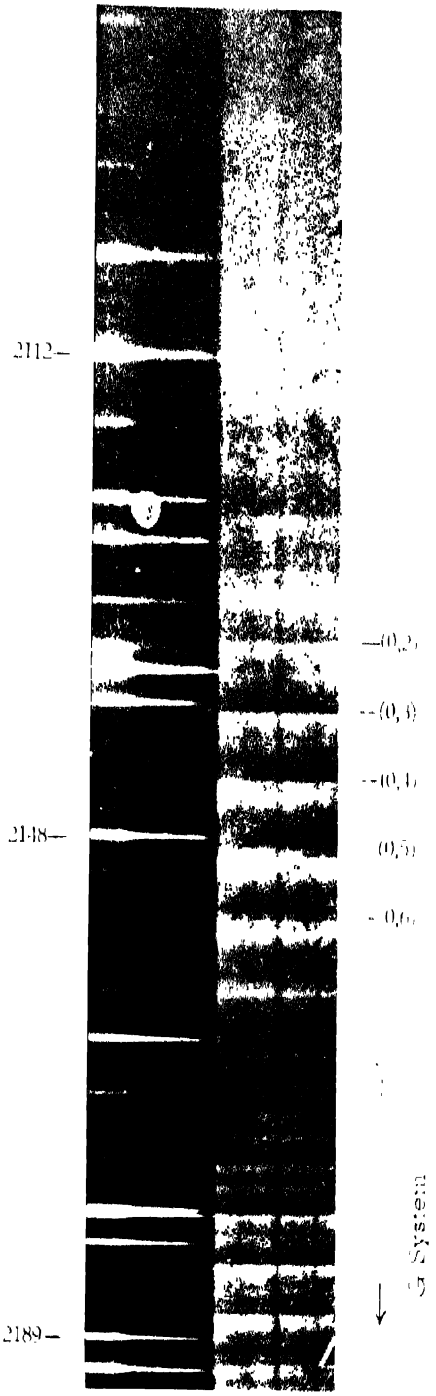

b

(*b*) H System Comparison.

to λ 2000. It might be mentioned here that this iodine H. F. discharge could as well be employed as a source of continuous spectrum in the ultra-violet absorption experiments in place of the usual hydrogen discharge tube. Such a source has, in fact, proved very easy to set up and convenient to work with and is being employed in our laboratory with success. A full description of this will be found elsewhere. The above experiments have led the authors to consider the mercury iodide molecule as the emitter of the G and H systems. A further confirmation is afforded by the vibrational analysis of the two systems suggested in the succeeding sections.

RESULTS

G System.—This system, lying between λλ 2230—2165, was first reported by Prilheshejewa (1932) who published measurements of 22 band heads which were from a low dispersion spectrogram in which the individual members of the sequences could not obviously have been sufficiently resolved. Even the direction of degradation of the bands was not definitely observed. No analysis or regularities were suggested by him. In the present work the dispersion used is about 5 A. U. per mm. in this region ; a much larger number of band heads, about fifty in all, are measured. They are found to be clearly red-degraded with sharp heads towards the violet side. A reproduction of this system is given in Plate IV which is a four-hour exposure with copper arc comparison.

The wave-lengths, intensities and wave-numbers of the band heads are given in Table I. The intensities are visual estimates. For comparison, the data reported by Prilheshejewa are also given in the first column. The analysis of the system is found to be comparatively easy as the heads are characteristically prominent and fairly resolved.

TABLE I

Band heads of the G-System.

Wave length		Int.	Wave number	Classification
Prilheshejewa	Authors			
2239.7				
2234.60	2234.30	0	44742.7	(4,10)
	2233.50	1	44758.7	(3,9)
	2232.60	1	44776.7	(2,8)
	2231.61	3	44796.7	(1,7)
	2229.22	0	44844.8	(4,9)
	2228.22	1	44861.9	(3,8)
2227.2	2227.37	2	44882.0	(2,7)
	2226.29	3	44903.7	(1,6)
	2225.21	0	44925.6	(0,5)
	2223.06	0	44969.0	(3,7)
	2221.88	2	44992.9	(2,6)

TABLE I (*contd.*)

Band heads of the G-system.

Wave length		Int.	Wave number	Classification
Prilheshejewa	Authors			
2220.5	2220.74	4	45016.0	(1,5)
	2219.38	3	45043.6	(0,4)
	2218.71	0	45057.2	—
	2215.02	4	45132.2	(1,4)
2213.2	2213.61	5	45161.0	(0,3)
	2212.08	2	45192.2	(3,5)
	2211.17	1	45210 8	(2,4)
	2210.86	0	45219.6	—
	2209 12	1	45252.7	(1,3)
2208.0	2207.78	6	45280.2	(0,2)
	2207.03	0	45295.6	(3,4)
2205.0	2205.12	3	45334.8	(2,3)
2204.6	2203.63	4	45365.5	(1,2)
	2202.56	0	45387.5	(4,4)
2202.4	2201.92	4	45400.7	(0,1)
	2201.00	2	45419.7	(3,3)
	2199.59	2	45448.7	(2,2)
2196.0	2197.67	6	45488.4	(1,1)
	2196.24	0	45518.1	—
	2195.12	4	45541.3	(3,2)
2193.3	2193.53	4	45574.3	(2,1)
	2192.50	3	45595.7	(5,3)
2191.5	2191.72	4	45611 9	(1,0)
2190.0	2190.94	2	45628.1	(4,2)
	2189.67	1	45654.6	(3,1)
	2188.45	3	45680.1	(6,3)
2188.2	2187.55	6	45698.8	(2,0)
	2187.01	0	45710.1	(5,2)
2185.3	2185.63	1	45739.1	(4,1)
	2184.23	0	45768.4	(7,3)
2183.5	2183 36	5	45786.5	(3,0)
	2181.02	3	45835.7	(5,1)
2180.7	2179.33	5	45871.3	(4,0)
	2178.64	0	45885.7	(7'2)
	2176.80	3	45924.6	(6,1)
2175.0	2175.13	4	45959.8	(5,0)
	2174.44	1	45974.3	(8,2)
	2173.75	1	45988.9	—
	2172.69	3	46011.4	(7,1)
2171 4	2171.06	2	46046.9	(6,0)
	2170.49	1	46058.1	(9,2)
	2169.68	0	46075.2	—
2168.5	2168.76	1	46094.8	(8,1)
2168.0	2168.05	0	46109.8	—
	2167.16	0	46128.8	(7,0)
	2166.60	00	46140.7	—
	2165.99	0	46153 7	—

TABLE II

Vibrational analysis of G-system HgI.

v'' / v'	0	1	2	3	4	5	6	7	8	9	10	
0		45400.7(4)	45280.2(6)	45161.0(5)	45043.6(3)	44925.6(0)						
1	45611.9(4)	45488.4(6)	45365 5(4)	45252.7(1)	45132.2(4)	45016.0(4)	44903.7(3)	44796.7(3)				87.7
2	45698.8(6)	45574.3(4)	45448.7(2)	45334.8(3)	46210.8(1)		44992.3(2)	44882.0(2)	44776.7(1)			84.4
3	45786.5(5)	45654.6(1)	45541.3(4)	45419.7(2)	45295.6(0)	45192.2(2)		44969 0(0)	44864.9(1)	44758.7(1)		86.3
4	45871.3(5)	45739.1(1)	45628.1(2)		45387.5(0)					44844.8(0)	44742.7(0)	86.6
5	45959.8(4)	45835.7(3)	45710.1(0)	45595.7(3)								89.9
6	46046.9(2)	45924.6(3)		45680.1(3)								86.8
7	46128 8(0)	46011.4(3)	45885 7(0)	65768 4(0)								85.7
8		46094.8(1)	45974 3(1)									86.6
9			46058.1(1)									83.8
	125.1	120.6	116.5	121.5	112.5	113.3	108.7	104.7	106.2	102.2		

TABLE III

v' \ v''	0	1	2	3
0	46625	46499	46382	46262
1	46846	46724		
2	47058	46930		
3	47262	47136		

Table II presents the bands in the usual diagonal array. It will be seen that most of the intense bands fall into the v' progression with $v''=0$ and v'' progressions with $v'=0$ and 1; the intensity distribution is such that the Frank-Condon parabola is very wide and open, the (0, 0) band being absent. The $x'_e w'_e$ values are not, in spite of the sharpness of the band heads, very regular; but the general scheme is believed to be correct. The following vibrational formula is calculated for the bands by plotting the $\Delta G(v)$ values against the quantum numbers and adopting the graphical method.

$$\nu = 45542.4 + (88.4\,u' - 0.2u'^2) - (125.7\,u'' - 1.2u''^2) \text{ where } u' = (v' + \tfrac{1}{2}) \text{ etc.}$$

The values 125.7 and 1.2 indicate that the lower state of this system is the same as that determined previously for the C and D systems.

H-System.—This system too was first reported by Prilheshejewa but the number of bands was only ten. The scheme in Table III was also tentatively suggested by the above author, which, according to the present work, appears to be very fragmentary and uncertain. Several bands reported as single by Prilheshejewa are observed to consist of blends of two or more heads and hence an altogether different vibrational analysis has been obtained. The new scheme is presented in Table IV and Table V gives the details of the measurements. Twenty-two band heads are measured between λλ 2170-2110. The degradation of the bands, as can be seen from the reproduction, Plate IV is definitely towards the red as in the G-System. This feature suggested the rearrangement of the heads shown in Table IV, which leads to a value of $w_e' < w_e''$, while the Prilheshejewa's scheme gives $w_e' > w_e''$ unusual for red-degraded bands. Further, if Prilheshejewa's analysis is adoped, many of the strong bands would be left out of the scheme. With our analysis all the bands can be represented by the formula,

$$\nu = 47110.2 + (97.1\,u' - 1.65u'^2) - (125.3\,u'' - 1.15\,u''^2)$$

The $\Delta G(v'')$ values for this system are much more regular than those for the G-system and the constants calculated for the lower state are considered as accurate. For the upper state the constants are derived from only two $\Delta G(v')$ values.

TABLE IV

Vibrational analysis of H-system HgI.

v' \ v''	0	1	2	3	4	5	6	7	8	9
0		46972.7(1) 120.0	46852.7(5) 117.2	46735.5(6) 115.7	46619.8(5) 114.4	46505.4(3) 112.2	46393.2(1)			
93.8		92.6	92.6		92.9	95.6	94.5			
1	47188.0(0) 122.7	47065.3(2)	46945.3(2)		46712.7(0) 111.7	46601.0(4) 113.3	46487.7(5) 108.8	46378.9(3) 107.1	46271.8(1)	
90.5		89.5			89.7			9.06	9.15	
2		47154.8(1)			46802.4(1)			46469.5(4) 106.2	46363.3(4) 106.2	46257.1(3)
	122.7	120.0	117.2	115.7	113.1	112.7	108.8	106.6	106.2	

TABLE V

Band heads of the H-system.

Wave length	Int.	Wave Number		Classification
		Authors	Prilheshcjewa	
2161.15	3	46257.1	46262	(3,9)
2160.46	2	46271.8		(1,8)
2156.20	4	46363.3		(2,8)
2155.48	3	46378.0	46382	(1,7)
2154.81	1	46393.2		(0,6)
2151.27	4	46469 5		(2,7)
2150.43	5	46487.7		(1,6)
2149.61	3	46505.4	46499	(0,5)
2145.20	4	46601.0		(1,5)
2144.33	5	46619.8	46625	(0,4)
2141.35	00	46684.8		(2,5)
2140.07	0	46712.7		(1,4)
2139.02	6	46735.5	46726	(0,3)
2135.96	1	46802.4		(2,4)
2134.62	00	46832.0		(1,3)
2133.67	5	46852.7	46846	(0,2)
2129.46	2	46945.8	46930	(1,2)
2128.22	3	46972.7		(0,1)
2124.03	2	47065.3	47058	(1,1)
2120.00	1	47154.8	47136	(2,1)
2118.51	0	47188.0		(1,0)
2114.82	00	47270.2	47262	(2,0)

The intensities of the bands present interesting peculiarities. Fig. 1 shows the potential curves drawn to scale, for the upper and lower states of this system and the transitions taking place according to Frank-Condon principle. The parabola of intensities thus obtained is indicated by a continuous line on the right side of the figure, inset in the small table giving the observed intensity distribution among the bands. It is a very wide and open one with the vertex shifted towards higher v'' values, the (0, 3) and (0, 4) bands being the most intense of the entire systems.

Another feature of this system is the existence of only three v'' progressions after which there is an abrupt termination of the bands ; there is no band with $v'>2$. This is considered to be an instance of predissociation, not found in any of the other systems of HgI so far analysed. The phenomenon of predissociation first observed in the S_2 bands has since been noted in band systems of several other molecules (cf. Jevons 'Report' 1932). In S_2, two points of predissociation were observed and abrupt changes in the appearance of the bands occur at these points ; further, the bands which have diffuse structure in

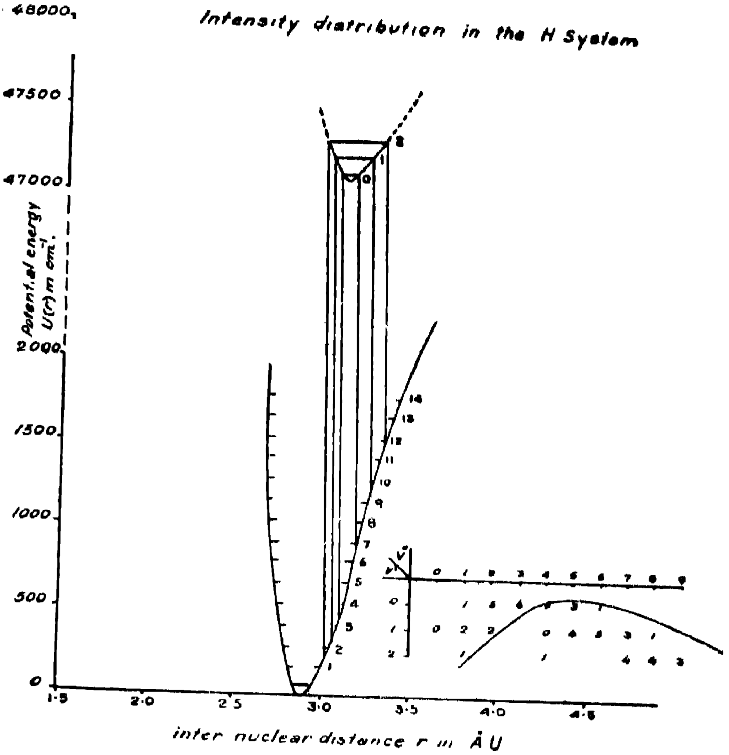
Intensity distribution in the H System
48000
47500
47000
Potential energy U(r) in cm⁻¹.
2000
1500
1000
500
0
1·5
2·0
2·5
3·0
3·5
4·0
4·5
inter nuclear distance r in ÅU
v″
v′

FIG. 1

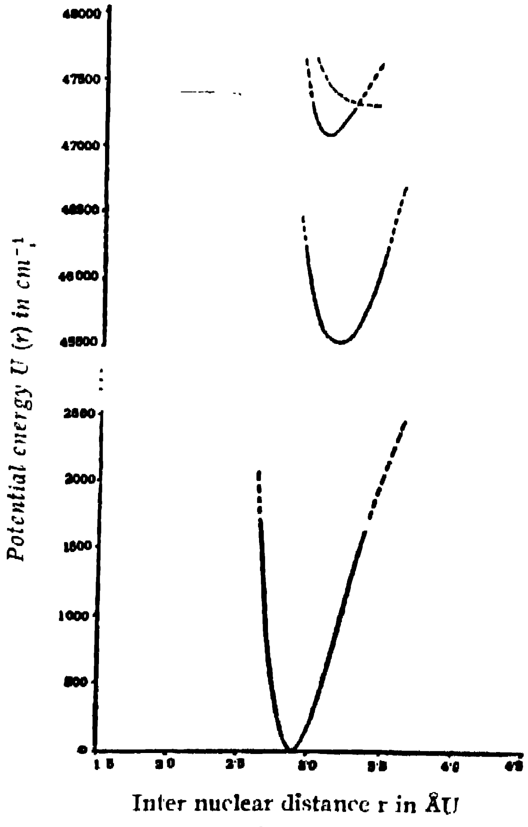
48000
47500
47000
46500
46000
45500
2500
2000
1500
1000
500
0
Potential energy U (r) in cm⁻¹.
1·5
2·0
2·5
3·0
3·5
4·0
4·5
Inter nuclear distance r in ÅU

FIG. 2

absorption do not at all occur in emission. Similarly in the β system of nitric oxide, bands with $v' > 4$ are observable in absorption but not in emission. In yet other bands, such as the v'' progression of the N_2 second positive system a sudden cut off occurs in emission and the systems do not occur even in absorption. All these characteristics have been interpreted as due to the interaction of the upper state with an unstable electronic state of the molecule giving rise to radiationless transitions. The repulsive curve of such a possible electronic state, intersecting the curve for the upper state of the H-system is indicated in Fig. 2 which shows the potential energy curves for the G and H-systems of the HgI molecule.' A complete understanding of the nature of the predissociation is not yet possible unless the absorption of HgI in this region is also studied in detail. Experiments with a view to studying this particular feature are in progress and further discussion will be presented later.

The vibrational constants, the estimated value of the dissociation energy and E(atom) for the upper and lower states are given in Table VI. The values indicate a common lower state, same as that for the C and D systems. The nature of the upper electronic state is difficult to determine. Some of the bands of the G-system are accompanied by fainter sub-bands which cannot be of isotopic origin. They are probably P components if the upper electronic state of this system is a $^2\pi$. For the H-system, the upper state is probably a $^2\Sigma$.

TABLE VI

System	ω_e'	ω_e''	D′	D″	E_{atom}	Dissociation products of the upper state,
G	88.4	125.7	1.21	0.44	6.48	$Hg(^1P) + I(^2P)$
H	97.1	125.3	0.16	0.44	5.63	$Hg(^2P) + I(^2P)$

PHYSICS DEPARTMENT
ANDHRA UNIVERSITY
WALTAIR.

REFERENCES

Curtis and Evans (1933) *Proc. Roy. Soc. A* **141**, 603.
Howell (1943) *Proc. Roy. Soc. A* **182**, 95.
Jevons (1932) Report on Band Spectra, Page 201.
Prilbeshejewa (1932) *Phy. Z. Sowjet.* **1** 189.
Rao, Sastry and Krishnamurty (1944) *Ind. Jour. Phys.* **18**, 323
Rao snd Ramachandra Rao (1944) *Current Science*, **13**, 279
Ramkrishna Rao and Rao (1946) *Ind. Jour. Phys.* **20**, 148.
Venkateswarlu (1946) *Ind. Acad. Sci.* **24 A**, 473.
Venkateswarlu (1946) *Ibid.* **24A**, 480.
Warren (1935) *Phy. Rev.* **47**, 1.

17

INTER-ELECTRODE CAPACITANCES OF TRIODE VALVES AT ULTRA-HIGH FREQUENCY AND THEIR DEPENDENCE ON THE OPERATING CONDITIONS

By D. K. GANGULI and S. R. KHASTGIR *

(Received for publication, June 18, 1947)

ABSTRACT. The inter-electrode capacitances of six triode valves and their dependence on the usual operating conditions were measured on a Lecher wire system with ultra-high frequency field. The basic principles of the method of measurements, experimental procedure and the results obtained are embodied in the present paper. No grid bias was employed and the effect of varying the filament current and anode current for three anode voltages on the inter-electrode capacitances was studied. The filament and anode voltages were suited to the individual valves employed in the investigation. The main features of the experimental results have been fully discussed and their interpretation given in a general way.

INTRODUCTION

Any method of measuring very small capacities can be adopted for the measurements of inter-electrode capacitances of thermionic valves without much difficulty, when they are not in working condition. The heterodyne method or any A. C. balanced bridge method is usually employed. For the inter-electrode capacitances which are extremely small, as in small receiving valves, screen-grid valves, ultra-short wave valves and the midget valves of the 'Acorn' type, suitable methods have been devised from time to time by various workers. These methods give accurate values of the inter-electrode capacitances under non-operating conditions of the valves. Some measurements have also been made under operating conditions. Jones' (1937) measurments in the region of radio-frequency (1 Mc/s) by a bridge method with several triode valves having different anode voltages and varying filament and anode currents within the working range of the valves, furnished some interesting results. Following a double-beat resonance method, measurements of the grid-filament, anode-grid and anode-filament capacitances were carried out by Mitra and Khastgir (1946) for eight different triode valves for various anode currents with three specified anode voltages. The method was essentially a heterodyne method for the measurement of small values of capacities. For accuracy of resonance adjustments, the heterodyne whistle was made to beat with an audible note of fixed frequency, the exact resonance point having been obtained by the no-beat adjustment. Mesurements were made with a field of 1 Mc/s, as in the work of Jones.

Although there was a general agreement between the experimental results of Jones and those of Mitra and Khastgir regarding the nature of the variations of the grid-filament and anode-grid capacitances with anode current, yet there appeared in general an important difference in the sequence of the increase of grid-filament capacitance or of decrease of the anode-grid capacitance with the amount of anode voltage, for the same anode current. Similar measurements of inter-electrode capacitances were, therefore, thought desirable with ultra-high frequency fields, to see whether the same features, as observed with 1 Mc/s, prevailed in the range of ultra-high frequencies. The measurements of course were effected on a pair of Lecher wires, the terminal condenser being a 'grouped' capacitance, having any one of the three inter-electrode capacitances in one branch of the parallel system. The short-circuiting bridge was adjusted for maximum voltage across the terminal condenser of the Lecher wires. With such voltage resonance, the effect of the electrical conductivity of the electronic medium on the resonance length was eliminated. The inter electrode capacitances and their variations with different anode currents under different specified anode voltages were measured with an ultra-high frequency field of 66.76 Mc/s (wave-length λ = 440. 4 cm.) for the following six triode valves :—

---

* Fellow of the Indian Physical Society.

(1) Philips B 405.
(2) Philips E 406.
(3) Cossor 41 MP.
(4) Hivac PX 230.
(5) Mazda PP 3 /250.
(6) 'Acorn' tube.

The make, name and other details of the valves are given in Table I.

TABLE I

Make. Name	Fil. voltage (volts)	Fil. current m. a)	Anode voltage (volts)	Anode curr. (m. a)	Plate resis. (ohm)	Mutual conductance
Philips B 405	4	150	250	21	6000	1.6
Philips E 406 N	4	1000	500	2X20	2000	3
Cossor 41 M.P.	4	1000	200	24	2,500	7.5
Hivac PX 230	2	300	150	17.5	1,850	3.5
Mazda PP$_3$/250	4	1000	300	48	1,000	6 5
'Acorn'	4	310	150	3 8	2,700	.1

In all the mesurements with these valves, no bias voltage was applied to the grid.

EQUIVALENT NETWORK OF A TRIODE

To explain the method of obtaining the individual values of the three inter-electrode capacitances, some theoretical considerations regarding equivalent network of a triode will be of help.

A triode may be represented as a network with Z_a and Z_g the external impedance of the anode-filament and grid-filament circuits respectively: Let C_{gf}, C_{ag}, C_{af} denote the grid filament, anode-grid and the anode-filament capacitances respectively. Representing the A.C. resistance between the filament and the anode by r_p which is in parallel with the anode-filament capacitance C_{af}, and remembering that an alternating potential e_g impressed on the grid introduces an e. m. f. equal to $\mu_0\, e_g$ (μ_0 being the amplification factor of the valve) in the anode circuit, the input impedance can be obtained by including in the anode circuit a fictitious generator giving a voltage $\mu_0 e_g$ and solving the Kirchoff equations for the network.

For very low frequencies ($w < 10^6$), the anode-filament capacitance C_{af} can be neglected, as it is shunted by r_p which is small compared with the reactance offered by C_{af}. Breaking the impedance into resistance and reactance and assuming that the external impedance is inductive, expressions for the input resistance and input capacity comes out to be

$$C_g = C_{gf} + C_{ag}\left(1 + \frac{\mu_0 \cdot r_a}{r_p + r_a}\right) \qquad \dots \quad (1)$$

where r_a = resistance in the anode circuit

When $r_a \approx 0$, the input capacity reduces to $C_{gf} + C_{ag}$.

For high frequencies ($w > 10^6$) the anode-filament capacity C_{af} cannot be neglected. Since w is large, we can neglect, however, the w-terms of lower order in comparison with those of the higher orders. The input resistance can then be shown to be zero and the input capacity will then have a value given by

$$C_g = C_{gf} + \frac{C_{ag} \cdot C_{af}}{C_{ag} + C_{af}} \qquad \dots \quad (2)$$

Thus at very high radio frequencies the input capacity of a triode network is practically independent of the constants of the external output circuits. The effective capacitance between the grid and the filament of the triode network can, therefore, be looked upon as a 'grouped' capacitance consisting of the grid-filament capacitance placed in parallel with the series combination of the anode-grid and anode-filament capacitances. This effective grouped capacitance will evidently vary when the individual inter-electrode capacitances change with the change of the working conditions.

DETERMINATION OF THE INDIVIDUAL VALUES OF THE INTER-ELECTRODE CAPACITANCES

(a) *Under Non-Operating Condition of the Valve.*

Three separate observations of the 'grouped' capacitances, specified below were made for the evaluations of the three individual inter-electrode capacitances without difficulty.

(*i*) For the first observation, the anode and the filament were shorted. Under such condition the effective capacitance across the grid and the filament would be a grouped capacitance of value C_1 given by

$$C_1 = C_{gf} + C_{ag} \qquad \cdots \quad (3)$$

(*ii*) For the second observation, the anode and the grid were shorted. Under this condition the effective capacitance across the grid and filament would be C_2 given by

$$C_2 = C_{gf} + C_{af} \qquad \cdots \quad (4)$$

(*iii*) For the third observation the grid and the filament are joined, so that the effective capacitance across the anode and the grid would be C_3 given by

$$C_3 = C_{ag} + C_{af} \qquad \cdots \quad (5)$$

From (3), (4) and (5), we get

$$\left.\begin{aligned} C_{gf} &= \tfrac{1}{2}\left[C_1 + C_2 - C_3\right] \\ C_{ag} &= \tfrac{1}{2}\left[C_1 - C_2 + C_3\right] \\ C_{af} &= \tfrac{1}{2}\left[C_2 + C_3 - C_1\right] \end{aligned}\right\} \qquad \cdots \quad (6)$$

By measuring C_1, C_2 and C_3, the individual values of the inter-electrode capacitances C_{gf}, C_{ag} and C_{af} can be determined from (6).

(*b*) *Under operating conditions of the value*

The input capacity of a triode network operated at very high radio frequencies has been shown approximately to be the same as the effective capacitance across the grid and the filament under non-operating condition. Thus for high radio-frequencies the same procedure of determining the inter-electrode capacitances of a triode can be adopted under operating condition, provided a suitable large capacity is employed across anode and filament in case (*i*), or across the anode and grid in case (*ii*). The large capacity serves a double purpose. First, if the anode and the filament are shorted just by a connecting wire as in case (*i*), the high tension battery will be shorted; the insertion of the large capacity prevents this short-circuiting. If, again, the anode and grid are shorted by a connecting wire as in case (*ii*), the H. T. voltage will be supplied to the grid as well; the large capacity across the anode and the grid acts as a 'blocking' condenser. Secondly, the insertion of a comparatively large capacity, in either case, is tantamount to short-circuiting, as far as high radio frequency is concerned, so that for both the cases (*i*) and (*ii*), the input capacity would be given by the same simple formulae as (3) and (4). When the grid and filament are shorted by a connecting wire or a large capacity, the effective capacitance across the anode and the grid would be also be given by the same formula (5).

Thus the individual inter-electrode capacitances of a triode can be determined from the set of formulae which are the same as (6).

METHOD OF MEASUREMENT WITH ULTRAHIGH FREQUENCY FIELD

(a) *Experimental procedure and details*

The electrical connections showing the insertion of a condenser of comparatively large capacity in the circuit of the triode under examination are illustrated in Fig. 1. The effective capacitances across the input terminals marked C_1, C_2 and C_3 in the diagrams were measured on a pair of Lecher wires (Fig. 2).

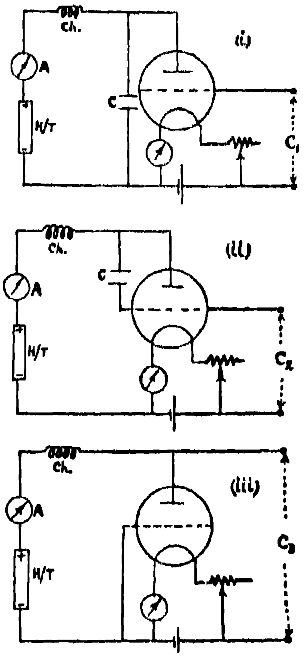

FIG. 1

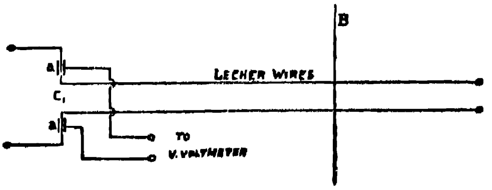

FIG. 2

It is to be noted that a suitable high frequency choke was inserted in the anode circuit of the experimental valve. This was done to avoid short-circuiting of C_{af} through the H. T. battery and the milliammeter A in the anode circuit, each of which has a negligible resistance. In the filament circuit there was a variable resistance and a suitable milliammeter. Each of the grouped capacitances C_1, C_2, C_3 served as a terminal condenser of a pair of Lecher wires. Ultra-high frequency oscillations from the inductance coil L of the oscillator were induced into the Lecher wire system. The short circuiting bridge B was adjusted till the r.f. voltage across the terminal condenser was maximum. This voltage resonance was indicated by means of a valve-voltmeter unit coupled to Lecher wire system at the input end by means of two small condensers consisting of copper tubes insulated from the Lecher wires by glass sleeves. Particular precaution was taken to avoid the effect of the neighbouring oscillator directly on the valve voltmeter unit by enclosing the voltmeter in a shielded box. In case (*iii*) where the Lecher wires, at the input end, were connected to the anode and grid (grid and filament being shorted), a suitable fixed condenser K (0 001 μf) in the bridge prevented short-circuiting of the anode and the grid of the experimental valve. The fixed condenser was conveniently mounted across two stout copper wires fixed on an ebonite frame with a handle. In cases (*i*) and (*ii*), the fixed condenser was not necessary, and the short-circuiting bridge was merely a stout copper wire mounted on the ebonite frame.

The reading for the tuning position could be noted with the help of an index pin fixed on the ebonite frame and pointing towards a long wooden scale running parallel to the Lecher wires.

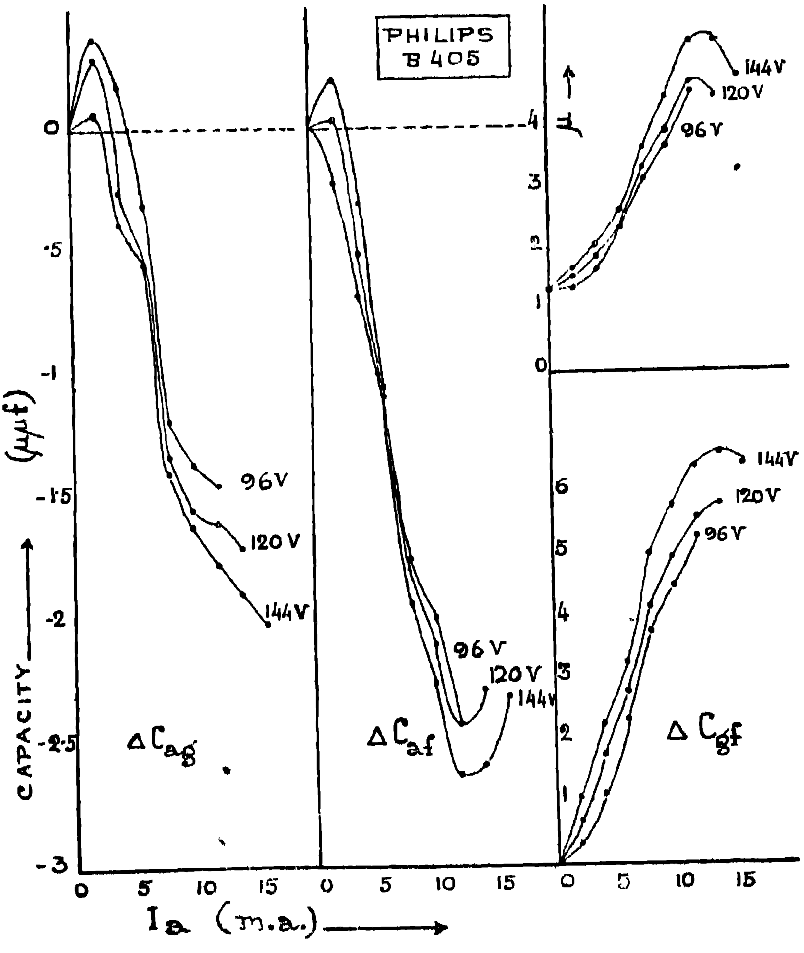

Fig. 3

The Lecher wire system consisted of two parallel S.W.G. No. 18 bare copper wires placed horizontally with a separation of 7.6 cm. between them. The surge impedance Z_0 of the line was calculated to be 579. 8 ohms.

(*b*) *Working Formulae for the Determination*

Let Z_0 be the surge impedance of the Lecher wire system and C be the terminal capacity which is any one of the grouped capacitances C_1, C_2, C_3. If ω be the angular frequency of the oscillations induced into the Lecher wire system then the condition for current resonance, neglecting the resistance of the wire and assuming no leakage across them, is given by

$$Z_0 \tan \frac{2\pi l}{\lambda} = \frac{1}{\omega C}$$

or

$$\cot \frac{2\pi l}{\lambda} = \omega C Z_0 \qquad \dots (7)$$

where l is the resonance length for wavelength λ corresponding to the angular frequency ω of the oscillations.

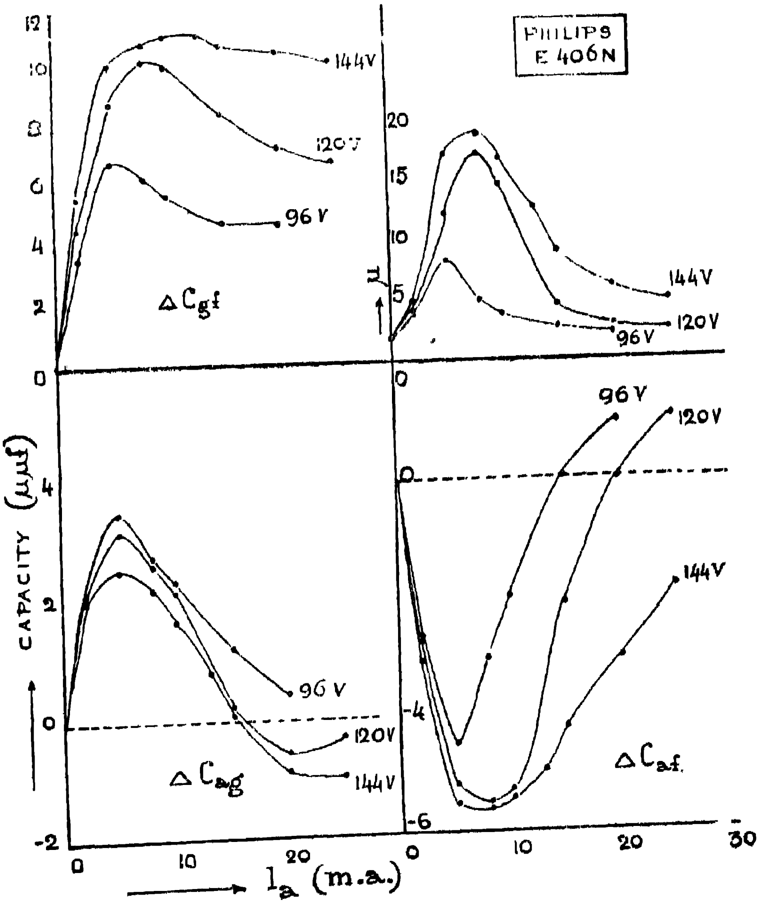

FIG. 4

In the present experiment the length was adjusted for maximum voltage across the terminal condenser. It is, however, known that this voltage resonance condition is the same as the current resonance condition, provided the distribution of electrons inside the terminal condenser is uniform. Neglecting here the slight non-uniformity in the electronic medium, the voltage resonance condition could be taken the same as that for current resonance given by (7).

In case (*iii*) where the short-circuiting bridge comprised of a fixed condenser K, the condition of resonance would be given by

$$\frac{Z_0}{\omega K Z_0 + \tan(2\pi l/\lambda)}\left[\omega K Z_0 \tan\frac{2\pi l}{\lambda} - 1\right] = \frac{1}{\omega C} \qquad \ldots (8)$$

When $\omega K Z_0 \gg \tan\frac{2\pi l}{\lambda}$ this would reduce to (7)

viz., $$\cot\frac{2\pi l}{\lambda} = \omega C Z_0$$

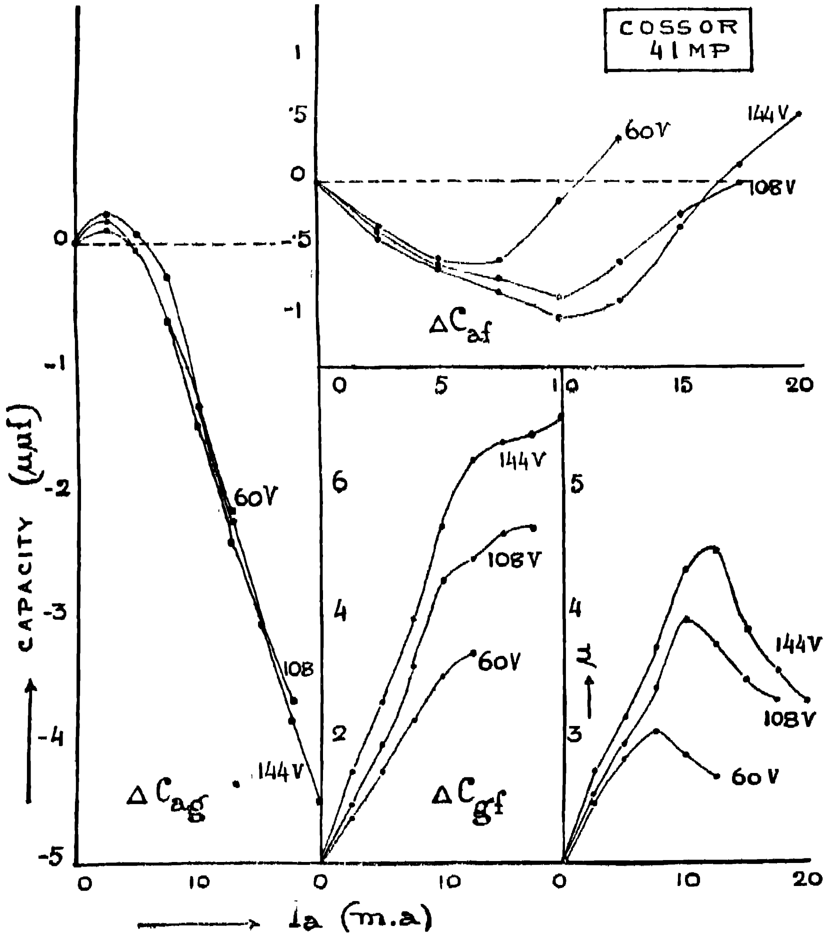

FIG. 5

(c) *Procedure in the mesurement of Inter-electrode capacitances under the non-operating condition of the valves :*

The triode valve was suitably mounted on a wooden base so that the pins were on the level of the plane of the Lecher wires. For cases (*i*) and (*ii*) short leads were taken from the grid and filament to two mercury cups suitably placed. For case (*iii*) leads were taken from the anode and the grid to the same two mercury cups.

With any one 'grouped' capacitance C_1, C_2, or C_3 resonance lengths were obtained by adjusting the short-circuiting bridge. The value of C_1, C_2 or C_3 was then obtained from (7), which may be written here as:

$$C_{1,2,3} = \frac{1}{\omega . Z_0} \cot . \frac{2\pi l}{\lambda}$$

From the values of C_1, C_2, C_3, for any triode valve, the individual values of C_{gf}, C_{ag}, and C_{af} were obtained under non-operating condition from (6)

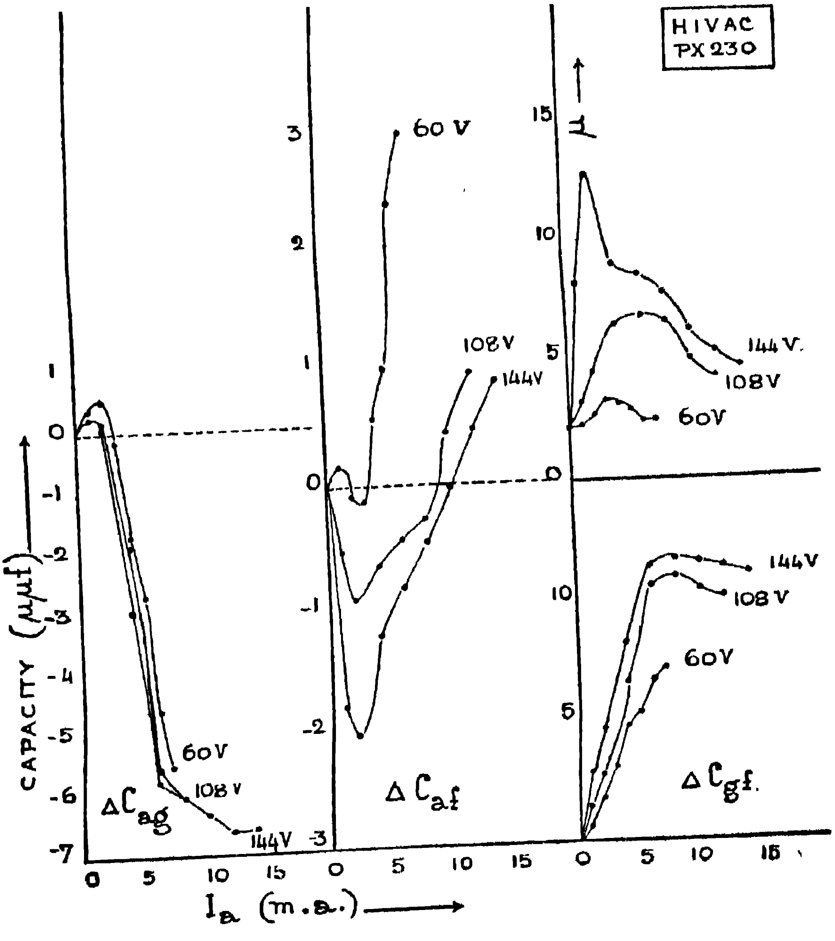

FIG. 6

(d) *Procedure in the measurements under the operating condition*

In these measurements the experimental arrangements were made as in Figs. 1 and 2. Under the operating conditions also there were three cases (*i*), (*ii*) and (*iii*). First, with anode voltage on but with no filament and anode currents, the resonance length l was found in each case. Then for a certain anode current i_a, the resonance length changed to a value l'. The change in the required grouped capacitance C_1, C_2 or C_3 in cases (*i*), (*ii*) or (*iii*) was then given by

$$\Delta c = \frac{1}{k}\left[\cot\frac{2\pi l}{\lambda} \sim \cot\frac{2\pi l'}{\lambda}\right], \qquad \ldots (9)$$

where $k = \omega Z_0$

An increase in l means a decrease in capacity, and a decrease in l indicates an increase of the same.

It was thus possible to measure C_1, C_2 and C_3 for various values of the anode current from (9) for any triode valve. From these data, the changes

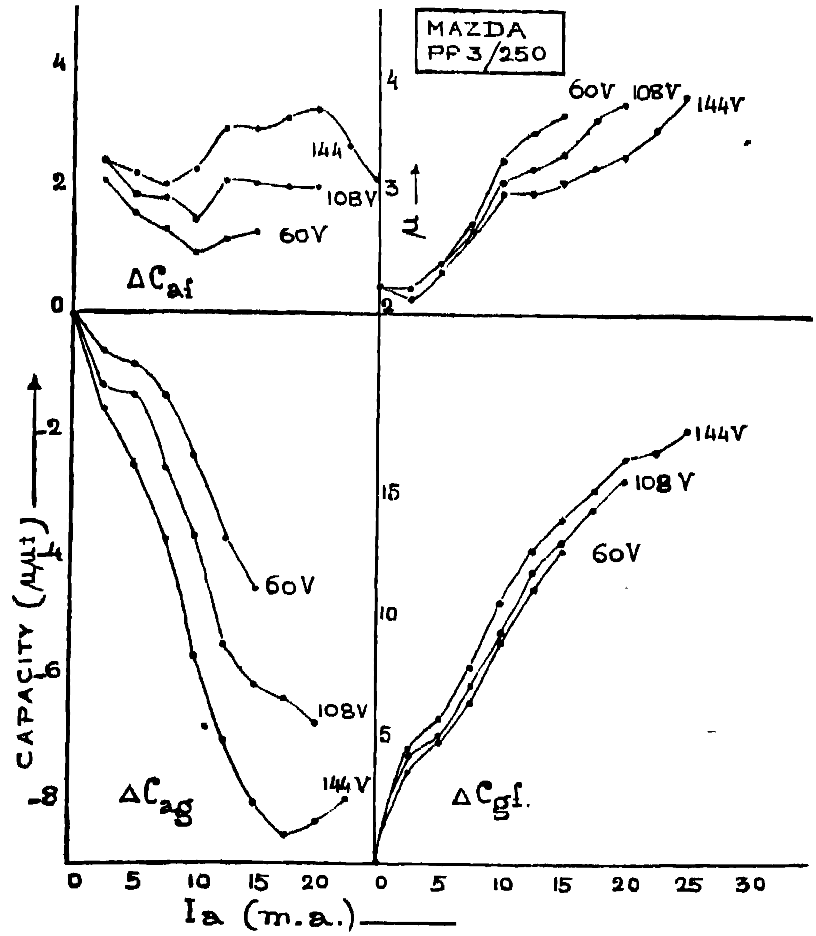

FIG. 7

in the inter-electrode capacitances ΔC_{gf}, ΔC_{ag}, and ΔC_{af} were determined with the help of (6).

Having previously measured the individual values of inter-electrode capacitances under non-operating conditions, their actual values for various anode currents could easily be evaluated.

EXPERIMENTAL RESULTS

(a) *Measurements of the 'cold' values of inter-electrode capacitances*

The 'cold' values of inter-electrode capacitances obtained experimentally for six triodes are given in Table II.

The values of the amplification factor as obtained from the ratio C_{gf}/C_{af} are also entered in the table.

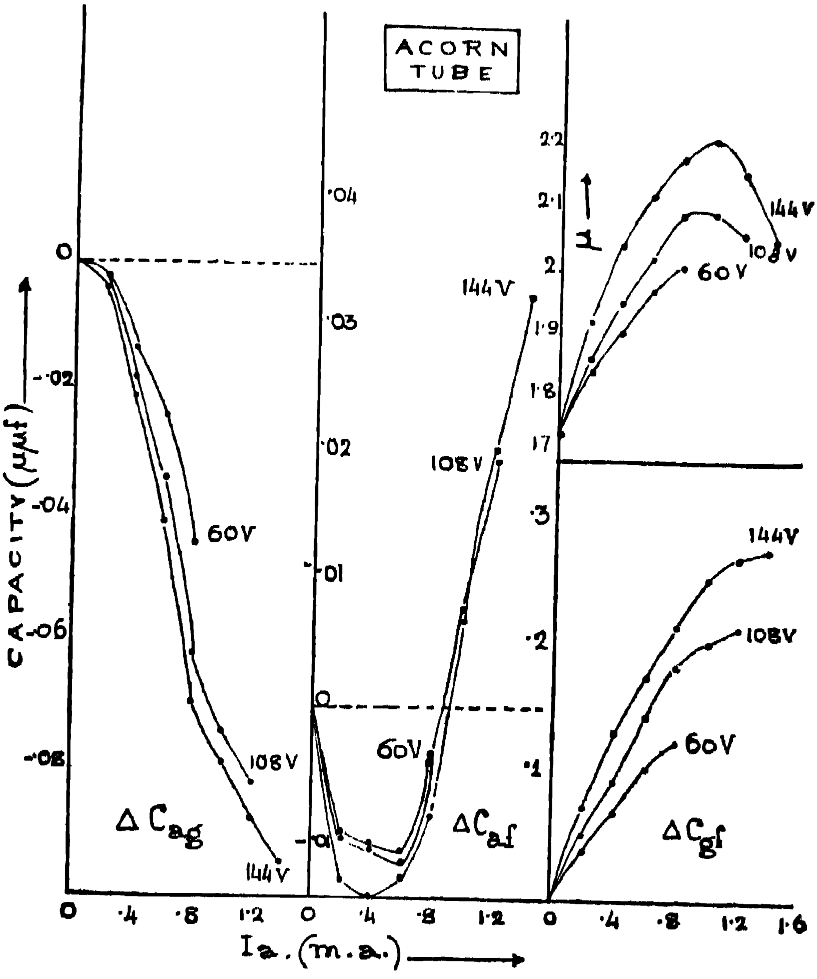

FIG. 8

TABLE II

Name of triode.	C_{gf} $(\mu\mu f)$	C_{ag} $(\mu\mu f)$	C_{af} $(\mu\mu f)$	$\mu_0 = \frac{C_{gf}}{C_{af}}$
Philips B405	6.9	5.1	5.1	1.35
Philips E406N	12.49	11.61	6.81	2.0
Cossor 41 M.P.	9.52	8.9	4.51	2.11
Hivac PX230	6.2	8.4	2.02	2.12
Mazda PP3/250	12.305	13.015	5.525	2.22
'Acorn' (with base)	·94	1.24	·54	1.74

(b) *Variations of Inter-electrode Capacitances with anode current*

The experimental results for all the six triodes are illustrated in figures 3 to 8. The changes in the individual capacitances *i.e.*, ΔC_{gf}, ΔC_{ag} and ΔC_{af} and the values of μ_0 obtained from C_{gf}/C_{af} for different anode currents are shewn in the diagrams. Variations of the inter-electrode capacitances with anode current for three fixed anode voltages were studied,

SUMMARY OF EXPERIMENTAL RESULTS

Summing up all the experimental results, the following generalisations can be made.

I. (*a*) There was a large and steady increase of the grid-filament capacitance with the increase of anode current, followed in some cases by a slow decrease with further increase of anode current.

(*b*) For the same anode current, the observed increase of the grid-filament capacitance was larger for a larger anode voltage.

II. (*a*) Usually there was a comparatively slow decrease of the anode-grid capacitance with the increase of anode current. In some cases, a slight increase was observed for small values of anode current, followed by the usual decrease with further increase of anode current.

(*b*) For the same anode current, the observed decrease of the anode-grid capacitance was larger for a larger anode-voltage.

III. Usually there was a steady decrease of anode-filament capacitance with increase of anode current, with an occasional increase with further increase of anode-current. In some cases, there was indication of slight increase for small values of anode current.

IV. There was a rapid rise in the amplification factor as obtained from the ratio of the grid-filament capacitance to anode-filament capacitance followed by a slow decrease in most cases. Thus for a certain value of anode current there appeared, in most cases, a maximum value of amplification factor.

V. The increase of grid-filament capacitance and the decrease of anode-grid capacitance for each of the six triodes for maximum change in anode current for a given voltage (144 volts) are tabulated below.

TABLE III.

V_a = 144 volts

Valve	'Cold' value		Δi_a (m a)	ΔC_{gf} ($\mu\mu f$)	$\frac{\Delta C_{gf}}{C_{gf}}$	ΔC_{ag} ($\mu\mu f$)	$\frac{\Delta C_{ag}}{C_{ag}}$
	C_{gf}($\mu\mu f$)	C_{ag}($\mu\mu f$)					
Philips B405	6.9	5.1	0–16	6.52	.94	−2.01	−.39
Philips E406N	12.49	11.61	0–25	10.28	.82	−0.05	−.08
Cossor 41 M.P.	9.52	8.0	0–20	7.2	.75	−4.48	−.50
Hivac Px230	6.2	8.4	0–14	11.12	1.8	−6.58	−.78
Mazda PP3/250	12.31	13.02	0–25	17.78	1.44	−7.98	−.61
'Acorn'	0.91	1.24	0–1.4	28	.3	−0.094	−.075

DISCUSSION AND INTERPRETATION OF EXPERIMENTAL RESULTS

The electrons inside the inter-electrode space in a valve usually bring about two effects.—(1) a reduction in the dielectric constant of the electronic medium, and (2) a conductivity effect across the electrodes. The latter is, however, eliminated in our measurements, where lengths were adjusted on the Lecher wires for maximum voltage across the terminal condenser. Thus we should normally expect a decrease in the inter-electrode capacitance with increasing anode current due to a gradual reduction of dielectric constant of the electronic medium. This normal feature is usually observed in the case of the *anode-grid capacitance.* In the case of the *gridfilament capacitance* we have to consider, in addition, the effect of the space-charge. The effect of the space-charge is to diminish the effective distance between the anode and the filament. With a fixed anode voltage, as anode current increases on increasing the filament current, the space-charge increases. Thus the effective distance between the anode and the filament would decrease, *i.e.*, the inter-electrode capacity would increase with increasing anode current. The rate of this increase would evidently slow down, and the inter-electrode capacitance would approach a saturation value with larger values of increasing anode current.

Considering the gradual reduction of dielectric constant of the electronic medium with the increase of anode current, it is evident that the reduction of the effective capacity due to the decrease of dielectric constant would only appear for very large values of the anode current. It is therefore expected that the inter-electrode capacitance would show a gradual increase with the increasing anode current followed by a decrease with further increase of anode current. In the case of grid-filament capacitance this was actually observed. In some cases, however, the subsequent decrease was not observed within the range of the anode current.

If the observed increase of the grid-filament capacitance with increasing anode current is a space-charge effect, then it is evident that the increase of grid-filament capacitance for a given anode current would be less for a higher value of the anode voltage. With all the six triodes examined in the ultra-high frequency field, the sequence was, however, found completely reversed. As already explained by Mitra and Khastgir (*loc. cit*) this was most likely due to the emission of secondary electrons at higher voltages. When secondary emission takes place at the grid surface, the latter acquires a positive potential. With a perceptible positive potential on the grid, the electrons flowing from the filament to the grid would move faster with a positive than with a neutral grid. Hence for a given thermionic current, N. e. v., the average electron density would be less, as the velocity of the electrons would be larger, so that the decrease of the grid-filament capacitance due to the change of the dielectric constant would be smaller for the higher anode voltages, for which there is secondary emission. The increase of the grid-filament capacitance due to space-charge would therefore, appear larger.

The positive potential on the grid would, on the other hand, retard the electrons going from the grid to the anode. As a consequence, with a higher anode voltage producing secondary emission, for the same anode current, the electron density would be larger. This would cause a larger decrease of the anode-grid capacitance for higher anode voltages, for the same value of the anode current. This was actually observed with all the valves.

Some test experiments were performed to find whether the observed variations of the inter-electrode capacitances were partly, at any rate, due to the change in the inter-electrode distance or dimensions as a result of the heating effect in several valves. In these experiments, the valve under test was used without any anode voltage. The grid and the filament were connected to the input terminals of the Lecher wire system, and with no filament current, the short-circuiting bridge was adjusted for voltage resonance in the usual way. As soon as the filament current was switched on, and there was only a small fraction of a milliampere flowing in the anode circuit of the valve, a shift of the tuning position was observed. With further increase of filament current, however, there was no further perceptible change in the tuning position. The shift was found in the direction which indicated an increase in the capacity of the terminal condenser of the Lecher wires. It can be conjectured that as soon as the filament current was switched on, some stray capacitance was suddenly introduced due to the L.T. battery and connecting wires, etc., thus causing a shift in the tuning position in the direction indicating an increase in the capacity of the terminal condenser of the Lecher wires. That this shift was not due to a change in the inter-electrode distance or dimensions on account of heating is evident from the fact that there had been no further shift of tuning position when the filament current was increased considerably.

The initial slight increase of the anode-grid capacitance observed with some valves within very small values of the anode current may perhaps be associated with the shift of the tuning position observed on switching on the filament circuit. It is evident that the apparent slight increase of capacitance due to this extraneous cause would show itself only when the observed decrease of the anode-grid capacitance with anode current was indeed small in magnitude. In the case of the observed increase of the grid-filament capacitance with anode current, the observation in the neighbourhood of small values of anode current obviously included the slight increase due to the extraneous cause.

As already remarked by Mitra and Khastgir *loc. cit.*, other factors may also affect the variation of inter-electrode capacitances. The works of Schottky (1914), Epstein (1910), Fry (1920) and others showed that the increase of the grid-filament capacitance of a valve depended on inter-electrode distances. The effective values of the inter-electrode capacitances may thus, to some extent, be affected by the relative positions of the electrodes inside the valve.

PHYSICS DEPARTMENT,
DACCA UNIVERSITY.

REFERENCES

Epstein (1919), *Deutsch. Phys. Gesel. verh*, **21**, 85.
Fry (1920), *Vide* Van der Bijl's Thermionic vacuum Tubes, p. 63.
Jones (1937), *Jour. I. E. E.*, **81**, 658.
Mitra and Khastgir (1946), *Ind. Jour. Physics*, **20**, 81.
Schottky, (1914), *Phys. Zeitscht*, **15**.

SOME DIRECTIONAL OBSERVATIONS OF ATMOSPHERICS ON 1000 METRES DURING SUNSET TIME

By S. R. KHASTGIR,* M. K. DAS GUPTA AND D. K. GANGULI

(Received for publication, May, 5, 1947)

ABSTRACT. The theory of sunrise and sunset maxima in the number and strength of atmospherics, as given by Khastgir, is elaborated in this paper. A simple method, based on this theory, is worked out for the location of a thunderstorm centre which gives rise to atmospherics, by observing the time of occurrence of the atmospherics maximum, when the distant thunderstorm prevails over a length of time covering the time of sunrise or sunset. The results of some directional observations of atmospherics taken in May-June 1946 with a cathode-ray tube direction-finder are also given in the paper. The positions of the observed maxima with reference to ground sunset enabled determinations of the locations and distances of the thunderstorm centres active during the period. The results indicated that most of the thunderstorm areas were on the eastern side of Dacca, in Burma and a few on the western side. The distances were found to range from about 190 to 1750 Km.

INTRODUCTION

It was long known that there were anomalies observed in the number and in the intensity of *distant* atmospherics during the sunrise and the sunset periods. Eccles (1918) reported observation of a sunset minimum and this was confirmed by other investigators. Espenschied, Anderson and Bailey's (1926) observations, however, indicated an increase of atmospherics during the sunrise and sunset times. Potter's (1931, 1932) work on atmospherics received in frequency channels from 5 MC/S to 20 MC/S, also revealed intensity maxima during the periods of sunrise and sunset. Double peaks were also observed by him about the time of sunrise on some occasions. The preliminary investigations on distant atmospherics received in medium frequencies by Khastgir and Kameswar Rao (1940) and Khastgir and Ray (1940) in this laboratory showed an unmistakable maximum during the sunset time. Later observations on very high radio frequencies by Khastgir and Innas Ali (1942) and on medium frequencies by Khastgir and Basak (1942) showed in many cases maxima in the region of ground sunrise and sunset times. Usually one maximum (and sometimes two maxima) was observed some minutes *before* the ground sunrise time. One maximum was also observed some minutes *after* the ground sunset time. Occasionally there was indication of a maximum at the time of the ground sunset. The effect of sunset on atmospherics was also reported in a paper by Subba Rao (1941). Venkata Rao Telang's (1941) records of the atmospheric electric field also indicated anomalies during the sunset time.

---

* Fellow of the Indian Physical Society

Potter (1931) attempted a general explanation of the sunrise and sunset effects observed and also of the double peak ; but this explanation does not seem to be at all satisfactory in view of the present knowledge of the ionosphere. For very long waves, Namba (1933) gave an explanation of the sunset and sunrise effects on atmospherics. According to his view, the reflexion at the ionized layer is *metallic* before sunset and *dielectric* after sunset ; and the sunset and sunrise effects are due to the transition in the reflection characteristics of the layer. A general explanation of the phenomenon was also offered by Khastgir (1942). The object of the present paper is to elaborate this explanation into a theory and to show that on this theory a simple method can be devised for the location of a thunderstorm centre which gives rise to atmospherics by observing the time of occurrence of the maximum in the strength of the atmospherics, when the distant thunderstorm prevails over a length of time covering the sunrise or sunset time. The results of some directional observations of atmospherics about the sunset time are also given in the paper.

THEORY OF ATMOSPHERICS MAXIMA DURING SUNRISE AND SUNSET PERIODS

A lightning stroke gives rise to damped pulses of electromagnetic waves. When a lightning takes place on the earth's surface or somewhere within the troposphere, the electromagnetic pulses arrive at the receiver situated at some distance after reflexion from the ionospheric layer. In the small hours of the morning, it is evident, the intensity of downcoming wave, originally coming from the distant source of atmospherics, increases gradually with the slowly decreasing ionization in the E-layer, till on the incidence of the solar rays, at sunrise, there is a great increase in the ionization causing a large fall in the intensity owing to a larger absorption in the layer and also to a greater deviation of the rays due to higher electron concentration. This causes a maximum in the strength of the atmospherics about the time of sunrise. Before sunset, again, the intensity of the downcoming waves gradually increases due to a continuous decrease in ionospheric absorption till at the instant of the withdrawal of the solar rays at sunset the intensity suddenly falls. This is because when the ionizing solar rays are withdrawn, there is a perceptible decrease in the E-layer ionization and the downcoming waves are much less deviated and necessarily fail to reach the receiving point. This gives a maximum in the strength of the atmospherics about sunset time. Subsequently, however, the smaller ionospheric absorption asserts itself causing at first a slow decrease of intensity and ultimately an increase.

The work on the early morning increase of E-layer ionization by Mitra (1938) has shown that the ionization begins to increase *not* when the early morning solar rays strike the E-layer by grazing the earth's surface *but* when the rays strike the layer by grazing the surface of the ozonosphere at a height of 35 Km. from the earth. The sun's rays, in order to produce ionization in the E-layer should therefore pass over the ozone region, so as not to have the radiations of the shorter wavelengths absorbed by the ozone. Keeping this conclusion in view, the time of occurrence of the increase of ionization in the E-layer by sun's rays at dawn or of the decrease of ionization when the solar rays are withdrawn at dusk, can be found with reference to the ground sunrise and sunset times. This would correspond to the time of occurrence of the atmospherics maximum observed about the time of sunrise or sunset. The double peaks which were usually observed on higher frequencies before the ground sunrise can be explained in terms of the two layers E and F. It is known that the F-layer ionization also indicates a rapid increase in value about the sunrise (in the layer) and also a sharp fall about the sunset (in the layer).

POSITION OF THE SUNRISE AND SUNSET MAXIMA AND THE LOCATION OF THUNDERSTORM CENTRES

For simplicity in treatment, let us first consider the *particular case*, when the source of the atmospheric disturbance and the receiving point are in the east-west plane. Let S and R represent the source of atmospherics and R the receiving point. The damped electromagnetic pulses from the source of the atmospherics would reach the receiving point after reflexion at A in the ionospheric layer. It is evident from fig. 1 that the ionization in the region A would begin to increase only when the sun's rays would pass over the tangent from A to the top of the ozone layer. The ground sunrise or sunset at the receiving point is of course easily determined by drawing a tangent plane on the earth's surface at the receiving

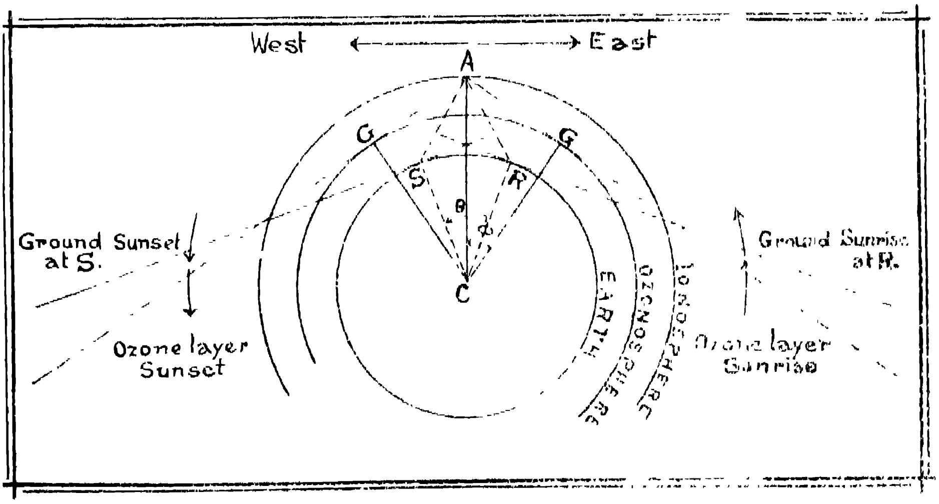

FIG. 1

site R. From A where the ionospheric reflexion takes place, let us now draw a tangent AG touching the ozone layer at G. Denoting the angular distance between the noise source and the receiving point by θ and the angle ACG by ϕ, it can be easily seen that the instant when the sun's rays would begin to produce ionization in the region A by grazing the top of the ozone layer it would be earlier or later than the ground sunrise at R, according as $\phi >$ or $< \frac{\theta}{2}$. This is true whether R is to the east or west of S. It is also evident that the difference between the instant of ground sunrise at the receiving point and the instant when the ionization begins to increase in the region A would be given by

$$\Delta T = (4\phi \mp 2\theta) \text{ minutes} \tag{1}$$

The signs of the difference and summation refer respectively to the cases when the receiving point R is to the east and to the west of the noise source S.

Similar arguments would apply to the case of the sunset. It should be noted that the sunset maximum would appear *after* the ground sunset, provided $\phi > \frac{\theta}{2}$, whereas under the same condition the sunrise maximum would appear *before* the ground sunrise. The difference between the instant of ground sunset at the receiving point and the time of occurrence of sunset maximum would be given by the same formula. It should be noted that the signs of difference and summation would in the case of sunset refer respectively to the cases when the receiving point R is to the west and to the east of the noise source S.

We shall now consider the *general case* where the source of the atmospheric disturbance and the receiving point lie in any plane, as in Fig. 2.

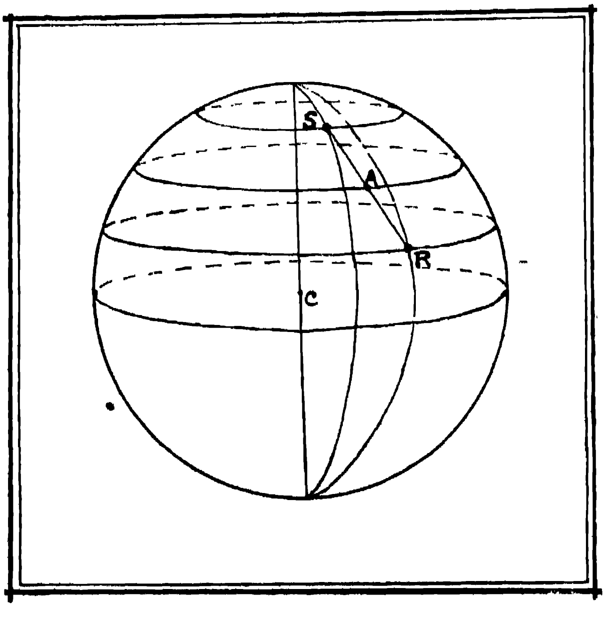

FIG. 2

Let SR make an angle with the north-south line at the receiving point R. The point at which reflexion at the ionosphere takes place is now directly above a small circle corresponding to the latitude of A ; In Fig. 1 the tangent plane drawn from A to the ozonosphere touches it at G. The straight line GC drawn from this point G to the centre C of the small circle makes now an angle with CA, given by

$$\cos\phi = \frac{R\cos\frac{\lambda_s+\lambda_r}{2} + H_o}{R\cos\frac{\lambda_s+\lambda_r}{2} + H_i}$$

where λ_s and λ_r are the latitudes of the source of atmospherics and the receiving point, H_o and H_i the heights of the ozone layer and the E-layer respectively and R the radius of the earth. We are assuming here that the sun follows a path in a plane parallel to the equatorial plane. The assumption does not materially alter the calculation with which we are concerned. Approximately, however, when the source of atmospherics is not too distant, we can write

$$\cos\phi = \frac{R\cos\lambda_r + H_o}{R\cos\lambda_s + H_i} \qquad (2)$$

Again if l_s and l_r are the longitudes of the source S of atmospherics and the receiving point R, the difference between the instant of ground sunrise (or sunset) and the instant when the ionization begins to increase (or decrease) in the region A would be given by

$$\Delta T = 4\phi \mp 2(l_s - l_r) \text{ minutes} \qquad \ldots \quad (3)$$

Further, we have

$$\tan\alpha = \frac{\lambda_r \sim \lambda_s}{l_r \sim l_s} \qquad (4)$$

where α is the direction of arrival of the atmospherics at the receiving point with respect to north-south.

Thus if for the receiving point the latitude λ_r and longitude l_r are known, it is possible to find the latitude λ_s and longitude l_s of the thunderstorm centre from (2), (3) and (4), if the time of occurrence of the sunrise (or sunset) maximum relative to ground sunrise (or sunset) and the direction of arrival of the atmospherics are known. The angular distance of the thunderstorm centre from the receiving point can then be obtained from the formula :

$$\widehat{SCR} = \cos^{-1}[\sin\lambda_s . \sin\lambda_r + \cos\lambda_s . \cos\lambda_r . \cos(l_s - l_r)] \qquad \ldots \quad (5)$$

The actual distance is easily determined by multiplying the angular distance by the radius of the earth.

For Dacca as the receiving point

and taking the following data :

Radius of the earth

Reflexion height in the E-layer from the earth's sur

Ozone layer height

we get $\phi=\cdot 7^{\circ}$

With this value of ϕ and with the observed val

centres can be easily calculated.

TIME OF OCCURRENCE OF SUNRISE MAXIMA OF ATMOSPHERICS PARTICULAR CASES

East-West direction For the east-west directio

evident $\lambda_s=\lambda_r$. So long as the source of atmospherics is

receiving point *i.e.*, $l_s > l_r$, and the distance is within th $)=2\phi$, the atmospherics maximum is expected to appear *before* ground sunrise and *after* ground sunset. Within this limit, the greater is the distance between the receiving point and the noise source, the smaller is the difference in time between ground sunrise (or sunset) and the time of occurrence of the atmospherics maximum. When the distance is such that $2(l_s-l_r)=4\phi$, a maximum is expected at the ground sunrise (or sunset). When the distance exceeds this limit, the atmospherics maximum appears *after* the ground sunrise and *before* the ground sunset.

When the source of atmospherics is to the *west* of the receiving point $l_s < l_r$, and the distance is within the limit $(l_r-l_s)=2\phi$, the maximum would appear *after* the ground sunrise and *before* the ground sunset. Within this limit, the greater is the distance between the noise source and the receiving point, the smaller is the difference in time between ground sunrise (or sunset) and the time of occurrence of the maximum. In the same way, again, when $2(l_r-l_s)=4\phi$, a maximum would appear at the ground sunrise (or sunset). When the distance exceeds this limit the maximum would appear *before* the ground sunrise and *after* ground sunset.

North-South direction.—For the N-S direction *i.e.*, it is evident $l_s=l_r$. Thus the atmospherics maximum is always expected at 4ϕ min. before ground sunrise or 4ϕ min. after ground set.

SUCCESSIVE REFLEXIONS FROM THE IONOSPHERE

Successive reflexions from the ionosphere would, however, cause atmospherics maxima to appear one after another at regular intervals of time. For this, the location of thunderstorm centre requires careful consideration. Let

S and R denote respectively the source of atmospherics and the receiving point in the E-W plane. For a single ionospheric reflexion, A is the point where such reflexion takes place (Fig. 3). For double reflexion, X and Y are the points where reflexion occurs. For a single reflexion, the difference of time between ground sunrise (or sunset) and the time of occurrence of maximum is given by

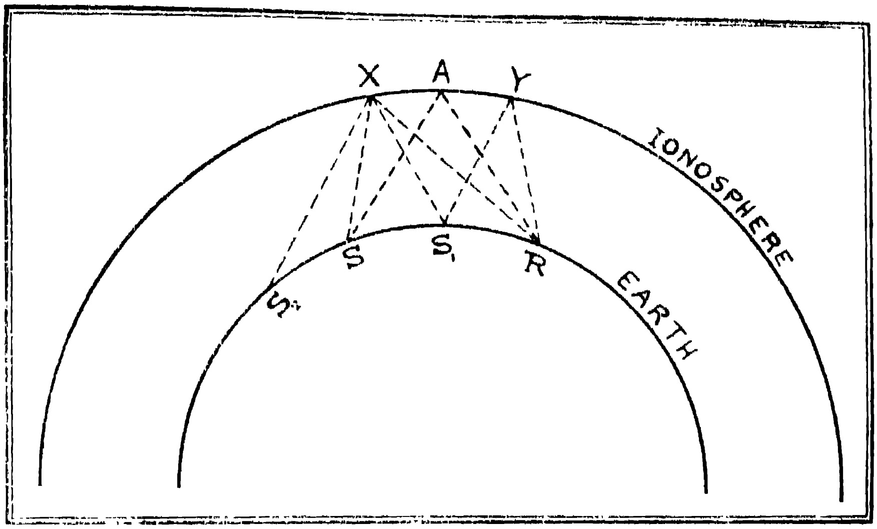

FIG. 3

$$\Delta T = 4\phi - 2\theta,$$

where θ is the angular distance between S and R.

In the case of successive double reflexion, for the *second* reflexion at Y, $(\Delta T)_2 = 4\phi - \theta$, the 'virtual' source being at S_1, whereas, for the *first* reflexion at X, $(\Delta T)_1 = 4\phi - 3\theta$, the virtual source being at S_2. The difference of $(\Delta T)_2$ and $(\Delta T)_1 = 2\theta$ min. Thus if single as well as successive double reflexions occur simultaneously between S and R, three maxima will appear successively at $(\Delta T) = 4\phi - \theta$, $4\phi - 2\theta$ and $4\phi - 3\theta$, the successive intervals of time being θ min.

In locating thunderstorms centres from directional observations of distant atmospherics, the above considerations are of importance.

THE D/F EQUIPMENT AND EXPERIMENTAL PROCEDURE

The D/F equipment

Briefly the D/F equipment consisted of the following :—

(1) A pair of 'crossed' loop, 6 ft. sq. with 10 turns of S.W. No. 7/22 stranded copper wire. The plane of one aerial was in the N-S direction and that of the other in the E-W direction. Each was tuned to 1000 metres.

(2) The two loop aerials were connected to two similar H/F amplifier units. The circuit diagram of each is shown in Fig. 4.

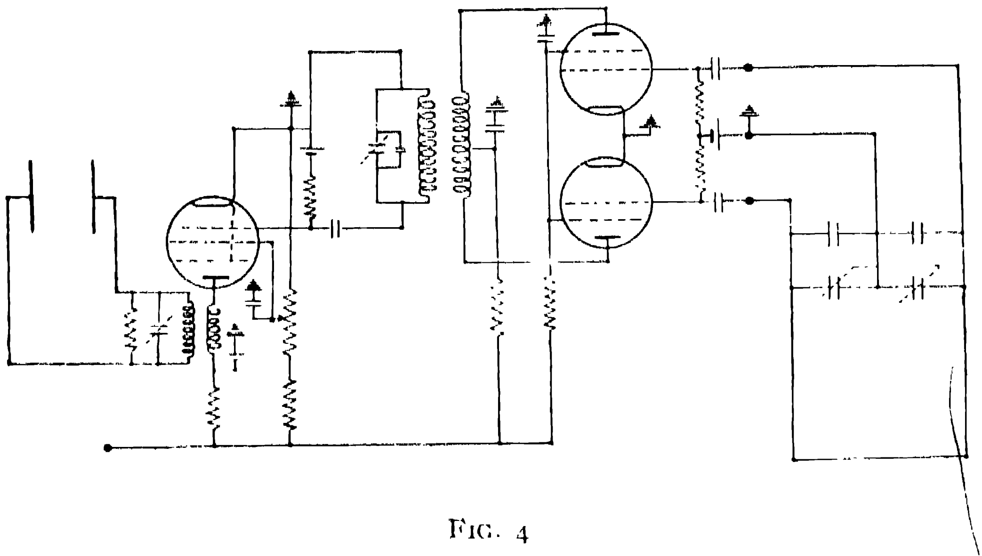

FIG. 4

(3) *The Oscilloscope.*—To a pair of the deflecting plates was connected the output of one amplifier and to the other pair was connected the output of the other amplifier.

When the atmospheric pulse was received by the aerial-system, currents were induced into the two aerials each tuned to 1000 metres. The voltages developed across the tuning condensers were then amplified and the amplified voltages applied across the two pairs of deflecting plates in rectangular directions yielded a straight line on the oscillograph screen. The inclination of the straight line gave the direction of arrival of the atmospherics for which the particular straight line response was obtained. In the experimental arrangement, the straight line sweep on the oscillograph screen in the vertical direction indicated 0° representing N-S. The orientation of the line in the clock-wise direction indicated increasing angles towards the E-W. The directions were obtained on a transparent scale held in contact with the surface of the oscillograph screen.

(4) *Balanced Oscillator.*—For proper adjustment of the D/F equipment, an oscillator producing oscillations corresponding to 1000 metres with 'pairs' of balanced 'bleeder' resistances in the output circuit was employed. With equal voltages obtained from the pair of bleeder resistances and applied across the tuning condensers of the two loop aerials, the linear response on the oscillograph screen was noted and by adjusting the gain of one or the other of the amplifiers, the straight line response was made to point exactly in the direction of 45°. The 45° alignment was made each time before a set of directional observations of atmospherics was taken.

EXPERIMENTAL PROCEDURE

Each day when sunset observations were decided upon, it was arranged to take continuous observations of the directions and magnitudes of the linear responses for 10 mins. before and 30 to

40 mins. after the ground sunset for the day. On the transparent scale was marked straight lines in ink showing directions at intervals of 10° round the centre which coincided with the undeviated central spot on the oscillograph screen. The number of atmospherics recorded in 2′ mins. was then counted for each direction. The sum of the magnitudes of the linear responses for the same 2′ mins. was also found for each direction. This measured what may be called the *atmospherics activity*, during the period of 2′ mins. The number and the 'activity' of the atmospherics were then separately plotted against time for the different directions. From the time of occurrence of the observed maxima with reference to the ground sunset time, the locations of the source of atmospherics was found in the way already explained.[1]

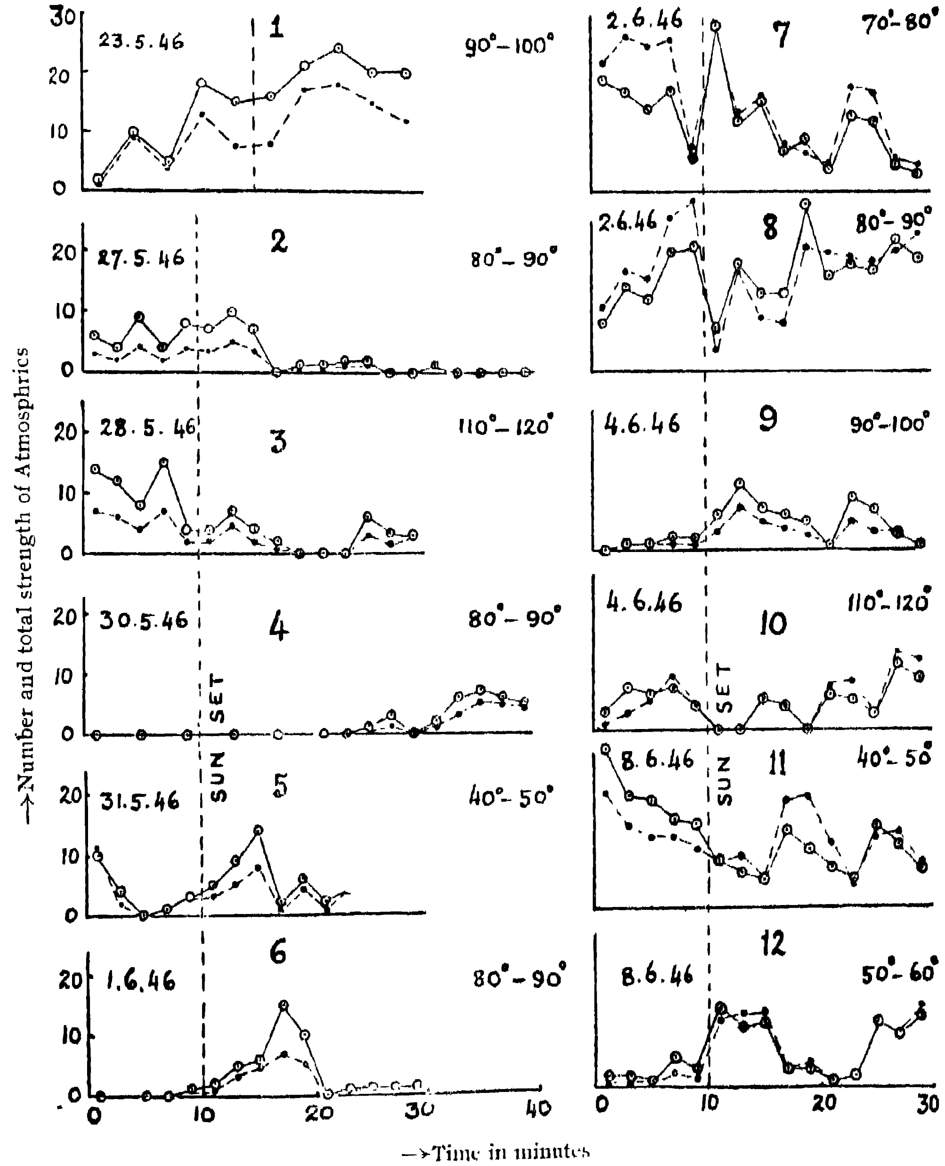

FIG. 5

EXPERIMENTAL RESULTS

Some typical directional observations out of a large number taken during the course of about a month in May-June, 1946, are given here. The twelve sets of observations for atmospherics coming from different directions are illustrated in Fig. 5. The graphs clearly show the maxima in *number* and *activity* of the atmospherics during sunset period. *Usually* the positions of the maxima coincide for atmospherics number and activity. Due to comparatively long period of observations after the sunset and only a short period before it, the maxima after senset were observed more than those before sunset. It is evident from theoretical considerations that the maximum after ground sunset *usually* denotes the arrival of the atmospherics after ionospheric reflexion from a thunderstorm centre on the eastern side of the receiving point and similarly the maximum before sunset usually indicates the arrival of the atmospherics from the western side of the receiving point, except for *very distant* atmospherics which are too feeble to be recorded on the oscillograph.

One distinct case of successive double reflexion simultaneously occurring with the usual single reflexion between the source of atmospherics and receiving point is shown in curve No. 10, where there are three successive peaks at regular intervals. The location of the source of atmospherics is in such cases obtained with reference to the middle peak. It is likely that the curves Nos. 9 and 11 represent two other similar cases where possibly the farthest of the three successive peaks was not observed.

LOCATIONS AND DISTANCES OF THUNDERSTORM CENTRES

In Table I are entered the locations and distances of thunderstorm centres for the twelve cases as calculated from the observed times of occurrence of the atmospherics maximum after or before the ground sunset time. The interval of time is taken as positive or negative according as the maximum occurred after or before the ground sunset.

TABLE I

T (min)	Location of Thunder-storm centres	Distance	Remarks
1. (*a*) 7.5	100°.65 E 22°.8 N	1034 Km.	
(*b*) − 5.0	78°.9 E 22°.7 N	1190 Km	
(*c*) − 10.5	81°.65 E 22°.9 N	900.7 Km	
2. (*a*) + 3	102°.9 E 24°.8 N	1278 Km.	

TABLE I (*contd.*)

	(*b*)− 5	78°.9 E 24°.7 N	1179 Km	
3.	(*a*)+15	96°.9 E 20°.7 N	756.1 Km.	
	(*b*)+ 3	102°.9 E 17°.9 N	1156 Km.	
	(*c*)− 3	77°.9 E 17°.9 N	1456 Km.	
4.	(*a*)+25	91°.4 E 23°.8 N	180.0 Km	
	(*b*)+17	95°.9 E 24°.2 N	975.2 Km	
5.	(*a*)+ 9	99°.9 E 14°.2 N	1456 Km	
	(*b*)+ 5	101°.9 E 12°.2 N	1764 Km	
6.	+ 7	100°.9 E 24°.6 N	1068 Km	
7.	(*a*)+13	97°.9 E 25°.7 N	705 Km	
	(*b*)+ 5	101°.9 E 26°.8 N	1268 Km	
	(*c*)+ 1	103°.9 E 20°.1 N	1431 Km.	
8.	(*a*)+ 9	99°.9 E 24°.5 N	98[illegible].9 Km	
	(*b*)+ 3	102°.9 E 24°.8 N	1276 Km	
9	(*a*) . (*b*)+13 (*c*)+ 3	97°.9 E 23°.0 N	773.9 Km	Multiple reflexion
10.	(*a*)+17 (*b*)+11 (*c*)+ 5	98°.9 E 23°.3 N	867.4 Km.	Multiple reflexion
11.	(*a*) ... (*b*)+15 (*c*)+ 7	96°.9 E 30°.2 N	967.4 Km.	Multiple reflexion
12	(*a*)+15	96°.9 E 28°.3 N	834.1 Km.	
	(*b*)+ 5	101°.9 E 31°.8 N	1445 Km.	
	(*c*)− 3	77°.9 E 32°.5 N	1575 Km	

CONCLUSION

The thunderstorm centres on the eastern side of Dacca were mostly in Burma near the Shan States. Few records showed that the atmospherics originated in the western side of Dacca were mostly from Central India. The thunderstorm centres as found from the twelve sets of atmospherics records ranged from 189 to 1764 Km.

ACKNOWLEDGEMENT

The measurements were carried out at the Dacca Atmospherics Research Station with the D/F equipment of the Council of Scientific and Industrial Research to whom our thanks are due. We also sincerely thank Mr. N. C. Dhar, M.Sc., Meteorological Assistant, for technical help in these observations.*

Physics Department
Dacca University.

---

* A summary of the paper has recently been published in (*Nature*, 26, April. 1947.)

REFERENCES

Eccles, (1918), Handbook of Wireless Telegraphy and Telephony, 176.
Espenschied, Anderson and Bailey, (1926), *Proc. I R.E.*, **14**, 7.
Khastgir, (1942), *Science and Culture*, **11**, 233 .
Khastgir and Basak, (1942), *Current Science*, **11**, 392.
Khastgir and Kameswar Rao, (1940), *Proc. I.R.E.*, **28**, 511
Khastgir and Innas Ali, (1942), *Ind. J. Physics*, **16**, Part 6, 399.
Khastgir and Majumdar, (1942), *Science and Culture*, **11**, 235.
Khastgir and Ray, (1940), *Science and Culture*, **5**, 772.
Mitra, (1938), *Science and Culture*, **3**, 496
Namba, (1933), *Proc. I.R.E.*, **21**, 238.
Potter, (1931), *Proc. I.R.E* , **12**, 1731
,, (1932), *Proc. I.R.E.*, **20**, 1512.
Subba Rao, (1941), *Proc. Nat Acad. Science (India)*, **14**, No. 2, Sec. B.
Venkata Rao Telang, (1941), *Proc. Ind. Science Congress*, Paper No. 20, Physics Section.

ON THE PROPAGATION OF E.M. WAVES THROUGH THE UPPER ATMOSPHERE

BY M. N. SAHA,* B. K. BANERJEA AND U. C. GUHA

ABSTRACT. This paper reports a comprehensive working of the problems of an ionised atmosphere, traversed by a magnetic field, as in the case of the Earth's atmosphere. Expressions are deduced for electrical polarisation and complex conductivity for such an atmosphere when traversed by radio waves, in a tensor-form, as first suggested by Darwin. The equations of propagation of radio frequency waves through such a medium are obtained by the use of cardinal axes, and then the equations of vertical propagation are deduced Expressions are obtained for refractive indices of ordinary and extraordinary waves, which agree with the expressions given by Appleton. Expressions are obtained for polarisation, absorption etc. of the radio waves travelling in the ionosphere. Curves are given for the polarisation ratio and refractive indices of the two waves as functions of the magnetic latitude of the place of observation.

1 INTRODUCTION

Ever since the classical works of Appleton (1932) and Hartree (1932), the problem of the propagation of e.m. waves in the ionosphere has received attention from numerous workers Summaries of these works are available in various reports. Recently B. K. Banerjea (1947) made a critical and comparative study of the fundamental methods of Appleton (1932), Hartree (1932), Saha, Rai and Mathur (1937) and Saha and Banerjea (1945) and showed that these various methods can be deduced as special cases of a general method developed according to Darwin's (1925) suggestion of treating the e.m. properties of the medium as tensor quantities. The present paper continues the treatment further and aims at giving a true wave formulation of the general problem. For the convenience of the reader some results of the previous works carried out by the senior author and his early collaborators are included so that no further references to these papers are needed. Part of the results mentioned in the earlier parts are not new, but have been derived in a novel, easier and unitary way.

The Displacement of the Ions in the Ionosphere

The equation of motion of the charged ions referred to any system of co-ordinates can be written as :

$$\frac{d^2\rho}{dt^2}+\nu\frac{d\rho}{dt}+\frac{e}{mc}\left[\mathrm{H}\times\frac{d\rho}{dt}\right]=\frac{e}{m}\boldsymbol{E} \qquad (1.1)$$

---

* Fellow of the Indian Physical Society.

where ρ = displacement vector with components (ξ, η, ζ)

e, m = magnitude of the charge and mass of the ion respectively.

ν = collision frequency of the ions.

H = Earth's magnetic field.

$\boldsymbol{E} = \boldsymbol{E}_0 \cos pt$, electric vector of the incident electromagnetic wave.

The effect of the magnetic vector and the space charges have been omitted as usual. The notation conforms as closely as possible to those used by Appleton (1932) and Saha, Rai and Mathur (1937) and B. K. Banerjea (1947).

It can easily be verified that the solution of the above equation with $\boldsymbol{E} = \boldsymbol{E}_0 \cos pt$ is the real part of the solution obtained with $\boldsymbol{E} = \boldsymbol{E}_0 e^{ipt}$; we use $\boldsymbol{E}$ in this latter form because solution is then easy to obtain. The quantity analogous to the static conductivity now comes out as complex (Stratton, 1942), whose real part gives ordinary refractive index and the imaginary part gives deviation of the refractive index from unity.

Introducing the polarisation vector $\boldsymbol{P} = 4\pi N e\rho$ where N is the ion-concentration and using the abbreviations,

$$\frac{mp^2}{Ne^2} = \frac{4\pi p^2}{p_0^2} = \frac{4\pi}{r}, \quad p_0^2 = \frac{4\pi N e^2}{m}, \quad r = \frac{p_0^2}{p^2},$$

$$\nu/p = \delta, \qquad 1 - i\delta = \beta, \qquad \dots \quad (1.2)$$

$$\frac{eH}{mc} = \mathbf{p}_h, \qquad \frac{\mathbf{p}_h}{p} = \omega \text{ with components } \omega_x, \omega_y, \omega_z.$$

We get from equation (1.1) replacing $\rho\ (\xi, \eta, \zeta)$ by $\frac{1}{4\pi N e}(P_x, P_y, P_z)$

$$\begin{aligned} \beta P_x + i\omega_z P_y - i\omega_y P_z &= -E_x \\ -i\omega_z P_x + \beta P_y + i\omega_x P_z &= -E_y \qquad \dots \quad (1.3) \\ i\omega_y P_x - i\omega_x P_y + \beta P_z &= -E_z \end{aligned}$$

The solution of these equations can be briefly written as

$$P = A\,\Delta.E \qquad \dots \quad (1.4)$$

where $A = \frac{r}{\beta(\beta^2 - \omega^2)}$ and Δ is a tensor given by the matrix,

$$\Delta = \begin{vmatrix} \omega_x^2 - \beta^2 & \omega_x\omega_y + i\beta\omega_z & \omega_x\omega_z - i\beta\omega_y \\ \omega_y\omega_x - i\beta\omega_z & \omega_y^2 - \beta^2 & \omega_y\omega_z + i\beta\omega_x \\ \omega_z\omega_x + i\beta\omega_y & \omega_z\omega_y - i\beta\omega_x & \omega_z^2 - \beta^2 \end{vmatrix} \qquad \dots \quad (1.5)$$

It has been shown by Saha and Banerjea (1945) that the tensor possesses certain "Cardinal Axes" which may be denoted by 1, 2, 3. "1" is the direction of the earth's magnetic field, "2" is the line perpendicular to the magnetic meridian, and "3" is the line perpendicular to "1" lying in the magnetic meridian. The relation between these axes and the axes commonly used in ionospheric problems with XZ as magnetic meridian and OZ as vertical is shown in the diagram below :

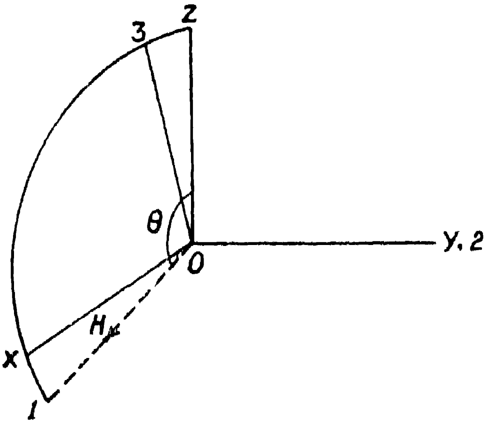

FIG. 1

Shows disposition of cardinal axes (1, 2, 3) with axes used generally in considering vertical propagation.

In this figure $\theta = \angle ZO1$ is called the angle of propagation. The axis O1 is always along the positive direction of H. In general literature on ionospheric problems, the positive direction of H is generally not expressed quite clearly, with the result that the sense of rotation of the electric and magnetic vectors of the returning radio wave is left unclarified. In what follows the positive direction of H is along the positive direction of the magnetic lines of force, *i.e.* in the northern hemisphere it is downward and in the southern the reverse is the case.

Choice of these axes is equivalent to putting

$$\omega_1 = \omega, \quad \omega_2 = \omega_3 = 0,$$

where ω_1, ω_2, ω_3 are the components of ω along (1, 2, 3) axes. We have then

$$\Delta = - \begin{vmatrix} \beta^2 - \omega^2 & 0 & 0 \\ 0 & \beta^2 & i\beta w \\ 0 & -i\beta w & \beta^2 \end{vmatrix} \qquad \ldots \quad (1.6)$$

The complex conductivity σ of the medium, defined by the equation

$\boldsymbol{\sigma}.\boldsymbol{E} = \text{current} = -Ne\dfrac{d\boldsymbol{\rho}}{dt} = -ipNe\boldsymbol{\rho} = -\dfrac{ip}{4\pi}\boldsymbol{P} = -\dfrac{ipA}{4\pi}\Delta.\boldsymbol{E}$ is a tensor quantity defined by the matrix,

$$\boldsymbol{\sigma}=\frac{iNe^2}{m}\begin{vmatrix}\frac{1}{p-i\nu} & 0 & 0\\ 0 & \frac{p-i\nu}{(p-i\nu)^2-p_h^2} & \frac{-ip_h}{(p-i\nu)^2-p_h^2}\\ 0 & \frac{ip_h}{(p-i\nu)^2-p_h^2} & \frac{p-i\nu}{(p-i\nu)^2-p_h^2}\end{vmatrix} \qquad \dots (1.7)$$

The steady current conductivity σ^* is obtained from above by putting $p=0$. We have

$$\boldsymbol{\sigma}^*=\frac{Ne^2}{m}\begin{vmatrix}\frac{1}{\nu} & 0 & 0\\ 0 & \frac{\nu}{p_h^2+\nu^2} & \frac{p_h}{p_h^2+\nu^2}\\ 0 & \frac{-p_h}{p_h^2+\nu^2} & \frac{\nu}{p_h^2+\nu^2}\end{vmatrix} \qquad \dots (1.8)$$

Thus in the direction of the magnetic field, the steady current conductivity is $\frac{Ne^2}{m\nu}$. We have the components of current as

$$i_1=\frac{Ne^2}{m\nu}E_1$$

$$i_2=\frac{Ne^2}{m(p_h^2+\nu^2)}(\nu E_2+p_h E_3) \qquad \dots (1.9)$$

$$i_3=\frac{Ne^2}{m(p_h^2+\nu^2)}(-p_h E_2+\nu E_3)$$

If $E_3=0$, we have $i_2=\frac{Ne^2}{m(p_h^2+\nu^2)}\nu E_2$. The quantity $\frac{Ne^2\nu}{m(p_h^2+\nu^2)}$ is known as transverse conductivity. We have besides, the current $i_3=-\frac{Ne^2p_h}{m(p_h^2+\nu^2)}E_2$ along the Z axis, though there may be no e.m.f. in that direction

The Polarisation Vector.—The polarisation vector $\boldsymbol{P}$ is defined as

$$\boldsymbol{P}=\frac{4\pi i}{p}\boldsymbol{\sigma}.\boldsymbol{E}$$

and we can easily deduce that

$$E_1=-\frac{\beta}{r}P_1,\quad E_2\pm iE_3=-\frac{\beta\mp w}{r}(P_2\pm iP_3) \qquad \dots (1.10)$$

The Electric Displacement Vector and the Complex Dielectric Tensor.—The electric displacement vector $\boldsymbol{D}=\boldsymbol{E}+\boldsymbol{P}$ may be expressed as $\boldsymbol{D}=\mathsf{K}.\boldsymbol{E}$., where K is the complex dielectric tensor given by the matrix,

$$\mathbf{K}=\begin{vmatrix} 1-r/\beta & 0 & 0 \\ 0 & 1-r\beta/(\beta^2-\omega^2) & ir\omega/(\beta^2-\omega^2) \\ 0 & -ir\omega/(\beta^2-\omega^2) & 1-r\beta/(\beta^2-\omega^2) \end{vmatrix} \qquad \dots \quad (1.11)$$

2. THE MAXWELLIAN EQUATIONS

From the Maxwellian equations :

$$\nabla\times\boldsymbol{H}=\frac{1}{c}\frac{\partial\boldsymbol{D}}{\partial t},\quad \nabla\times\boldsymbol{E}=-\frac{1}{c}\frac{\partial\boldsymbol{H}}{\partial t},\quad \nabla.\boldsymbol{D}=\nabla.\boldsymbol{H}=0 \qquad \dots \quad (2.1)$$

We get by the usual methods, the equations of propagation for the electric and magnetic vectors in the form :

$$\Delta^2E_1+\frac{p^2}{c^2}(1-r/\beta)E_1=0$$

$$\nabla^2(E_2\pm iE_3)+\frac{p^2}{c^2}\left(1-r/(\beta\pm\omega)\right)(E_2\pm iE_3)=0 \qquad \dots \quad (2.2)$$

$$\nabla^2\boldsymbol{H}+\frac{p^2}{c^2}\boldsymbol{H}=-\frac{4\pi}{c}\nabla\times(\boldsymbol{\sigma}.\boldsymbol{E})$$

The Wave Equations for Vertical Propagation in any Latitude:—Let us first confine ourselves to the propagation along the vertical Z-axis, so that ∇ and ∇^2 simply reduce to $\frac{d}{dz}$ and $\frac{d^2}{dz^2}$. Introducing the new variable $u=pz/c$, we get from (2.2)

$$\frac{d^2E_1}{du^2}+\left(1-\frac{r}{\beta}\right)E_1=0 \qquad \dots \quad (2.3a)$$

$$\frac{d^2}{du^2}(E_2+iE_3)+\left(1-\frac{r}{\beta-\omega}\right)(E_2+iE_3)=0 \qquad \dots \quad (2.3b)$$

$$\frac{d^2}{du^2}(E_2-iE_3)+\left(1-\frac{r}{\beta+\omega}\right)(E_2-iE_3)=0 \qquad \dots \quad (2.3c)$$

The components of the vector E in two systems (1, 2, 3) and with XZ-plane as magnetic meridian and OZ as vertical are related as :

$$\left.\begin{aligned} &E_1=E_x\sin\theta+E_z\cos\theta; && E_x=E_1\sin\theta-E_3\cos\theta. \\ &E_2=E_y; && E_y=E_2. \\ &E_3=-E_x\cos\theta+E_z\sin\theta; && E_z=E_1\cos\theta+E_3\sin\theta. \\ &\omega_x=\omega\sin\theta,\quad \omega_y=0, && \omega_z=-\omega\cos\theta \end{aligned}\right\} \qquad \dots \quad (2.4)$$

The equations (2.3) as such are not suitable for use when we consider the propagation of plane waves, for such cases we have to use in conjunction with (2.2), the Maxwellian condition $\nabla.\boldsymbol{D}=0$. For vertical propagation, this reduces to $\frac{d}{dz}D_z = 0$, *i.e.*, $D_z = 0$, since the steady components of **D**, if any, are unimportant in the study of the wave propagation :

From $D_z = 0$ and (1.4) and (1.5) we have eliminating P_x, P_y, P_z and putting $w_y = 0$.

$$E_z = \frac{iw_x}{C'}(-w_z E_x + i\beta E_y) \qquad \ldots \quad (2.5)$$

where $C' = \beta(\beta^2 - w^2) - r(\beta^2 - w_z^2)$.

Multiplying (2.3a) by $\sin\theta$ and the difference of (2.3b) and (2.3c) by $-\cos\theta$, adding the results and then replacing E_1, E_2, E_3 by their equivalent expressions in terms of E_x, E_y, E_z from (2.4) we get after some simplification,

$$\frac{d^2E_x}{du^2} + \mathrm{K}_1 E_x - i\mathrm{L}E_y = 0 \qquad \ldots \quad (2.6)$$

where

$$\left.\begin{aligned} \mathrm{K}_1 &= 1 - r\frac{\beta^2 - r\beta - \omega^2\sin^2\theta}{C'} \\ \mathrm{L} &= \frac{-i(\beta - r)\omega\cos\theta}{C'} \end{aligned}\right\} \qquad \ldots \quad (2.7)$$

Again replacing E_2 and E_3 by E_x, E_y, E_z in equation (2.3b) from (2.4) and E_z by E_x and E_y from (2.2), we have after some work,

$$\frac{d^2E_y}{du^2} + \mathrm{K}_2 E_y + i\mathrm{L}E_x = 0. \qquad \ldots \quad (2.8)$$

where

$$\mathrm{K}_2 = 1 - r\frac{\beta^2 - r\beta}{C'} \qquad \ldots \quad (2.9)$$

Equation (2.6) and (2.8) were obtained explicitly in this form by Saha, Rai and Mathur (1937). Equivalent equations with vector components of the ordinary and extraordinary waves intermixed in each equation were obtained by Rydbeck (1944). But equations in this form do not help much in the understanding of the phenomena, unless the coupling term L between the variables vanishes. This takes place at $\theta = \pi/2$, *i.e.*, at the magnetic equator, where the equations of propagation become,

$$\frac{d^2E_x}{du^2} + \left(1 - \frac{r}{\beta}\right)E_x = 0 \qquad \ldots \quad (2.10)$$

$$\frac{d^2E_y}{du^2} + \left(1 - \frac{r}{\beta - \frac{\omega}{\beta - r}}\right)E_y = 0$$

For the magnetic poles, $\theta = \pi$ and 0, and for these values of θ, $\mathrm{K}_1 = \mathrm{K}_2$; for $\theta = \pi$, *i.e.*, mag N-pole, the equation of propagation takes the form :

$$\frac{d^2}{du^2}(E_x \pm iE_y) + \left(1 - \frac{r}{\beta \mp \omega}\right)(E_x \pm iE_y) = 0 \qquad \ldots \quad (2.11)$$

For $\theta=0$, *i.e.*, mag. S-Pole, the equation similarly reduces to

$$\frac{d^2}{du^2}(E_x \pm iE_y) + \left(1 - \frac{}{\beta+\omega}\right)(E_x \pm iE_y) = 0 \qquad (2.11a)$$

Equation in these forms were studied by Saha and Rai (1937), for the case when damping is negligible, *i.e.*, $\beta=1$, from the wave mechanical point of view. The Chapman layer of ion-distribution was treated as a potential barrier and the penetration of the waves under certain simplifying assumptions were studied in the same way as Gamow did in his famous work on the "Penetration of the Potential Barrier of Nuclei of Atoms by High Energy Particles." Recently Rydbeck (1942) has studied these equations when the coupling term L vanishes; he has given an elaborate treatment of the wave equations for magnetic equator and taking a parabolic ion-layer and using Weber's parabolic functions he has obtained expressions for the reflection co-efficient, transmission co-efficient and phase retardation of the wave in a thin friction free parabolic layer. In the ray treatment of Appleton we practically confine ourselves to these two limiting cases, *viz.*, their quasi-longitudinal case is for $\theta=\pi$, 0, *i.e.*, $K_1=K_2$ and their quasi-transverse case, *i.e.*, $\theta=\frac{\pi}{2}$, $L=0$.

The following method will be found applicable to all stations. Multiplying both sides of (2.8) by "iF," and adding to (2.6), where F is an indeterminate multiplier to be presently determined, we have

$$\frac{d^2E_x}{du^2} + iF\frac{d^2E_y}{du^2} + (K_1 - FL)E_x + \left(K_2 - \frac{L}{F}\right)iFE_x = 0 \qquad \dots \quad (2.12)$$

Now choose F in such a way that $K_1 - FL = K_2 - \frac{L}{F}$

so that F is given by the equation

$$F^2 - \frac{K_1 - K_2}{L}F - 1 = 0 \qquad \dots \quad (2.13)$$

Put
$$\frac{K_1 - K_2}{L} = \frac{\omega \sin^2\theta}{(r-\beta)\cos\theta} = 2G = 2g\cos\alpha e^{i\alpha},$$

where
$$g = \frac{\omega \sin^2\theta}{(r-1)\cos\theta}, \quad \tan\alpha = \frac{\delta}{1-r} \qquad \dots \quad (2.14)$$

Let F_1, F_2 be the roots of equation (2.13). Then

$$F_1, F_2 = G \pm \sqrt{1+G^2}$$

$$= g \pm \sqrt{1+g^2} \qquad \text{for } \delta=0 \qquad \dots \quad (2.15)$$

Now turning to equation (2.12) we can rewrite it in the form

$$\frac{d^2}{du^2}(E_x + iFE_y) + q^2(E_x + iFE_y) - 2i\frac{dF}{du}\frac{dE_y}{du} - i\frac{d^2F}{du^2}E_y = 0 \dots \quad (2.16)$$

where q has the two values given by

$$q_1{}^2 = K_2 - \frac{L}{F_1} = K_2 + LF_2 = 1 - \frac{r}{C'}(\beta - \gamma)(\beta + \omega \cos\theta\, F_2)$$

$$= 1 - \frac{r}{\beta + \omega\cos\theta\, F_1}. \qquad \dots \quad (2.17)$$

$$q_2{}^2 = K_1 - \frac{L}{F_2} = K_1 + LF_1 = 1 - \frac{r}{C'}(\beta - r)(\beta + \omega\cos\theta\, F_1)$$

$$= 1 - \frac{r}{\beta + \omega\cos\theta\, F_2}. \qquad \dots \quad (2.18)$$

for $C' = (\beta - r)(\beta + \omega\cos\theta\, F_1)(\beta + \omega\cos\theta\, F_2)$.

In those cases where the quantities $\frac{dF}{du}$, $\frac{d^2F}{du^2}$ can be neglected, the equations can be written as

$$\frac{d^2}{du^2}(E_x + iF_1E_y) + q_1{}^2(E_x + iF_1E_y) = 0 \qquad \dots \quad (2.16a)$$

$$\frac{d^2}{du^2}(E_x + iF_2E_y) + q_2{}^2(E_x + iF_2E_y) = 0$$

These signify that the beam is broken up into two, with the refractive indices q_1, and q_2, and polarisations determined by F_1 and F_2 (*Vide* §4).

We next proceed to discuss the case of friction free atmosphere. In this case we have

$$q_1{}^2 = 1 - \frac{r}{1 + \omega\cos\theta\, F_1} \qquad \dots \quad (2.17a)$$

$$q_2{}^2 = 1 - \frac{r}{1 + \omega\cos\theta\, F_2} \qquad \dots \quad (2.18a)$$

Both q_1, q_2 are to be continuous functions of r. We find from the expression for g, that for $r \longrightarrow 1$, $g \longrightarrow \infty$. At this point, $q_1{}^2$, $q_2{}^2$ should obey the condition of continuity, *i.e.*,

$$\underset{r=1-0}{\mathrm{Lt}}(q_1{}^2,\ q_2{}^2) = \underset{r=1+0}{\mathrm{Lt}}(q_1{}^2,\ q_2{}^2)$$

Taking first q_1, we find that if we take for the region $r=0$ to $r=1$

$$F_1 = g - \sqrt{1+g^2}, \text{ consequently } q_1{}^2 = 1 - \frac{}{1 - \omega\cos\theta\,(\sqrt{1+g^2} - g)} \qquad (2.17b)$$

Then q_1 varies from 1 to 0 in the domain $r=0$ to 1. As the value is to be continuous, and since g on crossing over to $r = 1+0$, becomes negative, we find that for this region ($r > 0$) we should put

$$F_1 = \sqrt{1+g^2} - |g|$$

$$i.e., \ q_1{}^2 = 1 - \frac{}{1 + \omega\cos\theta\,(\sqrt{1+g^2} - |g|)} \qquad \dots \quad (2.17c)$$

These expressions for q_1^2 has no singularity at any point and it is identical with the expression for the refractive index of the ordinary wave as given by Appleton. A $(1-q_1^2)$ curve for different values of θ from expressions (2.17 *b*, *c*) is given in Fig. 2, for $\omega < 1$, and $\omega > 1$.

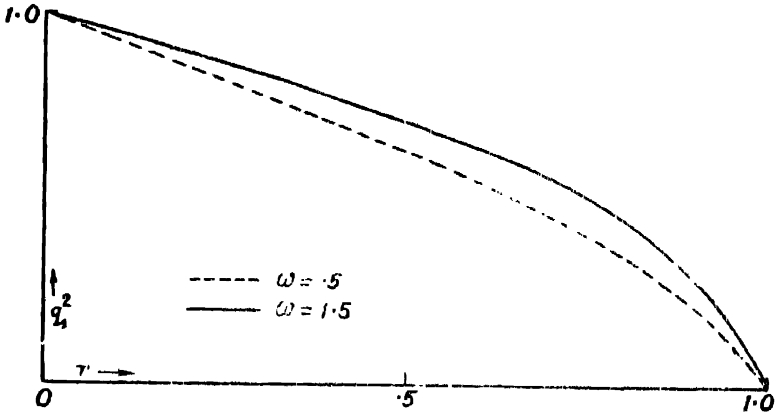

Fig. 2

Variation of the square of the refractive index for the o-wave with electron concentration $\left(r = \frac{4\pi e^2}{mp^2} N\right)$, for p_h/p $\omega < 1$ (here .5) and $\omega > 1$ (here 1.5)

For the other beam we can now substitute the corresponding value of F_2, we obtain :

$$q_2^2 = 1 - \frac{r}{1+\omega \cos\theta \, F_2} = 1 - \frac{r}{1+\omega\cos\theta(\sqrt{1+g^2}+g)} \quad \text{for } r<1 \quad \dots (2.18b)$$

$$= 1 - \frac{r}{1-\omega\cos\theta(\sqrt{1+g^2}+|g|)} \quad \text{for } r>1 \quad \dots \quad (218c)$$

It can be easily shown that for $\omega < 1$, $(1-q_2^2)$-curve starts from (o, 1) passes through $(1-\omega, 0)$ and a point of infinite singularity at $r = \frac{1-\omega^2\cos^2\theta}{1-\omega^2}$ where it passes from $-\infty$ to $+\infty$, passes through the point (1, 1) and $(1+\omega, 0)$ for all values of θ.

q_2^2 has therefore to be identified with the square of the refractive index of the extraordinary wave (Fig. 3).

For $\omega > 1$, we find that the curve passes through (o, 1) and (1, 1), between $r = 0$, and 1, $q_2^2 > 1$ but after (1, 1) the value of q_2^2 becomes less than unity and gradually tends to the value zero at $r = 1+\omega$, after which it is negative (Fig. 3).

The quantities $g(\omega, r, \theta)$, $-F = \sqrt{1+g^2} - |g|$ which occur in this work are functions of ω, r and θ.

In Table I, the function $g(\omega, 0, \theta)$ has been given for various values of ω and θ. To obtain $g(\omega, r, \theta)$ we have to divide $g(\omega, 0, \theta)$ by $(r-1)$.

TABLE I

$$g = \omega \cos^2\theta/2 \sin\theta, \quad r = 0$$

θ°	ω = .1	ω = 2	ω = .3	ω = .5	ω = .8	ω = 1.0	ω = 1.5	ω = 2	ω = 5	ω = 10	ω = 20	ω = 50	ω 100
91°	2.8640	5.7270	8.591	14.315	22.908	28.635	42.955	57,270	143.15	286.35	572.70	1431.5	2863.5
92°	1.4310	2.8620	4.293	7.155	11.448	14.310	21.465	28.020	71.55	143.10	286.20	715.5	1431.0
93°	.9525	1.9050	2.858	4.763	7.620	9.525	14.290	19.050	47.63	95.25	190.50	476.3	952.5
94°	.7135	1.4270	2.141	3.568	5.708	7.135	10.705	14.270	35.68	71.35	142.70	356.8	713.5
95°	.5695	1.1390	1.709	2.845	4.556	5.695	8.545	11.390	28.48	56.95	113.90	284.8	569.5
190°	.2793	.5586	.838	1.397	2.234	2.793	4.190	5.586	13.97	27,93	55.86	139.7	279.3
105°	.1802	.3604	.541	.901	1.142	1.802	2.795	3.604	9.01	18.02	36.04	90.1	180.2
110°	.1291	.2581	.387	.645	1.032	1.291	1.935	2.581	6.45	12.91	25.81	64.5	129.1
115°	0972	.1944	.292	.486	.777	.972	1.460	1.944	4.86	9.72	19.44	48.6	97.2
120°	.0750	.1500	225	.375	.600	.750	1.113	1.500	3.75	7.50	15.00	37.5	75.0
125°	.0585	.1170	.176	.293	.468	.485	880	1.170	2.93	5.85	11.70	29.3	58.5
130°	.0457	.0913	.137	.228	.365	.457	.685	.913	2.28	4.57	9.13	22.8	45.7
135°	.0354	0707	.106	.177	.283	.354	.530	.707	1.77	3.54	7.07	17.7	35.4
140°	.0270	.0539	.081	.135	.216	.270	495	530	1.35	2.70	5.39	13.5	27.0
145°	.0201	0402	.060	.100	.161	201	.300	.402	1.00	2.01	4.02	10.0	20.1
150°	.0144	0289	.043	.072	.115	.144	.215	.289	.72	1.44	2.89	7.20	14.4
155°	.0099	.0197	.030	.049	.079	.099	.150	.197	40	.99	1.97	4.90	9.9
160°	,0062	.0125	.019	.031	.050	.062	.095	.125	.31	62	1.25	3.11	6.2
165°	.0035	.0069	.010	.017	.028	.035	.050	.069	.17	.35	.69	1.72	3.5
170°	.0015	.0031	.005	.008	.012	.015	.025	.031	.08	.15	.31	80	1.5
175°	.9004	.0008	.001	.002	.003	004	.005	.008	.02	.04	.08	21	.4
176°	.0002	.0004	.001	.001	.002	.002	.004	.004	.01	.02	.04	.10	.2
177°	.0001	.0003	.000	,001	.001	.001	.002	.003	.00(5)	.01	.02	.05	.1
178°	.0001	.0001	.000	.000	.000	,001	.001	.001	.00(3)	.00(6)	.01	03	.016
179°	.0000	.0000	.000	.000	.000	.000	.000	.000	.00	00	,00	.00	.00
180°	.0000	.0000	.000	.000	.000	.000	.000	.000	.00	00	.00	.00	.00

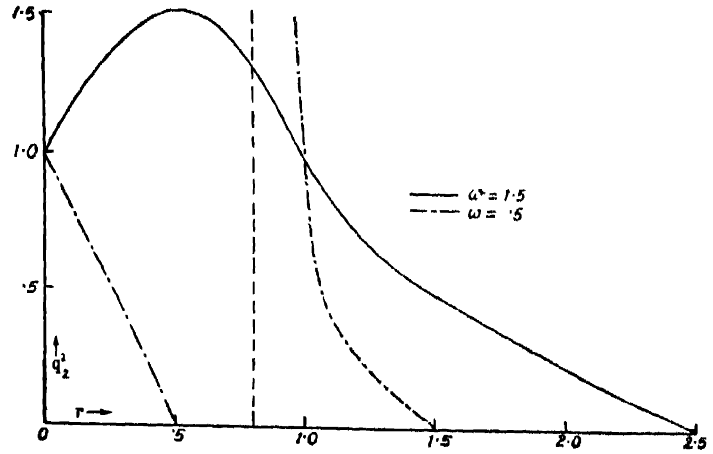

FIG. 3

Variation of the square of the refractive index for the e-wave with electron concentration $\left(r \quad \frac{4\pi e^2}{mp^2}N\right)$ for $p_0/p = \omega < 1$ (here ·5) and $p_0/p = \omega > 1$ (here 1·5)

3 FINITE DAMPING

We next discuss the case when $\delta > 0$, and in so doing we have to formulate the expressions for polarisation ratios and refractive indices in such a way that if $\delta \rightarrow 0$, these general expressions should reduce to those discussed in the previous section.

In this case F_1 and F_2 are complex roots of the equation (2.13). Let us put

$$F_1 = -\rho\, e^{i\phi}, \text{ and consequently } F_2 = \frac{1}{\rho}\, e^{-i\phi} \qquad \ldots \quad (3.1)$$

since $F_1F_2 = -1$, with the condition that ρ is always positive. In the particular case $\delta = 0$, we have $\phi = 0$ or π. Since F_1 is negative for $r < 1$, therefore $\phi = 0$ for $r < 1$. Again F_1 is positive for $r > 1$, therefore, $\phi = \pi$ for $r > 1$. So we get for $\delta = 0$,

$$\rho = \sqrt{1 + g^2} - |g| \text{ for } r >. =, < 1.$$

Now

$$F_1 + F_2 = \frac{1}{\rho}\, e^{i\phi} - \rho\, e^{-i\phi} = 2g \cos \alpha\, e^{i\alpha} = 2G$$

Equating real and imaginary parts,

$$(1 - r) \cos \phi \left(\frac{1}{\rho} - \rho\right) - \delta \sin \phi \left(\frac{1}{\rho} + \rho\right) = -\frac{\omega \sin^2\theta}{\cos \theta}$$

$$(3.2)$$

$$\delta \cos \phi \left(\frac{1}{\rho} - \rho\right) + (1 - r) \sin \phi \left(\frac{1}{\rho} + \rho\right) = 0$$

or $\cos\phi\{(1/\rho)-\rho\}=2g\cos^2\alpha,\quad \sin\phi\{(1/\rho)+\rho\}=-2g\sin\alpha\cos\alpha.$

Solving the above equations (3.2) we get

$$\sin^2\phi=\frac{2g^2\sin^2\alpha}{1+g^2+\sqrt{1+2g^2\cos 2\alpha+g^4}},\qquad \tan\phi=-\frac{1-\rho^2}{1+\rho^2}\tan\sigma \ldots \quad (3.3)$$

and
$$\rho=\pm\sqrt{1+g^2\cos^2\alpha-\sin^2\phi}\pm\sqrt{g^2\cos^2\alpha-\sin^2\phi} \quad \ldots \quad (3.4)$$

This expression for ρ can reduce to the corresponding relation for $\delta=0$ only if we take

$$\rho=\sqrt{1+g^2\cos^2\alpha-\sin^2\phi}-\sqrt{g^2\cos^2\alpha-\sin^2\phi} \quad \ldots \quad (3.4a)$$

Hence $1/\rho-\rho=2\sqrt{g^2\cos^2\alpha-\sin^2\phi}>0$, for all values of α and g. Thus $\rho<1$. Then returning to the equations (3.2), we have for northern hemisphere for the region $r<1$, *i.e.*, $g>0$

$$\cos\phi>0,\quad \sin\phi<0,\quad i.e.,\ 3\pi/2<\phi<2\pi$$

and for the region $r>1$, *i.e.*, $g<0$

$$\cos\phi<0,\quad \sin\phi<0,\quad i.e.,\ \pi<\phi<3\pi/2.$$

The case in the southern hemisphere is just the opposite. The results can be tabulated as :

TABLE II

θ	r	$g=\dfrac{\omega\sin^2\theta}{2(r-1)\cos\theta}$	$\delta=0$		$\delta>0$	
			$\rho=-F_1$	ϕ	ρ	ϕ
N. H.	<1	$(+)$	$\sqrt{1+g^2}-g$	0	$\sqrt{1+g^2\cos^2\alpha-\sin^2\phi}-\sqrt{g^2\cos^2\alpha-\sin^2\phi}$	$3/2\pi<\phi\leq 2\pi$
$\pi/2\leq\theta\leq\pi$	>1	$(-)$	$\sqrt{1+g^2}+\lvert g\rvert$	π		$\pi\leq\phi\leq 3/2\pi$
S. H.	<1	$(-)$	$\sqrt{1+g^2}+\lvert g\rvert$	π		$0<\phi<\pi/2$
$0\leq\theta\leq\pi/2$	>1	$(+)$	$\sqrt{1+g^2}-g$	0		$\pi/2<\phi\leq\pi$

With these complex expressions for F_1 and F_2 which reduce to the expressions discussed in the previous chapter, we get the ordinary and extraordinary complex refractive indices as

$$q_0^2=1-\frac{r}{\beta+\omega\cos\theta F_1}=1-\frac{r}{\beta-\omega\rho\cos\theta e^{i\phi}}=1-\frac{r}{X_0-iY_0} \quad \ldots \quad (3.5)$$

where $X_0=1-\omega\rho\cos\theta\cos\phi,\quad Y_0=\delta+\omega\rho\cos\theta\sin\phi.$

$$q_e^2=1-\frac{r}{\beta+\omega\cos\theta F_2}=1-\frac{r}{\beta+\omega/\rho\cos\theta e^{-i\phi}}=1-\frac{r}{X_e-iY_e} \quad \ldots \quad (3.6)$$

where $X_e=1+\omega/\rho\cos\theta\cos\phi,\quad Y_e=\delta+\omega/\rho\cos\theta\sin\phi,$

Following Booker, we may put $q=\mu-(ick/p)$

Then
$$\mu^2-\frac{c^2k^2}{p^2}=1-\frac{rX}{X^2+Y^2},\qquad \frac{2\mu ck}{p}=\frac{rX}{X^2+Y^2}\qquad \dots\quad (3.7)$$

and for the non-deviating region, where $ck/p<<1$

$$k=\frac{p}{2c}\left(\frac{1}{\mu}-\mu\right)\frac{Y}{X},\qquad \mu^2=1-\frac{rX}{X^2+Y^2}$$

We have thus for the non-deviating region :

$$\left.\begin{aligned}\mu_0^2&=1-r\frac{1-\omega\rho\cos\theta\cos\phi}{(1-\omega\rho\cos\theta\cos\phi)^2+(\delta+\rho\omega\cos\theta\sin\phi)^2}\\ k_0&=\frac{p}{2c}\left(\frac{1}{\mu}-\mu\right)\frac{\delta+\rho\omega\cos\theta\sin\phi}{1-\omega\rho\cos\theta\cos\phi}\end{aligned}\right\}\qquad \dots\quad (3.8)$$

$$\left.\begin{aligned}\mu_e^2&=1-r\frac{1+\omega/\rho\cos\theta\cos\phi}{(1+\omega/\rho\cos\theta\cos\phi)^2+(\delta+\omega/\rho\cos\theta\sin\phi)^2}\\ k_e&=\frac{p}{2c}\left(\frac{1}{\mu_e}-\mu_e\right)\frac{\delta+\omega/\rho\cos\theta\sin\phi}{(1+\omega/\rho\cos\theta\cos\phi)}\end{aligned}\right\}\qquad \dots\quad (3.9)$$

The correctness of the above expressions can be tested for special cases .

For the magnetic equator, $\theta=\pi/2$ we have from (3.4*a*), $\rho=0$ and $\frac{\sin\theta}{\rho}e^{-i\phi}=\frac{\omega}{\beta-i}$. Hence, we get the equations (2.10), as special cases of (2.16*a*), For the magnetic north pole, $\theta=\pi$, $\rho=1$, $\phi=\pi$, hence (2.16*a*) reduce to equations (2.11). For the magnetic south pole $\theta=0$, $\rho=1$, $\phi=0$, hence (2.16*a*) reduce to equations (2.11*a*).

4. POLARISATION.

Let us next discuss the polarisation of the down-coming wave for any station for a stratified, slowly varying ionosphere with finite damping. Since the e.m. waves which are propagated in such a medium are not transverse in the electric vector $\boldsymbol{E}$, but are transverse in the magnetic vector $\boldsymbol{H}$ and in the method of detection, the $\boldsymbol{H}$ vector is utilized, it is customary to express the polarisation of the waves with respect to the latter. So we start with the equations of propagation of the magnetic vector, *viz.*,

$$\frac{d^2H_x}{du^2}+K_2H_x-iLH_y=0\qquad \dots\quad (4.1)$$

$$\frac{d^2H_y}{du^2}+K_1H_y+iLH_x=0\qquad \dots\quad (4.2)$$

in place of the corresponding equations (2.6) and (2.8) for the electric vector. Equations (4.1) and (4.2) follow immediately from (2.6) and (2.8) and (2.1). Eliminating H_y and H_x from (4.2) and (4.3) respectively we get

$$\frac{d^4H_x}{du^4}+(K_1+K_2)\frac{d^2H_x}{du^2}+(K_1K_2-L^2)H_x=0 \qquad \dots \quad (4,3)$$

and

$$\frac{d^4H_y}{du^4}+(K_1+K_2)\frac{d^2H_y}{du^2}+(K_1K_2-L^2)H_y=0 \qquad \dots \quad (4\cdot4)$$

where the derivatives of K_1, K_2 and L have been neglected as before. The general solutions of (4.3) and (4.4) are

$$H_x = A_1e^{is_1u} + A_2e^{+is_2u} + A_3e^{-is_1u} + A_4e^{-is_2u}$$

$$H_y = B_1e^{is_1u} + B_2e^{+is_2u} + B_3e^{-is_1u} + B_4e^{-is_2u}$$

where

$$s_1^2 = \frac{K_1+K_2-\sqrt{(K_1-K_2)^2+4L^2}}{2}$$

$$s_2^2 = \frac{K_1+K_2+\sqrt{(K_1-K_2)^2+4K^2}}{2}$$

It can be easily shown that

$$s_1^2 = q_1^2, \qquad s_2^2 = q_2^2$$

Retaining only the solutions for the down-coming waves, we get

$$H_x=A_1\,e^{iq_2u}+A_2\,e^{iq_1u} \qquad \dots \quad (4\cdot5)$$

$$H_y=B_1\,e^{iq_2u}+B_2\,e^{iq_1u} \qquad \dots \quad (4\cdot6)$$

where q_1 and q_2 are those roots of s_1^2 and s_2^2 respectively which have the imaginary parts positive. Substituting (4.5) and (4.6) in (4.1) we get,

$$(-q_1^2\,A_2+K_2\,A_2-iLB_2)\,e^{iq_1u}+(-q_2^2\,A_1+K_2\,A_1-iLB_1)\,e^{iq_2u}=0$$

which being an identity in u yields

$$-q_1^2\,A_2+K_2\,A_2-iL\,B_2=0$$

$$-q_2^2\,A_1+K_2\,A_1-iL\,B_1=0$$

whence we have, referring back to (4.1) and (4.2),

$$\frac{B_1}{A_1}=i\frac{q_2^2-K_2}{L}\;;\quad \frac{B_2}{A_2}=i\frac{q_1^2-K_2}{L} \qquad \dots \quad (4\cdot7)$$

From the general solutions of (4.1) and (4.2) it is evident that these equations represent two waves given by

$$H_x^{(1)}=A_1\,e^{iq_2u},\quad H_y^{(1)}=B_1\,e^{iq_1u}$$

$$H_x^{(2)}=A_2\,e^{iq_1u},\quad H_y^{(2)}=B_2\,e^{iq_1u}$$

travelling with complex phase velocities c/q_2 and c/q_1 respectively. Following the nomenclature adopted before $H_x^{(1)}$ & $H_y^{(1)}$ combine to give the down coming extra-ordinary wave and $H_x^{(2)}$ & $H_y^{(2)}$ give the downcoming ordinary wave, and the polarisation ratios for the two waves are

$$\frac{H_y^{(0)}}{H_x^{(0)}} = -\frac{B_2}{A_2} = i\,\frac{q_1^2-K_2}{L} = iF_1$$

$$\frac{H_y^e}{H_x^e} = -\frac{B_1}{A_1} = i\,\frac{q_2^2-K_2}{L} = iF_2$$

Taking $H_x^{(0)} = R_{0x}\, e^{i(\gamma_{0x}+pt)}$, $H_y^{(0)} = R_{0y}\, e^{i(\gamma_{0y}+pt)}$

where R_{0x}, R_{0y}, γ_{0x} and γ_{0y} are real functions of u, we get

$$H_x^{(0)} = R_{0x} \cos(\gamma_{0x}+pt), \quad H_y^{(0)} = R_{0y} \cos(\gamma_{0y}+pt)$$

as the two true solutions of the problem with

$$\boldsymbol{E} = \boldsymbol{E}_0 \cos pt \text{ in place of } \boldsymbol{E} = \boldsymbol{E}_0\, e^{ipt}$$

Hence $\dfrac{H_y^{(0)}}{H_x^{(0)}} = \dfrac{R_{0y}}{R_{0x}} e^{i(\gamma_{0y}-\gamma_{0x})} = iF_1 = -i\rho\, e^{i\phi} = \rho\, e^{i(\phi-\pi/2)}$

whence $$\rho = \frac{R_{0y}}{R_{0x}}$$

and $$\gamma_{0y} - \gamma_{0x} = \phi - \frac{\pi}{2}.$$

are the ratio of the axes and the constant phase difference between the y and x components of the magnetic vector respectively. The equation of the polarisation ellipse for the ordinary wave follows immediately by eliminating "pt" between the two equations in (4.8): We have

$$H_x^{(0)2} - \frac{2H_x^{(0)}H_y^{(0)}}{\rho}\sin\phi + \frac{H_y^{(0)2}}{\rho} = R_{0x}^2 \cos^2\phi \qquad \dots \quad (4.9)$$

This equation shows that the axes of the ellipse are tilted to the respective y and x axes, the amount ψ_0 of tilt to the y axis being given by

$$\tan 2\psi_0 = -\frac{2\rho\sin\phi}{1-\rho^2} \qquad \dots \quad (4.10)$$

The points of contact of this ellipse with the circumscribed rectangle are (FIG. 4) respectively $(\pm R_{0x}\sin\phi,\ \pm R_{0x}\,\rho)$ and $(\pm R_{0x},\ \pm\rho\, R_{0x}\sin\phi)$

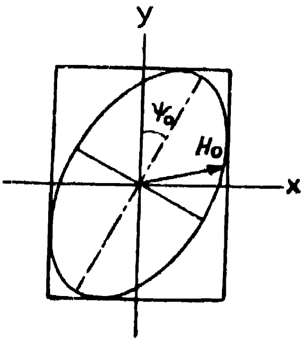

FIG. 4

Polarisation ellipse for the reflected O-wave (northern hemisphere)

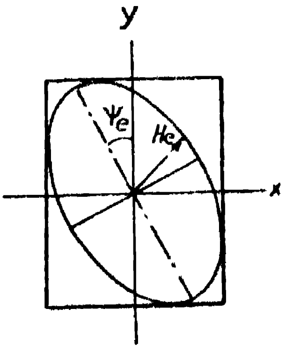

FIG. 5

Polarisation ellipse for the reflected O-wave (southern hemisphere)

For the other wave

$$\rho_e = \frac{R_{ey}}{R_{ex}}, \quad \gamma_{ey} - \gamma_{ex} = \phi + \frac{\pi}{2}$$

and it can easily be shown that

$$\rho_e = \frac{1}{\rho} \text{ and } (\gamma_{ey} - \gamma_{ex}) - (\gamma_{oy} - \gamma_{ox}) = \pi \qquad \ldots \quad (4.11)$$

consequently the equation of the polarisation ellipse for the e-wave is

$$\frac{H_x^{e\,2}}{\rho^2} + \frac{2H_x^e H_y^e}{\rho} \sin\phi + H_y^{e\,2} = \frac{R_{ex}^2}{\rho^2} \cos^2\phi$$

which shows the same ellipse rotated through an angle $\pi/2$. For this ellipse (FIG. 5) the angle of tilt and the points of contact with the circumscribed rectangle are given by :

$$\tan 2\psi_e = -\frac{2\rho \sin\phi}{1-\rho^2} = \tan(2\psi_o + \pi) \qquad \ldots \quad (4.13)$$

and $$\left(\pm R_{ex} \sin\phi, \ \pm \frac{R_{ex}}{\rho}\right), \quad \left(\pm R_{ex}, \pm \frac{R_{ex}}{\rho} \sin\phi\right),$$

In the experimental methods of determining the ratio of the axes of the polarisation ellipse, it is generally assumed that the polarisation of the downcoming wave is mainly determined by the lowest layers of the ionosphere where N the ion concentration tends to vanish. Recently Eckersly (1945) has determined the polarisation of the downcoming waves for $p = 6.1$, 6.4 and 7.6 Mc. and has remarked that in order to agree with his experimental results, the polarisation of the downcoming wave should be determined not by the lowest layer of the ionised strata but somewhere inside. Since there is as yet no definite and convincing evidence either experimental or theoretical, of the particular strata or the entire layer fixing the polarisation, we have plotted ρ, the ratio of the axes for the o-wave as a function of $\theta' = \theta - \frac{\pi}{2}$, the magnetic latitude of the place of observations for various values of ω, for ν, *i.e.*, N⟶0.

Sense of rotation of the polarisation ellipse can be inferred from equations (4.8). Since the damping has no effect on the sense of rotation of the magnetic vector, we infer the sense of rotation for the case where damping is absent. In this case for northern hemisphere $\phi = 0$ and hence equation (4.8) gives

$$H_x^{\circ} = R_{ox} \cos(\gamma_{ox} + pt)$$

$$H_y^{(o)} = \rho R_{ox} \sin(\gamma_{ox} + pt).$$

Hence as t increases from 0, H_x° decreases from $R_{ox} \cos\gamma_{ox}$ to 0 and remains positive, while $H_y^{(o)}$ increases from $\rho R_{ox} \sin\gamma_{ox}$ to ρR_{ox} showing that the vector H_r°, whose components are H_x° and H_y° and which describes the ellipse given by (4.9) is moving in the anticlockwise direction. Thus for all waves received in the northern hemisphere the down-

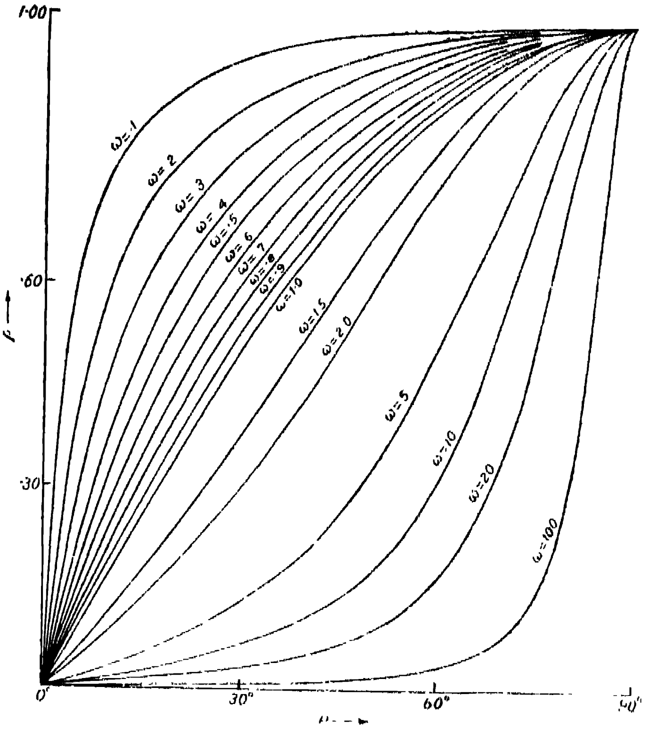

FIG. 9

Variation of the polarisation ratio $\rho = \sqrt{1+g^2} - |g|$ where $g = \frac{\omega \sin^2\theta}{2\cos\theta}$ for various values of $\omega = p_0/p$, for different angles of propagation $\rho \rightarrow 1$ means circular polarisation.

coming ordinary wave is polarised in the anticlock-wise direction as viewed along the direction of propagation. For the extraordinary wave,

$$H_x^e = R_{e,x} \cos(\gamma_{e,x} + pt)$$

$$H_y^e = -\frac{R_{e,x}}{\rho} \sin(\gamma_{e,x} + pt)$$

Hence as t increases from 0, H_x^e decreases as before but H_y^e becomes more and more negative showing that the vector H^e whose components are H_x^e and H_y^e and which describes the ellipse given by (4.12) moves in the clockwise direction. Thus for all stations in the northern hemisphere, the downcoming e-wave is polarised right handed as viewed along the direction of propagation.

For the southern hemisphere the sense of the rotation of the two ellipses will be just opposite since $\phi = \pi$ for $\delta = 0$ in the southern hemisphere in place of $\phi = 0$ for $\delta = 0$ in the northern hemisphere.

ACKNOWLEDGMENT

Two of us, B. K. Banerjea and U. C. Guha, have been the recipients of two Research scholarships from the Radio Research Committee of the Council

of Scientific and Industrial Research (India) and wish to express their thanks to the Council for facility to work and permission to publish this paper.

Palit Laboratory of Physics,
Calcutta University.

REFERENCES

Appleton 1932, *Jour Inst. Elec. Eng.*, **71**, 646
Banerjea 1947, *Proc. Roy. Soc. A*, **196**, 67.
Booker 1936, *Proc. Roy Soc. A.*, **156**, 235.
Eckersley 1945 *Proc. Roy Soc A.*, **184**, 196.
Darwin 1925, *Trans. Camb. Phil. Soc.*, **23**, 137.
Hartree 1932, *Proc. Camb. Phil. Soc.*, **29**, 143.
Rydbeck 1940, *J. Applied Physics*, **13**, 577
Saha, Rai and Mathur 1937, *Nat. Inst. Sci. (India)*, **4**, 53.
Saha and Rai 1937, *Nat Inst, Sci. (India)*, **4**, 319.
Saha and Banerjea 1945, *Ind. Journ. Phy.*, **19**, 159.
Stratton 1942, Electomagnetic Theory, p 326.

20

ON THE CONDITIONS OF ESCAPE OF MICROWAVES OF RADIO-FREQUENCY RANGE FROM THE SUN

BY PROF. M. N. SAHA,* B. K. BANERJEA AND U. C. GUHA

(*Received for publication, Sept. 15, 1947*)

ABSTRACT. In this paper, we have discussed the conditions of escape of radio-frequency waves from the solar atmosphere with the aid of magneto-ionic theories of propagation of radio-waves through an ionised atmosphere traversed by a magnetic field. It has been shown from these theories that the magnetic field of the spots actually enables the e-component of the waves to escape from deeper layers of the solar atmosphere and thus provides an explanation of the observational fact that radio-waves are actually emitted by the spot regions themselves It is shown that the same theories give a general and satisfactory explanation of all the facts observed so far, *e g.*, the circular polarisation, and sudden intensification of emission with the onset of radio flares Programmes for further work are indicated.

1. INTRODUCTION

In several communications to *Nature* and elsewhere, various British, Australian and New Zealander workers have described experiments which prove conclusively that during times of solar disturbance, there are large outbursts of radio-frequency energy from the sun. The wave-lengths of the radio waves, as observed by these workers, vary from 1.5 to 30 metres (200 Mc/sec to 10 Mc/sec) and there is short account of a solitary work in the centimetre region (Dicke and Beringer, 1946), in which emission has been measured by a different technique.

The communications are mostly short. The most complete account has so far been given by Appleton and Hey (1946). Relevant points from their account are given below.

The observations were made when there was outburst of sun-spot activity which started on 22nd February, 1946. According to their statement the sunspot crossed the solar disc at a heliographic latitude 22°N, central meridian passage occurring on 28th February, 1946. The maximum size of the spot was some two thousand millionth part of the sun's hemisphere. A very extensive and brilliant solar flare occurred from approximately 12 hours to 15-03 hours on 28th February, and the accompanying radio fadeout which began just after 12 hours lasted till 20-0-0 hours. A great magnetic storm broke out with great activity at 7-22 hours on 2nd March. The days of greatest intensity of solar noise, *i.e.*, 27th and 28th February, occurred when the sun-spot was near the central meridian passage and at the time of intense sun-spot activity several solar flares were observed in addition to the most brilliant one to which reference has already been made. The sun-spot decreased in size after the 28th February and at the same time solar noise subsided.

---

* Fellow of the Indian Physical Society.

The reports so far published make it clear that the metre range microwave radiations are emitted only during times of solar activity. In fact a close statistical correspondence between the sun-spot activity and metre range microwave emission has been established by Pawsey, Payne-Scott and MacReady (1947) and others.

This close correspondence is further confirmed by the experiments of Ryle and Vonberg (1946) who, by an ingenious adaptation of the famous Michelson-Pease method of measuring stellar diameters, showed that the actual region from which these radio-waves are coming subtends an angle not greater than 10′ of arc, the solar diameter being 32′ of arc. The size of the radio-wave generating regions, thus determined, is of the same order of, though somewhat larger than, the size of the large sun-spot groups (3′ of an arc). Pawsey *et al* find by a different method that the diameter is about 6′.

The main characteristics of these solar radio noise, as determined by the various workers, can be summarised as follows:—

(*i*) The radiation is closely connected with sun-spots, appearing and disappearing with the latter.

(*ii*) The radiation has the characteristics of random noise, the intensity of the spectrum is neither steady with time nor continuous in wave-length, nor monochromatic.

(*iii*) The intensity of radio-emission is extraordinarily high.—Appleton and Hey working on 4.7 metres, found that the radio flux from the active area was 10^3 times that associated with black body radiation from the disc as a whole. Supposing that only 1/200th part of the sun's hemisphere is active, the intensity increases to 2.10^5 times the black body radiation from the sun's disc.

(*iv*) The intensity is subject to sudden fluctuations occurring generally with the onset of flares or other disturbances.

(*v*) Polarisation.—Experiments on the polarisation of the radio noise have been carried out by Appleton and Hey (1946) in London, by Ryle and Vonberg (1946) in Cambridge and Martyn (1946) in Canberra. They have all found that the radio noise is invariably circularly polarised, but otherwise the descriptions are confusing. Describing the polarisation of waves from the sun-spot groups of July 27 to August 3, 1946, Ryle and Vonberg say:—

"Measurements taken over the period July 27 to August 3rd, showed the polarisation to be anticlockwise, viewed along the positive direction of propagation (left handed). Between August 3 and August 7, the degree of polarisation diminished, being virtually completely random on August 7. On August 8, 40% polarisation was observed again but with right-handed polarity, the result presumably of increased activity in a subsidiary sun-spot."

Martyn (1946) working in the southern latitudes (35°S Canberra) while observing the same sun-spots occurring in the last week of July 1946 noted:—

> "It was found that the right-handed circularly polarised power received was some seven times greater than that received when the system accepted only left-handed polarised radiation. Three days later, when this sun-spot group crossed the meridian these conditions were reversed ; five times more power being then received on the left-handed than on the right-handed system".

Thus simultaneously observing the same sun-spot groups the sense of rotation of the polarised signal in the two hemispheres were found by the observers to be opposite.

As will be made clear later, it will be helpful to the understanding of the phenomenon if, simultaneously with the recording of the polarisation, all the characteristics of sun-spots (heliographic latitude and longitude, distance from the centre of the disc, magnetic field strength, classification, etc.) are given.

Measurements for radiation below metre range

Appleton and Hey state that they could not detect any enhancement of solar noise on wave-lengths as short as 1/10 metre. Similar observations by the T.R.E. establishment on a 3/10 metre yielded a negative result. The radio noise associated with the sun-spot activity becomes significant, without very special technique, when the wave-lengths approach 1.5 metres. The results are in accordance with the observations of MacReady, Pawsey, Payne-Scott (1946). On the otherhand Dicke and Beringer (1945) working in the centimetre range and using special technique found that microwaves of 1.25 cm. length are emitted during times of solar activity, the corresponding black body temperature being 11000°K.

2. PRELIMINARY ATTEMPTS AT A THEORY OF THE PHENOMENON

The problem is to find out the physical mechanism which gives rise to the radio-frequency waves in the sun and also to discuss how these waves are propagated through the solar atmosphere. Let us first confine ourselves to the second aspect of the problem, for whatever may be the physical mechanism giving rise to the radio-waves, it is clear that their passage through the various layers of the solar atmosphere would be regulated by the laws of electro-magnetism. As is well-known, the various layers of the solar atmosphere are highly ionised, the electron-density, according to well-tested astrophysical theories, being 10^{14}/c.c. for the photospheric level, 10^{11}/c.c. for the base of the chromosphere (500 km above photosphere) which fall to 3.5×10^{8}/c.c. at the top of the chromosphere (14500 km). The density thereafter falls slowly throughout the whole corona, but is $\simeq 10^{3}$/c.c. even at distance of 10 solar diameters.

The quiescent sun has, like the Earth, a permanent magnetic field, the existence of which was first indicated by the investigations of G. E. Hale. On account of its small value, the reality of the effect has been sometimes called into question, but recent investigations by Thiessen (1946) appear to have satisfied the astrophysicists that the field is real. The value is 25 gauss at the solar magnetic equator, and 50 gauss at the magnetic poles. According to Hale and Thiessen the magnetic axis is inclined at an angle of 6° to the sun's axis, but for our purpose we can take the two axes to be identical. Besides this small permanent magnetic field, magnetic fields of a higher order are developed in spot regions during times of solar activity.

The conditions in the sun are, therefore, somewhat similar to those prevailing in the Earth's atmosphere (ionosphere) for transmission of radio-waves through it, and the same mathematical methods which have been developed by Appleton, Hartree and others, can be used in the present case

The authors (Saha, Banerjea and Guha, 1947) have, however, completely recast the mathematical treatment of propagation of radio-waves through an ionised atmosphere which is traversed by a magnetic field, and results from this paper are freely used in the present one. The main conclusions of Appleton are, however, quite sufficient for a preliminary survey of the problem.

According to these workers, a beam of unpolarized radio-waves on entry into the ionosphere is split up into two waves, which are styled ordinary (shortly called o-wave), and extraordinary (shortly called e-wave). They travel with different velocities, *i.e.*, refractive indices, have different states of polarisation and are absorbed to different degrees. These quantities, *viz.*, the refractive indices, polarisation and absorption are functions of electron density N, damping, field-strength H, and θ, the angle of propagation which is the angle between the magnetic field and the direction of propagation. In the case when damping can be neglected the refractive indices for the two waves are functions of N, H, and θ and decrease steadily as N increases. When μ becomes zero, the wave can no longer proceed forward, but is reflected back. The limiting conditions (Appleton-conditions) for penetration are for the

$$\text{o-wave,}\quad N < \frac{\pi m}{c^2} f^2 < 1.21 \times 10^{-8} f^2 \qquad (2.1)$$

$$\text{e-wave,}\quad N < \frac{\pi m}{c^2} f\,(f \pm f_h) < 1.21 \times 10^{-8} f(f \pm f_h) \qquad (2.2)$$

where f = wave frequency = c/λ

f_h = gyromagnetic frequency for a field H

$$= \frac{eH}{2\pi mc}$$

$$= 2.8 \times 10^6 H$$

These conditions are independent of θ.

Let us apply these conditions to the solar atmosphere. For the o-wave,

$$
\begin{aligned}
N &< 1.25 \times 10^{-8} \times f^2 \\
&\left.\begin{aligned}
&< 1.25 \times 10^{6} \quad \text{for} \quad f = 10 \text{ Mc/sec}, \quad \lambda = 30 \text{ m} \\
&< 5 \times 10^{8} \quad \text{for} \quad f = 200 \text{ Mc/sec}, \quad \lambda = 1.5 \text{ m}
\end{aligned}\right\} \quad \ldots \quad (2.1a)
\end{aligned}
$$

This shows that the o-component of the metre waves cannot escape from the sun unless they originate in the corona, and that so progressively in the upper layers, as we take larger waves. The o-component of 30 metre waves can come only from beyond a distance of several diameters of the sun.

The e-wave should satisfy two conditions :

(*a*) f should be $> f_h$

(*b*) N should be $< 1.25 \times 10^{-8} \times f(f - f_h)$

(*a*) shows that the e-component of microwaves cannot escape from the quiescent sun unless $f > 100$ Mc/sec, $\lambda < 3$ metres, but microwaves of longer wave-length have been detected. (*b*) states that e-microwaves satisfying condition (*a*) would have to originate even in higher layers, *i.e.*, their probability of escape from deeper layers is much less than that of o-waves.

These difficulties have been sought to be explained with the aid of the hypothesis that the microwaves actually originate in the higher corona to which a temperature of the order of a million degree is ascribed. But the hypothesis does not explain why the microwaves are so copiously emitted during times of solar spottedness and are actually emitted, as now appears almost certain, from the spots themselves and not from the quiescent regions, unless we make the very improbable assumption that it is only the spots which develop the million degree temperature. The assumption is extremely improbable in view of the fact that spectroscopic evidence shows that spots are regions of much lower temperature than even the photosphere. This necessitates the investigation of the problem from an altogether different point of view.

Sunspots and microwave emission

The sun-spots, according to the classical investigations of Hale and Nicholson (1925), are found to show magnetic fields of entirely different order of magnitude than the quiescent sun, from a few hundred gauss for tiny spots to about 4000 gauss for the largest ones. Their direction is normal to the solar surface at the centre of the spot, but becomes inclined to the surface as we go outwards to the penumbral regions, as shown in Fig. 1. The largest number of spots occur in close pairs, showing opposite polarity, and even those which are apparently single, appear to have an invisible companion, having opposite polarity somewhere inside the surface. In fact, the spots are known to be hydrodynamical vortices, passing underneath the apparent surface, the two ends of the vortices being the two components of the bifocal spots. Spot groups show very complicated forms for which reference may be made to original sources (Nicholson, 1938) and reports (Nicolet, 1942).

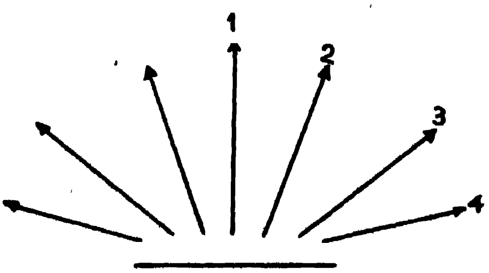

FIG. 1

Schematic representation of lines of force of the magnetic field in the region above a sun-spot (Nicholson).

Let us now apply the Appleton-conditions for escape of radio-waves from the spots, supposing that they originate somewhere within the spots.

For the o-component, since its condition of escape does not depend on the magnetic field, the conditions (2.1) will continue to apply, *i.e.*, the o-component of microwaves cannot escape from the sun, unless they originate in the corona over the spots.

We observe that $f_h = 2.8 \times 10^9 k,$

where k = value of the magnetic field in kilogausses: so that $\lambda_h = \frac{10.7}{k}$ cms. It is well known from Appleton's theory that the polarisation and refractive index of the e-component depend very largely on the quantity $\omega = f_h/f = \lambda/\lambda_h$. We have for the sunspots $\omega = 9.3km$, where m = length of the microwave emitted in metres. Taking $k = 1$, $m = 2.1$, $\omega \cong 20$, but the value may be much larger for longer waves and larger fields. Taking an average value of 20 for ω, we can easily draw the following conclusions:

Since $\omega >> 1$, the condition that the square of the refractive index vanishes at the point where the electron concentration is given by the formula $4\pi Ne^2/m < p(p-p_h)$ is absent. If we plot the value of the refractive index for the e-wave in the case $\omega > 1$ as a function of electron concentration, we find that, when damping is neglected, the $(\mu_e^2 - N)$ curve is a smooth one, decreasing gradully to zero at $N = \frac{e^2}{\pi m} f(f+f_h)$ (*vide* Fig. 2), while μ_0^2 reaches the zero value at $N = \frac{e^2}{\pi m} f^2$.

Since the wave can proceed till this condition is satisfied the limiting concentration for escape of the e-wave is given by

$$N \lesssim 1.25 \times 10^{-8} f(f+f_h) \qquad (2.3)$$

Taking $f = 1.5 \times 10^8$ ($\lambda = 2$ metres)

We should have $N \lesssim 1.25 \times 10^{-8} \times 1.5 \times 10^8 \times 2.8 \times 10^9 k$

$$\lesssim 6.6 \times 10^9 k$$

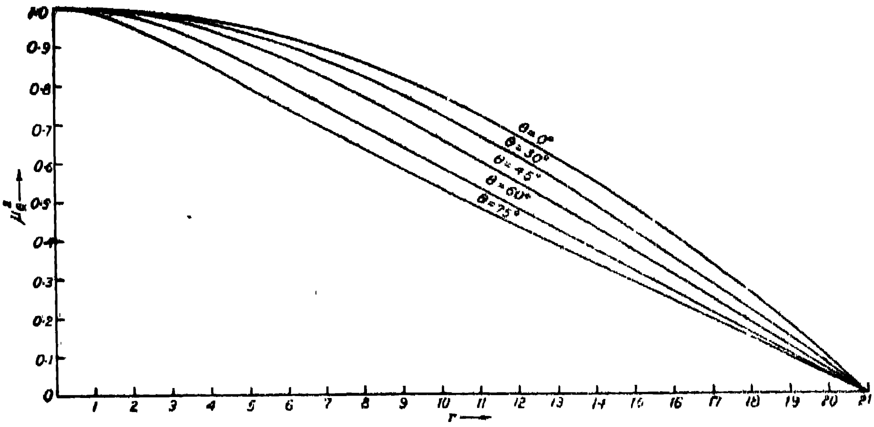

FIG. 2

Variation of the square of the refractive index of the extraordinary wave with electron concentration for different angles of propagation (for $\omega = 20$).

The calculation shows that the e-component can come from far deeper layers than the o-component, in fact from deep chromospheric layers, where the electron density is $(1 + \omega) \simeq 21$ times the limiting density for o-waves.

The magnetic field measured for the spots refer to the lowest layers—in fact, as will be shown later for the reversing layer of the spots. The field above and below must be very different. We have given in §3, plausible formulae for the variation of the field above the reversing layer, and these formulae may probably be experimentally verified as suggested by Hale long ago (*vide* appendix).

But these methods are not applicable for finding out the value of the magnetic field below the reversing layer, for which we have to fall back upon some speculative theories. If the spots are hydrodynamical vortices, they should funnel out on reaching the chromosphere, but their cross-sections must be very small just below the reversing layer, and according to Chapman (1944), fields may reach enormous values of the order of a million gauss. If this be correct the e-component can escape from far deeper layers.

3. CHARACTERISTICS OF THE SPOT ATMOSPHERE

Though the ideas outlined in the previous paragraphs make it clear that it is the strong magnetic field of the sunspots, which allows only one component of microwave beams to come out from very deep layers, the application of the above ideas to the actual problem of emission requires a more detailed knowledge of the physical conditions prevailing in various layers of the spot-region.

The physical quantities of which knowledge is particularly needed in this connection, are:

(1) The concentration of different kinds of atoms and molecules at different levels.

(2) The electron concentration at different levels.

(3) The magnetic field and its variation with height.

Methods, based on sound physical theories, have been developed for determining the various physical characteristics of the normal solar atmosphere. with the aid of data obtained from astrophysical observations, account of which will be found in Unsöld's *Sternatmosphäre* and Stromgren's analysis of the composition of the solar atmosphere. The term "Solar atmosphere" is used in a comprehensive sense after Rosseland to denote the totality of the phenomena known under the terms: the Reversing Layer, the Chromosphere and the Corona, and they are treated together, because, inspite of the fact that the nomenclature had their origin in different groups of observational data, the problems of the three layers easily pass into one another.

It is well-known that the sun-spot and its neighbourhood show very great deviations from the normal solar atmosphere, marked by fall of temperature, development of magnetic fields, and radial, transverse and vertical motion of the solar gases, giving rise to difficult hydrodynamical problems. A comprehensive theory, explaining the whole history and physical characteristics of spots, is still wanting, but our requirements, as given above, are limited. But even here, information is very scanty. The elaborate methods, which have been used for finding out the concentration of various types of atoms and electron density of the normal solar atmosphere in different layers, can be applied also to spots, but this has not yet been done. Only indirect methods of comparison with the normal atmosphere are available (Moore 1931, Richardson 1931). For these reasons, it is necessary to review critically the methods used for the normal solar atmosphere.

The normal reversing layer is a region extending from the level of the photosphere to the base of the chromosphere, a distance of 300-500 km. The Fraunhofer lines mostly originate from absorption of continuous photospheric light by the atoms and molecules contained in this layer.

Several methods are available for finding out the composition of the reversing layer, but the results, though of the same order, do not tally with each other. According to Russell (1928) the composition (percentege of atoms) is 91% H, probably 3% He, 3% O, 1.5% other elements of which Fe forms the preponderating part, and 1.5% electrons. The atmosphere is nearly purely hydrogen, and becomes more so as we ascend upwards. The to number of H-atoms over 1 c.c. of photosphere is given by Russell as 1.8×10^{22}/c.c.

The electrons in the reversing layers and the chromosphere are mostly derived from the thermal ionisation of metals.

For the chromosphere very extensive investigation by Wildt (1947), based on analysis of flash spectrum data, is available, from which Table I has been compiled :

According to Wildt (1947) the concentration of H-atoms in the chromsophere is given by the formula :

$$n_H = 6.76 \times 10^{15} . e^{-.92 \times 10^{-8} z} \text{ (in cms).}$$

The hydrostatic density gradient, on the assumption of a temperature of 5000°K is 6.9×10^{-8}cm^{-1}. It is, as if the weight of hydrogen has dimnished to $.92/6.9 = 1/7.5$ of its value or the temperature has risen to nearly 35000°K.

The electron-density at any point within the chromosphere can be obtained by extrapolation; assuming the exponential law to hold good, calculation shows that $n = n'_e e^{-\beta z}$ (in cms), where $\beta = .43 \times 10^{-8}$cm^{-1}. The gradient is almost half that of H, as electrons are not obtained only from the ionisation of H but also from the metallic elements which are almost completely ionised.

The values of electron density in the corona (from 20,000 km upwards) are given by Bumbauch (1937). These are obtained from a thorough discussion of numerous measurements of the brightness of the corona, on the basis of K. Schwarzschild's hypothesis, generally accepted, that the continuous spectrum of the solar corona is due to photospheric light scattered by free electrons. Bumbauch's calculations (Unsöld, p. 440) extend from 20000 km to nearly ten times the solar radius, and the density varies from 4×10^8 to nearly 10^5/c.c. The figure for the top of the chromosphere (14500 km) has been extrapolated by Wildt from Bumbauch's figure. Another calculation based on extrapolation of hydrogen densities, gives $n_e = 2 \times 10^{11}$/c.c. at this height. Bumbauch's figures have recently been revised by Allen (1946) and van der Hulst (1947).

TABLE I

Locality	Level above Photosphere	Hydrogen density	Electron density
Reversing layer	0 to 500 km	6.76×10^{15}	10^{14}
Base of chromosphere	500 km	4×10^{15}	1.6×10^{11}
Top of chromosphere	14,500 km	2×10^{10}	3.5×10^{8}
Corona	> 20,000 km		3×10^{8} to 10^{4}

THE MAGNETIC FIELD IN THE SPOT REGIONS

Magnetic field of sun-spots has been systematically measured in the Moun Wilson Observatory since the great discovery by Hale in 1908, as part of th routine programme of the observatory and the results are available in publications of the observatory and in various reports.

For the measurement of the field, the iron line $\lambda = 6173{\cdot}346$ Å, which is exceptionally sharp, has been generally used. As this is a line of intensity 5 on the Rowland scale, and in the chromosphere spectrum reaches only a height of 400 km, it can be taken that the fields measured refer to the lowest level of the spot.

But for the purposes of this paper, we require the value of the spot field at higher levels, and away from the axis of the field. There appears to be no systematic observation on this point, though Hale (1908) was aware of the necessity of such observations. He states :

> " We have already seen that the strength of the field in spots apparently changes very rapidly along a solar radius, and is small at the upper level of the chromosphere."

We have given in Appendix the full passage from the original paper of Hale which suggests a programme for measurement of the magnetic field at various levels above the reversing layer of spots. To our knowledge these suggestions have not been worked out but they are worth a trial.

Two different and indirect methods, based on Mount Wilson measurement of the field over various distances from the centre of the umbra, are available. These are given below :—

(1) Broxon (1942) while observing the effect of the spot fields on cosmic rays suggested that the magnetic fields of unipolar spots may be fairly approximately represented by the field of a vertically placed magnet having a dipole moment $\mu = \sqrt{2}aH_0/8$ situated at a depth of $a/\sqrt{2}$ with the axis coinciding with the axis of the spot, where a = radius of the spot and H_0 is the field strength at the spot centre. For complete mapping of such a field,

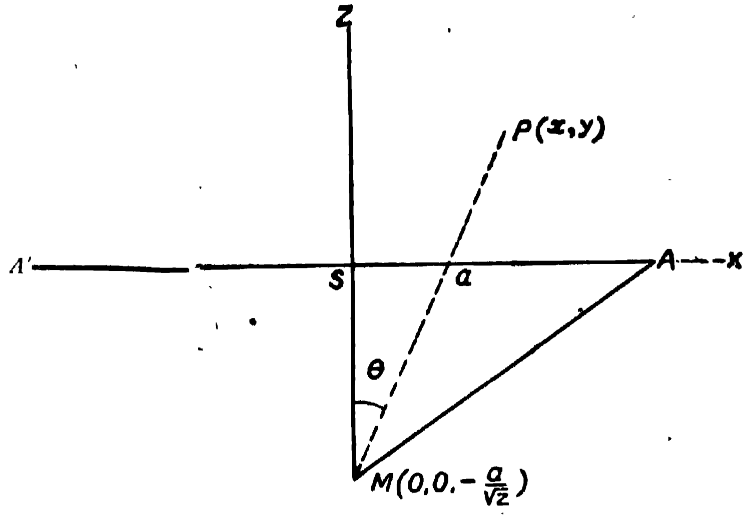

FIG. 3

The co-ordinate system for a circular spot (broxon type) let A′SA be the plane of the spot and MS the axis of the spot, with the dipole at M. We chose the frame work XYZ, with X-axis along SA, Z-axis along MSM′ and Y-axis perpendicular to the plane of the paper (Fig. 3). As the field is symmetrical about the axis let us find out the field at any point $P(x, o, z)$ in the XZ plane. Let also $R = MP$ and $\phi = \angle PMS$ be the polar co-ordinates of P with $M(o.o, -a/\sqrt{2})$ as origin.

Then the potential Ω at P is given by

$$\left.\begin{array}{l}
\Omega = \dfrac{\mu\cos\phi}{R^2} = \mu\dfrac{(z+a/\sqrt{2})}{\{x^2+(z+a/\sqrt{2})^2\}^{\frac{3}{2}}} \\[2ex]
H_R = -2\dfrac{\mu\cos\phi}{R^3}, \quad H_x = \dfrac{3\sqrt{2}}{8}H_0\dfrac{\xi(\zeta+1/\sqrt{2})}{\{\xi^2+(\zeta+1/\sqrt{2})^2\}^{\frac{5}{2}}} \\[2ex]
H_\phi = -\dfrac{\mu\sin\phi}{R^3}; \quad H_z = \dfrac{H_0}{4\sqrt{2}}\cdot\dfrac{2(\zeta+1/\sqrt{2})^2-\xi^2}{\{\xi^2+(\zeta+1\sqrt{2})^2\}^{\frac{5}{2}}} \\[2ex]
H = \dfrac{H_0}{4\sqrt{2}}\cdot\dfrac{\sqrt{\xi^2+4(\zeta+1/\sqrt{2})^2}}{\{\xi^2+(\zeta+1/\sqrt{2})^2\}^2} = \dfrac{\mu}{R^3}\sqrt{1+3\cos^2\phi}
\end{array}\right\} \quad \dots \quad (3.1)$$

with $x = \alpha\xi, \quad z = a\zeta.$

Since in the above co-ordinate systems,

$$\left.\begin{array}{l}
\tan\phi = x/(z+a/\sqrt{2}) = \dfrac{\xi\sqrt{2}}{(1+\zeta\sqrt{2})} \\[2ex]
\text{we have} \quad \cot\psi = H_z/H_x = \cot\phi - \dfrac{1}{3\sin\phi\cos\phi}
\end{array}\right\} \quad \dots \quad (3.2)$$

Expression (3.1) gives the magnitude of the magnetic field at any point on or above the spot and to get field direction, we plot the curves representing lines of force given by

$$R = A\sin^2\phi, \qquad A = \text{arbitary costant.}$$

To show how the field intensity varies with distance from the spot centre and with height, the quantity H/H_0 has been plotted (Fig. 4) against ξ for values of $\zeta = 0, \cdot 1, \cdot 5, \cdot 6, 1\cdot 0$. The topmost curve for $\zeta = 0$ gives H at different points along the spot surface. At the edge of the spot H/H_0 becomes nearly 14% whereas it ought to be zero. The other curves for $\zeta = \cdot 1, \cdot 3, \cdot 6$ and $1\cdot 0$ give the field intensities at different points on planes parallel to the spot surface at heights of $\frac{1}{10}$, $\frac{3}{10}$, $\frac{6}{10}$ and unit times the spot radius. As we go higher and higher above the spot surface, the field becomes more or less constant over the entire plane as is evident from the lowest curve for $\zeta = 1$, which is situated at a height equal to the spot radius.

Fig. 5 gives the lines of force at different points The tangent to these curves at any point gives the direction of the magnetic field at that point. The thick line SA is the spot surface. From (3.2) we note that ϕ-constant lines are the lines of constant ψ. Values of ψ for certain different values of ϕ are represented by arrows in the diagram. $\psi = 0$ is the line coinciding

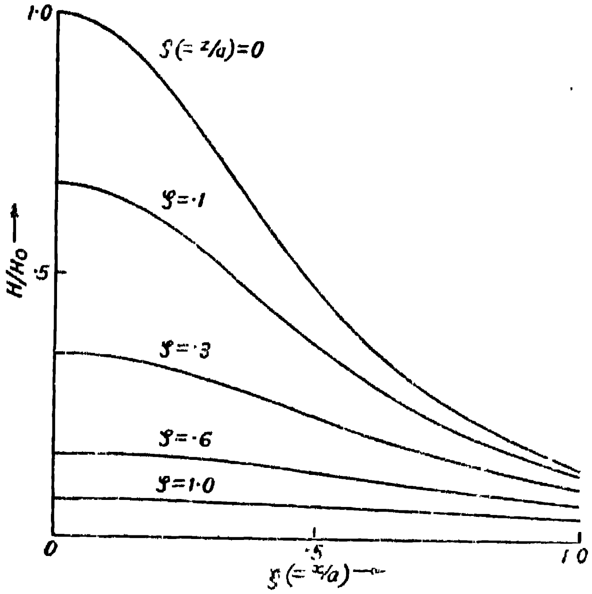

Variation of the intensity of the magnetic field along and above the spot surface (Broxon type).

Fig. 4

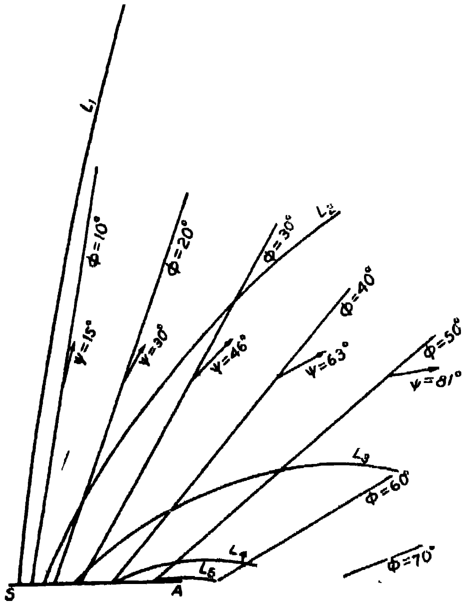

Lines of force of the spot field according to Broxon.

M

Fig. 5

with the central line $\phi=0$ Gradually as ϕ increases, ψ also increases, and at the periphery $\psi=\pi/2$, showing that the z-component of the magnetic field is absent at the edges, *i.e.*, the field is perfectly horizontal at the edges.

(2) Chapman (1943) has given another approach to the problem. For finding out the spot fields at different points, he argues as follows :

"If the two ends, whether of the straight or semicircular magnet, are sufficiently far apart, we can calculate the magnetic field near each as if the other were not there. Suppose the surface density σ (of magnetic poles) over the end depends only on the distance r from the centre of the spot ; and the magnetic intensity H and its inclination ψ, will likewise depend only on r. I have calculated ψ for various relationships between σ and r in order to find out what distribution of σ would agree approximately with Nicholson's measurement of ψ for a sun-spot. The details are omitted here. I give only the results for the assumed variation of surface density,

$$\sigma = \frac{H_0}{2\pi}\left(1-\frac{r^2}{a^2}\right)^2 \quad . \qquad \ldots \quad (3.3)$$

Taking the same axes as before, the magnetic pontential at a point P (x, o, z) is given by

$$\Omega = \frac{H_0 a}{2\pi}\int_0^1\int_0^{2\pi}(1-\rho^2)^2 \frac{\rho\, d\rho\, d\phi}{\sqrt{\lambda^2-2\lambda\rho\cos\phi\cos\psi+\rho^2}} \qquad \ldots \quad (3.4)$$

where $\lambda^2 = \dfrac{x^2+z^2}{a^2}$, $\tan\psi = \dfrac{x}{z}$, $r/a=\rho$

This is an elliptic function in λ."

Since for our purpose of investigating the propagation of e.m. waves in the solar atmosphere, we are not much concerned with the actual variation of the field over the surface of the spot, but mainly with the order of magnitude of H on and above the spot and as our line of argument will be the same for different kinds of variations of the magnetic fields, we do not

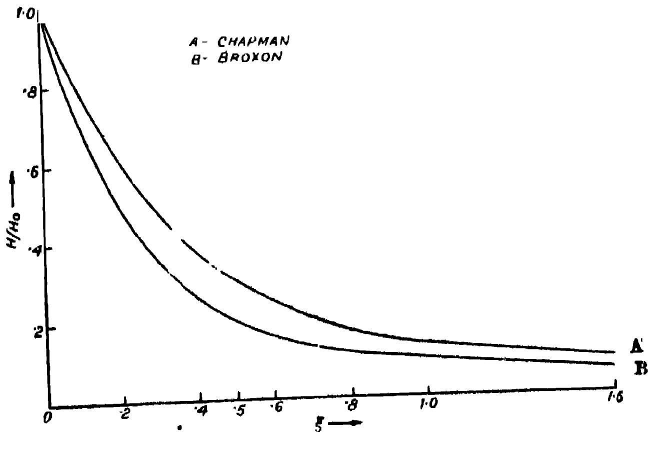

FIG. 6

Variation of the value of the magnetic field along the axis of a spot according to Chapman (A) and Broxon (B). ($\zeta=z/a$), z=distance along the axis, a=radius of spot.

proceed further with Chapman's assumptions, but stop here merely comparing the variation of H for the axial case for Chapman and Bioxon fields. For the axial case expression (3.4) gives

$$H_z = \frac{H_0}{3} \; . \; \{(8\zeta^4 + 12\zeta^2 + 3) - 8\zeta(1+\zeta^2)^{\frac{3}{2}}\} \qquad \ldots \quad (3.5)$$

Values of H/H_0 have been plotted against ζ for $\xi = 0$ (axial case) for Chapman fields (A) and Bioxon fields (B) in Fig. 6. The general trend of the two curves is the same, but Chapman's values are somewhat higher. We find that in both the cases, for large spots of radius $a = 28{,}000$ km, and $H_0 = 3600\ \Gamma$, large fields of the order of 1000 Γ persist at heights of the order of 15,000 km, *i.e.*, the top of the chromosphere. For such spots the fields reduce to approximately 13 to 10% at 30,000 km.

4. PROPAGATION OF E.M. WAVES

We are now in a position to discuss the actual problem of propagation of radio-waves through the solar atmosphere surrounding the spots, on the supposition that these waves have their origin deep within the spots, and are consequent on the physical processes taking place within the sun which give rise to spots.

As mentioned before, the propagation depends on: N, the electron density, H, the magnetic field, δ the damping coefficient $= \nu/p$ where ν is the number of collisions suffered by an electron per sec, p = pulsatance $= 2\pi f$, θ the angle of propagation, which is the angle between the direction of propagation and the positive direction of lines of force. We have discussed N and H, we shall now discuss the other quantities.

(*a*) The damping factor $\delta = \nu/p$

In the reversing layer (500 kms), we have $T \simeq 6000°$K, n = concentration of atoms mostly hydrogen $= 4.10^{15}$/c.c., n_e = electron density $\simeq 10^{14}$ per c.c. The mean free path of electrons is, therefore, $L_e = 4\sqrt{2}\ L$, where L is the mean free path of heavy particles.

Hence $$L_e = 4\sqrt{2}\,\frac{1}{\sqrt{2}\,\pi n \sigma^2} = \frac{4}{\pi .\ 4.10^{15} .\ 10^{-16}} \simeq 3 \text{ cms.}$$

$$c = \text{mean molecular velocity of electrons}$$

$$= \sqrt{\frac{3kT}{m_e}} \simeq 5.10^7 \text{ cms.}$$

Hence $\nu = \bar{c}/L_e \simeq 2.10^7\ \text{sec}^{-1}$.

Taking $\lambda = 2m,\ f = 1.5.10^8,\ p = 2\pi f$

and $\delta = \nu/p \simeq 2.10^{-2}$.

The value of δ is thus seen to be very small even on the reversing layer. In the higher layers δ falls very rapidly and therefore it is justifiable to neglect damping altogether.

(*b*) The angle of propagation

Let the globe represent the sun, C its body centre and CE the direction of the Earth. E is the centre of the visible disc. Let S be the position of the centre of the umbra of the spot.

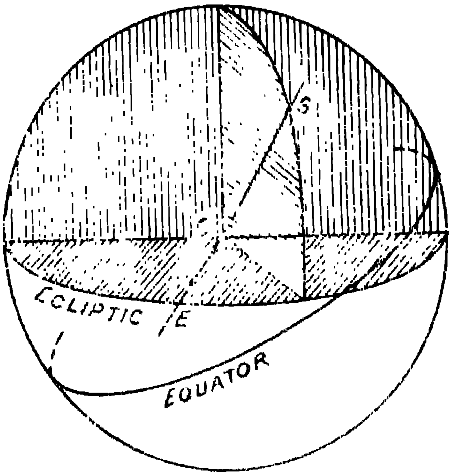

FIG. 7

Position of spot as seen from the earth S-position of the spot on sun (after Smart, *Spherical Astronomy*).

Then the direction of the spot axis, and of the central magnetic field of the spot is along CS. The angle ECS, which is generally denoted by ρ (but we shall denote it by χ as ρ has been used in a different sense), can be obtained by calculation from daily observation of the spot (*vide* Smart, *Spherical Astronomy*, p. 172). When the spot first appears on the east limb, $\chi = 90^\circ$, but there is hardly any observation available at the first appearance of the spot. Observations generally start after a day, when $\chi \simeq 75^\circ$, then gradually χ diminishes day by day, but even during central meridian passage χ is generally different from zero, except on very rare occasions. After central meridian passage, χ again increases day by day till it is 90° when the spot disappears on the west limb.

Choice of Axes.—The plane ECS may be taken as the (XZ) plane, CE being the axis of Z, the axis of X being perpendicular to CE in the plane ECS. The axis of Y is perpendicular to the plane of ECS (Fig. 8).

Angle of propagation.—(See Fig. 8) According to our assumption, the source of radio-waves is the funnel shaped volume about S, with CS as axis. The volume comprises the whole conical space of the solar atmosphere with the spot as the base, which is traversed by the lines of force. If the lines of force were everywhere parellel to CS, $\theta = \chi$ if the polarity of the spot were R (lines of force away from the surface) and $= |\pi - \chi|$ if the polarity were V (lines of force passing into the surface).

But such is not the case, as the lines of force curve away from the direction of CS, as discussed in §3. Let us find out the angle θ for any point P $(a\xi, a\eta, a\zeta)$ within the spot. This is the angle between CE, and the tangent to the lines of force at P. These make an angle ψ defined by (3.2) with CS, at an azimuth $\alpha=\tan^{-1}\eta/\xi$.

θ varies between $\chi+\psi$, $\chi-\psi$ as α varies between 0 and 2π.

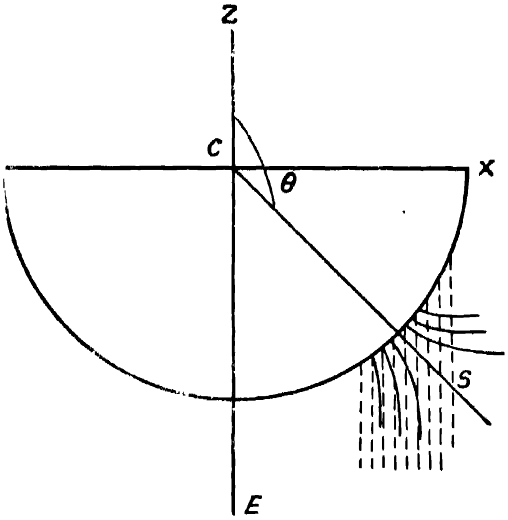

FIG. 8

Plane through Earth, Sun's centre and spot centre, showing how angle of propagation of waves varies in the neighbourhood of spot.

The equations of propagation of the radio-waves through the spot atmosphere can now be written, using the symbols of the previous paper. They are:

$$\left.\begin{aligned}&\frac{d^2}{du^2}(E_x+iF_1E_y)+q_0^2(E_x+iF_1E_y)=0\\&\qquad\text{for the o-wave}\\\text{and }&\frac{d^2}{du^2}(E_x+iF_2E_y)+q_e^2(E_x+iF_2E_y)=0\\&\qquad\text{for the e-wave}\end{aligned}\right\}\quad\cdots\quad(4.1)$$

where $u=2\pi z/\lambda$, $F_1=\sqrt{1+g^2}-|g|$, $F_2=\sqrt{1+g^2}+|g|$,

$$g=\omega\sin 2\theta/2\cos\theta\ (r-1)$$

and

$$\left.\begin{aligned}q_0^2&=1-\frac{r}{1+\omega\sin\theta\,(\sqrt{1+g^2}-|g|)}\quad\text{for } r<1\\&=1-\frac{r}{1-\omega\sin\theta\,(\sqrt{1+g^2}-|g|)}\quad\text{for }>1\end{aligned}\right\}\quad\cdots\quad(4.2)$$

$$q_e^{\,2} = 1 - \frac{}{1 - \omega \sin\theta\,(\sqrt{1+g^2} + |g|)} \quad \text{for } r < 1$$

$$= 1 - \frac{}{1 + \omega \sin\theta\,(\sqrt{1+g^2} + |g|)} \quad \text{for } r > 1 \qquad (4.8)$$

The waves will be able to come out as long as q_0^2 and q_e^2 are > 0. Let us first investigate the probable values of q_0^2 and q_e^2 in the spot region. They vary from point to point and we give the values of the relevant quantities for $\lambda = 1.5m$, $f = 2.10^8$/sec.

We have $N_0 = \frac{mp^2}{4\pi e^2} = 5.10^8$, $\omega = 1.4 \times 10^{-2}$ H.

Reference to paper (I)* shows that whatever the values of ω and θ, q_0^2 always tends to zero at $r = 1$. This happens at a height of 13500 km. So all o-waves coming from below this height are turned back.

As regards the e-wave, the transparency extends to the point where $r = 1 + \omega$. For the present case, we assume that N, the ion-concentration varies according to the law $N = N_0 e^{-\beta z}$ (*vide* Table II). The e-wave can leak out from levels where $r \leq 1 + \omega$. For the present case this happens at $z > 3900$ kms. So the whole column, above a height of 3900 km, would be transparent to the e-waves of wave-length 2m (Fig. 9).

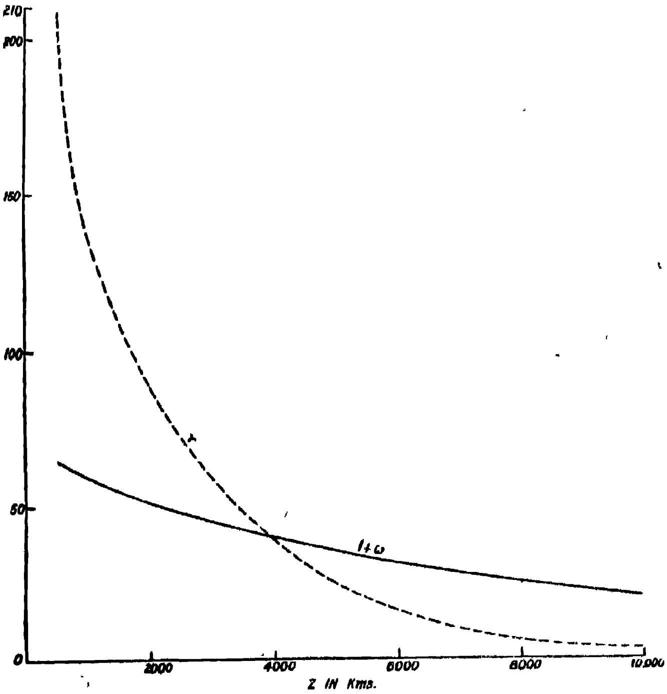

FIG. 9

The dotted curve shows the variation of $r = \frac{4\pi Ne^2}{mp^2}$ with height over the spot for $\lambda = 2m$

The other curve gives $(1 + \omega)$ as a function of height.

---

* Saha, Banerjea and Guha, 1947, Ind. J. Phys., 21, 181.

It is easy to see that the shorter waves would be able to come from correspondingly deeper layers.

Polarisation and sense of polarisation of the waves.—Detailed description of measurements of polarisation is not available ; but in all the short notes which have been published it is stated that the polarisation is circular, even when the spots are close to the limb. Some state that the sense of polarisation changes on crossing the meridian (Martyn, 1946), while others do not find any such change (Bowen, 1946).

TABLE II

Level above photosphere in km	N_e	(r)		H (Broxon)	ω
		Normal Atmosphere	Spot Atmosphere		
0	$1.6.10^{11}$ cc	320	176	3600Γ	50.4
500	$1.29.10^{11}$,,	258	141.9	3330 ,,	46.6
1,000	$1.04.10^{11}$,,	208	114.4	3063 ,,	42.9
1,500	$8\ 37.10^{10}$,,	167	91.85	2885 ,,	40.39
2,000	$6.80.10^{10}$,,	136	74.80	2720 ,,	38.8
3,000	$4.42.10^{10}$,,	88	48.40	2364 ,,	35.10
5,000	$1\ 86.10^{10}$,,	37	20.35	1830 ,,	25.62
8.000	$5.12.10^{8}$,,	10	5.50	1296 ,,	18.14
10,000	$2.14.10^{8}$,,	5	2.75	1068 ,,	15.00
14,500*	3.10^{8} ,,	.66	.53	720 ,,	10.80
$20,000^1$	$2.9.10^{8}$,	.64	.35	618 ,,	8.65
30,000	$2.5.10^{8}$,,	.50	.28	360 ,,	5 04
40,000	$2.1.10^{8}$,,	.46	.25	187 ,,	2.62
50.000	$1.7.10^{8}$,,	.34	.19	104 ,,	1.46
100,000	$.85.10^{8}$,,	.20	.11	14 ,,	.20
1000,000	$.11.10^{6}$,,	.00	.00	0	0

* This value is not extrapolated from the curve $n = n_0 e^{-\beta z}$, but is an experimental value obtained from coronal data.

(1) These values are taken from extrapolation of the values of electron concentration in the corona obtained from scattering of light by free electrons given by Bambauch (See Physik der Stern-atmosphäre, page 440, 1938) and recently corrected by Allen (1946), and Van de Hulst (1947).

It is only possible to make some general statements about polarisation from our theory. We have $H_y/H_x = \sqrt{1+g^2} - |g|$ both for the o-wave, and the e-wave. Since g is changing at every point, so polarisation of the wave, as it is propagated through the solar atmosphere, is constantly changing. A large $|g|$ means "linear polarisation", a small $|g|$ means circular polarisation Inside the chromosphere $|g|$ is large, hence the waves will be "linearly polarised". But as the waves pass through the corona both ω and r tend to vanish and $\omega \sin^2 \theta/2(r-1) \cos\theta$ is a very small quantity, *e.g.*, it is .066 for $\theta = 120°$ at a height of 10^6 km above the photosphere and hence $\rho \rightarrow 1$, and the waves become circular. Table II gives the values of r and ω for the spot atmosphere at various heights.

The sense of polarisation would depend upon the value of θ.

The waves have to pass through the Earth's ionosphere before we receive them. But in this case

$$r = \frac{4\pi N e^2}{m p^2} = \frac{N}{5 \cdot 10^8} \simeq 10^{-2}, \quad \omega = f_h/f = {\cdot}7.10^{-2}, \quad g = {\cdot}0035 \cos^2\theta \simeq 0.$$

Hence $F_1 = F_2 = 1$, *i.e.*, the magnetic field is too weak to cause any change in the polarisation of the micro-waves from the sun.

5. GENERAL DEDUCTIONS

It is not possible to penetrate more deeply into the phenomena with the aid of our theory, unless the observations become more refined and the technique is improved, but some general statements can be made.

The equations of propagation show that the escape of waves and the sense of their circular polarisation are extremely sensitive to the value of the spot field and the concentration of electrons. In our treatment we have taken the source to be single spot (α-type), but observations have shown that majority of spots are bipolar, consisting of a leader and a follower with opposite polarity, whose field-strength undergoes rapid changes with the age. Let us quote from Chapman (1943) :

> " Sun-spot Dipole Moments.—Hale found that most sunspot groups at some stage in their life-history, show bipolarity that is to say, they include two spots, or two regions or groups of spots, of opposite magnetic polarity, one red (R) and the other violet (V). At other stages, however, there is often only one spot, of like polarity over all its area ; this is called a unipolar spot.
>
> A typical spot group begins as two small spots, or two groups of spots, of opposite polarity, nearly in the same latitude, and 3° or 4° apart in longitude. The two principal spots grow rapidly and separate in longitude to a distance of 10° or more; the rear spot attains its maximum area in 3 or 4 days ; the leader attains a larger maximum area in 7, 8 or 9 days, many smaller spots develop within the group, mostly near the two main ones. The dipole moment of the group is greatest when the spots are largest and furthest apart.

Consider a notable case, that of the great bipolar group M. W. 6725, 8° S, consisting of two great spots each of radius 20,000 km, about 14° apart, together with many smaller spots between; for this group $H=3900\Gamma$; considering only the two large spots, the dipole moment is 5×10^{16} km^3, *i.e.*, 600,00 times as great as the Earth's dipole moment, and about 1/170 of that of the sun. The sun-spot dipole moment is of course horizontal, and nearly parallel to the sun's equator, though the leading spot is generally somewhat nearer to the equator than is the follower. At the equator the dipole axis is along the equator, and according to W. Brunner its inclination to the equator increases with latitude to about 16° at 30° latitude."

Many of the spots whose radio emission had been under investigation during the last and the present year, appear to have been of this type.

In such cases, each one of the component spots with different polarity will emit microwaves of different intensity and with circular polarisation of opposite sense. Though the waves from each spot may be co-herent, the waves from the two spots may not be co-herent, like light from two distinct sources. This appears to explain in a general way the observations of Ryle and Vonberg, Martyn, and of Appleton and Hey. But it is desirable that radio observations be coupled with simultaneous observations of the polarity and field strength of the component spots.

When the spot group is of the γ-type (multipolar and without demarcation) the polarisation may be random.

Sudden changes in intensity.—Sudden changes in intensity are expected when H and N change suddenly. This happens during flares which, as Geovanelli (1945) has shown, are connected with the γ-type of spots, where the field strength undergoes rapid changes. This may affect microwave emission in two ways, (1) sudden increase in the value of H, will allow the e-component of the microwave to come from deeper layers and vice versa, (2) if the physical mechanism of emission given out by the senior author (Saha, 1946) be correct, sudden fluctuations of magnetic field will induce more copious emission of microwaves. But this point requires further investigation.

APPENDIX 1

The line $\lambda = 6173.346$ is the weakest member of a $d^7p^5D—d^7p^5P$ multiplet of Fe. Its position is given in table mentioned below :

The multiplet is $d^7s^5D-d^7s^5P$ according to Russell. The excitation potential of the $^5D_0$ level is 4.21 volts ($\nu = 34121$ cm^{-1}). The other lines of the multiplet, notably 6137.005, and 6151.630 etc. are also sometimes used for measurement of the sunspot fields.

The theoretical Zeemann-pattern of 6173.32 is given by $\Delta\nu = \pm a(0, 5/2)$. This is also experimentally verified. The Mount Wilson values of magnetic field are obtained from comparison of laboratory data with observational data, and are therefore independent of particular Zeemann-pattern.

	${}^5D_0$	${}^5D_1$	${}^5D_2$	${}^5D_3$	${}^5D_4$
${}^5P_1$	1 6173·346 16194·19 (400)	5 6213·44 16089·79 (500)	5 6297·83 15874·16 (500)		
${}^5P_2$		1 6137·005 16290·00 (200)	6 6219·190 16074·59 (500)	10 6335·34 15780·11 (500)	
${}^5P_3$			1 6151·630 16251·35 (350)	6 6265·145 15956·02 (500)	10 6430·86 15543·73 (800)

Hale's suggestion for measurement of magnetic field in the higher layers of the spot

" On considerations it will be seen, however, that the separation of the doublets must depend, in some degree on the distribution of the absorbing vapor in the solar atmosphere, and on the coefficient of absorption of the particular line employed. A striking instance of this kind, affecting lines of the same series, is illustrated in the case of hydrogen, described in a previous paper.* Although the Hα line extends to the upper part of the chromosphere and prominences, the mean level represented by its absorption is much lower than that given by Hα. The consequence is that Hα enables us to photograph the solar vortices, the characteristic stream lines of which do not appear at the lower Hδ level. Similarly, if the intensity of a given titanium line falls off rapidly, the level represented by this line may be comparatively low. If, on the other hand, its intensity curve is of such a form as to indicate that the absorption at higher elevations plays an important part, the mean level represented by the line may be considerably higher than in the previous case. To settle this question we must know :

(1) The range of elevation in the spot of the vapors of iron, titanium, and other elements:

(2) The intensities of the lines of these elements at different levels ;

(3) The rate at which the strength of the field decreases upward.

In the absence of information regarding the first two points, we may enquire as to the probable relative behavior of titanium, iron, and other elements if the distribution of the vapors at different levels were the same as in the chromosphere. From a discussion of a large number of photographs of the flash spectrum, made by different observers at several eclipses, Jewell has compiled a table showing the heights above the sun's limb attained by various lines in the blue and violet*. "The heights for titanium range from 100 miles (160 km) for 4466.0 to 3500 miles (5640 km) for 4466.7, while certain strong enhanced lines in the ultra-violet reach elevations of 6000 or 8000 miles (9660 or 12,880 km). For iron the minimum height is 200 miles (320 km) for 4482.4 and the maximum 1000 miles (1610 km) for 4584.0. Chromium ranges from 100 miles for 4280.2 to 1200 miles (1930 km) for 4275.0 ; manganese from "100 miles or more" for 4451.8 to "800 miles (1290 km) or more" for 4030.9 ; vanadium from 100 miles for 4390.1 to 200 miles for 4379.4 . It thus appears that the range in level represented by the titanium lines is much greater than for the lines of iron, chromium, manganese, and vanadium. If the vapors were similarly distributed in spots, the maximum strength of field indicated by the titanium lines should therefore correspond with the maximum value for iron, but some titanium lines, produced by absorption at higher mean levels, should give lower field strength. Chromium should agree more nearly with iron. Vanadium, if the less refrangible lines reach no greater elevations, should give closely accordant (maximum) values for the field strength. It will perhaps be possible, with the aid of the 30 feet spectrograph, to determine the relative levels in the chromosphere attained by most of the lines in question, but it is a much more difficult matter to do this for sun spots. I hope, however, that our new spectroheliograph of 30 feet focal length may throw some light on this subject."

---

* Solar Vortices.

It is evident that these considerations will have no bearing on the present problem unless the field strength decreases very rapidly upward in spots. That this probably occurs is shown by the fact that the D-lines of sodium and the b-lines of magnesium are usually but slightly affected in the spot spectrum,† and are displaced through a very small distance when the Nicol is rotated. Thus, at the level represented by these lines, which attain elevations in the chromosphere probably not exceeding 5000 miles, the field strength is reduced to a small fraction of its maximum value.

ACKNOWLEDGMENT

Two of us, B. K. Banerjea and U. C. Guha have been the recipients of two Research Scholarships from the Radio Research Committee of the Council of Scientific & Industrial Research (India) and wish to express their thanks to the Council for facility to work and permission to publish this paper.

PALIT LABORATORY OF PHYSICS
CALCUTTA UNIVERSITY.

---

* "Total Solar Eclipses of May, 28, 1900, and May 17, 1901." Publications of the U.S. Naval Observatory Series, Vol. IV, Appendix 1.

† Except for the strengthening of the wings, which may be produced by some cause other than a magnetic field.

REFERENCE

Allen, 1946, M.N.R.A.S., 106, 137.

Appleton and Hey, 1946, *Phil. Mag.*, **37**, 73.

Broxon, 1942, *Phy. Rev.*, **62**, 521.

Bumbauch, 1937, *A N.*, 263.

Chapman, 1943, *M.N.R.A.S.*, **103**, 117.

Dicke and Berringer, 1946, *Astro. Journ.*, **103**, 76.

Geo-vanelli, 1946, *Nature*, **158**, 87.

Hale and Nicholson, 1925, Magnetic observations of Sun's spots.

Hale, 1935, *Nature*, **36**, 703.

Hartree, 1931, *Proc. Camb. Phil. Soc.*, **27**, 143.

Hulst, 1947, *Astro. Journ.*, 105, 431.

Pawsey, MacReady and Payne-Scott, 1946, *Nature*, **157**, 158.

Pawsey, MacReady and Payne-Scott, 1947, *Proc. Roy. Soc.*, **190**, 357.

Martyn, 1946, *Nature*, **158**, 308

Moore, 1931, *Astro. Journ.*, **75**, 222, 298

Nicholson, 1926, *Pub Ast. Soc. Pac* , **38**, 347.

Nicolet, Le Soleil, page 51, fig. 30.

Richardson, 1931, *Astro. Journ* , **73**, 216.

Russell, 1929, *Astro. Journ.*, **70**, 11.

,, 1934, *Astro. Journ.*, **78**, 239.

Ryle and Vonberg, 1946, *Nature*, **158**, 339.

Saha, 1946, *Nature*, **158**, 717.

Saha, Banerjea and Guha, 1947, *Ind. J. Phys* , **21**, 181.

Thiessen 1946, *Ann de Astro. Physi.*, **9**, 101.

Wildt, 1947, *Astro. Journ.*, **106**, 43.

X-RAY STUDIES OF ALKALI CHLORIDES DISSOLVED IN B_2O_3—GLASS

By SUBODH KUMAR MAJUMDAR and BHUPATI KUMAR BANERJEE

(*Received for publication, Aug. 6, 1947*)

(Plates VIIA, VIIB and VIIC)

ABSTRACT. X-ray investigation is made of $NaCl$-B_2O_3, KCl-B_2O_3 and $RbCl$-B_2O_3 glass systems and the effect of different concentrations of alkali chloride in B_2O_3 glass has also been studied.

It is found that alkali chloride retains its characteristic structure and in some cases it induces crystallinity in the glass itself.

INTRODUCTION

In previous communications, Majumdar and co-workers (1942, 45, 46) have published the results of X-ray diffraction of alkali halides dissolved in boric oxide and borax-glasses. The salts investigated have all polar linkages and the equilibrium in such cases, according to the simpler electro-static theory of Born and others (1938), is the result of mainly two forces, *viz.*, the Coulomb forces between the ions obeying the inverse square law and the short distance repulsive forces. It is well-known that in aqueous solutions the lattice is destroyed primarily on account of the weakening of the electrostatic forces in a medium of high dielectric constant, such as water, and the so-called ionisation occurs. It is conceivable therefore that if these polar salts could be dissolved in a medium possessing not such a high dielectric constant as water (lying between 6.5−7.5), the weakening of the electrostatic forces may not be so great as to cause ionisation but large enough to produce an enlargement of the lattice. It was with this object that alkali chlorides were dissolved in boric oxide and borax glasses and the properties, of the melt after solidification were studied in various ways, *viz.*, refractometrically, by X-ray diffraction and by studying their diamagnetic susceptibilities.

The earlier investigations led one of us (Majumdar, *loc. cit.*) to believe that there was an actual enlargement of the lattice of these crystals when dissolved in the above-mentioned glasses. The subject has since been studied using more refined methods and using more powerful X-ray generator and the results are recorded in the present paper.

NaCl-B_2O_3

Sample

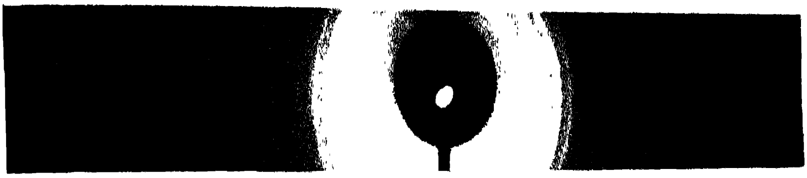

A_1

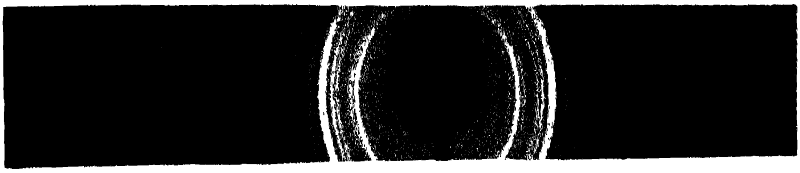

A_2

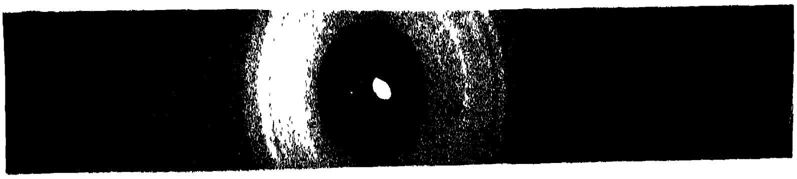

A_3

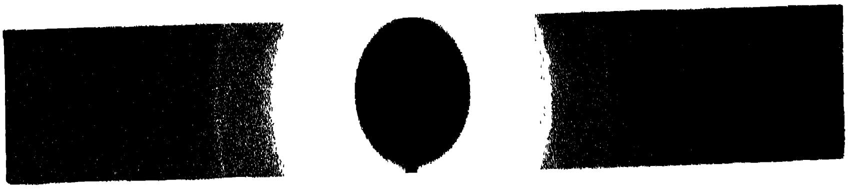

A_4

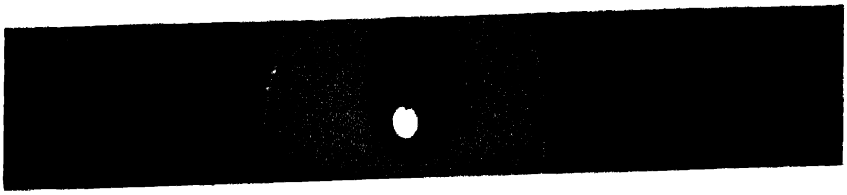

A_5

KCl-B_2O_3

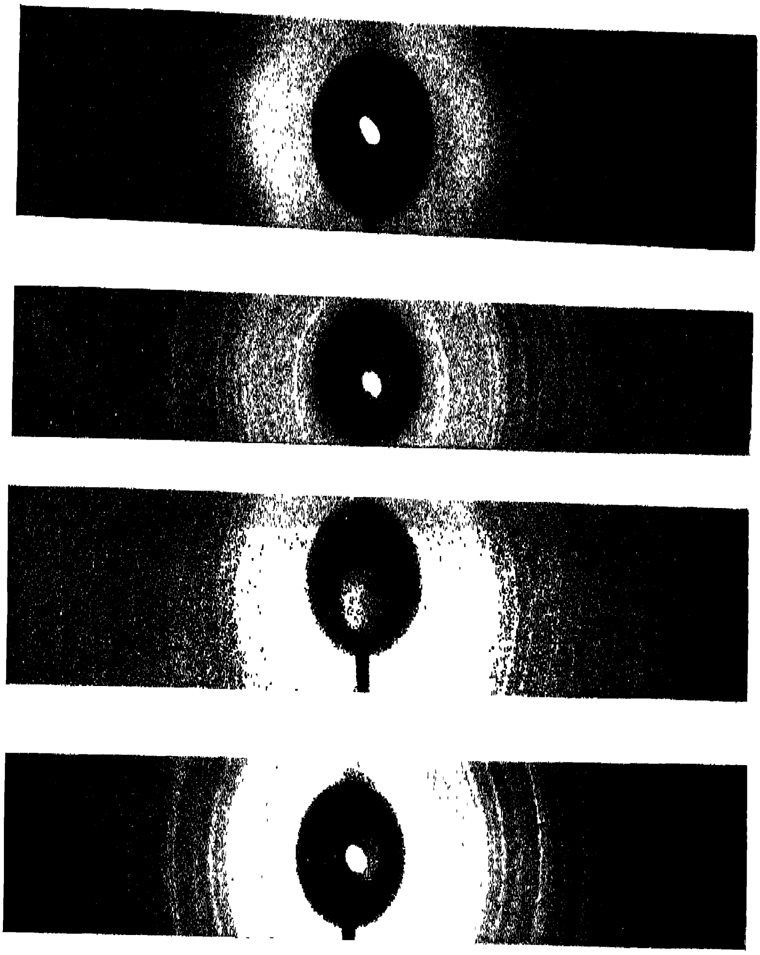

RbCl B_2O_3

Sample

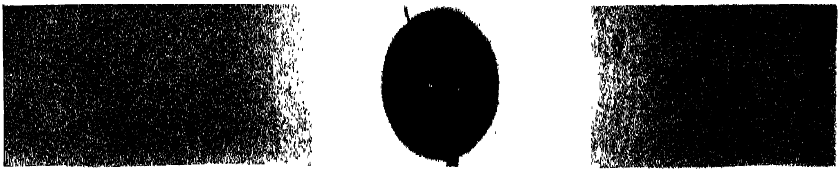

C_1

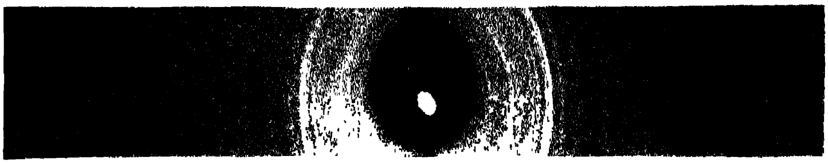

C_2

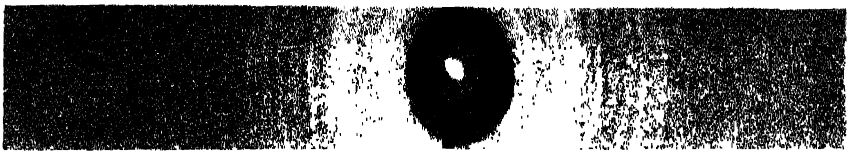

C_3

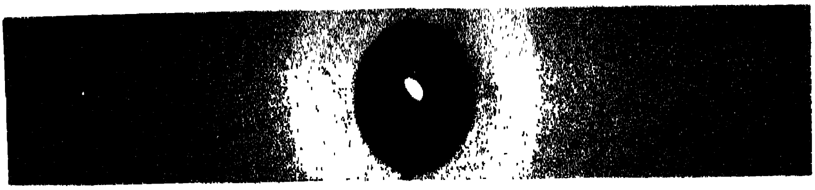

C_4

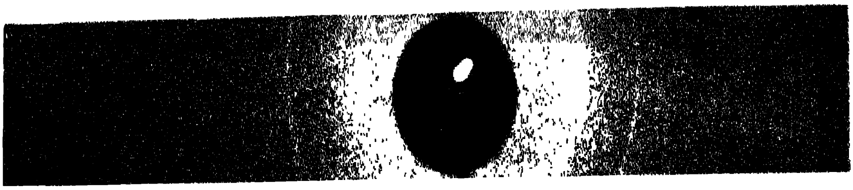

C_5

According to modern conception regarding structure of glass due to Zachariasen (1932), Warren and others (1938), a sort of *non-repeating* network exists in the glass as opposed to the regular space-lattice obtaining in a true crystal. And hence haloes or diffuse lines are obtained with a glass in X-ray diffraction experiments instead of sharp lines obtained with true crystals. It is of interest, therefore, to examine if the X-ray diffraction patterns of crystals dissolved in a glass reveal sharp lines due to the dissolved crystal and the faint haloes due to the glass. As a result of a large number of experiments this expectation has been realised in every case.

Warren and his co-workers (1037) have studied the diffraction photographs given by B_2O_3-glass, using Fourier analysis method and have come to the conclusion that in the glass, each boron atom is linked with three other oxygen atoms, in a triangular arrangement. Warren and Loring studied the SiO_2-Na_2O-glass system with Na_2O content varying from O to 46% Na_2O. With small Na_2O-contents, the pattern shows a single strong peak at $\frac{\sin}{\lambda}=0.12$, but with increasing Na_2O-content, the peak diminishes in intensity, while a new peak at $\frac{\sin}{\lambda}=0.18$ appears in the picture and this peak becomes more pronounced with increasing soda-content. It was also found by these authors that with increasing alkali oxide content, B-O-B distance changes and there is a shift from the planar threefold configuration to fourfold tetrahedral configuration. The present communication records the results of the following systems :—$NaCl$-B_2O_3 ; KCl-B_2O_3 ; $RbCl$-B_2O_3.

EXPERIMENTAL

The salts as well as boric acid of Merck Pro-Analyse quality were recrystallised from conductivity water and carefully dehydrated first in an air oven and then in a vacuum desiccator for several days. The presence of traces of moisture was tested by taking a sample in absolute alcohol and treating with anhydrous copper sulphate.

The anhydrous B_2O_3 and the salt were then quickly powered and heated in a platinum crucible over a Mecker burner for several hours until a homogeneous melt was obtained. The crucible was then chilled and the solid extracted. Each piece was tested in a polarisation microscope for optical isotropy. The samples were then powdered, enclosed in a thin-walled capillary tube and the Debye-Scherrer photograph taken. The alkali-content was determined by estimating chlorine volumetrically by back titration method, and in some cases checked by gravimetric method.

X-ray from a Hadding tube with copper anti-cathode run at a voltage of about 40 KV and a tube current of 4.5−5.5 milliamp, after collimation through narrow circular slits was made incident on the sample in the form of a stick of 1 mm diam. placed along the axis of a cylindrical camera of 3.90 cm. radius. The glancing angle θ in degrees is obtained from the equation, $\theta=\frac{x}{4r}\times 57.3$ degrees, where x is the distance in cm. between two similar lines in the negative and r, the radius of the camera.

An exposure of 10–12 hours was necessary. The analysis of the results are shown in the following tables, in which *s* stands for strong, *m* for medium, *w* for weak and *v* for very. θ_α and θ_β stand for angles due K_α (1.539 A) and K_β (1.389 A) due to copper radiation.

TABLE I

$NaCl-B_2O_3$ (Sample A_1 – 3.53% NaCl)

Int.	Observed θ	Calc. NaCl		B_2O_3		$Na_2B_4O_7$	
		θ	Plane	θ	Int.	θ	Int.
mw	6°58′	...	...	6°45′	(2)	...	...
w	8°27′	...	...	...	...	...	...
s	9°26′	...	...	...	...	...	...
ms	10°6′	...	...	...	...	9°56′	(2)
w	10°27′	...	...	...	...	10°47′	(2)
ms	11°33′	...	...	11°52′	(1)	...	...
s	12°28′	...	...	12°25′	(½)	...	...
s	13°13′	...	...	13°16′	(10)	...	...
s	13°46′	...	...	14° 7′	(10)	...	...
vw	14°19′	14°19′	$(200)_\beta$	...	...	...	...
m	14°57′	...	...	...	...	14°42′	(4)
w	15°25′	...	...	15°24′	(1)	...	...
mw	16° 9′	15°52′	(200)	...	...	...	...
m	17° 4′	...	...	...	...	17°17′	(½)
w	18°27′	...	...	...	...	18°35′	(1)
mw	19°39′	...	...	...	...	19°46′	(½)
w	20°12′	...	...	20° 7′	(2)	...	...
mw	20°39′	20°27′	$(220)_\beta$	...	...	...	...
w	21° 7′	...	...	21° 6′	(½)	...	...
w	21°51′	...	...	...	...	22° 9′	(½)
w	22°34′	...	...	...	...	22°54′	(1)
ms	22°57′	22°45′	(220)	...	...	...	...
ms	24°25′	...	...	...	...	24°35′	(1)
mw	24°58′	...	...	24°38′	(½)	...	...
w	26° 1′	...	...	...	...	25°44′	(1)
ms	27°26′	...	...	27°28′	(½)	27°19′	(½)
w	28°38′	28°17′	(222)	...	...	...	...
w	30°29′	...	...	30°36′	(½)	...	...
w	37°38′	37°42′	(420)	...	...	...	...
w	42°13′	42° 5′	(422)	...	...	...	...

TABLE II

NaCl – B_2O_3 (Sample A_2 – 5.23% NaCl)

Int.	Observed θ	Calc. NaCl		B_2O_3		$Na_2B_4O_7$	
		θ	Plane	θ	I	θ	I
m	6°28′	...	...	6°45′	(5)	...	...
m	7°19′	...	...	7°30′	(5)	...	...
mw	8°26′	...	...	...	...	...	...
s	9°37′	...	...	...	...	9°57′	(2)
m	10°28′	...	...	...	...	10°46′	(2)
s	11°33′	...	...	11°52′	(2)	...	...
s	12°28′	...	...	12°25′	(1)	...	..
vs	13° 7′	...	...	13°16′	(10)	...	...
vs	13°57′	13°42′	(111)	14° 7′	(10)	...	...
w	14°19′	14°19′	(200)β	...	...	...	...
ms	15° 3′	...	...	15°24′	(1)	...	...
s	16°20′	15°52′	(200)	...	...	...	...
mw	17°15′	...	..	...	...	...	...
m	18°21′	...		..	...	18°34′	(1)
ms	19°27′	...	...	...	...	19°46′	(½)
mw	20°34′	20°27′	(220)β	20° 7′	(2)	...	...
w	21°51′	...	...	...	...	22° 9′	(½)
ms	22°57′	22°45′	(220)	...	...	...	...
m	24°25′	...	...	24°38′	(½)	24°35′	(1)
w	25°19′	...	...	...	...	25°44′	(1)
m	27°21′	26°59′	(311)	27°28′	(½)	27°19′	(½)
w	28° 5′	28°17′	(222)	...	...	...	...
w	29°39′	...	...	...	...	29°48′	(½)
w	37°49′	37°42′	(420)	...	...	...	...
w	42°36′	42°51′	(422)	...	...	...	...

TABLE III

NaCl – B_2O_3 (Sample A_3 – 7.83% NaCl)

Int.	Observed θ	Calc. NaCl		Calc. B_2O_3		$Na_2B_4O_7$	
		θ	Plane	θ	I	θ	I
w	8°22′	...	...	...	...	...	...
s	9°42′	...	...	..	..	9°56′	(2)
w	10°22′	...	...	...	...	10°47′	(2)
mw	12° 7′	...	...	12°25′	(1)	...	...
m	12°51′	...	...	...	...	13°10′	(2)
m	13°31′	...	...	13°16′	(10)	...	...
s	14°19′	...	...	14° 7′	(10)	...	...
w	14°41′	14°19′	(200)	...	...	...	...
mw	15°25′	...	...	...	...	15°42′	(1)
m	16° 9′	15°52′	(200)	...	...	...	...
w	16°58′	...	...	16°42′	(½)	16°33′	(1)
m	17°37′	...	...	...	...	17°47′	(½)
mw	18°55′	...	...	...	...	18°35′	(1)
m	20°12′	20°27′	(220)β	...	...	...	...
s	23° 2′	22°45′	(220)	...	...	...	...
w	23°58′	...	...	...	...	23°53′	(½)
ms	25°30′	...	...	...	...	25°44′	(1)
s	28°22′	28°17′	(222)	...	...	...	.
mw	33°36′	33°10′	(400)	...	...	...	...
mw	38° 1′	37°42′	(420)	...	...	...	...
mw	42°17′	42° 5′	(422)	...	...	...	...

TABLE IV

NaCl—B_2O_3 (Sample A_4—14.00% NaCl)

Intensity	Observed	Calculated	
	θ	θ	Plane
s	15° 58′	15° 52′	(200)
w	20° 33′	20° 27′	$(220)_\beta$
s	22° 46′	22° 45′	(220)
m	28° 16′	28° 17′	(222)
mw	33° 25′	33° 10′	(400)
m	37° 56′	37° 42′	(420)
mw	42° 13′	42° 5′	(422)

TABLE V

NaCl—B_2O_3 (Sample A_5—23.52% NaCl)

Intensity	Observed	Calc. NaCl	
	θ	θ	Plane
m	14° 23′	14° 19′	$(200)_\beta$
vs	16° 0′	15° 52′	(200)
w	20° 36′	20° 27′	$(220)_\beta$
vs	22° 51′	22° 45′	(220)
m	28° 14′	28° 17′	(222)
w	33° 10′	33° 10′	(400)
s	37° 46′	37° 42′	(420)
s	42° 5′	42° 5′	(422)

TABLE VI

KCl—B_2O_3 (Sample—B_1—1.01% KCl)

Intensity	Observed	Calculated KCl		B_2O_3	
	θ	θ	Plane	θ	Plane
m	13° 57′	14° 12′	(200)	14° 7′	10
w	15° 10′	...	...	15° 24′	1
vw	17° 52′	...	...	18° 5′	½
w	20° 12′	20° 17′	(220)	...	...
w	25° 5′	25° 8′	(222)	...	...

TABLE VII

KCl—B_2O_3 (Sample B_2—5.09% KCl)

Intensity	Observed	Calc. KCl		B_2O_3	
	θ	θ	Plane	θ	I
mw	7° 12′	...	...	7° 30′	(5)
s	8° 11′	...	...	...	...
w	11° 31′	...	...	11° 52′	(1)
s	12° 43′	12° 47′	$(200)_\beta$	12° 25′	(1)
s	13° 21′	...	...	13° 16′	(10)
ms	14° 9′	14° 12′	(200)	14° 7′	(10)
mw	15° 14′	...	...	15° 24′	(1)
s	16° 23′	...	...	16° 42′	(½)
mw	17° 57′	18° 3′	$(220)_\beta$	...	...
w	18° 55′	...	...	18° 54′	(½)
w	20° 17′	...	...	20° 17′	(2)
ms	20° 40′	20° 17′	(220)	..	...
w	21° 27′	...	...	21° 6′	(½)
mw	22° 48′	22° 32′	$(222)_\beta$	..	...
w	24° 19′	...	...	24° 38′	(½)
m	25° 9′	25° 8′	(222)	...	...
mw	28° 40′	..	...	28° 58′	(½)
m	29° 45′	29° 22′	(400)	...	...
m	33° 10′	33° 14′	(420)	. .	...
m	36° 58′	36° 56′	(422)	...	...

TABLE VIII

KCl—B_2O_3 (Sample B_3—8.77% KCl)

Intensity	Observed	Calc. KCl		B_2O_3	
	θ	θ	Plane	θ	I
m	7° 15′	...	...	7° 30′	(5)
s	8° 14′	...	...	...	...
w	11° 27′	...	...	11° 52′	(1)
s	12° 13′	...	...	12° 25′	(1)
s	12° 56′	12° 47′	$(200)_\beta$	13° 16′	(10)
ms	13° 46′	14° 12′	(200)	14° 7′	(10)
mw	15° 3′	...	...	15° 24′	(1)
ms	16° 13′	.	...	16° 42′	(½)
mw	17° 48′	18° 3′	$(220)_\beta$	...	...
w	18° 43′	...	...	18° 54′	(½)
w	20° 0′	...	.	20° 7′	(2)
ms	20° 22′	20° 17′	(220)	...	...
w	21° 0′	...	...	21° 6′	(½)
mw	22° 46′	22° 32′	$(222)_\beta$	...	...
w	24° 13′	...	...	24° 38′	(½)
m	24° 58′	25° 8	(222)	...	...
mw	28° 33′	...	...	28° 58′	(½)
m	29° 45′	29° 22′	(400)	...	...
m	33° 14′	33° 14′	(420)	...	...
ms	36° 38′	36° 56′	(422)	...	...

TABLE IX

$KCl—B_2O_3$ (Sample B_4—13.53 KCl)

Intensity	Observed	Calc. KCl		B_2O_3	
	θ	θ	Plane	θ	I
w	7° 28	...	...	7° 30′	(5)
s	8° 12′	...	..	...	...
m	11° 30′	...	...	11° 52′	(1)
s	12° 42′	...	...	12° 25′	(1)
s	13° 22′	12° 47′	$(200)_\beta$	13° 16′	(10)
s	14° 12′	14° 12′	(200)	14° 7′	(10)
w	15° 19′	...	...	15° 24′	(1)
s	16° 16′	...	...	16° 42′	(½)
m	17° 56′	18° 3′	$(220)_\beta$	...	...
w	18° 52′	...	...	18° 54′	(½)
s	20° 16′	20° 17′	(220)	...	..
w	21° 20′	...	...	21° 6′	(½)
mw	22° 48′	22° 32′	$(222)_\beta$	...	...
w	24° 28′	...	...	24° 38′	(½)
s	25° 13′	25° 8′	(222)	...	...
m	28° 58′	29° 22′	(400)	...	...
w	29° 54′	29° 38′	$(420)_\beta$	...	...
s	33° 17′	33° 14′	(420)	...	...
s	37°	36° 56′	(422)	...	...

TABLE X

$RbCl—B_2O_3$ (Sample C_1—1.44% RbCl)

Intensity	Observed	Calc. RbCl		B_2O_3	
	θ	θ	Plane	θ	I
ms	6° 57′	...	...	6° 45′	(5)
ms	7° 50′	...	...	7° 30′	(5)
m	11° 27′	11° 42′	(111)	...	...
s	12° 51′	...	...	13° 16′	(10)
s	13° 40′	13° 33′	(200)	14° 7′	(10)
m	15° 48′	...	...	15° 24	(1)
mw	17° 44′	17° 23′	$(220)_\beta$	...	...
ms	19° 27′	19° 21′	(220)	...	...
mw	20° 55′	20° 31′	$(311)_\beta$	20° 7′	(2)
vw	21° 50′	21° 29′	$(222)_\beta$	...	...
m	22° 57′	22° 52′	(311)	...	...
mw	24° 14′	23° 57′	(222)	...	...
w	28° 10′	27° 57′	(400)	...	...
w	31° 56′	31° 36′	(420)	...	...

TABLE XI

RbCl—B_2O_3 (Sample C_2—2.07% RbCl)

Int.	Observed θ	Calc. RbCl		B_2O_3	
		θ	Plane	θ	I
m	7° 9'			7°30'	(5)
w	8°31'				
s	9°25'				
w	10°11'				
w	11°45'	11°42'	(111)	11°52'	(1)
m	12°29'	12°12'	(200)β	12°25'	(1)
m	13°13'			13°16'	(10)
s	13°51'	13°33'	(200)		
w	14°24'			14° 7'	(10)
m	15° 9'			15°24'	(1)
w	16°31'			16°42'	(1/2)
mw	17°15'	17°23'	(220)β		
m	19°39'	19°21'	(220)		
w	20°39'	20°31'	(311)β	20° 7'	(2)
w	21°40'	21°29'	(222)β		
mw	23° 7'	23° 1'	(311)		
m	24°15'	23°57'	(222)		
mw	27°36'	27°57'	(400)		
m	31°57'	31°36'	(420)		
w	34°53'	35°1'	(422)		

TABLE XII

RbCl—B_2O_3 (Sample C_3—3.154% RbCl)

Int.	Observed θ	Calc. RbCl		B_2O_3	
		θ	Plane	θ	I
m	7°20'			7°30'	(5)
s	8° 4'				
mw	9°32'				
ms	11°22'	11°42'	(111)	11°52'	(1)
w	12° 7'	12°12'	(200)β		
s	12°40'			12°25'	(1)
m	13°24'	13°33'	(200)	13°16'	(10)
w	14°30'			14° 7'	(10)
s	15°47'			15°24'	(1)
mw	17°48'	17°23'	(220)β		
s	19°33'	19°21'	(220)		
s	20°23'			20° 7'	(2)
s	21° 7'			21° 6'	(1/2)
w	21°51'	21°29'	(222)β		
mw	22°40'	22°52'	(311)		
mw	24°14'	23°57'	(222)		
mw	25° 7'	25° 1'	(400)β	24°38'	(1/2)
w	28°16'	27°57'	(400)		
w	31°37'	31°39'	(420)		

TABLE XIII

RbCl – B_2O_3 (Sample C_4 – 6.95% RbCl)

Int.	Observed	Calc. RbCl		B_2O_3	
	θ	θ	Plane	θ	I
w	12°25′	12°12′	(200 β		
s	13°44′	13°33′	(200)		
w	15°42′			15°24′	(1)
w	17°34′	17°23′	(220)β		
s	19°21′	19°21′	(220)		
w	21° 7′	21°29′	(222)β		
w	22°48′	22°52′	(311)		
m	24° 7′	23°57′	(222)		
w	27°40′	27°57′	(400)		
m	31°58′	31°36′	(420)		
mw	35° 3′	35° 1′	(422)		

TABLE XIV

RbCl – B_2O_3 (Sample C_5 – 7.98% RbCl)

Int.	Observed	Calc. RbCl	
	θ	θ	Plane
w	11°22′	11°42′	(111)
w	12°18′	12°12′	(200)β
s	13°30′	13°33′	(200)
mw	17°15′	17°23′	(220 β
s	19°16′	19°21′	(220)
vw	21°8′	21°29′	(222)β
w	22°40′	22°52′	(311)
mw	23°41′	23°57′	(222)
w	27°32′	27°57′	(400)
mw	31°18′	31°36′	(420)
mw	34°42′	35° 1′	(422)

DISCUSSION

- It is clear from the tables that the lines due to the pure salts appear in every case in the dispersed glass system and certain foreign lines are present in many cases . It should be stated here that no lines other than the characteristic haloes were obtained with pure B_2O_3 & $Na_2B_4O_7$-glasses respectively prepared under exactly similar conditions.

The analysis was carried out in the following indirect way. Granting that the main lines were due to the dissolved alkali salts, the values of θ for different planes were calculated from the known radius of the camera and also checked in many cases with the negatives of the pure salts themselves and these values were compared with the experimental values. It was found that barring a number of lines, the values remarkably agreed with the experimental values, as will be seen from the tables given before. The discrepancy in the case of some of the extra lines was sought to be explained in a number of ways . The lines correspond to any of the well-known crystalline borates for with experimental data are available. It was found however that Cole, and Taylor (1934) and Cole, Taylor and Scholes (1935) had measured the diffraction lines of crystalline anhydrous B_2O_3 and crystalline anhydrous $Na_2B_4O_7$. Tables in their paper give the values of for these substances and the intensities according to their own scale the strongest corresponding to 10 and the weakest 1/2. It is thus seen that with NaCl, the main lines are due to the salt and the extra lines are due to anhydrous B_2O_3 and anhydrous $Na_2B_4O_7$. Further, the foreign lines persist at higher concentiations of the salts. This is also true of KCl more or less. With RbCl however at higher concentrations of the salt the foreign lines are remarkably absent.

The question now arises whether the systems studied represent true solutions or merely non-homogeneous suspensions of the salt in the glass medium. Ultramicroscopic observations with such systems and with gold and platinum dispersed in similar medium (Nature) failed to detect any diffraction cones. The sharpness of the lines however indicates that the size of the particles are bigger than the colloidal suspension for example of gold and platinum studied by Zsigmondy. The existence of the lattice in the glass systems further raises the question whether the ions of the alkali halides take up their respective positions within the non-repeating hollows of B_2O_3-glass (Warren) or they exist as definite clusters , more or less of the nature of a true collodial suspension. In the former case, the lattice dimensions are liable to be altered on account of the dielectric effect of the glass medium on the Coulomb and short distance forces (Majumdar and Palit) and this would lead us to expect an enlargement of the lattice. The results recorded in this paper shows however that there is no appreceable alteration of the lattice dimensions of the dissolved salts in the glass.

The question why there is a partial devitrification of the glass (B_2O_3) when fused with the salts requires explanation. It should be stated that in blank experiments with the B_2O_3-glass alone, no evidence of devitrification was obtained and further with strong concentrations of RbCl also, no such devitrification was noticeable. Similar results have been obtained with gold and platinum dispersed in B_2O_3 and $Na_2B_4O_7$-glasses. The ability of the dissolved substance to release the instability of the glass therefore is in some way connected with its structure and physical properties like dipole moment in the salts and atomic number in the case of the dispersed metals. This point is being further pursued.

Our best thanks are due to the authorities of the Indian Association for the Cultivation of Science, Bowbazar, Calcutta, for permission to use the apparatus and to Dr. K. Banerjee, D.Sc., for help and suggestions and to Mr. R. K. Sen, M.Sc., for help in course of the work. Our thanks are also due to the Council of the Board of Scientific and Industrial Research of the Government of India for award of a money grant.

REFERENCE

Born, 1938, *Verhandl deuts physikal Gesellsch*, **20**, 21
Majumder, S. K. 1942, *J. Ind. Chem. Soc.*, **19**, 241
" 1945, " **2**, 117
" 1940 **23**,
" 1946, *Ind. Jour. Phys.*, **20**, 918
Cole and Taylor, 1934, *J. Ame. Chem. Soc.*, **56**, 1648
Cole, Taylor and Shole, 1935, *J. Ame. Cer. Soc.*, **18**(2), 55, **18**(3) 79
Majumdar, S. K. 1942, *J. Ind. Chem. Soc.*, **19**(11) 461
1945, *Nature*, **156**, 423
" 1946, *Nature*, **158**, 754 (1946)
Warren, 1936, *J. Ame. Cer. Soc.*, **21**(8) 287
Warren, 1937, *J. Ame. Cer. Soc.*, **19**(7) 202
Warren and Loring, 1938, *J. Ame. Cer. Soc.*, **18**, 269
Zachariasen, 1932, *J. Ame. Chem. Soc.*, **54**, 3841

ON THE RAMAN SPECTRA OF SOLUTIONS OF ETHYLENE DIBROMIDE IN DIFFERENT SOLVENTS*

By B. M. BISHUI and S. B. SANYAL†

(Received for publication, Aug. 11, 1947)

(Plate VI)

ABSTRACT, The Raman spectra of moderately dilute solutions of ethylene dibromide in different solvents, *e. g.*, methyl alcohol, carbon tetrachloride, benzene, toluene and hexane have been studied and the relative intensities of the Raman lines 551 cm^{-1} and 660 cm^{-1} have been determined with help of blackening-log-intensity curves in each case as well as in the case of the pure liquid. The values of the ratio $I_{660}:I_{551}$ observed in the different cases are as follows. For pure liquid it is 100:17.5, for solution in methyl alcohol 100:24, in carbon tetrachloride, 100:17, in benzene, 100:23, in toluene 100:22 and in hexane it is 100:10. These results have been discussed in the light of the hypotheses put forward by Mizushima *et al* (1934) and by Sirkar and Bishui (1945). It is pointed out that it is difficult to explain all the observed facts with the help of the former hypothesis.

INTRODUCTION

The permanent electric moment (m) of ethylene dichloride and ethylene dibromide dissolved in different solvents was measured by Mizushima, Morino and Higasi (1934), the solvents used for the purpose being hexane, heptane, ether, benzene, toluene and amylene in the former case and hexane, benzene, carbon disulphide and carbon tetrachloride in the latter case. It was observed by them that the value of m for $C_2H_4Cl_2$ increases from the value 1.14×10^{-18} at $-70°C$ to about 1.38×10^{-18} at about $30°C$ in the case of solutions in hexane, heptane and amylene, while it remains almost constant at different temperatures in the solutions in benzene and toluene, the values in these two cases being 1.75×10^{-18} and 1.7×10^{-18} respectively. In order to explain this dependence of m on temperature they have assumed that the CH_2Cl group in the $C_2H_4Cl_2$ molecule is always executing rotatory oscillations about the trans configuration, the angular amplitude ϕ of this oscillation being determined by the Maxwell Boltzmann distribution law. The potential energy U has been assumed to be equal to $\beta\,(1-\cos\phi)$ and different values have been given to β in the case of different solvents in order to explain the observed variation of m with temperature. The higher value of m observed in the case of benzene is explained on the assumption that benzene acts as a polar solvent and the value of ϕ is very large for the majority of the molecules in solution in benzene as in the solutions in methyl alcohol or ether. They could not, however, explain satisfactorily why the value of *m* of the $C_2H_4Cl_2$ molecule dissolved in benzene is independent of temperature and is only slightly larger than that observed in the case of solution in hexane, although the value of the ratio $I_{653} : I_{752}$ in the latter case is only one third that in the former case. It was, therefore, thought worth while to determine the relative intensities of the corresponding Raman lines of $C_2H_4Br_2$ dissolved in different solvents, employing the more accurate method of photographic photometry in order to understand the significance of the changes observed with the change in the solvent.

---

* Communicated by Dr. S. C. Sirkar.

† Fellow of the Indian Physical Society.

EXPERIMENTAL

Kahlbaum's pure ethylene dibromide was used in the present investigation. It was distilled in vacuum before it was used for making the solutions. The solvents were also obtained either from Merck's or from Kahlbaum's original packing and each of them had to be distilled repeatedly in vacuum in order to get rid of continuous background in the Raman spectra. The molecular concentrations of $C_2H_4Br_2$ in the solutions in different solvents are: in benzene 0.35, in toluene 0.55, in hexane 0.43, in methyl alcohol 0.19 and in carbon tetrachloride 0.35. The Raman spectra of the pure liquid and of the solutions were photographed on Ilford Selochrome plates taken from the same packet and the plates were developed under identical conditions. A Fuess spectrograph with optical parts of glass was used. The intensity marks were taken on some of the plates, using different known slit-widths and a strip of white card board illuminated by light from a tungsten filament lamp as source of light. The purity of the solvents was tested by photographing their Raman spectra. Microphotometric records were then obtained for the lines 551 cm^{-1} and 660 cm^{-1} in all the spectrograms and also for the intensity marks, using a Moll's self-registering microphotometer. For the pure liquid spectrograms with different times of exposure were obtained in order that the density of the line 660 cm^{-1} in the spectrograms due to the mixtures might be almost the same as that in one of these different spectrograms for the pure liquid.

Blackening-log-intensity curves were then drawn for the wavelengths corresponding to the lines 551 cm^{-1} and 660 cm^{-1} excited by the Hg line 4358 A. U. and with the help of the blackening-log-intensity curves the relative intensities of these two lines were determined in each case. If I_1 and I'_1 be the intensities of the line 551 cm^{-1} in the spectrograms due to the pure liquid and one of the solutions respectively, and I_2 and I'_2 those for the line 660 cm^{-1}, we have

$$I_1/I'_1 = c_1,\ I_2/I'_2 = c_2$$

$$\therefore\ \frac{I_1}{I_2} = \frac{c_1}{c_2} \cdot \frac{I'_1}{I'_2}.$$

Thus it is easy to find out whether the ratio $\frac{I_1}{I_2}$ undergoes any change on dissolving the liquid in any solvent.

In determining the intensities of the lines, the total intensity at the peak of the line and that of the background were found out. On subtracting the latter from the former, the true intensity of the line was obtained. While obtaining the microphotometric records, the deflection due to the unexposed part of the plate was recorded, so that the intensity of the background referred to this unexposed part could be determined. The line of infinite density was also recorded on all the records. Some of these microphotometric records are reproduced in Plate VI. It can be seen from Figs. 1 and 2 that the ratio $I_{551}:I_{660}$ is less in the case of hexane than in the pure liquid. The actual values observed in the different cases are given in Table I.

TABLE I

Ethylene dibromide

State	$I_{660}:I_{551}$	$m \times 10^{-18}$
Pure liquid	100 : 17.5	......
Solution in CCl_4	100 : 17	0.86 (20°C)
Solution in CH_3OH	100 : 24	......
Solution in benzene	100 : 23	1.18 (20°C) 1.20 (50°C)
Solution in toluene	100 : 22	.....
Solution in hexane	100 : 10	0.91 (25°C) 0.79 (0°C)

The values of permanent electric moment *m* observed in the different cases by Mizushima *et al* (1934) are given in the last column of Table I. The corresponding results obtained in the case of ethylene dichloride by those authors are given in Table II for comparison.

TABLE II

Ethylene dichloride

State	$I_{752}:I_{653}$	$m \times 10^{-18}$
Pure liquid	100 : 71	1.12 × (gas at 30°C)
Solution in CH_3OH	100 : 83	......
Solution in ethyl alcohol	100 : 75	......
Solution in ether	100 : 50	1.49 (20°C)
Solution in hexane	100 : 20	1.36 (25°C)
Solution in benzene	100 : 67	1.75 (30°–50°C)

It can be seen from Table I that the ratio $I_{551}:I_{660}$ increases considerably when ethylene dibromide is dissolved in methyl alcohol, benzene or toluene, but it remains unchanged when carbon tetrachloride is used as the solvent. Again in solution in hexane the value of the intensity ratio diminishes to about half the original value. The values of *m* given in the last column can not be reconciled with those of this intensity ratio on the hypothesis put forward by Mizushima *et al* (1934) that the number of molecules in the trans configuration diminishes when the liquid is dissolved in solvents of high dielectric constant and the lines 660 cm^{-1} and 551 cm^{-1} are the corresponding lines due to the trans and oscillating configurations of the molecule respectively. The trans configuration has no permanent electric moment and the value of *m* in the case of solution in hexane is slightly higher than that for solution in carbon tetrachloride. Hence according to the hypothesis put forward by Mizushima *et al* (1934) the ratio $I_{551}:I_{660}$ ought to have been slightly higher in the case of solution in hexane than in the solution in carbon tetrachloride. On the contrary the ratio is observed to be 1:10 in the former case which is less than 1:7·10 observed in the latter case. Such a discrepancy also occurs in the case of ethylene dichloride as can be seen from results reported by Mizushima *et al* (1934) and quoted in Table II. In the case of solution in benzene the corresponding ratio $I_{653}:I_{752}$ is 1:1·5 and the value of *m* is $1{\cdot}75\times10^{-18}$, but in the case of solution in hexane the ratio is 1:5 while the value of *m* is $1{\cdot}36\times10^{-18}$. Since the permanent moment is wholly due to the molecules in the configuration other than the trans configuration the value of *m* in solution in hexane ought to have been much less than $1{\cdot}36\times10^{-18}$. It has been pointed out by them that this anomaly is not due to the presence of associated molecules of $C_2H_4Cl_2$ in the solution in benzene, because according to the cryoscopic measurements carried by Harada* the molecule has normal molecular weight in dilute solution in benzene. They have not, however, given any satisfactory explanation of this anomaly.

The hypothesis put forward by Mizushima *et al* (1934) mentioned above cannot explain also some changes in the Raman spectra which are observed when these two liquids are solidified at low temperatures. If the Raman lines which disappear with the solidification of the liquids would be due to the non-planar configurations of the molecule and those which persist in the solid state be due to the trans configuration, we would expect the lines which disappear to be polarised because the non-planar configurations, have no symmetry element and they do not postulate the existence of large number of molecules of this type in the liquid state. Actually, however, some of the lines which disappear in the solid state are totally depolarised in the liquid state. Again the line 3012 cm^{-1} which is totally depolarised in the liquid state is evidently due to some antisymmetric valence oscillation of the C-H groups. This line persists in the solid state, but such an oscillation is totally forbidden in the Raman effect in the case of the trans configuration. Hence this line cannot be due to any antisymmetric oscillation of the single $C_2H_4Cl_2$ molecule in the trans configuration. We have, therefore, to assume the existence of some other configuration of the molecule in the liquid and solid states to explain these observed facts.

---

* Unpublished

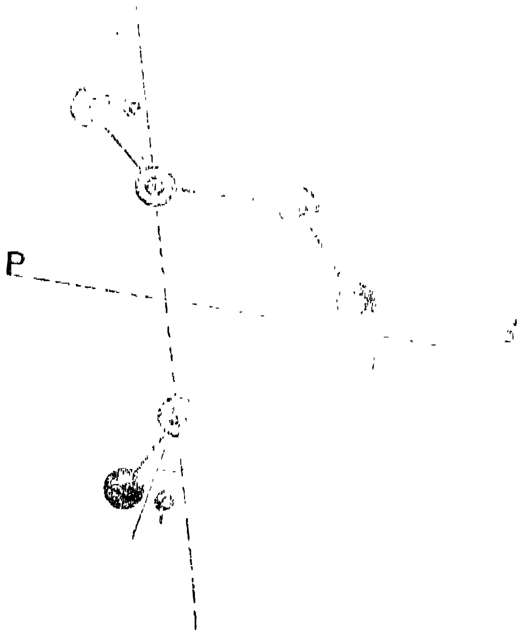

Fig. 8

It has already been pointed out by Sirkar and Bishui (1945) that the presence of associated molecules may be responsible for the changes in the Raman spectra which occur with the change of state of these substances. As regards the change in the relative intensities of the lines 551 cm^{-1} and 660 cm^{-1} of ethylene dibromide observed in the present investigation it can be seen that if the line 551 cm^{-1} is due to the associated molecules, the number of such molecules increases when the liquid is dissolved in benzene, toluene and methyl alcohol and it diminishes when hexane is used as the solvent. The permanent electric moment, however, remains almost unchanged when the liquid is dissolved in hexane and it increases in solutions in benzene, toluene and methyl alcohol. We have, therefore, to assume the shape of the associated molecule in solution in benzene to be non-planar as shown in Fig. 8 so that the value of m for the single molecule is much less than that for the cis configuration but the value of m for the associated molecule being the resultant of two such moments inclined at an angle slightly less than 90°, is greater than that for the single molecule. The increase in the value of m with temperature may be due to the increase in the angle ϕ made by the C-CH_2Cl plane with the plane of trans configuration. In the case of solution in cyclohexane the angle of inclination of the permanent moments of the two constituent $C_2H_4Cl_2$ molecules with each other at about 20°C is such that the value of the resultant moment is almost the same as that for the single molecule. Hence the value of m does not change appreciably even when the number of associated molecules diminishes. With the rise of temperature the angle diminishes slightly so that the value of the resultant increases a little. It may also so happen that the value of ϕ is larger in the solution in hexane than in the pure liquid.

Thus the observed facts can be explained by assuming the existence of associated molecules of static model postulated by Sirkar and Bishui (1945). In the solid state probably the structure of the molecule changes to a centro-symmetrical one as pointed out by them. On the other hand the structure postulated by Mizushima *et al* is of dynamic type oscillating about the trans configuration. There is other difficulties besides those mentioned above in postulating the existence of molecules of such a dynamic structure. The frequencies of such rotatory oscillations of the molecules about the trans configuration are expected to be much higher than that of the applied electric field used in the measurement of dielectric constant, as can be seen from the values of β given by Mizushima *et al* (1934). Hence only the mean square value of m is expected to be observed from the polarisation measured experimentally. They have assumed that the value of m is given by

$$m^2 = 4\mu^2 \sin^2\theta \cdot \frac{\int_{-\pi}^{+\pi} e^{-U/kT} \sin^2 \frac{\phi}{2}\, d\phi}{\int_{-\pi}^{+\pi} e^{-U/kT}\, d\phi} \qquad \dots (1)$$

where θ is the angle between the C-C line and the dipole moment of CH_2Cl or CH_2Br group, μ is the moment of the group and $U = \beta\ (1 - \cos\ \phi)$. It is evident that equation (1) gives the value of m^2 only when the static model is assumed and the value of ϕ is governed by the Maxwell-Boltzmann distribution law. The value of m^2 for the dynamic model oscillating with frequency higher than that of the applied field is not given by (1). Hence the values of m calculated by them with the help of (1) cannot be those for the dynamic model.

The relative intensities of the Raman lines 653 cm^{-1} and 752 cm^{-1} of ethylene dichloride dissolved in various solvents are being measured with the help of blackening log intensity curves and the discussion of the results obtained for that substance by Mizushima *et al* is reserved for a future communication.

ACKNOWLEDGMENT

The authors are indebted to Dr. S. C. Sirkar for kindly suggesting the problem and for his guidance and to Prof. M. N. Saha, F.R.S., for kindly providing facilities for carrying out the investigations in the Palit Laboratory of the Physics Department, Calcutta University.

Dept of Physics,
University College of Science,
Calcutta.

REFERENCES

Mizushima, S., Morino, Y. and Higasi, K. (1934). *Phys. Zeit.*, **35**, 905.
Sirkar, S. C. and Bishui, B. M. (1945), *Ind. J. Phys.*, **19**, 24.

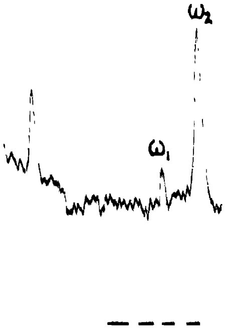

Fig. 1

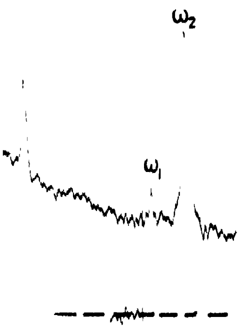

Fig. 2

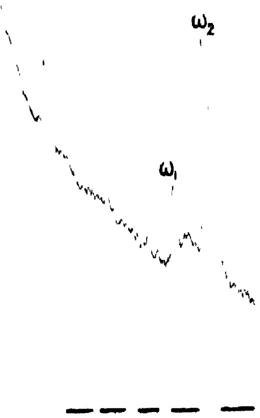

Fig. 3

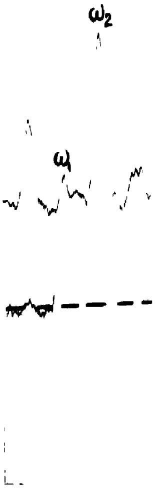

Fig. 4

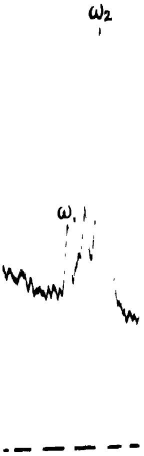

Fig. 5

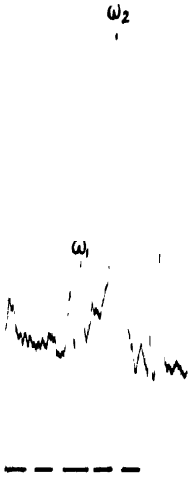

Fig. 6

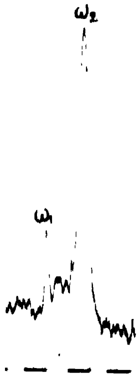

Fig. 7

MICROPHOTOMETRIC RECORDS OF RAMAN SPECTRA.

Fig. 1 Pure $C_2H_4Br_2$

Fig. 2 Solution in hexane

Fig. 3 " " CH_3OH

Fig. 4 " " CCl_4

Fig. 5 Solution in C_6H_6

Fig 6 " " toluene

Fig 7 Pure $C_2H_4Br_2$

$\omega_1 = 551 cm^{-1}$, $\omega_2 = 660 cm^{-1}$

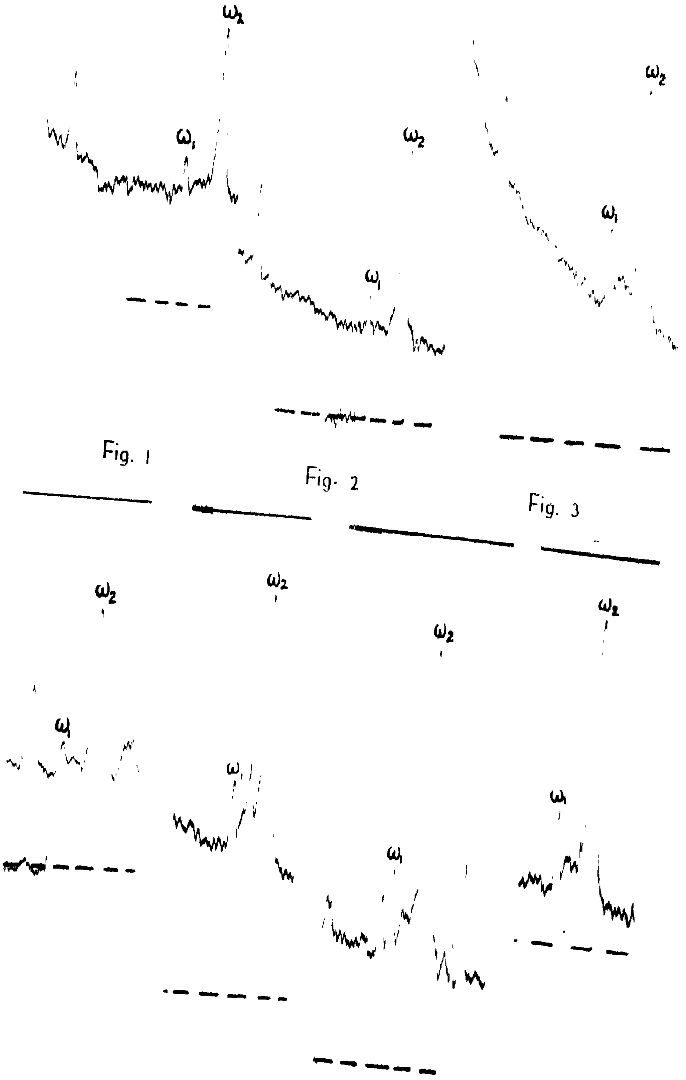

Fig. 1 Fig. 2 Fig. 3

Fig. 4 Fig. 5 Fig. 6 Fig. 7

MICROPHOTOMETRIC RECORDS OF RAMAN SPECTRA.

Fig. 1 Pure $C_2H_4Br_2$

Fig. 2 Solution in hexane

Fig. 3 " " CH_3OH

Fig. 4 " " CCl_4

Fig. 5 Solution in C_6H_6

Fig. 6 " " toluene

Fig. 7 Pure $C_2H_4Br_2$

$\omega_1 = 551\text{cm}^{-1}$, $\omega_2 = 660\text{cm}^{-1}$

MEASUREMENTS OF 'INHERENT' NOISE IN RADIO RECEIVERS

By M. K. DASGUPTA, J. RAY AND S. R. KHASTGIR*

(*Received for publication, June 30, 1947*)

ABSTRACT. In the present investigation, the 'inherent' noise in a radio receiver was measured in terms of *the equivalent noise voltage* at the input of the receiver. Measurements of equivalent noise voltages at the input of six different A.C.-D.C. commercial receivers (Philips 313H, Ambassador, G E. 6U5, Ferranti, G.E.C BC 3977 and G.E.C. (BC 4337) were made for a wide range of frequency channels from about 1 Mc/S to 20 Mc/S over a widely varying carrier voltages from about 0.02 μV to about 10^3 μV. The main results are briefly the following:

(*i*) The equivalent noise voltages were found to be of the order of one micro-volt for a carrier input voltage of one micro-volt.

(*ii*) For all the frequency channels, excepting the medium frequency, the equivalent noise voltage was found to increase *linearly* with the increase of input voltage up to a certain value of the latter It appears likely that this limit of the input voltage marked the beginning of the A.V.C. operation in a receiver.

Beyond this limit, the rate of increase of noise was found to be decidedly less. For higher input voltages there was perceptible increase of noise due to the A.V.C. action.

(*iii*) The equivalent noise voltage was found, in general, to be higher for the higher frequency channels.

(*iv*) A comparison of the six different receivers under test has been made in regard to their signal-to-noise ratio values.

(*v*) The effect of imperfect filtering of the line noise was shown by a comparison of the noise measurements when a receiver was worked from the D.C. mains and when it was worked from a dry H.T. battery of the same voltage.

(*vi*) Equivalent noise voltage measurements were made, for comparison, with a receiver operated by 220 volts, A.C. obtained by converting the D.C. mains voltage by a rotary converter.

All the measurements were made by adopting E.J.T. Moore's method with certain modifications. The method has been fully described and the experimental results discussed in a general way.

INTRODUCTION

In India, as in many parts of Asia and other countries like Australia, there are only a few high-powered transmitting stations and the various transmitting stations are all situated at great distances. Day-time reception is therefore, demanded over very long distances. For good reception under such condition, the receiver should not only have high sensitivity and fidelity, but also a high signal-to-noise ratio over a wide range of broadcast frequencies. The 'inherent' noises in receivers may sometimes be so amplified as to swamp out any received signal or at least to produce a disturbance too great for reasonable reception. As the sensitivity of receivers is governed primarily by the noises in the receivers, the rating of receivers with respect to the signal-to-noise ratio is an important factor in the design of receivers. Measurements of 'inherent' noise and a study of the signal-to-noise ratio in receivers are, therefore, of great value

---

* Fellow of the Indian Physical Society.

THE NATURE OF THE 'INHERENT' NOISES IN RECEIVERS

What are called the 'inherent' noises in a receiver consist mainly of three distinct types of noises due to (*a*) shot effect, (*b*) thermal effect and (*c*) ionization effect,

(*a*) *The Shot Effect.*—This was discovered and first studied by Schottky (1918). It relates to the irregular emission of electrons from the filament to the anode of any thermionic valve causing a corresponding fluctuation in anode current. The fluctuating anode current, when sufficiently amplified, produces noise at the output. The shot noise voltage in a valve can be represented by the formula

$$V_n^2 = 2ke\,\Gamma\Delta f\cdot\frac{i_a}{g^2}, \qquad \ldots \quad (1)$$

where e = electronic charge
i_a = anode-current under working condition
g = mutual conductance
Δf = band-width of the receiver
k = constant
F = factor depending on operating condition.

With a temperature-limited cathode $\Gamma = 1$, in a valve, such as a triode where the space-charge acts as a reservoir, the noise is considerably reduced and F has a value of about 0.05.

(*b*) *The Thermal Effect.*—The haphazard thermal agitation of the electrons, in a conductor or in an electronic medium like a thermionic valve, produces voltages of minute order between any two points in the conducting medium. These voltages when sufficiently amplified produce noise. This thermal noise was studied theoretically by Johnson (1926-28) and is often called Johnson noise. Works on the same line have also been done by Nyquist (1928), Llewellyn (1930), London (1936) and others. The Johnson noise voltage is given by

$$V_n^2 = 4kT\int_{f_1}^{f_2} R_s\,df,$$

where k = Boltzmann constant

$= 1{\cdot}374 \times 10^{-23}$

T = Kelvin temperature

R = Resistance component of input impedance

f_1 and f_2 are the frequency limits of the receiver.

When R is constant and does not vary with f

$$V_n^2 = 4\ k\text{TR}\ \Delta f \qquad \ldots \quad (2)$$

Here the resistance R refers to a conducting wire-circuit or to any conducting medium. In the case of a tuned circuit consisting of a capacity C in parallel with a coil having an inductance L and resistance r, the dynamic resistance given by $L/C.r$ should be substituted in the formula.

(*c*) *The Ionization Effect.*—In a thermionic valve there is always some residual gas. The electrons from the filament on their passage to the anode, produce ions by bombardment with the atoms of the residual gas. These ions may either strike the filament and produce an irregularity in the emission or they may strike the grid causing an irregularity in the electronic flow. These irregularities produce minute voltages which, when sufficiently amplified, cause noise at the output. Ionization noise is usually associated with soft thermionic valves.

All the three types of noise may be classified under '*fluctuation*' noise. As these noises are caused by a large number of irregular impulses, they evidently constitute a continuous spectrum in which there are all frequencies ranging from zero to infinity and the relative phases of the various components having no discernible relationships with one another and may be said to have *random* values. In the presence of a signal carrier, the components appear as side-bands of the signal. It is to be noted that the 'fluctuation' noise side bands on either side of the signal frequency are unrelated in phase, unlike the signal-modulation side-bands which are related in phase. The 'fluctuation' noise may, therefore, be termed 'random' noise.

It is evident that the fluctuation phenomena, which give rise to noises in receivers, are mainly those that occur in the first valve and in circuits preceding the first. Any slight fluctuations occurring in these circuits have the chance of being sufficiently amplified so as to produce an output voltage comparable with the signal output. In considering the 'inherent' noise in the receiver circuits, it is customary to express noise in terms of resistance, such that the energy expended on such resistance is equal to the noise-energy Considering first the input circuit to which the antenna is coupled, the 'noise-resistance' of the input circuit depends upon its resistance and temperature and also on the coupling. The next important source of 'inherent' noise after the input circuit is the R/F valve. To define this valve noise we are to substitute the valve by an imaginary 'noiseless' valve, in the grid circuit of which we place a resistor of such a value that the loudspeaker gives the same amount of noise-energy as the original valve. Thus in view of (1) and (2), the noise-resistance of a valve can be expressed by

$$R = \frac{e.F}{2T} \cdot \frac{i_a}{g^2} = k . \frac{i_a}{g^2} \tag{3}$$

where $k = \frac{e.F}{2T}$ = a multiplier characteristic of the type of the valve,

i_a = anode current,

and g = mutual conductance of the valve.

It is therefore, evident that when the valve is worked on a smaller slope, the noise is expected to increase. This happens when the A.V.C. is applied.

In short wave bands the noise-resistance of a R/F valve is usually much larger than the noise-resistance of the input circuit.

The anode circuit of the R/F valve also causes some noise. This equivalent to a fictitious noise-resistance in the grid-circuit of the valve giving the same noise-energy at the output end of the receiver. This imaginary resistance is equal to the noise-resistance of the anode circuit divided by the square of the amplification factor of the valve. It is to be noted that when A.V.C. is applied the amplification is thereby decreased, the equivalent noise-resistance of the anode circuit imagined in the grid of the valve is increased to a great extent.

After the R/F valve comes the noise-resistance of the R/F coupling which may be of the order of a thousand ohms. In any superheterodyne receiver, the 'mixer' valve is to be considered in a manner similar to that of the R/F valve. Here also with the application of the A.V.C., the noise-resistance of the 'mixer' valve is considerably increased. A block diagram is shown in Fig. 1 representing the various noise-resistances which have already been mentioned.

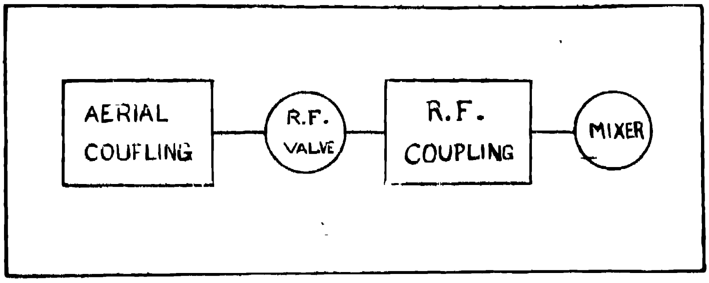

Fig. 1

METHODS OF MEASURING THE 'INHERENT' NOISE IN RELATION TO SIGNAL STRENGTH IN RECEIVERS

In the accepted standard method of rating a radio receiver, the signal-to-noise ratio is determined by measuring the output voltages. when a modulated carrier voltage and an unmodulated carrier voltage of the same value are applied one after another at the input end. The signal-to-noise measurement by this method is, however, open to certain objections. The method has, therefore, been replaced by a more equitable method developed by the Standard Committee of the Institute of Radio Engineers, U. S. A. (1938). This is known as "Equivalent Noise Side-band Input" or ENSI using its shortened form. The ENSI is the equivalent input magnitude of all random noise which is transferred to the output and therefore, of all such noise within the side-bands passed by the receiver. For the purpose of actual measurement the Equivalent Noise Side-band Input is taken equal to the input of a single side-band of 400 cycles modulation which produces the same audio output from the receiver. It has been put forward that the value of ENSI can be obtained from

$$E_n = m.E_s.\left(\frac{E'_s}{E'_n}\right) \qquad \ldots \quad (4)$$

where E_n = ENSI-voltage

E_s = signal carrier voltage

m = signal modulation depth

E'_n = output voltage of noise only

E'_s = output voltage of signal only.

Although the expression for the Equivalent Noise Side-band Input voltage has the advantage that its value in many receivers does not depend critically on the carrier input voltage, the sensitivity of the receiver or the volume control setting, the method does not allow for differences in audio response curves between different receivers. Again in this method, there is little or no indication of other design features, especially the effect of the A.V.C. on the R/F stage. To indicate the secondary causes of noise, such as the A.V.C. effect, E.J.T. Moore (1938) devised a method of measuring the 'inherent' noise voltage which is based upon the measurement of *equivalent noise voltage* at the input of the receiver.

The equivalent noise voltage at the input is defined as $V_n = mE$, where m is the noise modulation depth of an R/F carrier voltage E which is modulated by sinusoidal A/F (400 or 1000 cycles/sec.) voltage, the modulated signal voltage applied to the input producing the same A/F current in the loudspeaker voice coil as that produced by the same R/F voltage modulated by the 'inherent' noise of the receiver. Following the above definition, the equivalent noise voltages in some Australian or American radio receivers were measured by Moore on some medium and short wave channels for a range of carrier input voltage.

SCOPE OF THE PRESENT INVESTIGATION

In the present investigation equivalent noise voltage measurements were carried out with some commercial radio receivers adopting Moore's method with certain modifications. Measurements were undertaken for a wide range of frequency channels from about 1 Mc/S to 20 Mc/S over a widely varying input carrier voltages from about 0.02μV to about $10^3\mu$V.

The following six superhet sets were tested :—

TABLE I

Name and make	Years of use	Name and make	Years of use
(1) Philips 313H	8	(4) Ferranti	New
(2) 'Ambassador' (British make)	New	(5) G.E.C. (BC 3977)	5
(3) G.E. 6U5	8	(6) G.E.C. (BC 4337)	New

All the receiving sets were A.C./D.C. sets. Usually the D.C. voltage 220V from the mains was employed to work the receivers. With one new receiver—the Ambassador—measurements were carried out when the set was worked with a D.C. voltage of 220V from dry battery for comparison with the measurements when the line voltage was used to work the receiver. Measurements were also made for the same set when it was worked with 220 A.C. obtained by converting the line D.C. with the help of a smoothly running shielded rotary converter.

The measurements of the 'inherent' noise were made, usually at night or during the early part of the morning in order to avoid electrical interferences from electric fans and other electrical machines. Measurements were made only under good weather condition when there were no atmospherics.

THEORY OF THE METHOD EMPLOYED IN MEASURING EQUIVALENT NOISE VOLTAGE

In an ideal noise-free receiver there should not be any A/F voltage across the receiver output if the receiver is tuned to an unmodulated carrier potential from a standard signal generator. But as there is always some 'inherent' noise in a receiver, a small A/F voltage is developed at the output. A high gain A/F amplifier is used to amplify this voltage. The output terminals of the amplifier are then connected to any linear-scale voltmeter-unit giving a deflection directly proportional to the A/F voltage at the output of the amplifier. Let us suppose that θ is the deflection observed in the linear-scale meter when the R/F carrier voltage E modulated by the 'inherent' noise of the receiver is applied across the receiver input. Using a modulator unit the R/F carrier potential is then modulated at 1000 cycles/sec. obtained from an A/F oscillator. By varying the A/F voltage across the input terminals of the modulator unit the modulation A/F voltage at the output of the modulator or at the input of the receiver is then varied till the deflection in the linear-scale meter is 20. This A/F modulation voltage V_m at the receiver input should then be equal to the equivalent noise voltage of the receiver given by $V_n = mE$, where m is the depth of modulation which can be measured. Thus $V_n = V_m$.

Let us now find the relation between the modulation voltage V_m at the output of the modulator and the A/F voltage V applied across the input terminals of the modulator unit.

The voltage at the input of the modulator unit is given by

$$v = V_0 + E \sin pt + V \sin \omega t \qquad \ldots \quad (5)$$

where E is the R/F carrier voltage of frequency $p/2\pi$, V the applied A/F voltage of frequency $\omega/2\pi$ and V_0 the grid-bias voltage. If now the characteristic of the modulator valve is given by

$$i = \alpha + \beta v + \gamma v^2,$$

the R/F component of the anode current having a frequency $p/2\pi$ will be:

$$i = (\beta + 2\gamma.V_0)\left[1 + \frac{2\gamma}{\beta + 2\gamma.V_0} . V \sin \omega t\right] E \sin pt \qquad \ldots \quad (6)$$

The output circuit of the modulator unit is the secondary coil of a R/F transformer, the primary coil being in the anode circuit of the modulator valve. The anode circuit is tuned to the carrier frequency by a variable condenser placed in parallel with the primary coil. Thus the current in the secondary circuit which can only be an R/F current of frequency $p/2\pi$ will be obtained by multiplying the expression as given in (6) by the transformation ratio T of the R/F transformer. If now the impedance of the secondary coil be Z_B, then the voltage across the output terminals of the modulator unit will be

$$E_1 = k(\beta + 2\gamma V_0).E[1 + m \sin \omega t] \sin pt \qquad \ldots \quad (7)$$

where $k = TZ_B$ = a circuit constant and m = modulation depth

$$= \frac{2\gamma}{\beta + 2\gamma V_0} .V$$

It is evident that the degree of modulation m is independent of the carrier input voltage E and is directly proportional to the A/F voltage V applied at the input terminals of the modulator unit. The degree of modulation per volt denoted by $M(= m/V)$ is thus a constant quantity which can be determined experimentally.

When $\quad m = 0,$

we get $\quad E_1 = k(\beta + 2\gamma V_0).E \sin pt$

or $\quad |E_1| = k(\beta + 2\gamma V_0).E$

$$= A_m E \qquad \ldots \quad (8)$$

where $\quad A_m = k(\beta + 2\gamma V_0).$

Usually there is a loss of R/F signal in the modulator. Clearly A_m in (8) will represent the modulation loss factor which can be found by experiment. The modulation voltage V_m at the output of the modulator is thus obtained from

$$m \quad \frac{V_m}{A_m . E} \quad M.V.$$

This gives $$V_m = A_m .M.V.E. \tag{9}$$

Since $V_n = V_m$, the equivalent noise-voltage is obtained from the equation (9).

In the actual experimental set-up, a dummy aerial was inserted in the aerial input lead of the receiver under test. For a common basis of noise evaluation for all receivers, a band pass filter, with the frequency band between 500 and 1100 cycles per sec., was used after the receiver and just before the A/F amplifier. As the filter was not ideal, a correction factor was necessarily introduced. The output voltage of the attenuator also needed a correction due to inexact matching. The value of the A/F voltage V, obtained after necessary corrections, was used in the evaluation of the equivalent noise-voltage from (9).

DETAILS OF EXPERIMENTAL ARRANGEMENT

The experimental set-up for the measurement of equivalent noise-voltage is illustrated in the block diagram in Fig. 2. The essential parts of the assemblage are the following :

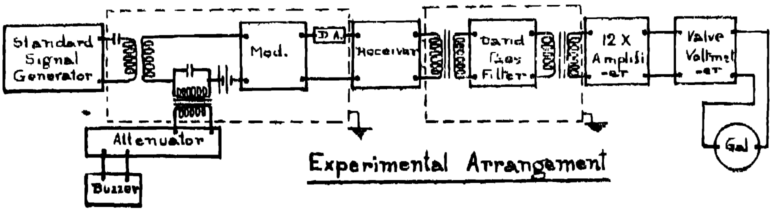

FIG. 2

(1) *Standard Signal Generator.*—A signal generator with output meter was worked with 220 volts A.C.

(2) *Audio Oscillator.*—An oscillator of the induction buzzer type giving 1000 cycles/sec. was employed.

(3) *Attenuator.*—A well-shielded variable A/F attenuator with a characteristic impedance of 600 ohms, enabled application of smaller A/F voltages.

(4) *Coupling link.*—The R/F voltage from the signal generator and the A/F voltage from the audio oscillator were induced into the coupled circuit through suitable R/F and A/F transformers respectively. The secondary coils of the R/F and the A/F transformers were in series and connected across the input terminals of the modulator unit. The primary of the R/F transformer was connected across the output of the signal generator. The

primary of the A/F transformer placed across the output of the attenuator was such that the output impedance of the attenuator was nearly equal to its characteristic impedance. The secondary coil of the A/F transformer was shunted by a suitable condenser. The coupling link was properly shielded.

(5) *Modulator Unit.*—The modulator valve was made to work about the bend near the cut-off voltage. The anode circuit comprised the primary coil of an R/F transformer tuned by a variable condenser placed in parallel. The output voltage was obtained across the secondary terminals.

(6) *Dummy aerial.*—A dummy aerial consisting of a capacity of $200\mu\mu f$, a self-inductance of $20\mu H$ and a resistance of 25 ohms, all enclosed in a shielded box, was used for all frequency channels excepting 20 Mc/S, in which case a 500-ohm resistance was inserted.

(7) *Receivers.*—The six receivers were all of superheterodyne A.C./D.C. type.

(8) *Band-pass filter.*—A band-pass filter with frequency band between 500-1100 cycles/sec. was placed between the receiver under test and the A.F. amplifier, the input and output connections having been made through matched A/F transformers.

(9) *Collin's* 12X *A/F amplifier.*

(10) *Linear-scale meter.*—A valve-voltmeter constructed with a 6H6 valve gave output anode current directly proportional to the input voltage.

(11) *A moving coil galvanometer.*—The output of the valve-voltmeter was connected across the galvanometer.

EXPERIMENTAL PROCEDURE

The experimental procedure was as follows :

(*i*) The receiver under test was tuned to the desired frequency of the standard signal generator. The modulation was used for adjustment and then switched off.

(*ii*) The 12X amplifier was adjusted for some convenient value to give a suitable galvanometer deflection θ. The A/F oscillator was not worked during the adjustment.

(*iii*) The audio oscillator was then switched on and the attenuator was adjusted for a suitable A/F voltage V at its output which was applied to the input of the modulator unit till the deflection was 2θ.

(*iv*) The modulation voltage V_m at the input of the receiver was then equal to the equivalent noise-voltage V_n .

The equivalent noise voltage was thus obtained from (9) in terms of the A/F voltage V at the output of the attenuator.

CORRECTION FACTORS FOR EXACT EVALUATION OF NOISE

(1) *Attenuator-Loss.*—As *exact* matching condition was not fulfilled, the attenuator output voltage in *db* needed a correction. The correction was effected by the actual measurements of the input and output voltages of the attenuator with the same input and output connections as were used during the noise measurements. The *corrected* attenuator output voltage (V_{att}) multiplied by the transformation ratio A_t of the A/F transformer in the coupling link gave the value of the A/F voltage V applied at the input of the modulator unit. Thus we can write $V = A_t \times V_{att}$. In the present arrangement $A_t = 0.92$.

(2) *Modulator-Loss.*—The loss of the R/F signal in the modulator was found in the usual manner with the standard signal generator and the receiver, the A/F voltage at the receiver output being measured by a suitable meter.

For different frequency channels, the R/F transformer in the coupling link and the R/F transformer at the output of the modulator had to be changed. The modulator-loss was found to depend on these replacements. In Table II are given the average values of the modulator-loss factor A_m obtained experimentally for the different frequency channels:

TABLE II

Frequency Channel in Mc/s	Modulator-loss factor
1.13	.024
4.0	.012
6.5	.010
8.5	.013
14.0	.029
20.0	.027

(3) *Band-Pass filter Correction.*—The attenuation characteristic of the band pass filter was obtained in the usual way.

From the attenuation characteristic curve, the *average* value of the filter loss within the pass band was found to be 6.02 *db*. In other words the *average* ratio of the output to input voltage of the filter within the pass band was .50.

It should be noted here that in the experimental procedure for the measurement of equivalent noise voltage, a suitable galvanometer deflection θ was observed, when unmodulated carrier voltage was applied to the input of the receiver under test. This deflection was due to the noise voltage with frequencies limited by the pass band of the filter. When 1000 cycles-modulation was employed and the attenuator adjusted until the valve-voltmeter galvanometer deflection was 2θ, half of this deflection was due to the equivalent noise voltage V_n, the other half due to the modulation voltage V_m at the input of the receiver corresponding to 1000 cycles sec. If the filter was an ideal one, *i.e.*, if the filter-loss was the same of all frequencies, it would have been possible to write $V_n = V_m$. But in the present case, the ratio of the output to input voltage of the filter for 1000 cycles/sec., as computed from the attenuation characteristic was found to be .60, whereas the corresponding *average* value was .50. Thus for the same galvanometer deflection, the modulation voltage V_m should be put equal to 5/6 times the noise voltage V_n. Thus we can write

$$V_n = 6/5 V_m = A_f . V_m ,$$

where A_f = band-pass-filter correction factor = 1.2.

Thus taking into account the correction factors, the expression for the equivalent noise voltage as given by (9) resolves itself to—

$$V_n = A_m . A_f . A_t . M . V_{att} . E_{\mu v} \qquad \dots \quad (10)$$

where A_m = modulation loss factor

A_f = band-pass filter correction factor

A_t = transformation ratio of the A/F transformer in the coupling link = 0.92.

V_{att} = A/F voltage at the output of the attenuator corrected for in exact termination.

$E_{\mu v}$ = carrier voltage in μV

and M = modulation depth per volt.

All calculations of equivalent noise voltage were made with the help of (10).

MEASUREMENT OF MODULATION DEPTH PER VOLT

Using the same audio oscillator worked with the variable A/F attenuator and applying a suitable known voltage to the input of the modulator unit which was worked under exactly the same condition as during the time of noise measurements, the waveform of the modulated voltage at the output of the modulator was suitably amplified and studied after proper synchronization on the fluorescent screen of an oscilloscope. With different frequencies of the carrier, the measured values of modulation depth per volt of the applied A/F voltage at the input of the modulator were found to be nearly the same. The average value of the modulation depth per volt was found to be

$$M = \frac{m}{V} = 2.06$$

EXPERIMENTAL RESULTS WITH RECEIVERS WORKED WITH D/C VOLTAGE FROM THE MAINS.

For the two receivers (Philips 313H and Ambassador) the measurements of equivalent noise-voltage were carried out for the following frequency channels'

	Frequency Mc/s	Wavelength Metres
(1)	1.13	265.5
(2)	4.0	75.0
(3)	6.5	46.1
(4)	8.5	35.3
(5)	14.0	21.4
(6)	20.0	15.0

For the other four receivers, *viz.*, G. E. (6U5), Ferranti, G. E. C. (BC 3977) and G. E. C. (BC 4337), measurements were made for three frequency channels only, *viz.*, 1.1 Mc/s, 4Mc/s and 20 Mc/s. The results are shown in curves plotting the logarithms of the equivalent noise-voltage against the logarithms of the carrier input voltages for any frequency channel. The signal to noise ratio curves are also drawn. For Philips 313H and Ambassador sets, the experimental results are shown in Figs. 3(*a*) & 3(*b*) and 4(*a*) & 4(*b*).

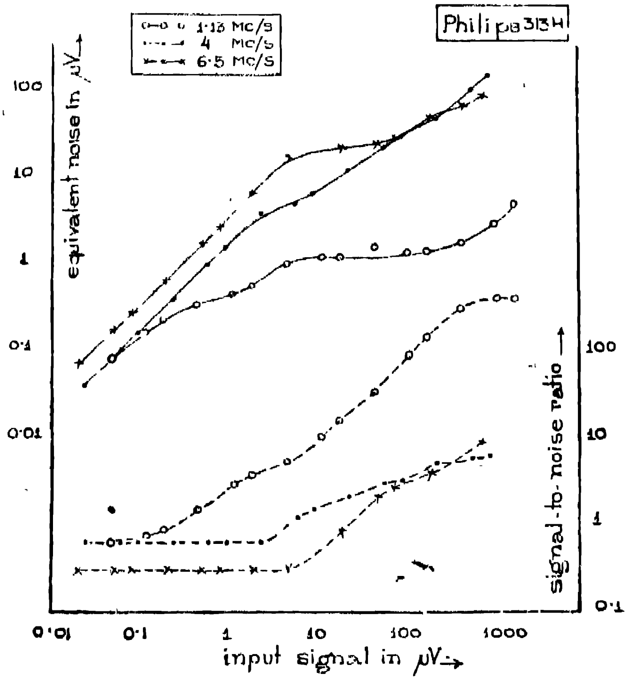

FIG. 3(a)

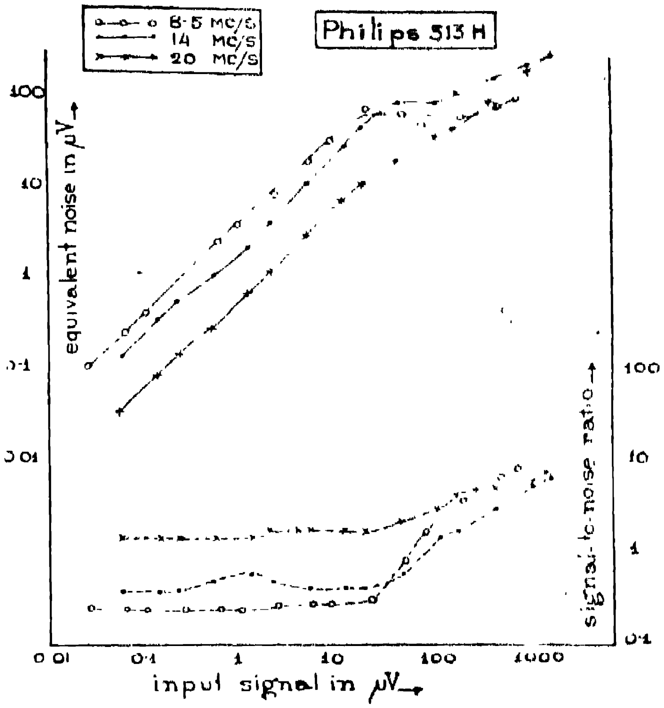

o—o—o 8·5 Mc/s
—•—•— 14 Mc/s
—×—×— 20 Mc/s
Philips 513 H
equivalent noise in μV→
100
10
1
0·1
0·01
signal-to-noise ratio→
100
10
1
0·1
0·01
0·1
1
10
100
1000
input signal in μV→

FIG. 3(b)

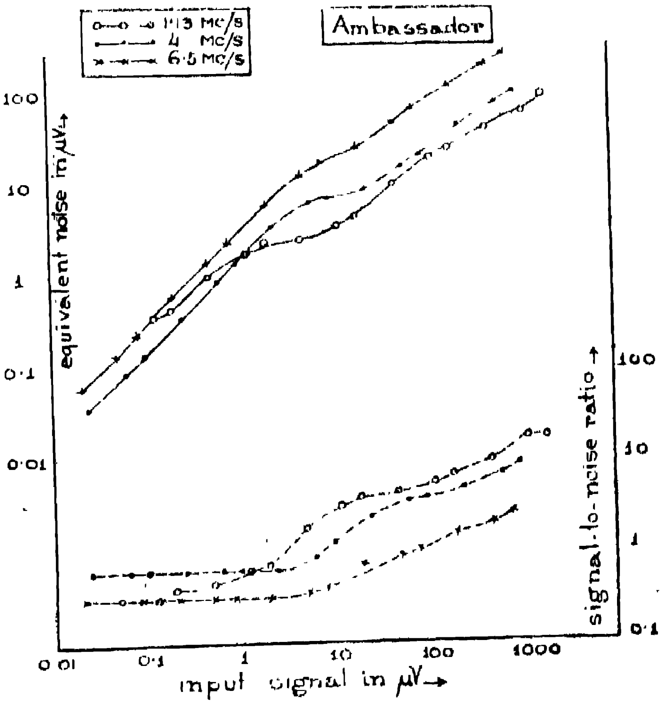

o—o—o 1·13 Mc/s
—•—•— 4 Mc/s
—×—×— 6·5 Mc/s
Ambassador
equivalent noise in μV→
100
10
1
0·1
0·01
signal-to-noise ratio →
100
10
1
0·1
0·01
0·1
1
10
100
1000
input signal in μV→

FIG. 4(a)

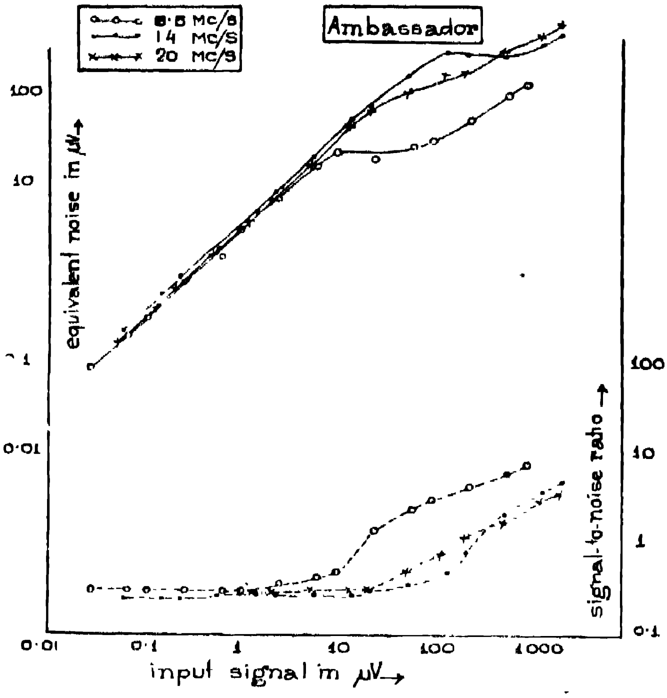

Fig. 4(b)

For the other four receivers the results are illustrated in Figs. 5-8.

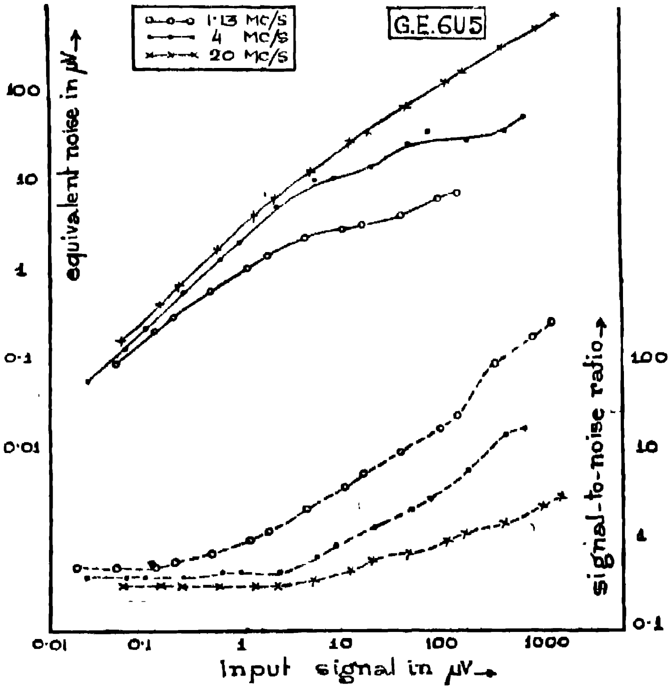

Fig. 5

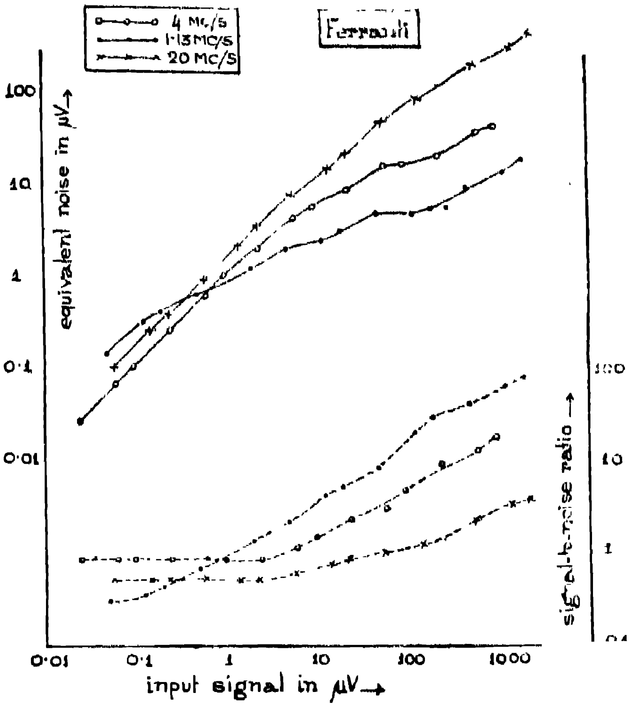
4 Mc/s
1·13 Mc/s
20 Mc/S
Ferranti
100
10
1
0·1
0·01
equivalent noise in μV→
100
10
1
0·1
signal-to-noise ratio →
0·01
0·1
1
10
100
1000
input signal in μV→

FIG. 6

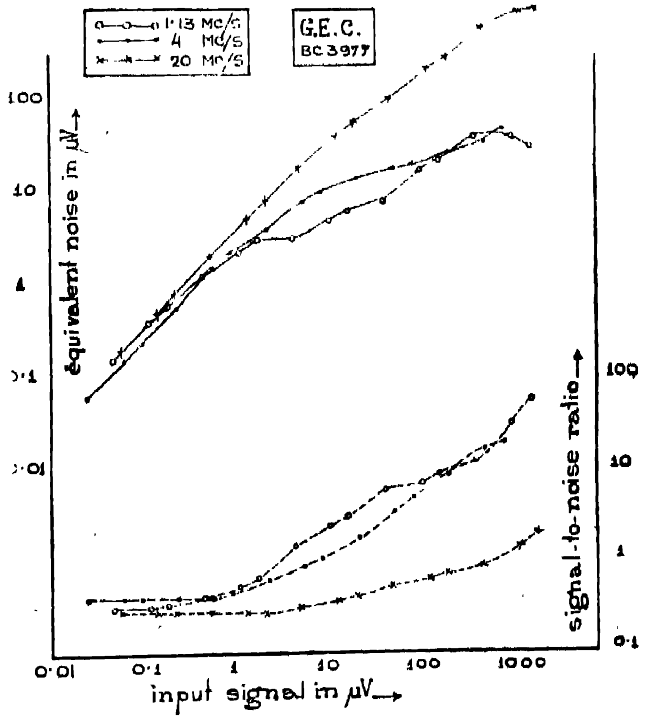
1·13 Mc/s
4 Mc/s
20 Mc/S
G.E.C.
BC 3977
100
10
1
0·1
0·01
equivalent noise in μV→
100
10
1
0·1
signal-to-noise ratio→
0·01
0·1
1
10
100
1000
input signal in μV→

FIG. 7

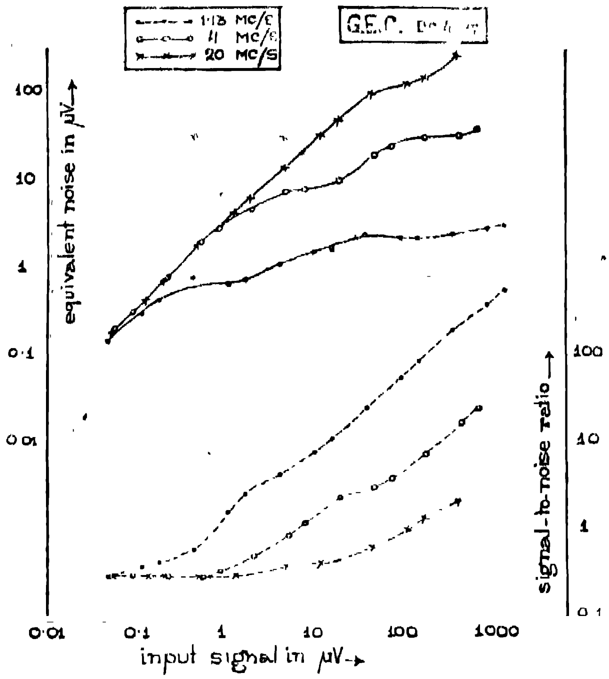

FIG. 8

COMPARISON OF EQUIVALENT NOISE VOLTAGES IN A RECEIVER (a) WHEN WORKED FROM D/C MAINS (b) WHEN WORKED WITH EQUAL VOLTAGE FROM DRY HT BATTERY AND (c) WHEN WORKED WITH A/C VOLTAGE OF THE SAME VALUE

The Ambassador receiver was worked with 220 Volts D/C obtained from dry H. T. The measurements of noise were then carried out on a frequency 4 Mc/s. Similar measurements were made on the same frequency channel when the receiver was worked from the D/C mains and also when the receiver was worked with 220 volts A/C obtained by converting the D/C mains voltage by a rotary converter. The results are shown in Fig. 9.

ANALYSIS OF EXPERIMENTAL RESULTS

I. The equivalent noise voltages were found to be of the order of one micro-volt for a carrier input voltage of one microvolt.

II. For all the frequency channels, *excepting the medium frequency* (1·13 Mc/s), the equivalent noise voltage was found to increase *linearly* with the increase of the input voltage up to a certain value of the latter, beyond which the rate of increase of noise was found to be decidedly less. The linear variation of the equivalent noise voltage for smaller input voltages is prominently displayed in the signal-to-noise curves. The *horizontal* straight lines in these curves correspond to the *inclined* straight lines in the equivalent noise-voltage curves. The change from the horizontality in the signal-to-noise curves is

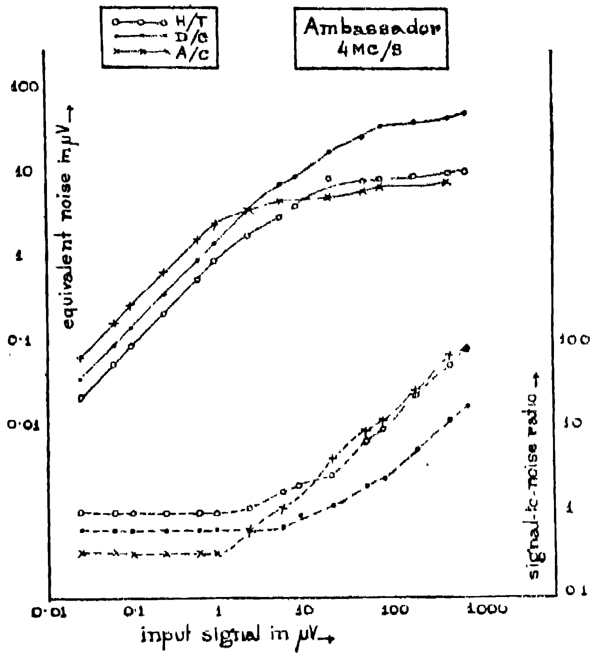

FIG. 9

found to occur at a particular value of the carrier input voltage. The values of the input voltage up to which the equivalent noise was found to increase linearly with the input voltage for all the receivers under test and for different frequencies are given in Table III.

TABLE III

Carrier input voltages up to which the 'inherent' noise was directly proportional to the input voltage.

Frequency channel	Philips 313H	Ambassador	G.E. 6U5	Ferranti	G.E.C. BC 3977	G.E.C. BC. 4337
4 Mc/s	2.4 μV	2.4 μV	2.4 μV	2.4 μV	.6 μV	.60 μV
6.5 ,,	5.0 ,,	2.0 ,, 5.0 ,,				
8.4 ,,	10.4 ,,	10.4 ,,				
14 ,,	23.2 ,,	14.5 ,,				
20 ,,	>21.6 ,, <54 ,,	>13.5 ,, <21.6 ,,	>2.16 ,, <5.4 ,,	>2.16 ,, <5.4 ,,	2.16 ,,	1.35 ,,

For each receiver the limiting voltage appeared, in general, to increase with the increase of frequency, the value lying within about 25 μv.

III. The equivalent noise voltage was found, in general, to be higher for the highest frequencies. In other words the signal-to-noise ratio was found, in general, to decrease with increasing frequencies. The only exception was 20 Mc/s in the case of Philips 313 H.

IV. The values of the signal-to-noise ratio for the three different orders of carrier input voltage are shown in Table IV for (a) medium radio frequency and (b) 20 Mc/s frequency for all the receivers under test.

TABLE IV

Receivers	Carrier input (μV)	Signal-to-noise ratio			
		1.13 Mc/s		20 Mc/s	
		ratio	db	ratio	db
1. Philips (313H)	1 10 100	2.4 9.3 22.9	7.6 19.4 27.2	1.66 1 74 3.92	4.4 4.8 9.6
2. Ambassador	1 10 100	.58 2.95 5.4	− 4.8 9.4 14.6	.31 .31 .63	−10.2 −10.2 − 4.0
3. G.E.C. (B.C. 3997)	1 10 100	.50 1.8 6.9	− 6.0 5.2 16.8	.30 .32 .63	−10.4 −10.0 − 5.0
4. G.E. (6U5)	1 10 100	.98 3.4 17.8	− .2 10.6 25.0	.525 .66 1.41	− 5.6 − 3.6 3.0
5. G.E.C. (B.C. 4337)	1 10 100	1.48 7.2 50.1	3.4 17.2 34.0	.30 .33 .85	−10.4 − 9.6 − 1.4
6. Ferranti	1 10 100	.93 3.6 19.35	− .6 11.2 26.0	.525 .66 1.41	− 5.6 − 3.6 3.0

V. The equivalent noise voltage in a receiver was found to be definitely less when worked with a dry H. T. battery of the same voltage than when worked from the D. C. mains. Imperfect filtering of the line noise was responsible for the greater noise when the receiver was worked from the mains voltage.

In the case of the A.C-operation, the equivalent noise was found to be smaller for the higher carrier voltages and larger for the smaller carrier voltages than when the receiver was D. C. - operated.

DISCUSSION OF EXPERIMENTAL RESULTS

While there is a general agreement of our experimental results with those of Moore (1938) for high input voltages, there is an important difference in the region of low input voltages. Starting from a very small input voltage up to a certain value of the latter, Moore's measurements with some Australian and American receivers showed a constancy in the value of the equivalent noise voltage, whereas with all the receivers under our test the equivalent noise voltage was found to increase linearly with the input voltage up to a certain value beyond which the rate of increase of noise was found to be decidedly less.

It appears likely that the limit of the input voltage up to which the equivalent noise was found to increase linearly with the input voltage marks the beginning of the A. V. C. operation in the receiver. When the A. V. C. begins to function, the noise voltage, however, gets limited in the same way as the signal voltage. This explains the slow increase of equivalent noise beyond the observed limiting input voltage.

It may be said in a general way that the value of the input voltage when the A . V . C . begins to function should increase with the increase of frequency. For a fixed receiver input, the amplified H.F. voltage impressed at the input of the detector is usually smaller for the higher frequencies, since the voltage-gain is smaller. Thus for a higher frequency, a higher receiver input voltage would be required to start the working of the A. V. C. This appears to be in general agreement with our observations.

It is difficult to explain the observed linear increase of the equivalent noise voltage with the carrier input voltage for the small values of the latter. It can only be conjectured that the valve-noise, which constitutes the major part of the inherent' noise in a receiver, increases with the amplitude of the oscillations. Any stray noise impressed at the grid of the modulator valve would, indeed, cause a noise voltage at the output which would increase proportionately with the carrier input. Particular care was, however, taken about shielding and even inspite of it if there was any stray effect it must have been extremely small in the region of small input voltage. When the input voltage was fairly high, it is likely that the extraneous noise produced some effect. It is significant to observe that the inclined straight line representing the observed increase of equivalent noise voltage with the input voltage clearly passes through the origin.

All the equivalent noise curves clearly show the expected increase of noise due to A. V. C. action at higher input voltages inspite of the smoothing down of the noise voltage due to A. V. C.

The observed increased of equivalent noise voltage in a receiver with the frequency of the carrier for a given voltage of the latter can be explained in a general way. The thermal noise in a circuit or valve as well as the shot noise in a valve depend on the resistance of the circuit and the valve. Since the resistance of either increases with frequency, the 'inherent' noise in a receiver would necessarily increase with the increase of the frequency channel.

ACKNOWLEDGMENT

In conclusion we record our grateful thanks to the Radio Engineers of the A. I. R., Dacca for their technical help and co operation.

PHYSICS DEPARTMENT,
DACCA UNIVERSITY.

REFERENCES

Committee of the Standards- Report on Radio Receivers, (1938), *Proc. I.R.E.*

Johnson (1926), *Phys. Rev.* **26**, No. 1, July

„ (1927), *Phys. Rev.* **29**, Feb.

„ (1928), *Phys. Rev.* **32**, July

„ (1927), *Nature*, **119**, Jan. 8

Johnson and Llewellyn (1934), *Elec. Eng.* **53**, 1449, (Nov.)

London (1936), *Proc. I.R.E.*, **24**, 1514, (Nov.)

Llewellyn (1930), *Proc. I.R.E.*, **18**, 243 (Feb.)

Moore, E.J.T. (1938), *Proc.* All-World Radio Convention (Australia)

Nyquist (1928), *Phys. Rev.* **32**, 110 (July).

Schottky (1925), *vide* paper by Fry in *Jour. Frank. Inst.* **199**, 203.

24

X-RAY STUDY OF VEGETABLE FIBRES

By BHUPATI KUMAR BANERJEE

(Received for publication, Sept. 4, 1947)

(Plates VIII A and VIII B)

ABSTRACT. Some vegetable fibres have been studied by means of X-rays and it is found that the orientation of cellulose crystallites is not same in all cases. In some fibres the major axis of the unit cell is almost parallel to the fibre axis and in some the major axis is at some spiral angle to the fibre axis while in an extreme case the cellulose crystallites are randomly distributed.

INTRODUCTION

Much progress has been made during the last few years regarding the knowledge of the structure of cellulose fibre from various sources of investigations—specially due to the correct interpretation of X-ray photograph, correlating the chemical information supplied by Haworth.

Cellulose is the main constituent of cotton, ramie, flax, jute, etc. and practically it builds up the frame-work of all vegetable tissues. It has been shown by various workers that the fundamental structures of cellulose derived from these various sources are identical. The elementary unit of cellulose is monoclinic with $a = 8{\cdot}35$A, $b = 10.3$A and $c = 7{\cdot}9$A and $\beta = 84^\circ$. The space group is C_2^2 with four glucose units in the unit cell. The cellulose fibre is a crystalline aggregate consisting of small crystallites separated by amorphous or intercrystalline areas. The crystal area is built up by repetition of the unit cell arrangement of glucose units in space.

X-ray investigation of jute fibre has been made by Banerjee and Roy, (1941) Sarkar, Rudra and Saha (1944) and Banerjee, Basak and Sen (1945). Some vegetable fibres were also studied by Bose and Ahmed (1946). In the present investigation a number of vegetable fibres—Pandanus., Annanus sativus, Sesbania aculeas, Hibiscus esculantus, Calotropis jigantea, coma on the seed of Calotropis jigantea, Hibiscus mutabilis, Musa sapientum, Crotalania juncea, Agave Americana, Coir A which had been isolated from green-cocoanut and coir B which had been isolated from dried cocoanut—have been studied by X-rays.

The fibres of Hibiscus esculantus and Crotalania juncea were, however, previously studied by Bose and Ahmed and the Coir B has been studied by Astbury. There are, however, considerable difference between the X-ray photographs of cellulose derived from different sources regarding the diffuseness and directions of extensions of the spots indicating differences in the internal order among the ultimate fibres and extents over which regularity of arrangement occurs.

A narrow pencil of X-rays from a Hadding-Seigbahn type of X-ray tube with Cu anti-cathode run at a voltage of 40.KV and a tube current of 5-7 milliamps was incident on a thin bundle of fibre (about 1 mm. diameter) normal to the length of the fibre. The diffracted X-rays were received on a cylindrical film of radius 3 cm. Exposures of about 8 hours were given. The photographs obtained are reproduced in the Plates VIII A and VIII B.

The angular co-ordinates θ and μ of the spots were obtained in the usual way and the glancing angle was obtained from the following relation $\cos\theta \cos\mu = \cos 2\theta_0$. The identification of spots were made by comparing the experimental glancing angle with the calculated Bragg angles of various planes the index K being known from the layer line in which the spots occur.

Crotalaria Juncea

Indices	Intensity	Character
(101)	S	Sharp and well resolved
(002)	S	Sharp and distinct
(004)	m	Slightly extended along the radial direction
(311 (212	S	Well resolved
(120 (021	S	Sharp and distinct
(221 (122	m	Slightly broad
(130)	m	Diffuse and broad
(032)	S	Sharp and extended along the radial direction
(232)	m	Diffuse

Calotropis jigantea

Indices	Intensity	Character
(101)	S	Sharp and long
$(10\bar{1})$	S	Sharp and long
$(002)_\beta$	m	Discrete line of uniform width
(002)	VS	Sharp and slightly bended in the form of an arc.
(004)	m	Elongated to a certain length.
(311 (013	S	Sharp and slightly bended.
(021)	S	Sharp and well resolved.
(221 (122	W	Diffuse.
(131)	m	Diffuse and broad.
(231 (032	S	Sharp and slightly bended along the arc of a circle
(331)	mw	Diffuse and elongated to a certain length along the radial direction.
(042 (241	m	Diffuse and elongated along the circumference of the diffuse ring

Sesbania aculeas

Indices	Intensity	Character
$(10\bar{1})$	S	Sharp and well resolved.
(002)	S	Distinct and bended along the arc of the circle on which the spots lie.
(004)	W	Very diffuse.
(013)	S	Bended to an arc.
(021)	S	Sharp and well resolved.
(130)	W	Broad and diffuse
(032 (231	S	Sharp and bended along the circumference of a circle on which the spots lie.

Hibiscus mutabilis

dices	Intensity	Character
(101)	S	Sharp and well resolved
(002)	S	Sharp and long
(004)	m	Very diffuse
(212) (311)	S	Drawn into a long arc
(021) (120)	S	Sharp and discrete
(130)	W	Diffuse and broad
(032)	S	Extended along the radial direction

Hibiscus esculantus

dices	Intensity	Character
(101)	S	Sharp and well-resolved
(002)	S	Sharp and bended to a long arc
(004)	W	Very diffuse
(212) (311)	S	Extended to a long arc
(120) (021)	S	Sharp and elongated along the radial direction
(130)	W	Diffuse and broad
(032)	S	Extended to a considerable length along the circumference of the circle on which the spots lie.

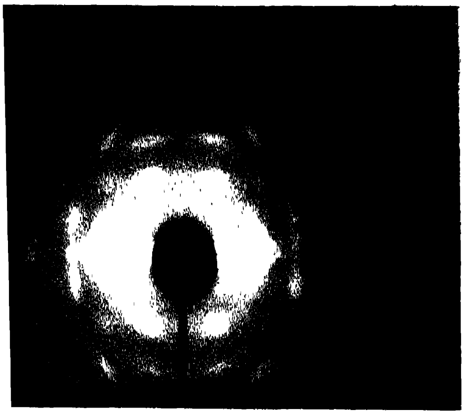

(1) Crotalaria juncea.

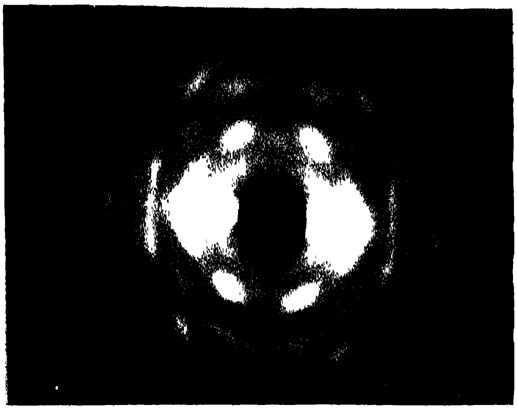

(2) Calotropis gigantea.

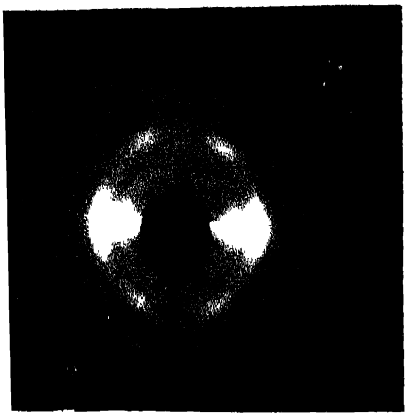

(3) Sesbania aculeas.

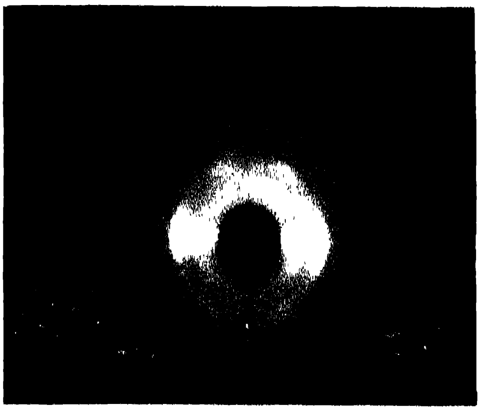

(4) Hibiscus mutabilis.

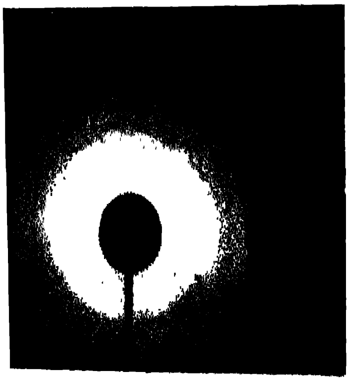

5) Hibiscus esculantus.

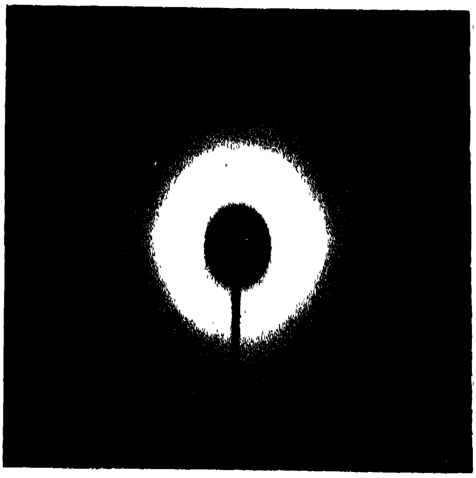

(6) Annanus sativus.

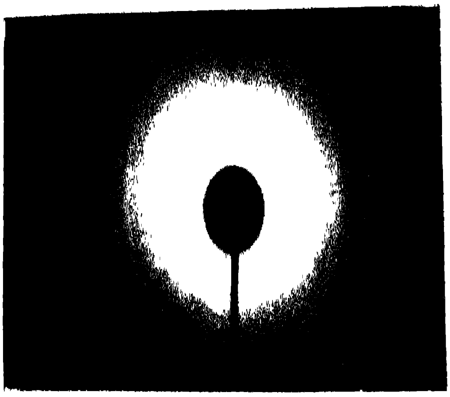

(7) Pandanus.

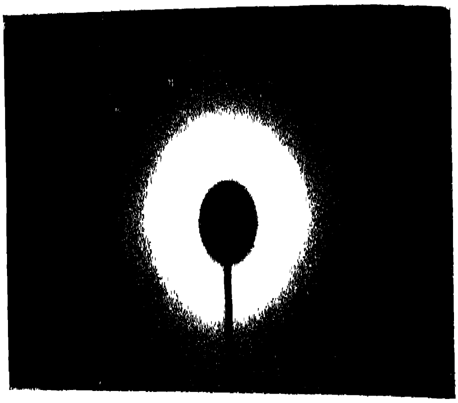

(8) Musa sapientum.

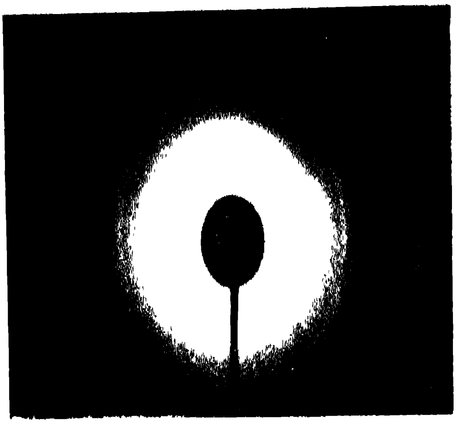

(9) Agave Americana.

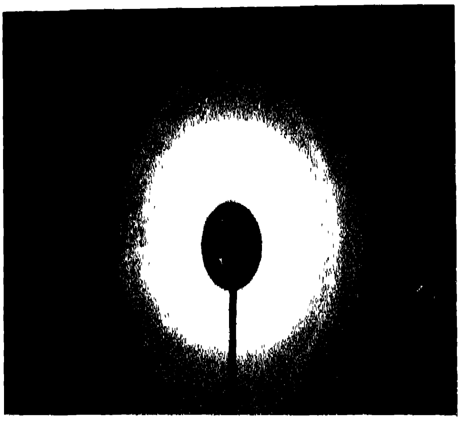

(10) Coir-A.

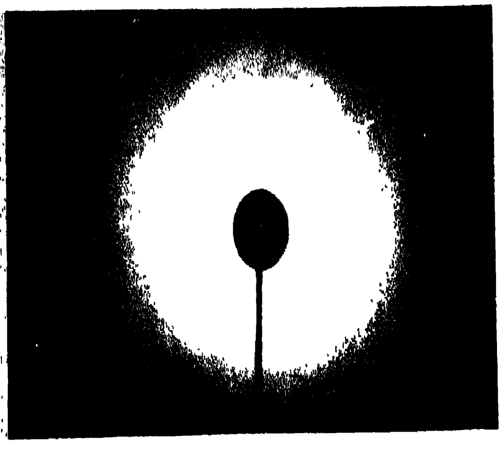

(11) Coir-B.

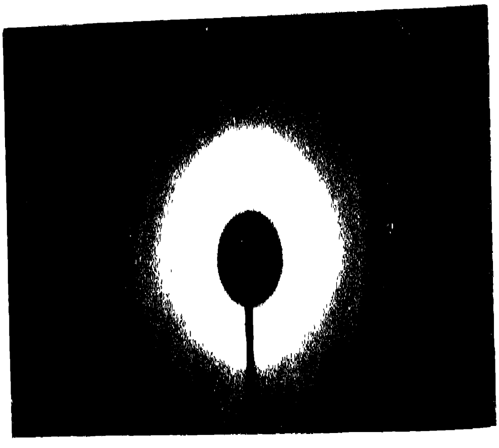

(12) Coma on the seed of Calotropis jigantia.

Annanus Sativus

Indices	Intensity	Character
(101)	S	Sharp and well resolved
(002)	S	Sharp and bended along the radial direction
(212) (312)	m	Drawn into a longer arc
(021)	m	Not well resolved
(032) (231)	m	Drawn into a ring

Pandanus

Indices	Intensity	Character
(101)	S	Sharp and long
(002)	Vs	Sharp and bended to form a part of a ring
(103)	m	Marked intense portion of the continuous ring is taken as the position of the spot.
(004)	W	Diffuse

Musa sapientum

Indices	Intensity	Character
(101)	ms	Not well resolved
(002)	S	Sharp and extended to a considerable length along the radial direction.
(103)	m	Intense portion of the ring is taken as the position of the spot.

Agave Americana

Indices	Intensity	Character
(101)	S	Extended to a sharp arc
(002)	VS	Elongated into a sharp arc which is a part of a relatively less intense continuous circle.
(103)	m	Drawn into a complete ring of uniform intensity
(004)	W	Drawn into a continuous diffuse band

Coma on the seed of Calotropis jigantea

Indices	Intensity	Character
(101) (101)	m	Not distinct
(002)	S	Drawn into a complete ring of almost uniform intensity.
(103)	ms	Drawn into ring of uniform intensity
(004)	W	Diffuse band

DISCUSSION

It has been mentioned before that the cellulose is the chief constituent of all fibres. But the X-ray pictures of all fibres studied in this paper reveal that the degree of orientations of cellulose crystallites are not the same. The major axis of the unit cell of cellulose may be oriented either parallel to the fibre axis or at some spiral angle to the fibre axis or the crystallites may be randomly distributed. The example of each case mentioned above can be had in the X-ray photographs of various fibres in this paper.

The X-ray diffraction pattern of Crotalania juncea is similar to that of ramie or jute. It is just like the single rotation photograph. The spots are discrete and the resolution is perfect. The pattern of the picture as well as the shape and size of the spots indicate that the crystallinity extends over domains nearly of the same dimensions as those in ramie for which Mark and Meyer estimated an average dimension of about 50A thick but at least 600A long. The orientation of the '*b*' axis of crystallites also are approximately parallel to the fibre axis.

The X-ray diffraction pattern of Calotropis jigantea is very similar to that of above except that in this case there is a slight back-ground scattering and the spots are rather broader and a little elongated. So the domains of crystallinity are slightly smaller than and the orientations of crystallites are rather inferior to those of Crotalaria juncea.

The diffraction pattern of Sesbania aculeas and Hibiscus mutabilis have strong similarity to one another. The pattern and the positions of the spots are same as above but the shape and size of the spots are quite distinct from those of Crotalaria juncea or Calotropis jigantea The spots retain their sharpness along the radial directions but extend along the directions of Debye-Scherrer rings so as to form arcs. This indicates that the orientation of crystallites of cellulose parallel to the fibre axis is partially deranged.

The pattern and the positions of the spots of Hibiscus esculantus are quite similar to those of Hibiscus mutabilis except that in this case the spots are drawn into still longer arcs. This indicates that the alignment of the crystallites of cellulose is considerably deranged from parallelism.

The X-ray diffraction pattern of Annanus sativus is interesting. In this case the spots are completely drawn into arcs forming continuous Debye-Scherrer rings and the positions of the spots in the rings are indicated by the intense sharp portions in the rings. The spots on the equatorial line are quite sharp. All this indicates that there is a very wide disorientation of the crystallites of cellulose from parallelism to the fibre axis. The maxima of intensity on the rings, however, indicates that the tendency towards orientation still prevails.

There are some rings in the X-ray photographs of Pandanus and Musa sapientum and the spots on the equatorial layer line lie on the rings. Spots on the other layer lines are absent. This also indicates the disordered arrangement of the fibre molecule.

The diffraction pattern of Agave Americana produces some rings followed by diffuse bands. The first two rings are so marked with greater intensity on the equator that they give rise to two strong arcs which bend along the circumference of the respective ring. This picture is quite distinct from that of Calotropis jigantea or Hibiscus mutabilis where we get discrete spots in the diffraction pattern. This indicates that the cellulose crystallites are irregularly distributed in the fibre.

Coir A and Coir B give the same type of X-ray photograph. There are two strong arcs followed by diffuse rings but the ends of each arc are more intense than the middle portion of it. The distribution of intensity of the first arc of Coir A changes so abruptly at the ends that it gives rise to two spots It is known that in Coir B the crystallites of cellulose are at some spiral angle to the fibre axis. As the diffraction patterns of Coir-A and Coir-B are almost identical, so it can be legitimately concluded that in Coir A cellulose crystallites are at some spiral angle to the fibre axis.

In the X-ray pattern of Coma on the seed of Calotropis jigantea there are some rings with diffuse bands. This photograph is similar to the usual powder photograph. It indicates that the cellulose crystallites are randomly distributed in this fibre. This picture is quite different from other fibres studied and is very similar to the young cotton fibre below 35-days where the evidence of cellulose orientation was absent.

The fibres studied in this paper have not been delignified and so there is a slight back ground scattering in every photograph.

Works are in progress to determine the size of cellulose miscelles as well as the nature and the degree of disorientation of cellulose crystallites to the fibre axis.

ACKNOWLEDGMENTS

In conclusion the author desires to offer his best thanks to Prof. K. Banerjee for his keen interest in the work and to Mr. R. K. Sen for the kind help in course of the work.

INDIAN ASSOCIATION FOR THE
CULTIVATION OF SCIENCE
210, BOWBAZAR STREET,
CALCUTTA

REFERENCES

Banerjee and Roy (1941) *Proc. Nat. Inst. Sci.* (India) **7**, 375.
Banerjee, Basak and Sen (1945) *Ind. Jour. Phys.* **19**, 217.
Bose and Ahmed (1946) *Ind. Jour. Phys.* **20**, 105.
Sarkar, Rudra and Saha (1944), *Proc. Nat. Inst. Sci.* (India) **10**, 325.

THE BAND SPECTRUM OF CADMIUM CHLORIDE

By C. RAMASASTRY

(Received for publication, Sept. 5, 1947)

(Plate IX)

ABSTRACT. The spectrum of CdCl as excited by a H. F oscillator is investigated from the red down to λ1850. The Cornell system between λλ2240−2181 has been extended, altogether 19 bands being recorded. These are arranged into four v' progressions which enabled the determination of the vibrational constants chiefly of the upper state. The constants are

$$\nu_e = 45398.2 \qquad \begin{matrix} \omega' = 204.0 & x'\omega' = 7.5 \\ \omega'' = 330.0 & x''\omega'' = 1.0 \end{matrix}$$

The peculiar appearance of the bands is interpreted as due to the predissociation in the upper state at some high rotational level of $v' = 2$.

There is no evidence, in emission, of the bands recorded by Walter and Barratt in absorption in the region λλ3181−3018. A new emission system is observed in the visible region consisting of 23 red-degraded bands from 4800A−4000A, some of these bands indicated a rotational structure even under small dispersion.

INTRODUCTION

Wieland (1929) was the first to investigate the band spectrum of cadmium chloride in the course of his extensive study of the halides of zinc, cadmium and mercury, as excited by a high frequency oscillator. While the halides of mercury were found to give several systems, Wieland reported a comparatively fewer systems for the halides of zinc and cadmium. For cadmium chloride he had only mentioned the existence of two groups of bands, (1) between λ6400−λ3300 which are diffuse and red degraded; (2) an overlapping group between λ3400−3300 which are sharp and violet degraded. Walter and Barratt (1929) photographed the absorption spectra associated with Zn, Cd and Hg, in the near ultra-violet and reported three groups of bands which might possibly be ascribed to Cd + Cl, (1) λ3181 to λ3135 (2) λ3104 to λ3077 (3) λ3074 to 3018; altogether twenty seven band heads were measured. The data were in agreement with the earlier observation by Mohler and Moore (1927). Oeser (1935) made a more systematic work, specially on the absorption and fluorescence spectra of the halides of zinc and cadmium, and confirmed the assignment of bands in the region 3181A to 3018A to the cadmium chloride molecule. He also gave measurements of twelve absorption bands in the far ultra-violet between λ2163−λ1774. The wavenumber interval between these bands was shown to increase successively from 850 cms.$^{-1}$ to about 1000 cms.$^{-1}$ Cornell (1938) got the ultra-violet band spectra of the chlorides of zinc, cadmium and mercury, excited by a high frequency power oscillator. In CdCl, he reported a brief system consisting of seven red degraded bands between λ2240 − λ2185 and arranged them into two progressions with $v' = 0$ and $v' = 1$. The constants for the lower state were estimated as $\omega''_e = 330.5$ cm.$^{-1}$ and $x''_e \omega''_e = 1.2$ cm.$^{-1}$, but those for the upper state could not be calculated as no bands were observed involving $v' > 1$. Isotopic components were measured for the (0, 1) and (1, 2) bands and shown to occur in the expected positions. In an attempt to systematise the band systems of zinc, cadmium and mercury halides, Howell (1943) arranged the Walter and Barratt's three groups of bands of cadmium chloride (λλ3181 − 3080) into a doublet system represented by the transition $^2\Pi \longrightarrow {}^2\Sigma$ with a $^2\Pi$ interval of 1115 cm^{-1} which is in agreement with the predicted value of 1140 cm.$^{-1}$ The constants for the lower $^2\Sigma$ state of this system are in fair agreement with those of the lower state of the Cornell system.

Summarising our present knowledge of the band spectrum of the CdCl molecule, the following systems may be stated to have been definitely established :

	Region	Transition	Occurrence
1. Cornell System	λλ2240 − 2181	$^2\Sigma \longrightarrow {}^2\Sigma$	in emission only
2. Howell System	λλ3181 − 3018	$^2\Pi \longrightarrow {}^2\Sigma$	in absorption only

In the course of a series of investigations on the spectra of the halides of Group II-*b* elements, Zn, Cd, and Hg, the emission spectrum of cadmium chloride was studied by the author from the visible region down to λ1850, as a result of which the Cornell system, mentioned above, could be much extended. Also the visible bands, the existence of which was just reported by Wieland, could be photographed and measured. The purpose of the present paper is to record these observations.

EXPERIMENTAL

The spectrum of cadmium chloride is excited in a Pyrex tube with external electrodes by means of a H. F. oscillator described by the author (Ramasastry, 1947). Strong heating with an etna burner was found necessary between and beyond the electrodes. No trace of N_2 or NO bands is observed when fresh crystalline salt is heated in the tube though the OH bands are invariably present (Plate X-*a*). But, if fused salt is reheated N_2 and NO bands do predominate (Plate X-*b*).

The dispersing instruments employed are the Hilger constant deviation, small and medium-quartz spectrographs. Ilford Selo-Chrome plates, sensitised with mobil oil (Ramasastry and Rao, 1947), are used to record the spectrum in the ultraviolet,

TABLE I

avelength	Int.	Wavenumber (Author)	Wavenumber (Cornell)	Classification	Obs.-Cal.
2191.85	4	45609.3	45609.9	1,0	−2.8
2196.15	2	45519.0	...	2,1	+1.8
2201.80	1	45403.2	...	3,2	−0.0
2205.05	10	45366.8	45363.4	0,0	+3.7
2207.40	8	45287.4	45282.9	1,1	+4.2
2212.07	2	45190.5	...	2,2	+0.3
2217.50	1	45081.8	...	3,3	−2.5
2219.90	6	45033.7	45033.9	0,1	−0.5
2223.55	5	44959.4	44956.3	1,2	+3.2
2228.05	2	44868.3	..	2,3	+3.0
2233.36	1	44761.3	..	3,4	−0.1
2236.07	4	44706.8	44708.0	0,2	−0.4
2239.90	5	44630.2	44632.8	1,3	−1.1
2243.90	1	44541.6	...	2,4	−0.8
2249.20	0	44446.8	...	3,5	+6.2
2252.45	1	44282.5	...	0,3	+0.2
2256.30	2	44306.1	...	1,4	−3.1
2260.86	0	44217.2	...	2,5	−4.3
2272.75	0	43985.0	...	1,5	−2.5

TABLE II

...	0	1	2	3	4	5
0	10	6	4	1		
1	4	8	5	5	2	0
2		2	2	2	1	0
3			1	1	1	1

TABLE III*

(v′, v″)	ν	Obs. shift	Calc. shift
(0, 1)	45033.7	7.5	7.6
(1, 2)	44959.4	0.1	9.4
(0, 2)	44706.8	15.0	14.3
(1, 3)	44630.2	15.0	17.1

RESULTS

Cornell System.—As many as 19 bands are measured in this system, reproduced in Plate X(*a*) obtained with Hilger small quartz instrument of dispersion 14Å/mm at λ2200 The wavelength, intensity, wavenumber data and classification of the bands are given in Table I together with Cornell's values. The spectrum taken with the larger Hilger instrument (Plate X-*b*), clearly showed the isotopic components of (0, 2), (1; 3) bands, in addition to those of (0, 1) and (1, 2) measured by Cornell.

---

* The large difference in the (1, 3) band may be due to overlapping by NO bands.

Table II gives the vibrational analysis of the bands (each band is represented by its intensity) which is an extension of the Cornell's scheme.

The new data enabled the determination of the vibrational constants of the upper state as well, which could not be obtained by Cornell. The constants are:

$$\nu_e = 45398.2 \qquad \begin{matrix} \omega_e' = 264.0 & \qquad x_e'\omega_e' = 7.5 \\ \omega_e'' = 330.9 & \qquad x_e''\omega_e'' = 1.0 \end{matrix}$$

Table III gives the observed and calculated isotope shifts for the different bands. The agreement confirms the vibrational assignments.

Failure to observe progressions of these bands with $v' > 1$ led Cornell to suggest the occurrence of predissociation in the upper state for vibrational level of higher quantum numbers In order to examine this feature clearly, the author has taken a number of exposures. Although there are bands involving higher quantum numbers, still the system exhibits a peculiar appearance. The heads, forming the progressions $v' = 0$ and $v' = 1$, are clearly red-degraded but the extent of shading off, *i.e.*, the extent of rotational structure, diminishes very rapidly so that the bands with $v' = 2$ are narrow and those with $v' = 3$ are line-like and very faint. This might, in all probability, be accounted for by the occurrence of predissociation strongly in the upper state starting at 3 stage corresponding to some high rotational level associated with $v' = 2$.

Howell System.—This system is not observed in emission by the author; Cornell made no mention of it. It was observed only in absorption. Howell analysed it as due to $^2\Pi - {}^2\Sigma$ electronic transition, on the analogy of the other halides of Hg, and Cd. The sharp and violet-degraded emission bands, briefly referred to by Wieland, could not be detected, even when special precaution was taken to avoid the OH bands in this region by keeping phosphorous pentoxide in a side bulb of the evacuated discharge tube for two days.

Visible Bands.—Examination of the spectrum in the visible region revealed another system between λ4770 – λ4050 which does not appear to have been recorded by any of the previous investigators except Wieland, who made but a mere mention of it. About 23 bands are listed in all, of which only 14 could be measured from the constant deviation spectrograph, the rest being from pictures taken with small quartz instrument. Even under the small dispersion of the constant deviation the rotational structure of the more refrangible bands could be observed. Some are double headed probably due to the chlorine isotopes. Approximate measurements of the band heads are given in Table IV. The interval between alternate bands is only about

C_D C_L emission bands.

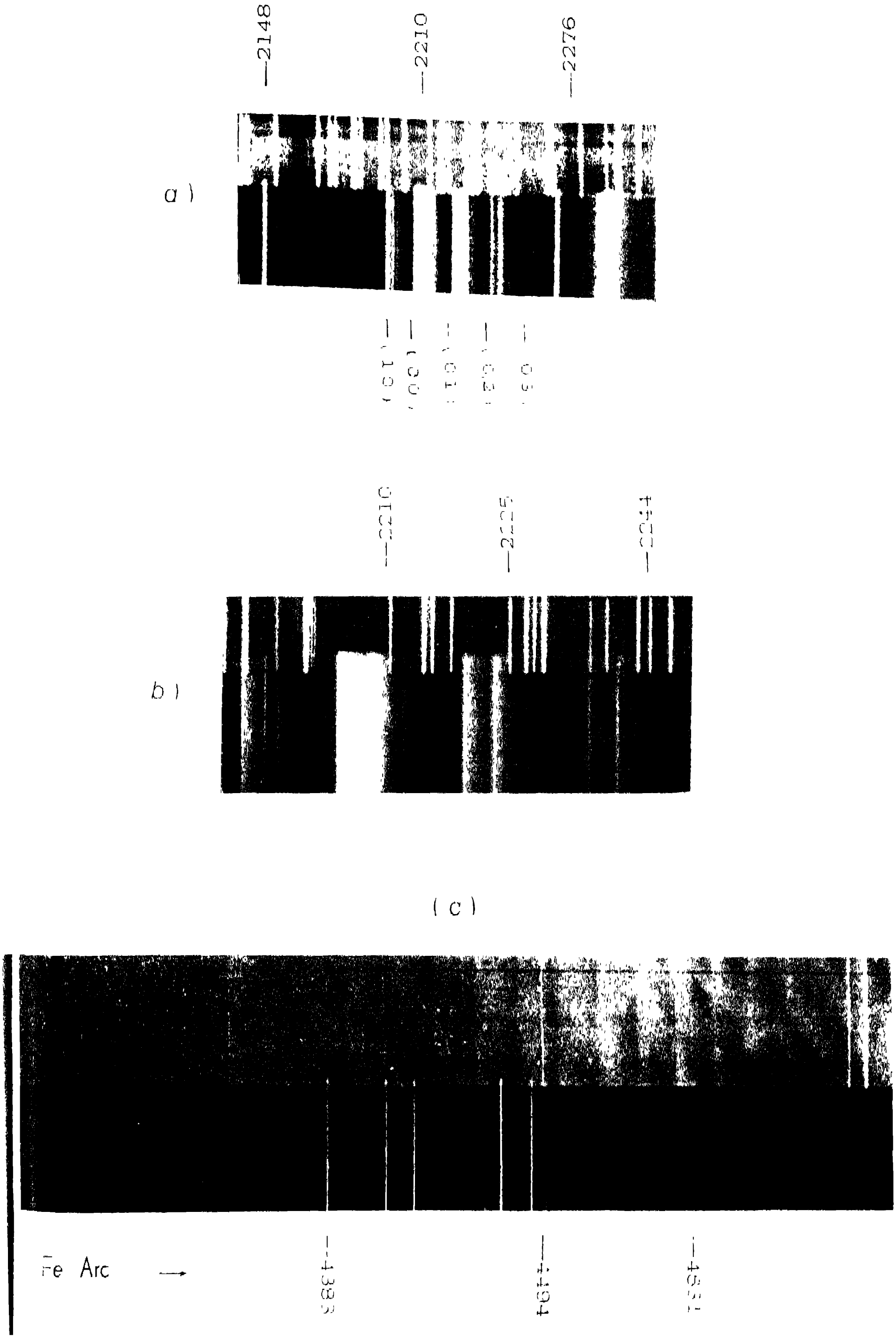

TABLE IV

Wavelength	Int.	Wavenumber	Wavelength	Int.	Wavenumber
4058	0	24636	4395.6	4	22744
4081	1	24497	4425.9	5	22588
4104	1	24360	4455.0	5	22440
4131	1	24200	4483.5	6	22298
4152	1	24078	4514.5	6	22145
4176	1	23940	4542.5	7	22008
4213	1	23729	4572.1	6	21866
4233	1	23617	4605.7	4	21706
4311.3	1	23188	4638.2	4	21554
4323.2	2	23125	4735.3	2	21112
4338.4	3	23044	4769.8	2	20959
4367.8	4	22888	...	..	..

300 cm, whereas the frequency of the ground state of the CdCl molecule is 330.9 cm. A second group of bands in the visible can also be clearly observed between λ6400 – λ5400 in a high dispersion spectrogram (15A per mm.). There are altogether about fifteen bands; they are red degraded and diffuse but not measurable. Further work on these visible bands, chiefly to study their rotational structure, is in progress.

ACKNOWLEDGMENTS

The author wishes to express his grateful thanks to Prof. K. R. Rao under whose inspiring guidance the work is being carried on.

ANDHRA UNIVERSITY,
WALTAIR.

REFERENCES

Cornell (1938), *Phy. Rev.*, **54**, 341.
Howell (1943), *Proc. Roy. Soc. (London)*, **182**, 95.
Mohler and Moore (1927), *J. Opt. Soc. Amer.*, **15**, 74.
Oeser (1935), *Zeits. f. Physik*, **95**, 699.
Ramasastry (1947), *Ind. J. Phys.* (communicated).
Ramasastry and Rao (1947), *Ind. J. Phys.* (in the press).
Walter and Barratt (1929), *Proc. Roy. Soc.*, **A122**, 201.
Wieland (1929), *Helv. Phys. Acta.*, **2**, 46 and **2**, 77

A SOURCE OF CONTINUOUS SPECTRUM IN THE ULTRA-VIOLET

By C. RAMASASTRY

(Received for publication, Sept. 5, 1947).

(Plate X)

ABSTRACT · The set up of H.T. discharge through iodine vapour is described as a simple source of continuous spectrum in the region λ3000-λ1950.

A number of sources of continuous spectrum have been described by several investigators for use in the ultra-violet.

1. The under-water spark The under-water spark between aluminium electrodes seems at one time to be very extensively used, but it is inconvenient to work with as the electrodes fall off very quickly and the source requires constant attention.

2. The Helium Continuum. The helium continuum is particularly useful for studies in absorption in the vacuum grating region between λλ900-600.

3. Burning magnesium ribbon.
4. Continuum emitted by flames such as CS_2.
5. A high current tungsten filament (Beutler and Metropolis, 1940).
6. Electrically exploded mercury (Knauss and Bryan, 1935).
7. Spark between mixed metallic electrodes.

The sources 3 to 7 are occasionally used for particular regions of the spectrum.

The main sources of continuous spectrum that are most generally employed are the Lyman capillary discharge and the hydrodgen discharge. A convenient modification of the original Lyman discharge tube was described in detail by Collins and Price (1934). For a set up of this source the requirements are : a transformer, giving 15 to 20,000 volts at the secondary, a rectifier, a condenser of capacity one micro-farad capable of withstanding a high voltage and a millimeter bore pyrex or quartz capillary discharge tube. In spite of its high intensity and the extent of the spectrum (from visible down to λ200), its chief disadvantages are the early wearing out and the consequent replacement of the capillary tube through which the condensed discharge passes and the erratic nature of the discharge which makes it unsuitable for spectro-photometric work. The hydrogen discharge tube, on the other hand, runs smoothly and with a suitable source of electrical excitation gives a fairly intense continuous spectrum which can be used even for quantitative spectrophotometric investigations over an extensive range of

the spectrum from visible down to λ1600. In recent years this is being used invariably in preference to every other type of source.

In the course the author's investigations on the band spectra of certain diatomic and triatomic molecules, it became necessary to devise a very simple and convenient source of continuous spectrum, as the hydrogen source could not be set up on account of inadequate laboratory facilities during the war period. The spectrum of the high frequency discharge through iodine vapour was then under investigation by him as a part of systematic experiments made to ascertain the origin of the bands of the various iodide molecules. The H. F. iodine discharge showed an intense continuous spectrum from the region λ3000 to λ1950 under the conditions of excitation described below.

A quartz window is attached with shellac to one end of a thin walled pyrex or quartz tube of about half to three-fourth inch internal diameter, the other end being drawn into an adaptor to be connected to an evacuating pump through a series of absorption towers to prevent iodine vapour from entering the pumping system. The R. F. voltage (about 125 volts) available at the ends of the tank circuit of Hartley shunt-fed valve oscillator (frequency of about 5 megacycles) is applied to the tube by means of external electrodes of brass or tin foil. The distance between the electrodes can be altered by sliding the electrodes along the tube. Details of the electrical set up are shown in figure 1. A wet cloth or cotton, wrapped round the tube near the window, serves the double purpose of not only preventing iodine from

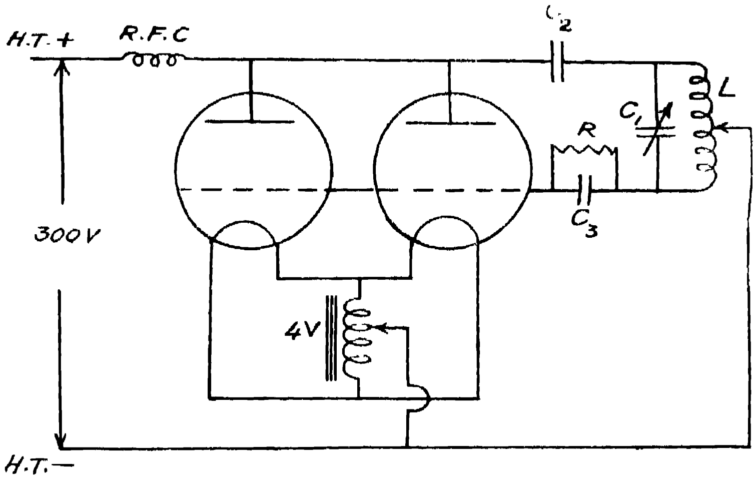

FIG. 1

Hartley Shunt-fed circuit with two Osram PX_4 valves in parallel

C_1 = 100 m m.f. variable, 2 m m air gap.
C_2 = 0.005 m.f. mica.
C_3 = 0.002 m.f. mica.
R = Two 25,000 ohms 1 watt carbon resistors in parallel.
L = 10 turns of copper wire (1 m.m. diam.) on octagonal wooden former (10 cm. diam.).

26

A SOURCE OF CONTINUOUS SPECTRUM IN THE ULTRA-VIOLET

By C. RAMASASTRY

(Received for publication, Sept. 5, 1947).

(Plate X)

ABSTRACT The set up of H. T. discharge through iodine vapour is described as a simple source of continuous spectrum in the region λ3000-λ1950.

A number of sources of continuous spectrum have been described by several investigators for use in the ultra-violet.

1. The under-water spark. The under-water spark between aluminium electrodes seems at one time to be very extensively used, but it is inconvenient to work with as the electrodes fall off very quickly and the source requires constant attention.

2. The Helium Continuum. The helium continuum is particularly useful for studies in absorption in the vacuum grating region between λλ900-600.

3. Burning magnesium ribbon.
4. Continuum emitted by flames such as CS_2.
5. A high current tungsten filament (Beuller and Metropolis, 1940).
6. Electrically exploded mercury (Knauss and Bryan, 1935).
7. Spark between mixed metallic electrodes.

The sources 3 to 7 are occasionally used for particular regions of the spectrum.

The main sources of continuous spectrum that are most generally employed are the Lyman capillary discharge and the hydrodgen discharge. A convenient modification of the original Lyman discharge tube was described in detail by Collins and Price (1934). For a set up of this source the requirements are, a transformer, giving 15 to 20,000 volts at the secondary, a rectifier, a condenser of capacity one micro-farad capable of withstanding a high voltage and a millimeter bore pyrex or quartz capillary discharge tube. In spite of its high intensity and the extent of the spectrum (from visible down to λ200), its chief disadvantages are the early wearing out and the consequent replacement of the capillary tube through which the condensed discharge passes and the erratic nature of the discharge which makes it unsuitable for spectro-photometric work. The hydrogen discharge tube, on the other hand, runs smoothly and with a suitable source of electrical excitation gives a fairly intense continuous spectrum which can be used even for quantitative spectrophotometric investigations over an extensive range of

the spectrum from visible down to λ1600. In recent years this is being used invariably in preference to every other type of source.

In the course the author's investigations on the band spectra of certain diatomic and triatomic molecules, it became necessary to devise a very simple and convenient source of continuous spectrum, as the hydrogen source could not be set up on account of inadequate laboratory facilities during the war period. The spectrum of the high frequency discharge through iodine vapour was then under investigation by him as a part of systematic experiments made to ascertain the origin of the bands of the various iodide molecules. The H. F. iodine discharge showed an intense continuous spectrum from the region λ3000 to λ1950 under the conditions of excitation described below.

A quartz window is attached with shellac to one end of a thin walled pyrex or quartz tube of about half to three-fourth inch internal diameter, the other end being drawn into an adaptor to be connected to an evacuating pump through a series of absorption towers to prevent iodine vapour from entering the pumping system. The R. F. voltage (about 125 volts) available at the ends of the tank circuit of Hartley shunt-fed valve oscillator (frequency of about 5 megacycles) is applied to the tube by means of external electrodes of brass or tin foil. The distance between the electrodes can be altered by sliding the electrodes along the tube. Details of the electrical set up are shown in figure 1. A wet cloth or cotton, wrapped round the tube near the window, serves the double purpose of not only preventing iodine from

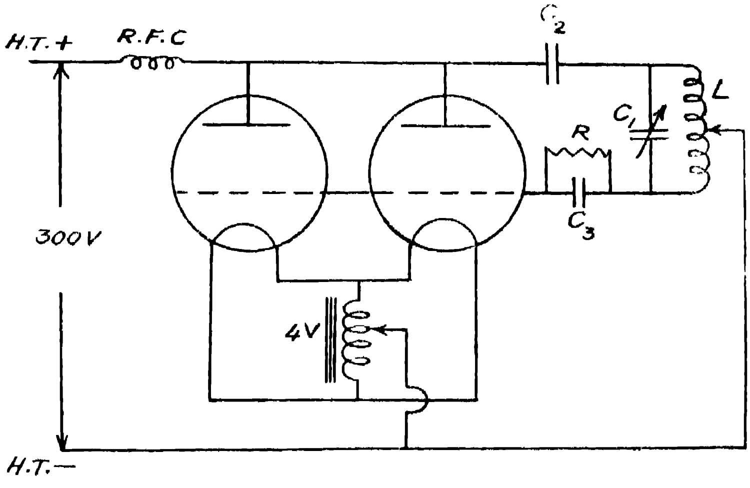

FIG. 1

Hartley Shunt-fed circuit with two Osram PX_1 valves in parallel

C_1 = 100 m m.f. variable, 2 m m air gap.
C_2=0.005 m.f. mica.
C_3=0.002 m.f. mica.
R = Two 25,000 ohms 1 watt carbon resistors in parallel.
L = 10 turns of copper wire (1 m.m. diam.) on octagonal wooden former (10 cm. diam.).

A SOURCE OF CONTINUOUS SPECTRUM IN THE ULTRA-VIOLET

By C. RAMASASTRY

(Received for publication, Sept. 5, 1947).

(Plate X)

ABSTRACT The set up of H. F. discharge through iodine vapour is described as a simple source of continuous spectrum in the region λ3000-λ1950.

A number of sources of continuous spectrum have been described by several investigators for use in the ultra-violet.

1. The under-water spark: The under-water spark between aluminium electrodes seems at one time to be very extensively used, but it is inconvenient to work with as the electrodes fall off very quickly and the source requires constant attention.

2. The Helium Continuum. The helium continuum is particularly useful for studies in absorption in the vacuum grating region between λλ1000 600.

3. Burning magnesium ribbon.
4. Continuum emitted by flames such as CS_2.
5. A high current tungsten filament (Beuller and Metropolis, 1940).
6. Electrically exploded mercury (Knauss and Bryan, 1935).
7. Spark between mixed metallic electrodes.

The sources 3 to 7 are occasionally used for particular regions of the spectrum.

The main sources of continuous spectrum that are most generally employed are the Lyman capillary discharge and the hydrodgen discharge. A convenient modification of the original Lyman discharge tube was described in detail by Collins and Price (1934). For a set up of this source the requirements are: a transformer, giving 15 to 20,000 volts at the secondary, a rectifier, a condenser of capacity one micro-farad capable of withstanding a high voltage and a millimeter bore pyrex or quartz capillary discharge tube. In spite of its high intensity and the extent of the spectrum (from visible down to λ200), its chief disadvantages are the early wearing out and the consequent replacement of the capillary tube through which the condensed discharge passes and the erratic nature of the discharge which makes it unsuitable for spectro-photometric work. The hydrogen discharge tube, on the other hand, runs smoothly and with a suitable source of electrical excitation gives a fairly intense continuous spectrum which can be used even for quantitative spectrophotometric investigations over an extensive range of

the spectrum from visible down to λ1600. In recent years this is being used invariably in preference to every other type of source.

In the course the author's investigations on the band spectra of certain diatomic and triatomic molecules, it became necessary to devise a very simple and convenient source of continuous spectrum, as the hydrogen source could not be set up on account of inadequate laboratory facilities during the war period. The spectrum of the high frequency discharge through iodine vapour was then under investigation by him as a part of systematic experiments made to ascertain the origin of the bands of the various iodide molecules. The H. F. iodine discharge showed an intense continuous spectrum from the region λ3000 to λ1950 under the conditions of excitation described below.

A quartz window is attached with shellac to one end of a thin walled pyrex or quartz tube of about half to three-fourth inch internal diameter, the other end being drawn into an adaptor to be connected to an evacuating pump through a series of absorption towers to prevent iodine vapour from entering the pumping system. The R. F. voltage (about 125 volts) available at the ends of the tank circuit of Hartley shunt-fed valve oscillator (frequency of about 5 megacycles) is applied to the tube by means of external electrodes of brass or tin foil. The distance between the electrodes can be altered by sliding the electrodes along the tube. Details of the electrical set up are shown in figure 1. A wet cloth or cotton, wrapped round the tube near the window, serves the double purpose of not only preventing iodine from

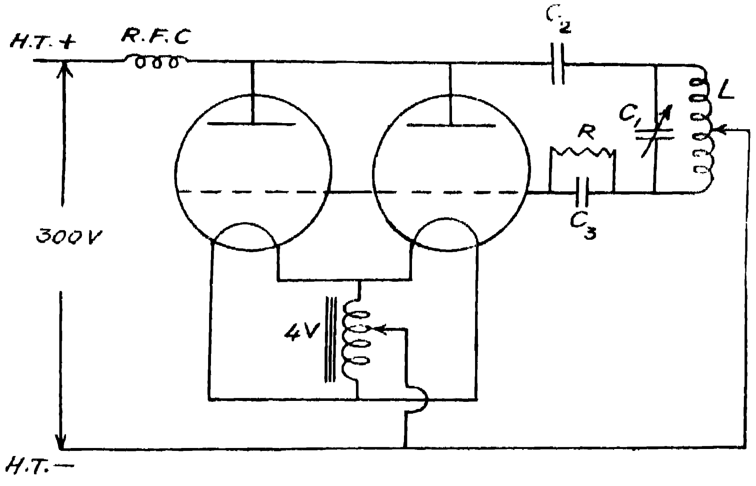

FIG. 1

Hartley Shunt-fed circuit with two Osram PX_1 valves in parallel

C_1 = 100 m m.f. variable, 2 m m air gap.

C_2 = 0.005 m.f. mica.

C_3 = 0.002 m.f mica.

R = Two 25,000 ohms 1 watt carbon resistors in parallel.

L = 10 turns of copper wire (1 m.m. diam) on octagonal wooden former (10 cm. diam.).

condensing on the window but also ensures a steady supply of vapour from iodine crystals deposited underneath it. No heating is necessary as the heat of the discharge itself is sufficient to produce enough vapour pressure of iodine. The continuous spectrum is most intense with an optimum electrode distance and high iodine vapour pressure. If at any time the iodine deposited itself on the window a gentle heating with a spirit lamp is enough to clear the window. When iodine gets exhausted in the discharge tube it becomes necessary to introduce a few crystals again.

With a Hilger medium quartz spectrograph exposures of even three minutes were found sufficient to obtain the continuous spectrum down to λ2062 with the discharge tube facing the slit directly. It shows the well-known iodine bands in the visible. The characteristic iodine continua and diffuse bands above λ3000 (Curtis and Evans, 1933; P. Venkateswarlu, 1946 and 1947) are observable. The other system of diffuse emission bands below λ3000 are probably masked entirely by the continuous spectrum such that the spectrum runs quite uninterrupted down to the resonance line of iodine at λ2052. Reproduction of the region of the spectrum below λ3000 is shown in two sections in Plate XI—*a* and *b*. The continuous spectrum, however, showed signs of extending much below this resonance line. A moderate exposure with a Hilger small quartz instrument gives the continuous spectrum down to the limit of the instrument at about λ1850, the atmospheric absorption bands also being recorded (Plate XI—*c*).

An ordinary uncondensed transformer discharge through iodine vapour also is found to develop this continuous spectrum though it is comparatively fainter. A similar continuous spectrum is observed in the H. F. discharge through bromine as well (Plate XI—*d*). Perhaps, it is a characteristic of the halogen molecules and is analogous to the continuous spectrum emitted by hydrogen.

ACKNOWLEDGMENTS

My thanks are due to Prof. K. R. Rao for his constant guidance and encouragement.

ANDHRA UNIVERSITY,
WALTAIR.

REFERENCES

Beutler and Metropolis (1940), *Jour. Opt. Soc.*, **30**, 115.
Collins and Price (1934), *Rev. Sci. Inst.*, **5**, 423.
Curtis and Evans (1933), *Proc. Roy. Soc. Lond.* A **141**, 603.
Knauss and Bryan (1935), *Phy. Rev.*, **47**, 842.
Venkateswarlu (1946), *Proc. Ind. Acad. Sci.*, **24A**, 480.
Venkateswarlu (1947), *Ibid*, **25A**, 119.
Venkateswarlu (1947), *Ibid*, **25A**, 133.

RAMASASTRY

PLATE X

Continuous Spectrum of Iodine and Cu arc comparison.

(*a*)

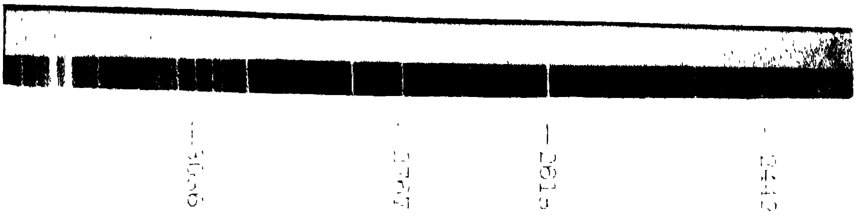

(*b*)

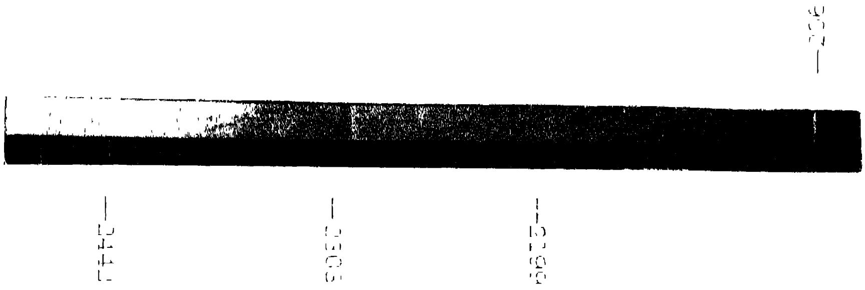

(*c*)

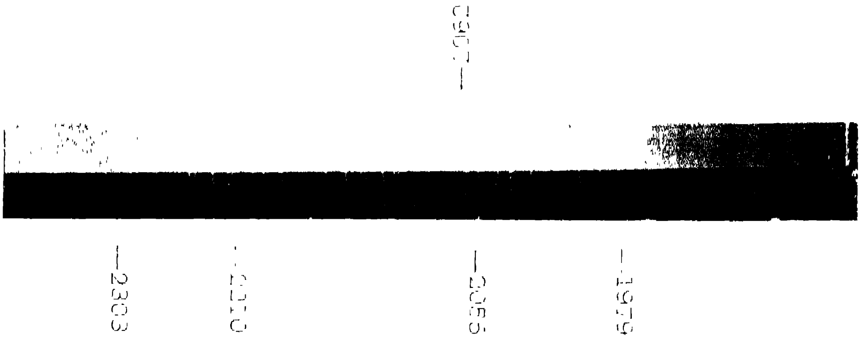

Continuous Spectrum of Bromine and Fe arc comparison.

(*d*)

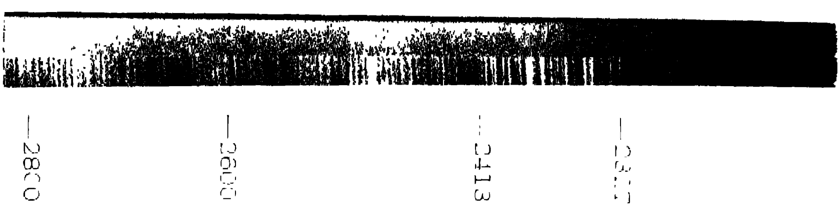

A NEW CRYOSTAT OF THE GASFLOWTYPE AND A QUARTZ FIBRE MICROBALANCE ADOPTED FOR MAGNE-CRYSTALLINE MEASUREMENTS *

By AKSHAYANANDA BOSE

(Received for publication, Oct. 3, 1947)

ABSTRACT. In the first part of the paper a description of a new form of automatically controlled gas flow type of cryostat, working between 300°K and 80°K, is given. The cryostat is suited to magnetic measurements on single crystals at low temperatures. The temperature can be maintained steady to about 0.01°C with its help for long periods. In the latter parts the techniques for the measurement of anisotropies and that of principal susceptibilities at low temperatures is described. A quartz fibre torsion microbalance has been devised, specially for this latter measurement, with the help of which the forces on a crystal in an inhomogeneous field can be quickly and accurately measured. The same techniques could be extended down to liquid hydrogen or helium temperatures when available.

INTRODUCTION

In the course of the investigations on the low temperature behaviour of the paramagnetic salts of the iron group undertaken by the author in this laboratory, he developed the technique of the magnetic measurements on single crystals at low temperatures down to the liquid air temperature. The technique presents certain new features, in the design of the cryostat and of the torsionbalance for the measurements of absolute susceptibilities of crystals and also in the arrangements used for the measurements of anisotropies. The present paper gives the details of these low temperature techniques which have since been used by a large number of workers in this laboratory working on similar lines.

THE CRYOSTAT

The original type of cryostat designed by the author and used by various workers (Krishnan and co-workers 1936-1939) in this laboratory for magnetic measurements on crystals at low temperatures, was of the liquid bath type. Petroleum ether of low boiling point was used as the bath liquid and its temperature was kept constant at any desired low temperature within a range of 0.1°C by an automatic relay system controlling the cooling or the heating of the bath. Details of the cryostat are to be found in the papers already mentioned. As was pointed out in these papers the main disadvantage of such a cryostat was that the available range of temperature was limited to within about 140° K, since at lower temperatures the liquid became highly viscous making it difficult to maintain a uniform temperature by stirring.

---

* Part of thesis approved for the D.Sc. degree of the Dacca University.

In order to get over this and a few other minor defects, a new cryostat (Bose, 1940) of the gas flow type was designed and used in our present

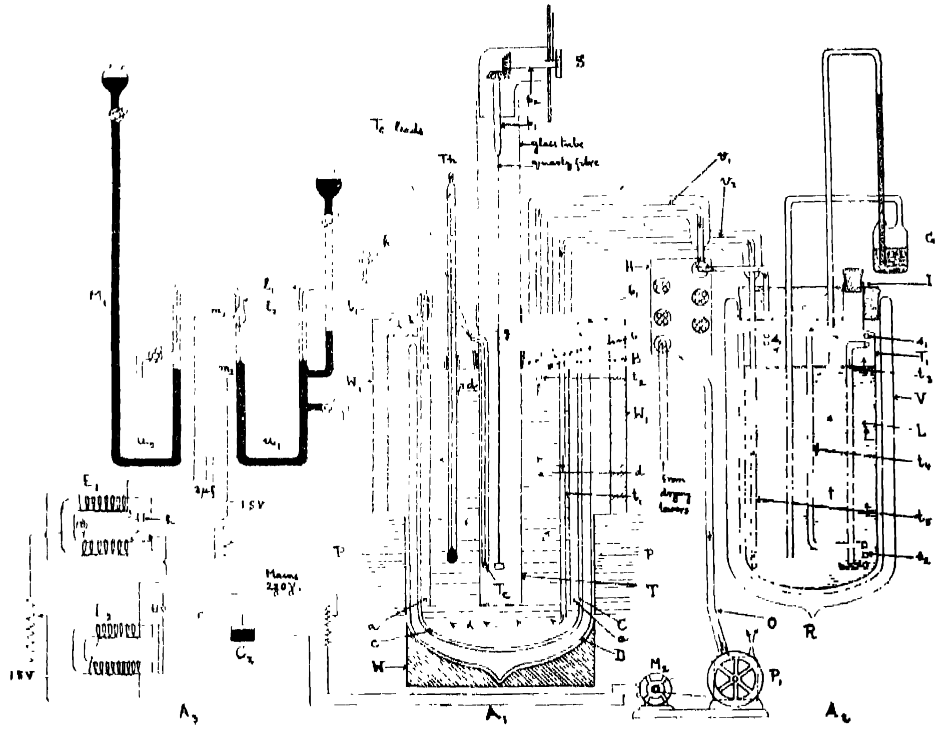

FIG. 1

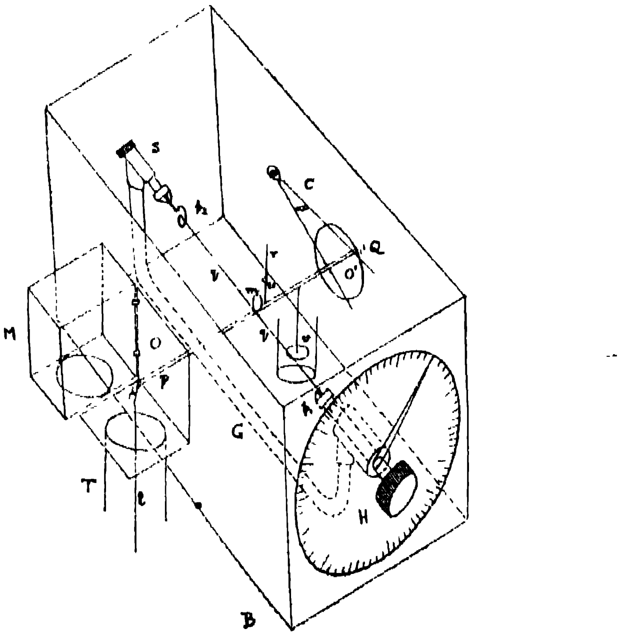

FIG. 2

measurements. From a diagram of this cryostat (Fig. 1) it will be seen that the main parts of the new cryostat are: (1) the thermostatic system, appearing in the middle portion of the diagram and marked A_1, in which the temperature is maintained constant for magnetic measurements; (2) the arrangement for the supply of dry cold air to the thermostatic system, marked A_2, on the right hand side; (3) the control system A_3, on the left which regulates the supply of cold air into the thermostat; (4) the arrangements for the measurement of the low temperatures; and (5) the arrangements for magnetic measurements at these low temperatures. These various parts will be described in the following paragraphs.

(1) The cryostatic chamber where the temperature is maintained constant consists of a cylindrical double walled vessel the bottom of which, however, is single walled and cupshaped. This chamber fits snugly inside the cylindrical Dewar vessel *D*, of internal diameter about 5 cms. The walls of the chamber are of thin copper sheet about ½ mm. thick and the top of the chamber is closed by a brass disc *B*, with a central hole through which the experimental tube is fitted leaktight with a conical collar arrangement, *b*. The annular space, *a*, of width about 3 mm. between the two walls, is closed at both ends and serves as the bulb of a constant volume air thermometer. It is connected by a capillary Pyrex tubing, l_1, to the manometric system of the temperature control device.

The usual disadvantages in these gas flow types of cryostat are the difficulty of maintaining the temperature in different parts of the chamber uniform, and affording an efficient exchange of heat between the flowing gas and the walls of the chamber. In the present arrangement these difficulties were overcome by the following simple device.

The chamber is cooled by a flow of cold air from the refrigerant system, *R*, led into the bottom of the chamber by the tube t_1, and out of the chamber by the exit tube t_2, at the top. The whole of the space inside the chamber contains a series of 50 discs of thin copper, *d*, of the same diameter as the inner cylinder of the chamber, and disposed perpendicularly to the axis of the cylinder at equal intervals. These discs have a large number of holes each about 1 mm. diameter through which the cold air is drawn up from the bottom of the chamber. The discs are, however, so arranged that the holes in the adjacent discs were never vertically above one another and in consequence the flow of cold air is rendered turbulent by the successive interruption to its straight passage.

(2) The circulation of the cold air is maintained and controlled by a suction pump, P_1, the speed of which can be adjusted. Atmospheric air dried by passing through lime and caustic potash towers is precooled at first by its passage through four copper tubings enclosed in a single wide copper tubing through which, on the other hand, the cold waste air from the cryostat chamber is made to circulate in an opposite direction to the ingoing air in

the four narrow copper tubings. The tubings are of sufficient length to provide an efficient heat exchange between the incoming atmospheric air and the outgoing waste air. This countercurrent heat-exchanger system is marked H, in the diagram.

Next, this precooled air is *progressively* cooled practically to the temperature of liquid air by its passage through a system of copper tubings in the form of spirals kept inside the refrigerant chamber R. This chamber consists of a cylindrical tank, T_1, made of thin brass sheet, containing liquid air, L, and placed inside a large Dewar flask, V. The level of the liquid air in the tank is indicated by the glycerine pressure gauge, G, so that it may be replenished in time through the inlet, I, usually kept closed with a cork. The first copper spiral, s_1, which the incoming air encounters is placed above the level of liquid air in the tank and is cooled only by the vapour rising from the liquid. The end of this spiral is immersed under the liquid air and the incoming air bubbles out at this end through the liquid and mixes with the vapour above, cooling fresh lots of incoming air in the spiral, s_1. From this space the cold air then enters the next spiral s_2, immersed in liquid air through the end of the spiral kept above the level of the liquid. The air is here intensely cooled down to the temperature of liquid air and passes on through the other end of the spiral, through the double walled vacuum jacketed Pyrex tube, V_2, and through the inlet tube, I_1, to the bottom of the cryostat chamber. It then passes upwards through the perforated plates, d, already mentioned, cooling the whole system and thence through the vacuum jacketed tube, V_1, enters the countercurrent heat-exchanger, H, where it gives up the residual cold to the ingoing air from the drying towers, and is finally sucked out by the pump, P_1, through the outlet O. Due to the turbulent flow at the perforated copper discs and the high conductivity of copper a thorough exchange of heat takes place between the cold air, the copper discs and the walls of the chamber, and this serves to give a fair uniformity of temperature over the experimental tube. Further, the heat insulation of the system is so good and its thermal capacity so adjusted that the temperature may be kept moderately steady, even without the help of any controlling system, and at the same time the liquid air consumption is quite moderate.

(3) The temperature control device is essentially the same as described in our previous paper in connection with the original form of the cryostat, except for a few modifications to increase its sensitivity and to secure its smooth working over a long run. The various parts of the system may be easily followed from Fig. 1. The interspace, a, between the two walls of the cryostat chamber, as has already been mentioned serves as the bulb of a constant volume air thermometer. Due to its annular shape the present arrangement in addition to economising space, conduces to a quicker and larger response to the fluctuations of temperature inside the cryostat chamber.

In the barometer portion of the control system, long pressure tubing connections were as far as possible avoided, replacing them by glass U-tubes, u_1 and u_2, since mercury surface became fouled by long contact with rubber. The capillary tube, l_1, is of Pyrex glass to prevent breakage due to intense cooling. But the capillary l_2, is of ordinary glass so that the platinum electrodes, m_1 and m_2, serving to close the relay circuit, may be sealed into it. Previous experience showed that tungsten contacts used earlier were a constant source of trouble due to rapid formation of a high resistance oxide, very difficult to remove. The barometer column, M_1, and tubes u_2, l_2, u_1 and l_1, meet end to end and are connected to one another by short pieces of rubber tubing and contain requisite amounts of clean mercury.

The mercury level in the tube u_1, is so adjusted that it just touches the upper platinum electrode, m_1, while the other electrode, m_2, remains always under the mercury. A relay, E_1, of the magnetic control type actuated by a feeble current of about 5 milliamperes is connected across the electrodes m_1 and m_2, and makes the circuit of a second relay, E_2, so long as the contact at the mercury level is kept closed. The second relay of gravity control type, in its turn, carrying a heavier current of about 0.02 amperes, closes the circuit of the motor pump which sucks cold air through the cryostat chamber, cooling it thereby. The stopcock, k, is kept open in the meanwhile connecting the interspace, a, with the atmosphere. Thus there is no change of pressure within the interspace and the level of mercury stays on touching the electrode m_1, the pump runs on, and the temperature inside the cryostat chamber goes on falling. When a desired temperature has been attained the stopcock, k, is closed and the fall of pressure due to any further cooling of the enclosed air, at once breaks the mercury contact and the pump is shut off. The small heat leakage from outside is just enough, however, to start the pump very soon and the rate of suction of cold air is so adjusted that the cooling just balances this heating and a very steady temperature inside the cryostat chamber (within about 0.01 C) is soon attained. The mercury surfaces at the platinum contact m_1, and in the cup C_2, are covered with glycerine so as to avoid oxidation of the surfaces. A condenser of 2 micro-farad capacity is connected in parallel with the platinum electrodes, m_1 and m_2 to damp out any sparking. A complete set of magnetic measurements between 300°K and 80°K at intervals of about 25° and lasting over about 4 hours required about 1½ litres of liquid air including losses at the start, and an extra quarter litre was found to be enough for taking a second set of observations over the same range starting from 80°K and going up to room temperature. The second set of measurements acted as a check on the first, and served further to reveal any permanent modification in the crystalline form that might have occurred at the lower temperatures.

(4) *Measurement of temperatures.*—A rough indication of temperature inside the cryostat chamber, for initial adjustments may be obtained with the

pentane thermometer, *Th*, inserted through a hole at the top of the chamber. For an accurate determination of the temperature of the crystal, however, a copper constantan couple was used one junction, *Tc*, of which, sheathed in a narrow Pyrex glass tube was kept inside the experimental tube, side by side with the crystal; the other junction of the couple also similarly sheathed being kept at the temperature of melting ice, in a Dewar flask. The thermocouple was calibrated in the usual manner using the following standard temperatures (See International Critical Tables, Vol I, p. 53).

(*a*) The temperature of steam from water boiling under atmospheric pressure *p*, namely,

$$100\cdot000^\circ\mathrm{C} + 0\cdot0367(p-760)^\circ\mathrm{C}\,,$$

(*b*) The temperature of the room measured with a calibrated mercury thermometer reading directly to 1/10° C;

(*c*) The temperature of pure melting ice. The null E. M. F. observed at this temperature serves as a check for the absence of any extraneous E. M. F.

(*d*) The temperature of a mixture of solid carbon dioxide and ethyl ether evaporating under atmospheric pressure namely,

$$-78\cdot51^\circ\mathrm{C} + 0\cdot0105(p-760)^\circ\mathrm{C}\,;$$

(*e*) The temperature of liquid oxygen boiling under atmospheric pressure namely,

$$183\cdot00^\circ\mathrm{C} + 0\cdot0126(p-760)^\circ\mathrm{C}.$$

To measure the E. M. F of the thermocouple at various temperatures, it was balanced against the E. M. F. of a standard Weston-Cadmium cell with a Leeds and Northrup dual type potentiometer reading to a microvolt, and a five constant formula of the type

$$E = a + bt + ct^2 + dt^3 + et^4$$

was used giving the relationship between the E. M. F. of the thermocouple and the temperature of the cold junction in degrees Centigrade.

The temperature inside the experimental tube was found to be constant within about 0.01° C when the relay system was working smoothly, and the vertical gradient of temperature in the region occupied by the crystal inside the tube was negligible.

THE MEASUREMENT OF MAGNETIC ANISOTROPIES

The experimental technique adopted for the measurement of the magnetic anisotropies of single crystals is essentially the same as that adopted in our previous work (1939). In the experimental arrangement the crystal was suspended inside the experimental chamber *T*, inserted well within the cryostat chamber so that the crystal might be suspended in the central portion of the uniform horizontal magnetic field between the large flat polepieces *P*, *P*, of a powerful electro-magnet. The suspension fibre (see Fig. 1) was made in two halves, the upper part, a fine quartz fibre lying entirely outside the cryostat chamber and the lower part a stout rigid glass fibre lying partly outside but mostly inside the chamber. Thus the torsional constant of the whole suspension fibre was practically that of the fine quartz fibre alone and remained constant whatever might be the temperature of the crystal. At the same time, a small glass index *g*, fixed horizontally to the upper end of the rigid part of the suspension, served to indicate the movements of the crystal which is invisible from outside. The torsion head *S*, to which the quartz suspension is attached, is of the vertical disc type already used in our previous works (1930) in which the rotation of the crystal about the vertical axis is observed as a rotation about a horizontal axis with the help of a suitable cross-pinion arrangement P_1, P_2. The value of the anisotropy $\Delta\chi$ per gm. molecule, in the horizontal plane is given by :

$$\frac{1}{2}\frac{m}{Mc}H^2\Delta\chi=\lambda \text{ (say)}$$

$$=\frac{\alpha_c-\frac{\pi}{4}-\sigma_c}{\cos 2\sigma_c} \qquad \dots \quad (1a)$$

where

$$\sin 2\sigma_c=\frac{1}{2\lambda} \qquad \dots \quad (1b)$$

in which m is the mass of the crystal, M its gm. molecular weight, H the magnetic field on the crystal, α_c is the critical angle of torsion on the fibre, observed on the torsion head, and $\frac{\pi}{4}+\sigma_c$ is the critical angle through which the crystal turns in the meanwhile from its initial position in the field ; both these angles being measured from the initial state in the magnetic field when there is no torsion in the fibre to the state when the equilibrium of the crystal becomes unstable.

MEASUREMENT OF ABSOLUTE SUSCEPTIBILITIES WITH A MICROBALANCE

For the measurement of the absolute susceptibility of a crystal for a given direction, the following method was adopted. When the crystal is placed with freedom to rotate about a vertical axis in a horizontal field H, with a vertical gradient $\frac{\partial H}{\partial h}$, as can be obtained near the middle of the upper edges of the pair of large rectangular flat and parallel polepieces used in the measurement of anisotropy, the crystal sets itself with the direction of its maximum susceptibility in the horizontal plane, along the direction of the field. At the same time it experiences a force in the vertical direction given by the relation,

$$F=\tfrac{1}{2}(k-k_a)H\frac{\partial H}{\partial h}, \qquad \dots \quad (2)$$

where k and k_a are volume susceptibilities of the crystal in the direction of the field and that of the surrounding air respectively. The thermal expansion of the crystal being small the integrated value of $H\dfrac{\partial H}{\partial h}$, over the volume of the crystal, may be considered as proportional to this volume, provided the crystal always remains in the same position. Then it may be shown that

$$\frac{F_T}{F_\Theta} = \frac{\chi_T}{\chi_\Theta}\left[1 + \frac{k_{a\Theta}}{k_\Theta}\left(1 - \gamma\Theta\right)\left(1 - \frac{\Theta}{T}\right)\right] \qquad \dots \quad (3)$$

where F_T and F_Θ are the vertical forces on the crystal at any temperature T and room temperature Θ, respectively, temperatures being measured on absolute scale, χ_T and χ_Θ are the gram-molecular susceptibilities of the crystal along the direction of the field at those temperatures; $k_{a\Theta}$ the volume susceptibility of air and k_Θ that of the crystal in the field direction, both at room temperature, and γ is the coefficient of thermal volume expansion of the crystal. Thus, if the forces F_T at different temperatures are measured, knowing the absolute susceptibility of the crystal in the direction concerned at room temperature, the values of the absolute susceptibilities at other temperatures can be calculated.

The vertical forces on the crystal due to the inhomogeneous field mentioned above, were measured with the help of a quartz microbalance developed for this purpose (Fig. 2). The beam, PQ, of the balance consists of a thin walled quartz tube about 12 cms long and 2 mm. diameter weighing about 0.25 gms, the two ends of which are drawn out in the form of hooks. The beam is suspended exactly at the centre with two pieces of fine quartz fibre, one from either side of the beam, at right angles to the beam, so that the beam and the two pieces of fibre q, q, lie in the same horizontal plane. The further end of one fibre is then attached to a stout quartz spiral p_2, which itself is clamped to a screw-slide S, with which a constant tension on the quartz fibre could be maintained. The further end of the other quartz fibre is also attached to the pin p_1, of a torsion head H. The torsion head and the screw-slide are mounted on a U-shaped Pyrex tube frame G, the plane of which contains the quartz fibres and is at right angles to the quartz beam. Evidently, a rotation on the torsion head produces a twist mainly on the fibre attached to it, and causes the beam to rotate about this horizontal axis of torsion. Thus, a vertical force upon the end of the beam, such as is produced here by the attraction of the inhomogeneous magnetic field on a crystal suspended from one hook of the balance, may be counterbalanced by rotating the torsion head suitably. The system is enclosed within a rectangular wooden box B, with a sliding glass panel at the top. The two ends of the beam project through windows O, O', on two opposite sides of the box and are protected from air-draughts with suitable removable glass faced covers to accommodate the projecting ends of the beam. Thus, a pencil of light passing through the glass front of the cover *M*, and reflected back from a small mirror *m*, mounted at right angles to and on the middle of the balance beam, magnifies its movements. In actual practice, the usual scale and telescope arrangement is used to bring back the balance beam to its original position by rotating the torsion head when the beam is deflected. A mica damping vane *v*, efficiently damps the oscillations of the beam. The torsion pin with its housing passes through one small side of the box, the graduated disc and the torsion head remaining outside the box for convenience of manipulation. When not in use the balance beam may be arrested by the spring catch *C*, worked from outside.

The crystal is suspended from one arm of the balance with a fine quartz fibre *l*, having very small torsion constant, passing through a hole at the bottom of the window cover, and protected on its way to the crystal chamber by a glass tube *T*. The length of the fibre is such that the crystal is a little above the upper edge of the large parallel pole-pieces *P P*. (Fig. 1) of the electromagnet, but at the same time well within the crystal chamber where the temperature is practically uniform. The suspension fibre being very thin, there being practically no horizontal gradient of the field and the crystal so chosen as to have very little anisotropy of shape, the crystal sets practically with its maximum direction of susceptibility in the horizontal plane, along the field. Further, there is no lateral shift of the crystal and the translational force on it is entirely due to the vertical gradient. This force is balanced by twisting the microbalance fibre when the crystal is brought back to the same position as before, as indicated by the scale and telescope arrangement already mentioned. Thus, the conditions necessary for equation (2) to hold are obtained to a high degree of accuracy and forces on the crystal known from the angle of torsion of the fibre. It was found that the force and the angle of torsion were proportional even with such a high torsion of the fibre as corresponded to five complete rotations of the torsion head. The forces on the crystal are thus measured at various temperatures and the absolute susceptibilities along the field direction at these temperatures calculated from (3).

CONCLUSION

With the help of the experimental techniques described above the author made measurements on the magnetic anisotropy and absolute susceptibilities of a large number of single crystals of the paramagnetic salts of the iron group of elements. The results of these experiments have been published in the form of a memoir (1946), a discussion of which will be published in subsequent papers. Other works in these directions are in progress in this laboratory. The same techniques could be easily adopted for work down to liquid hydrogen or helium temperatures but as there is no arrangement to obtain liquid hydrogen or helium in this laboratory or elsewhere in India, the author had to be content with the measurements in the liquid air range.

ACKNOWLEDGMENTS

The author is grateful for the kind interest taken in the work by Prof. K. S. Krishnan, F R.S., and also to the authorities of Indian Association for the Cultivation of Science for all facilities provided. Due to unavoidable circumstances the publication of the work of which the present paper is a part, and which was done before 1941, has been considerably delayed.

INDIAN ASSOCIATION FOR THE CULTIVATION OF SCIENCE,
CALCUTTA.

REFERENCES

Bose, A, 1940, *Proceedings of the Indian Science Congress.*

Bose, A, 1940, Paramagnetism of Single Crystals of the Salts of the iron Group of Elements at Low Temperatures (Hindusthan Printing Works, Dacca.)

Krishnan, K S , Mukherji, A., and Bose, A , 1939, *Phil Trans Roy. Soc* (A), **238**, 125.

Krishnan, K S., and Ganguli, N., 1939. *Zeit. f. Krist.*, **100**, 530.

Krishnan, K. S., and Mukherji, A., 1936-38, *Phys. Rev.*, **50**, 860 ; **54**, 533 ; **54**, 841.

EXTRA REFLECTIONS IN LAUE PHOTOGRAPHS OF BENZIL

By R. K. SEN

(Received for publication, October 4, 1947)

ABSTRACT. In the present paper the results of the accurate measurements of the positions of extra spots and streaks observed in Laue photographs of benzil have been reported. From these measurements it has been shown that the reciprocal lattice points of benzil have planer extensions parallel to a^*c^* planes with sharp extension along a^* axes. It has also been shown that the shape of the scattering domains around the reciprocal lattice points depends on the direction of the incident beam. The nature of the derrangement waves giving rise to the extra reflections have been discussed.

INTRODUCTION

Lonsdale and Smith (1941) published a few very interesting Laue photographs of benzil showing fairly sharp continuous streaks and extra spots. The continuous streaks observed in the photograph taken with the X-ray beam along the [0001] axis, correspond with the layer lines due to rotation around the three two-fold axes. The streaks extend through moderately large distances (*e.g.*, from the [3302] Bragg reflection to the $[\bar{3}121]$ extra spot and from the $[\bar{3}121]$ extra spot to the $[02\bar{2}1]$ extra spot. In the case of the photograph taken with the incident X-ray beam along the $[10\bar{1}0]$ direction (the [0001] axis being vertical), streaks coinciding with the layer lines due to rotation about two two-fold axes (*i.e.*, $[1\bar{2}10]$ and $[11\bar{2}0]$ axes) and the [0001] axis are present. In this photograph Lonsdale and Smith could observe up to the third order layer line streaks corresponding to rotation around the two-fold axes. Banerjee, Khan and the author (1945), using cylindrical film, observed the beautiful fourth order layer line streaks. They determined the positions of the pair of extra spots from the $[04\bar{4}0]$ plane when the incident beam makes 0°, 1° and 2° with the [1010] directions. These measurements have shown that the $[04\bar{4}0]$ extra spots lie at the position of the intersection of the fourth order layer lines which could have been obtained by rotation around the two-fold axes with the equatorial layer line which would be produced by rotation around the [0001] axis. In the present investigation the positions of a large number of extra spots for a number of different orientations have been measured very accurately and the Fourier transforms of the results of these measurements are discussed.

EXPERIMENTS

A small single crystal of benzil, crystallised from ether, was mounted with the [0001] axis vertical on the axis of the camera. Unfiltered X-rays from a Hadding-Siegbhan type of X-ray tube run at a voltage of 50 k.v. and a tube current from 7 to 10 m amps., after being collimated through a slit .5 mm. in diameter and 7 cm long, was incident on the crystal along the [1010] direction in the first photograph. The diffracted beams were received on the cylindrical film. Photographs were then taken with the X ray beam making various angles with the [1010] direction. In each of these Laue photographs over and above the Laue spots and the extra reflections a number of aluminium powder diffraction lines, obtained by the scattering of X-rays by a small amount of aluminium powder dusted on the crystal, were also recorded. The indices of the planes giving rise to the Laue spots and the associated extra spots were assigned with the help of the Laue equations according to the method of Ganguly (1952). For the assignment of indices to the extra spots, the points in the reciprocal space corresponding to the maxima on the spots are obtained from Fourier transform. The method of obtaining such a representation on the reciprocal lattice is shown, as for example, for the reflections corresponding to the photograph taken with the incident X-ray beam along [1010] direction, in Fig. 2. From this figure it is observed that the reciprocal lattice points [0440] and [4400] are silghtly away from the surface of the sphere of reflection, so there arises the probablity of the [0440] and [4400] extra spots occurring in the photograph. Now, in this setting of the crystal the [0110] and (1100) faces make an angle of 30° with the incident beam, so at an angle of 60° on the two sides of the incident beam, we shall have the Laue reflection from the [0110] and [1100] planes. Again since the reciprocal lattice points [0440] and [4400] falls inside the sphere of reflection, the extra reflections from [0440] and [4400] planes will appear at angles smaller than that of the corresponding Laue spots. Actually in the photograph along the equatorial line on the two sides of the incident X-ray beam, there are two Laue spots an angle of 60 and immediately after each of the Laue spots on the smaller angle side there is a pair of extra spots. So these double extra spots are from the [0440] and [4400] planes. In a similar way the correct indices of the other extra spots have been assigned to them.

The positions of maximum intensity inside the extra spots were determined with the help of a non-recording photo-electric photometer. The scanning spot of light was allowed to traverse the extra spot and two aluminium powder lines in a single traversal along the equatorial line through the centre of the extra spot. The traversal was carried on by sliding the photograph in a direction perpendicular to the direction of the scanning light with the help of a screw driven by the hand. The deflection in the galvanometer after every .5 mm. was noted. Then the difference between this deflection and the deflection corresponding to the clear background was plotted against the distance traversed. Three photometric curves—one corresponding to the extra spot and two very sharp curves corresponding to the aluminium lines were obtained. From these photometric curves the distance 'd' between the aluminium lines (corresponding to the aluminium peaks) and the distance 'd_1' of the peak corresponding to the extra spot from one of the aluminium lines can be obtained accurately. Then the angle of diffraction θ_m corresponding to the maximum intensity in the extra spot is found from the relation, $(\theta_m \sim \theta_1) = d_1 / d(\theta_2 - \theta_1)$ where θ_1 and θ_2 are the known angles $(\theta_2 > \theta_1)$ of diffractions corresponding to the aluminium lines. For spots lying above or below the equatorial layer line, the extra spot was once scanned through its centre parallel to the equatorial line and again it was scanned along the perpendicular direction through the position in the spot corresponding to the peak of the first scanning. From the photometric records of the above-mentioned scannings, the angular co-ordinates of the extra spot was found out and from them the angle of diffraction θ_m was obtained. The observed values of θ_m are shown in Tables I, II, and III.

RESULTS

We have represented geometrically the observed results in the Ewald's reciprocal lattice. For this purpose we constructed first the lattice with vectors b_1, b_2, b_3 where $b_1 = \frac{a_2 \times a_3}{V}$, $b_2 = \frac{a_3 \times a_1}{V}$ and $b_3 = \frac{a_1 \times a_2}{V}$; a_1, a_2, a_3 being the primitive translations of the crystal and V being the volume of the unit cell. A sphere was then drawn with C as centre and radius $CO = 1/\lambda$, (Fig 1), where λ is the wave length used, CO is the direction of the incident beam. If this sphere, known as the sphere, of reflection passes through a reciprocal lattice point P, there will be a selective Bragg reflection, the direction of reflection being given by CP. Now, in the case of an ideal crystal in which the atoms are at rest at the correct lattice points these are the only reflections possible, but in actual crystals, the atoms are neither regularly arranged everywhere nor at rest. In consequence, notable scattering of X-rays occurs even if the sphere of reflection do not pass through a reciprocal lattice point. In fact around the reciprocal lattice points there exists a region of scattering such that if the sphere of reflection passes through any portion of this region, X-ray reflections of notable intensity is observed. In order to get an idea of the domain of scattering, we therefore proceeded in the following way. The directions of scattering corresponding to the different points in the extra spots were drawn on the reciprocal lattice. Then at the points, where the directions of scattering meet the sphere of reflection, weights proportional to the intensity of scattering at the points concerned were put. On representing the present measurement in the reciprocal lattice in this way it is observed that the positions of maximum intensity in the extra spots correspond to points lying on the a* axes of the reciprocal lattice. This is shown in the cases of the equatorial $(0\bar{4}40)$ extra spot in figure 2.

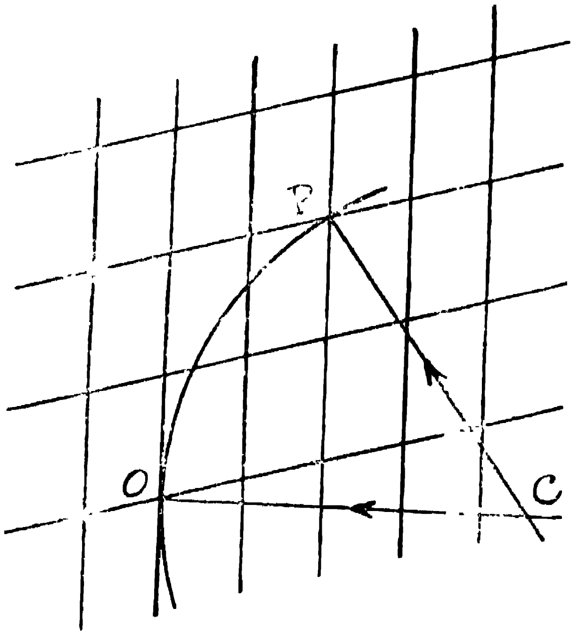

FIG. 1

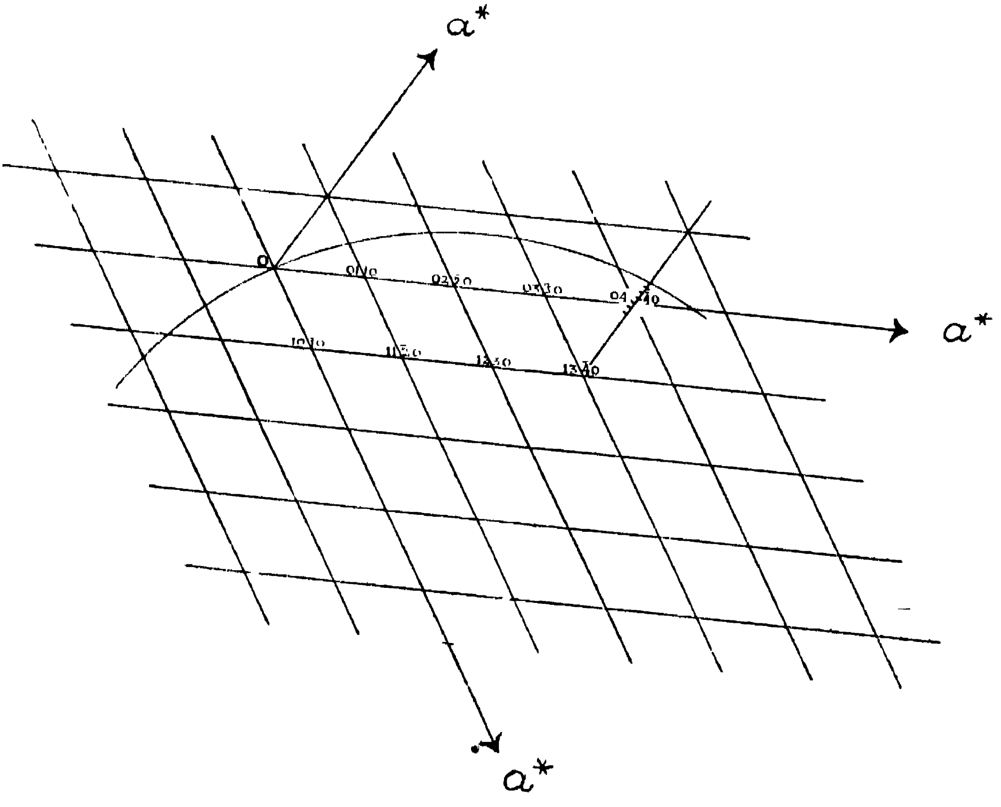

FIG. 2

The diagram represents points where the directions corresponding to the extra maxima meet the sphere of reflection

In the case of the streaks it is observed that in a particular photograph the different points of maximum intensity in the streaks (along the length of the streak) correspond to points of the reciprocal lattice lying on the line of intersection of the planes parallel to a*c* planes by the sphere of reflection. The present measurements, therefore, show that the reflecting regions around the reciprocal lattice points are like plane sheets parallel to the a*c* planes with regions of much stronger scattering along the a* axes. The small dimensions of the extra spots indicate that the strong scattering regions are fairly sharp extensions along the a* axes.

Again it will be seen from Tables I, II and III that the observed positions of the extra spots agree with the calculated positions of the intersections of the hypothetical layer lines due to rotation about the $[11\bar{2}0]$ axis and the [0001] axis. The angular co-ordinates μ and ϕ corresponding to the intersections of the hypothetical layer lines dues to rotation about [1120] axis and the [0001] axis were calculated from the relations,

$$\cos\alpha = \frac{h\lambda}{a} + \cos\alpha_0,$$

$$\sin\mu = \frac{l\lambda}{},$$

and

$$\cos\alpha = \cos\mu\cos\chi$$

where α = the angles between [1120] axis and the scattered rays ;

$90-\mu$ = the angle between the [0001] axis and the scattered rays ;

h, l, are the integers representing the respective orders of layer lines,

χ = projection of α in the equatorial plane (Fig 3)

$= \pm(\alpha_0 - \phi)$, α_0 being the angle between the $[11\bar{2}0]$ axis and the incident ray.

Now, the hypothetical layer lines due to rotation about $[11\bar{2}0]$ axis correspond in the reciprocal lattice to planer extensions of the reciprocal lattice points parallel to the plane normal to the $[1\bar{1}20]$ axis, *i.e.*, parallel to a*c* planes. Similarly the layer lines due to rotation about the [0001] axis correspond to planer extensions of the reciprocal lattice points parallel to the basal planes perpendicular to the [0001] axis. The intersections of these two sets of layer lines, therefore, correspond to points on the a* axes (*i.e.*, the line along which the basal planes and the a*c* planes meet). So the agreement between the observed and the calculated positions in Tables I, II and III, also proves that the extra spots are given by more or less sharp extensions of the reciprocal lattice points along the a* reciprocal lattice axes. The shape of the scattering domain around the reciprocal lattice points, therefore, shows that the derangement waves, (whether of thermal or other origin), responsible for the extra reflections, are restricted to planes parallel to the a^*c^* planes and those travelling along the a^* axes are more drastic.

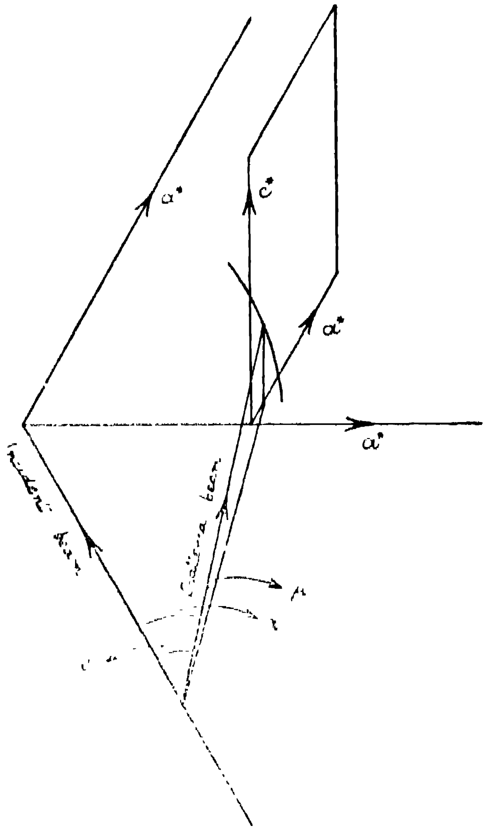

FIG. 3

DISCUSSION

From the present measurements, it has been observed that the reciprocal lattice points have sharp extensions along the a^* axes only. The extra maxima, corresponding to the intersections of the extensions parallel to c^* axes with the sphere of reflection, do not appear in any of these photographs. But in the case of the photographs taken with the X-ray beam along the [0001] axis, measurements of the angles of diffraction of the extra maxima from the photograph reproduced by Lonsdale and Smith (*loc cit*) shows that the extra maxima correspond to points where lines parallel to the c^* axes meet the sphere of reflection. Moreover, extra maxima corresponding to the points where lines parallel to a^* axes meet the sphere of reflection are not present in this photograph taken with the incident X-ray beam along the [0001] direction. The crystal used by Lonsdale and Smith is fairly large, so the extra spots are large in dimensions and consequently the presence of an extra spot separated from another by small angles cannot be decided unambiguously. In the present investigation, therefore, photographs have been taken with a very small crystal. From these photographs also, it is observed that when the X-ray beam is incident along the [0001] axis, the reciprocal lattice have extensions along c* and have no extension along a* axes. For example, in our photograph taken

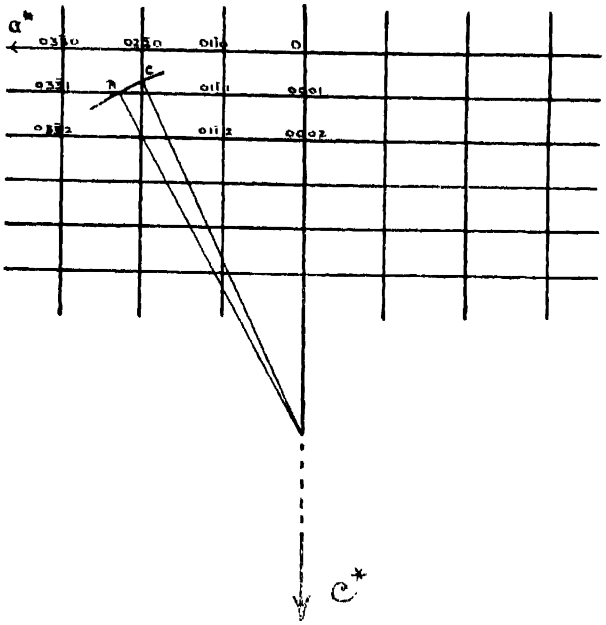

with the X-ray beam exactly along the [0001] axis, it will be observed that the position of the (0221) extra spot agrees with the position in the photograph corresponding to the intersection of the sphere of reflection with lines drawn from the (02$\bar{2}$1) reciprocal lattice point parallel to the c* axis but the extra spots corresponding to the intersection of the sphere of reflection with lines drawn from the same reciprocal lattice point parallel to a* axes are absent. Similarly in the photographs taken with the incident X-ray beam making different angles with the [0001] axis it has been obseved that the extra spots are single spots corresponding to the intersection of the sphere of reflection with the extensions of the reciprocal lattice points parallel to c* axes. From these observations it may therefore be concluded that the reciprocal lattice points have sharp extensions parallel to c* axes or a* axes according as the incident beam is perpendicular to the basal planes (planes normal to *c* axis) or lies in the basal planes.

Now, according to the thermal theories the scattering domain around the reciprocal lattice points depends only on the temperature of the crystal and it does not depend on the direction of the incident beam. The present observations, therefore, show that the extra spots do not owe their origin to the thermal vibrations. Since the pattern of extra spots of benzil depend on the direction of the beam, it is very likely that the extra spots in this case are due to vibrations set up by the incident X-ray beam. The vibrations set up are probably elastic vibrations which are quenced at the temperature of the liquid air. This will account for the disappearance of the extra spots of benzil at the temperature of the liquid air observed by Lonsdale and Smith.

TABLE I

Showing positions of the $(0\bar{4}40)$ and $(4\bar{4}00)$ extra spots

Angle between the incident X-ray beam and the [1010] axis	Angle of mis-setting $\Delta(\theta_1-\theta_0)$	Observed angle of diffraction corresponding to the extra maxima	Calculated angles corresponding to the intersection of the hypothetical layer lines due to rotation about [11$\bar{2}$0] axis and [0001] axis	Calculated angles corresponding to the intersection of the hypothetical layer lines due to rotation about [1210] axis and the [0001] axis
0°6′	4°48′	47°25′	47° 22′	......
0°6′	4°48′	52°18′	......	52°26′
0°6′	5° 0′	47°18′	47° 17′	......
0°6′	5° 0′	52°25′	......	52°32′
1°0′	3°54′	47°59′	47°50′	......
1°0′	3°54′	51°59′	......	52° 0′
1°0′	5°54′	46°44′	46°53′	......
1°0′	5°54′	53° 0′	......	52°59′
2°0′	2°54′	48°13′	48°22′	......
2°0′	2°54′	51°10′	......	51°31′
2°0′	6°54′	46°30′	46°27′	......
2°0′	6°54′	53°21′	......	53°30′
3°0′	1°54′	50°53′	......	51° 3′
3°0′	7°54′	53°58′	......	54° 2′
6°0′	−1° 6′	49°35′	......	49°46′
8°0′	−3° 6′	49° 2′	......	48°58′
10°0′	−5° 6′	48°17′	......	48°14′
12°0′	−7° 6′	47°40′	......	47°33′
15°0′	−10°6′	46°31′	......	46°37′

R. K. SEN

PLATE X

LAUE PHOTOGRAPHS OF BENZIL

[0001] Vertical

Cylindrical Camera Radius 5 cm

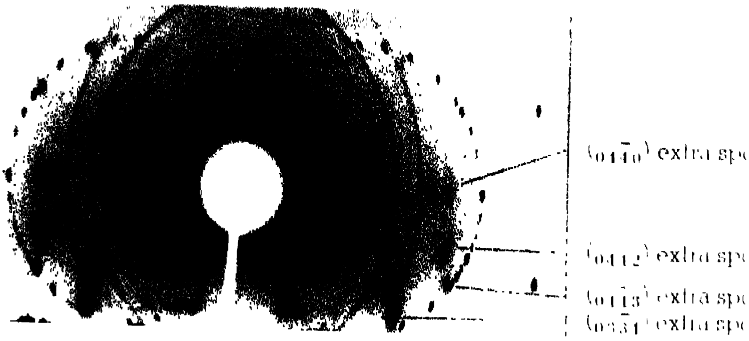

X-ray beam along $[10\bar{1}0]$ direction

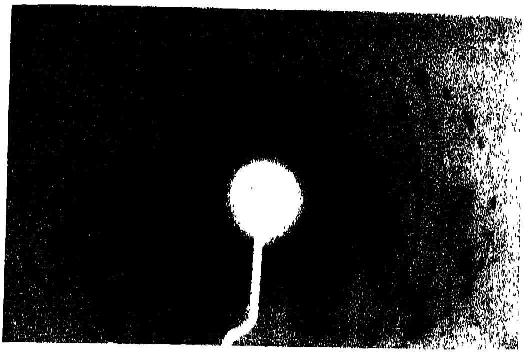

X ray beam making 1° with $[10\bar{1}0]$.

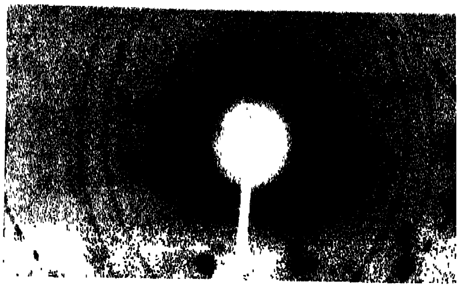

X-ray beam making with $[10\bar{1}0]$.

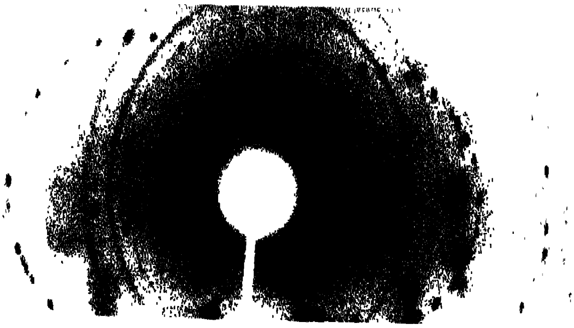

X-ray beam making 2° with $[10\bar{1}0]$

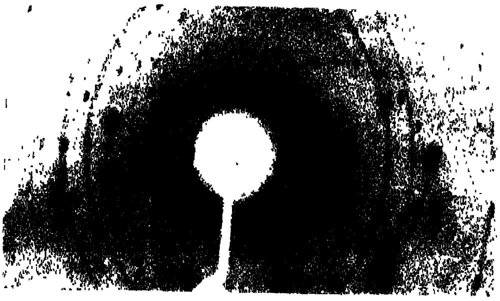

LAUE PHOTOGRAPHS OF BENZIL

[0001] Vertical

Cylindrical Camera—Radius 5 cm

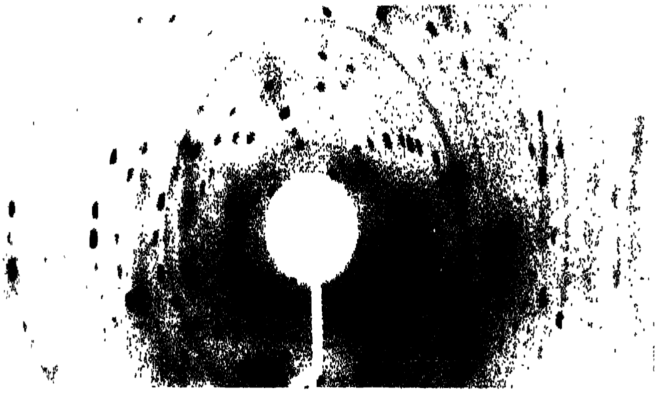

X-ray beam making 10 with [1010].

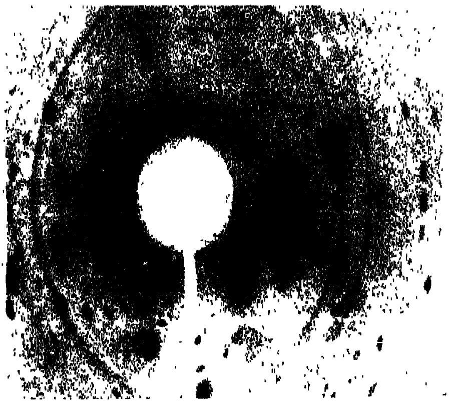

X-ray beam making 12° with [10$\bar{1}$0]

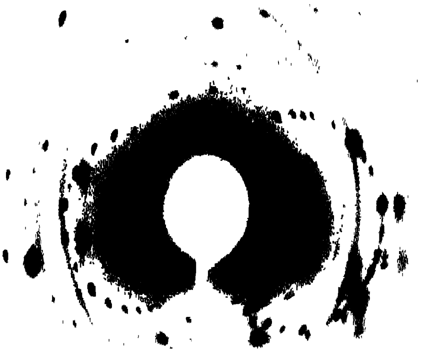

X-ray beam making 8° with [10$\bar{1}$0].

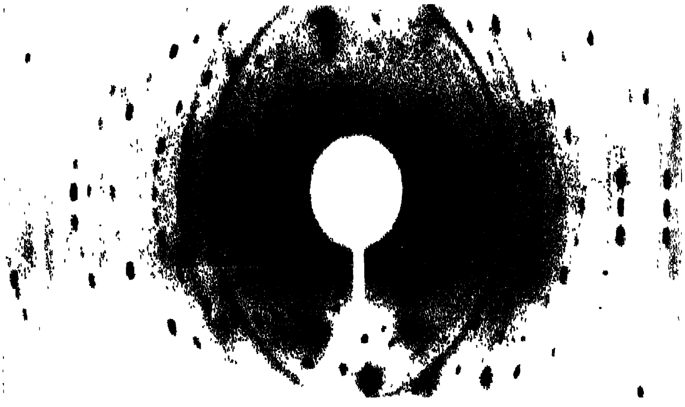

X-ray beam making 15 with [10$\bar{1}$0].

TABLE II

Showing positions of the non-equatorial extra spots from (0442), (0332), and (0333) planes

Angle between the incident X-ray beam and the [1010] axis	Indices of the planes giving rise to the extra spots	Observed horizontal angular co-ordinates ϕ of the extra maxima	Calculated values of ϕ corresponding to the intersection of the hypothetical layer lines due to rotation about the [1210] and [0001] axes	Observed vertical angular coordinates μ of the extra axima	Calculated values of μ corresponding to the hypothetical layer lines due to rotation about [0001] axis
0°6′	(0442)	52°4′	52°14′	12°43′	12°55′
1°0′	(0442)	51°30′	51°48′	12°43′	12°55′
2°0′	$(0\bar{4}42)$	50°56′	51°20′	12°43′	12°55′
3°0′	$(0\bar{4}42)$	50°41′	50°53′	12°56′	12°55′
6°0′	$(0\bar{4}42)$	50° 0′	49°52′	12°44′	12°55′
6°0′	$(0\bar{3}33)$	37°52′	38° 7′	10°45′	19°36′
8°0′	$(0\overline{44}2)$	49°14′	48°53′	12°43′	12°55′
8°0′	$(0\bar{3}32)$	37°53′	37°56′	12°56′	12°55′
10°0′	$(0\bar{3}33)$	37° 0′	36°49′	19°34′	19°36′

TABLE III

Showing positions of the non-equatorial $(0\bar{1}13)$ and $(0\bar{1}\bar{1}4)$ extra spots

Angle between the incident X-ray beam and the $[10\bar{1}0]$ axis	Indices of the plane giving rise to the extra spot	Observed horizontal coordinates ϕ of the extra maxima	Calculated values of ϕ corresponding to the intersection of the hypothetical layer lines due to rotation about the $[11\bar{2}0]$ and [0001] axes	Observed vertical angles of coordinates μ of the extra maxima	Calculated values of μ corresponding to the hypothetical layer lines due to rotation about the [0001] axis
0°6′	(0114)	12°22′	12° 8′	26°26′	26°33′
1°0′	$(0\bar{1}13)$	11°47′	11°21′	19°38′	19°36′
1°0′	(0114)	11°40′	12° 1′	26°33′	26°33′
3°0′	$(0\bar{1}14)$	11°57′	12°18′	26°27′	26°33′
8°0′	$(0\bar{1}13)$	12°15′	12° 3′	19°31′	19°36′

ACKNOWLEDGMENT

My thanks are due to Prof. K. Banerjee for suggesting the problem and his constant help during the progress of the work.

INDIAN ASSOCIATION FOR THE CULTIVATION OF SCIENCE,
210, BOWBAZAR STREET, CALCUTTA.

REFERENCES

Banerjee, K., Sen, R. K and Khan, Md. Ferdouse (1945), *Proc. Nat. Inst. Sci. Ind.*, **11**, 4.
Ganguly, M (1942), *Proc. Nat. Inst. Sci. Ind.*, **8**, 389.
Lonsdale, K. and Smith, H (1941), *Proc. Roy. Soc.*, **A 179**, 8.

COMPARATIVE STUDIES OF *JOSHI-EFFECT* UNDER SINGLE AND BI-PHASE HALF-WAVE DETECTION

By BIND BASNI PRASAD

(Received for publication June [illegible])

ABSTRACT. Production of *Joshi-effect* Δi, *viz.*, an instantaneous and reversible photo-variation (usually diminution) of current i in chlorine excited by a 50 cycle transformer discharge, has been studied under single and bi-phase half-wave detection with a double diode (6H6). The current in dark in the latter was comparatively low, while net and relative *Joshi-effect* were greater. Based on a partial interference of even harmonics of i an explanation is developed for the observed decrease of conductivity and increase of Δi and $\%\Delta i$ under bi-phase detection.

INTRODUCTION

The marked significance of this effect Δi in halogens and some other gases due to a given exciting potential V (Joshi, 1942, 1943*a*), as a hitherto unrecognised factor in current theories of photo-electric and discharge phenomena; and especially the dependence of its magnitude on the nature of the current indicator, have been emphasised by Joshi (1943*a*, 1945*a* 1945*b*). The latter influence was observed in a striking manner by the writer in a study of this effect under uni- and bi-electrode excitations (Prasad, 1946). In the present work, a study has been made of the influence of the nature of the impedance of the current indicator on the corresponding value of the *Joshi-effect* in single and bi-phase detections, which correspond to half and full-wave detections.

EXPERIMENTAL

The general experimental arrangement and the circuit employed are shown in Fig. 1. A Siemens' type ozoniser filled at about 300 mm pressure with purified chlorine, was excited at potentials varied in the range 4 to 10 kV (r. m. s.) at 50 cycle frequency. The discharge current i was admitted to the primary of a Bell transformer. A double diode 6H6 (RCA) was used as the detector; its cathodes were connected together through a D. C. millimeter to the centre of the transformer secondary. Three series of observations under single and bi-phase detections, of the plate current were carried out when the ozoniser in dark (i_D), and irradiated (i_L), with the arrangements (*ii*), (*iii*), (*iv*) described later. Using each of these circuits, the net *Joshi-effect* Δi is given by $i_D - i_L$; $100\,\Delta i/i_D$ denotes the relative *Joshi-effect* $\%\Delta i$.

Only one of the typical sets of these results is returned in Tables I, II and III and (in part) expressed graphically in Figs. 2, 3 and 4.

(*ii*) The diode was coupled inductively with the low tension line of the ozoniser circuit by means of the Bell transformer. In single phase detection, both the plates were connected at α in Fig. 1 to the same secondary.

Fig. 1 Joshi-effect under Single and Bi-phase Detection

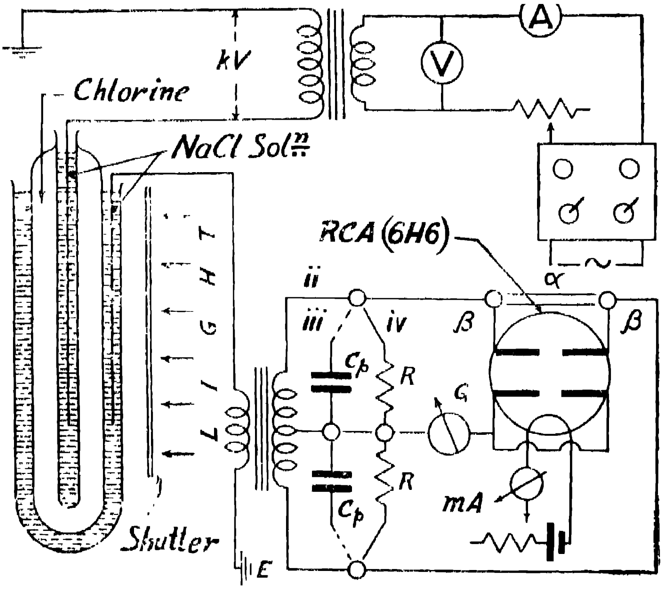

Fig. 2 Single and Bi-phase Detection of Joshi-effect (Inductive Coupling)

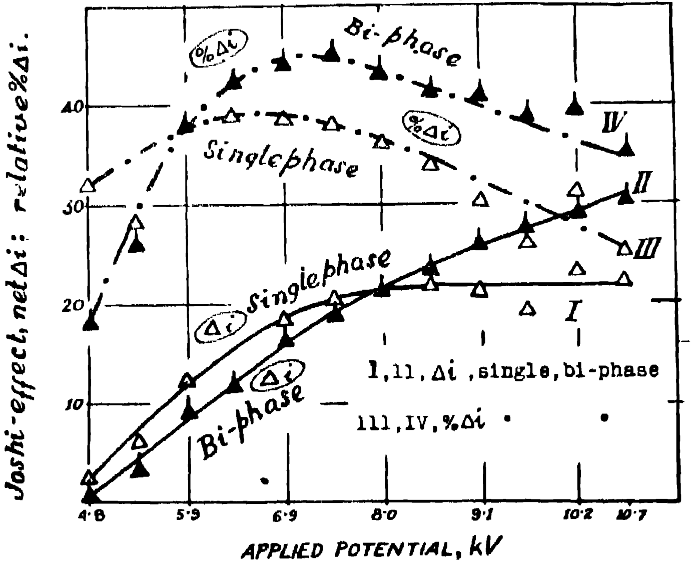

Fig.3 Single and Bi-phase Detection of Joshi-effect (Inductive-Capacitative Coupling)

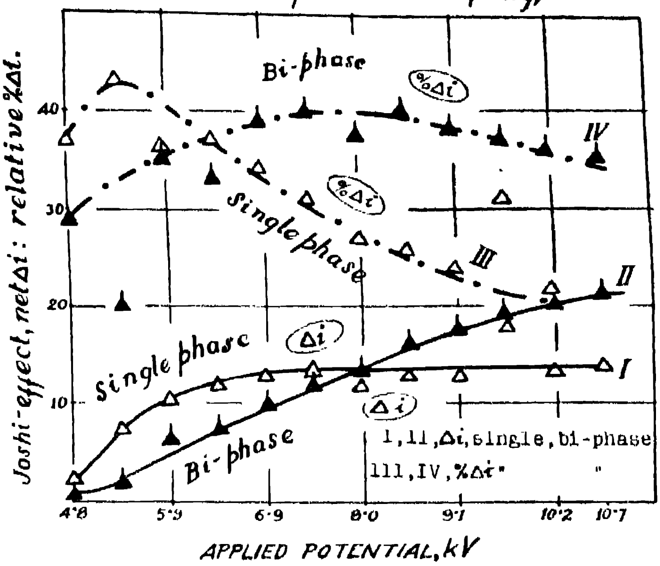

TABLE I

Potential-variation of the *Joshi-effect* in Single and Bi-phase half-wave Detection : Inductive Coupling

kV	i_0		i_1		Δi		$\%\Delta i$	
	$^1\phi$	$^2\phi$	$^1\phi$	$^2\phi$	$^1\phi$	$^2\phi$	$^1\phi$	$^2\phi$
4.8	8.5	3.3	5.8	2.7	2.7	0.6	31.8	18.2
5.3	21.5	11.7	15.5	8.7	6.0	3.0	27.9	25.6
5.9	33.0	23.0	20.5	14.3	12.5	8.7	37.9	37.8
6.4	41.5	27.5	25.5	16.0	16.0	11.5	38.6	41.8
6.9	48.0	36.0	29.5	20.0	18.5	16.0	38.5	44.4
7.5	53.5	42.0	33.0	23.0	20.5	19.0	38.3	45.2
8.0	58.5	49.0	37.5	28.0	21.0	21.0	35.9	42.9
8.5	64.5	56.0	42.5	33.0	22.0	23.0	34.1	41.1
9.1	69.5	63.0	48.5	37.5	21.0	25.5	30.2	40.5
9.6	74.0	70.0	55.0	43.0	19.0	27.0	25.7	38.6
10,2	79.5	79.0	56.5	48.0	23.0	31.0	28.9	39.2
10.7	87.5	85.0	65.5	55.0	22.0	30.0	25.1	35.3

$^1\phi$ = Single phase ; $^2\phi$ = Bi-phase

Fig. 4 Single and Bi-phase Detection of Joshi-effect (Inductive-Resistive Coupling)

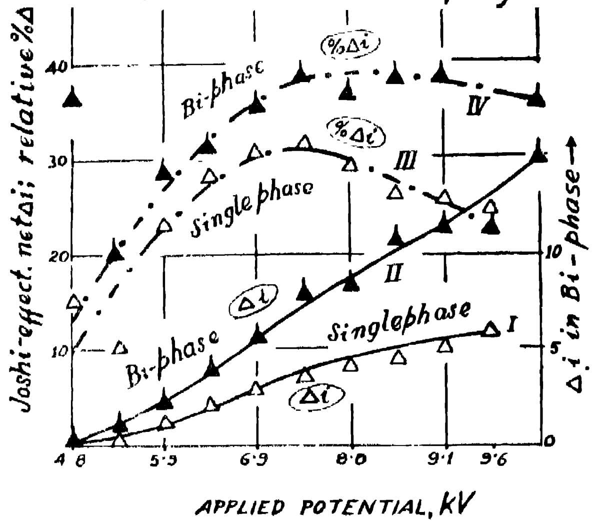

TABLE II

Potential-variation of the *Joshi-effect* in Single and Bi-phase half-wave Detection : Inductive-Capacitative Coupling

kV	i_0		i_L		Δi		$\%\Delta i$	
	$^1\phi$	$^2\phi$	$^1\phi$	$^2\phi$	$^1\phi$	$^2\phi$	$^1\phi$	$^2\phi$
4.8	5.4	3.1	3.4	2.2	2.0	0.9	37.0	29.0
5.3	17.2	9.0	9.7	7.2	7.5	1.8	43.6	20.0
5.9	28.0	16.5	18.0	10.5	10.0	6.0	35.7	36.3
6.4	32.5	22.2	20.5	14.8	12.0	7.4	36.9	33.3
6.9	37.5	25.5	24.5	15.5	13.0	10.0	34.7	39.2
7.5	41.5	30.0	28.5	18.0	13.0	12.0	31.3	40.0
8.0	44.5	35.0	32.5	22.0	12.0	13.0	26.9	37.1
8.5	49.5	41.0	36.5	24.5	13.0	16.5	26.3	40.2
9.1	53.5	45.5	40.5	28.0	13.0	17.5	24.3	38.5
9.6	57.0	50.5	38.5	31.5	18.5	19.0	31.6	37.6
10.2	61.5	55.0	48.0	35.0	13.5	20.0	21.9	36.4
10.7	65.5	60.0	51.5	39.0	14.0	21.0	21.3	35.0

$^1\phi$ = Single phase ; $^2\phi$ = Bi phase

In the bi-phase detection, they were connected separately at β, β. One of the series of results for i_0, i_L, Δi and $\%\Delta i$ in single phase and bi-phase detection using this circuit, in the potential range mentioned above, is shown in Table 1. In Fig. 2 the variation of Δi and $\%\Delta i$ under both detections are shown gra-phically as a function of the applied potential in kV.

TABLE III

Potential-variation of the *Joshi-effect* in Single and Bi-phase half-wave Detection : Inductive-Resistive Coupling

kV	i_0		i_L		Δi		$\%\Delta i$	
	$^1\phi$	$^2\phi$	$^1\phi$	$^2\phi$	$^1\phi$	$^2\phi$	$^1\phi$	$^2\phi$
4 8	2 7	1.1	2 3	0 7	0.4	0 4	14.8	36.4
5 3	6.0	4.0	5.4	3 2	0.6	0.8	10.0	20.0
5.9	11 0	8 4	8.5	6 0	2 5	2.4	22.7	28.6
6 4	16 0	12 5	11.5	8 6	4 5	3.9	28.1	31.2
6.9	20.9	16.1	14.5	10 4	6 4	5 7	30.6	35.4
7.5	24.6	20 0	17.2	12.3	7.4	7 7	30.8	38.5
8.0	29 5	22.8	20.9	14.5	8,6	8.3	29.2	36.4
8.5	35.0	27.8	26.0	17.0	9 0	10.5	25.7	37.8
9.1	41.0	30.0	30.5	18.5	10 5	11.5	25.6	38.3
9.6	49.0	36.2	37.0	25.0	12.0	11.2	24.5	30.9
10.2	...	42.0	...	27.0	...	15.0	...	35.7
10.7	...	...	...	...	...	...	...	...

$^1\phi$ = Single phase ; $^2\phi$ = Bi-phase

(*iii*) In this arrangement, the circuit in (*ii*) was modified by introducing a by-pass, 100 $\mu\mu$F, condenser between the plates and the cathode-line before the D. C. indicator, in single phase detection ; in bi-phase detection, at the same position two equal condensers of 100 $\mu\mu$F were connected to the plates on either side of the cathode-line as shown in Fig. 1 (*iii*). These results are returned in Table II and by curves for Δi and $\%\Delta i$ against kV in Fig. 3.

(*iv*) The centre of the transformer secondary was left un-connected and the capacities were replaced by equal Dubilier resistances of 4 kilo-ohms at *iv* in Fig. 1. The results are shown in Table III and graphically in Fig. 4.

DISCUSSION

The threshold potential V_m (Joshi, 1929, 1944*a*) near which the system breaks down as a dielectric and below which Δi is not appreciable was found

STUDIES OF THE OPTICAL PROPERTIES OF SOME ORGANIC CRYSTALS

By M. N. DATTA

Received for publication, Oct 1, 1947

ABSTRACT. The directions of the optical principal directions of the monoclinic crystals anthraquinone and naphthalene tetrachloride have been determined for three different wave-lengths in the green, yellow and red regions of the spectrum The principal refractive indices for these wave lengths have been determined for the crystals of anthraquinone meta-dinitrobenzene, phloroglucine dihydrate and naphthalene tetrachloride.

INTRODUCTION

The optical properties of crystals have attracted the attention of physicists and mineralogists from very early days of science. Recently the subject is receiving renewed interest owing to its importance in the determination of the atomic arrangements inside crystals. This can particularly be said about aromatic organic crystals where the optical properties give indications of the orientations of the benzene rings inside the crystals. Accordingly, a systematic investigation into the optical properties of organic crystals have been undertaken in this laboratory.

Of the four crystals that we have studied, two, namely, anthraquinone and naphthalene-tetrachloride belong to the monoclinic system and other two, namely metadinitrobenzene and phloroglucine dihydrate belong to the orthorhombic system. So, for the former crystals it has been necessary to determine the directions of the principal axes, while in the latter they are fixed along the directions of the crystallographic axes. For the monoclinic crystals, however, the monoclinic axis is one of the principal axes while the other two, which are at right angles to each other, lie in a plane normal to this axis. For the determination of the directions of these basal axes, the crystal was mounted on Fedorov stage, placed between crossed nicols of a polarising microscope, and the crystal was rotated about the direction until extinction was observed. The angle between the direction of the electric vector of the polarised light and a crystal edge is measured accurately and hence the directions of the principal axes are fixed. For the determination of the principal refractive indices, the Becke method has been utilised. For this purpose the crystal is immersed in a drop of a liquid, whose refractive index is intermediate between two principal indices of the crystal, and is mounted on the Fedorov stage with the plane containing the two principal directions normal to the axis of the optical system. The crystal is illuminated by polarised light and is rotated about the axis of the optical system until the Becke line just disappears. This is repeated for another liquid of intermediate refractive index. The two principal refractive indices α and β are given by the relation,

$$(i)\quad \alpha^2 = \frac{n_1^2 n_2^2 \cos^2\theta_2 \sin^2\theta_1 - n_1^2 n_2^2 \sin^2\theta_2 \cos^2\theta}{n_1^2 \sin^2\theta_1 - n_2^2 \sin^2\theta_2}$$

$$(ii)\quad \beta^2 = \frac{n_1^2 n_2^2 \cos^2\theta_1 \sin^2\theta_2 - n_1^2 n_2^2 \cos^2\theta_2 \sin^2\theta_1}{n_1^2 \cos^2\theta_1 - n_2^2 \cos^2\theta_2}$$

where n_1 and n_2 are the refractive indices of the two liquids and θ_1 and θ_2 are the angles between the first principal axis and the directions of the electric vectors for the disappearance of the Becke lines.

In some crystals it is not convenient to determine all the three refractive indices by this method. In such cases the optic axial angle is determined on the Fedorov stage. This gives us a further relation between the principal refractive indices, α, β and γ,

$$\frac{\gamma}{\alpha}\sqrt{\frac{\alpha^2 - \beta^2}{\beta^2 - \gamma^2}} = \operatorname{Tan} V_\alpha$$

where V_α is half the optic-axial angle

All the measurements were carried out for three parts of the spectrum namely, red, yellow and green. Red light was obtained from an incandescent electric lamp by filtering through two parallel walled glass vessels, (each 15 mm. thick) one containing .005 gm of crystallised violet and the other 10 gms. of potassium chromate both dissolved in 100 cc. of water.

The mean wave-length of the transmitted light is 656 μμ. Yellow light was obtained from a sodium arc lamp which gives a wave-length of 589 μμ. For the green light a mercury arc with a filter of three parallel walled glass vessels (each 15 mm. thick), one containing 10 gms. of potassium chromate, and each of the other two 0.025 gms. of potassium permanganate, each of them dissolved in in 100 c.c. of water was used. The transmitted wave-length is 546 μμ.

OPTICAL PROPERTIES OF ANTHRAQUINONE

Anthraquinone crystal was previously regarded as belonging to the orthorhombic system but Sen from his X-ray studies (1940) found that it really belongs to the monoclinic system which was confirmed by goniometric and optical measurements. The c-axis, according to Groth's terminology, has been found to be the only symmetry direction and so this is one of the principal optical directions. The directions designated by *a* and *b* of Groth were considered, in conformity with the supposed orthorhombic character of the crystal, to be the other two principal axes. It was shown by Sen that for sodium light the real principal axes in this plane make an angle of 16° with these two axes respectively. The results that have been obtained by us for the three different wave-lengths with the improved method of measurement are given in Table I.

TABLE I

Mean λ	Angle between Groth's '*a*' axis and a principal optic direction	Semi-optic-axial angle
546μμ	15°35′40″	71°23′
589μμ	16° 5′40″	71°45′
656μμ	17°35′40″	72° 6′

The optic axial plane was found to be normal to the principal direction nearest to Groth's '*a*' axis and the semi-optic-axial angle V is given in the third column of the Table I.

The refractive indices along the principal directions normal to the symmetry axis were determined by the Becke method and the other direction by utilising the value of V determined as above. The results are given in Table II. The refractive index along the principal direction nearest to Groth's '*a*' axis has the highest value and hence it is designated as α according to the usual convention. The symmetry axis has the lowest refractive index which is accordingly designated as γ.

TABLE II

Mean λ	α	β	γ
589μμ	1·816	1·698	1·506
656μμ	1·806	1·690	1·500

These results indicate that the planes of the benzene rings are very close to the α-direction while they are nearer to the β-direction than to the γ-direction. These results agree with those obtained by Sen.

OPTICAL PROPERTIES OF *m*-DINITROBENZENE

Crystallographic data

Orthorhomb. Bipyr. V_h^{16}

$Z=4$

$a=13{\cdot}27$A, $b=14{\cdot}00$A, $c=3{\cdot}82$A.

Measurement.—Face angles of *m*-dinitrobenzene were measured by one circle goniometer and its axes were recognised. A single crystal with its *c*-axis (long axis) horizontal is placed on flat face *a* on Fedorov universal stage between the crossed nicols. The principal refractive indices, along the *b*-axis and *c*-axis were determined by the method of disappearance of Becke line as described above.

Refractive index along the remaining principal direction was determined from the variation in refractive index with change of angular position in a symmetry plane of the triaxial ellipsoid.

The maximum and minimum refractive indices were found to be along the *c* and the *a*-axes respectively. The values of the principal refractive indices are given in Table III where α, β and γ according to convention represent refractive indices along the *c*, *b*, and *a*-axes respectively.

TABLE III

Mean λ	α	β	γ
546μμ	1·434	1·707	1·842
589μμ	1·432	1.766	1·839
656μμ	1·430	1·764	1·835

OPTICAL PROPERTIES OF PHLOROGLUCINON DIHYDRATE

Measurement of the principal refractive indices were carried by the same method as that used for metadinitrobenzene.

The maximum and minimum refractive indices are along the *b* and the *a* axes respectively and hence according to usual convention α, β and γ represent the principal refractive indices along *b*, *c* and *a*-directions. The refractive indices are given in Table IV.

TABLE IV

Mean λ	α	β	γ
546μμ	1·692	1·689	1·499
589μμ	1·659	1·648	1·481
656μμ	1·629	1·607	1·464

OPTICAL PROPERTIES OF NAPHTHALENE TETRACHLORIDE

The angle between the crystallographic axes and the principal axes in the plane (010) were measured in the same way as was done in the case of anthraquinone crystal. The angle between principal plane with *m*-face (110 or 1̄10) is actually measured and from that angle with *a*-axis is calculated as angle between the *m*-face and the *a*-axis. The results are given in Table V.

TABLE V

Mean λ	Angle between a principle direction and '*a*' axis
546μμ	2°16′
589μμ	1°28′
656μμ	0°34′

The three principal refractive indices were determined by the same method as in the cases of metadinitrobenzene and phloroglucine dihydrate the results are given Table VI.

TABLE VI

Mean λ	α	β	γ
546μμ	1·793	1·775	1·534
589μμ	1·786	1·766	1·528
656μμ	1·779	1 756	1·523

α_1, β and γ represent the refractive indices corresponding to the principal directions close to the *a* and *c*-axes and along the *b*-axis respectively.

ACKNOWLEDGMENTS

Thanks are due to Prof. K. Banerjee for suggesting the problem and his constant help during the progress of the work. Thanks are also due to the authorities of the Indian Association for the Cultivation of Science for awarding the author a scholarship.

INDIAN ASSOCIATION FOR THE CULTIVATION OF SCIENCE,
CALCUTTA.

REFERENCE

Sen, S. N., 1940, *Science and Culture*, **5**, 719

A NOTE ON THERMAL FLUCTUATION

By DULEH SINGH KOTHARI and LAXMAN SINGH KOTHARI

(*Received for publication, July [illegible], 1947*)

ABSTRACT. In the present note the problem of fluctuation of energy in a stream of radiation and particles has been treated on the basis of the general distribution law, for Bose-Einstein and Fermi Dirac Statistics. Section 1 mentions the distribution law and gives values of several constants for the extreme relativistic and non-relativistic cases. In section 2 is discussed the energy fluctuation in a fixed volume. The expressions for the fluctuations in energy in a beam crossing an area, are derived in the next section. The last section deals with the entropy of a beam It is noted therein that the entropy is finite for a beam of zero intensity and also that a beam of finite intensity but zero entropy is possible.

1. INTRODUCTION

In a recent paper by W. B. Lewis (1947) entitled 'Fluctuations in a Stream of Thermal Radiation,' expressions have been derived for fluctuations of energy in a radiation beam and for the minimum detectable power by an isolated body, connected to surroundings only by radiation. In the present note the problem is discussed on the basis of the general distribution law

$$n(\epsilon)d\epsilon = \frac{D\epsilon^{s-1}d\epsilon}{(e^{\epsilon/kT}+\beta)}, \qquad \dots \quad (1)$$

where $n(\epsilon)d\epsilon$ is the number of particles lying within the energy range ϵ and $\epsilon+d\epsilon$; in volume v, of an assembly which is assumed to be at a temperature T, k is Boltzmann's constant, $\beta=1$ for Fermi-Dirac Statistics and $\beta=-1$ for Bose-Einstein Statistics, s is a positive number exceeding unity, and D is another constant whose value depends upon the specific character of the particles constituting the assembly. The values of D and s for the cases of interest are given below:

(*a*) $D=\frac{4\pi v g}{h^3}$; $s=3$ where g is the weight factor. This is the extreme relativistic case and writing $\beta=-1$ and $\epsilon=h\nu$ we get the Planck's Radiation formula.

(*b*) $D=\frac{(4\sqrt{2})\pi m^{\frac{3}{2}}v}{h^3}g$; $s=\frac{3}{2}$, where m is the mass of the particle and g its weight factor due to spin. This corresponds to the extreme non-relativistic case.

The general case corresponding to the distribution law, $n(\epsilon)d\epsilon=\frac{D\epsilon^{s-1}d\epsilon}{(\frac{1}{A}e^{\epsilon/kT}+\beta)}$ (A being the degeneracy parameter) will be discussed in a subsequent paper.

The last section deals with the entropy of a stream of particles (or quanta). We shall follow as far as possible Lewis' treatment

2. ENERGY FLUCTUATION IN A FIXED VOLUME

From the theory of fluctuations it is known that the mean-square fluctuation of the number of particles (or quanta) confined to the volume v is

$$\Delta n^2 = \left(n - \beta \frac{n^2}{N} \right), \qquad \ldots \quad (2)$$

where N is the total number of independent cells in the relevant phase-space and n the number of particles (or quanta). The mean-square energy fluctuation of the particles of energy ϵ is given by

$$E^2 = \epsilon^2 \Delta n^2.$$

From the equations (1) and (2), we have

$$\overline{E^2} = n\epsilon^2 - \beta \frac{n^2 \epsilon^{s+1}}{D} \frac{1}{d\epsilon}, \qquad \ldots \quad (3)$$

Taking η_0 to be the mean energy, we write

$$\eta_0 = n\epsilon. \qquad \ldots \quad (4)$$

The general distribution law then yields

$$\eta_0 = \frac{D\epsilon^s d\epsilon}{(e^{\epsilon/kT} + \beta)}, \qquad \ldots \quad (5)$$

Making proper substitutions from the equations (4) and (5), the relation (3) becomes

$$\overline{E^2} = \eta_0 \epsilon \left[1 - \frac{\beta}{e^{\epsilon/kT} + \beta} \right]. \qquad \ldots \quad (6)$$

In this expression if we put $\beta = 1$, we get $\overline{E^2}$ for a Fermi-Dirac assembly and if β is taken to be -1, Lewis' expression for radiation is obtained.

It may be noted that in case $\epsilon >> kT$, the second term in (6) is negligible and $E^2 = \eta_0 \epsilon$, which is the classical result. However, the second term predominates if $\epsilon << kT$.

Now to obtain the total energy fluctuation we substitute the value of η_0 from (5) in (6) and integrating over the entire range we get

$$\overline{\Delta E_v^2} = D \int_0^\infty \frac{\epsilon^{s+1} e^{\epsilon/kT}}{(e^{\epsilon/kT} + \beta)^2} d\epsilon.$$

Putting $\xi = \frac{\epsilon}{kT}$ the above equation becomes

$$\overline{\Delta E_v^2} = D(kT)^{s+2} \int_0^\infty \frac{\xi^{s+1} e^\xi d\xi}{(e^\xi + \beta)^2}. \qquad \ldots \quad (7)$$

writing $y=\dfrac{\xi^{s+1}}{c\xi+\beta}$, we have

$$\overline{\Delta E_v^{\,2}}=D(kT)^{s+2}\left[\int_0^{\infty}\frac{(s+1)\xi^{s}\,d\xi}{c\xi+\beta}-\int_0^{\infty}dy\right].$$

The second integral vanishes at both the limits and so

$$\overline{\Delta E_v^{\,2}}=D(s+1).(kT)^{s+2}\int_0^{\infty}\frac{\xi^{s}\,d\xi}{(c\xi+\beta)}. \qquad \ldots \quad (8)$$

It may be noted that

$$\int_0^{\infty}\frac{\xi^{s}\,d\xi}{(c\xi+\beta)}=\lfloor\!\overline{s+1}\,\zeta(s+1)\ldots\ldots(\text{B. E. S.})=(1-\tfrac{1}{2}s)\lfloor\!\overline{s+1}\,\zeta(s+1)\ldots\ldots(\text{F. D. S.}),$$

where ζ is the Reimann-Zeta function : $\zeta(s)=\sum\limits_{n=1}^{\infty}\dfrac{1}{n^{s}}$

In this equation if we put the values of the various constants corresponding to the B. E. S., we get (which is Lewis' equation (8))

$$\overline{\Delta E_v^{\,2}}=\frac{(2\pi kT)^5}{15c^3h^3}\,v.$$

By the application of Stefan's law we have $\overline{\Delta E_v^{\,2}}=4E_T kTv$, where E_T is the energy density of full black-body radiation of temperature T.

In the extreme non-relativistic case equation (8), on substituting the values of the various constants, reduces to

$$\overline{\Delta E_v^{\,2}}=\frac{8\sqrt{2}\,\pi m^{\frac{3}{2}}}{h^3}\,v(kT)^{\frac{7}{2}}\frac{5}{2}\left(1-\frac{1}{2\sqrt{2}}\right)\lfloor\!\overline{\tfrac{5}{2}}\,\zeta(\tfrac{5}{2})$$

$$=\tfrac{5}{2}B_1 v\frac{(kT)^{\frac{7}{2}}}{h^3}\cdot m^{\frac{3}{2}} \qquad \ldots \quad (9)$$

where $$B_1=8\sqrt{2}\,\pi\left(1-\frac{1}{2\sqrt{2}}\right)\lfloor\!\overline{\tfrac{5}{2}}\,\zeta'(\tfrac{5}{2}).$$

To express $\overline{\Delta E_v^{\,2}}$ in terms of the energy density, we proceed to find an expression for the same. The energy density is

$$E_T=\frac{8\sqrt{2}\,\pi m^{\frac{3}{2}}}{h^3}\int^{\infty}\frac{\epsilon^{\frac{3}{2}}}{e^{\epsilon/kT}+1}\,d\epsilon.$$

writing $\xi=\dfrac{\epsilon}{kT}$, we have

$$E_T=\frac{8\sqrt{2}\,\pi}{h^3}(kT)^{\frac{5}{2}}m^{\frac{3}{2}}\int_0^{\infty}\frac{\xi^{\frac{3}{2}}}{c\xi+1}\,d\xi=\frac{B_1 m^{\frac{3}{2}}(kT)^{\frac{5}{2}}}{h^3}. \qquad \ldots \quad (10)$$

Equations (9) and (10) yield

$$\overline{\Delta E_v^{\,2}}=\tfrac{5}{2}E_T kTv. \qquad \ldots \quad (11)$$

3. ENERGY FLUCTUATION IN A BEAM CROSSING AN AREA

Considering particles (or quanta) of energy ϵ moving in all directions with a velocity u, the number crossing an area a in unit time is $\frac{1}{4}n_1 ua$, where n_1 is the number per unit volume. The mean-square fluctuation of energy crossing the area is given by

$$\Delta E_a^2 = \frac{1}{4} n_1 ua\epsilon^2\left(1 - \beta\frac{n}{N}\right).$$

Since $n_0 = n_1\epsilon\tau$ we get (from equation (5)) the total energy fluctuation

$$\Delta E_a^2 = \frac{1}{4}\frac{Da}{\tau}\int_0^\infty \frac{u\epsilon^{s+1}e^{\epsilon/kT}}{(e^{\epsilon/kT}+\beta)^2}d\epsilon. \qquad \ldots \quad (12)$$

Noting that in the case of radiation $u=c$, we arrive at

$$\Delta E_a^2 = \frac{ca}{4}\frac{(2\pi kT)^5}{15c^3h^3}.$$

For particles in the non-relativistic case $u = \sqrt{\frac{2\epsilon}{m}}$ and equation (12) becomes

$$\Delta E_a^2 = \frac{4\pi ma}{h^3}\int_0^\infty \frac{\epsilon^3 e^{\epsilon/kT}}{(e^{\epsilon/kT}+1)^2}d\epsilon.$$

Writing $\xi = \epsilon/kT$ and treating the above integral in the manner adopted in evaluating the integral occurring in (7), we find

$$\Delta E_a^2 = \frac{4ma}{h^3}(kT)^4\int_0^\infty \frac{\xi^2 d\xi}{(e^\xi+1)} = B_2\frac{ma}{h^3}(kT)^4,$$

where $$B_2 = 4\pi\left(1-\frac{1}{2^2}\right)3\zeta(3).$$

Expressing the value of the total energy fluctuation across a in terms of the energy density, we get from eqn. (10).

$$\Delta E_a^2 = \frac{B_2}{B_1}\left(\frac{kT}{m}\right)^{\frac{1}{2}} kTE_r a. \qquad \ldots \quad (13)$$

It may be of interest to note the expression for time variation of fluctuation in a beam. If ω_a is the rate of flow of energy or power crossing area a, it can be shown that

$$\Delta\omega_{a\,t}^2 = 2\frac{B_2}{B_1}\left(\frac{kT}{m}\right)^{\frac{1}{2}} kTE_r a\Delta f,$$

where Δf is the frequency interval.

In case the amount of energy radiated by a body at temperature T is equal to the energy received, the effective mean square fluctuation of energy is doubled, and we get

$$\overline{\Delta\omega_{a\,t}^2} = 4\frac{B_2}{B_1}\left(\frac{kT}{m}\right)^{\frac{1}{2}} kTE_r a\Delta f.$$

Putting the value of E, from (10) we have

$$\sqrt{\Delta\omega^2_{r,t}} = 2\left(\frac{kT}{h}\right)^2 \sqrt{B_{2}\pi m h\Delta t} \qquad \ldots \quad (14)$$

4. ENTROPY OF A BEAM

In this section we shall derive an expression for the entropy of a beam of particles (or quanta). To simplify the problem we take the beam to be isotropic with respect to direction and concentrated within a small solid angle Δo. The energy density of such a beam is given by

$$\rho = \frac{Df\epsilon\,\Delta\epsilon\,\Delta o}{4\pi c},$$

where $f = \frac{1}{e^{\epsilon/kT}+\beta}$ and $\Delta\epsilon$ is a small interval in which the energy of the particles is confined. The intensity of such a beam is given by

$$I = \frac{Df\epsilon\,u\cos\theta}{4\pi c}\,\Delta\epsilon.\Delta o = f.\epsilon.\Delta T,$$

where $\Delta T = \frac{D\epsilon^{-1}u\cos\theta\,\Delta\epsilon.\Delta o}{4\pi c}$, θ is the angle between the direction of the beam and the normal to the area considered and u is the velocity of the particles (or quanta).

The entropy of this beam passing through unit area in unit time is given by the formula

$$S = -k\{\beta(1-\beta f)\ln(1-\beta f) + f\ln f\}\Delta T.$$

In order to find the ratio of entropy and intensity of the beam, a dimensionless quantity Q is defined by the relation

$$Q = \frac{S/k}{I/\epsilon}.$$

Using the expressions for S and I, we have

$$Q = -\frac{1}{f}\left\{\beta(1-\beta f)\ln(1-\beta f) + f\ln f\right\}. \qquad \ldots \quad (15)$$

To get a better picture we only discuss the two extreme cases. Taking the first case in which $\epsilon >> kT$ (*i.e.*, $f = e^{-\epsilon/kT} << 1$) we obtain from (15)

$$Q = \left\{1 - \beta\frac{f}{2} - \ln f\right\} = -\ln f. \qquad \ldots \quad (16)$$

Thus we find that both for particles and quanta Q tends to infinity. This signifies that the entropy is finite even for a beam of zero intensity.

Considering the other extreme case in which $\epsilon << kT$, we note that $f = 1$ in the F. D. case and corresponding to the B. E. case it is equal to $\frac{kT}{h\nu}$ $(>>1)$. Thus the two cases have to be treated separately.

In case of particles the equation (15) yields

$$Q=(1-f)\ln(1-f)=1-f. \tag{17}$$

The value of Q for photons is easily seen to be

$$Q=-\frac{\ln f}{f}.$$

We, therefore, note that both for particles and photons a beam of finite intensity but zero entropy is possible the case of photons has already been treated by Landau (1946) recently.

MAHARANA BHUPAL COLLEGE,
UDAIPUR.

REFERENCES

Landau, L., 1946, *Journal of Physics* (U. S. S. R.), Vol. X, No. 6.
Lewis, W. B., 1947, *Proc. Phys. Soc.*, **59**, 34.

BAND SPECTRUM OF CARBON DISULPHIDE—PART I. (TRIATOMIC MOLECULE, CS_2)

By C RAMASASTRY and K. R. RAO *

(*Received for publication, Sept 5, 1957*)

(Plates XIA and XIB)

ABSTRACT. The absorption bands of the vapour of carbon disulphide are photographed under different conditions of pressure and temperature in the ultra-violet using Hilger small and medium quartz instruments The behaviour of the characteristic bands of the CS_2 molecule between λλ2300-1940 has been examined and wave-length data of this system are presented in detail. Two prominent progressions are detected among the bands, only one of which was reported previously by Price and Simpson. While the Price and Simpson progression can be represented as the transition $(v, 0, 0)' \leftarrow (0, 0, 0)''$, the new progression is interpreted as corresponding to $(v, 2, 0)' \leftarrow (0, 0, 0)''$. This leads to the suggestion of a value of 235 cm^{-1} for the deformation frequency of the upper electronic state of the molecule which has a value of 400 cm^{-1} for the corresponding frequency in the ground state.

INTRODUCTION

CS_2 is one of the few polyatomic molecules, the band spectra of which have been the subject of a number of investigations. Two systems are well established in the absorption spectrum of carbon disulphide in the quartz ultra-violet. The first lies between λ3800 and λ2900. The earliest extensive work on this system is that of Wilson, (1929) who photographed the absorption bands with a Hilger quartz E 1 spectrograph under various conditions of temperature and pressure and reported wave-lengths of about 650 bands. Jenkins (1929) photographed the same bands with a 21-foot grating but could report only a partially resolved rotational structure of some of the bands. Mulliken (1941) ascribed this system to a forbidden electronic transition which becomes allowed by the vibronic selection rules, if the molecule is assumed to be slightly bent in the excited state. This explains the rotational structure of the bands, consisting of simple P and R branches, resembling those of a diatomic molecule. This rotational structure was obtained for six bands of the system by Lieberman (1941), who established them as originating from the transition ${}^1\Sigma_u^+ - {}^1\Sigma_g^+$. The vibrational analysis of the system is still far from complete as it presents an unusually large number of bands, the behaviour of which varies considerably with the temperature and pressure conditions of the vapour. But all workers who have attempted this analysis have found evidence of a frequency of about 270 cm^{-1}

---

* Fellow of the Indian Physical Society.

[Wilson (1929), Jenkins$_2$ (1929), Watson and Parker (1931), Kusch and Loomis, (1930), and Lieberman (1941)]. This frequency was supposed to be probably corresponding to ν_1' in the excited state by all the investigators except Lieberman, who has suggested that from the relative intensities of the two progressions $\nu_2''=0$ and $\nu_2''=2$, it is more likely to be the ν_2' vibration On account of the complicated nature of the spectrum no definite assignment would be possible until a complete analysis is known.

The second system, lying in the region between λ2300-λ1850, is much more intense than the first, no trace of the latter being found under conditions when intense bands are recorded at λ2100, (Plate XIB(*b*)). Mulliken (1941) attributed this system to an allowed electronic transition.

$$(\Pi\sigma\Pi)^{3}(\Pi\Pi\bar{\Pi})^{1}\ {}^1\Sigma_u^+ \leftarrow (\Pi\sigma\bar{\Pi})^{4}(\Pi\Pi\Pi)^{0}\ {}^1\Sigma_g^+$$

Besides the early work by Bruhat and Pautheimer (1924) and by Nielson (1936) the most important investigation on this system is that due to Price and Simpson (1938) These authors photographed the bands with a vacuum spectrograph in the region below λ2300 and reported the occurrence of a long progression of about sixteen bands with the mean wave-number interval of 410 cm^{-1}. The first member of this progression was located at λ 2175 or ν 45950, from experiments on temperature variation of intensities of the bands. The mean recurring value of 410 cm^{-1} was definitely assigned to the symmetrical valence frequency, $\nu_1{}'$, of the upper state, which has a value 656 cm^{-1} in the ground state, from a consideration of the selection rules and the appearance of the spectrum. Price and Simpson have also indicated that each band of this system is really built up of many components; the band at λ2080, for example, shows several heads with intervals of 40 cm^{-1}. The multiplicity of the heads was explained as due to rotational structure which arises as a result of the molecule becoming slightly bent in the upper state (about 2 or 3 degrees) and acquiring a relatively low moment of inertia. The red degradation and rotational spacing are shown to be compatible with this hypothesis.

In addition to the above mentioned two systems, Price and Simpson have obtained several other absorption bands of carbon disulphide further down below λ2000; (1) a strong band at λ1815 consisting of two components (2) a progression of seven bands between λ1750 – λ1650 with a separation of about 830 cm^{-1} (3) four bands between λ1612-λ1550, each showing a rotational structure with rotational spacing as wide as 79 cm^{-1} and (4) a complicated set of bands between λ1535 and λ1450 crowded together without any obvious regularities and various sets of diffuse bands below λ1200. Many of these extreme ultra-violet band systems* exhibit little or no vibrational structure and are ascribed to transitions of comparatively non-bonding electrons to excited orbitals which are mainly atomic in character. In contrast to this, the first two systems, mentioned earlier, are suggested to correspond to

Absorption Spectra of CS_2 (Cu arc comparison.

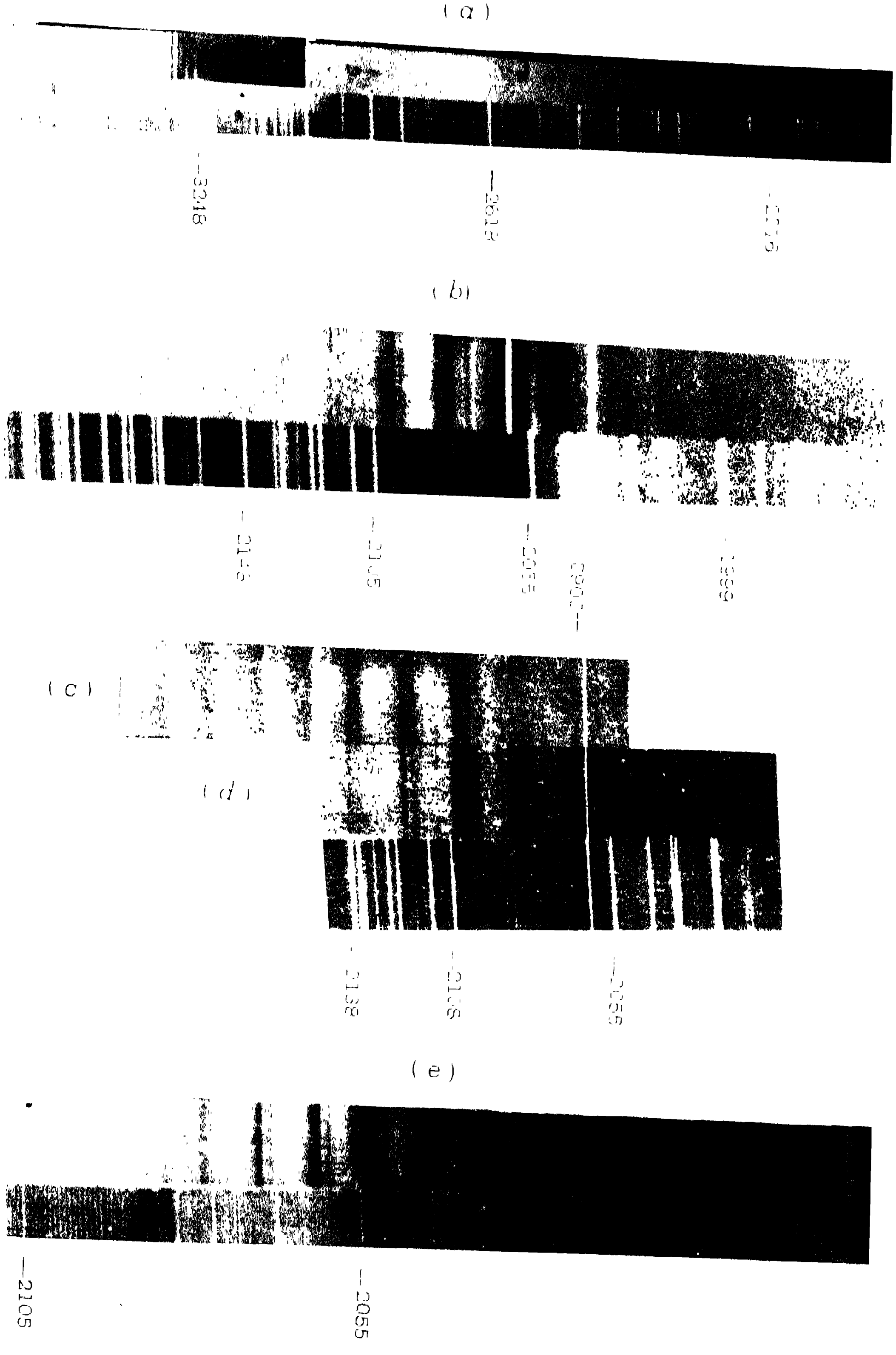

Absorption Spectra of CS_2 (Cu arc comparison.)

(a)

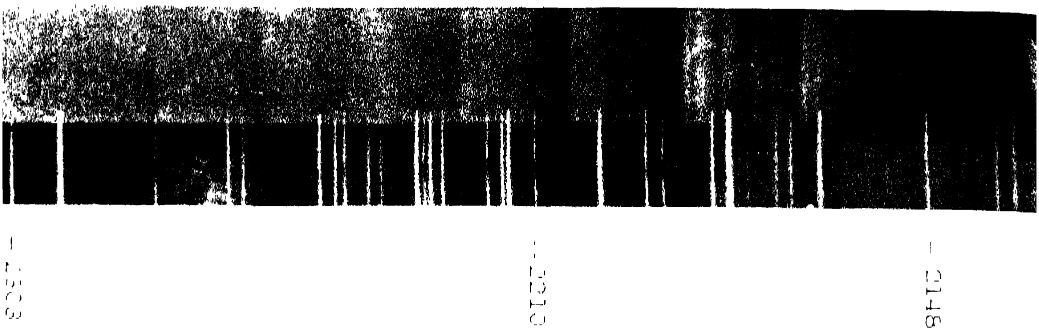

(b)

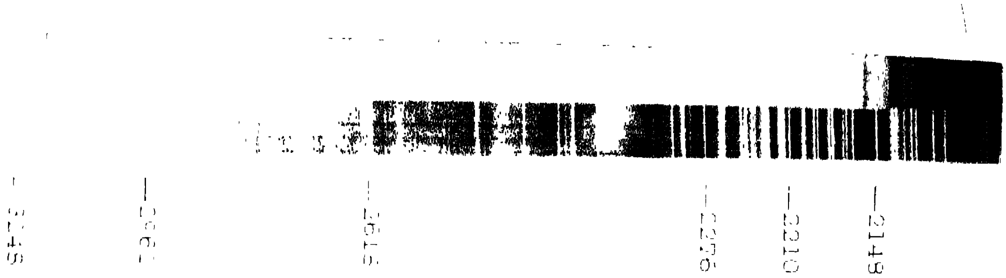

(c)

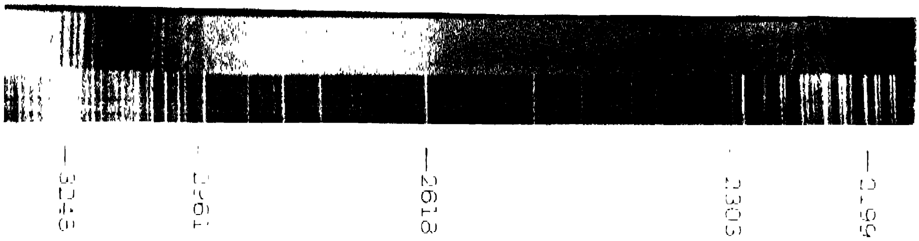

(d)

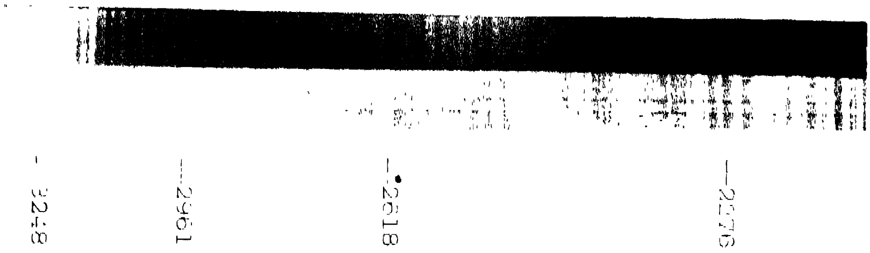

transitions to anti-bonding molecular orbitals. No complete analysis exists for any of the band systems indicated above and the need for further investigation is obvious, on account of the particular interest of the CS_2 absorption in connection with the structure of the spectra of triatomic molecules. The present paper describes the results of a detailed study of the second absorption system of CS_2 molecule in the region λ2300 to λ1000 and presents an interpretation of a new progression detected among the bands.

EXPERIMENTAL

Three absorption tubes of lengths 25 cms , 15 cms., and 5 cms., made of half-inch bore Pyrex glass tubing are used. Plane quartz windows are attached at either end with shellac (N. C. B. C. Pure No 1 Brand, made in India). The absorption tube is provided with two side tubes for maintaining a constant flow of the vapour which is necessary and essential in experiments with polyatomic molecules that easily decompose. To one of the side tubes a CS_2 container with a long and narrow stem is connected by means of a short length of pressure tubing ; the other side tube is connected to an evacuating pump. The flow of the vapour is regulated by two screw pinch cocks. It is very important that the pressure condition in the tube should be constant during an exposure. Hence with each absorption tube two definite and reproducible pressure conditions are adjusted and maintained. In one case, the pinch cock on the container side is almost completely closed and that on the pump side fully opened. This is found to give a very steady condition, the slow capillary flow of the vapour at the pinch cock on the container side admitting enough vapour into the absorption tube to ensure a steady stream through it. Under these conditions the bands at the short wave-length end of the system are photographed. In the second case, the pinch cock on the container side is fully opened, while that on the pump side is very slightly opened, the quantity of vapour drawn off by the pump being reduced considerably. This condition is expected to correspond to the saturation vapour pressure of the liquid at the temperature of the container. This arrangement could be used to study the absorption at different pressures by immersion of the container in various temperature baths. Experiments were carried out by surrounding the container with ice-salt mixtures giving temperatures between 0° to −20°C. The chief difficulty met with in this case is that within a few minutes a solid deposit is formed on the window nearer the source of continuous spectrum, so that further exposure becomes ineffective. Hence it is found advantageous to screw the pinch cock on the pump side only partially but not completely. In spite of this precaution, the quartz window had to be removed, cleaned and attached again three or four times during an exposure, taking care not to disturb the pinch cocks.

The source of continuous spectrum is a high frequency discharge through iodine vapour described elsewhere and found very easy to set up and convenient to work with even when fairly large exposures are required. For photographing the spectrum two instruments are mainly used. (1) Hilger small quartz E $\genfrac{}{}{0pt}{}{31302}{29322}$ having a dispersion of 12 Å per mm. at λ2000. (2) Hilger medium quartz spectrograph E315 giving a dispersion of 5 Å per mm. at λ2200. As the spectrum occurs below λ2400 the photographic plates had to be specially sensitised for the extreme ultra-violet. Of the various sensitisers that are usually recommended and adopted the ordinary double shell mobil oil was found to be very satisfactory. A thin film of oil was spread on the plate before exposure. The plate was bathed in benzene before development for five minutes to completely dissolve away the oil film and then developed using the caustic soda alkali-developer.

RESULTS

A preliminary study of the band spectrum under the varied experimental conditions described above indicated that the region of absorption is determined largely by the pressure conditions of the vapour. With the lowest pressure used, (Plate XIA(*c*)) the extreme bands below λ2000 were developed, and the bands at longer wave lengths could be photographed only when the vapour pressure was raised considerably. But under these conditions (Plate XIA(*a*)) the shorter wave-length side of the band system was found merged in a continuous absorption. By no adjustment of the pressure it was found possible to get the entire system from λ3000 to λ1850 at a single exposure. The width of each band also depends on the pressure condition in the absorption tube at any particular temperature. Seemingly narrow bands at certain pressures appear as wide and red degraded as the vapour pressure is changed and even split up into a number of components even at the low dispersion used (for example λ2005) (Plate XIA*c* and *d*).

This leads to a difficulty in estimating the relative intensities of the bands. But by successive comparison made over short ranges of the spectrum, it can be stated that in general, the intensity of the system is greatest in the region λ2050 and falls off on either side—a distribution of intensity which may be regarded as corresponding to Franck-Condon variation.

Plates XIA and XIB show a series of photographs of the bands under different conditions, the details of which are explained at the end. There are a number of very characteristic features of these bands which might prove helpful in interpreting their structure.

1. The system presents the unmistakable appearance of a long progression consisting of many members. (Plate XI) A.

2. The bands are generally degraded towards the red end and many of them distinctly show very composite structure, consisting of a number of widely spaced sub-heads; as many as eight of these sub-heads were measured in two or three of these members. The association of the sub-heads to the

main member may be uncertain and cannot be decided until the rotational structure is known. These sub-heads probably form the rotational structure of the bands.

3. Apart from the accompanying sub-heads, each member consists of two main components one of which is much more intense than the other. The less intense component too appears to be resolvable under high dispersion; it becomes broader like the main component with change of vapour pressure and has a sharp violet edge. This feature is observed clearly in Plate XIA(*e*).

EXPLANATION OF THE PLATES

Plate XIA-*a* 25 cms absorption tube, saturation v p of CS_2 at 30° (highest effective path length used, bands observed only in the 3300 region but no bands in the 2150 region)

Plate XIA-*b* 25 cms. tube; pump continuously working (the 3300A system is not present)

Plate XIA-*c* 15 cms tube, at saturation v p of CS_2 at 30

Plate XIA-*d* ,, with the pump continuously working

Plate XIA-*e* 5 cms tube, with the pump continuously working (lowest effective path length used)

Plate XIB-*a* medium quartz spectrogram, 15 cms. tube, s v.p. of CS_2 (prominent SO_2 bands are also seen)

Plate XIB-*b*, *c* and *d* 15 cms tube; continuous evacuation, at temp 30°, 120° and 150°c (*b* shows only the 2300 system, *c* and *d* show bands in the 3300A region also due to CS_2, CS, SO_2, SO, S etc.)

TABLE I

Absorption Bands of Carbon disulphide

Wave-length	Intensity	Wave-number
†2296.55	0	43529
82.92	00	43790
†76.26	1	43917
†57.01	2	44293
54.47	1	44342
41.51	0	599
†38.53	2	659
31.40	0	801
29.28	0	843
23.40	3	962
†22.67	2	976
20.00	1	45029
18.85	1	053
16.81	0	096
14.59	1	141
07.52	1	286
06.76	5	300
†05.27	4	331
†02.22	1	395
00.70	1	426
2199.68	1	447
98.02	4	482
97.33	1	496
96.11	4	521
95.77	0	527
95.11	3	542
92.86	4	587
90.89	0	629
90.32	0	642
89.65	1	654
88.95	0	669
88.28	1	683
87.80	3	694
87.22	3	706
86.29	3	725
84.72	3	759
2180.18	6	45853
79.14	0	870
78.98	0	878
77.32	6	914
75.49	6	952
†73.17	6	46001

(† SO_2 bands occurring as impurity).

The measurements given below are from Hilger small quartz spectrograph.

Wave-length	Intensity	Wave number	Wave-length	Intensity	Wave number
2196.2	00	45519	2074.0	3	48201
			70.1	2	291
81.4	0	705	68.1	2	338
80.1	1	855	62.9	10	460
75.5	3	952	60.8	8	509
72.8	1	46009			
			54.1	0	667
64.2	[illegible]	192	50.1	0	755
61.3	2	254			
59.-	[illegible]	290	46.8	2	841
56.0	5	368	45.9	4	862
54.9	3	391	43.8	2	913
50.8	3	480	38.5	1	49040
48.6	2	527			
46.0	3	584	31.4	1	139
42.3	4	664			
37.8	8	762	28.8	5	274
35.0	6	824	25.7	2	350
31.8	3	894	19.7	1	496
29.3	2	919			
27.4	2	991	11.7	3	693
25.1	1	47042	08.4	4	775
23.5	2	074			
19.3	8	170	04.8	0	861
16.0	6	244			
13.3	3	304	01.3	0	951
08.6	5	410	1997.2	8	50055
			95.5	8	098
02.2	0	554	92.4	1	170
00.2	8	599			
2098.1	8	647	80.5	8	477
95.3	10	711	75.9	2	594
92.1	1	784			
			68.6	4	785
83.5	10	981	63.7	10	909
78.4	10	48099			
2076.5	5	48143	49.3	10	51285
			1932.2	10	51738

4. A number of sharper bands are observed which have a somewhat line-like appearance and occur mostly above λ2180 (Plate XIB*a*) λ2108 is one such band XIA(*c*). It persists as line-like and does not change in appearance with pressure. It may be an atomic absorption line but could not be identified with any such known line.

A complete catalogue of the wave-lengths of all the observed band heads is given in Table (I). The intensity values cannot be taken as determined on uniform comparison. At best, they give relative values of bands which occur close together. Down to λ2173 the wave-lengths are determined from the Hilger medium quartz plate and the rest from the small instrument. There is an over-lapping region between the two sets of measurements; the differences are due, chiefly, to the partial resolution of the rotational structure in the larger dispersion. Plate XIB(*a*) shows the spectrum with the medium quartz instrument between $\lambda 2300$ and $\lambda 2140$. It indicates, specially, the desirability of further investigation with a still higher dispersion. Some prominent heads are also seen, which are due to SO_2, occurring as an impurity in some exposures. Such bands are indicated in the table by an asterisk.

DISCUSSION

The intense bands are arranged by Price and Simpson to form into a progression with a mean frequency of about 410 cm^{-1}. For convenience, the wave-numbers of these bands are given below, (Table II) together with the corresponding values from our meas-urements. Although there appear to be large discrepancies in the successive wave-number intervals, the evidence from the photographs shows that there can be no doubt as to the reality of the progression itself. The discrepancies may be due to the unresolved rotational structure and the low dispersion of the spectrograph.

TABLE II

CS_2 Progression (Price and Simpson)

Price and Simpson		Author	
Wave-number (int.)		Wave-number	$\Delta\nu$
45950 (00)	420	45542	410
46370 (0)	420	45952	416
46790 (0)	410	46368	394
47200 (1)	410	46762	408
47610 (1)	410	47170	429
48020 (2)	420	47599	382
48440 (3)	430	47981	479
48870 (5)	420	48460	402
49290 (6)	420	48862	412
49710 (7)	400	49274	419
50110 (7)	370	49693	405
50480 (8)	420	50098	379
50900 (9)	380	50477	432
51280 (10)	440	50909	376
51720 (8)	420	51285	445
52140 (7)	...	51730	...

The first band of this progression was located by Price and Simpson at ν 45950. Our photographs definitely indicate the occurrence of at least one more member and the origin is more probably at ν 45542. The behaviour of the band at different temperatures—chiefly at very low temperatures—is yet to be determined.

The relation of this characteristic frequency to the fundamental frequencies in the CS_2 molecule was discussed by Price and Simpson. In the ground state, Raman Effect and Infra-red data have established the fundamental frequencies of this molecule as

Symmetrical valence frequency or breathing frequency ... $\nu_1 = 656$
Deformation or bending frequency ... ... $\nu_2 = 400$
Anti-symmetrical frequency ... ... $\nu_3 = 1523$

Of these, ν_1 is the only totally symmetrical frequency, the two remaining being non-totally symmetrical. Herzberg and Teller's selection rules for an allowed electronic transition are :

1. Totally symmetrical vibration can undergo any change

$$\Delta v = \pm 0,\ 1,\ 2, \cdots$$

2. Non-totally symmetrical vibrations will change in even values,

$$i.e.,\ \Delta v = \pm 0,\ 2,\ 4, \cdots$$

In spite of the agreement of the frequency 410 cm^{-1} with the deformation or bending frequency ν_2'' in the ground state, still it has to be assigned to the upper state of the molecule, as the selection rules permit only the totally symmetrical vibration frequencies to appear in absorption from the vibrationless ground state. Further, if this progression were to arise from vibrating ground state, the intensity distribution among the bands should be determined by the Boltzman factors, which would make the bands at the long wave-length end quite weak. The observed intensity, namely, a gradual rise and a gradual fall, is more in accordance with the Franck-Condon principle. From the above considerations, this frequency of 410 cm^{-1} is to be identified with the symmetrical valence frequency ν_1' of the upper state.

In addition to the above mentioned progression, detected by Price and Simpson, the photographs have revealed the existence of another, which has not been reported by any of the previous investigators. It was mentioned earlier that each of the intense members of the Price and Simpson progression is accompanied by a less intense but very prominent component, occurring at about × 60 or 70 cm^{-1} towards the shorter wave-length side of each. There are two possibilities of interpreting these bands; one is to regard them as components of a doublet electronic level (the intense heads forming the other component); but the CS_2 molecule cannot give rise to doublet electronic states. They cannot also form part of the rotational structure, because the heads occur towards the shorter wave-length of the main bands whereas the main bands are degraded to the red. The other possibility is to consider them as forming another progression having approximately the same frequency difference 410 cm^{-1}. For clearness, these band heads are shown below:

New CS_2 Progression

ν	$\Delta\nu$	ν	$\Delta\nu$
46009	382	48509	404
46391	433	48913	437
46824	420	49350	425
47244	403	49775	401
47647	454	50176	418
48090	410	50594	...

In spite of the irregularities in the wavenumber intervals, the reality of this progression cannot be doubted. The interval between this and the Price and Simpson progression may be 70 cm^{-1}, or 470 cm^{-1}, 870 cm^{-1}. This shows that the bands do not arise from vibrating ground states. If, however, the interval of 470 $cms.^{-1}$ is regarded as corresponding to two quanta of (twice 235 $cms.^{-1}$), the deformation frequency of the upper state, the new progression can be interpreted as due to the transition $(v, 2, 0)' \leftarrow (0, 0, 0)''$ while the main progression (Price and Simpson's) can be represented as $(v, 0, 0)' \leftarrow (0, 0, 0)''$. Our photographs have indicated, besides these two progressions, the existence of several line-like bands; the explanation of these is not yet clear; they will, perhaps, be understood when the rotational structure, the variation of intensity with temperature, and other characteristics of the bands are studied and the third frequency of the upper state is established. Attempts in this direction are in progress.

ANDHRA UNIVERSITY,
WALTAIR.

REFERENCES

Bruhat and Pautheimer (1924), *Comp. Rend.*, **179**, 154.
Jenkins (1929), *Astrophy. J.*, **70**, 191.
Kusch and Loomis (1939), *Phy. Rev.*, **55**, 850.
Lieberman (1941), *Phy. Rev.*, **60**, 496.
Mulliken (1941), *Phy. Rev.*, **60**, 512.
Nielson (1936), *Phy. Rev.*, **49**, 413.
Price and Simpson (1938), *Proc. Roy. Soc.*, **A165**, 272.
Ramasastry (1947), *Ind. J. Phys.* (Communicated).
Watson and Parker (1931), *Phy. Rev.*, **37**, 1013(A).
Wilson (1929), *Astrophy. J.*, **69**, 34.